



# ICAROB 2015

## PROCEEDINGS OF THE 2015 INTERNATIONAL CONFERENCE ON ARTIFICIAL LIFE AND ROBOTICS

January 10-12, 2015  
Horuto Hall, Oita, JAPAN  
International Meeting Series

Editor-in-Chief

Masanori Sugisaka

Editors: Takao Ito, Ju-Jang Lee, Yingmin Jia

ISBN 978-4-9902880-9-9

The 2015 International Conference on Artificial Life and Robotics (ICAROB 2015), Horuto Hall, Oita, Japan, January 10-12, 2015

Proceedings of the 2015 International Conference on  
**ARTIFICIAL LIFE AND ROBOTICS**  
**(ICAROB2015)**

January 10-12, 2015  
Horuto Hall Oita, Japan

Editor-in-Chief: Masanori Sugisaka  
Editors: Takao Ito, Ju-Jang Lee, Yingmin Jia  
ICAROB 2015 ISBN 978-4-9902880-9-9



# Contents

1	Organization, etc.	1
2	Messages	6
3	Time Table	10
4	Opening Ceremony	13
5	Technical paper index	14
6	Abstracts	26
6-1	PS abstracts	26
6-2	IS abstracts	27
6-3	OS abstracts	28
6-4	GS abstracts	43
7	Authors index	62
8	Conference room	68

## **SPONSERED**

AROB (ALife Robotics Corporation Ltd.)



## **ORGANIZED BY**

International Steering Committee of International Conference on Artificial Life and Robotics (ICAROB)

## **TECHNICAL Co-SPONSORED BY**

IEEE Fukuoka Section (Japan)

## **CO-ORGANIZED BY**

Chinese Association for Artificial Intelligence (CAAI, P. R. China)  
University of Sultan Zainal Abidin (UniSZA) (Malaysia)

## **ADVISORY COMMITTEE CHAIR**

Moshe Kam (New Jersey Institute of Technology, Former IEEE President, USA)

## **ADVISORY COMMITTEE**

F. Harashima (Tokyo Metropolitan University, President, Japan)  
B. Eisenstein (Drexel University, Former IEEE President, USA)  
H. Kimura (RIKEN, Japan)  
M. Tomizuka (University of California Berkeley, USA)  
M. Kam (New Jersey Institute of Technology, Former IEEE President, USA)  
A. Grzech (Wrocław University of Technology, Poland)  
K. Aihara (The University of Tokyo, Japan)  
D. J.G. James (Coventry University, United Kingdom)  
J. Johnson (The Open University, UK)  
K. Kyuma (Mitsubishi Electric Corporation, Japan)  
S. Rasmussen (University of Southern Denmark, Denmark)  
J. M. Epstein (The Johns Hopkins University, USA)  
J. Świątek (Wrocław University of Technology, Poland)  
P. Kalata (Drexel University, USA)  
P. Oh (Drexel University, USA)  
R. Fischl (Drexel University, USA)  
T. Fukuda (Meijo University, Japan)  
Kai-Tai Song (National Chiao Tung University, Taiwan)

## **GENERAL CHAIRS**

Masanori Sugisaka (Alife Robotics Corporation Ltd.(Japan), Open Univesity(UK), University of Sultan Zainal Abidin (UniSZA), University of Malaysia-Peris(Malaysia))

## **Co GENERAL CHAIRS**

Yingmin Jia (Beihang Univesty, P. R. China)  
Takao Ito (Hiroshima University, Japan)  
Ju-Jang Lee (KAIST, Korea)

## **VICE GENERAL CHAIR**

C. Zhang (Tinghua Univesity, P. R. China)  
H. H. Lund (Technical University of Denmark, Denmark)  
J. L. Casti (International Institute for Applied Systems Analysis, Austria)  
J.M. Lee (Pusan National University, Korea)  
Y. G. Zhang (Academia Sinica, P. R. China)

## **PROGRAM CHAIRMAN**

Makoto Sakamoto (University of Miyazaki, Japan)

## **SUB PROGRAM CHAIR**

M. Oswald (The Vienna University of Technology, Austria)

## **INTERNATIONAL ORGANIZING COMMITTEE**

E. Hayashi (Kyushu Institute of Technology, Japan)  
H. Desa (University of Malaysia, Perlis, Malaysia)  
H. Suzuki (The University of Tokyo, Japan)  
H. Furutani (The University of Miyazaki)  
H. Matsuno (Yamaguchi University, Japan)  
J. Wang (Beijing Jiaotong University, P. R. China)  
K. Shimohara (Doshisha University, Japan)  
K. Ohtsu (Tokyo University of Marine Science and Technology)  
K-L. Su (National Yunlin University of Science and Technology, Taiwan)  
M. Kubo (National Defense Academy of Japan, Japan)  
M. Obayashi (Yamaguchi University, Japan)  
M. Yamashita (Kyushu University, Japan)  
M. Rajiv (New Jersey Institute of Technology)  
M. Rizon (University of Sultan Zainal Abidin, Malaysia)  
P. Sapaty (Ukrainian Academy of Science, Ukraine)

Q. Yanbin (Harbin Institute of Technology, P. R. China)  
S. Ishikawa (Kyushu Institute of Technology, Japan)  
T. Kohno (The University of Tokyo, Japan)  
T. Hattori (Kagawa University, Japan)  
T. S. Ray (University of Oklahoma, USA)  
V. Berdonosov (Komsomolsk-on-Amur State University of Technology, Russia)  
Y. Yoshitomi (Kyoto Prefectural University, Japan)

#### **INTERNATIONAL PROGRAM COMMITTEE**

A. Nakamura (AIST, Japan)  
A. Selamat (University of Technology of Malaysia (UTM), Malaysia)  
B. Fu (Shanghai Jiatong University, P. R. China)  
D. Ai (University of Science & Technology Beijing, China)  
E. Joelianto (Bandung Institute of Technology, Indonesia)  
F. Dai (Tianjin University of Science & Technology, P. R. China)  
H. Ogai (Waseda University, Japan)  
H. Yanagimoto (Osaka Prefecture University, Japan)  
H. Umeo (Osaka Electro-Communication University, Japan)  
H. Iizuka (Osaka University, Japan)  
H. Zhao (Shanghai Institute of Technology, P. R. China)  
H. Abbass (University of New South Wales and ADFA, Australia)  
I. Tanev (Doshisha University, Japan)  
J. Zhao (Beijing Jiaotong University, P. R. China)  
K. E. Merrick (University of New South Wales and ADFA, Australia)  
K. Kobayashi (Aichi Prefectural University)  
K. Kurashige (Muroran Institute Technology, Japan)  
K. Sugawara (Tohoku Gakuin University, Japan)  
L. Pagliarini (Technical University of Denmark, Denmark)  
M. Eaton (University of Limerick, Ireland)  
M. Yokomichi (The University of Miyazaki, Japan)  
M. Tabuse (Kyoto Prefectural University, Japan)  
M. Hatakeyama (university of Zurich, Switzerland)  
M. Svinin (Kyushyu University, Japan)  
M. Watanabe (Kagoshima University, Japan)  
N. Mokhtar (University of Malaya, Malaysia)  
P. S. Sapaty (National Academy of Sciences of Ukraine, Ukraine)  
S. Ikeda (The University of Miyazaki, Japan)  
S. S. Joshi (College of Engineering, UCLA, USA)  
S. Omatu (Osaka Institute of Technology, Japan)  
S-M Chen (National Taichung University of Education, Taiwan)  
T. Zhang (Tsinghua University, P. R. China)  
T. Iwamoto (Mitsubishi Electric Corporation, Advanced Technology R&D Center, Japan)  
T. Katayama (the University of Miyazaki, Japan)  
T. Yoshinaga (Tokuyama National College of Technology)

Y. Fan (University of California-Davis, USA)

Y. Liu (University of Aizu, Japan)

Y. I. Cho (The University of Suwon, Korea)

S. Mabu (Yamaguchi University, Japan)

H. Matsushita (Kagawa University, Japan)

## **LOCAL ARRANGEMENT COMMITTEE**

M. Sakamoto (University of Miyazaki, Japan)

M. Sugisaka (ALife Robotics Co., Ltd., Japan,

Open University, UK,

University of Sultan Zainal Abidin (UniSZA), University of Malaysia-Peris, Malaysia)

Takao Ito (Hiroshima University, Japan)

## **HISTORY**

This symposium was founded in 1996 by the support of Science and International Affairs Bureau, Ministry of Education, Culture, Sports, Science and Technology, Japanese Government. Since then, this symposium has been held every year at B-Con Plaza, Beppu, Oita, Japan except in Oita, Japan (AROB 5th '00) and in Tokyo, Japan (AROB 6th '01). We changed this symposium name as The International Conference on Artificial Life and Robotics newly. This conference invites you all.

## **OBJECTIVE**

The objective of this conference is the development of new technologies for artificial life and robotics which have been recently born in Japan and are expected to be applied in various fields. This conference will discuss new results in the field of artificial life and robotics.

## **GENERAL SESSION TOPICS**

**GS1** Artificial intelligence(4)

**GS2** Complexity(4)

**GS3** Evolutionary computation(3)

**GS4** Intelligent control(4)

**GS5** Neuromorphic systems(4)

**GS6** Poster Sessions(14)

**GS7** Pattern recognition (3)

**GS8**Robotics I (5)

**GS9** Robotics II (5)

**GS10**Robotics III (5)

## **ORGANIZED SESSION TOPICS**

**OS1**Intelligent Control(5)

**OS2**Software Development Support Method (6)

**OS3**Image Analysis, Human Interface, and Text Mining(5)

**OS4**Graph Theory and Its Application(3)

**OS5** Bio-Inspired Algorithms and Their Applications(3)

**OS6** Computer Science and Information Processing(4)

**OS7** Computer Network and Security(3) **OS8** Kansei Engineering(5)

### **COPYRIGHTS**

Accepted papers will be published in the proceeding of The 2015 International Conference on Artificial Life and Robotics (ICAROB 2015). Some of high quality papers in the proceeding will be requested to re-submit their papers for the consideration of publication in an international journal ROBOTICS, NETWORKING AND ARTIFICIAL LIFE under agreement of both Editor-in-Chief and 3 reviewers. All correspondence related to the conference should be addressed to ICAROB Office.

### **ICAROB Office**

**ALife Robotics Corporation Ltd.**

**3661-8 Oaza Shimohanda, Oita 870-1112, JAPAN**

**TEL/FAX: +81-97-597-7760**

**E-MAIL:**

[icarob@alife-robotics.co.jp](mailto:icarob@alife-robotics.co.jp)

**Home Page :** <http://alife-robotics.co.jp/>

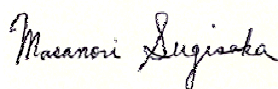
## MESSAGES



**Masanori Sugisaka**

**General Char**

**(Professors, Open  
Univesity(UK),University of Sultan  
Zainal Abidin, University of  
Malaysia-Peris(Malaysia) and  
President of Alife Robotics Co.,  
Ltd..(Japan))**

A handwritten signature in black ink that reads "Masanori Sugisaka". The signature is written in a cursive, flowing style.

**Masanori Sugisaka**

**General Chair of ICAROB**

It is my great honor to invite you all to The International Conference on Artificial Life and Robotics (ICAROB 2015).

This Conference is changed as the old symposium from the first (1996) to the Eighteenth(2013) anually which were organized by Oita University, Nippon Bunri University(NBU), and ALife Robotics Corporation Ltd. under the sponsorship of the Science and Technology Policy Bureau, the Ministry of Education, Science, Sports, and Culture (Monbusho), presently, the Ministry of Education, Culture, Sports, Science, and Technology (monkasho), Japanese Government, Japan Society for the Promotion of Science (JSPS), The Commemorative Organization for the Japan World Exposition ('70), Air Force Office of Scientific Research, Asian Office of Aerospace Research and Development (AFOSR/AOARD), USA. I would like to express my sincere thanks to not only Monkasho (annually fund support from 1996 to 2013) but also JSPS, the Commemorative Organization for the Japan World Exposition ('70) , Japanese companies for their repeated support.

The old symposium was organized by International Organizing Committee of AROB and was co-operated by the Santa Fe Institute (USA), RSJ, IEEJ, ICASE (Now ICROS) (Korea), CAAI (P. R. China), ISCIE, IEICE, IEEE (Japan Council), JARA, and SICE.The old AROB symposium was growing up by absorbing many new knowledge and technologies into it.

This history and character was inherited also from ICAROB 2014(The 2014 International Conference on Artificial Life and Robotics) now.From now on, ALife Robotics Corporation Ltd. is in charge of management. This year we haveThe 2015 InternationalConference on Artificial Life and Robotics (ICAROB 2015).The future of The ICAROB is brilliant from a point of view of yielding new technologies to human society in 21st century.

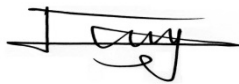
I hope that fruitful discussions and exchange of ideas between researchers during Conference(ICAROB 2015) will yield new merged technologies for happiness of human beings and, hence, will facilitate the establishment of an international joint research institute on Artificial Life and Robotics in future.

**Yingmin Jia**

**Co-General Chair of ICAROB**



**Yingmin Jia**  
**Co-General Chair**  
**(Professor,**  
**Beihang University,**  
**R .P. China)**

A handwritten signature in black ink, appearing to read 'Yingmin Jia', written over a horizontal line.

It is my great pleasure to invite you to the 2015 International Conference on Artificial Life and Robotics (ICAROB 2015), in Oita City, Oita, Japan from Jan. 10th to 12th, 2015.

ICAROB develops from the AROB that was created in 1996 by Prof. Masanori Sugisaka and celebrated her birthday of 19th years old in 1996. Doubtless, new mission and big challenges in the field of artificial life and robotics will promote ICAROB to start a new stage and attract wide interests among scientist, researchers, and engineers around the world.

For a successful meeting, many people have contributed their great efforts to ICAROB. Here, I would like to express my special thanks to all authors and speakers, and the meeting organizing team for their excellent works.

Looking forward to meeting you at ICAROB in Oita City and wishing you enjoy your stay in Japan.





**Takao Ito**  
**Co-General Chair**  
**(Professor Hiroshima**  
**university, Japan)**

A handwritten signature in black ink that reads "Takao Ito". The signature is written in a cursive, flowing style.

## **Takao Ito**

### **CoGeneral Chair of ICAROB**

It is my great honor to invite you all to The 2015 International Conference on Artificial Life and Robotics (ICAROB 2015). This Conference is changed as the old symposium from the first (1996) to the Eighteenth I am pleased to welcome you to the 2015 International Conference on Artificial Life and Robotics in the wonderful city of Oita, Japan

The ICAROB has long history. The former organization of the ICAROB was developed under the strong leadership of the President, Professor. Masanori Sugisaka, the father of AROB. We gathered many researchers, faculty members, graduate students from all over the world, and published numerous high-quality proceedings and journals every year.

Over the years, dramatic improvements have been made in the field of artificial life and its applications. The ICAROB has becoming the unifying the exchange of scientific information on the study of man-made systems that exhibit the behavioral characteristic of natural living systems including software, hardware and/or wetware. Our conference shapes the development of artificial life, extending our empirical research beyond the territory circumscribed by life-as-we-know-it and into the domain of life-as-it-could-be. It will provide us a good place to present our new research results, good ideas, and valuable information about artificial intelligence, complex systems theories, robotics, management of technology, etc.

In order to provide an outstanding technical level for the presentations at the conference, we have invited more than 60 distinguished experts in the field of artificial life in the organizing committee and program committee. We will have 22 sessions during 3 days of conference, including 4 invited sessions.

The conference site is the Horuto Hall, one of the finest congress centers in Oita. It is situated near the center of the city and in front of Oita railway station. You can find many fantastic scenic spots and splendid hot-springs. Enjoy your stay and take your time to visit the city of Oita.

I am looking forward to meeting you in Oita during ICAROB 2015 and to sharing a most pleasant, interesting and fruitful conference

**Ju-Jang Lee**



**Ju-Jang Lee**  
**Co-General Chair**  
**(Professor, KAIST)**

A handwritten signature in black ink, appearing to read 'J. Lee'.

**Co-General Chair of ICAROB**

The First International Conference on Artificial Life and Robotics (ICAROB) was held in Oita City, Oita, Japan from Jan. 11th to 13th, 2014. This year's Conference will be held amidst the high expectation of the increasingly important role of the new interdisciplinary paradigm of science and engineering represented by the field of artificial life and robotics that continuously attracts wide interests among scientist, researchers, and engineers around the globe.

Distinguished researchers and technologists from around the world are looking forward to attending and meeting at ICAROB. ICAROB is becoming the annual excellent forum that represents a unique opportunity for the academic and industrial communities to meet and assess the latest developments in this fast growing artificial life and robotics field. ICAROB enables them to address new challenges, share solutions, discuss research directions for the future, exchange views and ideas, view the results of applied research, present and discuss the latest development of new technologies and relevant applications.

In addition, ICAROB offers the opportunity of hearing the opinions of well-known leading experts in the field through the keynote sessions, provides the bases for regional and international collaborative research, and enables to foresee the future evolution of new scientific paradigms and theories contributed by the field of artificial life and robotics and associated research area. The twenty-first century will become the century of artificial life and intelligent machines in support of humankind and ICAROB is contributing through wide technical topics of interest that support this direction.

It is a great honor for me as a Co-General Chair of the 2nd ICAROB 2015 to welcome everyone to this important event. Also, I would like to extend my special thanks to all authors and speakers for contributing their research works, the participants, and the organizing team of the 2nd ICAROB.

I'm looking forward to meeting you at the 2nd ICAROB in Oita City and wishing you all the best.

### TIME TABLE (1/10)

1/10	Room404	Room406	Room407
9:30~	Registration		
10:00-11:40		GS8(5)Robotics I Chair T. Sethaput	GS2(4)Complexity Chair K. Kobayashi
11:40-11:50	Coffee break		
11:50-12:10	Opening Ceremony (Room405)		
12:10-13:00	Lunch		
13:00-14:00		GS7(3)Pattern Recognition Chair J. Wang	GS3(3)Evolutionary Computation Chair S. Mabu
14:00-14:20	Coffee break		
14:20-16:00		GS9(5)Robotics II Chair Y. Morita	GS5(4)Neuromorphic Systems Chair T. Kondo
16:00-16:20	Coffee break		
16:20-18:00		GS10(5)Robotics III Chair S. Kim	GS4(4)Intelligent Control Chair J-M Lee.
<p><b>GS1 Artificial intelligence(4)</b>  <b>GS2 Complexity(4)</b>  <b>GS3 Evolutionary computation(3)</b>  <b>GS4 Intelligent control(4)</b>  <b>GS5 Neuromorphic systems (4)</b>  <b>GS6 Poster Sessions(14)</b>  <b>GS7 Pattern recognition (3)</b>  <b>GS8 Robotics I (5)</b>  <b>GS9 Robotics II (5)</b>  <b>GS10 Robotics III(5)</b></p> <p><b>OS1 Intelligent Control(5)</b>  <b>OS2 Software Development Support Method (6)</b>  <b>OS3 Image Analysis, Human Interface, and Text Mining(5)</b>  <b>OS4 Graph Theory and Its Application(3)</b>  <b>OS5 Bio-Inspired Algorithms and Their Applications(3)</b>  <b>OS6 Computer Science and Information Processing(4)</b>  <b>OS7 Computer Network and Security(3)</b>  <b>OS8 Kansei Engineering(5)</b></p>			

### TIME TEBLE (1/11)

1/11	Room404	Room405	Room406	Room407
9:30~	Registration			
10:00-11:00		GS6(14)Poster Chair J.J. Lee and J. Wang.	Room403	
			Plenary Speech	
			Prof. Kai-Tai Song	
11:00-12:30			Invited Speech(403) Prof. Henrik H. Lund Prof. Luigi Pagliarini Dr. Jovana Jovan Jovic	
12:30-13:20	Lunch			
13:20-15:00		GS6(14)Poster	GS1(4)Artificial Intelligence Chair M.Kubo	OS8(5)Kansei Engineering Chair T.Hattori
15:00-15:20	Coffee break			
15:20-17:00		GS6(14)Poster	OS1(5) Intelligent Control Chair Y.Jia	OS3(5)Image Analysis, Human Interface, and Text Mining Chair: Y. Yoshitomi
18:00-20:00	Banquet: HOTEL HOKKE CLUB OITA			

### TIME TABLE (1/12)

1/12	Room404	Room406	Room407
9:30~	Registration		
10:00-10:30		Room403	
		Plenary Speech	
		Prof. Kenji Hashimoto	
10:40-12:40		OS5(3)+OS7(3) Chair H. Furutani Chair H. Yamaba	OS2(6) Chair T. Katayama
12:40-13:10	Lunch		
13:10-15:30		OS6(4)+OS4(3) Chair M. Sakamoto Chair: T. Ito	
15:40-16:40	Farewell Party (3rd Floor: Restaurant)		

# **The International Conference on ARTIFICIAL LIFE AND ROBOTICS 2015 (ICAROB2015 )**

## **January 10 (Saturday)**

**Room 405 11:50-12:10**

### **Opening Ceremony**

**Chair: M. Sakamoto (University of Miyazaki, Japan)**

#### **Welcome Addresses**

- 1. General Chairman of ICAROB** M. Sugisaka (ALife Robotics Co., Ltd. Japan, The Open University, UK, University of Sultan Zainal Abidin (UniSZA), Malaysia, University of Malaysia-Perlis, Malaysia (UniMAP))
- 2. Co-General Chairman of ICAROB** Y. M. Jia (Beihang University, China)
- 3. Co-General Chairman of ICAROB** T. Ito (Hiroshima University, Japan)
- 4. Co-General Chairman of ICAROB** J. J. Lee (KAIST, Korea)

## **January 11 (Sunday)**

**HOTEL HOKKE CLUB OITA**

**18:00-20:00**

### **Banquet**

**Chair: J.M. Lee (Pusan National University, Korea)**

#### **Welcome Addresses**

- K.T. Song (National Chiao Tung University (NCTU), Taiwan)  
H.H. Lund (Denmark Technical University of Denmark, Denmark)  
J.J. Jovic (AIST, Japan),

## TECHNICAL PAPER INDEX

### January 10 (Saturday)

#### 9:30- Registration (Room404)

#### Room 406

#### 10:00-11:40 GS8(5)Robotics I

Chair: Thunyaseth Sethaput (Thammasat University, Thailand)

GS8-1 *Production effects by form changes of autonomous decentralized FMSs with mind*  
Kakeru Yokoi, Hidehiko Yamamoto, and Takayoshi Yamada (Gifu University, Japan)

GS8-2 *Development of an autonomous-drive personal robot*  
*"Improve the accuracy of object area determination by boundary detection"*  
Mikiko Hirai, Eiji Hayashi (Kyusyu Institute of Technology, Japan)

GS8-3 *Construction of a supermicro sense of force feedback and vision for micro-objects:*  
*development of a haptic device*  
Yusei Ishii, Eiji Hayashi (Kyushu Institute of Technology, Japan)

GS8-4 *Error Recovery of Pick-and-Place Tasks in Consideration of Reusability of Planning*  
Akira Nakamura, Kazuyuki Nagata, Kensuke Harada and Natsuki Yamanobe  
(National Institute of Advanced Industrial Science and Technology (AIST), Japan)

GS8-5 *Design of Sliding Mode Controller for Droplet Position in EWOD Microfluidic System*  
Thunyaseth Sethaput (Thammasat University, Thailand), Arsit Boonyaprapasorn  
(Chulachomkloa Royal Military Academy, Thailand)

#### 13:00-14:00 GS7(3) Pattern Recognition

Chair: Jiwu Wang (Beijing Jiaotong University, China)

GS7-1 *Fast motion detection based on cross correlation*  
Panca Mudjirahardjo, Joo Kooi Tan, Hyungseop Kim and Seiji Ishikawa  
(Kyushu Institute of Technology, Japan)

GS7-2 *Detecting moving objects on a video having a dynamic background*  
FX Arinto Setyawan, Joo Kooi Tan, Hyungseop Kim, Seiji Ishikawa  
(Kyushu Institute of Technology, Japan)

GS7-3 *Study on the Target Recognition and Location Technology of industrial Sorting Robot based on Machine Vision*

Jiwu Wang, Xianwen Zhang, HuazheDou( Beijing Jiaotong University, China)  
Sugisaka Masanori (Alife Robotics Corporation Ltd, Japan, Open University, United Kingdom)

### **14:20-16:00 GS9(5)Robotics II**

**Chair: Yoshifumi Morita (Nagoya Institute of Technology, RIKEN-RSC, Japan)**

- GS9-1 *Mechanism Designs for Bio-inspired Flapping Wing Robots*  
Palakorn Tantrakool, Eakkachai Pengwang  
(King Mongkut's University of Technology Thonburi, Thailand)
- GS9-2 *Effective rocking motion for inducing sleep in adults– Verification of effect of mother's embrace and rocking motion –*  
Keishi Ashida, Yoshifumi Morita (Nagoya Institute of Technology, RIKEN-RSC, Japan)  
Ryojun Ikeura (Mie University, RIKEN-RSC, Japan)  
Kiyoko Yokoyama (Nagoya City University, RIKEN-RSC, Japan)  
Ming Ding, Yuki Mori (RIKEN-RSC)
- GS9-3 *Postural Sway Response to Local Vibratory Stimulation in Young, Middle-aged and Elderly People in Standing Position*  
Ayaka Yamada, Eishi Nakamura, Noritaka Sato, Yoshifumi Morita  
(Nagoya Institute of Technology, Japan)  
Tadashi Ito, Yoshihito Sakai (National Center for Geriatrics and Gerontology, Japan)  
Kazunori Yamazaki (Fujita Health University, Japan)
- GS9-4 *Development of Unmanned Transport System for automated systems*  
Hyunhak Cho, Jungwon Yu, Yeongsang Jeong, Hansoo Lee, Sungshin Kim  
(Pusan National University, Korea)
- GS9-5 *Localization method for AGV using magnetic devices and IMU*  
Moonho Park, EunKyeong Kim, Yeongsang Jeong, Hansoo Lee, Jungwon Yu,  
Sungshin Kim (Pusan National University, Korea)

### **16:20-18:00 GS10(5)Robotics III**

**Chair: Sungshin Kim (Pusan National University, Korea)**

- GS10-1 *On the Effects of Epigenetic Programming on the Efficiency of Incremental Evolution Of the Simulated Khepera Robot*  
Yasuto Nishiwaki, Ivan Tanev and Katsunori Shimohara  
(University of Doshisha, Japan)
- GS10-2 *The Effect of Duration of Both Stages of Incremental Genetic Programming on its Efficiency of Evolution of Snakebot*  
N. Mukosaka, I. Tanev, K. Shimohara (Doshisha University, Japan)



- GS10-3 *Design of an effective shoulder joint mechanism for an upper-limb exoskeleton robot*  
Masahito Akiyama, Kazuo Kiguchi (Kyushu University, Japan)
- GS10-4 *A Machine Learning Approach to a Lateral Continuous Force Estimation for a Walking Biped Robot*  
Yeoun-Jae Kim, Jun-Yong Lee and Ju-Jang Lee (KAIST, Korea)
- GS10-5 *The Improvement of Robust Robot SLAM Algorithm Based on Sensor Fusion*  
Jiwu Wang, Shunkai Zheng, Fangbo Liao (Beijing Jiaotong University, China)  
Sugisaka Masanori (Alife Robotics Corporation Ltd, Japan and Open University, United Kingdom)

## **Room 407**

### **10:00-11:40 GS2(4) Complexity**

**Chair: Kunikazu Kobayashi (Aichi Prefectural University, Japan)**

- GS2-1 *Interactive musical editing system to support human errors and offer personal preferences for an automatic piano*  
Kenji Tsunenari, Eiji Hayashi (Kyushu Institute of Technology, Japan)
- GS2-2 *Modeling of collaboration in design process Based on Channel Theory*  
Patchanee Patitad, Hidetsugu Suto (Muroran Institute of Technology, Japan)
- GS2-3 *Sterilizing system of ballast water using an arc discharge*  
Piao shengxu, Jae-cheol Lee, Zheng Tao, Heeje Kim (Pusan National University, Korea)
- GS2-4 *The design of medical ruby laser power supply system using LLC resonant converter*  
Jaecheol Lee, Piao shengxu, Zheng Tao, Heeje Kim (Pusan National University, Korea)

### **13:00-14:00 GS3(3) Evolutionary Computation**

**Chair: Shingo Mabu (Yamaguchi University, Japan)**

- GS3-1 *Online Rule Updating System Using Evolutionary Computation for Managing Distributed Database*  
Wirarama Wedashwara, Shingo Mabu, Masanao Obayashi and Takashi Kuremoto (Yamaguchi University, Japan)
- GS3-2 *Reinforcement Learning with Symbiotic Relationships for Multiagent Environments*  
Shingo Mabu, Masanao Obayashi and Takashi Kuremoto, (Yamaguchi University, Japan)
- GS3-3 *Development of a Dividual Model Using a Modular Neural Network for Human-Robot Interaction*  
Toshiyuki Tanaka and Kunikazu Kobayashi (Aichi Prefectural University, Japan)

### **14:20-16:00GS5(4)Neuromorphic Systems**

**Chair: Tadashi Kondo (Tokushima University, Japan)**

- GS5-1 *Associative Memory with Class I and II Izhikevich Model*  
Yoshika Osawa, Takashi Kohno (University of Tokyo, Japan)
- GS5-2 *Medical image recognition of heart regions by deep multi-layered GMDH-type neural network using principal component-regression analysis*  
Tadashi Kondo, Junji Ueno and Shoichiro Takao (Tokushima University, Japan)
- GS5-3 *Deep feedback GMDH-type neural network using principal component-regression Analysis and its application to medical image recognition of abdominal multi-organs*  
Tadashi Kondo, Junji Ueno and Shoichiro Takao (Tokushima University, Japan)
- GS5-4 *Synchronized Response to Grayscale Image Inputs in the Chaotic Cellular Neural Network*  
Masayuki Fujiwara, Akihiro Yamaguchi (Fukuoka Institute of Technology, Japan)  
Masao Kubo (National Defense Academy of Japan, Japan)

### **16:20-17:40GS4(4)Intelligent Control**

**Chair: Jang-Myung Lee (Pusan National University, South Korea)**

- GS4-1 *Design of 1/40 scale simulator to apply the Flying Touch Method in hot rolling process*  
Sung-jin Kim, Hyun-hee Kim, Min-cheol Lee (Pusan National University, South Korea)
- GS4-2 *Improving Accuracy of Inertial Measurement unit using Discrete Wavelet Transform*  
Jae-Hoon Jung, Dong-Hyuk Lee, Jang-Myung Lee  
(Pusan National University, South Korea)
- GS4-3 *Outdoor Localization for Quad-rotor using Kalman Filter and Path Planning*  
Chen-Hu, Yo-Seop Hwang, Jang-Myung Lee (Pusan National University, South Korea)
- GS4-4 *Distributed Terminal Backstepping Control for Multi-Agent Euler-Lagrange Systems*  
Seong-Ik Han, Yun-Ki Kim, Jang-Myung Lee (Pusan National University, South Korea)

## **January 11 (Sunday)**

### **9:30- Registration (Room404)**

### **Room 403**

#### **10:00-11:00 Plenary Speech**

**Chair: Ju-Jang Lee (KAIST, Korea)**

#### **PS-1: Kai-Tai Song(National Chiao Tung University, Taiwan)**

PS-1 *Vision-Based Grasp Planning and Experiments of a Mobile Manipulator*  
Yi-Fu Chiu and Kai-Tai Song(National Chiao Tung University, Taiwan)

#### **11:00-12:30 Invited Speech**

**Chair: Yingmin Jia (Beihang University, China)**

**IS-1: Henrik Hautop Lund(Centre for Playware,Technical University of Denmark, Denmark)**

**IS-2: Luigi Pagliarini (Centre for Playware, Technical University of Denmark, Denmark,  
Academy of Fine Arts of Macerata, Italy)**

**IS-3: Jovana Jovic (AIST, Japan)**

IS-1 *Combining playware exergaming with a mobile fitness app*  
Emmanouil Giannisakis, Henrik Hautop Lund  
(Technical University of Denmark, Denmark)

IS-2 *Parallel Relational Universes – experiments in modularity*  
Luigi Pagliarini (Centre for Playware, Technical University of Denmark, Denmark  
Academy of Fine Arts of Macerata, Italy)  
Henrik Hautop Lund (Centre for Playware, Technical University of Denmark,Denmark)

IS-3 *Identifying humanoid and human physical parameters*  
Jovana Jovic, Eiichi Yoshida (AIST, Japan), Gentiane Venture (TUAT, Japan)

### **Room 405**

#### **10:00-17:00GS6 Poster Session(14)**

**Chair: J. J. Lee (KAIST, Korea)**

**Jiwu Wang(Beijing Jiaotong University, China)**

GS6-1 *The construction of evaluation index system for graduate course*  
Ai Dongmei, Wen Jiawei, Ning Xiaojun  
(University of Science and Technology Beijing, China)

- GS6-2 *Extracting Pattern of Arm Movements based on EMG Signal for Stroke Therapy*  
Khairunizam Wan, Rashidah Suhaimi, Aswad A.R (Universiti Malaysia Perlis, MALAYSIA)  
D. Hazry, Zuradzman M. Razlan, Shahrman AB (Universiti Malaysia Perlis, MALAYSIA)  
Mohd Asri Ariffin and Haslina M (Universiti Sains Malaysia, MALAYSIA)
- GS6-3 *Cascade Controller Design for Steering Control of Nonholonomic Autonomous Mobile Robot Vehicle*  
S. Faiz Ahmed, D. Hazry (Universiti Malaysia Perlis (UniMAP), Malaysia)  
F. Azim (Hamdard University, Pakistan)
- GS6-4 *Research on Iris Recognition Based on the BP Neural Network*  
Fengzhi DAI, Li FAN, Chunyu YU, Bo LIU
- GS6-5 *Synchronization Control of a Four-wing Fractional-Order Chaotic System and Its Analog Circuit Design*  
Hongyan Jia, Qian Tao, Jinfang Li, Wei Xue  
(Tianjin University of Science & technology, PR China)
- GS6-6 *A fractional-order hyper-chaotic system and its circuit implementation*  
Wei Xue, HuiXiao, Jinkang Xu, Hongyan Jia  
(Tianjin University of Science and Technology, PR China)
- GS6-7 *Research on Early Crop Monitoring Using Photosynthetic Production Index in China*  
Fengzhi DAI<sup>1</sup>, Li FAN<sup>1</sup>, Daijiro KANEKO, Nozomu HIROSE, Chunyu YU<sup>1</sup>  
(<sup>1</sup>Tianjin University of Science & technology, China)
- GS6-8 *Design and Implementation of Motor Test System based on Virtual Instrument*  
Yulong Xia, Huailin Zhao (Shanghai Institute of Technology, China)  
Jihong Zhu, Yang He (Tsinghua University, China)
- GS6-9 *Consensus Problem of Distributed Multi-agent System*  
Huailin Zhao (Shanghai Institute of Technology, China) Wei Ren (UCR, USA),  
Masanori Sugisaka (Alife Robotics Corporation LTD, Japan)
- GS6-10 *Dingle's Model-based EEG Peak Detection using a Rule-based Classifier*  
Asrul Adam, Norrima Mohktar, Marizan Mubin (University of Malaya, Malaysia),  
Zuwairie Ibrahim (Universiti Malaysia Pahang, Malaysia),  
Mohd Ibrahim Shapiai (Malaysia-Japan International Institute of Technology Universiti  
Teknologi Malaysia, Malaysia)
- GS6-11 *Different Learning Functions for Weighted Kernel Regression in Solving Small Sample Problem with Noise*  
Zuwairie Ibrahim, Nurul Wahidah Arshad (Universiti Malaysia Pahang, Malaysia),  
Mohd Ibrahim Shapiai  
(Malaysia-Japan International Institute of Technology Universiti Teknologi Malaysia,  
Malaysia),

Norrima Mokhtar(University of Malaya,Malaysia)

GS6-12 *Simultaneous Computation of Model Order and Parameter Estimation of a Heating System Based on Particle Swarm Optimization for Autoregressivewith Exogenous Model : An Analysis*

Teoh Shin Yee, Zuwairie Ibrahim, Kamil Zakwan Mohd Azmi  
(Universiti Malaysia Pahang, Malaysia),  
Norrima Mokhtar (University of Malaya,Malaysia)

GS6-13 *Maximum Probability Algorithm for Fault Diagnosis*

Fengzhi DAI, Li FAN, Bo LIU (Tianjin University of Science & technology, China)

GS6-14 *The Fractional Order Hyperchaotic Generalized Augmented Lü System and its Circuit Implementation*

Wei Xue, Jinkang Xu, Hongyan Jia  
( Tianjin University of Science and Technology, PR China)

## Room 406

### 13:20-14:40 GS1(4)Artificial intelligence

**Chair: Masao. Kubo (National Defense Academy of Japan, Japan)**

GS1-1 *Selecting Words and Notation Using Literary Data in the Integrated Narrative GenerationSystem*

Jumpei Ono, Takashi Ogata (Iwate Prefectural University, Japan)

GS1-2 *Evaluation of a Narrative Discourse Generation System Based on the Concept of "Norm and Deviation"*

Taisuke Akimoto (The University of Electro-Communications, Japan)  
Takashi Ogata (Iwate Prefectural University, Japan)

GS1-3 *An aggregating approach of target enclosure of robot swarm*

Masao KUBO, Hiroshi SATO, Akira Namatame  
(National Defense Academy of Japan, Japan)  
Akihiro Yamaguchi(Fukuoka Institute of Technology, Japan)

GS1-4 *Probability of mixing up a nearest neighbor robot under target enclosure by robot swarm*

Masao KUBO, Hiroshi SATO, Akira Namatame  
(National Defense Academy of Japan, Japan),  
Akihiro Yamaguchi (Fukuoka Institute of Technology, Japan)

**15:20-17:00 OS1(5) Intelligent Control**

**Chair: Yingmin Jia (Beihang University, P.R.China )**

**Co-Chair: Weicun Zhang (University of Science and Technology Beijing, P.R.China)**

- OS1-1 *Adaptive Multiple-Model Control of a Class of Nonlinear Systems*  
Chao Yang and Yingmin Jia (Beihang University, P.R.China)
- OS1-2 *Attitude reorientation of spacecraft with attitude forbidden zones*  
XuhuiLu and Yingmin Jia ( Beihang University, P.R.China)
- OS1-3 *Weighted Multiple Model Adaptive Control of Slowly Time-Varying Systems*  
Weicun Zhang, Qing Li (University of Science and Technology Beijing, P.R.China)
- OS1-4 *A Reduced-Complexity Interacting Multiple Model Algorithm for Location Tracking in Heterogeneous Observation*  
Xiaoyan Fu and Yuanyuan Shang (Capital Normal University, P.R.China)
- OS1-5 *Single Image Dehazing on Mobile Device based on GPU Rendering Technology*  
Yuanyuan Shang, Yue Meng, Xiuzhuang Zhou, Xiaoyan Fu, and Hui Ding  
(Capital Normal University, P. R. China)

**Room407**

**13:20-15:00 OS8(5) Kansei Engineering**

**Chair: Tetsuo Hattori (Kagawa University, Japan)**

**Co-Chair: Hiromichi Kawano ( NTT AT, Japan)**

- OS8-1 *Investigation of Feature Quantity in Sound Signal and Feeling Impression Using PCA*  
Yusuke Kawakami, Tetsuo Hattori (Kagawa University, Japan),  
Hiromichi Kawano (NTT AT, Japan), Tetsuya Izumi (Micro-Technica Co., Ltd., Japan)
- OS8-2 *Automated Color Image Arrangement Method Using Curvature Computation in Histogram Matching*  
Yusuke Kawakami, Tetsuo Hattori, Yoshiro Imai, Haruna Matsushita (Kagawa University, Japan), Hiromichi Kawano (NTT AT, Japan),  
R.P.C. Janaka Rajapakse (Tainan National University of the Arts, Taiwan)
- OS8-3 *Change Detection Experimentation for Time Series data by New Sequential Probability Ratio*  
Yoshihide KOYAMA, Tetsuo HATTORI (Kagawa University, Japan)  
Hiromichi KAWANO (NTT AT, Japan) Katsunori TAKEDA (Canon IT Solutions Inc., Japan)
- OS8-4 *Analysis of Navier-Stokes Equation from the Viewpoint of Advection Diffusion (I)*  
--- Analytical Solution of Diffusion Equation ---  
Hiroki SAKAMOTO, Tetsuo HATTORI (Kagawa University, Japan)

Akiomi TADA (Japan)Vanhoa NGUYEN (Japan)Hiromichi KAWANO (NTT AT, Japan)

OS8-5 *Analysis of Navier-Stokes Equation from the Viewpoint of Advection Diffusion (II)*  
--- Approximate Solution ---

Hiroki SAKAMOTO, Tetsuo HATTORI (Kagawa University, Japan)

Akiomi TADA (Japan)Vanhoa NGUYEN (Japan)Hiromichi KAWANO (NTT AT, Japan)

### **15:20-17:00 OS3(5)Image Analysis, Human Interface, and Text Mining**

**Chair: Yasunari Yoshitomi (Kyoto Prefectural University, Japan )**

**Co-Chairman: Masayoshi Tabuse (Kyoto Prefectural University, Japan)**

OS3-1 *Development of Mouse Cursor Control System Based on Face Direction Using Kinect*

Masayoshi Tabuse (Kyoto Prefectural Univ., Japan)

Kaori Tamura (ISI Software Corp., Japan)

OS3-2 *Quantitative Evaluation of Facial Expressions and Movements of Persons While Using Video Phone*

Taro Asada, Yasunari Yoshitomi, Ryota Kato, Masayoshi Tabuse,  
(Kyoto Prefectural University, Japan)

Jin Narumoto (Kyoto Prefectural University of Medicine, Japan)

OS3-3 *Facial Expression Recognition Using Facial Expression Intensity Characteristics of Thermal Image*

Yasunari Yoshitomi, Taro Asada, Ryota Kato, and Masayoshi Tabuse  
(Kyoto Prefectural University, Japan)

OS3-4 *Method for Character Domain Extraction from Image Using Wavelet Transform*

Taiki Taniguchi (ZENSHO HOLDINGS Co., Ltd., Japan)

Yasunari Yoshitomi (Kyoto Prefectural University, Japan)

OS3-5 *Classification of Japanese Documents and Ranking of Representative Documents Using Characteristic of Frequencies of Words*

Jun Kimura(JustSystems Corp., Japan)

Yasunari Yoshitomi, Masayoshi Tabuse(Kyoto Prefectural University, Japan)

## **January 12 (Monday)**

**9:30- Registration (Room 404)**

### **Room403**

**10:00-10:30 Plenary Speech**

**Chair: Takao Ito (Hiroshima University, Japan)**

## **PS-2:Kenji Hashimoto (Waseda University, Japan)**

- PS-2 *Biped Robot Research at Waseda University*  
Kenji Hashimoto, Atsuo Takanishi (Waseda University, Japan)

## **Room 406**

### **10:40-12:40 OS5(3) + OS7(3)**

#### **OS5(3) Bio-Inspired Algorithms and Their Applications**

**Chair Hiroshi Furutani (University of Miyazaki, Japan)**

**Co-Chair Kenji Aoki (University of Miyazaki, Japan)**

- OS5-1 *Analysis of Genetic Disease Haemophilia A by Using Machine Learning*  
Kenji Aoki, Makoto Sakamoto, Hiroshi Furutani (University of Miyazaki, Japan)
- OS5-2 *Analysis of Asymmetric Mutation Model in Random Local Search*  
Hiroshi Furutani, Yifei Du, Kenji Aoki, Makoto Sakamoto (University of Miyazaki, Japan)
- OS5-3 *Hitting Time Analysis of OneMax Problem in Genetic Algorithm*  
Y. Du, Q. Ma, k. Aoki, M. Sakamoto, H. Furutani (University of Miyazaki, Japan)  
Y. Zhang (Qinghai University, China)

#### **OS7(3) Computer Network and Security**

**Chair Hisaaki Yamaba (University of Miyazaki, Japan)**

**Co-Chair Kentaro Aburada (Oita National College of Technology, Japan)**

- OS7-1 *An Authentication Method for Mobile Devices that is Independent of Tap-Operation on a Touchscreen*  
Hisaaki Yamaba, So Nagatomo, Shinichiro Kubota, Tetsuro Katayama, Naonobu Okazaki (University of Miyazaki, Japan)  
Kentaro Aburada (Oita National College of Technology, Japan)  
Mirang Park (Kanagawa Institute of Technology, Japan)
- OS7-2 *Proposal of Security Evaluation System using User's Reviews and Permissions for Android Application*  
Naonobu Okazaki (University of Miyazaki, Japan)  
Yoshihiro Kita (Kanagawa Institute of Technology, Japan)  
Kentaro Aburada (Oita National College of Technology, Japan)  
Mirang Park (Kanagawa Institute of Technology)
- OS7-3 *Evaluation of Neighbors Based Routing for ad hoc networks*  
Kentaro Aburada (Oita National College of Technology, Japan)  
Hisaaki Yamaba, Shinichiro Kubota, Tetsuro Katayama, Naonobu Okazaki (University of Miyazaki, Japan)  
Mirang Park (Kanagawa Institute of Technology, Japan)



**13:10-15:30 OS6(4)+OS4(3)**

**OS6(4) Computer Science and Information Processing**

**Chair Makoto Sakamoto (University of Miyazaki, Japan)**

**Co-Chair Yasuo Uchida (Ube National College of Technology, Japan)**

OS6-1 *Sufficient spaces for seven-way four-dimensional Turing machines to simulate four-dimensional one-marker automata*

Makoto Nagatomo, Makoto Sakamoto, Hikaru Susaki, Tuo Zhang, Satoshi Ikeda, and Hiroshi Furutani (University of Miyazaki, Japan)  
Takao Ito (Hiroshima University, Japan)  
Yasuo Uchida (Ube National College of Technology, Japan)  
Tsunehiro Yoshinaga (Tokuyama College of Technology, Japan)

OS6-2 *Some Properties of k-Neighborhood Template A-Type Three-Dimensional Bounded Cellular Acceptors*

Makoto Sakamoto, Makoto Nagatomo, Hikaru Susaki, Tuo Zhang, Satoshi Ikeda, and Hiroshi Furutani (University of Miyazaki, Japan)  
Takao Ito (Hiroshima University, Japan)  
Yasuo Uchida (Ube National College of Technology, Japan)  
Tsunehiro Yoshinaga (Tokuyama College of Technology, Japan)

OS6-3 *Perfect Analysis in miniature Othello*

Yuki Takeshita, Satoshi Ikeda, Makoto Sakamoto (Miyazaki University, Japan)  
Takao Ito (Hiroshima University, Japan)

OS6-4 *A proposal for teaching programming through the Five-Step Method*

Y. Uchida, S. Matsuno (National Institute of Technology, Ube College, Japan)  
T. Ito (Hiroshima University, Japan)  
M. Sakamoto (University of Miyazaki, Japan)

**OS4(3) Graph Theory and Its Application**

**Chair Takao Ito (Hiroshima University, Japan)**

**Co-Chair K. Ogata (University of Nagasaki, Japan)**

OS4-1 *The Role of National Standards Setter in the Global Convergence Era -In the Case of the Japanese Setter during the first decade-*  
Ogata, K. (University of Nagasaki, Japan)

OS4-2 *An Empirical Research on Inter-firm Capital Relationship in Yokokai using IDE Spatial Model*

Takao Ito (Hiroshima University, Japan)  
Makoto Sakamoto, S. Ikeda (University of Miyazaki, Japan)  
R. Mehta (New Jersey Institute of Technology, U.S.A)  
Tsutomu Ito (Hino Motors, Ltd. Japan)

OS4-3 *Design and Experimental Evaluation of a Human Skill-Based PID Controller*  
Yuntao Liao, Yamamoto Toru (Hiroshima University, Japan)

## **Room407**

### **10:40-12:40 OS2(6)Software Development Support Method**

**Chair: Tetsuro Katayama (University of Miyazaki, Japan)**

**Co-Chair: Makoto Sakamoto (University of Miyazaki, Japan)**

- OS2-1 *Prototype of a Supporting Tool to Generate Testing Communication Diagram*  
Tetsuro Katayama, Seiya Urata, Yohei Ogata, Hisaaki Yamaba, and Naonobu Okazaki  
(University of Miyazaki, Japan)  
Yoshihiro Kita, (Kanagawa Institute of Technology, Japan)  
Kentaro Aburada (Oita National College of Technology, Japan)
- OS2-2 *Code Coverage Visualization on a Web-Based Testing Tool for Java Programs*  
Mochamad Chandra Saputra (Universitas Brawijaya, Indonesia)  
Tetsuro Katayama (University of Miyazaki, Japan)
- OS2-3 *TFVIS: a Supporting Debugging Tool for Java Programs by Visualizing Data Transitions and Execution Flows*  
Hiroto Nakamura, Tetsuro Katayama, Hisaaki Yamaba, Naonobu Okazaki  
(University of Miyazaki, Japan)  
Yoshihiro Kita (Kanagawa Institute of Technology, Japan)  
Kentaro Aburada (Oita National College of Technology, Japan)
- OS2-4 *Proposal of a testing method using similarity of interleaving for Java multi-threaded programs*  
Shoichiro Kitano, Tetsuro Katayama, Hisaaki Yamaba, and Naonobu Okazaki  
(University of Miyazaki, Miyazaki, Japan)  
Yoshihiro Kita (Kanagawa Institute of Technology, Japan)  
Kentaro Aburada (Oita National College of Technology, Japan)
- OS2-5 *Proposal of a Modification Method of a Source Code to Correspond with a Modified Model in MDA.*  
Yuuki Kikkawa, Tetsuro Katayama, Hisaaki Yamaba, and Naonobu Okazaki  
(University of Miyazaki, Japan)  
Yoshihiro Kita (Kanagawa Institute of Technology, Japan)  
Kentaro Aburada (Oita National College of Technology, Japan)
- OS2-6 *Prototype of a Decision Table Generation Tool from the Formal Specification*  
Kenta Nishikawa, Tetsuro Katayama, Hisaaki Yamaba and Naonobu Okazaki  
(University of Miyazaki, Japan)  
Yoshihiro Kita (Kanagawa Institute of Technology, Japan)  
Kentaro Aburada (Oita National College of Technology, Japan)

## Abstract

### Plenary Speech

#### PS-1 Vision-Based Grasp Planning and Experiments of a Mobile Manipulator

Yi-Fu Chiu and Kai-Tai Song (National Chiao Tung University, Taiwan)  
ivan790721.ece01g@nctu.edu.tw, ktsong@mail.nctu.edu.tw

In this paper, a motion planner is designed and implemented for of a mobile manipulator to travel to a spot for grasping of an object. In this work, the probability of successful grasping inside the workspace of the robot arm is used for grasping planning. A vision SLAM system is combined with reachability calculation to figure out the grasping position. Using a laboratory dual-arm robot, we conducted experiments in different conditions to verify the effectiveness of the developed system.



#### PS-2 Biped Robot Research at Waseda University

Kenji Hashimoto, Atsuo Takanishi (Waseda University, Japan)  
contact@takanishi.mech.waseda.ac.jp

Waseda University has researched on biped robots since 1967. In this talk I will introduce our latest biped robots, WABIAN-2, a running robot and WL-16. WABIAN-2 has 41-DOF, and its height is 1480 mm with 63.8 kg weight. WABIAN-2 has realized a human-like walk with the knees stretched, heel-contact and toe-off motion by utilizing a foot mechanism having a passive toe joint and a 2-DOF (Roll, Yaw) waist mimicking a human's pelvis motion. Now we are going to build a new biped humanoid robot capable of running and walking in order to study human running and other features. The running robot can jump by utilizing a pelvic movement and leg elasticity. WL-16 is a human-carrying biped vehicle consisting of two Stewart Platform type legs and waist with a passenger seat. WL-16 can be used as a substitute for a wheel chair.



## Invited Speech

### IS-1 Combining playware exergaming with a mobile fitness app

Emmanouil Giannidakis, Henrik Hautop Lund  
(Technical University of Denmark, Denmark)

We propose a novel playware as a merge between exergames and mobile fitness apps to engage the users in physical exercises, not only as competitive play, but also in the form of cooperative play. The concept connects modular interactive tiles with radio communication to Android tablets and smart phones, which can connect to the Internet. This allows the players to monitor their playware exergaming performance on the smart device(s). The test subjects playing the games were school children (12-13 years old). As a social playware, we investigated how the playware mediated cooperative and competitive play amongst the users. It was found that the majority of game play involved social interaction between players, and that 8 out of 10 pupils on the top-10 were girls. The playware seemed to motivate the girls to become physically active.

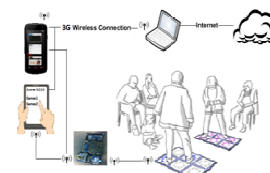


Figure 1. Modular tiles connected to smart devices and internet.

### IS-2 Parallel Relational Universes – experiments in modularity

Luigi Pagliarini<sup>1,2</sup> Henrik Hautop Lund<sup>1</sup>  
(<sup>1</sup> Centre for Playware, Technical University of Denmark, Denmark)  
(<sup>2</sup> Academy of Fine Arts of Macerata, Italy)

We here describe Parallel Relational Universes, an artistic method used for both the psychological analysis of group dynamics and speculations on aesthetics. The design of the artistic system, which mediates group dynamics, emerges from our former experiments on modular playware and remixing playware. Inspired from consolidated psychological and artistic practice and founded on the remixing modular Playware logic, where users remix samples in the form of physical and functional modules, we created an artistic instantiation of such a concept with the Parallel Relational Universes, allowing arts alumni to remix artistic expressions. Here, we report the data emerged from a first pre-test, run with gymnasium's alumni. We then report both the artistic and the psychological findings. We finally discuss possible variations of such an instrument under the light of modern technologies. Between an art piece and a psychological test, at a first cognitive analysis, it seems to be a promising research tool.

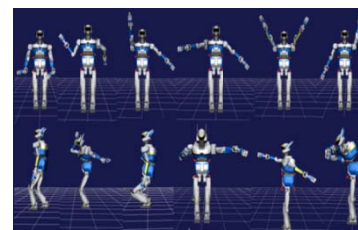


Figure 1. An example outcome of Parallel Relational Universes

### IS-3 Identifying humanoid and human physical parameters

Jovana Jovic<sup>1</sup>, Eiichi Yoshida<sup>1</sup>, Gentiane Venture<sup>2</sup>  
(<sup>1</sup>AIST, Japan),  
(<sup>2</sup>TUAT, Japan)

Dynamical and kinematic analysis of humanoid and human movements require accurate estimation of segment mass parameters (mass, center of mass, and inertia matrix), and their misinterpretation can lead to significant variation in estimated joint kinematics. In the field of robotics, several methods have been developed for estimation of mass parameters of humanoid robots, as well as human subjects, based on linear properties of dynamic equation of bipedal systems with respect to the set of mass parameters. This talk will focus on those methods addressing the state-of-the-art research in the topic. Examples of both human and humanoid robots mass parameters estimation will be given. Identified mass parameters improve output of human dynamic analysis and humanoid simulation and model-based control.



Examples of exciting trajectories used for the mass parameters estimation.

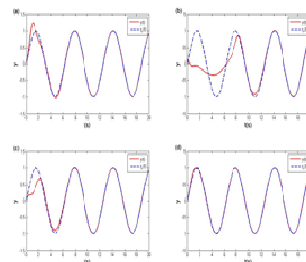
## OS

### OS1: Intelligent Control

#### OS1-1 Adaptive Multiple-Model Control of a Class of Nonlinear Systems

Chao Yang and Yingmin Jia  
(Beihang University, P.R.China)

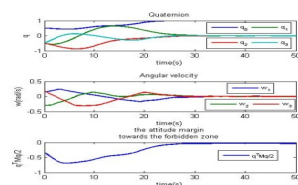
In this paper, an adaptive multiple-model controller is developed for nonlinear systems in parametric-strict-feedback form. Unlike the previous results, a switching scheme is not required here to switch to the most appropriate model. The new scheme reduces the number of identification models and uses information from all the models more efficiently via convex combination of estimates of parameters. The parameter convergence and global asymptotic stability of tracking errors in the closed-loop system are guaranteed. A simulation example is included to demonstrate the effectiveness of the obtained results.



#### OS1-2 Attitude reorientation of spacecraft with attitude forbidden zones

Xuhui Lu and Yingmin Jia  
(Beihang University, P.R.China)

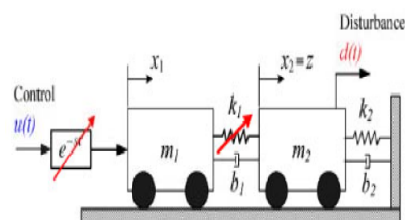
This paper investigates the attitude reorientation control scheme for spacecraft, considering attitude forbidden zone and external disturbances. Here a novel potential function is proposed. Besides a dynamical scaling factor and backstepping technique are synthesized to accommodate the avoidance of attitude forbidden zones and the disturbance attenuation. Simulation results are given to verify the effectiveness of the proposed method.



#### OS1-3 Weighted Multiple Model Adaptive Control of Slowly Time-Varying Systems

Weicun Zhang, Qing Li  
(University of Science and Technology Beijing, P.R.China)

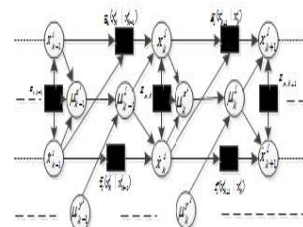
Weighted multiple model adaptive control (WMMAC) is a combination of off-line design and online decision, which combines a finite number of simple controllers by weighting algorithm. This paper presents an improved weighting algorithm of slowly time-varying systems and a new method to partition model uncertainty using  $v$ -Gap metric. The effectiveness of the proposed method is verified through Matlab simulation results.



### OS1-4 A Reduced-Complexity Interacting Multiple Model Algorithm for Location Tracking in Heterogeneous Observation

Xiaoyan Fu and Yuanyuan Shang  
(Capital Normal University, P.R.China)

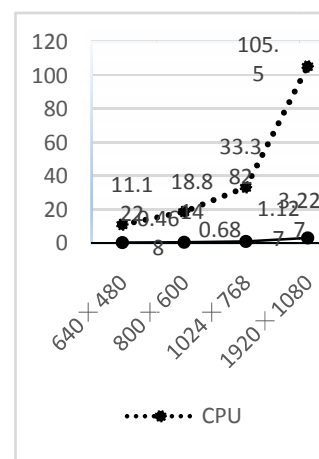
This paper is devoted to the problem of state estimate of discrete-time stochastic systems with Markov jump parameters. A low-complexity and high accuracy algorithm is presented to reduce the computational load of the traditional interacting multiple model algorithm with heterogeneous observations for location tracking. By decoupling the x and y dimensions to simplify the implementation of location and formulating the problem in a factor graph framework, updated information is iteratively passed based on an adaptive fusion decision to obtain the state estimation of maneuvering target. Extensive Monte Carlo simulations show that the proposed algorithm is more computationally attractive than existing multiple model methods.



### OS1-5 Single Image Dehazing on Mobile Device based on GPU Rendering Technology

Yuanyuan Shang, Yue Meng, Xiuzhuang Zhou, Xiaoyan Fu, and Hui Ding  
(Capital Normal University, China)

Images captured in bad weather conditions such as haze, dust, fog, and rain are often substandard because of the attendant poor visibility and low intensity contrast. Over the past few years, image dehazing has become popular in imaging science communities because of its potential application in many vision tasks. Image dehazing utilizes a very complex algorithm that requires intensive filtering and floating-point arithmetic operations. Consequently, processing speed is the most significant bottleneck in its application in some vision tasks such as mobile platforms. On the other hand, graphic processing unit (GPU) rendering technology is widely used in image processing applications to speed up image processing algorithms. In this paper, we propose an optimized single image parallel processing dehazing algorithm for mobile platforms and implement it on a Windows Phone device based on GPU rendering technology. Experimental results on hazy images demonstrate the efficacy and effectiveness of our proposed approach in improving image quality.



## OS2 Software Development Support Method

### OS2-1 Prototype of a Supporting Tool to Generate Testing Communication Diagram

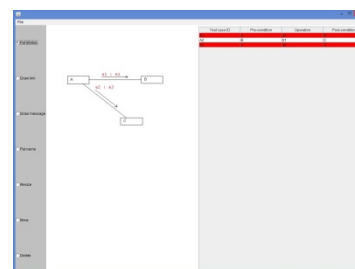
Tetsuro Katayama<sup>\*</sup>, Seiya Urata<sup>\*</sup>, Yohei Ogata<sup>\*</sup>, Yoshihiro Kita<sup>†</sup>,  
Hisaki Yamaba<sup>\*</sup>, Kentaro Aburada<sup>‡</sup> and Naonobu Okazaki<sup>\*</sup>

(<sup>\*</sup>University of Miyazaki, Japan)

(<sup>†</sup>Kanagawa Institute of Technology, Japan)

(<sup>‡</sup>Oita National College of Technology, Japan)

This research has implemented a prototype of a supporting tool to generate testing communication diagram. The testing communication diagram visualizes messages, which are written in a part of test cases, between objects in software system and helps a developer to understand where the software system is tested by a large quantity of test cases written in text. The testing communication diagram is generated by adding the information of test cases to communication diagram in UML (Unified Modeling Language). The implemented prototype can support that a developer draws testing communication diagram. Moreover, it can detect more efficiently deficiency and/or contradiction in communication diagram and/or test cases.



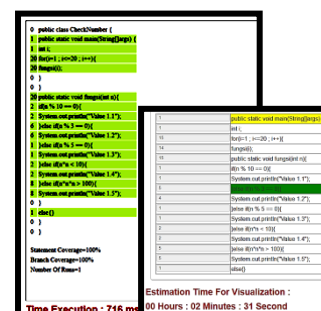
### OS2-2 Code Coverage Visualization on a Web-Based Testing Tool for Java Programs

Mochamad Chandra Saputra<sup>\*</sup>, Tetsuro Katayama<sup>†</sup>

(<sup>\*</sup>Universitas Brawijaya, Indonesia)

(<sup>†</sup>University of Miyazaki, Japan)

This research implements a web-based testing tool which displays code coverage visualization result testing for java programs using statement coverage (C0) and branch coverage (C1). The result displays for visual information have been highlighted in bright green as information of executed lines, bright yellow for C0 and dark green for C1. The testing tool informs the user using visualization to understand the behavior of the tested code as a sequence of the executed lines. The results of testing are satisfied C0 and C1 100%, it's meant the testing tool successfully checked each line and verified as a true condition of all based on the covering status of a statement and branch coverage. The testing tool significantly reduces the time for testing a sample software code, 716 ms using our testing tool and over 4 minutes using manual testing.

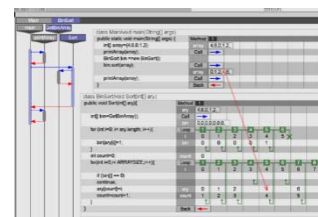




## OS2-3TFVIS: a Supporting Debugging Tool for Java Programs by Visualizing Data Transitions and Execution Flows

Hiroto Nakamura<sup>\*</sup>, Tetsuro Katayama<sup>\*</sup>, Yoshihiro Kita<sup>†</sup>,  
Hisaki Yamaba<sup>\*</sup>, Kentaro Aburada<sup>‡</sup> and Naonobu Okazaki<sup>\*</sup>  
(<sup>\*</sup>University of Miyazaki, Japan)  
(<sup>†</sup>Kanagawa Institute of Technology, Japan)  
(<sup>‡</sup>Oita National College of Technology, Japan)

We have developed TFVIS in order to improve efficiency of debugging for Java programs. TFVIS can perform the visualization of data transitions and the visualization of execution flows. The visualization of data transitions shows the flow of variable renewals in executing programs. It becomes easier to grasp the behavior in executing the programs whose behavior is unexpected by a bug. The visualization of execution flows shows an entire flow of the execution. It is useful to select the part where users want the visualization of the data transitions. When we use the visualization of the data transitions based on the source code, the visualization of execution flows supports to grasp behavior of the program and the place where users visualize. At last, the efficiency of TFVIS is shown.



## OS2-4 Proposal of a testing method using similarity of interleaving for Java multi-threaded programs

Shoichiro Kitano<sup>\*</sup>, Tetsuro Katayama<sup>\*</sup>, Yoshihiro Kita<sup>†</sup>,  
Hisaki Yamaba<sup>\*</sup>, Kentaro Aburada<sup>‡</sup> and Naonobu Okazaki<sup>\*</sup>  
(<sup>\*</sup>University of Miyazaki, Japan)  
(<sup>†</sup>Kanagawa Institute of Technology, Japan)  
(<sup>‡</sup>Oita National College of Technology, Japan)

In order to improve the efficiency of testing Java multi-threaded programs, this research proposes a testing method to detect order violation in them using similarity of interleaving. Order violation is one of the distinctive bug patterns in concurrent programs. This pattern means that some threads can be executed as an access to a certain memory in an unexpected order. Our proposed method improves the efficiency of testing by executing interleaving which can test the places where lead the order violation easily in source codes and by reducing interleaving which is similar to executed one already. The efficiency of our method is shown by experiments for confirmation.

```
class OnePrinter extends Thread {
    public void run() {
        PreemptionPointer.preemptionPoint(0);
        System.out.println(1);
        PreemptionPointer.preemptionPoint(1);
    }
}

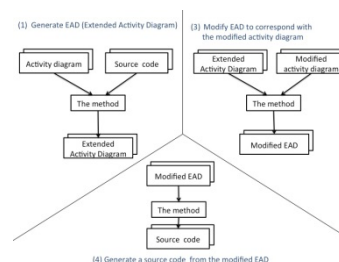
class TwoPrinter extends Thread {
    public void run() {
        PreemptionPointer.preemptionPoint(2);
        System.out.println(2);
        PreemptionPointer.preemptionPoint(3);
    }
}
```



## OS2-5 Proposal of a Modification Method of a Source Code to Correspond with a Modified Model in MDA.

Yuuki Kikkawa<sup>\*</sup>, Tetsuro Katayama<sup>\*</sup>, Yoshihiro Kita<sup>†</sup>,  
 Hisaaki Yamaba<sup>\*</sup>, Kentaro Aburada<sup>‡</sup> and Naonobu Okazaki<sup>\*</sup>  
 (<sup>\*</sup>University of Miyazaki, Japan)  
 (<sup>†</sup>Kanagawa Institute of Technology, Japan)  
 (<sup>‡</sup>Oita National College of Technology, Japan)

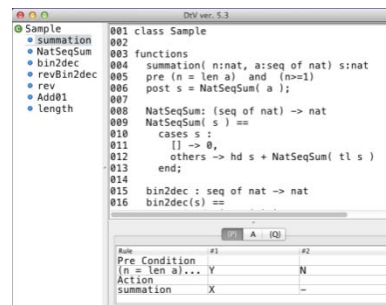
This study improves efficiency of software development using MDA. This paper proposes a method that reduces time and effort to keep consistency between models and a source code after requirement specification is modified. The proposed method consists of four steps as below. (1) The method generates EAD (Extended Activity Diagram) from an activity diagram and a source code added detail specification. EAD is a diagram that adds a part of the source code which has the detail specification to the activity diagram. Here, the detail specification is information omitted in drawing an activity diagram. (2) A developer modifies the activity diagram to fit the changed requirement specification. (3) The method modifies EAD to correspond with the modified activity diagram. (4) The method generates a new source code from the modified EAD.



## OS2-6 Prototype of a Decision Table Generation Tool from the Formal Specification

Kenta Nishikawa<sup>\*</sup>, Tetsuro Katayama<sup>\*</sup>, Yoshihiro Kita<sup>†</sup>,  
 Hisaaki Yamaba<sup>\*</sup>, Kentaro Aburada<sup>‡</sup> and Naonobu Okazaki<sup>\*</sup>  
 (<sup>\*</sup>University of Miyazaki, Japan)  
 (<sup>†</sup>Kanagawa Institute of Technology, Japan)  
 (<sup>‡</sup>Oita National College of Technology, Japan)

This research has implemented a prototype of a decision table generation tool from the specification (the formal specification) described in a formal specification language. This paper uses the formal specification description language VDM++ which is the lightweight formal methods VDM (Vienna Development Method) to write the formal specification. This prototype generates a decision table from the specifications of VDM++, and displays it. We applied some general specifications to the prototype, in order to evaluate its usefulness. This prototype could generate decision tables from each of the applied specifications. We confirmed that this prototype works properly. As a result, the prototype has improved the efficiency in test design with formal methods.



## OS3 Image Analysis, Human Interface, and Text Mining

### OS3-1 Development of Mouse Cursor Control System Based on Face Direction Using Kinect

Masayoshi Tabuse<sup>1</sup>, Kaori Tamura<sup>2</sup>  
(<sup>1</sup>Kyoto Prefectural Univ., Japan)  
(<sup>2</sup>ISI Software Corp., Japan)

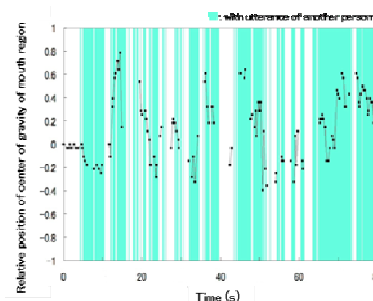
We propose a method of operating mouse cursor and controlling television based on face direction using Kinect. Using our system anyone can control television by motion of a user easily and cheaply. It is not necessary to fix a user's head or to restrict user's head movement. Therefore, it can ease a user's burden compared with conventional devices. Furthermore, a person with trouble in a hand can control television easily. Our system measures face direction and controls mouse cursor using 4 face directions of rightward, leftward, upward and downward directions using Kinect. It changes a television's channel and volume by controlling mouse cursor based on face direction using Kinect in a range with distance less than 4 meters between a user and Kinect. It is also applicable to operation of other application software controlled by mouse cursor.



### OS3-2 Quantitative Evaluation of Facial Expressions and Movements of Persons While Using Video Phone

Taro Asada<sup>1</sup>, Yasunari Yoshitomi<sup>1</sup>, Ryota Kato<sup>1</sup>, Masayoshi Tabuse<sup>1</sup>, and Jin Narumoto<sup>2</sup>  
(<sup>1</sup>Kyoto Prefectural University, Japan)  
(<sup>2</sup>Kyoto Prefectural University of Medicine, Japan)

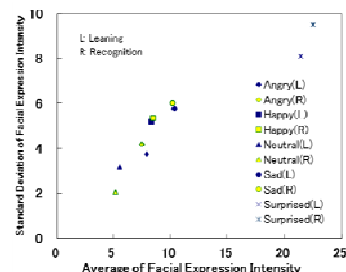
We have developed a method for analyzing facial expressions and movements of a person while speaking with another person using a video phone to improve the QOL of elderly people living in care facility, or at home. In the present study, the video is analyzed using image processing software (OpenCV) and the newly proposed feature parameters of facial expressions and movements, which are extracted in the mouth-part area. The feature parameter for expressing facial expression is defined as the average of facial expression intensity. The feature parameter for expressing facial movement is defined as the average of absolute value of vertical coordinate for the center of gravity of mouth area in the relative coordinate system. The experimental result shows the usefulness of the proposed method.



### OS3-3 Facial Expression Recognition Using Facial Expression Intensity Characteristics of Thermal Image

Yasunari Yoshitomi, Taro Asada, Ryota Kato, and Masayoshi Tabuse  
(Kyoto Prefectural University, Japan)

In the present study, we proposed a method for recognizing facial expressions. The recorded video is analyzed by thermal image processing and the feature vector of facial expression, which is extracted in the area of mouth and jaw by applying 2D-DCT (Discrete Cosine Transform) for each domain having  $8 \times 8$  pixels in the area of mouth and jaw. The facial expression intensity defined as the norm of difference vector between the feature vector of neutral facial expression and that of observed one can be used for analyzing a chance of facial expression. The average and the standard deviation of facial expression intensities are used for recognizing facial expression. The average and the standard deviation of time of utterance are helpful for recognizing facial expression. The experimental results show the usefulness of the proposed method.



### OS3-4 Method for Character Domain Extraction from Image Using Wavelet Transform

Taiki Taniguchi<sup>1</sup> and Yasunari Yoshitomi<sup>2</sup>  
(<sup>1</sup>ZENSHO HOLDINGS Co., Ltd., Japan)  
(<sup>2</sup>Kyoto Prefectural University, Japan)

The number of images having private information and/or URL of illegal Web site has been increasing in the cyber space on the Internet. These images might cause infringement of human right and/or criminal act. In the present study, a method for extracting the region(s) having characters on an image has been developed using Wavelet Transform (WT) and the empirical knowledge that a character has strong vertical and/or horizontal element(s). Finally, the output RGB image is generated by the operation that the color of the pixel on the original RGB image is changed into white when the value of corresponding pixel on the mask image made by the proposed method is '0', resulting in extracting the region(s) having characters on the original RGB image. The experimental results show the usefulness of the proposed method.



## OS3-5 Classification of Japanese Documents and Ranking of Representative Documents Using Characteristic of Frequencies of Words

Jun Kimura<sup>1</sup>, Yasunari Yoshitomi<sup>2</sup>, and Masayoshi Tabuse<sup>2</sup>

(<sup>1</sup>JustSystems Corp.,Japan)

(<sup>2</sup>Kyoto Prefectural University, Japan)

It is very difficult to read through all of Web pages in which we are interested. A Web page has some kinds of media, such as document, image, and sound. We have developed a method for classification of Japanese documents and ranking of representative documents using characteristic of frequencies of words. All nouns in a document are extracted with use of MeCab (<http://mecab.sourceforge.net/>) with which the document is resolved into several morphemes. For clustering, we use ward method. The representative document is defined as the document whose feature vector is the closest to the center of gravity of the class in the feature vector space among all documents belonging to the class. The ranking of the representative documents is decided in the descending order of the number of documents belonging to the class.

Order of Clustering	Document No.	Number of Document in Cluster	Ranking
1	7	20	1
2	3	11	2
2	11	9	3
3	3	11	—
3	6	5	4
3	15	4	5
4	3	8	—
4	6	5	—
4	15	4	—
4	17	3	6

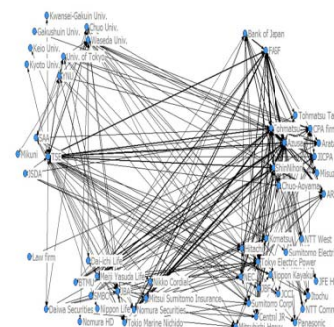
Ranking : 7=>3=>11=>6=>15=>17

## OS4 Graph Theory and Its Application

### OS4-1 The Role of National Standards Setter in the Global Convergence Era -In the Case of the Japanese Setter during the first decade-

Ogata, K. (University of Nagasaki,Japan)

An aim of this paper is to explain that the change of standard-setting activities of ASBJ, Japanese accounting standard setter, in the 2000s was caused by its own standard-setting development strategy. Researches on accounting standard-setting processes have had two different ideas about characteristics of the setters: the pluralistic organization regarded as a political forum of some stakeholders related to accounting standards, and the autonomous organization regarded as an actor which behave with a will to achieve desirable policy purposes. Through an analysis of organizational structure using graph theory, we show that the ASBJ strategically alter its structure, and that the structure can trigger the change of setting activities. It means that the ASBJ has a nature not so much pluralistic as autonomous organization.



## OS4-2 An Empirical Research on Inter-firm Capital Relationship in Yokokai using IDE Spatial Model

Takao Ito<sup>1</sup>, Makoto Sakamoto<sup>3</sup>, R. Mehta<sup>2</sup>, Tsutomu Ito<sup>4</sup>, and S. Ikeda<sup>3</sup>

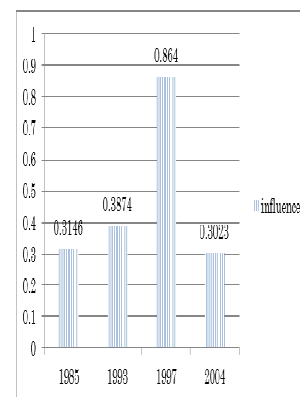
(1 Hiroshima University, Japan)

(2 New Jersey Institute of Technology, U.S.A)

(3 University of Miyazaki, Japan)

(4 Hino Motors, Ltd. Japan)

This paper introduces recent fundamental modifications to Japanese alliance system known as the keiretsu, and analyses how these changes have affected corporate performance. Specially, the performance of Japanese auto manufacturers, such as Toyota, Nissan and others, has significantly improved due to sophisticated production system technologies, highly productive workers, and recurring transaction relationship with other partners in their network family. One possible determinant of their success could be due to their unique organization forms –the keiretsu– which provides a strong platform to forge their strategic alliance relationship with their parts suppliers as well as collaboration in research and development with other automobile makers. After economic bubble of the 1990', the strong ties between automobile makers and their supplier partners experienced significant changes, which are known as “keiretsu loosening”. Consequently, what is the status quo of automotive keiretsus? Does cross-shareholding, which is one specific form of capital relationship in keiretsu, still contribute to improving corporate performance? To answer these questions, this paper reports the results of a study that collected data on cross-shareholdings to shed light on the relationship between inter-firm capital relationship and corporate performance. The findings of this empirical investigation reveal that: (1) Keiretsu is a flexible, highly adaptive organizational form; its scale changes in response to economic situations; (2) Capital relationship is still a significant determinant of increasing profits for keiretsu partners even after the bubble burst in the 1990s..

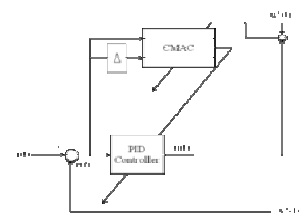


Influence in Yokokai from 1985 to 2004.

## OS4-3 Design and Experimental Evaluation of a Human Skill-Based PID Controller

Yuntao Liao, Yamamoto Toru(Hiroshima University,Japan)

Nowadays less and less people are willing to do hard works. Which model articulation controller (CMAC) is a kind of neural networks (NNs) that can easily solve problems of nonlinear system. Compared with other NNs the advantage of CMAC is that it takes shorter learning time. Moreover because of the widely used of PID controller a human skill-based PID controller using CMACs has been proposed in this paper.

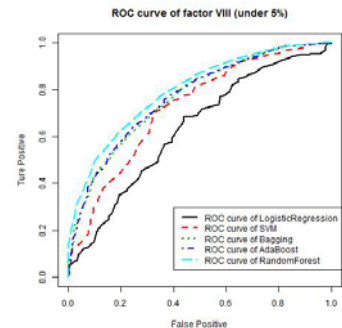


## OS5 Bio-Inspired Algorithms and Their Applications

### OS5-1 Analysis of Genetic Disease Haemophilia A by Using Machine Learning

Kenji Aoki, Makoto Sakamoto, Hiroshi Furutani  
(University of Miyazaki, Japan)

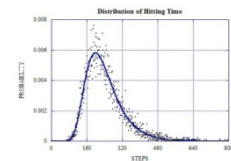
Haemophilia A is a genetic disease resulting from deficiency of factor VIII. The database of mutations causing haemophilia A has been developed by the world wide collaboration. In this study, we examined the relation between activity of factor VIII and the missense mutation by using machine learning. As parameters, we used four physical-chemical parameters of amino acids. We predicted the severity of haemophilia A by using machine learning in factor VIII. As the result, logistic regression is not better than other methods in the prediction of haemophilia A severity. The result of the prediction improved in order to SVM, Bagging, AdaBoost, RandomForest. These results suggested that we can predict the haemophilia severity by using these methods, and Random Forest was the best method in these five methods to predict the haemophilia A severity.



### OS5-2 Analysis of Asymmetric Mutation Model in Random Local Search

Hiroshi Furutani, Yifei Du, Kenji Aoki, Makoto Sakamoto  
(University of Miyazaki, Japan)

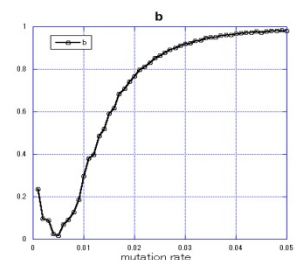
There are many reports that the asymmetric mutation model is a very powerful strategy in EAs to obtain better solutions more efficiently. In this paper, we report stochastic behaviors of algorithms that are asymmetric mutation models of Random Local Search (RLS). The mathematical structure of asymmetry model can be derived in terms of a finite Markov chain. We demonstrate some useful results representing the effects of asymmetric mutation.



### OS5-3 Hitting Time Analysis of OneMax Problem in Genetic Algorithm

Y. Du<sup>1</sup>, Q. Ma<sup>1</sup>, k. Aoki<sup>1</sup>, M. Sakamoto<sup>1</sup>, H. Furutani<sup>1</sup>, Y. Zhang<sup>2</sup>  
(<sup>1</sup>University of Miyazaki, Japan)  
(<sup>2</sup>Qinghai University, China)

Genetic algorithms (GAs) are stochastic optimization techniques, and we have studied the effects of stochastic fluctuation in the process of GA evolution. A mathematical study was carried out for GA on OneMax function within the framework of Markov chain model. We treated the task of estimating convergence time of the Markov chain for OneMax problem. Next, in order to study hitting time, we study the state after convergence. Our results demonstrate that the hitting time distribution  $h(t)$  has an exponential form, and the logarithmic of  $h(t)$  is linearly decreasing function.



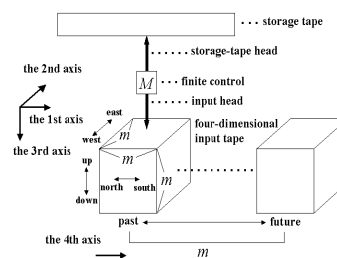


## OS6 Computer Science and Information Processing

### OS6-1 Sufficient spaces for seven-way four-dimensional Turing machines to simulate four-dimensional one-marker automata

Makoto Nagatomo<sup>1</sup>, Makoto Sakamoto<sup>1</sup>, Hikaru Susaki<sup>1</sup>, Tuo Zhang<sup>1</sup>, Takao Ito<sup>2</sup>, Yasuo Uchida<sup>3</sup>,  
 Tsunehiro Yoshinaga<sup>4</sup>, Satoshi Ikeda<sup>1</sup>, and Hiroshi Furutani<sup>1</sup>  
 (1:University of Miyazaki, Japan)(2:Hiroshima University, Japan)  
 (3:Ube National College of Technology, Japan)(4:Tokuyama College of Technology, Japan)

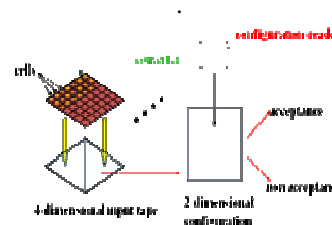
We think that recently, due to the advances in many application areas such as motion image processing, computer animation, and so on, it is very useful for analyzing computational complexity of multi-dimensional information processing to explicate the properties of four-dimensional automata, i.e., three-dimensional automata with the time axis. As far as we know, there is no investigation about four-dimensional automata. Then, in 2002, we first introduced four-dimensional finite automata in the world. In 2003, we investigated four-dimensional alternating Turing machines. In this paper, we continue the investigations, and deal with sufficient spaces for four-dimensional Turing machines to simulate one-marker automata.



### OS6-2 Some Properties of k-Neighborhood Template A-Type Three-Dimensional Bounded Cellular Acceptors

Makoto Sakamoto<sup>1</sup>, Makoto Nagatomo<sup>1</sup>, Hikaru Susaki<sup>1</sup>, Tuo Zhang<sup>1</sup>, Takao Ito<sup>2</sup>,  
 Yasuo Uchida<sup>3</sup>, Tsunehiro Yoshinaga<sup>4</sup>, Satoshi Ikeda<sup>1</sup> and Hiroshi Furutani<sup>1</sup>  
 (1)University of Miyazaki, Japan, (2)Hiroshima University, Japan,  
 (3)Ube National College of Technology, Japan, (4)Tokuyama College of Technology, Japan)

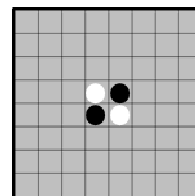
In this paper, we investigate multi-dimensional computational model, k-neighborhood template A-type three-dimensional bounded cellular acceptor on four-dimensional tapes, and discuss some basic properties. This model consists of a pair of a converter and a configuration-reader. The former converts the given four-dimensional tape to three-dimensional configuration. The latter determines whether or not the derived three-dimensional configuration is accepted, and concludes the acceptance or non-acceptance of given four-dimensional tape. We mainly investigate some open problems about k-neighborhood template A-type three-dimensional bounded cellular acceptor on four-dimensional tapes whose configuration-readers are L(m) space-bounded deterministic (nondeterministic) three-dimensional Turing machines.



### OS6-3 Perfect Analysis in miniature Othello

Yuki Takeshita<sup>1</sup>, Satoshi Ikeda<sup>2</sup>, Makoto Sakamoto<sup>3</sup>, Takao Ito<sup>4</sup>  
(<sup>1,2,3</sup>Miyazaki University, Japan)  
(<sup>4</sup>Hiroshima University, Japan)

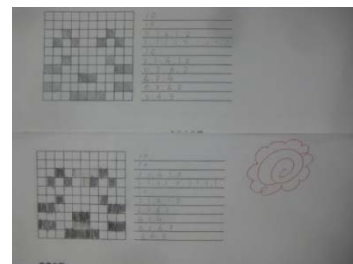
In 1993, mathematician Joel. Feinstein found that a perfect play on 6×6 board of Othello gives a 16-20 win for the second player; the perfect play is a score and the sequence in the case where both players were the best play. More than 20 years have passed since then, in a recent the mainstream board game study is computer game such as chess and Go, but standard 8×8 board of Othello has not been solved at this time. Therefore, we suppose the nature of the game from the perfect analysis of the board which is smaller than it. Additionally, this study also includes the meaning of the double-check, because we were not able to find the article that checked the result of Feinstein. In this paper, we show the perfect play of 4×4, 4×6, 4×8, 4×10 and 6×6 board. From this result, we discuss the nature of the game in 8×8 board or more board.



### OS6-4A proposal for teaching programming through the Five-Step Method

Y. Uchida<sup>1</sup>, S. Matsuno<sup>1</sup>, T. Ito<sup>2</sup>, M. Sakamoto<sup>3</sup>  
(<sup>1</sup>National Institute of Technology, Ube College, Japan)  
(<sup>2</sup>Hiroshima University, Japan)  
(<sup>3</sup>University of Miyazaki, Japan)

We teach computer programming to students aged 17 through 18 years. In the course, a few students consider themselves to have insufficient understanding of programming or think that they are not good at programming. In response, we adopted and implemented a part of the Computer Science Unplugged (CS Unplugged) method, which is considered an effective way of teaching information science. However, although CS Unplugged has generated considerable results in motivating students to learn and in initial learning, we feel that it is not sufficiently connected to full-fledged programming languages such as C and Java. Accordingly, we propose advancing from CS Unplugged to full-fledged programming through a new Five-Step Method. In this paper, we describe the thinking and concepts behind this proposed method.





## OS7 Computer Network and Security

### OS7-1 An Authentication Method for Mobile Devices

#### that is Independent of Tap-Operation on a Touchscreen

<sup>1</sup>Hisaaki Yamaba, <sup>1</sup>So Nagatomo, <sup>2</sup>Kentaro Aburada, <sup>1</sup>Shinichiro Kubota,

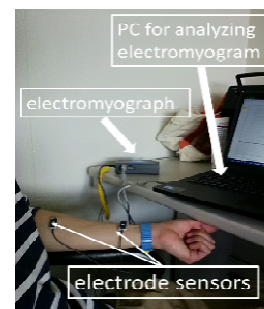
<sup>1</sup>Tetsuro Katayama, <sup>3</sup>Mirang Park, <sup>1</sup>Naonobu Okazaki

(<sup>1</sup>University of Miyazaki, Japan)

(<sup>2</sup>Oita National College of Technology, Japan)

(<sup>3</sup>Kanagawa Institute of Technology, Japan)

In these days, mobile devices such as tablet type PCs or smart phones widely penetrated. This causes a new need for authentication method that has tolerant to shoulder surfing. Under this situation, we are investigating a new user authentication method for mobile devices not using screen touching but using surface electromyogram signals. In this paper, a series of experiments were carried out in order to investigate the prospect of the authentication method using s-EMG. Concretely, several motion patterns of wrist are introduced, and s-EMG signals generated at each gesture were measured. And we compared the s-EMG signal patterns generated by the same subject and the patterns generated by different subjects. As a result, it was found that patterns of same subjects were similar and those of different ones were different each other.



### OS7-2 Proposal of Security Evaluation System using User's Reviews and Permissions for Android Application

Naonobu Okazaki, (University of Miyazaki, Japan)

Yoshihiro Kita, (Kanagawa Institute of Technology, Japan)

Kentaro Aburada, (Oita National College of Technology, Japan)

Mirang Park (Kanagawa Institute of Technology)

y.kita@ccy.kanagawa-it.ac.jp

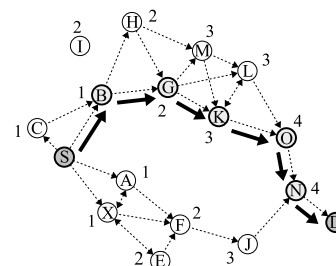
Leakage of the personal information in Android OS powered device by mal-applications is becoming the heavy matter. The Android OS users must be careful not to install mal-applications. The reviews and the using permissions of applications are useful by users to detect mal-application. However, the most of users read the reviews only. All users must be cautious about not only the using permissions but also the combination of them. In this paper, we propose the security evaluation system to prevent the installation of mal-applications on Android OS. This system indicates the user reviews with the using permission information of application to new users. Reviews have two types: positive reviews and negative reviews. Positive reviews include selling points or good features for the application. Negative reviews include wrong points or problems of the application. New user evaluates the one of reviews, and determines to download the application. The evaluation report of the review is transmitted to the reviewer which wrote it. Therefore, the reviewer can use the report as reference for the better.



### OS7-3 Evaluation of Neighbors Based Routing for ad hoc networks

Kentaro Aburada<sup>1</sup>, Hisaaki Yamaba<sup>2</sup>, Shinichiro Kubota<sup>2</sup>,  
Tetsuro Katayama<sup>2</sup>, Mirang Park<sup>3</sup>, Naonobu Okazaki<sup>2</sup>  
(<sup>1</sup> Oita National College of Technology, Japan)  
(<sup>2</sup> University of Miyazaki, Japan)  
(<sup>3</sup> Kanagawa Institute of Technology, Japan)

In ad hoc networks, due to the mobility of nodes, radio wave interference, and limited resources, such as batteries, communication links are unstable and restricted. As such, an efficient routing protocol is needed in order to solve these problems. The existing protocols cannot adapt to the route repair when the route is disconnected. In the present paper, we propose a neighbors-based routing (NBR) protocol by constructing paths in an area in which a large number of nodes exists. Simulations confirm that the proposed protocol has higher connectivity and a lower control overhead than existing protocols in topologies in which nodes move.

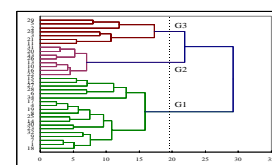


### OS8 Kansei Engineering

#### OS8-1 Investigation of Feature Quantity in Sound Signal and Feeling Impression Using PCA

Yusuke Kawakami, Tetsuo Hattori (Kagawa University, Japan),  
Hiromichi Kawano (NTT AT, Japan),  
Tetsuya Izumi (Micro-Technica Co., Ltd., Japan)

This paper investigates the relationship between feature quantity of sound signal and feeling impression using PCA (Principal Component Analysis). As the feature quantity, we use Fluctuation value and sum of squared errors (Residual) which is calculated by regression analysis of sound signal, in the same way as our previous paper. As a result, we have found that the feeling response of examinees can be classified into three groups by a clustering analysis. And also we have obtained the results of PCA for the feeling effects depending on each group of examinees and four kinds of frequency zone of sound signal. In this paper, we discuss the analysis results on the Kansei (or feeling) effect.



#### OS8-2 Automated Color Image Arrangement Method Using Curvature Computation in Histogram Matching

Yusuke Kawakami, Tetsuo Hattori, Yoshiro Imai, Haruna Matsushita (Kagawa University, Japan),  
Hiromichi Kawano (NTT AT, Japan),  
R.P.C. Janaka Rajapakse (Tainan National University of the Arts, Taiwan)

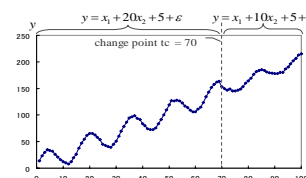
This paper proposes an improved method for automated color image arrangement method by using histogram curvature computation. The previous paper that we have presented the principle of our method using Histogram Matching based on Gaussian Distribution (HMGD), and how to detect input color image peakedness in its histogram. In this paper, we describe about Variance Estimated HMGD (VE-HMGD) as improvement HMGD. We also show how to estimate the histogram variance of original image based on the curvature computation. Moreover we compare processing results between VE-HMGD and HMGD through some experimentation. As the result, we show that, in the color, VE-HMGD is more natural than HMGD.



### OS8-3 Change Detection Experimentation for Time Series data by New Sequential Probability Ratio

Yoshihide KOYAMA, Tetsuo HATTORI (Kagawa University, Japan)  
 Hiromichi KAWANO (NTT AT, Japan)  
 Katsunori TAKEDA (Canon IT Solutions Inc., Japan)

Previously, we have proposed a novel method using New Sequential Probability Ratio (NSPR) for the structural change detection problem of ongoing time series data instead of using SPRT (Sequential Probability Ratio Test). In this paper, for comparison, we present the experimental results by applying the both methods, i.e., NSPR and SPRT, to time series data that are generated by a multiple regression model in the case where one explanatory variation is a periodic function (sine function). And also we discuss the effectiveness of the both methods.



### OS8-4 Analysis of Navier-Stokes Equation from the Viewpoint of Advection Diffusion (I) --- Analytical Solution of Diffusion Equation ---

Hiroki SAKAMOTO, Tetsuo HATTORI (Kagawa University, Japan)  
 Akiomi TADA (Japan)  
 Vanhoa NGUYEN (Japan)  
 Hiromichi KAWANO (NTT AT, Japan)

We propose an approximate analysis method for the Navier-Stokes Equation (NSE) based on the similarity between NSE and Advection Diffusion Equation (ADE). In this paper, we present an analytical solution and a Green function (integral kernel) which are obtained from the diffusion equation over uniform flow field (or velocity field) in three dimensional (3D) boundless region under arbitrary initial condition. The solution shows that the diffusion process is a Markov one and that the Green function becomes a Gaussian-like exponential function.

$$\frac{\partial C}{\partial t} = D_x \frac{\partial^2 C}{\partial x^2} + D_y \frac{\partial^2 C}{\partial y^2} + D_z \frac{\partial^2 C}{\partial z^2} - u \frac{\partial C}{\partial x} - v \frac{\partial C}{\partial y} - w \frac{\partial C}{\partial z} - \lambda C + Q \quad (\text{ADE})$$

### OS8-5 Analysis of Navier-Stokes Equation from the Viewpoint of Advection Diffusion (II) --- Approximate Solution ---

Hiroki SAKAMOTO, Tetsuo HATTORI (Kagawa University, Japan)  
 Akiomi TADA (Japan)  
 Vanhoa NGUYEN (Japan)  
 Hiromichi KAWANO (NTT AT, Japan)

We propose an approximate analysis method for the Navier-Stokes Equation (NSE) based on the similarity between NSE and Advection Diffusion Equation (ADE). In the preceding paper titled "Analysis of Navier-Stokes Equation from the Viewpoint of Advection Diffusion (I)", we have presented the analytical solution of the ADE. Subsequently in this paper, we point out the explicit similarity between NSE and ADE by illustrating the corresponding equations. Then, we show an approximate solution of NSE using the aforementioned analytical solution of ADE.

$$\frac{\partial C}{\partial t} = D \nabla^2 C - (\mathbf{v} \cdot \nabla) C - \lambda C + Q \quad (\text{ADE})$$

$$\left( D = D_x = D_y = D_z \right)$$

$$\frac{\partial \mathbf{v}}{\partial t} = k \nabla^2 \mathbf{v} - (\mathbf{v} \cdot \nabla) \mathbf{v} - \frac{\text{grad} p}{\rho} + \frac{\mathbf{f}}{\rho} \quad (\text{NSE})$$

$$\left( \text{div} \mathbf{v} = 0 \right)$$

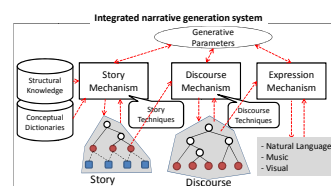
## GS

### GS1 Artificial intelligence

#### GS1-1 Selecting Words and Notation Using Literary Data in the Integrated Narrative Generation System

Jumpei Ono, Takashi Ogata  
(Iwate Prefectural University, Japan)

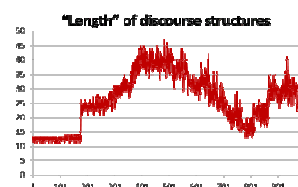
We have developed a narrative generation system called “Integrated Narrative Generation System: INGS”. The architecture of INGS has two types of macro level’s parts: “generation mechanism” and “knowledge mechanism”. The main elements of the latter “knowledge mechanism” are “conceptual dictionaries (for noun concepts and verb concepts)”, “language notation (or literation) dictionary”, and so on. Though the present mechanism of INGS randomly selects a noun concept from the choices, various types of noun concepts are mixed in a set such as old/new, ordinary/extraordinary, etc. This paper presents a common idea based on the frequency analysis of external texts’ words for the above two problems. For the first processing relevant to noun concepts, we automatically analyze frequency information of noun words in novels stored in “Aozora Bunko”, to select noun concepts according to the frequency information. For example, if we use noun concepts according to high-frequency noun words, the output text will be more readable. In this presentation, we will present the basic idea, text analysis programs with language parsing, several results, and the verification including comparing the results with the processing without the proposed mechanisms.



#### GS1-2 Evaluation of a Narrative Discourse Generation System Based on the Concept of “Norm and Deviation”

Taisuke Akimoto<sup>1</sup>, Takashi Ogata<sup>2</sup>  
(<sup>1</sup>The University of Electro-Communications, Japan)  
(<sup>2</sup>Iwate Prefectural University, Japan)

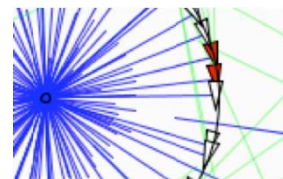
This paper deals with the verification of the narrative discourse system that automatically produces a variety of “discourse” structures from an inputted “story” structure through an iterative mutual action between a “narrator” mechanism and a “narratee” mechanism. We objectively consider the system’s behavior for identifying its achievements and issues to be addressed. In particular, we analyze a series of 10000 generated discourse structures according to their structural feature values by focusing on the diachronic alternation of “norm”, the narratee’s expectation in receiving discourses, caused by its “deviation” by the narrator. Overall, the mechanism produced a large number of different discourse structures through the restriction of generation space based on the norm at the time and the accumulation of small shifts in the norm.



### **GS1-3 An aggregating approach of target enclosure of robot swarm**

Masao KUBO<sup>1</sup>, Hiroshi SATO<sup>1</sup>, Akihiro Yamaguchi<sup>2</sup>, Akira Namatame<sup>1</sup>  
(<sup>1</sup>National Defense Academy of Japan, Japan)  
(<sup>2</sup>Fukuoka Institute of Technology, Japan)

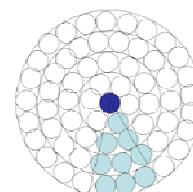
This paper presents a robot swarm model to enclose a target. The robots use information of the target and their neighbor information. In this paper, the robot observes the most robot dense direction as the neighbor information. We expect that this new approach makes the robot swarm more simple and robust for noisy environment. We confirm this model by computer simulations.



### **GS1-4 Probability of mixing up a nearest neighbor robot under target enclosure by robot swarm**

Masao KUBO<sup>1</sup>, Hiroshi SATO<sup>1</sup>, Akihiro Yamaguchi<sup>2</sup>, Akira Namatame<sup>1</sup>  
(<sup>1</sup>National Defense Academy of Japan, Japan)  
(<sup>2</sup>Fukuoka Institute of Technology, Japan)

This paper presents a robot swarm model to enclose a target. The robots use information of the target and their neighbor information. In this paper, the robot observes the most robot dense direction as the neighbor information. We expect that this new approach makes the robot swarm more simple and robust for noisy environment. We show a result of probabilistic analysis of this target enclosure approach.

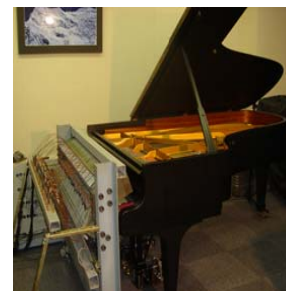


### **GS2 Complexity**

#### **GS2-1 Interactive musical editing system to support human errors and offer personal preferences for an automatic piano**

Kenji Tsunenari, Eiji Hayashi (Kyushu Institute of Technology, Japan)

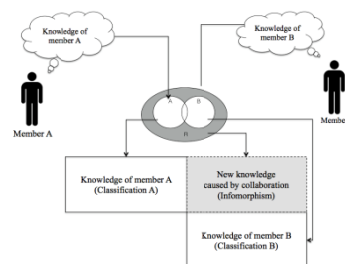
Recently, electronic musical instruments are achieving progress for development of electronics and seen everywhere. However, their sound quality and ambience are inferior to real musical instruments. Therefore, we developed automatic piano by using grand piano. Pre-edit is needed to play music in the manner of a live pianist. In the case of piano music, there are often 1000 or more notes in the score of even a short piece of music, requiring that an editor spend a huge amount of time to accurately simulate the emotionally expressive performance of a highly skilled pianist. Therefore, we have developed an interactive musical editing system that utilizes a database to edit music more efficiently.



## GS2-2 Modeling of collaboration in design process Based on Channel Theory

Patchanee Patitad, Hidetsugu Suto  
(Muroran Institute of Technology, Japan)

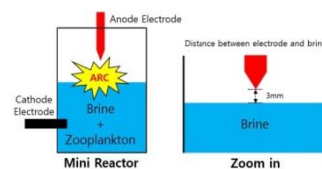
Collaboration is one of the effective approaches that help us to share knowledge together and exchange ideas within a team member. Sometimes, new helpful knowledge that is not held by the members emerges as a result of the collaboration. Such knowledge often contributes to get prime solutions during collaboration process. However, the way to generate such new knowledge is implicit. In this paper, a method of creating a model, which represents effects of collaboration in design process is proposed. By using this scheme, we can illustrate what new knowledge can be gotten from a collaboration and we can know the effect of the collaboration.



## GS2-3 Sterilizing system of ballast water using an arc discharge

Piao shengxu, Jae-cheol Lee, Zheng Tao, Heeje Kim  
(Pusan National University, Korea)

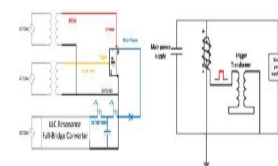
The inadvertent transfer of harmful aquatic organisms and pathogens in the ballast water of ships has been determined to cause a significant adverse impact to all around the world coastal regions. The recognition of these effects has made the ballast management system that is extremely important for protection of the marine environment. Recently, in order to solve this issue, a number of technologies have been developed and commercialized. Most of the treatment technologies are barely used independently. In addition, there are several combined methods to treat the ballast water. The overall aim of this study is to suggest one of the best ways of sterilization of ballast water using high voltage pulsed arc discharge.



## GS2-4 The design of medical ruby laser power supply system using LLC resonant converter

Jaecheol Lee, Piao shengxu, Zheng Tao, Heeje Kim  
(Pusan National University, Korea)

Because of its usability, the use of ruby laser for medical therapy has attracted a lot of interest. LLC resonant converter is used to control laser power density in ruby laser power supply. Zero voltage switching (ZVS) is implemented to minimize switching loss by LLC resonant converter. The power supply of solid state laser consists of trigger, simmer and main power supply. In this paper, simmer mode triggering circuit is used. It has advantage of miniaturizing a circuit and getting stability of a circuit by disconnecting trigger power supply from main power supply. We use DAB (Dual Active Bridge) to charge the capacitor. We obtained maximum laser output of 0.5J. Repetition of laser out is 3Hz.



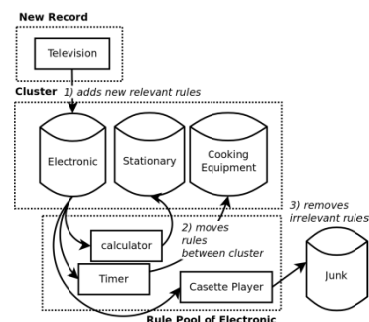


### GS3 Evolutionary computation

#### GS3-1 Online Rule Updating System Using Evolutionary Computation for Managing Distributed Database

Wirarama Wedashwara, Shingo Mabu, Masanao Obayashi and Takashi Kuremoto  
(Yamaguchi University, Japan)

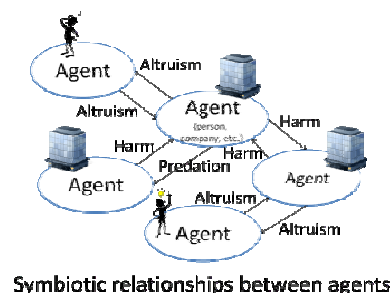
Research proposed decision support of database clusters optimization using genetic network programming (GNP) with on-line rule based clustering. GNP optimize cluster quality by reanalyze weak point of each cluster and maintain rules definition that stored on each cluster. Maintenance of rules definition includes : 1) adds new relevant rules, 2) moves rules between cluster and 3) removes irrelevant rules. Research simulation focused to optimize cluster quality response against several data unbalanced data growth to the data-set that already mapped with storage rules. Simulation results of proposed method shows better result and much lower iteration time.



#### GS3-2 Reinforcement Learning with Symbiotic Relationships for Multiagent Environments

Shingo Mabu, Masanao Obayashi and Takashi Kuremoto  
(Yamaguchi University, Japan)

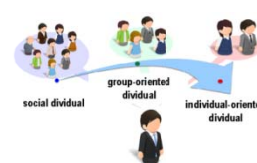
Studies on multiagent systems have been widely studied and realized cooperative behaviors between agents, where many agents are working together to achieve their objectives. In this paper, a new reinforcement learning framework considering the concept of Symbiosis in order to represent complicated relationships between agents and analyze the emerging behavior. In addition, distributed state-action value tables are also used to efficiently solve the multiagent problems with large number of state-action pairs. From the simulation results, it is clarified that the proposed method shows better performance comparing to the conventional reinforcement learning without considering symbiosis.



#### GS3-3 Development of a Dividual Model Using a Modular Neural Network for Human-Robot Interaction

Toshiyuki Tanaka and Kunikazu Kobayashi  
(Aichi Prefectural University, Japan)

Currently, in the field of human-robot interaction (HRI), robots have a problem that can only interact the same at all times with humans in a stereotypical way. We, therefore, introduce the concept called a dividual, which is originally proposed by Japanese novelist Keiichiro Hirano to interact properly with another human. We use two machine learning techniques, i.e. a modular neural network and an actor-critic reinforcement learning method, to construct a model of the dividual to grow through interactions with others. Through computer simulations, we confirmed a process to form an appropriate individual-oriented dividual.



## **GS4 Intelligent control**

### **GS4-1 Design of 1/40 scale simulator to apply the Flying Touch Method in hot rolling process**

Sung-jin Kim, Hyun-hee Kim, Min-cheol Lee  
(Pusan National University)

In the hot rolling process, scratches are occurred on the surface of a slab because of its strong friction. One of the methods to solve this scratches problem of slab is proposed which is the flying touch hot rolling process. This paper is focused on how the flying touch method can be applied to the gap control between upper and under roll in hot rolling process. This paper also introduces that the simulator of 40:1 size miniature model for applying flying touch method is manufactured to evaluate a performance of the flying touch method. Furthermore, it is evaluated by the simulator how much the flying touch hot rolling process can reduce the scratch.



### **GS4-2 Improving Accuracy of Inertial Measurement Unit using Discrete Wavelet Transform**

Jae-Hoon Jung, Dong-Hyuk Lee, Jang-Myung Lee  
(Pusan National University, South Korea)

In this paper, using discrete wavelet transform in the way of noise removal, and wavelet analysis has been used to denoise a digital image corrupted by noise in the acquisition step. This study proposed to minimize noise caused by internal characteristics and external factors of inertial measurement unit. By resolution decomposition which is characteristics of discrete wavelet transform, the noise can be removed actively with applying threshold. Previous studies use Low-pass filter or moving average filter for removing noise. But these filters are corresponded unsuitably for the rapidly changing data. This correspondence cause distortion of the original signal and cause another error for removing noise. In order to compensate for these disadvantages, discrete wavelet transform is applied.

### **GS4-3 Outdoor Localization for Quad-rotor using Kalman Filter and Path Planning**

Chen-Hu, Yo-Seop Hwang, Jang-Myung Lee  
(Pusan National University, South Korea)

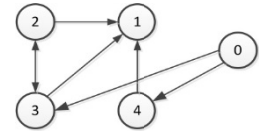
This paper proposes a new technique that produces the improved local information using low-cost GPS/INS system combined by Kalman filter and Path Planning when a Quad-rotor flies. Throughout the research, the low-cost GPS is combined with INS by using the Kalman filter in order to improve local information. However, this system has certain some disadvantages. In order to deal with these disadvantages, the algorithm based on the path planning can be adopted. When the quad-rotor flies outdoor, it is possible to predict that its moving path is short, since all the short moving paths of the quad-rotor can be assumed to be straight. Through the foregoing process, an improved kind of local information can be obtained when the quad-rotor flies. Also, the performance of the proposed system can be verified based on the outdoor experiments.



## GS4-4 Distributed Terminal Backstepping Control for Multi-Agent Euler-Lagrange Systems

Seong-Ik Han, Yun-Ki Kim, Jang-Myung Lee  
(Pusan National University, South Korea)

This paper presents a distributed terminal (finite-time) backstepping consensus control for multi-agent Euler-Lagrange systems. Terminal virtual error surfaces and virtual controls are proposed to guarantee the finite-time error consensus and formation convergence of a group of one-leader and multi-follower cooperative tracking Euler-Lagrange system. Finite-time stability including infinite-time stability was proved by the finite-time Lyapunov candidate function. Simulation example shows the effectiveness of the proposed finite-time backstepping coordinated tracking controller.

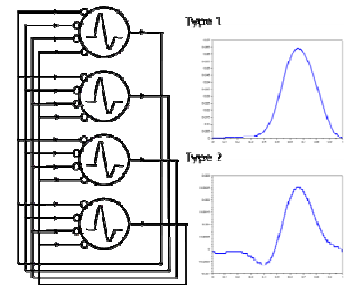


## GS5 Neuromorphic Systems

### GS5-1 Associative Memory with Class I and II Izhikevich Model

Yoshika Osawa, Takashi Kohno  
(University of Tokyo, Japan)

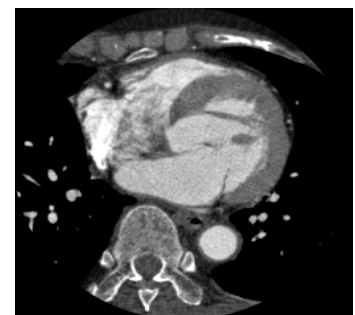
In the nervous system, information processing is performed by electrical signals, spikes, transmitted between the neurons. Spiking neural network is a system that qualitatively reproduce this complex behavior. It was shown in previous researches that the performance of associative memory task in all-to-all connected networks is higher when they are composed of Class II neurons than Class I neurons. The Izhikevich model in its Class II mode, however, does not have this performance boost. In this study, we focus on Phase Resetting Curve (PRC) as an index that reflects neuronal properties related to neuron classes more in detail and examined the relation between the shape of PRC and performance of associative memory task.



### GS5-2 Medical image recognition of heart regions by deep multi-layered GMDH-type neural network using principal component-regression analysis

Tadashi Kondo, Junji Ueno and Shoichiro Takao  
(Tokushima University, Japan)

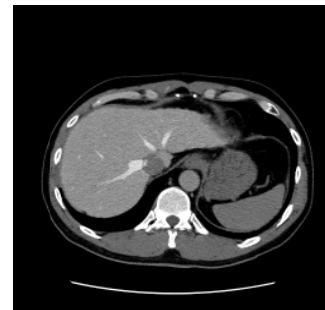
In this study, the deep multi-layered GMDH-type neural network algorithm using principal component-regression analysis is developed and applied to the medical image recognition of the heart regions. The multi-detector row CT (MDCT) images of the heart regions are used and the deep GMDH-type neural network architecture which has many hidden layers, is automatically organized from MDCT images of the heart regions so as to fit the complexity of the MDCT images of the heart regions. The deep GMDH-type neural network algorithm can automatically organize the deep neural network architectures so as to minimize the prediction error criterion defined as AIC or PSS.



### GS5-3 Deep feedback GMDH-type neural network using principal component-regression analysis and its application to medical image recognition of abdominal multi-organs

Tadashi Kondo, Junji Ueno and Shoichiro Takao  
(Tokushima University, Japan)

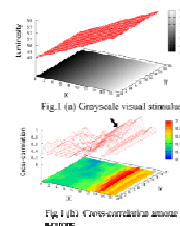
The deep Group Method of Data Handling (GMDH)-type neural network algorithms were proposed in our early works and can automatically organize the deep neural network architectures with many hidden layers by using heuristic self-organization method which is a type of the evolutionary computation. In this study, deep feedback GMDH-type neural network algorithm is developed and applied to medical image recognition of the abdominal multi-organs such as the liver and spleen. The recognition results are compared with those obtained by the conventional sigmoid function neural network trained using the back propagation method.



### GS5-4 Synchronized Response to Grayscale Image Inputs in the Chaotic Cellular Neural Network

Masayuki FUJIWARA<sup>1</sup>, Akihiro YAMAGUCHI<sup>1</sup>, Masao KUBO<sup>2</sup>  
(<sup>1</sup> Fukuoka Institute of Technology, Japan)  
(<sup>2</sup> National Defense Academy of Japan)

In this article, we study synchronized responses in the chaotic cellular neural network (Chaotic-CNN) for gray-scale visual stimulus. One fundamental goal of this study is to realize visual segmentation using chaotic neural synchronization. The Chaotic-CNN consists of chaotic spike response neurons that exhibits chaotic inter-spike intervals. Fig. 1 (a) is the gray-scale image pattern as visual stimulus. For this visual stimulus, a response of the Chaotic-CNN is numerically simulated. Then, the cross-correlation between one specific neuron that indicated by the arrow and others are calculated (Fig. 1 (b)). As shown in Fig. 1(b), high correlation is observed for the neurons in the direction of y axis and relatively lower correlation is observed for the others. Here, the neurons with the same input value form cell assembly for each input value. Each assembly is distinguished from the others in terms of cross-correlation. This result indicate a possibility of the visual segmentation using synchronized chaotic response.



## GS6 Poster Sessions

### GS6-1 The construction of evaluation index system for graduate course

Ai Dongmei, Wen Jiawei, Ning Xiaojun  
(University of Science and Technology Beijing, China)

Establishing the index system is the key to carry out the student assessment, evaluation of teaching largely quality depends on scientific index system. The related factors influencing the reliability and feasibility of teaching evaluation is analyzed in this article, and fair and scientific evaluation index system is established. Based on the summary of domestic and foreign existing evaluation index system, a set of new evaluation index system with our school teaching characteristics are established. Using the analytical hierarchy process to set up corresponding weights for each indicator, which makes the evaluation index system more complete and accurate.

$$A = \begin{pmatrix} 1 & a_{12} & \dots & a_{1n} \\ a_{21} & 1 & \dots & a_{2n} \\ \vdots & \vdots & \ddots & \vdots \\ a_{n1} & a_{n2} & \dots & 1 \end{pmatrix} = \begin{pmatrix} 1 & a_{12} & \dots & a_{1n} \\ \frac{1}{a_{12}} & 1 & \dots & a_{2n} \\ \vdots & \vdots & \ddots & \vdots \\ \frac{1}{a_{n1}} & \frac{1}{a_{n2}} & \dots & 1 \end{pmatrix}$$

### GS6-2 Extracting Pattern of Arm Movements based on EMG Signal for Stroke Therapy

Khairunizam Wan<sup>1</sup>, Rashidah Suhaimi<sup>1</sup>, Aswad A.R<sup>1</sup>, D. Hazry<sup>2</sup>, Zuradzman M. Razlan<sup>2</sup>,  
Shahriman AB<sup>2</sup>, Mohd Asri Ariffin<sup>3</sup> and Haslina M<sup>3</sup>  
(<sup>1</sup>Universiti Malaysia Perlis, MALAYSIA)  
(<sup>2</sup>Universiti Malaysia Perlis, MALAYSIA)  
(<sup>3</sup>Universiti Sains Malaysia, MALAYSIA)

This paper presents the investigation pattern of arm movements for the purpose of the rehabilitation for a stroke patient in the virtual reality (VR) environments. The investigation results are used to design the virtual objects in the virtual environments. The muscle activities are analyzed by using electromyography (EMG). Six EMG channels are attached to the right arm of the subject, which is at the location of deltoid anterior fibers, deltoid middle fibers, bicep, triceps, flexor and extensor while performing arm movements. The electrical signals acquired from EMG are analyzed to extract the signal's pattern by using signal processing technique. In the studies, several fundamental arm movements are performed by the subject and the acquired patterns of EMG signals are defined as muscle activities. The experimental results show that deltoid, bicep and triceps move with a significant value compared with flexor and extensor and are used to investigate the muscle activities, which is suitable to the stroke therapy.



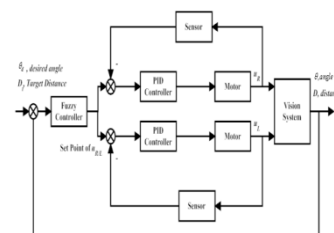
### GS6-3 Cascade Controller Design for Steering Control of Nonholonomic Autonomous Mobile Robot Vehicle

S. Faiz Ahmed<sup>1</sup>, D. Hazry<sup>1</sup>, F. Azim<sup>2</sup>

(<sup>1</sup>Universiti Malaysia Perlis(UniMAP), Malaysia.)

(<sup>2</sup>Hamdard University, Pakistan)

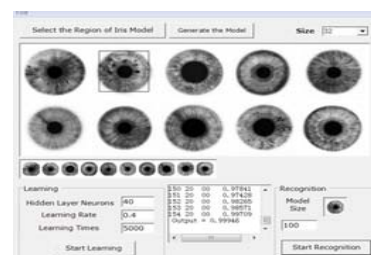
In this research article the cascade control system is presented for steering control of control of nonholonomic autonomous mobile robot vehicle. The propose system consist of a master controller and two slave controllers. The master controller is based on Fuzzy Logic Controller (FLC) which computes the required speed and angular speed needed by the two motors that drives the robot. Fuzzy logic is used to generate target trajectory movement. The two slave controllers are Proportional+Integral+Derivative (PID) controllers which ensured the desired speeds that needed for the both DC motors. PID controller parameters were tuned according to four ranges of speeds using model based tuning method. In addition, the control law is offered to select a suitable rule base for fuzzy controller in order to ensure the system is stable. The proposed cascaded controller is implemented on a nonholonomic mobile robot and the results have shown that, the proposed controller achieved the desired turning angle and the mobile robot tracks the target efficiently.



### GS6-4 Research on Iris Recognition Based on the BP Neural Network

Fengzhi DAI, Li FAN, Chunyu YU, Bo LIU

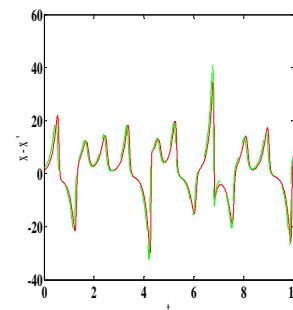
Iris recognition is the high confidence personal identification technology among the other biometrics recognition. This is not only because the iris's unique feature, but also due to its stability that the iris is immune to age and environment. In this paper, we design a feedforward neural network and use the back propagation algorithm to explore an elementary iris recognition system model. Ten iris samples that were pre-processed in a simple methodology are used as the recognition objects. Finally, the experiment demonstrates that though the recognition model is simply constructed, it has a high recognition rate and the recognition speed is reasonable. The proposed method provides a convenient way for iris recognition.



## GS6-5 Synchronization Control of a Four-wing Fractional-Order Chaotic System and Its Analog Circuit Design

Hongyan Jia, Qian Tao, Jinfang Li, Wei Xue  
(Tianjin University of Science & technology, PR China)

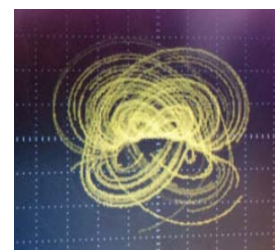
The four-wing fractional-order chaotic system is firstly introduced in this paper, and the state trajectories are given by using frequency domain approximate method. Then, a chaotic synchronization control of the four-wing fractional-order systems is also discussed, which is constructed by master-slave configuration with linear coupling. Simulation results are shown to verify the effectiveness of the proposed synchronization control, and the results from numerical analysis also show the chaotic synchronization control reported in the paper is simple and practical. At last, an analog circuit is designed to implement the synchronization control of the four-wing fractional-order system, and the results of circuit simulation are in agreement with those of numerical analysis, which probably provide a practical technology for application of fractional-order chaos, such as secure communication and image encryption.



## GS6-6 A fractional-order hyper-chaotic system and its circuit implementation

Wei Xue, HuiXiao, Jinkang Xu, Hongyan Jia  
(Tianjin University of Science and Technology, PR China)

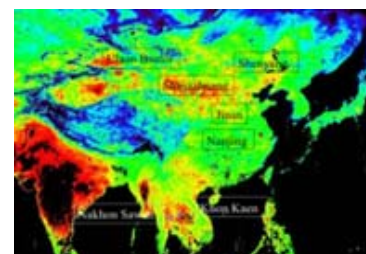
In this paper, the commensurate 3.6-order Qi hyper-chaotic system is investigated. Based on the predictor-corrector method, we obtain phase portraits, bifurcation diagrams, Lyapunov exponent spectra of the fractional-order system, and find that a four-wing hyper-chaotic attractor exists in the system when the system parameters change within certain ranges. On this basis, an analog circuit is designed to implement the fractional order hyper-chaotic system by using the method of approximation conversion from time domain to frequency domain, which verifies that the hyper-chaotic characteristic indeed exists in the fractional-order hyper-chaotic system on the physical level, and thus provides the technical basis for further application of the fractional-order hyper-chaotic system in engineering.



## GS6-7 Research on Early Crop Monitoring Using Photosynthetic Production Index in China

Fengzhi DAI<sup>1</sup>, Li FAN<sup>1</sup>, Daijiro KANEKO, Nozomu HIROSE, Chunyu YU<sup>1</sup>  
(<sup>1</sup>Tianjin University of Science & technology, China)

On the condition that there is great pressure on population growth and water resources shortage in China, aiming to monitor the early stage of crop growth, this paper presents a photosynthesis-based monitoring model for grain production. Not only the normalized difference vegetation index and elements such as the growing degree day are considered, the factors of sunshine and the cost of water resource are also considered in the model. Combined the meteorological data with the vegetation index that is adopted from remote-sensing, the model contains the elements of solar radiation, effective air temperature, vegetation biomass, stomatal opening, water stress, and the influence of temperature on grain plants, such as low-temperature sterility and high-temperature injury.



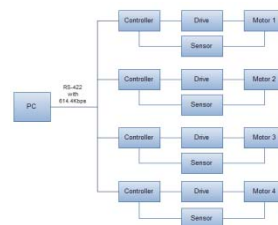
## GS6-8 Design and Implementation of Motor Test System based on Virtual Instrument

Yulong Xia<sup>1</sup>, Huailin Zhao<sup>1</sup>, Jihong Zhu<sup>2</sup> and Yang He<sup>2</sup>

(<sup>1</sup>Shanghai Institute of Technology, China)

(<sup>2</sup>Tsinghua University, China)

Most of the existing motor test systems based on the general computer with windows multimedia clock have problems of inaccurate timing and poor real-time capacity. A new motor test system is developed for improving the above problems and testing more motors simultaneously by serial communication with high baud rate. The test system software applies LabVIEW developing platform and is developed with the idea of the software engineering which makes each module functionally independent and improves the system reliability. Simultaneously the test system takes advantage of the characteristics of LabVIEW to complete relative accurate timing tasks and achieve excellent portability. To its communication, a professional serial port circuit is applied to support the high baud rate and bus connection. The experiment shows that the system is not only reliable, easy to operate, high availability and low test cost, but also satisfactory to the practical test.



## GS6-9 Consensus Problem of Distributed Multi-agent System

Huailin Zhao<sup>1</sup>, Wei Ren<sup>2</sup>, Masanori Sugisaka<sup>3</sup>

(<sup>1</sup>Shanghai Institute of Technology, China)

(<sup>2</sup>UCR, USA)

(<sup>3</sup>. Alife Robotics Corporation LTD, Japan)

This paper introduces the basic concept about the consensus of the distributed multi-agent systems. To a group of autonomous vehicles which are distributed, the consensus problem is the basic one in cooperative control to the multi-agent system. It discusses the problem based on the different conditions including the stochastic network topology, complex dynamic system, time delay effect, and the other ones. It gives the main research topics and some research achievements.



## GS6-10 Dingle's Model-based EEG Peak Detection using a Rule-based Classifier

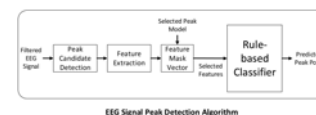
<sup>1</sup>Asrul Adam, <sup>2</sup>Zuwairie Ibrahim, <sup>1</sup>Norrima Mohktar, <sup>3</sup>Mohd Ibrahim Shapiai and <sup>1</sup>Marizan Mubin

(<sup>1</sup>University of Malaya, Malaysia)

(<sup>2</sup>Universiti Malaysia Pahang, Malaysia)

(<sup>3</sup>Universiti Teknologi Malaysia, Malaysia),

The employment of peak detection algorithm is prominent in several clinical applications such as diagnosis and treatment of epilepsy patients, assisting to determine patient syndrome, and guiding paralyzed patients to manage some devices. In this study, the performances of four different peak models of time domain approach which are Dumpala's, Acir's, Liu's, and Dingle's peak models are evaluated for EEG signal peak detection algorithm. The algorithm is developed into three stages: peak candidate detection, feature extraction, and classification. Rule-based classifier with an estimation technique based on particle swarm optimization (PSO) is employed in the classification stage. The evaluation result shows that the best peak model is Dingle's peak model with the highest test performance is 88.78%.

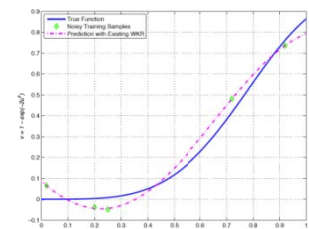




## GS6-11 Different Learning Functions for Weighted Kernel Regression in Solving Small Sample Problem with Noise

Zuwairie Ibrahim<sup>1</sup>, Nurul Wahidah Arshad<sup>1</sup>, Mohd Ibrahim Shapiai<sup>2</sup>, Norrima Mokhtar<sup>3</sup>  
(<sup>1</sup>Universiti Malaysia Pahang, Malaysia)  
(<sup>2</sup>Universiti Teknologi Malaysia, Malaysia)  
(<sup>3</sup>University of Malaya, Malaysia)

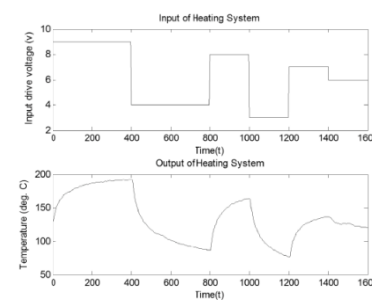
Previously, weighted kernel regression (WKR) for solving small samples problem has been reported. In the original WKR, the simple iterative learning technique and the formulated learning function in estimating weight parameters are designed only to solve non-noisy and small training samples problem. In this study, an extension of WKR in solving noisy and small training samples is investigated. The objective of the investigation is to extend the capability and effectiveness of WKR when solving various problems. Therefore, four new learning functions are proposed for estimating weight parameters. In general, the formulated learning functions are added with a regularization term instead of error term only as in the existing WKR. However, one free parameter associated to the regularization term has firstly to be predefined. Hence, a simple cross-validation technique is introduced to estimate this free parameter value. The improvement, in terms of the prediction accuracy as compared to existing WKR is presented through a series of experiments.



## GS6-12 Simultaneous Computation of Model Order and Parameter Estimation of a Heating System Based on Particle Swarm Optimization for Autoregressive with Exogenous Model : An Analysis

Teoh Shin Yee<sup>1</sup>, Zuwairie Ibrahim<sup>1</sup>, Kamil Zakwan Mohd Azmi<sup>1</sup>, Norrima Mokhtar<sup>2</sup>  
(<sup>1</sup>Universiti Malaysia Pahang, Malaysia),  
(<sup>2</sup>University of Malaya, Malaysia)

System identification is one of the method for solving a mathematical model of a system by performing on analysis only at its input and output behaviour. In system identification, the procedure of modelling the system is separated into four main parts. The first part is constructing an experiment to collect the input and output data of the system. Then, with some criteria, the model order and structure are selected. The next part is to estimate the parameters of the model. For the final part, the mathematical model is verified. Model order selection and parameter estimation are two important parts of finding the mathematical model for system identification. Previously, a technique called simultaneous model order and parameter estimation (SMOPE), which is based on Particle Swarm Optimisation (PSO) and ARX model, has been introduced to combine these two parts simultaneously. This technique, however, exclude the error term of ARX model. In this study, an analysis is shown to prove that the performance of SMOPE based on PSO and ARX model degraded as the magnitude of error increases.



### GS6-13 Maximum Probability Algorithm for Fault Diagnosis

Fengzhi DAI, Li FAN, Bo LIU

(Tianjin University of Science & technology, China)

This paper considers the fault diagnosis by outside fault phenomena. The method only depends on experience and statistical data to set up the fuzzy query relationship between the outside phenomena (fault characters) and the fault sources (fault patterns). From this relationship, the most probable fault sources can be located, and the standard fuzzy relationship matrix is stored as database.

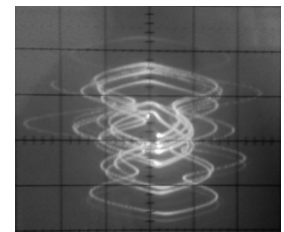
$\omega_{ip}$	$X_{ij}^f$			
	$x_{i1}$	$x_{i2}$	...	$x_{ip}$
$A_1$	$\omega_{11}$	$\omega_{12}$	...	$\omega_{1p}$
$A_2$	$\omega_{21}$	$\omega_{22}$	...	$\omega_{2p}$
...	...	...	...	...
$A_n$	$\omega_{n1}$	$\omega_{n2}$	...	$\omega_{np}$
...	...	...	...	...
$A_m$	$\omega_{m1}$	$\omega_{m2}$	...	$\omega_{mp}$

### GS6-14 The Fractional Order Hyperchaotic Generalized Augmented Lü System and its Circuit Implementation

Wei Xue, Jinkang Xu, Hongyan Jia

(Tianjin University of Science and Technology, PR China)

In this paper, a commensurate fractional-order hyperchaotic generalized augmented Lü system is investigated. We analyze its chaotic characteristics by drawing phase portraits, Poincaré maps, Lyapunov exponent spectra and power spectrum, and find that the system can present a four-wing hyperchaotic attractor. In addition, a circuit is designed for this system and the circuit implementation result shows the existence of the four-wing hyperchaotic attractor, which verifies the correctness of the theoretical analysis and provides the support for its application in engineering.



### GS7 Pattern Recognition

#### GS7-1 Fast motion detection based on cross correlation

Panca Mudjirahardjo, Joo Kooi Tan, Hyungseop Kim and Seiji Ishikawa

(Kyushu Institute of Technology)

**Abstract:** We present a fast motion detection as an abnormal motion based on cross correlation. Since the camera view is not in perpendicular with motion direction, the velocity of motion is not uniform spatially. Instead of object detection directly, we separate an image into several blocks. We calculate the cross correlation of the pixel intensity series in these blocks between current and previous frame. The maximum correlation is achieved at a certain delay. This delay shows a shift of a similar pattern between the current and previous frame. To localize the abnormal motion, we employ hierarchical block size. The performance of the proposed method is experimentally shown.

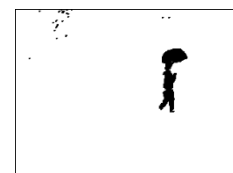




### GS7-2 Detecting moving objects on a video having a dynamic background

FX Arinto Setyawan, Joo Kooi Tan, Hyoungeop Kim, Seiji Ishikawa  
(Kyushu Institute of Technology, Japan)

This paper proposes a method of detecting moving objects in a video having a dynamic background using a method which infers the background sequentially. The proposed method performs the update of the pixel values in the background which are influenced by the value of the current pixel. The aim is to cope with changes in the value of the pixels in the background caused by the movement of the background objects such as the leaves swaying on trees, the water droplets of the rain or the change in light intensity according to the time lapse. The performance of the proposed method is shown experimentally using the video taken on a rainy and windy day.



### GS7-3 Study on the Target Recognition and Location Technology of industrial Sorting Robot based on Machine Vision

Jiwu Wang<sup>1</sup>, Xianwen Zhang<sup>1</sup>, Huazhe Dou<sup>1</sup>, Sugisaka Masanori<sup>2</sup>  
(<sup>1</sup>Beijing Jiaotong University)

(<sup>2</sup>Alife Robotics Corporation Ltd, Japan and Open University, United Kingdom)

In order to improve the applications for an industrial sorting robot, it is necessary to increase its flexibility and control accuracy. The prerequisites to automatically extract the multiple target positions accurately and robustly. The machine vision technology is an effective solution. Here an industrial robot arm is designed and set up for experiment simulation with machine vision. In order to reduce the influence of the size, deformation, and lighting etc., the target recognition and location method with fusion of scale invariant feature transform (SIFT) and moment invariants is developed. The experiments results showed that the developed image processing algorithms are robust, and the flexibility of the industrial robot can be improved by machine vision.

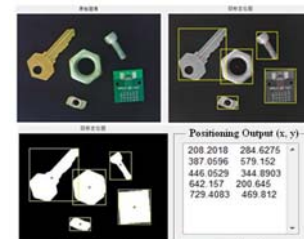


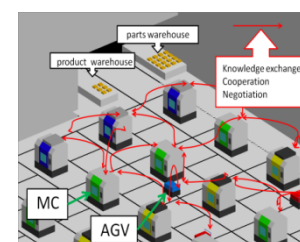
Fig.5 Illustration on the target positioning

### GS8Robotics I

#### GS8-1 Production effects by form changes of autonomous decentralized FMSs with mind

Kakeru Yokoi, Hidehiko Yamamoto, and Takayoshi Yamada  
(Gifu University, Japan)

An autonomous decentralized FMS does not have a management mechanism to control the entire factory and avoid the route interference of automatic guided vehicles (AGVs). This research aims to develop an autonomous decentralized FMS and focus on the development of the behavior control of AGVs to avoid the route interference, inspired by human mind; To express the mind, we propose the Minimum Unit of Mind (MUM) which has been used to simulate the production line in order to switching between arrogant and humble mind of AGVs. The result of simulation has shown it is possible to avoid the AGVs collisions. We examined the production line by applying different conditions such as changing the number of machining centers, AGVs and the position of products' warehouse.



## **GS8-2 Development of an autonomous-drive personal robot “Improve the accuracy of object area determination by boundary detection”**

Mikiko Hirai, Eiji Hayashi  
(Kyusyu Institute of Technology, Japan)

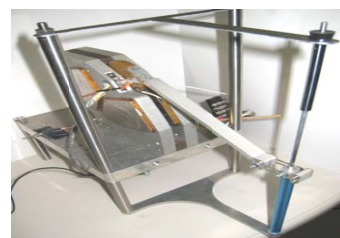
In the near future, autonomous self-driving robots are expected to provide various services in human living environments. The ability to work autonomously and accurately recognize surrounding objects are required for the autonomous robot. In previous research, the robot has enabled the recognition of the single object by the form, color, and the local characteristic of the object. In this paper, we present the system in the robot that enable to detect the single object area from plural objects in the camera image by using the function of the camera.



## **GS8-3 Construction of a supermicro sense of force feedback and vision for micro-objects: development of a haptic device**

Yusei Ishii, Eiji Hayashi  
(Kyushu Institute of Technology, Japan)

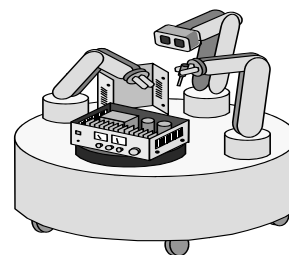
Recently, the technologies that can accurately perform minute work are now being sought for both medical treatments and in the field of manufacturing semiconductors. Such minute work is improved by using the micromanipulators, but their operation is difficult because the operator has no sense of force; he relies only on sight through microscope. As a result, a person skilled in the use of this technology is needed for all minute work. It is thought that the efficiency of minute work would be improved if the operator could obtain a sense of force while using a manipulator. We made and controlled the haptic device which shows the reaction force to the operator.



## **GS8-4 Error Recovery of Pick-and-Place Tasks in Consideration of Reusability of Planning**

Akira Nakamura, Kazuyuki Nagata, Kensuke Harada and Natsuki Yamanobe  
(National Institute of Advanced Industrial Science and Technology (AIST), Japan)

In manipulation tasks of complicated plant maintenance and industrial production, error recovery is an important research theme for robots that need to perform actual tasks. We have proposed error recovery using the concepts of both task stratification and error classification. Programming of error recovery will be simplified if the same planning can be used in many recovery paths. In this paper, reusability of planning in error recovery is verified by using pick-and-place tasks which are used frequently in plant maintenance and industrial production.

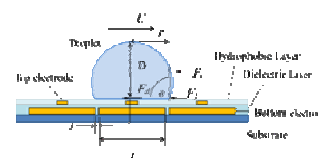


Maintenance Robot

## GS8-5 Design of Sliding Mode Controller for Droplet Position in EWOD Microfluidic System

Thunyaseth Sethaput(Thammasat University,Thailand),  
 Arsit Boonyaprasorn (Chulachomkloa Royal Military Academy,Thailand)

In microfluidic lab-on-chip devices, electrowetting on dielectric (EWOD) are widely used for various applications. To manipulate the micro droplet to achieve the desired path and accurate target position by using electrowetting technique are one of the common applications. In this paper, the motion of droplet is modeled as a single rigid body driven by both linear and nonlinear forces. In order to evaluate the potential of controller, the sliding mode controller is applied to this nonlinear microfluidic system. The effect of bounded disturbances is included in the designed controller. Simulation results provided the feasibility of the sliding mode controller for EWOD microfluidic manipulation under the effect of bounded disturbances.



The micro droplet motion on the EWOD plate.

## GS9Robotics II

### GS9-1 Mechanism Designs for Bio-inspired Flapping Wing Robots

Palakorn Tantrakool, Eakkachai Pengwang  
 (King Mongkut's University of Technology Thonburi, Thailand)

This paper presents the design of flapping systems for small air vehicle used in surveillance and surveying robot for an area that is hard to access. This paper also focuses on flapping mechanism of micro unmanned aerial robots that are similar to birds and insects. Our design consideration will have a wingspan up to 15 centimeters and a capability to hover. Enable technologies for fabrication of these designs are Computer-aided design (CAD) and 3D printers by using polymer materials with low density and weight. These structures are also connected by carbon rods for creating a crank-rocker mechanism. Characterizations of flapping wings are simulated and examined in this paper. With an external microcontroller board and power supply, this micro flapping wing robot will be tested and performed in real environments.



### GS9-2 Effective rocking motion for inducing sleep in adults

– Verification of effect of mother's embrace and rocking motion –

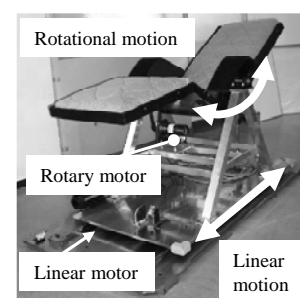
Keishi Ashida, Yoshifumi Morita (Nagoya Institute of Technology, RIKEN-RSC, Japan)

Ryojun Ikeura (Mie University, RIKEN-RSC, Japan)

Kiyoko Yokoyama (Nagoya City University, RIKEN-RSC, Japan)

Ming Ding, Yuki Mori (RIKEN-RSC)

The final goal of this research is to develop a relaxation machine for reducing stress and inducing sleep by using a rocking vibration. In our previous work, we measured the mother's embrace and rocking motion, constructed two types of the mother's rocking motion and developed an excitation apparatus simulating the mother's rocking motions. In this paper, we investigated the most effective rocking motion for inducing sleep in adults. We prepared ten types of rocking motion including two types of mother's rocking motions. The sleep-inducing effect of all the rocking motions was evaluated using Thurstone's paired comparison method (Case V). From statistical analysis of the subjective experimental results we found that, of the ten types of rocking motions, the linear

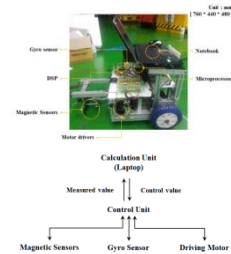




### GS9-5 Localization method for AGV using magnetic devices and IMU

Moonho Park, EunKyeong Kim, Yeongsang Jeong, Hansoo Lee, Jungwon Yu, Sungshin Kim  
(Pusan National University, Korea)

This paper is a research of the localization method for AGV (Autonomous Guided Vehicle) with a guidance system using magnetic localization devices. For navigation of AGV, an established magnetic guidance AGV detects a magnetic tape and follows the line. However, there are some weaknesses: disturbance and damage. To make up for the weak points, this paper proposed the localization method using two magnetic localization devices, a gyro sensor and encoders. In order to compensate global position, AGV's location and angle were compensated for a magnet position and gradient information using two magnetic localization devices. Between spot points, a relative position was calculated by kinematics with the devices. To verify the performance of the proposed method, it was compared with the method using a gyro sensor and encoders. As a result, the proposed method is more efficient than the existing one.

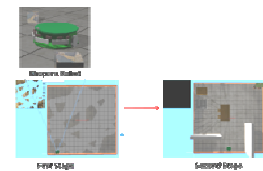


### GS10 Robotics III

#### GS10-1 On the Effects of Epigenetic Programming on the Efficiency of Incremental Evolution of the Simulated Khepera Robot

Yasuto Nishiwaki, Ivan Tanev, and Katsunori Shimohara  
(University of Doshisha, Japan)

The objective of this study is to develop an approach of Epigenetic Programming (EP) and to verify the feasibility of incorporating histones in genotype from both a computational and natural perspectives. In EP, we introduce histones as genetic ON and OFF “switches” that modify the gene expression by activating and deactivating the nodes in the tree representations (i.e., the “genotype”) of the controllers of simulated floor-cleaning Khepera robot, evolved via Genetic Programming (GP). We hypothesize that at the first stage of GP, when we evolve basic moving and cleaning abilities, histones inactivate genotypic areas that could be used during the second stage of evolution as a playground to evolve the novel obstacle-avoiding capabilities without damaging the already evolved basic abilities of the robot.



#### GS10-2 The Effect of Duration of Both Stages of Incremental Genetic Programming on its Efficiency of Evolution of Snakebot

N. Mukosaka, I. Tanev, K. Shimohara (Doshisha University, Japan)

The objective of our work is to investigate the optimal combination of durations of both stages of incremental Genetic Programming (IncGP) on the simulated Snake-like robots (Snakebots). In proposed IncGP we first evolve the bot in smooth terrain, and then evolve a population, partially seeded with these bots, in a challenging terrain. We experimented with various combinations of durations of both stages of IncGP, while fixing the total number of evolved generations. The obtained results suggest that neither the number of generations nor the obtained fitness value at the first stage of IncGP can be used as criteria for separating the two stages of IncGP. We hypothesized that another, qualitative criterion, such as the emergence of smooth sidewinding locomotion could be used instead, and conducted additional experiments that proved its worthiness.

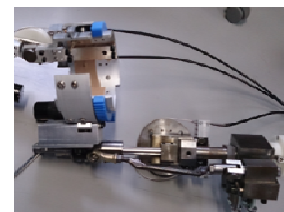




### GS10-3 Design of an effective shoulder joint mechanism for an upper-limb exoskeleton robot

Masahito Akiyama, Kazuo Kiguchi  
(Kyushu University, Japan)

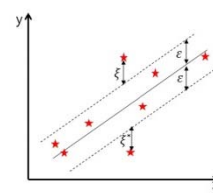
This paper proposes an effective shoulder joint mechanism for an upper-limb exoskeleton robot. A power-assist robot for human is regarded as one of the most promising machines which can assist labors in a heavy physical work, rehabilitation and so on. Human glenohumeral joint moves in 3-dimension in accordance with the movement of the upper-limb such as the shoulder flexion/extension and abduction/adduction motion. It makes the exoskeleton's shoulder mechanism complicated. In order to reduce the difference between the human glenohumeral joint position and the exoskeleton shoulder joint position, we propose a passive compensation mechanism which consists of links and sliders. This mechanism can imitate the movement of human glenohumeral joint without additional motors.



### GS10-4 A Machine Learning Approach to a Lateral Continuous Force Estimation for a Walking Biped Robot

Yeoun-Jae Kim, Jun-Yong Lee and Ju-Jang Lee (KAIST, Korea)

In this paper, a regressor for determining a lateral external continuous force applied upon a walking biped robot is investigated and verified by a numerical simulation. A pre-defined walking gait of a biped robot is constructed by the Tchebyshev method. And a continuous force-action classifier is generated. It determines whether the lateral external force is a continuous force or not. A regressor which estimates a lateral external continuous force acted upon a walking biped robot is constructed by SVR (Support Vector Regressor). The regressor is verified by a numerical simulation. We assumed that only lateral force is applied upon the COG (Center of Gravity) of the walking biped robot.



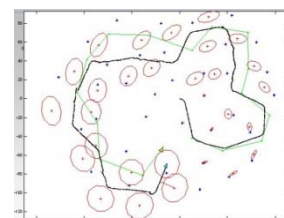
$$\begin{aligned} \text{Solution: } & y = wx + b \\ \text{Minimize: } & \frac{1}{2} \|w\|^2 + C \sum_{i=1}^N (\xi_i + \xi_i^*) \\ \text{Constraints: } & y_i - wx_i - b \leq \epsilon + \xi_i \\ & wx_i + b - y_i \leq \epsilon + \xi_i^* \\ & \xi_i, \xi_i^* \geq 0 \end{aligned}$$

### GS10-5 The Improvement of Robust Robot SLAM Algorithm Based on Sensor Fusion

Jiwu Wang<sup>1</sup>, Shunkai Zheng<sup>1</sup>, Fangbo Liao<sup>1</sup>, Sugisaka Masanori<sup>2</sup>  
(<sup>1</sup>Beijing Jiaotong University)

(<sup>2</sup>Alife Robotics Corporation Ltd, Japan and Open University, United Kingdom)

The Kinematic model of the robot is a very important part in SLAM, its error model will influence the positioning accuracy of robot and map building. Generally, the motion model relies simply on the data from encoder feedback. Due to cumulative error, the robot pose accuracy is relatively poor by mileage positioning with encoder. Here a new method is put forward based on data fusion of gyro sensor with the encoder data, and the robot pose accuracy is analyzed and improved. Then using the optimization Kinematic model on SLAM to verify the robustness.



## AUTHORS INDEX

### Notation of session name

**PS: Plenary Session, IS: Invited Session, OS: Organized Session, GS: General Session,**

Note: 33/90 =(page no. in Technical Paper Index) / (page no. in Abstracts)

	[A]			Cho	Hyunhak	GS9-4	15/59
AB	Shahriman	GS6-2	19/50				
Aburada	Kentaro	OS2-1	25/30	[D]			
		OS2-3	25/31	Dai	Fengzhi	GS6-4	19/51
		OS2-4	25/31			GS6-7	19/52
		OS2-5	25/32			GS6-13	20/55
		OS2-6	25/32	Ding	Hui	OS1-5	21/29
		OS7-1	23/40	Ding	Ming	GS9-2	15/58
		OS7-2	23/40	Dou	Huazhe	GS7-3	14/56
		OS7-3	23/41	Du	Yifei	OS5-2	23/37
Adam	Asrul	GS6-10	19/53			OS5-3	23/37
Ahmed	S. Faiz	GS6-3	19/51				
Ai	Dongmei	GS6-1	18/50	[F]			
Akimoto	Taisuke	GS1-2	20/43	Fan	Li	GS6-4	19/51
Akiyama	Masahito	GS10-3	16/61			GS6-7	19/52
Aoki	Kenji	OS5-1	23/37			GS6-13	20/55
		OS5-2	23/37	Fu	Xiaoyan	OS1-4	21/29
		OS5-3	23/37			OS1-5	21/29
Ariffin	Mohd Asri	GS6-2	19/50	Fujiwara	Masayuki	GS5-4	17/49
Arshad	Nurul	GS6-11	19/54	Furutani	Hiroshi	OS5-1	23/37
	Wahidah					OS5-2	23/37
Asada	Taro	OS3-2	22/33			OS5-3	23/37
		OS3-3	22/34			OS6-1	24/38
Ashida	Keishi	GS9-2	15/58			OS6-2	24/38
Azim	F.	GS6-3	19/51				
				[G]			
				Giannidakis	Emmanouil	IS-1-	18/27
	[B]						
Boonyaprasorn	Arsit	GS8-5	14/58				
				[H]			
				Han	Seong-Ik	GS4-4	17/48
	[C]			Harada	Kensuke	GS8-4	14/57
Chiu	Yi-Fu	PS-1	18/26				

Hashimoto	Kenji	PS-2	23/26	Ito	Tsutomu	OS4-2	24/36
Hattori	Tetsuo	OS8-1	21/41	Izumi	Tetsuya	OS8-1	21/41
		OS8-2	21/41				
		OS8-3	21/42				
		OS8-4	21/42	Jeong	Yeongsang	GS9-4	15/59
		OS8-5	22/42			GS9-5	15/60
Hayashi	Eiji	GS2-1	16/44	Jia	Hongyan	GS6-5	19/52
		GS8-2	14/57			GS6-6	19/52
		GS8-3	14/57			GS6-14	20/55
Hazry	D.	GS6-2	19/50	Jia	Yingmin	OS1-1	21/28
		GS6-3	19/51			OS1-2	21/28
He	Yang	GS6-8	19/53	Jovic	Jovana	IS-3	18/27
Hirai	Mikiko	GS8-2	14/57	Jung	Jae-Hoon	GS4-2	17/47
Hirose	Nozomu	GS6-7	19/52				
Hu	Chen	GS4-3	17/47				
Hwang	Yo-Seop	GS4-3	17/47				
				Kaneko	Daijiro	GS6-7	19/52
				Katayama	Tetsuro	OS2-1	25/30
						OS2-2	25/30
						OS2-3	25/31
						OS2-4	25/31
						OS2-5	25/32
						OS2-6	25/32
						OS7-1	23/40
						OS7-3	23/41
				Kato	Ryota	OS3-2	22/33
						OS3-3	22/34
Ikeura	Ryojun	GS9-2	15/58				
Imai	Yoshiro	OS8-2	21/41	Kawakami	Yusuke	OS8-1	21/41
Ishii	Yusei	GS8-3	14/57			OS8-2	21/41
Ishikawa	Seiji	GS7-1	14/55	Kawano	Hiromichi	OS8-1	21/41
		GS7-2	14/56			OS8-2	21/41
Ito	Tadashi	GS9-3	15/59			OS8-3	21/42
Ito	Takao	OS4-2	24/36			OS8-4	21/42
		OS6-1	24/38			OS8-5	22/42
		OS6-2	24/38	Kiguchi	Kazuo	GS10-3	16/61
		OS6-3	24/39	Kikkawa	Yuuki	OS2-5	25/32
		OS6-4	24/39	Kim	EunKyeong	GS9-5	15/60

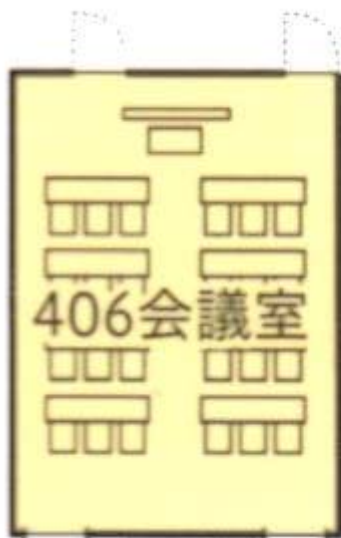
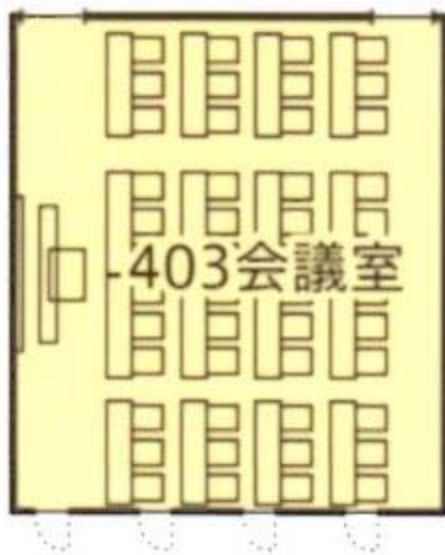
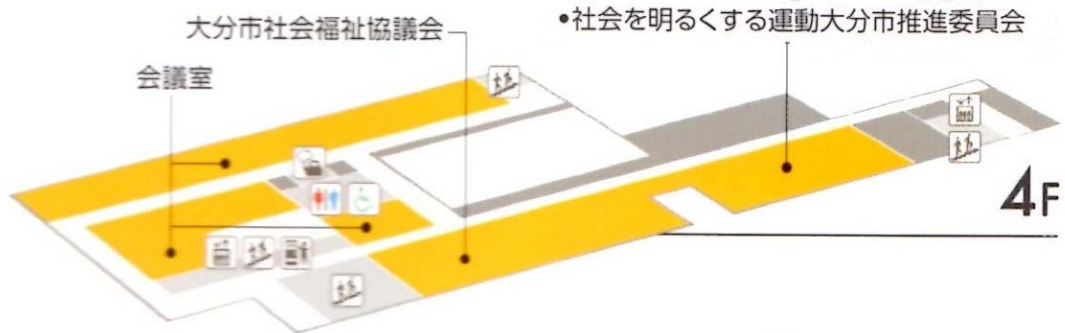


Kim	Heeje	<a href="#">GS2-3</a>	16/45			<a href="#">GS2-4</a>	16/45
		<a href="#">GS2-4</a>	16/45	Lee	Jang-Myung	<a href="#">GS4-2</a>	17/47
Kim	Hyoungseop	<a href="#">GS7-1</a>	14/55			<a href="#">GS4-3</a>	17/47
		<a href="#">GS7-2</a>	14/56			<a href="#">GS4-4</a>	17/48
Kim	Hyun-hee	<a href="#">GS4-1</a>	17/47	Lee	Ju-Jang	<a href="#">GS10-4</a>	16/61
Kim	Sung-jin	<a href="#">GS4-1</a>	17/47	Lee	Jun-Yong	<a href="#">GS10-4</a>	16/61
Kim	Sungshin	<a href="#">GS9-4</a>	15/59	Lee	Min-cheol	<a href="#">GS4-1</a>	17/47
		<a href="#">GS9-5</a>	15/60	Li	Jinfang	<a href="#">GS6-5</a>	19/52
Kim	Yeoun-Jae	<a href="#">GS10-4</a>	16/61	Li	Qing	<a href="#">OS1-3</a>	21/28
Kim	Yun-Ki	<a href="#">GS4-4</a>	17/48	Liao	Fangbo	<a href="#">GS10-5</a>	16/61
Kimura	Jun	<a href="#">OS3-5</a>	22/35	Liao	Yuntao	<a href="#">OS4-3</a>	24/36
Kita	Yoshihiro	<a href="#">OS2-1</a>	25/30	Liu	Bo	<a href="#">GS6-4</a>	19/51
		<a href="#">OS2-3</a>	25/31			<a href="#">GS6-13</a>	20/55
		<a href="#">OS2-4</a>	25/31	Lu	Xuhui	<a href="#">OS1-2</a>	21/28
		<a href="#">OS2-5</a>	25/32	Lund	Henrik	<a href="#">IS-1</a>	18/27
		<a href="#">OS2-6</a>	25/32		Hautop		
		<a href="#">OS7-2</a>	23/40			<a href="#">IS-2</a>	18/27
Kitano	Shoichiro	<a href="#">OS2-4</a>	25/31	[M]			
Kobayashi	Kunikazu	<a href="#">GS3-3</a>	16/46	M	Haslina	<a href="#">GS6-2</a>	19/50
Kohno	Takashi	<a href="#">GS5-1</a>	17/48	Ma.	Q.	<a href="#">OS5-3</a>	23/37
Kondo	Tadashi	<a href="#">GS5-2</a>	17/48	Mabu	Shingo	<a href="#">GS3-1</a>	16/46
		<a href="#">GS5-3</a>	17/49			<a href="#">GS3-2</a>	16/46
Koyama	Yoshihide	<a href="#">OS8-3</a>	21/42	Matsuno	S.	<a href="#">OS6-4</a>	24/39
Kubo	Masao	<a href="#">GS1-3</a>	20/44	Matsushita	Haruna	<a href="#">OS8-2</a>	21/41
		<a href="#">GS1-4</a>	20/44	Mehta	R.	<a href="#">OS4-2</a>	24/36
		<a href="#">GS5-4</a>	17/49	Meng	Yue	<a href="#">OS1-5</a>	21/29
Kubota	Shinichiro	<a href="#">OS7-1</a>	23/40	Mohd Azmi	Kamil	<a href="#">GS6-12</a>	20/54
		<a href="#">OS7-3</a>	23/41		Zakwan		
Kuremoto	Takashi	<a href="#">GS3-1</a>	16/46	Mohktar	Norrima	<a href="#">GS6-10</a>	19/53
		<a href="#">GS3-2</a>	16/46			<a href="#">GS6-11</a>	19/54
						<a href="#">GS6-12</a>	20/54
	[L]			Mori	Yuki	<a href="#">GS9-2</a>	15/58
Lee	Dong-Hyuk	<a href="#">GS4-2</a>	17/47	Morita	Yoshifumi	<a href="#">GS9-2</a>	15/58
Lee	Hansoo	<a href="#">GS9-4</a>	15/59			<a href="#">GS9-3</a>	15/59
		<a href="#">GS9-5</a>	15/60	Mubin	Marizan	<a href="#">GS6-10</a>	19/53
Lee	Jae-cheol	<a href="#">GS2-3</a>	16/45	Mudjirahardjo	Panca	<a href="#">GS7-1</a>	14/55



Sethaput	Thunyaseth	GS8-5	14/58	Taniguchi	Taiki	OS3-4	22/34
Setyawan	FX Arinto	GS7-2	14/56	Tantrakool	Palakorn	GS9-1	15/58
Shang	Yuanyuan	OS1-4	21/29	Tao	Qian	GS6-5	19/52
		OS1-5	21/29	Tsunenari	Kenji	GS2-1	16/44
Shapiai	Mohd	GS6-10	19/53				
	Ibrahim			[U]			
Shimohara	Katsunori	GS6-11	19/54	Uchida	Yasuo	OS6-1	24/38
		GS10-1	15/60			OS6-2	24/38
		GS10-2	15/60			OS6-4	24/39
Song	Kai-Tai	PS-1	18/26	Ueno	Junji	GS5-2	17/48
Sugisaka	Masanori	GS6-9	19/53			GS5-3	17/49
		GS7-3	14/56	Urata	Seiya	OS2-1	25/30
		GS10-5	16/61	Venture	Gentiane	IS-3	18/27
Suhaimi	Rashidah	GS6-2	18/52				
Susaki	Hikaru	OS6-1	24/38	[W]			
		OS6-2	24/38	WAN	Khairunizam	GS6-2	19/50
Suto	Hidetsugu	GS2-2	16/45	Wang	Jiwu	GS7-3	14/56
						GS10-5	16/61
[T]							
Tabuse	Masayoshi	OS3-1	22/33	Wedashwara	Wirarama	GS3-1	16/46
		OS3-2	22/33	Wen	Jiawei	GS6-1	18/50
		OS3-3	22/34				
		OS3-5	22/35	[X]			
Tada	Akiomi	OS8-4	21/42	Xia	Yulong	GS6-8	19/53
		OS8-5	22/42	Xiao	Hui	GS6-6	19/52
Takanishi	Atsuo	PS-2	23/26	Xu	Jinkang	GS6-6	19/52
Takao	Shoichiro	GS5-2	17/48			GS6-14	20/55
		GS5-3	17/49	Xue	Wei	GS6-5	19/52
Takeda	Katsunori	OS8-3	21/42			GS6-6	19/52
Takeshita	Yuki	OS6-3	24/39			GS6-14	20/55
Tamura	Kaori	OS3-1	22/33				
Tan	Joo Kooi	GS7-1	14/55	[Y]			
		GS7-2	14/56	Yamaba	Hisaaki	OS2-1	25/30
Tanaka	Toshiyuki	GS3-3	16/46			OS2-3	25/31
Tanev	Ivan	GS10-1	15/60			OS2-4	25/31
		GS10-2	15/60	Yamaba	Hisaaki	OS2-5	25/32

		OS2-6	25/32	Zhao	Huailin	GS6-8	19/53
		OS7-1	23/40			GS6-9	19/53
		OS7-3	23/41	Zheng	Shunkai	GS10-5	16/61
Yamada	Ayaka	GS9-3	5/59	Zheng	Tao	GS2-3	16/45
Yamada	Takayoshi	GS8-1	14/56			GS2-4	16/45
Yamaguchi	Akihiro	GS1-3	20/44	Zhou	Xiuzhuang	OS1-5	21/29
		GS1-4	20/44	Zhu	Jihong	GS6-8	19/53
		GS5-4	17/49				
Yamamoto	Hidehiko	GS8-1	14/56				
Yamamoto	Toru	OS4-3	24/36				
Yamanobe	Natsuki	GS8-4	14/57				
Yamazaki	Kazunori	GS9-3	15/59				
Yang	Chao	OS1-1	21/28				
Yee	Teoh Shin	GS6-12	20/54				
Yokoi	Kakeru	GS8-1	14/56				
Yokoyama	Kiyoko	GS9-2	15/58				
Yoshida	Eiichi	IS-3	18/27				
Yoshinaga	Tsunehiro	OS6-1	24/38				
		OS6-2	24/38				
Yoshitomi	Yasunari	OS3-2	22/33				
		OS3-3	22/34				
		OS3-4	22/34				
		OS3-5	22/35				
Yu	Chunyu	GS6-4	19/51				
		GS6-7	19/52				
Yu	Jungwon	GS9-4	15/59				
		GS9-5	15/60				
[Z]							
Zhang	Xianwen	GS7-3	14/56				
Zhang	Tuo	OS6-1	24/38				
		OS6-2	24/38				
Zhang	Weicun	OS1-3	21/28				
Zhang	Y.	OS5-3	23/37				





406会議室

# Production effects by form changes of autonomous decentralized FMSs with mind

**Kakeru Yokoi**

*Human Information Systems Engineering, Gifu University, 1-1, Yanagido, Gifu Japan*

**Hidehiko Yamamoto**

*Mechanical Engineering, Gifu University, 1-1, Yanagido, Gifu Japan*

**Takayoshi Yamada**

*Mechanical Engineering, Gifu University, 1-1, Yanagido, Gifu Japan*

*E-mail: yokoi1205@gmail.com, yam-h@gifu-u.ac.jp, yamt@gifu-u.ac.jp*

## Abstract

In autonomous decentralized FMS, the number of agents and constant installation position has been studied in previous studies. Therefore, in this study, we are considering to change the position of the warehouse and the number of AGVs to redesign the factory form and evaluate the changes in the production of autonomous decentralized FMS. By being inspired by human mind, we are proposing Minimum Unit of Mind (MUM), a new method of controlling the behavior of AGVs to avoid the unexpected collision in autonomous decentralized FMS.

## 1. Introduction

We need to avoid collision among AGVs when we use autonomous decentralized FMS. There are some rules to avoid collision, but these rules are not good enough to control the process of autonomous decentralized FMS because all situations can not be foreseen and rules are not described. Hence, the purpose of this study is to bring forward human mind to control the behavior of AGVs.

In fact there are some limitations to control autonomous decentralized FMS and avoiding the collision among AGVs, but in this study we are trying to improve the FMS process.

To improve and control the collision, we propose the development of behavioral control to avoid the collision by relying on the fact that simulating the human mind will help machines to make better decisions. In this study, we are considering to change the position of the product warehouse and change the number of AGVs to redesign the factory form and

evaluate the changes on the production of autonomous decentralized FMS.

### 2.1. Overview of autonomous decentralized FMS

Fig.1 illustrates an autonomous decentralized FMS factory scheme. As Fig1 shows, the factory floor is divided into grid patterns, and AGVs are moving along these lines to carry parts to the warehouse and machine centers which is representing the system of autonomous factory to carry out the production. The autonomous decentralized FMS does not have a management mechanism to integrate the entire system, (machining centers, AGV, product warehouse (PW), parts warehouse). Each agent that configures the system autonomously determines the act by recognizing the purpose of the system by cooperating and negotiating to other agent.<sup>1</sup>



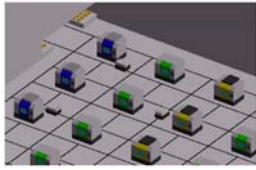


Fig.1: Autonomous Decentralized FMS Scheme

## 2.2. Model of the mind and behavior of the AGV

We describe the behavior of the AGV control of autonomous decentralized FMS factory. In autonomous decentralized FMS, each AGV determines the behavior autonomously. If any of the AGVs runs on the same line at the same time, they overlap and AGV path interference occurs. It is necessary to avoid such interference between AGVs and therefore, we have developed control rules for the system. If the number of AGVs increases, more unexpected events can occur because the rules become more complicated. Thus, it is impossible to generate rules that can be adapted to every situation in an autonomous decentralized FMS factory. This study focuses on the human mind, which can deal with unexpected events. We propose a mind model for the AGVs and develop a method to control their behavior by using a mind. The mind model considers two types of mind: an arrogant mind and a modest mind. AGV with arrogant mind takes the action approaching the destination forcibly. AGV with modest mind takes the action to give way to other AGV.

Fig.2 is a diagram about mind model. In this study, we call it Minimum Unit of Mind (MUM). Further, A1 and A2 is unit, X is load, and arrow is a stimulation vector. The threshold is determined by the unit.

If the internal value reaches the threshold, we call excited and if it does not reach, normal.

When a signal is sent to the unit, it sends a signal to the direction of the arrow when excited, and it is not sent when normal.

Load has the function to change the internal value of the unit. When the signal is sent to the load, the value of unit is decreased by the value of X.

Stimulation vector is a line connecting the load and the unit. It gives a signal to the load or unit when the signal comes, when A1 keeps excited, we call modest mind, and when normal, we call arrogant mind.

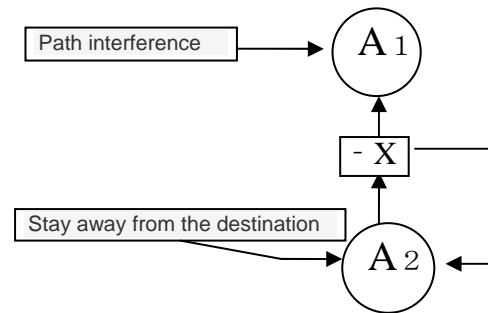


Fig2. Model of the mind

Next, we describe the internal functions of MUM. When the arrogant AGV has path interference, A1 is increased by 1. Keeping the situation of the interference and being increased by 1, the A1 value becomes the threshold value, and the AGV is changed to a modest one.

When AGVs with a modest mind keep giving a way, the value of A2 is increased by 1. When the situation is repeated an optional time and A2 becomes excited, a signal is sent to a load. The received load decreases the values of units A1 and A2 by optional values. Because of this, A1 and A2 are returned to normal and AGV with a modest mind is changed to one with an arrogant mind. In this way, when an arrogant mind is incorporated in the AGV, it is forceful in its motion. On the other hand, when a modest mind is incorporated in the AGV, it gives way to other AGVs.

## 3. Impact on production conditions and Change Agent

In this section we will investigate parameters such as capacity utilization, route interference and number of products by applying following conditions:

### 3.1. Changing the position of the products warehouse:

The product and part warehouses were immobilized in the previous studies and to prove that moveable warehouse method is effective, we decided to design five new factory layouts in this study.

### 3.2. Changing the number of machining centers and AGVs:

In the previous studies, the number of AGV was allocated to five AGVs and the number of the machining centers was done with 24 units. We will



change the AGV numbers from 2 to 9 AGVs, and we adopt 24 units of machining center and 16 units in this study.

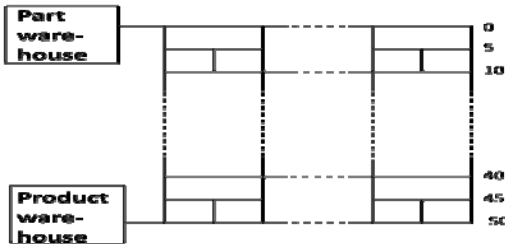


Fig3. Location of product warehouse (0, 50) layout

Fig.3: is a layout of the production floor when it was changed to the location of the product warehouse (0, 50).

#### 4. Simulation results

Figure 4, Table 1 and Table 2 are the results of the simulation of production when the number of machining centers and AGVs are being changed. As the result shown, the more number of AGVs, the more productions will be produced. However, we have gotten a result that shows a little difference when the number of machining centers are 24 units and 16 units. In addition, in the first 30 minutes of the starting the simulation there is a high route interference number as shown in the Fig 5. It is because, right after the starting the simulation, there is no part in the machine centers and all AGVs should go and pick the parts from the part warehouse simultaneously.

Table1. Production number of the case of 16 cars MC

AGV	2	3	4	5	6	7	8	9
data1	92	129	160	184	209	233	254	274
data2	89	129	156	184	212	233	256	273
data3	91	132	161	184	209	230	255	277

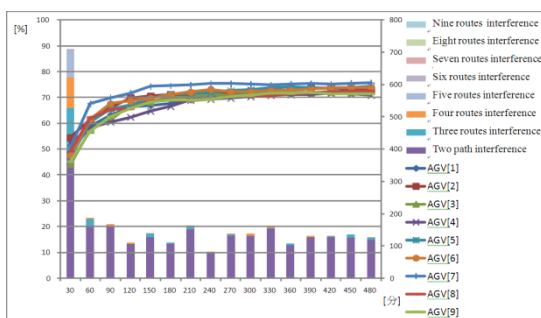


Fig4. AGV path interference and number of AGVs in every 30 minutes

Table2. Production number of the case of 24 cars MC

AGV	2	3	4	5	6	7	8	9
data1	84	122	151	184	214	235	257	274
data2	85	120	155	185	212	233	252	277
data3	84	118	155	185	210	232	252	280

Next, we show simulation results of autonomous decentralized FMS when the position of the product warehouse is changed to 5 different positions.

Table 3, 4 illustrate the utilization rate of MC when the number of AGVs are 8 and 5 and the number of MCs are set on 16.

Table3. Utilization rate when the AGV number is 5

Product warehouse	Capacity utilization
(0,10)	36.522
(0,25)	37.187
(0,50)	36.401
(60,0)	36.15
(60,25)	35.882
(60,50)	35.248

Table4. Utilization rate when the AGV number is 8

Product warehouse	Capacity utilization
(0,10)	49.864
(0,25)	50.136
(0,50)	50.306
(60,0)	50.293
(60,25)	50.075
(60,50)	49.235

When the AGVs number is 5 and the position of product warehouse is (0, 25) then the utilization rate of MC gives us a better result. Table 3, 4 are shown the results of this simulation. However, when the number of AGVs change to 8 and the position of PW change to (0, 50) then the utilization rate gets a little bit better than the previous condition. In the other hand, when the AGVs number is 5 or 8 and PW position is (60, 50) the utilization rate will be the lowest rate.

Table 5, 6 are shown the production number when the AGVs number is 5 and 8.

Table5. Production number when the AGV number is 5

Product warehouse	The production number
(0,10)	182
(0,25)	180
(0,50)	191
(60,0)	181
(60,25)	180
(60,50)	175

Table6. Production number in the case of 8 AGVs

Product warehouse	The production number
(0,10)	250
(0,25)	263
(0,50)	263
(60,0)	261
(60,25)	253
(60,50)	247

According to Table 5, 6 the PW with position (0, 50) has become the maximum production number when the AGVs number is 5 and 8. In case of having 5 AGVs the production number increasing but to compare with 8 AGVs the ratio of increasing the products is not significant. The lowest result of production number which we have got in simulation is about when the PW position is (60, 50) with both 5 and 8 AGVs.

Table 7, 8 illustrate the route interference number in case of 5 and 8 AGVs.

Table7. AGV route interference number of times in case of 5 AGVs

Product warehouse	Route interference number
(0,10)	997
(0,25)	912
(0,50)	729
(60,0)	833
(60,25)	850
(60,50)	731

Table8. AGV route interference number of times in case of 8 AGVs

Product warehouse	Route interference number
(0,10)	2668
(0,25)	2286
(0,50)	2134
(60,0)	2111
(60,25)	2113
(60,50)	1923

According to Table 7, 8 the route interference number is the lowest result in case of 5 and 8 AGVs and in the PW position (60, 50). As a result, the new production floors have a better result to compare with the previous production floors. Hence, Autonomous distributed system that was newly created by this simulation, and the results we have got through this simulation shows that the some layouts will be more efficient to use in the production floor.

## 5. Discussion

There are different rules and techniques which have been studied by other researchers, the number of AGVs

are limited so more number of AGVs cause more difficulties and collisions in the production floor in their study. In our research we have tried to improve the limitations and change the rules to be able to increase the number of AGVs as more as possible. To prove that our study is effective, we proposed MUM in this study.

In the following paragraphs we discuss the results of different layouts of the production floor, 5 and 8 AGVs, the number of parts, route interference number and MC utilization rate. According to mentioned Tables and Figures, the previous study with a PW position  $(x, y) = (0, 10)$  the path interference rate was high. In our study we change the layout of autonomous distributed system PW positions to (0, 25), (0, 50), (60, 0), (60, 25), (60, 50) and AGV route interference was reduced after applying changes. However the utilization rate of AGV is increased and interference number of AGV is reduced, but sometimes the number of production will be lower. Sometimes due to long distance between AGV to PW position the AGV takes a lot of time to move between two points which is time consuming.

In our study, the result of simulation shows that production floor with PW position (0, 50) with 5 and 8 AGVs will have a better performance and will get a better result; we expect the production efficiency by following this pattern. There are several ways to design the layout and change the number of AGVs and MCs, however we have got a good result which seems efficient, but we suspect that there can be other ways to make optimum. It has also been found that it is necessary to perform the simulation, depending on the different conditions.

## 6. Conclusions

In conclusion, changing the number of MC and AGVs affected the production rate and capacity utilization. Applying the new conditions and layout designs has improved the production line. Finding new optimal agent conditions by applying to autonomous decentralized FMS in order to improve the production efficiency should be done in a future work.

## Reference

- 1.Hidehiko Yamamoto, Jaber Abu Qudeiri and M.A. Jamali, Real-time Control of Decentralized Autonomous Flexible Manufacturing Systems by using Memory and Oblivion, Lecture Notes of Computer Science , Springer, pp.252-259, ISBN 978-3-540-46535-5, Nov., 2006.

# **Development of an Autonomous-Drive Personal Robot “Improve the Accuracy of Object Area Determination by Boundary Detection”**

**Mikiko Hirai**

*Department of Mechanical Information Science and Technology, Kyushu Institute of Technology,  
680-4, Kawazu, Iizuka-City, Fukuoka, 820-8502, Japan  
Email: hirai@mmcs.mse.kyutech.ac.jp*

**Eiji Hayashi**

*Department of Mechanical Information Science and Technology, Kyushu Institute of Technology,  
680-4, Kawazu, Iizuka-City, Fukuoka, 820-8502, Japan  
E-mail: haya@mse.kyutech.ac.jp*

## **Abstract**

We are developing an autonomous personal robot that able to perform practical tasks in a human environment based on information derived from camera images and the Laser Range Sensor (LRS). It is very important that the robot be able to move autonomously in a human environment, and to select a specific target object from among the many objects. This environmental recognition system is composed of an autonomous driving system and an object recognition system. So we confirmed the effectiveness of the object recognition system by the experimental results.

*Keywords:* Personal robot, Monocular camera, Image processing, Object recognition.

## **1. Introduction**

In the near future, some autonomous self-driving robots are expected to provide various services in human living environments. For this to occur, the robots will need to gain a grasp of the human environment. Therefore, the systems to provide environmental recognition based on image information are being widely studied. However, it is very difficult to recognize all driving environments from image information only. So far, no prospects for such a system have emerged. Here, we report on the development of an autonomous personal robot able to autonomously perform practical tasks in human environment based on the several information that are derived from the camera

images and the Laser Range Sensor (LRS) which is used to acquire two-dimensional distance information.

The system for this robot is composed of an autonomous run system for movement and an object recognition system for the recognition and grasping of an object. First, the autonomous run system decides upon a robot driving command based on information in the limited space map. Information such as walls and barricades are set to the map, and the data obtained from the CCD camera are compared against the map data. The route is decided, and the robot drives. The object recognition system is composed an object-recognition processing part and a location-information acquisition, processing part, both of which use the monocular

camera and the LRS. An object is recognized and identified using range information obtained from LRS in addition to the processed image data provided by the camera. The robot performs a grasping operation for the object according to this system.

This study is related to object recognition during an object manipulation process of the robot. Currently, the portion of the object manipulation, processing part is a problem of holding and judgment bottles were placed on the desk against the instructions of the user on whether or not the operation target object. In this study, we pay attention to work on object recognition of environment recognition processing parts, especially the object area determination processing of plastic bottles in the image obtained from the camera.

## 2. System of Robot

Our robot as shown in Fig.1 has a drive mechanism consisting of two front and two back wheels. The front wheels are attached to a motor that operates the wheels on either side independently, while the back wheels function as castor wheels. This method has the advantage of allowing a small turning radius. In addition, to acquire image information, both a single CCD camera with approximately 2,000,000 pixels and an LRS are installed on the head of the robot and can be rotated to all sides by two motors. DC servo motors are used in the robot's drive mechanism. The position and speed control are achieved by the control system of the drive mechanism. The robot also has two arms and hands equipped with sensors, which enable it to respond to the various demands of humans. Finally, an installed wireless LAN can provide remote control for humans. All devices are controlled by a Personal Computer (PC), and the lead batteries are used to supply the robot's electric power.

## 3. Object Recognition System

### 3.1. Outline of the autonomous system

We have developed an object recognition system for a robot that can acquire the target object position with image information captured by monocular CCD camera and range information obtained by LRS. This system

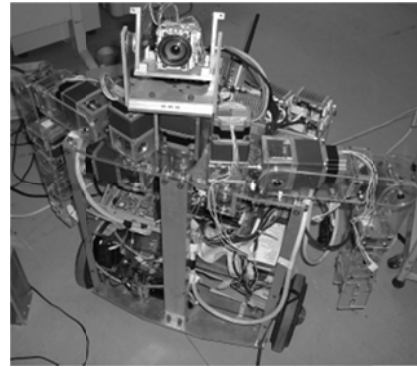


Fig.1. System Structure of Robot.

can acquire the object position on the assumption, for example, that the object is placed on a desk. First, the robot has recognized the single object in the form, the color and the local character of the object. Next, the system then acquires the location information of the object by using LRS with the recognized object. Afterwards, the arm is driven based on the location information, and the object can be grasped and held. The flow chart for the object recognition and holding object system is shown in Fig. 2.

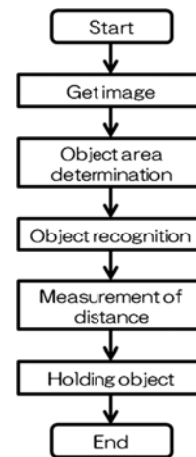


Fig.2. Flow chart of recognition and holding object.

### 3.2. The method for object recognition

In this section, we explain the method for object recognition and the process of the object recognition system is shown in Fig. 3.

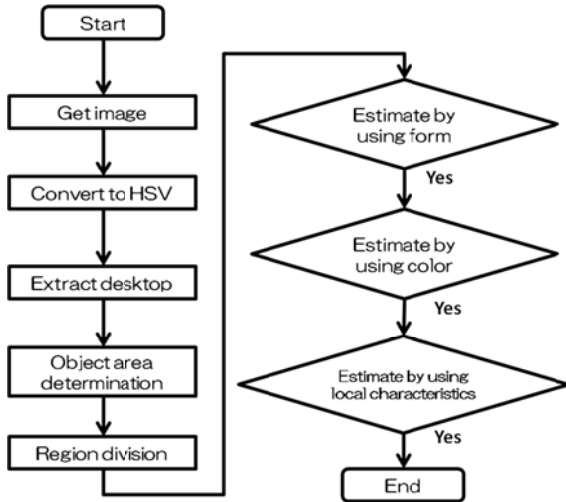


Fig.3. Process of object recognition system.

In this study, we pay attention to working on the object area determination processing of the plastic bottles in the image obtained from the camera. The robot requires to accurately recognize the object area when the object recognition. This processing is important in object recognition, because the robot cannot compare the form, the color and the local object characteristics in the image with the target object if the robot cannot recognize the object area exactly. The conventional object area determination processing is able to accurately recognize the object area when there is only one object or there are some objects which are not overlapping objects in the image. However, the object area determination processing has a problem that the robot cannot take out a plastic bottle area in the image if plural bottles overlap each other on the desk. In order to solve this problem, we attempt to add new processing that to detect the border between overlapping objects. So, we focused on the function of the camera, particularly the use of the zoom function. More specifically, we constructed a system that detects the boundary by displaying a border part between objects by using the camera zoom.

### 3.3. The method for object area determination

The flow for the processing to detect the border for determination the object area is shown in Fig. 4.

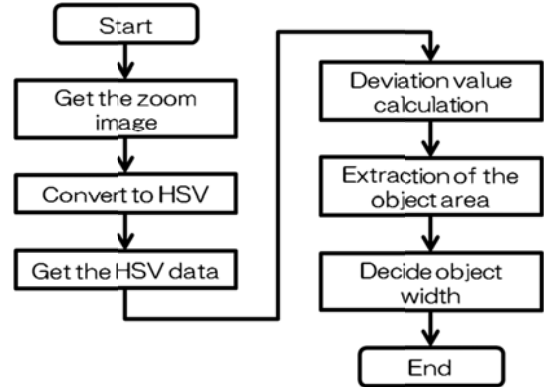


Fig.4. Process of detection the border flow.

#### 3.3.1. Convert to HSV processing part

This processing part converts images a color from RGB model to HSV model. The HSV color model means Hue, Saturation and Value. This model is often used by people who are selecting colors from a color wheel or palette, because it corresponds better to how people experience color than the RGB color space does.<sup>[1]</sup> The equations for conversion are shown in Eq. (1) ~ (4).

$$\begin{aligned} \max &= \max(R, G, B), \\ \min &= \min(R, G, B). \end{aligned} \quad (1)$$

Hue calculation

$$\begin{aligned} H &= 0 \quad (\max = \min), \\ H &= \left( \frac{G - B}{\max - \min} \right) \times 60 \quad (\max = R), \\ H &= \left( 2 + \frac{B - R}{\max - \min} \right) \times 60 \quad (\max = G), \\ H &= \left( 4 + \frac{R - G}{\max - \min} \right) \times 60 \quad (\max = B). \end{aligned} \quad (2)$$

Saturation calculation

$$\begin{aligned} S &= 0 \quad (\max = \min), \\ S &= \left( \frac{\max - \min}{\max} \right) \quad (\max \neq \min). \end{aligned} \quad (3)$$

Value calculation

$$V = \max. \quad (4)$$

### 3.3.2. Get the HSV data and deviation value calculation processing part

This processing part gets the HSV data and deviation value calculation. After the HSV conversion, set a rectangular area in the image. In addition, HSV data in the rectangular area are obtained and calculated each deviation value.

### 3.3.3. Extraction of the object area processing part

This processing part extracts the object area in the zoom image. First, this part compares the HSV data of the rectangular adjacency relationship for pixels with the deviation value. So, the rectangular adjacency pixels are considered to be an object same as the object in the rectangle, if the HSV data of the rectangular adjacency pixels are the value in the deviation value. The object area is extracted by repeatedly executing such processing.

### 3.3.4. Decide object width processing part

This processing part detects a border part between objects by detection the right and left ends of the object area. So, the object width is decided by the detection border.

## 4. Experiment of system evaluation

### 4.1. The method of experiment

We performed the following experiment to evaluate the performance of object area determination. Fig. 5 shows the experimental environment when the object is a plastic bottle. Its location was set three objects on a single-color desk in the laboratory. The detected object area is displayed on the image color classification. Getting result compares with the precedence research.

### 4.2. Result of experiment

The Fig. 6 shows the experimental result. This research can accurately recognize the single object area overlapping plural objects by detecting the border between objects.

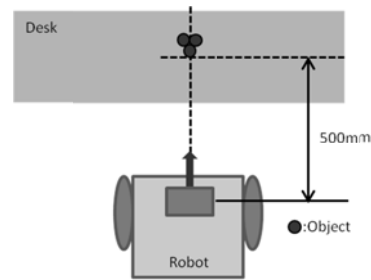


Fig. 5. The experimental environment.

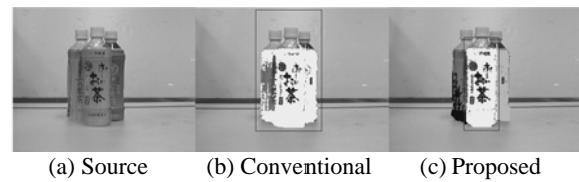


Fig. 6. Experiment results.

## 5. Conclusion

In this paper, we propose object recognition system that accurately recognizes the object area by detection the border between overlapping objects. This object recognition is detection the boundary by displaying a border part between objects by using the camera zoom. As a result, precision of object recognition improved. However, this system cannot recognize same objects. In the future we will try the solution to this problem.

## References

1. Convert from HSV to RGB Color Space, "<http://jp.mathworks.com/help/images/convert-from-hsv-to-rgb-color-space.html>" (accessed Nov 11th).
2. Y. Kibe and E. Hayashi, *Development of an autonomous-drive personal robot "An environment recognition system using image processing and an LSI"* (Journal of Artificial Life and Robotics, Springer 2011).
3. K. Ito and E. Hayashi, *Development of an autonomous-drive personal robot "An object recognition system using Self-Organizing Map"* (Journal of Artificial Life and Robotics, Springer 2014).

# Construction of a micro sense of force feedback and vision for micro-objects: development of a haptic device

**Yusei. Ishii**

*Graduate School of Computer Science  
and System Engineering  
Kyushu Institute of Technology  
680-4, Iizuka City, Fukuoka, Japan, 820-8502  
ishii@mmcs.mse.kyutech.ac.jp*

**Eiji. Hayashi**

*Department of Mechanical Information  
Science and Technology  
Kyushu Institute of Technology  
680-4, Iizuka City, Fukuoka, Japan, 820-8502  
haya@mmcs.mse.kyutech.ac.jp*

## Abstract

The purpose of this research was to develop a combined sense system that uses both force feedback and visual feedback to determine the shape of the microscopic features of a sample. We constructed a haptic device that gives a sense of that force to the operator when touching the sample. The experiment was tested for recreating touching force of salmon roe as the samples in a minute of the period time.

*Keywords:* force feedback, haptic interface, simulation.

## 1. Introduction

Technologies that can accurately perform minute work are now being sought for medical treatment and in the field of manufacturing semiconductors. Such minute work is improved by using micromanipulators, but their operation is difficult because the operator has no sense of force; he or she relies only on sight through a microscope. As a result, a person skilled in the use of this technology is needed for all minute work. The efficiency of minute work would be improved if the operator were able to have a sense of force while using a manipulator.

Here we describe the development of a more efficient system for minute operations. Our aim was to develop a system using not only the sense of sight through a microscope but also a sense of force from the manipulator. For this fundamental research, a system

was created to assess the reaction force when a minute sample was touched. A cantilever was used to touch the sample, and the reaction force was obtained from the degree to which the sample bent. In addition, we used a haptic device and amplified the force feedback from a minute sample of a virtual object.

## 2. System Structure

### 2-1. System summary

The system structure is shown in Fig. 1a, and a schematic view is shown in Fig. 1b. This system consists of a microscope with an automatic x-y stage, a piezo stage, a feedback stage controller to control the x-y stage, a piezo stage controller, a haptic device for transmitting force feedback (Fig. 2), a cantilever (Fig. 3), and a PC via which the user can control and operate these components. The sample was fixed on the x-y stage by an injector (Fig. 4) and a holding pipette (Fig. 5). When the cantilever, which was fixed to the piezo

© The 2015 International Conference on Artificial Life and Robotics (ICAROB 2015), Jan. 10-12, Oita, Japan

stage, touched the sample, the operator could maintain the cantilever's position by obtaining the value of the reaction force through the interface. The resolution of the piezo stage is 1 nm.

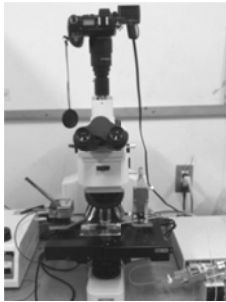


Fig. 1a. Photograph of the system structure.

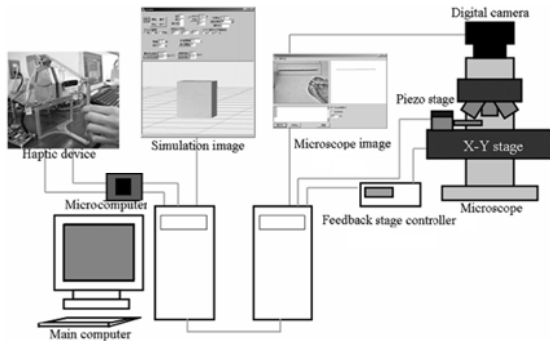


Fig. 1b. A schematic view of the system structure



Fig. 2. Haptic device.

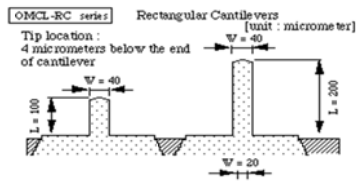


Fig. 3. Cantilever.



2-2. Haptic device

Figure 6 provides a diagram of the haptic device. It consists primarily of a rotor, a laser, PSD. We installed a coil on the rotor with a polarity magnet, which generated electromagnetic induction by an electric current and a magnetic force. The angle of the rotor can

be measured by the laser and the PSD. The rotor was able to follow any input waveform.

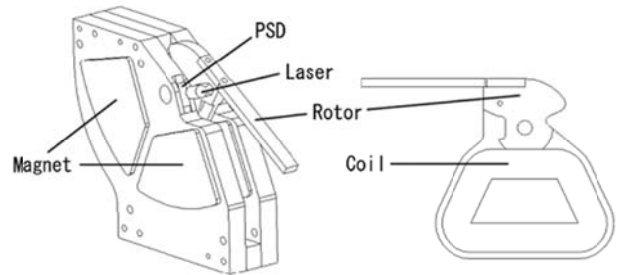


Fig. 6. Diagram of the haptic device.

The actuator is controlled by a servomechanism on the actuator. The system driving the actuator therefore consisted of four actuators: a microcomputer, an inputting AD/DA port, an outputting microcomputer, and a PC outputting order value. The system controls the actuator during each part of the process. Figure 7 shows the structure of the haptic device.

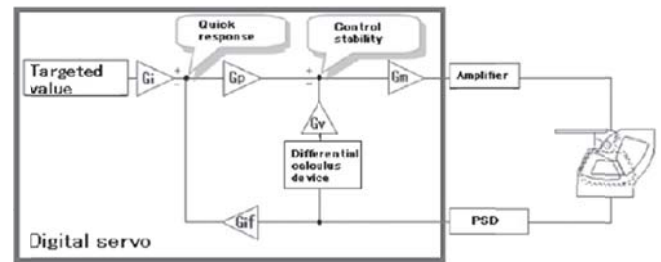


Fig. 7. Structure of the haptic device.

The actuator, whose actions are governed by the PD control, is operated through a digital differential calculus device. A transfer function for the quadratic function system shown in Fig. 8 is provided for the actuator servo system. The role of each parameter of the control system is to adjust the total offset to a master in  $G_i/G_f$ , to regulate the item viscosity/resonance point in  $G_p/G_v$ , and to regulate the total gain in  $G_m$ .

Table 1 provides a list of the control parameters of the servomechanism system.



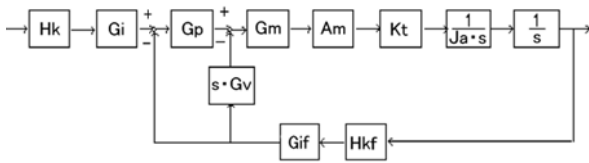


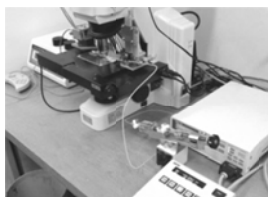
Fig. 8. Block diagram of the servomechanism system.

Table 1 Control parameters of the servomechanism system

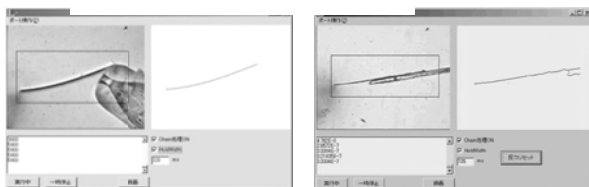
Parameter	Reference	Unit
Hk	Position Voltage Constant	18.56 [V/rad]
Hkf	Position Voltage Feedback Constant	18.56 [V/rad]
Am	Amplifier Constant	0.8986 [A/V]
Kt	Torque Constant	0.6141 [Nm/A]
Ja	Moment of Inertia	0.000581 [kg·m]
Gi	Controller Input Gain	1
Gif	Position Feedback Gain	1
Gp	Position Gain	adjusted value
Gv	Velocity Gain	adjusted value
Gm	Manipulation Gain	1

### 3. Measuring the reaction force

The reaction force was used to calculate the force applied by the minute object. In this experiment, we touched the minute object with the cantilever shown in Fig. 3, and the reaction force was obtained based on the degree of bend of the cantilever. The layout of the experiment is shown in Figs. 7 and 8, and the environment of the experiment is shown in Figs. 9. Based on this experiment, we were able to determine the reaction force applied by the minute object.



Experiment.



Simulating

Left of the figure 10 shows the cantilever touching the tip of the holding pipette. Right of the figure 10 shows the experiment that measures the reaction force of the downy hair. The image-processing speed of the cantilever was improved by the tracking process. The bend of the cantilever is assumed to be linear-elastic so that Hooke's law may be applied. The restoring force,  $F$ , of the bend of the cantilever is given by

$$F = kx \tag{1}$$

where  $x$  is the compression distance from the equilibrium position, and  $k$  is the spring constant.

### 4. Deforming the sample in simulation

In this study, we attempted to build a working system using a microscope, a haptic device, and a simulation. A fundamental element was simulating the deformation of a minute object. Figure 11 shows the graphical user interface (GUI) of the simulator. A graphic tool was created using OpenGL to draw the object and to choose the shape of the sample, for instance, a cube or sphere. The dynamic model of the sample consisted of a spring-mass array of mass points in both the vertical and horizontal directions. An example of the arrangement of mass points is shown in Fig. 12. When a force was applied at a mass point, the simulation calculated the speed of all mass points that had been affected. The image was renewed after every ten calculations.

We defined a spring as having a size but no weight, and a mass point as having a size, a weight, and a rigid body. An arbitrary mass object can be placed on a spring on a bitmap (Fig. 13). In addition, a sample can be seen from various viewpoints, and the deformation of the sample, which is impossible to observe by microscope, can be checked. The shape of this object can be either a cube or a sphere, and any point may be selected as a fixed point or an operating point.

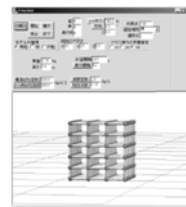


Fig. 11. Simulator.

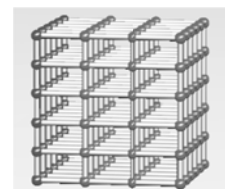


Fig. 12. Arrangement of mass points

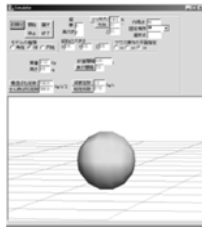


Fig. 13. Placing an arbitrary object on a bitmap.

**5. Characteristic measurements and a reappearance experiment for an object**

Dynamic characteristics of the object were measured and then recreated using the haptic device. The object used this time was salmon roe. We measured response of salmon roe and showed the displacement of its surface a figure. Figure14 shows the response of the salmon roe.

Salmon roe is 6 millimeters in diameter and we cannot precisely feel the sense of touch. Hence values in the figure are multiplied by 68 so that human can feel the sense of salmon roe’s touch. Figure15 shows that response of the salmon roe and haptic device. Table 2 shows the frequency, constant of spring, and damping coefficient in each ectopic focus.

In this experiment, there was a tendency for a touch feeling close to that of real and big salmon roe to be created when characteristic was recreated.

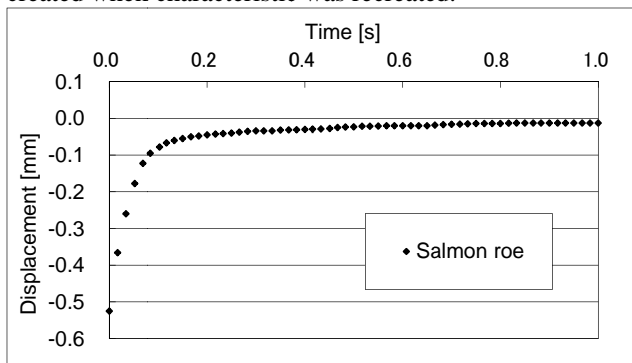


Fig.14. Time response of Salmon roe

Table2. Haptic device parameter of dynamic characteristic

Displacement [mm]	Frequency [Hz]	Spring constant [N/mm]	Damping ratio
0~6	6	0.072	2.6
6~35	6	0.072	1.0

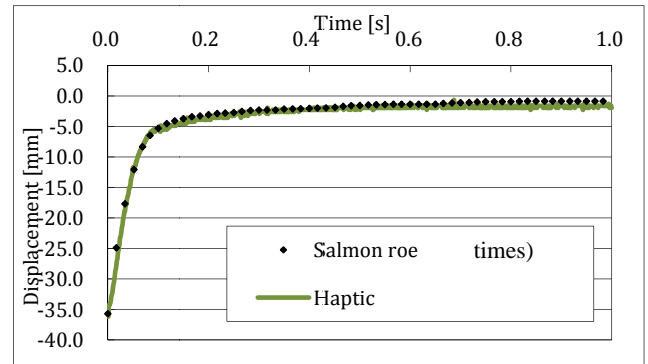


Fig.15. Time response of Salmon roe and Haptic device

**6. Conclusion**

In the present study the characteristics of salmon roe were measured and recreated, the evaluations were also carried out with regard to response and sense of force using a haptic device. The characteristics of various objects will be measured in the future, and the characteristics should recreate.

Future research should focus on building a system that allows a reaction force to be detected and shown more precisely. Such a system would make it possible to test smaller samples.

**7. Acknowledgement**

This research was partially supported by the Ministry of Education, Science, Sports and Culture, Grant-in-Aid for Scientific Research, 2012.

**References**

1. Miyamoto K (2007) Construction of super-micro sense of force feedback and vision for micro objects. Kyushu Institute of Technology.
2. Li X, Zhang Z (2008) Probe-type microforce sensor for micro/nano experimental mechanics. Trans Tech Publications, Stafa-Zurich, Switzerland
3. T.DOMOTO (2012) Construction of a sense of force feedback and vision for micro-objects: Recreate the response and a sense of force of objects. Kyushu Institute of Technology.
4. J. IMAHASE (2012) Construction of a sense of force feedback and vision for micro-objects: Developing AD converter. Kyushu Institute of Technology

# **Error Recovery of Pick-and-Place Tasks in Consideration of Reusability of Planning**

**Akira Nakamura, Kazuyuki Nagata, Kensuke Harada and Natsuki Yamanobe**  
*Intelligent Systems Research Institute*  
*National Institute of Advanced Industrial Science and Technology (AIST)*  
*Central 2, 1-1-1 Umezono, Tsukuba, Ibaraki, 305-8568 Japan*  
*E-mail: a-nakamura@aist.go.jp, k-nagata@aist.go.jp,*  
*kensuke.harada@aist.go.jp, n-yamanobe@aist.go.jp*  
*www.aist.go.jp*

## **Abstract**

Error recovery in robotic tasks is explored to enable robots to be used for complicated tasks. The authors' error recovery processes make use of the concepts of both task stratification and error classification. In this paper, the reusability of planning in error recovery is verified by using the typical pick-and-place tasks that are used in plant maintenance and industrial production.

*Keywords:* manipulation skill, error recovery, task stratification, error classification

## **1. Introduction**

In recent years, studies on robotic manipulation for performing tasks in various fields have been conducted. We have conducted many research studies on the robotic manipulation used to perform plant maintenance tasks and manufacture industrial products (Fig. 1). These manipulation tasks tend to be complex, necessitating that composition rules be devised for the entire work process.

By analyzing the assembly and disassembly sequences performed by humans, we found that those tasks tend to be composed of several significant motion primitives. We call each motion primitive a "skill" and have shown that most maintenance and production tasks can be composed of a number of skills.<sup>1-3</sup>

Ideally, a robotic task has to be successfully completed as planned. However, in the actual tasks of

complicated plant maintenance and industrial production, it is not rare for the execution of a task to terminate before completion. Therefore, error recovery is an important research theme for robots that need to perform such real-world tasks.<sup>4,5</sup>

We have explored error recovery in robotic tasks to enable robots to be used for complicated tasks.<sup>6-9</sup> Our error recovery processes make use of the concepts of both task stratification and error classification, and these techniques are based on the concept of skills.

Considering the use of various recovery paths, the reusability of task planning may become an important aspect of research on error recovery. In this paper, the reusability of planning in error recovery is verified by using the typical pick-and-place tasks that are used in plant maintenance and industrial production.

## **2. Stratification of Tasks**

© The 2015 International Conference on Artificial Life and Robotics (ICAROB 2015), Jan. 10-12, Oita, Japan

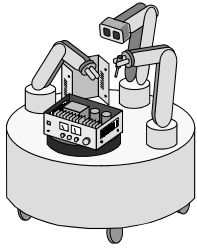


Fig. 1 Maintenance robot

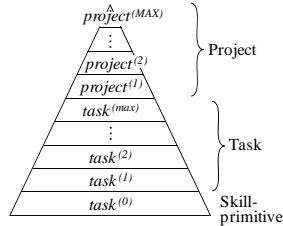


Fig. 2 Manipulation hierarchy

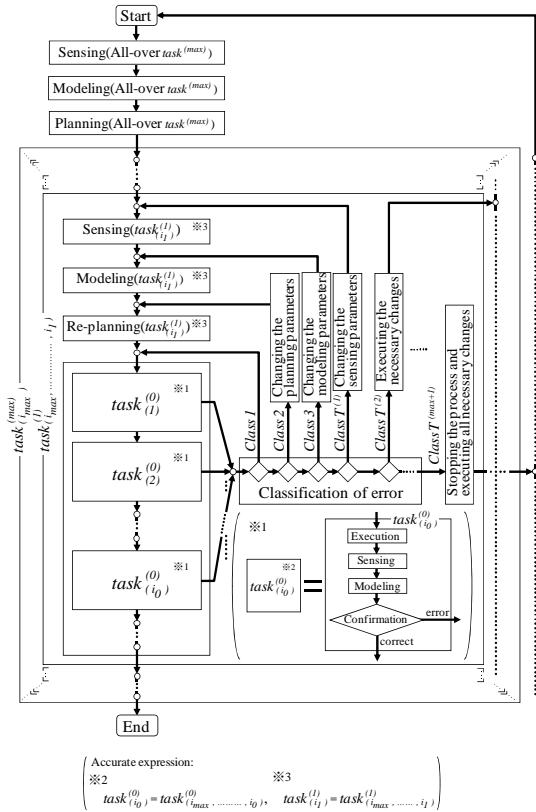


Fig. 3 Process flow with error recovery

This section explains our concept of skills and the stratification of tasks. See Refs. 1, 2 for more details.

### 2.1. Concept of skills

We analyzed human motions in such tasks as disassembly and reassembly and found that the movements consisted of several significant motion primitives. We call such motion primitives “skills<sup>1, 2</sup>”. We considered three fundamental skills: move-to-touch, rotate-to-level and rotate-to-insert, all of which play an

important part in those tasks. A specific task is composed of sequences of skill primitives such as these three skills. Moreover, many skills can be defined based on modified versions of these three fundamental skills<sup>3</sup>.

### 2.2. Stratification of tasks

Figure 2 shows a hierarchy of manipulation tasks<sup>6</sup>. If we ignore the servo layer, the *skill* layer, which consists of elements such as the move-to-touch and rotate-to-level skills, is located in the lowest layer called the  $task^{(0)}$  layer. One tier above the  $task^{(0)}$  layer is the  $task^{(1)}$  layer. Similarly,  $task^{(i+1)}$  is composed of sequences of  $task^{(i)}$  elements. The top layer, where the error recovery loop is closed, is called  $task^{(max)}$  and one tier above  $task^{(max)}$  is called the *project* layer. The *project* layer might also be hierarchized, but we will not discuss this here.

### 3. Error Recovery in Stratified Tasks

In an ideal environment, tasks are achieved without any errors occurring. In actual manipulation, however, errors often do occur from various causes. Our concept of error classification and process flow with error recovery in the task hierarchy are described in this section. See Ref. 6 for more details.

#### 3.1. Classification of errors

The causes of manipulation failures can be attributable to several kinds of errors. We group the error states into several classes of errors: execution, planning, modeling and sensing, according to the possible causes<sup>6</sup>.

Merely remedying the causes of these errors does not always solve the problem. It may be necessary to return to a previous step when the working environment is greatly changed by the error.

#### 3.2. Error recovery based on classification

A generalized process flow of stratified tasks that takes error recovery into account has been shown in Ref. 6. Figure 3 is an illustration of the central portion of Fig. 10 in Ref. 6. This process is performed based on recovery through a *backward correction process*. At the Confirmation step in each skill primitive  $task^{(0)}_{(i0)}$ , the result is judged to be correct or a failure by an automatic process or by a human operator. Error recovery is performed using the following error classification.

Class 1: When the error is judged to be an execution error,  $task^{(1)}_{(i1)}$  is executed again without correcting the parameter .

Class 2: When the error is judged to be a planning error,  $task^{(1)}_{(i1)}$  is executed again with a change in the planning parameters .

Class 3: When the error is judged to be a modeling error,  $task^{(1)}_{(i1)}$  is executed again with a change in the modeling parameters.

Class  $T^{(1)}$ : When the error is judged to be a sensing error,  $task^{(1)}_{(i1)}$  is executed again with a change in the sensing parameters.

Class  $T^{(2)}$ :  $task^{(2)}_{(i2)}$  is executed again after the execution of the necessary changes and returns to the start of one tier above the  $task^{(1)}_{(i1)}$  layer.

⋮

Class  $T^{(max)}$ :  $task^{(max)}_{(imax)}$  is executed again after the execution of the necessary changes and returns to the start of the  $(max - 1)$  tier above the  $task^{(1)}_{(i1)}$  layer.

Class  $T^{(max+1)}$ : When it is judged that too many changes will be required, the process being executed is interrupted and the process returns to the start of the all-over task.

## 4. Expanded Processes in Error Recovery

### 4.1. Forward correction process

To correct the robot's motions at each step, a manual operation module for robot control can be inserted in the terminal processing of each primitive motion. For example, slight errors concerning the position and orientation of the object after transition and the condition of the grasped object can be corrected<sup>8</sup>. This process is recovery through a *forward correction process* which differs from recovery through the *backward correction process* described in 3.2.

### 4.2. Additional tasks

Additional tasks may be necessary in some cases to perform the corrections of Class 2, 3 and 4 errors (Fig. 4).<sup>7</sup> For example, additional geometry modeling of the working environment may be necessary for a Class 2 error, and additional geometry modeling of the object

and the tool may be necessary for a Class 3 error. And additional geometry modeling of the working environment and calibration of the vision system may be necessary for a Class 4 error.

## 5. Planning with a View Toward Reusability

### 5.1. About reusability

Generally, a manipulation robot operates according to a computer program that is based on an ordered plan of operation. The tasks performed by a manipulation robot are varied and may involve such grasping tasks as gripper closing and opening, and transfer-related tasks such as lifting and approaching.

Similar tasks can be performed using a similar computer program. As such, in systems with error recovery functions, similar tasks can be performed in the recovery portions. Therefore, it is possible to use a similar program for similar kinds of tasks for the total system, not only for the main operation part but for the additional recovery parts as well. A system with high reusability—one in which many of the same programs in the whole system could be reused including the recovery parts—would provide a very efficient approach to system configuration.

### 5.2. How to improve reusability

Let us explain a method for improving reusability by using the tasks involved in repacking objects from a large box into a small box in a physical distribution scenario as shown in Fig. 5. See Ref. 9 for more details on this task.

Failures may occur due to various causes when performing the given tasks, and in various situations such as grasping, lifting, carrying and packing.

The failure in which a plastic (PET) beverage bottle is dropped during transfer is considered here. In most cases, the dropped object ends up in some sort of disordered position, for instance falling over to a horizontal posture from its original vertical orientation. While an object with the shape of a PET bottle topples in most cases, sometimes it remains standing upright.

Error recovery involves grasping the object and moving it to an objective destination. A movement about the postures in the task means keeping the object

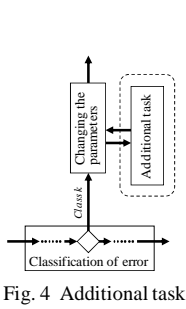


Fig. 4 Additional task

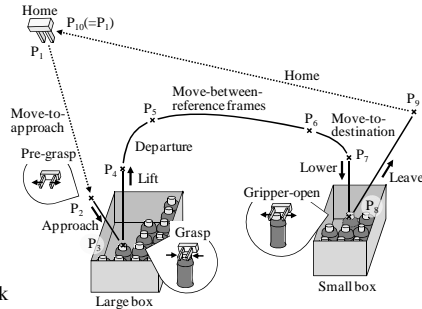


Fig. 5 Picking and placing task using a gripper

vertical when it is already vertical and standing upright, and righting it back to the vertical from a toppled horizontal position. In the original scenario, most pick-and-place tasks will not require restoring to vertical posture from an existing vertical orientation. In other words, the task is performed by a pick-and-place program that expresses a change in three degrees of freedom from the position without changing the orientation. The process of the error recovery when the failure occurred proceeds by planning the flow including a change in the orientation of grasping, carrying with that change of posture, and packing. That is, the task is performed by a pick-and-place program that expresses a change in six degrees of freedom of the position and orientation.

It is undesirable to have many programs involved even in a transfer task. This program represents one of pick-and-place that expresses a change in six degrees of freedom of the position and orientation. The change from the original scenario can be considered as change in three degrees of freedom of the position without a change in orientation.

Furthermore, it is desirable for the program to be one that is usable in a wide area as well as in a local domain. That is why calibration needs to be performed in a wide area. Global calibration means that not only the pick-and-place task of the original scenario but also the processes of error recovery can be performed by the same program. Reusability increases when as many common programs as possible can be used for the total manipulation tasks.

## 6. Conclusions

In this paper, we have discussed the reusability of planning in manipulation tasks including error recovery processes. The techniques and validity of the reusability of such programs have been presented and verified using pick-and-place tasks. Programming of the total task including error recovery will be simplified by using the same planning in the path of the original task and in multiple recovery paths.

In the future, we will conduct further research on optimum adjustment methods for the various parameters used in the error recovery paths and for selecting common programs. We will attempt to apply our techniques to actual maintenance robots.

## References

1. T. Hasegawa, T. Suehiro and K. Takase, A model-based manipulation system with skill-based execution, *IEEE Trans. Robot. Autom.*, **8**(5) (1992) 535-544.
2. A. Nakamura, T. Ogasawara, T. Suehiro and H. Tsukune, Skill-based backprojection for fine motion planning, in *Proc. IEEE/RSJ Int. Conf. on Intell. Robots Syst.*, (Osaka, Japan, 1996), **2**, 526-533.
3. A. Nakamura, T. Ogasawara, K. Kitagaki and T. Suehiro, Using robust and simplified geometric models in skill-based manipulation, in *Proc. IEEE/RSJ Int. Conf. on Intell. Robots Syst.*, (Hawaii, USA, 2001), **1**, 138-145.
4. B. R. Donald, Planning multi-step error detection and recovery strategies, *Int. J. Robot. Res.*, **9**(1) (1990) 3-60.
5. P. Pastor, M. Kalakrishnan, S. Chitta, E. Theodorou and S. Schaal, Skill learning and task outcome prediction for manipulation, in *Proc. IEEE Int. Conf. Robot. Autom.*, (Shanghai, China, 2011), 3828-3834.
6. A. Nakamura and T. Kotoku, Systematization of error recovery in skill-based manipulation, *Artificial Life and Robotics*, Springer, **14**(2) (2009) 203-208.
7. A. Nakamura and Y. Kawai, Recovery technique from classified errors in skill-based manipulation, in *Proc. 15th Int. Symp. on Artificial Life and Robotics (AROB 15th '10)*, (Oita, Japan, 2010), 1010-1013.
8. A. Nakamura, K. Nagata, K. Harada, N. Yamanobe, T. Tsuji, T. Foissotte and Y. Kawai, Error recovery using task stratification and error classification for manipulation robots in various fields, in *Proc IEEE/RSJ Int. Conf. on Intell. Robots Syst.*, (Tokyo, Japan, 2013), 3535-3542.
9. A. Nakamura, K. Nagata, K. Harada and N. Yamanobe, Error recovery using task stratification and error classification for manipulation robots in physical distribution, *Trans. Control and Mechanical Syst.*, **3** (2014) 122-131.

# Design of Sliding Mode Controller for Droplet Position in EWOD Microfluidic System

**Arsit Boonyaprapasorn**

*Dept. of Mechanical Engineering, Chulachomklao Royal Military Academy,  
Nakhon-Nayok, Thailand*

**Thunyaseth Sethaput**

*Dept. of Mechanical Engineering, Sirindhorn International Institute of Technology, Thammasat University,  
Pathum Thani, Thailand*

*E-mail: [urarl.urarl9@gmail.com](mailto:urarl.urarl9@gmail.com), [thunyaseth@siit.tu.ac.th](mailto:thunyaseth@siit.tu.ac.th)  
[www.siiit.tu.ac.th](http://www.siiit.tu.ac.th)*

## Abstract

In microfluidic lab-on-chip devices, electrowetting on dielectric (EWOD) are widely used for various applications. To manipulate the micro droplet to achieve the desired path and accurate target position by using electrowetting technique are one of the common applications. In this paper, the motion of droplet is modeled as a single rigid body driven by both linear and nonlinear forces. In order to evaluate the potential of controller, the sliding mode controller is applied to this nonlinear microfluidic system. The effect of bounded disturbances is included in the designed controller. Simulation results provided the feasibility of the sliding mode controller for EWOD microfluidic manipulation under the effect of bounded disturbances.

*Keywords:* Sliding mode control, Electro-wetting on Dielectric device, Lab-on-chip, Microfluidics.

## 1. Introduction

Electro-wetting on Dielectric (EWOD) is a microfluidic transport method utilizing the disturbance behavior of electrical field on the free surface energy and wet contact angle of a droplet. As shown in Fig. 1, the contact angle and droplet shape can be changed by applying voltages on one-side of a droplet, thus inducing the droplet to move. The technique is well-known for its precise manipulation of droplet movement. Currently, many lab-on-chip devices, equipped with EWOD micro-droplet transport are widely used for various applications such as in DNA sequencing [1], protein analysis and detection [2], Disease diagnosis [3, 6] molecular biology processes [4], detection of triglyceride in human fluid [5] and concentration detection of L-amino acid [7]. With its immense capability to precisely transport tiny droplets with little power consumption, EWOD technique has also been used in micro pumps [8] and micro-conveyors [9]. Pamula *et al.*

[10] created a micro-cooling system for IC circuit cooling, in which EWOD required less pumping power than typical mechanical pumps. In dealing with complicated analysis, diagnosis and detection processes, more complex array-typed EWOD devices have been created to support sophisticated lab-on-chip platforms. Multiple droplet manipulation becomes essential and enquires more precise control algorithms. Bhattacharjee and Najjara [11] mentioned about the need of feedback control of a single droplet position in a digital micro fluidic system (DMS) and presented simulation results of the feedback control system. Also, the work by Oprins *et al.* [12] proposed the modeling and control of droplet motion of the electro-wetting system. Based on the proposed models presented in [11] and [12], various nonlinear control techniques can be applied to control droplet position on top of a EWOD lab-on-chip platform.

© The 2015 International Conference on Artificial Life and Robotics (ICAROB 2015), Jan. 10-12, Oita, Japan



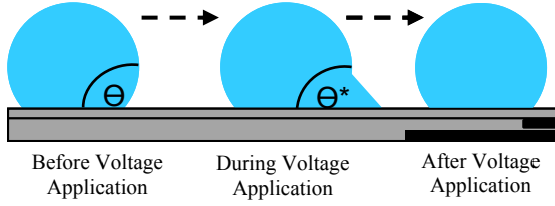


Fig. 1. Droplet movement by altering contact angle with applied voltage

This paper focuses on the design of sliding mode tracking controller to control the droplet position in the EWOD microfluidic system under the disturbance. The control system is simulated to evaluate the ability of this control technique.

## 2. EWOD Microfluidic System

### 2.1. Equation of Motion

In this study, the dynamic response of droplet is formulated as a simplified one-dimensional model based on the proposed by [11] and [12]. As shown in Fig. 2, the droplet is modeled as a single rigid body moving with velocity  $U$ . The motion of droplet is driven by the driving force ( $F_{dr}$ ) actuated by electrostatic force and its threshold ( $F_{thresh}$ ). The details of the threshold of electrostatic force can be determined from [13-15]. There are 3 sources of frictional force exerting against the motion of droplet including viscous dissipation due to internal fluid friction ( $F_d$ ), viscous drag due to moving through surrounding fluid ( $F_f$ ) and frictional force due to the contact line ( $F_c$ ). According to [11], the equation of droplet motion in EWOD configuration can be represented by

$$m \frac{d^2 x}{dt^2} = F_{dr} - F_{thresh} - F_d - F_f - F_c \quad (1)$$

where  $m$  and  $x$  are the mass and the displacement of the micro droplet, respectively. Assuming 5% overlap of adjacent electrodes [11], the droplet radius,  $a$  can be defined as  $a = L/2 + 0.05L$  where  $L$  is the electrode width and  $l$  is the gap between adjacent electrodes. As mentioned in [12], viscous drag due to moving through surrounding fluid ( $F_f$ ) can be neglected because air is the surrounding fluid. Thus, the motion of droplet in EWOD microfluidic system can be mathematically expressed as

$$m \frac{d^2 x}{dt^2} = F_{dr} - F_{thresh} - F_d - F_c \quad (2)$$

As presented in [14], the viscous dissipation due to internal fluid friction ( $F_d$ ) for the open EWOD configuration can be described as

$$F_d = \left( \frac{5\mu_d U}{2H} \right) (\pi a^2) \quad (3)$$

where  $\mu_d$  and  $H$  denote the droplet viscosity and height respectively.

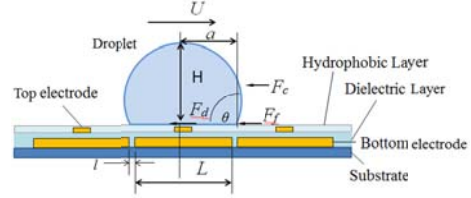


Fig. 2. The micro droplet motion on the EWOD plate

As presented in [11] and [12], frictional force due to the contact line ( $F_c$ ) can be expressed as

$$F_c = \zeta U^n (2\pi a) \quad (4)$$

where  $\zeta$  is the coefficient of contact-line friction based on kinetic-molecular theory.  $n$  is in the range from 0 to 2.

### 2.2. State Space Representation

The equation of motion in (2) can be presented in the form of first order nonlinear differential equation or the state equation and the output equation

$$\begin{aligned} \dot{x}_1 &= x_2 \\ \dot{x}_2 &= f(\bar{x}, t) + g(\bar{x}, t)u(t) + d(t) \\ y &= x_1 \end{aligned} \quad (5)$$

where  $g(\bar{x}, t) = \frac{1}{m}$

$$f(\bar{x}, t) = \frac{1}{m} \left[ - \left( \frac{5\mu_d x_2}{2H} \right) (\pi a^2) - \zeta x_2^n (2\pi a) \right]$$

The state variables  $x_1$  and  $x_2$  represent displacement,  $x$  and velocity of the micro droplet,  $\bar{x}$ . Also,  $\bar{x} = [x_1 \ x_2]^T$  is denoted as state vector. The control input,  $u(t)$  is  $F_{elect}$ . A  $d(\bar{x}, t)$  is bounded disturbance and  $|d(\bar{x}, t)| \leq M$  where  $M$  is a positive constant. The output variable is denoted by  $y$ .  $f(\bar{x}, t)$  is a nonlinear smooth function.

## 3. Controller Design

The sliding mode tracking controller was designed to track two types of desired signals: 1) step signal 2) sinusoidal signal. The step signal represents the case when micro droplet moves from the current electrode to the adjacent electrode. The sinusoidal signal was used to test the ability



of the controller to track the periodic motion of the droplet between two electrode plates.

According to (5), the sliding mode controller design with the selected reaching law as in [16] which can be shown as follows. First, the switching surface is defined as

$$s = e + ce \quad (6)$$

where  $c > 0$ .  $e$  and  $\dot{e}$  are denoted as tracking error and its derivative. Second, the Lyapunov function is defined as

$$V = \frac{1}{2}s^2 \quad (7)$$

From (6) and (7), the derivative of switching surface  $\dot{s}$

$$\dot{s} = \dot{e} + c\dot{e} = (\ddot{x}_r - \ddot{x}) + c(\dot{x}_r - \dot{x}) = (\ddot{x}_r - \ddot{x}_2) + c(\dot{x}_r - \dot{x}_1) \quad (8)$$

where  $x_r$  is the reference signal or desired displacement of the droplet. The exponential rate reaching law [16] or constant plus proportional rate reaching law [17] is selected

$$\dot{s} = -ks - \varepsilon \operatorname{sgn}(s) \quad (9)$$

where  $\varepsilon > 0$  and  $k > 0$ . Equating (8) and (9), the control input is determined as shown in (11).

$$-ks - \varepsilon \operatorname{sgn}(s) = [\ddot{x}_r - (f(\bar{x}, t) + g(\bar{x}, t)u(t) + d(t))] + c(\dot{x}_r - \dot{x}_2) \quad (10)$$

$$u(t) = \frac{1}{g(\bar{x}, t)} [ks + \varepsilon \operatorname{sgn}(s) + (\ddot{x}_r - f(\bar{x}, t) - d(t) - c(\dot{x}_r - \dot{x}_2))] \quad (11)$$

Based on the control input in (11), the stability of the control system can be verified as follows

$$\dot{V} = s\dot{s} \quad (12)$$

$$\dot{V} = s\{\ddot{x}_r - (f(\bar{x}, t) + g(\bar{x}, t)\frac{1}{g(\bar{x}, t)}[ks + \varepsilon \operatorname{sgn}(s) + (\ddot{x}_r - f(\bar{x}, t) - d(t) + c(\dot{x}_r - \dot{x}_2)]) + d(t) + c(\dot{x}_r - \dot{x}_2)\} \quad (13)$$

$$\dot{V} = s(-d - ks - \varepsilon \operatorname{sgn}(s)) = -sd - ks^2 - \varepsilon s \operatorname{sgn}(s) \quad (14)$$

If  $\varepsilon$  is selected such that  $\varepsilon \geq M$ , then the derivative of Lyapunov function satisfies the following condition.

$$\dot{V} = -sd - ks^2 - \varepsilon |s| \leq 0 \quad (15)$$

According to (15), It is clear that the designed control input is able to output signal to track the reference signal under disturbance.

## 4. Simulation Results and Discussions

Interesting points for tracking control problems in this research consists of two types of reference signals which are: 1) step function and 2) sinusoidal signal. The magnitude of the step function and sinusoidal function can be defined by the distance between centers of the first and the second electrode plate.

### 4.1. Simulation Example

The example of a EWOD microfluidic system is controlled by the designed controller in section 3 as shown in Fig. 3. The simulations of the control system for both cases are carried out in MATLAB program. The integration method is Runge-Kutta with sampling time of 0.00001 seconds. The water droplet is used in this simulation, and the system is operated at 20°C. The system parameters are presented as follows.

$$L = 1600 \times 10^{-6} \text{ m}, l = 70 \times 10^{-6} \text{ m}, \mu_d = 1.01 \times 10^{-3} \text{ Pa.s}, \\ \zeta = 0.08 \text{ Ns/m}^2, \rho_d = 1000 \text{ kg/m}^3, H = 0.0013 \text{ m} \\ a = 8.8 \times 10^{-4} \text{ m}, m = 2.5681 \times 10^{-6} \text{ kg}, n = 2, \\ \text{and } d(t) = 2000 \times 10^{-6} \sin(100t). F_{\text{thresh}} = 2.6541 \times 10^{-5} \text{ N}$$

The values of  $\zeta$ ,  $\rho_d$ , and  $C$  are from [11] and [12].  $L$  and  $l$  are from [18]. Assuming contact angel equal to  $\theta = 110^\circ$ ,  $H$  is determined from  $L$  based on [14].  $\mu_d$  is selected at the temperature equal to 20°C.  $m$  is calculated from the density,  $\rho_d$ , and volume of the droplet defined by  $a$  and  $H$ . According to [15], the value of  $F_{\text{thresh}}$  is the value of capillary force and is approximated based on the value of the contact angle,  $\theta = 110^\circ$ , the electrode width  $L$ , and the surface tension between water and air  $\gamma = 72 \text{ mN/m}$  [14], and the hysteresis angle  $\alpha = 7^\circ$  [14].

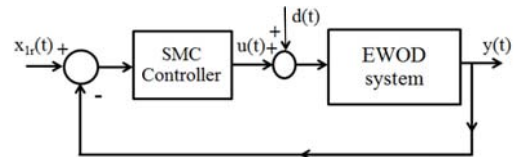


Fig. 3. The diagram of the feedback control system.

### 4.2. Step Reference Signal

The control EWOD microfluidic system has a step function as reference signal presented as

$$x_r(t) = \begin{cases} 1670 \times 10^{-6}, & t \geq 0 \\ 0, & t < 0 \end{cases} \quad (19)$$

with the initial condition  $\bar{x}(0) = [0 \ 0]^T$ . (20)

The control parameters are selected as follows,  $c=100$ ,  $k=90$  and  $\epsilon=3$ . The simulation results of droplet position and velocity are shown in Figs. 4(a) and 4(b). Position tracking error of the droplet is shown in Fig. 4(c). The control input signal is shown in Fig 4(d). Therefore, it is clear that the sliding mode controller is feasible to track the step reference signal accurately under the effect from the disturbance.

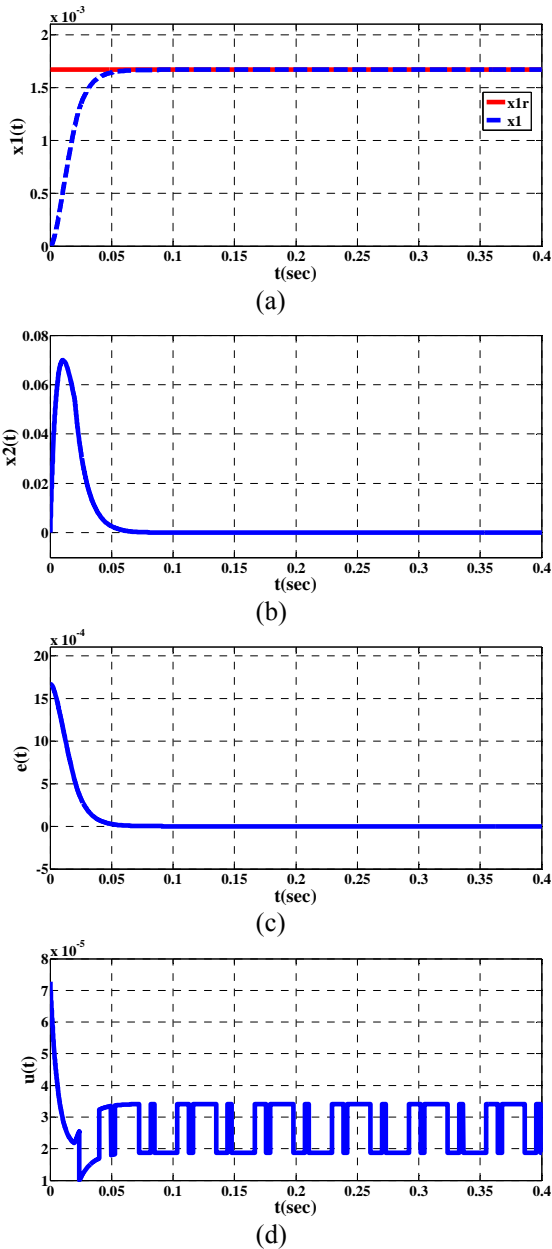


Fig. 4. Simulation results of tracking step reference signal

### 4.3. Sinusoidal Reference Signal

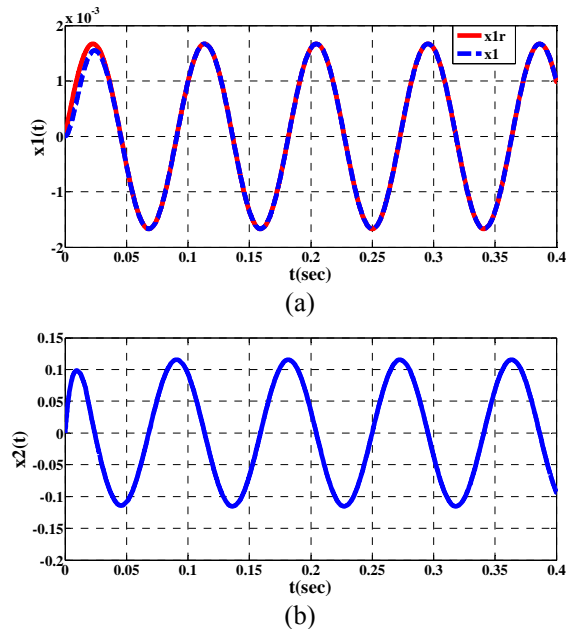
The sinusoidal function is the reference signal of the control EWOD microfluidic system expressed as

$$x_{1r}(t) = 1670 \times 10^{-6} \sin(\omega t) \quad (21)$$

where the frequency  $\omega = 22\pi \text{ rad} / \text{s}$

$$\text{with the initial condition } \bar{x}(0) = [0 \ 0]^T. \quad (22)$$

The control parameters,  $c$ ,  $k$  and  $\epsilon$  are selected as the same values in the previous case. The simulation results of droplet position and velocity as well as position tracking error of the droplet are shown in Fig. 5 (a), (b), and (c), respectively. The control input signal is shown in Fig. 5 (d). The controller with selected parameters is able to track the sinusoidal reference signal, so that the droplet can move along desire path as shown in Fig 5(a). The plot of velocity versus time is shown in Fig 5(b). At certain range of time for example  $t \geq 0.091 \text{ s}$ , the plot in figure 4 (b) is similar to the first derivative of the displacement in figure 4 (a) as considering from the amplitude and the phase difference of the plots from both figures. Thus, this plot is reasonable. The plot of position tracking error versus time in Fig 5(c) shows that the sliding mode control provides low position tracking error. Thus, the sliding mode controller is feasible to track the sinusoidal reference signal accurately even though the system is affected by the bounded disturbance. Therefore, the sliding mode controller is an appropriate technique for the position control of the micro droplet in the EWOD microfluidic system.



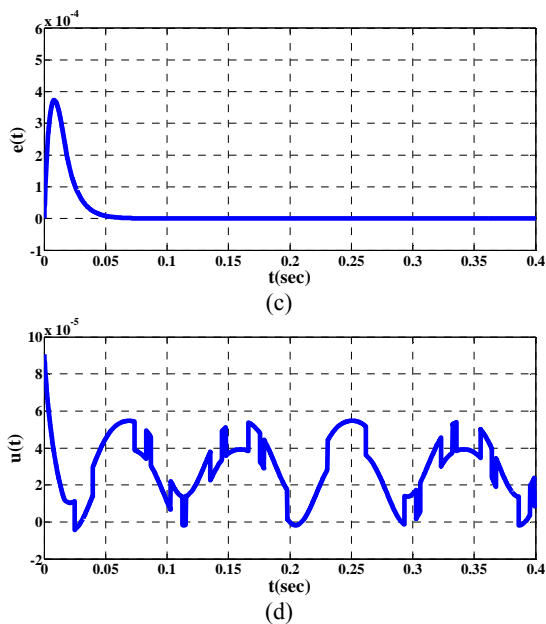


Fig. 5. Simulation results of tracking sinusoidal reference signal

## 5. Conclusions

The sliding mode control with exponential rate reaching law is feasible to control the microfluidic droplet motion in the EWOD microfluidic system under the effect of bounded disturbance signal. For the step reference signal, the controller provides the step response with no overshoot and tracks the reference signal accurately under the disturbance. In the case of the sinusoidal reference signal, the designed sliding mode controller can also provide accurate tracking.

## 6. References

- [1] K. Brady, "Electrowetting for DNA sequencing on chip", 2004 NNIN REU Research Accomplishments, pp. 26-27, 2004.
- [2] V. Srinivasan, V.K. Pamula, P. Paik, and R.B. Fair, "Protein stamping for MALDI mass spectrometry using an electrowetting-based microfluidic platform", in *Proc. of SPIE-The International Society for Optical Engineering*, vol. 5591, 2004, pp. 26-32.
- [3] V. Srinivasan, V.K. Pamula, M.G. Pollack, and R.B. Fair, "Clinical diagnostics on human whole blood, plasma, serum, urine, saliva, sweat, and tears on a digital microfluidic platform", in *Proc. the 7th International Conference on Miniaturized Chemical and Biochemical Analysis Systems*, Squaw Valley, California, U.S.A., 2003, pp.1287-1290.
- [4] M.G. Pollack, P.Y. Paik, A.D. Shenderov, V.K. Pamula, F.S. Dietrich, and R.B. Fair, "Investigation of electrowetting-based microfluidics for real-time PCR applications", in *Proc. the 7th International Conference on Miniaturized Chemical and Biochemical Analysis Systems*, Squaw Valley, California, U.S.A., 2003, pp.619-622.
- [5] C.S. Yu, M.Y. Lin, H.T. Hu, Y.C. Hu, and H.Y. Chou, "A droplet-based device for triglycerides colorimetric measurement", *Tamkang Journal of Science and Engineering*, vol. 8, no. 3, pp. 211-216, 2005.
- [6] V. Srinivasan, V. Pamula, M. Pollack, and R. Fair, "A digital microfluidic biosensor for multianalyte detection", in *Proc. of IEEE The Sixteenth Annual International Conference on Micro Electro Mechanical Machine (MEM-03Kyoto)*, Kyoto, Japan, 2003, pp. 327-330.
- [7] W. Satoh, H. Hosono, K. Morimoto and H. Suzuki, "Micro analysis system with an integrated microfluidic system based on electrowetting", in *Proc. of the fourth IEEE Conference on Sensors( IEEE SENSORS 2005)*, Irvine, CA, U.S.A., Oct. 30-Nov. 3, 2005, pp. 37-40.
- [8] K.S. Yun, I.J. Cho, J.U. Bu, G.H. Kim, Y.S. Jeon, C.J.(CJ) Kim, and E. Yoon, "A micropump driven by continuous electrowetting actuation for low voltage and low power operations", in *Proc. of the 14th IEEE international conference on Micro Electro Mechanical Systems (MEMS 2001)*, Interlaken, Switzerland, pp. 487-490.
- [9] I. Moon, and J. Kim "Using EWOD (electrowetting-on-dielectric) actuation in a micro conveyor system", *Sensor and Actuators A: Physical*, vol. 130-131, pp. 537-544, Aug. 2006.
- [10] V. K. Pamula and K. Chakrabarty, "Cooling of integrated circuits using droplet-based microfluidics", in *Proc. of the 13 th ACM Great Lakes Symposium on VLSI (GLSVLSI'03)*, Washington, DC, U.S.A., April 28-29, 2003, pp.1-4.
- [11] B. Bhattacharjee, and H. Najjaran, "Simulation of droplet position control in digital microfluidic systems", *Journal of Dynamic Systems, Measurement, and Control*, vol. 132, iss. 1, pp. 014501-1 - 014501-3, Jan. 2010.
- [12] H. Oprins, B. Vandevelde, and M. Baelmans, "Modeling and control of electrowetting induced droplet motion", *Micromachines*, (3)1, pp. 150-167, 2012.
- [13] H. Ren, R.B., Fair, M.g., Pollack, and E.J. Shaughnessy, "Dynamics of electro-d-wetting droplet transport ", *Sensor and Actuators B* 87 (2002), pp.201-206.
- [14] J. Berthier, *Microdrops and digital Microfluidics*, Norwich New York:William Andrew, 2008.
- [15] J. Berthier, P. Dubois, P. Clementz, P. Claustre, C. Peponet, Y. Fouillet, "Actuation potential and capillary forces in electrowetting based microsystem", *Sensor and Actuators A* 134 (2007) 471-479.
- [16] J. Liu, and X. Wang, "Advanced sliding mode control for mechanical systems" Beijing, Tsinghua University Press and Berlin Heidelberg, Springer-Verlag, 2011
- [17] W. Gao and J.C. Hung, "Variable Structure Control of Nonlinear Systems: A New Approach", *IEEE Transacstion on Industrial Electronics*, Vol. 40, No.1 February, 1993, pp. 45-55.
- [18] C. Phongsomboon, "Mobility control of a droplet on top of a flat plate", M.S. thesis, Dept. Mechanical Engineering, King Mongkut University of Technology Thonburi, Bangkok, Thailand, 2012. (in Thai)
- [19] R. W. Fox, P. J., Pritchard, and A. T., Macdonald, "Introduction to fluid mechanics", 7<sup>th</sup>edition, John Wiley and Sons, 2010.

## Fast motion detection based on cross correlation

PancaMudjirahardjo, JooKooi Tan, Hyoungseop Kim, Seiji Ishikawa

Dept. of Control Engineering, Kyushu Institute of Technology,

1-1 Sensui-cho, Tobata-ku, Kitakyushu-shi, Fukuoka, 804-8550, Japan

E-mail: {panca,etheltan,ishikawa}@ss10.cntl.kyutech.ac.jp, kim@cntl.kyutech.ac.jp

tel: 093-884-3191

### Abstract

We present a method of fast motion detection as an abnormal motion based on cross correlation. Since the camera view is not in perpendicular with motion direction, the velocity of motion is not uniform spatially. Instead of object detection directly, we separate an image into several blocks. We calculate the cross correlation of the pixel intensity series in these blocks between a current and a previous frame. The maximum correlation is achieved at certain delay. This delay shows a shift of a similar pattern between the current and the previous frame. To localize an abnormal motion, we employ a hierarchical block size. The performance of the proposed method is experimentally shown.

*Keywords:* Abnormal motion, cross correlation, delay, hierarchical block size.

### 1. Introduction

In recent years, abnormal motion detection has attracted great research attention in computer vision. Most current surveillance systems only provide *reactive* security by enabling the analysis of events after the event has already occurred — what is really needed by the security community is *proactive* security to help prevent future attacks.

Many approaches on video event analysis are based on the object trajectories extracted from video. Abnormal events can be detected through a prior learning of normal events or, without a learning process, by analyzing the trajectory result directly.

Jiang et al. [1] used spatial and temporal context and performed frequency-based analysis to detect anomalous video events. The normal observation is modeled by hidden Markov model (HMM). This research detected the anomalous car trajectory on the road from top view. Kiryati et al. [2] recognized an abnormal human behavior from high camera view.

Before the detection phase, they included a training phase for normal condition. Baranwal et al. [3] detected an abnormal indoor motion in a static background environment. They trained various motions using radial basis functions networks (RFBN). Park et al. [4] used clustering of motion based on similarity measurement of a feature space. They detected an abnormal motion, especially in a different direction case, from high camera view.

In this paper, we propose a fast motion detection with a camera view not in perpendicular with motion direction, as an abnormal motion among walking motion. We capture a scene from a 2 meter height and more for outdoor scenes, as shown in **Fig. 1**. Due to camera view not in perpendicular with motion direction, motion velocity in the image is not uniform spatially. We need to extend the method in [5,6].

It requires no foreground segmentation, no motion recognition and no object detection. We analyze the object's velocity through a certain delay where the maximum correlation occurred.

© The 2015 International Conference on Artificial Life and Robotics (ICAROB 2015), Jan. 10-12, Oita, Japan



Fig. 1. Scenes for performed experiment

## 2. Overview of the Proposed Method

A fast motion detection needs some velocity data. In this paper, we provide velocity data from cross correlation of pixel intensity series in the blocks between a current and a previous frame. The maximum correlation is achieved at a certain delay. This delay shows a shift of a similar pattern between the current and the previous frame.

Cross correlation is a standard method of estimating the degree to which two series of data are correlated. Consider two series  $x(i)$  and  $y(i)$  where  $i=0,1,2...N-1$ . The cross correlation  $r_{xy}$  at delay  $d$  is defined as [7],

$$r_{xy} = \frac{\sum_i [(x(i) - \bar{x})(y(i-d) - \bar{y})]}{\sqrt{\sum_i (x(i) - \bar{x})^2} \sqrt{\sum_i (y(i-d) - \bar{y})^2}} \quad (1)$$

where  $\bar{x}$  and  $\bar{y}$  are the means of the corresponding series.

The range of delay  $d$  and thus the length of the cross correlation series can be less than  $N$ , for example, to test correlation at short delays only. The denominator in the expression above serves to normalize the correlation coefficients so that  $-1 \leq r_{xy} \leq 1$  holds; the bounds

© The 2015 International Conference on Artificial Life and Robotics (ICAROB 2015), Jan. 10-12, Oita, Japan

indicating maximum correlation and 0 indicating no correlation. A high negative correlation indicates a high correlation but of the inverse of one of the series.

We describe the proposed method for fast motion detection based on cross correlation as depicted in Fig.2.

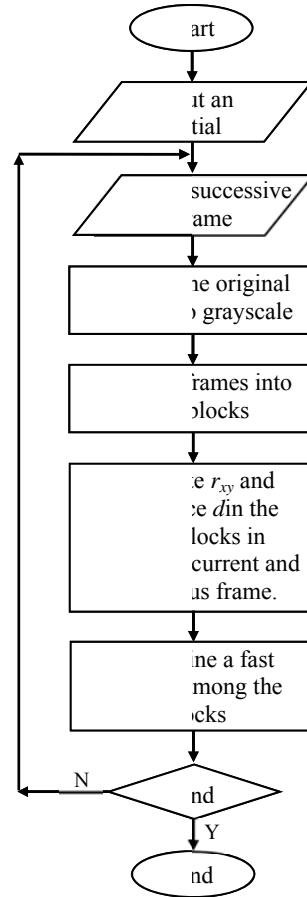


Fig. 2 Overview of the proposed method.

## 3. Method

In this section, we describe the proposed method in detail.

### 3.1. Preprocessing

First, we need to convert the original successive frames into grayscale images. Subsequently, we separate the images into  $m \times n$  blocks. The calculation of cross correlation in the same block between a current and a previous frame gives the information of shift of an object in this block.

### 3.2. Calculation of a shift magnitude based on cross correlation.

As was mentioned in section 2, cross correlation is a standard method of estimating the degree to which two series are correlated [7]. This calculation is one dimensional computation.

As a simple example, consider two rectangular pulses shown in Fig. 3, in blue and green. The correlation series is shown in red.

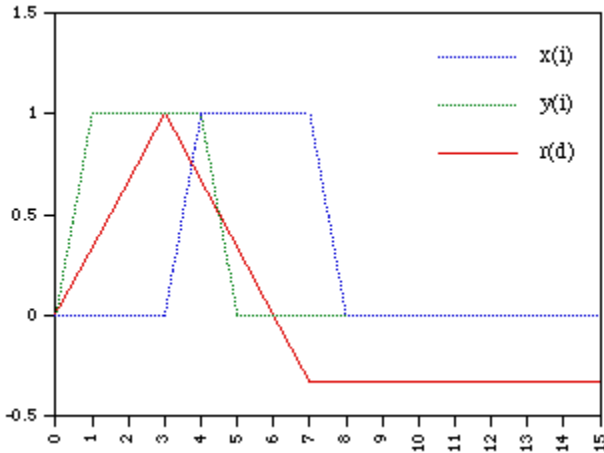


Fig.3. Example of cross correlation

The maximum correlation is achieved at a delay of 3. Considering the equations above, what is happening is that the second series is being slid past the first, at each shift the sum of the product of the newly lined up terms in the series is computed. This sum will be large when the shift (delay) is such that similar structure lines up.

Delay of the maximum correlation can be assumed as a shift of an object. This calculation of shift based on cross correlation is simpler than 2D correlation, because 2D correlation needs a template, then slides it over a specified range to get the maximum value. This calculation is also simpler than a method proposed in [6]. It is more accurate than optical flow based on Lucas-Kanade tracker which relies on feature points.

To provide one dimensional data series, we scan an image pixel as in Fig. 4.

To provide one dimensional data series as shown in Fig. 4, we perform the below algorithm, in which all the variables are in an integer type:

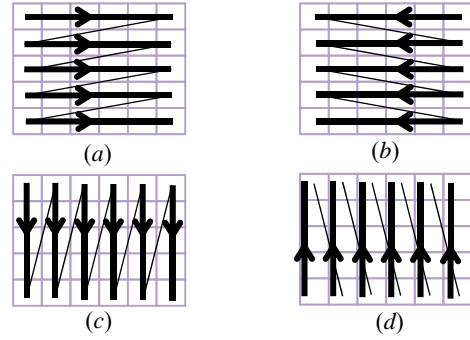


Fig. 4. Arrangement of pixel data to provide one dimensional data series.  
(a) hor\_1 (b) hor\_2 (c) ver\_1 (d) ver\_2

```

for (i = 0 : m×n)
    hor_1[i] = pixel[i/m][i-(i/m)×m];
    ver_1[i] = pixel[i mod n][i/n];
    hor_2[i] = pixel[i/m][(i/m+1)m-1-i];
    ver_2[i] = pixel[(i/n+1)n-1-i][i/m];
end for;

```

Here  $m$  and  $n$  are weight and height of an image block, respectively. **mod** is a modulo operation. Pixel[ $a$ ][ $b$ ] is a pixel intensity at  $a^{\text{th}}$  row and  $b^{\text{th}}$  column of the image block.

Then we calculate the cross correlation between current and previous image frame at the same image block. The maximum correlation is achieved at a certain delay. For example, the maximum correlation between  $\text{hor\_1}(t)$  and  $\text{hor\_1}(t-1)$  occurs at  $\text{delay}_{\text{hor\_1}}$ . We will get other delays, i.e.  $\text{delay}_{\text{hor\_2}}$ ,  $\text{delay}_{\text{ver\_1}}$ ,  $\text{delay}_{\text{ver\_2}}$ .

$$\text{delay}_{\text{hor}_\alpha} = \arg \max_d (r_{\text{hor}_\alpha(t), \text{hor}_\alpha(t-1)}) \quad (2a)$$

$$\text{delay}_{\text{ver}_\alpha} = \arg \max_d (r_{\text{ver}_\alpha(t), \text{ver}_\alpha(t-1)}) \quad (2b)$$

Where  $\alpha \in \{1, 2\}$ . Then the shift magnitude at a current image block is calculated as,

$$|\text{shift}| = \sum_\alpha \sqrt{\text{delay}_{\text{hor}_\alpha}^2 + \text{delay}_{\text{ver}_\alpha}^2} \quad (3)$$

Let us define the identity of  $|\text{shift}(i, j)|$ ,  $I_{(i, j)}$ , as below,

$$I_{(i, j)} = \begin{cases} 1 & \text{if } |\text{shift}(i, j)| > 0 \\ 0 & \text{otherwise} \end{cases} \quad (4)$$

Here,  $i$  and  $j$  are block's position at  $i$ -th row and  $j$ -th column, respectively.



### 3.3. Determining a fast motion

To detect a fast motion in a frame, we calculate the maximum of shift magnitude among the blocks within a frame. We do this search in hierarchical block sizes, as depicted in **Fig. 5**. First, block size  $m \times n$  pixels, we will detect a fast motion at  $block\_fast1$ . Second, block size  $m \times h$  pixels, we will detect a fast motion at  $block\_fast2$ . Finally, block size  $2m \times h$  pixels, we will detect a fast motion at  $block\_fast3$ , where  $h$  is image height.

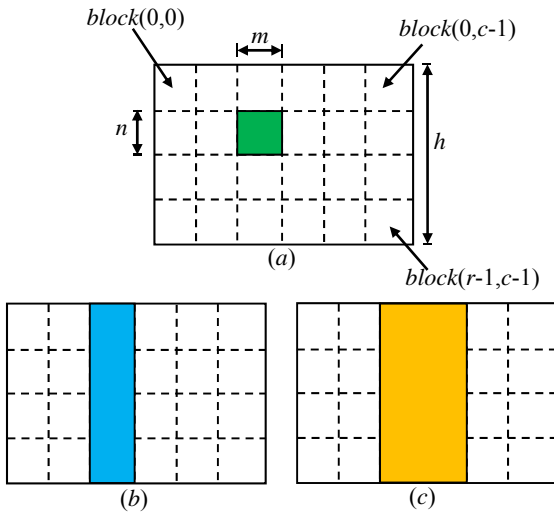


**Fig. 5.** Hierarchical block size.  
(a)  $m \times n$  (b)  $m \times h$  (c)  $2m \times h$

*Operation in  $m \times n$  block size level.* For each block, we have a shift magnitude,  $|shift(i, j)|$  defined by Eq. (3), where  $i \in \{0, \dots, r-1\}$  and  $j \in \{0, \dots, c-1\}$ . Then  $block\_fast1$  is defined by,

$$block\_fast1 = \max(|shift(i, j)|) \quad (5)$$

We record  $block\_fast1$  position at  $r_1$ -th row and  $c_1$ -th column.

*Operation in  $m \times h$  block size level.* For each column, we have an average of shift magnitude,  $avg\_shift_j$ , where  $j \in \{0, \dots, c-1\}$ .

$$f(j) = \sum_{i=0}^{r-1} |shift(i, j)| \quad (6a)$$

$$r_a(j) = \sum_{i=0}^{r-1} I_{(i, j)} \quad (6b)$$

$$avg\_shift_j = \begin{cases} \frac{f(j)}{r_a(j)} & \text{if } f(j) > 0 \\ 0 & \text{otherwise} \end{cases} \quad (6c)$$

Then  $block\_fast2$  is defined as,

$$block\_fast2 = \max(avg\_shift_j) \quad (7)$$

We get  $block\_fast2$  position at  $c_2$ -th column.

*Operation in  $2m \times h$  block size level.* For each column, we have an average of shift magnitude,  $avg\_shift_k$ , where  $k \in \{0, \dots, c-2\}$ .

$$f(k) = \sum_{j=k}^{k+1} \sum_{i=0}^{r-1} |shift(i, j)| \quad (8a)$$

$$r_b(k) = \sum_{j=k}^{k+1} \sum_{i=0}^{r-1} I_{(i, j)} \quad (8b)$$

$$avg\_shift_k = \begin{cases} \frac{f(k)}{r_b(k)} & \text{if } f(k) > 0 \\ 0 & \text{otherwise} \end{cases} \quad (8c)$$

Then  $block\_fast3$  is defined as,

$$block\_fast3 = \max(avg\_shift_k) \quad (9)$$

We get  $block\_fast3$  position at  $c_3$ -th column.

Finally, we will detect a fast motion at  $c_F$  column, if  $c_1 = c_2 = c_F$  or  $c_1 = c_3 = c_F$  or  $c_2 = c_3 = c_F$  or  $c_1 = c_2 = c_3 = c_F$ .

## 4. Experimental Result

The experimental environment is as follows: Operating system is Windows 7 ultimate; the processor is Intel® core™ i7 CPU 870 @2.93GHz and the used software is Microsoft Visual Studio 2010.

For experiment, we use outdoor scene, as **Fig. 1**, with many people do normal motion (walking) and a person does abnormal motion (running), with video frame rate and the size of a frame 30 fps and  $320 \times 180$  pixels, respectively.

We set  $m$  and  $n$  are 20 pixels, so we separate an image frame into  $16 \times 9$  blocks. For delay,  $d$ , we set 10. The experimental results are shown in **Fig. 6**.

**Table 1** shows the evaluation of performance, where TPR is true positive rate.

$$TPR = \frac{TP}{TP + FN} = \frac{TP}{GT} \times 100\% \quad (10)$$

Here :

$TP$  : true positive, fast motion is detected as fast motion.

$FN$  : false negative, fast motion is detected as normal motion.

$GT$  : ground truth.

**Table 1.** Evaluation of performance

scene	TPR (%)	Execution time (ms)
1	88.7	228.75
2	91.5	

## 5. Conclusion

In this paper, we propose a method of fast motion detection in a crowd, with camera view not in perpendicular with motion direction. Instead of object detection and to avoid foreground segmentation, we calculate the cross correlation between the current and the previous frame in the same image block.

To detect a fast motion, we employ hierarchical block sizes. There are three levels of hierarchical block sizes. The location of the fast motion is a column where two

or three detected blocks which contain fast motion are overlapping.

As future work, we are going to conduct experiments on the recognition of abnormal motion under stronger occlusion.

## References

- [1] F. Jiang, J. Yuan, S.A. Tsafaris, A.K. Katsaggelo, "Anomalous video event detection using spatiotemporal context". *Computer Vision and Image Understanding* 115, pp. 323-333, 2011.
- [2] N. Kiryati, T.R. Raviv, Y. Ivanchenko, S. Rochel, "Real-time abnormal motion detection in surveillance video". *Proceedings of ICPR*. 2008.
- [3] M. Baranwal, M.T. Khan, C.W. De Silva, "Abnormal motion detection in real time using video surveillance and body sensors". *International Journal of Information Acquisition*. Vol. 8, No. 2, pp. 103-116, 2011.
- [4] M. Park, J. K. Tan, Y. Nakashima, H. Kim, S. Ishikawa, "Detecting human flows on a road different from main flows". *Proceedings of AROB*. 2011.
- [5] P. Mudjirahardjo, J.K. Tan, H. Kim, S. Ishikawa, "Abnormal motion detection in an occlusive environment". *Proceeding of SICE Annual Conference 2013*, pp. 1398-1402. 2013.
- [6] P. Mudjirahardjo, J.K. Tan, H. Kim, S. Ishikawa, "Fast motion detection in a dynamic background". *Proceeding of International Symposium AROB 19<sup>th</sup> 2014*, pp. 896-900, 2014.
- [7] D. Lyon. "The discrete fourier transform, part 6: cross-correlation". *Journal of Object Technology*, Vol. 9, No. 2. Pp. 17-22, 2010.



**Fig.6.** Performance of fast motion detection from various scenes. A detected person with fast motion is indicated by red lines.



# Detecting moving objects on a video having a dynamic background

**FX Arinto Setyawan, Joo Kooi Tan, Hyoungeop Kim, Seiji Ishikawa**

*Dept. of Control Engineering, Kyushu Institute of Technology,*

*1-1 Sensui-cho, Tobata-ku, Kitakyushu-shi, Fukuoka, 804-8550, Japan*

*E-mail: {arinto,etheltan,ishikawa}@ss10.cntl.kyutech.ac.jp, kim@cntl.kyutech.ac.jp*

*tel: 093-884-3191*

## Abstract

This paper proposes a method of detecting moving objects in a video having a dynamic background using a method which infers the background sequentially. The proposed method performs the update of the pixel values in the background which are influenced by the value of the current pixel. The aim is to cope with changes in the value of the pixels in the background caused by the movement of the background objects such as the leaves swaying on trees, the water droplets of the rain or the change in light intensity according to the time lapse. The performance of the proposed method is shown experimentally using the video taken on a rainy and windy day.

*Keywords:* Object detection, foreground detection, background inference, Gaussian distribution.

## 1. Introduction

The increasing number of crimes and accidents that occur nowadays requires a reliable video surveillance system. The surveillance system can be realized by installing cameras in places vulnerable to crime and accidents. There are 3 types of video surveillance activities, i.e. manual (conventional), semi-autonomous and fully autonomous [1].

The conventional video surveillance systems can record what they see, but cannot find what is seen. In conventional surveillance systems, the task of video surveillance review was performed by trained security personnel. The increase of surveillance video data makes security officer jobs increasingly heavy. Solution by adding more security personnel is an option that spends much cost. A better solution is to replace a conventional video surveillance system by a fully autonomous system.

On the fully-autonomous system, the input is a video sequence taken in the spot where surveillance is

done, and, without human intervention, object detection and object tracking are done using computer [2]. The rapid development of computer, especially in terms of processing speed and a large amount of memory, allows the implementation of a fully autonomous surveillance system.

Detection of moving objects is one of the important tasks in many computer vision applications including a video surveillance system. A moving object detection system is a system that detects moving objects in a video taken with the use of surveillance cameras. A general approach used in the detection of moving objects is background subtraction [3,4,5]. The idea of the background subtraction is to compare the image scene at the current time with a reference of the background image model. Usually a reference of the background image model is the first image frame of the video and is updated all the time.

The other application of the detection of moving objects is for a traffic control system, application in the

field of sports, hospital patient monitoring, monitoring of students in a class, and others. Aslani and Nasab [6] performed a research on the application of detecting moving objects for a traffic monitoring system. Application on detecting moving objects in the field of sports was done by Manikandan and Ramakrishnan [5].

Much research on the detection of moving objects using a static camera has been done using the methods other than the background subtraction. Stauffer and Grimson [7] use Gaussian Mixture Model to address changes in the background such as changes in light intensity, slow-moving objects and the effects of moving elements in a scene. Aslani and Nasab [6] employ optical flow to detect and track a moving object. Keerthana, Ravichandran and Santhi [8] use Fuzzy-Extreme Learning Machine for detecting a moving object. Zhou, Yang and Yu [9] detect a moving object by a method of Detecting Contiguous Outliers in the Low-Rank Representation (DECOLOR).

In this paper, we propose a method of detecting a moving object in a video having a dynamic background. Pixel values on the background at all times are updated to get the model background. The updated value depends on how often the pixels are recognized as background or foreground. After moving object is detected, morphological operations are performed on the image frame in order to get better detection results. This method was tested on videos taken during a rainy and windy day in order to get a video that has a dynamic background.

## 2. Method

The flowchart on the method used in detecting moving objects in a video having a dynamic background is shown in Fig. 1. The first step of the proposed method is to convert an image at time  $T$  (abbr., image  $T$ ) from RGB to gray level. The purpose of this conversion is to reduce the computational load. Standard formula to convert RGB to grayscale is given as follows;

$$I = 0.2989R + 0.5870G + 0.1140B . \quad (1)$$

The second step is to determine the normal distribution model,  $N_T(f; \mu, \sigma)_{(x,y)}$ , of a pixel at  $(x,y)$  in the image frame. The normal distribution is formed using the following equation;

$$N_T(f; \mu, \sigma) = \frac{1}{\sqrt{2\pi} \sigma} e^{-\frac{1}{2}\left(\frac{f-\mu}{\sigma}\right)^2} \quad (2)$$

Here  $f$  is the value of the pixel intensity at pixel  $(x,y)$ , and  $\mu$  and  $\sigma$  are the mean and the variance of the pixel intensity. The value of the initial mean is the value of the intensity of the pixel in image  $T(=0)$  and the value of the initial variance is determined as 1 in the experiment.

The next step is the judgment if each pixel of the current image is in the background or on the foreground. This judgment is done by subtracting intensity of the current image pixel by the mean of previous image pixel. For the judgment, the following equation is employed;

$$\frac{|f_{T+1} - \mu_T|}{\sigma} \leq Th \quad (3)$$

Here  $f_{T+1}$  is the value of the pixel intensity in a current image frame and  $\mu_T$  is the mean value of the background pixel model.  $Th$  is a threshold. A pixel is regarded as the pixels in the background, if it satisfies Eq.(3): Otherwise it is regarded as the pixel on the foreground or on a moving object.

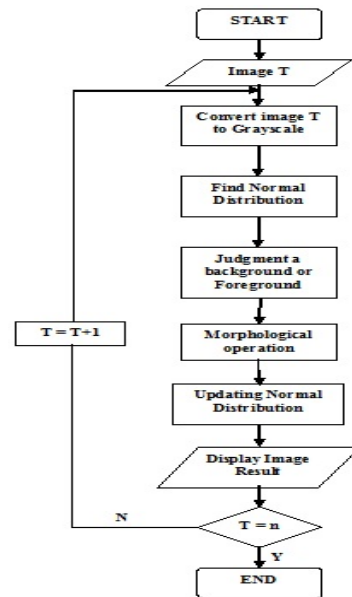


Fig. 1. Flowchart of the system.

After obtaining a set of pixels which represents a moving object, then a morphological operation is performed to those pixels on the image. The morphological operation used in the proposed method is the opening operation. The opening operation is a combination of erosion and dilation operations. They are performed in sequence, i.e., erosion is done to the original image and then dilation is applied to the result. The opening operation of an image  $f$  by a structuring element  $s$  is defined using the following equation:

$$g(x, y) = (f(x, y) \ominus s) \oplus s \quad (4)$$

An example of the result of the judgment followed by the morphological operation is shown in **Fig. 2**.

The next step is to update the normal distribution at each pixel in the background. The purpose of this update is to overcome the disturbance that occurs in the background caused by the change in light intensity, swaying leaves of trees, and slow-moving objects, etc. The mean and the variance of the normal distribution are updated using the following equations;

$$\mu_{T+1(x,y)} = \begin{cases} \rho * f_{T+1(x,y)} + (1 - \rho) * \mu_{T(x,y)} & \text{if } f_{T+1(x,y)} = \text{background} \\ (1 - \beta) * f_{T+1(x,y)} + \beta * \mu_{T(x,y)} & \text{if } f_{T+1(x,y)} = \text{foreground} \end{cases} \quad (5)$$

$$\sigma_{T+1(x,y)}^2 = \begin{cases} \rho * (f_{T+1(x,y)} - \mu_{T+1(x,y)})^2 + (1 - \rho) * \sigma_{T(x,y)}^2 & \text{if } f_{T+1(x,y)} = \text{background} \\ (1 - \beta) * (f_{T+1(x,y)} - \mu_{T+1(x,y)})^2 + \beta * \sigma_{T(x,y)}^2 & \text{if } f_{T+1(x,y)} = \text{foreground} \end{cases} \quad (6)$$



Fig. 2. Example of the performance: (a) Original image, (b) the moving object detection followed by the morphological operation.

$$\rho = c * N(f_{T+1}; \mu_T, \sigma_T^2) \quad (7)$$

$$\beta = \frac{1}{1 + k * C_{T+1}^2} \quad (8)$$

Here  $\rho$  is a variable learning rate. Constant  $c$  is defined so that the maximum value of  $\rho$  is 1.  $C_{T+1}$  is the number of successive frames where the pixel  $p(x,y)$  has been judged as a foreground pixel, and  $k$  is a constant. Each pixel is updated with different values depending on how often pixels are judged as foreground or background. These updated values affect the next judgment on the background or the foreground.

### 3. Experimental Results

For experiment, we use 2 video scenes. The video frame rate and the size of an image are 30 fps and  $320 \times 240$  pixels, respectively. The experimental environment is as follows: The operating system is Windows 7 Enterprise, the processor is Intel® core™ 2 Duo E7500, 4GB RAM, and the used software is MS Visual Studio 2008. The result of moving object detection on video 1 is shown in **Fig. 3**.

The effectiveness of the proposed method is evaluated by comparing the results with the ground truth, as shown in **Fig. 4**. In the resultant image of comparison between the result of the proposed method and the ground truth, the red areas are true positive (TP) that is an overlap part between the ground truth and detection results. Blue means the part which is included in the ground truth but not in the detection result and this part is False Negative (FN); Green means the part which is included in the detection result but not in the Ground Truth and this part is False Positive (FP).

The sensitivity of the proposed method is expressed using the popular parameters, Recall (R) and Precision (P), whereas the accuracy of the method is calculated using the F measure. They are defined by the following formula;

$$R = \frac{N_{TP}}{N_{TP} + N_{FN}} \quad (9)$$

$$P = \frac{N_{TP}}{N_{TP} + N_{FP}} \quad (10)$$

$$F = 2 \frac{Recall \times Precision}{Recall + Precision} \quad (11)$$

Here  $N_{TP}$  is the number of pixels in the true positive area; and  $N_{FP}$  is the number of pixels in the false positive area;  $N_{FN}$  is the number of pixels in the false negative area. The result on the evaluation of the proposed method is given in **Table 1**.

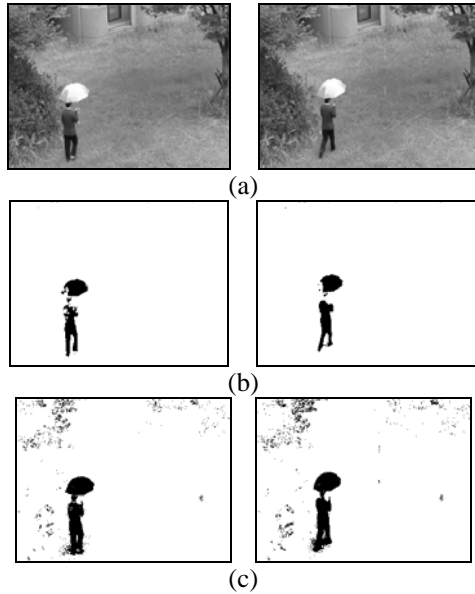


Fig. 3. The result of the moving object detection in video 1: (a) Original frames, frame 130 (the left) and frame 140 (the right), (b) the result of detection by the proposed method, (c) the result of detection using the background subtraction.

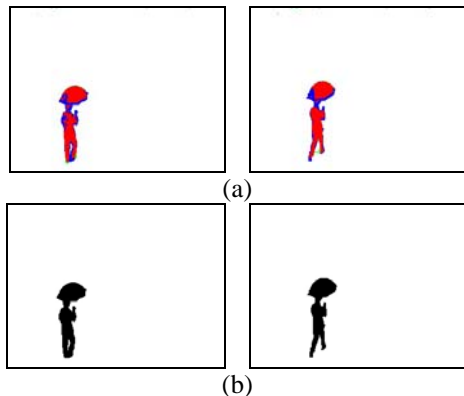


Fig. 4. Evaluation on the result shown in Fig. 3b: (a) Display of the TP (red), FN (blue) and FP (green), (b) the ground truth images.

© The 2015 International Conference on Artificial Life and Robotics (ICAROB 2015), Jan. 10-12, Oita, Japan

Table 1. Evaluation of the method.

Video	Evaluation values		
	$R(Recall)$	$P(Precision)$	$F(accuracy)$
Video 1	70.41	97.63	81.76
Video 2	67.84	86.66	75.97

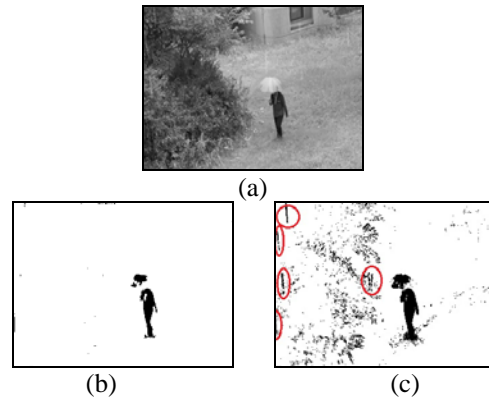


Fig. 5. Elimination of raindrops: (a) Original image containing raindrops, (b) the result by the proposed method, (c) the result by the background subtraction. The raindrops are marked in red.

#### 4. Discussion and Conclusion

The method used to detect a moving object on a video having a dynamic background is a background sequential inference. This method uses updating of the pixel values of the background based on how often the pixel is recognized as a background or foreground. The updating value of each pixel on a background is different with every pixel on the background. On the other hand, the threshold value, appearing in Eq.(3), to determine whether a pixel is in the background or on the foreground should probably be different with every region on the given image. But it is actually given an identical value such as 1 (equivalent to  $\sigma$ ) in the experiment and it gives satisfactory results.

The effectiveness of the proposed method was calculated using the parameters defined by Eqs.(9), (10) and (11). The method is considered effective, if the values of sensitivity, i.e., R and P, are greater than 50%. The used method achieved a high level of the precision

(P) and hence the accuracy (F) is also high. It has achieved the precision level greater than 80% and the accuracy greater than 75%.

Raindrops on a rainy day should be included in the background, since they don't have a particular meaning as objects. The proposed method can reduce raindrops effectively as shown in **Fig. 5**. Many raindrops are observed in the image of **Fig. 5a**. They are eliminated by the proposed method as shown in **Fig. 5b**, but some of them remain as in **Fig. 5c**, if a simple background subtraction is employed. The fields marked in red in **Fig. 5c** are raindrops.

The color of a moving object greatly affects the success of this technique. The color of an object that is very different from the background will be more easily recognized. The speed of a moving object also affects the success of this technique. If the object moves slowly or even it stands still in an image, it will be recognized as part of the background. But it is acceptable, as the topic of this paper is 'moving' object detection.

## References

- [1] I. S. Kim, H. S. Choi, K. M. Yi, J. Y. Choi, S. G. Kong, Intelligent visual surveillance - A survey, *International Journal of Control, Automation, and System*, **8**(5), (2010), pp. 926-936.
- [2] K. A. Joshi, D. G. Thakore, A survey on moving object detection and tracking in video surveillance system, *International Journal of Soft Computing and Engineering*, **2**(3), (2012), pp. 44-48.
- [3] T. Bouwmans, Recent advance on statistical background modeling for foreground detection: A systematic survey, *RCPS*, **4**(3), (2011), pp. 147-176.
- [4] C. Guyon, T. Bouwmans, E. Zahzah, Foreground detection based on low-rank and block-sparse matrix decomposition, *Proc. IEEE International Conference on Image Processing*, (2012), pp. 1225-1228.
- [5] R. Manikandan, R. Ramakrishnan, Human object detection and tracking using background subtraction for sports applications, *International Journal of Advanced Research in Computer and Communication Engineering*, **2**(10), (2013), pp. 4077-4080.
- [6] S. Aslani, H. M. Nasab, Optical flow based moving object detection and tracking for traffic surveillance, *International Journal of Electrical, Robotics, Electronics and Communications Engineering*, **7**(9), (2013), pp. 774-777.
- [7] C. Stauffer and W. E. L. Grimson, Adaptive background mixture models for real time tracking, *Conference on Computer Vision and Pattern Recognition*, Vol. 2, (1995), pp. 246-252.
- [8] N. Keerthana, K. S. Ravichandran, B. Santhi, Detecting the moving object in dynamic backgrounds by using fuzzy-extreme learning machine, *International Journal of Engineering and Technology*, **5**(2), (2013), pp. 749-754.
- [9] X. Zhou, C. Yang, and W. Yu, Moving object detection by detecting contiguous outliers in the low-rank representation, *IEEE Transactions on Pattern Analysis and Machine Intelligence*, **35**(3), (2013), pp. 597-610.

# Study on the Target Recognition and Location Technology of industrial Sorting Robot based on Machine Vision

Jiwu Wang<sup>1</sup>

*School of Mechanical, Electronic and Control Engineering, Beijing Jiaotong University  
Beijing 100044, China<sup>1</sup>*

Xianwen Zhang<sup>1</sup>, Huazhe Dou<sup>1</sup>

*School of Mechanical, Electronic and Control Engineering, Beijing Jiaotong University  
Beijing 100044, China<sup>1</sup>*

Sugisaka Masanori<sup>2</sup>

*Alife Robotics Corporation Ltd, Japan and Open University, United Kingdom<sup>2</sup>  
E-mail: jwwang@bjtu.edu.cn; sugisaka3@mocha.ocn.ne.jp*

## Abstract

In order to improve the applications for an industrial sorting robot, it is necessary to increase its flexibility and control accuracy. The prerequisite is to automatically extract the multiple target positions accurately and robustly. The machine vision technology is an effective solution. Here an industrial robot arm is designed and set up for experiment simulation with machine vision. In order to reduce the influence of the size, deformation, and lighting etc., the target recognition and location method with fusion of scale invariant feature transform (SIFT) and moment invariants is developed. The experiments results showed that the developed image processing algorithms are robust, and the flexibility of the industrial robot can be improved by machine vision.

*Keywords:* Arm robot, Target recognition, Flexible control, Machine vision

## 1. Introduction

Intelligent industrial robot, as the concentration and integration of advanced manufacturing technology, information technology and network technology etc., is getting more and more attention.<sup>1</sup> This is because a lot of robots and automated equipments will be required in the future applications.

Now, most of the traditional industrial robots can only work according to some fixed paths by an operator's

programming. The position of each target is predetermined, and robots only perform repetitive actions. But in the applications of the automated production line or a flexible manufacturing system,<sup>2</sup> such simple operations are not always satisfied to the practical request. It is necessary to obtain the position of each target automatically, and then adjust the angle of each joint correspondingly. Increasing industrial robot's flexibility and improving its repetitive positioning accuracy is the focus for their further applications.<sup>3</sup> In

order to realize above functions, the prerequisite is to get the target position accurately and reliably.

Machine vision is a good solution. A CCD camera can provide more information than other sensors. And some pattern recognition algorithms can be used to extract the target and calculate its position automatically in one captured image. Moreover, multiple targets and their positions can be determined at the same time, which makes robots to be flexibly controlled possible.

In order to get the position of each target, the target should be recognized first. Due to the influence of lighting, size, rotation and small scale perspective transformation etc., some target recognition algorithms are not robust. It will cause target positioning unreliable. The SIFT algorithm can effectively improve target recognition capability. In this paper, the SIFT algorithm is used for target recognition, and the target position is calculated with moment invariant method.

## 2. Target Recognition Based on Image Matching

For pattern recognition, some scale and grayscale transformation can not be avoided. It will make some matching algorithm unreliable. The algorithm of the scale invariant feature transform<sup>4</sup> (SIFT) is a local feature detection algorithm. It is based on matching image feature points to realize target recognition. Even in a complex environment, the target can be quickly and accurately recognized.

The kernel of SIFT algorithm is to search key points in the different scale space, and calculate their direction. The feature points in SIFT are those points, such as corners, edges, dark spot and bright spot etc., which will not be affected by illumination, viewpoint or occlusion. The process of SIFT algorithm is shown in figure 1.

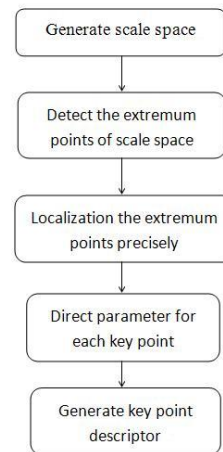


Fig.1.Illustration of SIFT algorithm steps

Image recognition is to identify the target image with the source images in the sample library. Compared with other pattern recognition algorithms, the necessary step is to input the sample target image in the sample library, which simplifies the complex operation for image processing. The target recognition process is shown in figure 2.

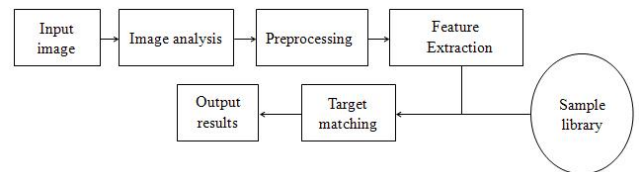


Fig.2. The flow chart of target recognition

In order to verify above algorithms, the following experiments are carried. We take a picture for all sample targets as the sample library, as shown in figure 3. We try to use the targets with different color and shape, even brightness.



Fig.3. Sample target image library

The matching results are shown in figure 4.

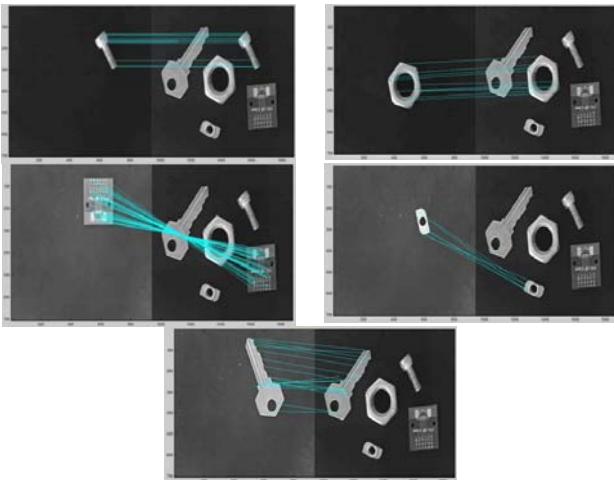


Fig.4 Illustration on the matching results

In figure 4, the scale and orientation transformation of the target are studied. Moreover, the influence of viewpoint and brightness modification is studied too. As shown in figure 4, with the SIFT algorithm, the matching results are robust and reliable. For each picture in this group, the left side is the input image to be detected, and the right side is the sample library. Their relationship is shown by connecting lines between the extracted feature points.

After the target is extracted by matching with SIFT algorithm, the next step is to determine its position. Generally, the center is necessary for each object, so the moment invariant algorithm is developed. As shown in figure 5, each target area is marked with rectangle, and its center is marked with a dot. Their coordinates are also given in unit of pixel.

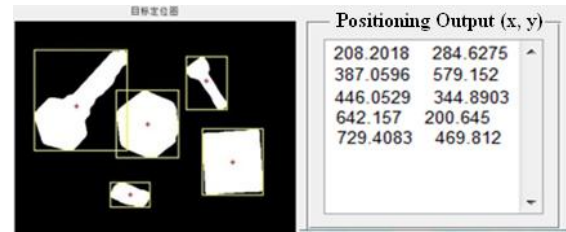


Fig.5 Illustration on the target positioning

### 3. Experiments

Based on the above target positioning with image processing algorithms of SIFT and moment invariants, the positioning control experiment with our arm robot is carried on. The experiment setting is as shown in figure 6. The CCD camera is fixed in the arm robot coordinate system. Thus the target position can be easily transformed to the end pose of the manipulator. With inverse kinematics equations, the angle of each joint can be calculated.

The experiment results show that the flexible control for multiple target operations can be performed with image processing methods developed in my lab. Moreover, with SIFT and moment algorithms, the influence of lighting and scale is low to the target position calculation.

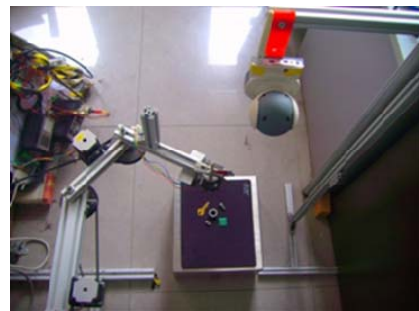


Fig.6. Control experiment with vision matching and positioning

### 4. Conclusions

system based on a CCD camera is developed. Multiple target control operations are performed with our lab arm robot. By algorithm fusion of SIFT and moment invariants, the multiple targets can be extracted robust and their positions can be calculated accurately.



Moreover, it can effectively control the influence of lighting and scale etc.

## References

1. Y. B. Wang, Y. Z. Hu, and M. Y. Lu, Siemens machine vision system and its application in automobile engine assembly line, *Automation systems engineering*, vol.1 (2006) 20-22.
2. K. L. Zhuang, J. Z. Wang, and J. Zhou, Application of machine vision in angle inspection, *Equipment Manufacturing Technology*, vol.4 (2011) 4-10.
3. G. L. David, Distinctive image features from scale-invariant key points. *Int. Journal of Computer Vision*, vol.2(60)(2004) 91-110.
4. A. Khotanzad, Y. Huahong, Rotation invariant image recognition using features selected via a systematic method, *Pattern recognition*, vol.23(10)(1990) 1089-1101.
5. M. Sugisaka, X. Wang, Intelligent control of a mobile vehicle using on-line learning, *System science*, vol.25(1999) 41-50.
6. M. Sugisaka, X. Wang, J. Lee, Intelligent control strategy for a mobile vehicle, *Applied mathematics and computation*, vol.20(1998) 91-98.

# Mechanism Designs for Bio-inspired Flapping Wing Robots

**Palakorn Tantrakool**

*Institute of Field roBOTics (FIBO), King Mongkut's University of Technology Thonburi,  
126 Pracha-Utid Road, Bangmod, Thrung Kru, Bangkok, 10140 Thailand*

**Eakkachai Pengwang**

*Micro Robotics Laboratory, Institute of Field roBOTics (FIBO), King Mongkut's University of Technology Thonburi,  
126 Pracha-Utid Road, Bangmod, Thrung Kru, Bangkok, 10140 Thailand  
E-mail: pingpong\_ray2@hotmail.com, eakkachai@fibo.kmutt.ac.th  
www.fibo.kmutt.ac.th*

## Abstract

This paper presents the design of flapping systems for small air vehicle used in surveying robot for an area that is hard to access. This paper also focuses on flapping mechanism of micro unmanned aerial robots that are similar to birds and insects. Our design consideration will have a wingspan up to 15 centimeters. Enable technologies for fabrication of these designs are 3D printers by using polymer materials with low density and weight. Characterizations of flapping wings are simulated and examined in this paper. This micro flapping wing robot will be tested and performed in real environments.

*Keywords:* Micro Robots, Flying Robots, 3D Printers, Surveying Robot

## 1. Introduction

Flapping wing robots are inspired from nature and developed for several mechanisms. Main objective is to improve flying characteristics by imitating the flight of birds and insects [1-2]. Recent challenges are volume of devices, accessibilities, strength of material, and stability control of the flight. Designs of flapping wing robots are studied for many perspectives, for example, geometry and materials of wings, flapping mechanism, mechanical structure, radio system control, CFD (Computational fluid dynamics) analysis and power sources. Flapping mechanisms are investigated by using several methods. By using a commercial 3D printer, C. Richter and H. Lipson [3] fabricated a four-wing robot with a total weight of 3.89 grams. For analysis of aerodynamics of flapping wing robots, H. Liu *et. al.* [4]

has built a flapping wing robot and studied flow of air when the flapping robot is moving. This robot contains a clap and fling mechanism. Moreover, D. Mueller and J. W. Gerdes [5] designed a flapping wing robot by using a crack rocker mechanism. This study examined several folding mechanism for measuring a lift force in each design. J. H. Han *et. al.* [6] has reviewed information about flapping wing robots for a wing structure, flapping wing mechanism, flight control, and power source. H. Y. Chao *et. al.* [7] has compared specifications on microcontroller boards. For a power supply of flapping wing robots, M. Karpelson *et. al.* [8] has collected information about advantages and disadvantages in each type of power source. This study focuses on the mechanism design for bio-inspired flapping wing robots with a 3D-printer construction.

Different mechanism designs are evaluated and tested for the lift force measurements.

## 2. Design

### 2.1. First Generation Design

Our first design of flapping wing system is a Scotch yoke mechanism. The structure of this robot is made of ABS (Acrylonitrile Butadiene Styrene) plastics. In this study, the Scotch yoke mechanism is chosen for movement because this mechanism can move continuously and generate a high transmission force. This design consists of linkages to a DC motor and a

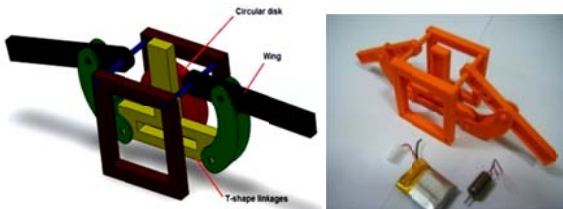


Fig. 1. The first generation of mechanism design for the flapping-wing robot. (a) CAD model (b) Fabricated prototype.

circular disc. Figure 1 shows a concept design of the first generation. When the circular disc is rotating, the T-shape linkage and the wing will consequently move upward and downward.

A testing result for the first generation showed that the T-shape linkage can move upward and downward in a slot wall. However, the gap distance between the slots of the upper part is larger than the width of the T-shape structure. This issue causes the inefficiency of the manipulation and the two wings cannot move simultaneously. Moreover, the T-shape linkage also moves with a high friction from the slot wall. It is also observed that the speed of flapping is reduced when the width of the slot is smaller.

### 2.2. Second Generation Design

As a testing result from the first generation, the second generation design is modified by using a crank rocker mechanism to reduce a friction in the assembly. In addition, the size and weight of the second design are reduced. Figure 2 shows a concept design of the second generation. The total weight of this design is eight

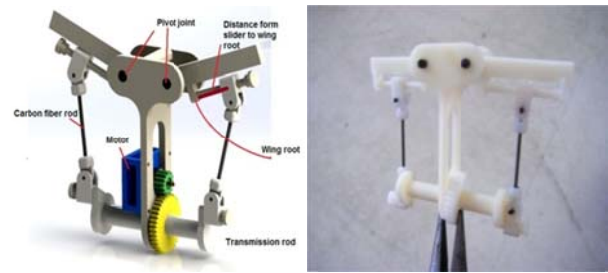


Fig. 2. The second generation of mechanism design for the flapping-wing robot. (a) CAD model (b) Fabricated prototype

grams. For these modifications, the point of rotation consists of two pivots and four joints to reduce the forces that act at wing.

When a DC motor rotates, the pinion gear drives the driver gear which is connected to a transmission rod. Two sides of transmission rod are linked to the carbon fiber rods that are connected to flapping wings. Carbon fiber is chosen for assembling this structure because it has a low weight and a high durability for external force. When the transmission rod rotates, carbon fiber rods push and pull a connected wing for upward and downward motions.

### 2.3. Third Generation Design

As a result from the testing, the second generation design still has a heavy weight. This design is improved



Fig. 3. The third generation of mechanism design for the flapping-wing robot.

for the size and weight. Material for this mechanism has also been changed from ABS plastics to a carbon fiber rod. The total weight of this design is reduced to six grams as shown in Figure 3.

### 3. Theoretical and Testing Analysis

Mechanical structures of the flapping-wing robots are analyzed for flight characteristics. Main parameter for this study is to analyze a wingspan angle. These wingspan angles are influenced by the length of carbon fiber rods and the distance from pivot points to the carbon fiber joints. This location is on a sliding bar that is connected to the wing. Mainly, the second generation design is characterized for a wingspan angle that is an angle of wing between upstroke and downstroke flight. The mathematical calculations are formulated by using Crank-rocker theorem in Gashof law and cosine rule.

This experimental results of wingspan angle correspond to the theoretical analysis. In figure 4, the different length of carbon fiber rods does not significantly affect to the values of wingspan angles. The range of averaged values of wingspan angles is

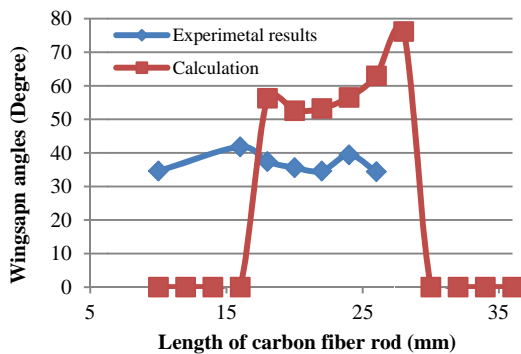


Fig. 4. Comparison between calculation and experimental results for different lengths of carbon fiber rod (when the distance from slider to wing root is 12 millimeters).

between 35 and 40 degrees. In figure 5, the distance from slider to wing root affects to wingspan angles. It is observed that increasing distance from slider to wing root will result to a decreasing wingspan angles.

### 4. Wing Design and Testing Flight

For a flight take-off, micro gear motor (gear ratio of 14:9) is used for an electrical actuator. The length of carbon fiber rod is 20 millimeters and the distance from slider to wing root is 10 millimeters. Flapping wing robots are assembled to wings that are made of plastic sheet. The length of wing is 15 centimeters. The structure of the wing is a plus-like shape. Two conditions of wing structure are evaluated for a testing flight. The first design is the wing structure with only carbon fiber. The second wing structure has rubber rods for a bending area when a robot is flapping. The objective of rubber rods is to enhance a wingspan angle. Figure 5 shows these two concept designs of the wing structure. It is assumed that the wing can collect more air under the wing with the rubber rods. This air collection under the wing becomes a thrust force for a flapping wing robot. Figure 6 shows the prototype is set up wing.

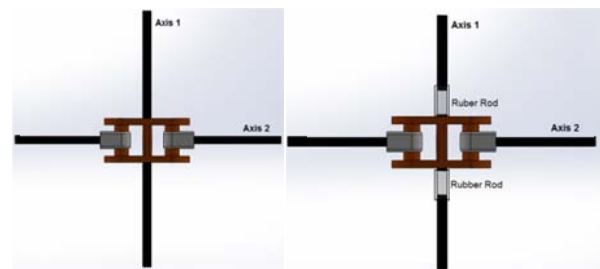


Fig. 5. Layout of two different wing structure (a) with only carbon fibers. (b) with rubber rods for a flexible wing.



Fig. 6. Third prototype is setup with the second design of wing structure. Wing is made from plastic sheet with a wingspan of 15 centimeters.

In testing flight, the measurement of lift force is evaluated for these bio-inspired flapping wing robots. The values of lift forces are approximated for the change in weight on a precise scale. The robots are hanged on a suspension and a rope is used to connect these robots to the scale as shown in Figure 7. When a robot is flapping, a tension force from the rope changes the weight value on the scale. This change in weight represents an approximated lift force of the flapping

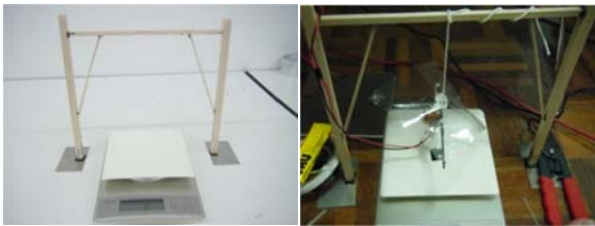


Fig. 7. A test setup with a suspension beam and a precise scale for measuring a lift force for bio-inspired flapping wing robots.

wing robot.

As a testing result, the first wing structure can generate an averaged lift force at 1.5 grams. The second wing structure that contains rubber rods can generate an averaged lift force at 2.5 grams. The performances are compared in Table 1.

**Table 1** Comparison on performances of bio-inspired flapping wing robots for difference wing structures at 5 V.

Wing Structures	Wing span (cm)	Flapping angle at axis 1	Total weight (g)	Avg. lift force (g)
Using only carbon fiber	15	0	6.6	1.5
Adding rubber rods for a flexible joints	15	15	6.7	2.5

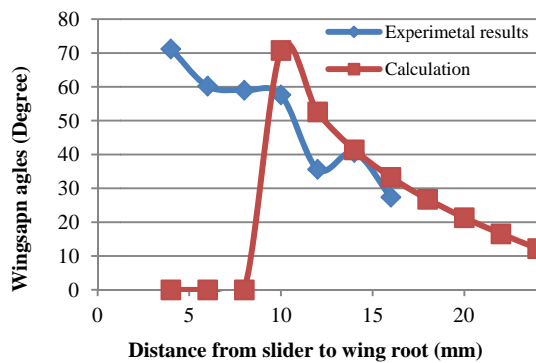


Fig. 5. Comparison between calculation and experimental results for different distance from slider to wing root (when the length of carbon fiber rod is 20 millimeters).

### 5. Conclusion

This study shows the design of bio-inspired flapping wing robots by using a 3D printer. The final design has a total weight of 6.6 grams. Moreover, the two different wing structures are analyzed for a lift. It is observed that the flexible joint with rubber rods can generate a higher lift force than the rigid wing structure. Hence, a flexible joint can increase a lift force for a bio-inspired flapping wing robot. However, these structures cannot generate an efficient lift force to overcome a weight of the robot. The modifications of motor speed and wingspan length will be implemented to improve the performance of these robots.

### Acknowledgements

This work is financially supported from the King Mongkut’s University of Technology Thonburi grant for new researchers. Authors also would like to thank to Professor Ben Parslew from University of Manchester and Professor Sutthipong Srijarom from University of Glasgow Singapore for intellectual discussions.

### References

1. T. J. Mueller, “Fixed and flapping wing aerodynamics for micro air vehicle applications”, Reston: Progress in astronautics and aeronautics, vol. 195, 2001.
2. B. W. Tobalske, D. R. Warrick, C. J. Clark, D. R. Powers, T. L. Hedrick, G. A. Hyder and A. A. Biewener, “Three-dimensional kinematics of hummingbird flight”, The Journal of Experimental Biology, The company of Biologists, pp. 2368-2382, 2007.
3. C. Richter and H. Lipson, “Untethered Hovering Flapping Flight of a 3D-Printed Mechanical Insect”, in Proc. A life XII Conference, Odense, Denmark, 2010.

4. H. Liu, X. Wang and T. Nakata, "Aerodynamics and Flight Stability of A Prototype Flapping Micro Air Vehicle", in Proc. International Conference on Complex Medical Engineering, Japan, 2012.
5. D. Mueller and J. W. Gerdes, "Incorporation of Passive Wing Folding in Flapping Wing Miniature Air Vehicles", in Proc. ASME Mechanism and Robotics Conference, San Diego, USA, 2009.
6. J. H. Han, J. S. Lee and D. K. Kim "Bio-inspired Flapping UAV Design: A University Perspective", in Proc. SPIE Conference Proceedings Vol.72951, 2009.
7. H. Y. Chao, Y. C. Cao and Y. Q. Chen, "Autopilots for Small Unmanned Aerial Vehicles: A Survey", International Journal of Control, Automation and Systems, pp. 36-44, 2010.
8. M. Karpelson, G. Y. Wei and R. J. Wood, "A Review of Actuation and Power Electronics Options for Flapping-Wing Robotic Insects", in Proc. IEEE International Conference on Robotics and Automation 2008, May 19-23, 2008.

## Effective rocking motion for inducing sleep in adults - Verification of effect of mother's embrace and rocking motion -

Keishi Ashida\*\*\*, Yoshifumi Morita\*\*\*, Ryojun Ikeura\*\*\*\*\*, Kiyoko Yokoyama\*\*\*\*\*, Ming Ding \*\*, Yuki Mori\*\*

\*Department of Computer Science and Engineering, Nagoya Institute of Technology  
Gokiso, Syouwa, Nagoya, Aichi 466-8555, Japan

E-mail: [k.ashida.353@stn.nitech.ac.jp](mailto:k.ashida.353@stn.nitech.ac.jp) / [morita@nitech.ac.jp](mailto:morita@nitech.ac.jp)

\*\*RIKEN- SUMITOMORIKO Collaboration Center for Human-Interactive Robot Research (RSC RIKEN)  
2271-130 Anagahora, Shimoshidami, Moriyama, Nagoya, Aichi 463-0003, Japan

\*\*\*Department of Mechanical Engineering, Mie University  
1577 Kurimamachiyacho, Tsu, Mie 514-8507, Japan

\*\*\*\*Department of Design and Architecture, Nagoya City University  
2-1-10 Kitachikusa, Chikusa, Nagoya, Aichi 463-0083, Japan

### Abstract

We investigated the most effective rocking motion for inducing sleep in adults. We prepared ten types of rocking motions, including two types of mother's rocking motions. The sleep-inducing effect of all the rocking motions was evaluated using Thurstone's paired comparison method (Case V). From statistical analysis of the subjective experimental results we found that, of the ten types of rocking motions, the linear motion component of a mother's rocking motions (Type 2) was the most effective for inducing sleep in adults.

*Keywords:* Rocking motion, Mother's rocking motion, Sleep-inducing effect, Thurstone's paired comparison method

### 1. Introduction

Recently, the number of people suffering from high levels of stress has increased, a phenomenon that has been called a *stressful society*.<sup>1</sup> Every year, more and more people suffer from stress-related illnesses. Moreover, sleep disorders are becoming more widespread in modern society because stress is one of the causes of insomnia. In nursing homes, it is a large burden for caregivers to assist patients to ensure the wellbeing of people who suffer from these problems.<sup>2</sup> Therefore, stress reduction and sleep induction are necessary for many people in modern society. It is generally known that when a baby is embraced and rocked by his or her mother, the baby feels comfortable

and falls asleep quickly. Therefore, we hypothesized that a rocking motion simulating a mother's embrace and rocking motion would have the same effects on adults. Against this background, the aim of our project is to develop a relaxation machine for reducing stress and inducing sleep by using a rocking motion simulating that of a mother. We expect that our research results will be used for other relaxation systems or robots in the future, for example the Robot for Interactive Body Assistance (RIBA), which is designed to assist caregivers by lifting patients in and out of their beds and wheelchairs.<sup>3</sup>

In our previous study, we analyzed a mother's embrace and rocking motion, and we designed and constructed an excitation apparatus simulating a mother's rocking motion. We found that there are two

© The 2015 International Conference on Artificial Life and Robotics (ICAROB 2015), Jan. 10-12, Oita, Japan

types of rocking motions given by a mother, and we constructed two models of these rocking motions.<sup>4</sup> From analysis of brain signals and subjective assessment, we found that the mother's rocking motions were more effective for inducing sleep in two healthy adults than in the case without rocking.<sup>5</sup> However, there were two problems with that study. One is that the number of subjects was small, and the other is that the sleep-inducing effects of different rocking motions have to be investigated.

In the work described in this paper, in addition to the two types of mother's rocking motions mentioned above, we prepared eight types of rocking motions to find the rocking motion that is most effective for inducing sleep in adults. We performed three experiments and evaluated the sleep-inducing effect by using Thurstone's paired comparison method.

## 2. Excitation apparatus simulating a mother's rocking motion

In our previous work we analyzed a mother's embrace and rocking motion to identify the features of the motion. From the results, we modeled a mother's rocking motion. The model of a mother's rocking motion is represented by

$$\begin{cases} x^{ref}(t) = A_x \sin(2\pi f_x t), \\ \theta^{ref}(t) = A_\theta \sin(2\pi f_\theta t + \phi) + B_\theta, \end{cases} \quad (1)$$

where  $x^{ref}(t)$  and  $\theta^{ref}(t)$  are the position and the angle of the center of gravity of the baby, respectively, and  $B_\theta$  was determined from the angle of a comfortable sitting position reported in Ref. 6. Then, we realized this rocking motion using the excitation apparatus shown in Fig. 1. The excitation apparatus has two degrees of freedom, one for linear motion and one for rotational motion. The rocking chair is driven by a linear motor and a rotary motor. The rotary motor is connected to the chair through a timing belt for rotation. The drive systems of the excitation apparatus are composed of speed-reference-type servo amplifiers for the linear and rotary motors, linear and rotary encoders, and a DSP board (dSPACE DS1104). The DSP board is used to implement the controllers for the linear and rotary motors. We designed controllers for the excitation apparatus using PD control and feed-forward control in

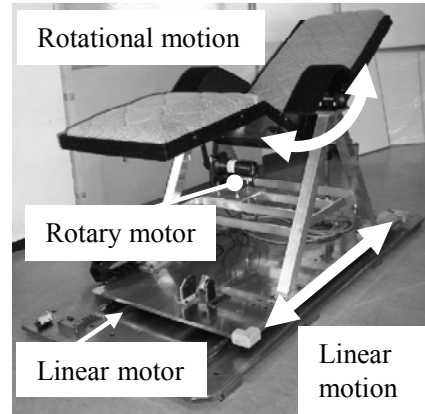


Fig. 1. Photograph of excitation apparatus.

order to simulate a mother's rocking motions in the excitation apparatus.

## 3. Experimental method

We performed experiments for finding the most-effective rocking motion for inducing sleep. The sleep-inducing effect of each rocking motion was evaluated on a numerical scale using Thurstone's paired comparison method (Case V)<sup>7,8</sup>. We verified the validity of adopting this method by using Mosteller's goodness-of-fit test. Moreover, we evaluated the confidence of the scale values.

The subjects were nine healthy males (average age, 25.4 years). The subjects wore ear muffs for sound insulation during the experiment, had their eyes closed, and rested in a supine position on the chair which was rocked by the excitation apparatus. The experimental protocol is shown in Fig. 2. R1, R2, R3, and R4 denote the types of rocking motions used in the experiment. After every two rocking motions, the subjects answered the question, "Which of the two rocking motions was more effective for inducing sleep?". The evaluation was performed with six different combinations of four rocking motions for each experiment. In order to reduce the influence of an order effect, we divided the subjects into two groups and used six combinations (Types R1 and R2, Types R1 and R3, Types R1 and R4, Types R2 and R3, Types R2 and R4, and Types R3 and R4) in two different orders, namely, Procedure 1 and Procedure 2, as shown in Fig. 2.



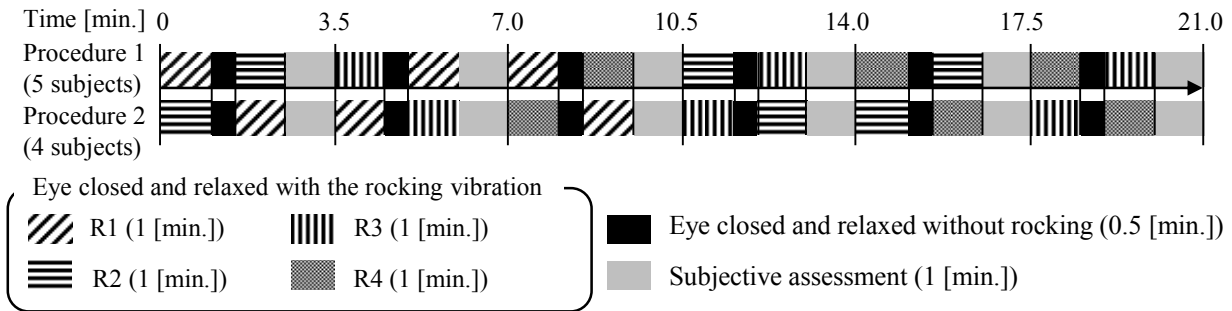


Fig. 2. Experimental protocol for finding the most-effective rocking motion in Experiments I, II, and III.

#### 4. Experiments

We performed three different experiments, Experiments I, II, and III, which are detailed below.

##### 4.1. Rocking motions used in Experiment I

We prepared four types of rocking motions, namely two types of mother’s rocking motions (Type 1 and Type 2), a rocking motion imitating the motion of a rocking chair (Type 3), and a rocking motion that has a high correlation with motion sickness (Type 4). In Fig. 2, R1, R2, R3, and R4 correspond to Type 1, Type 2, Type 3, and Type 4, respectively. Type 3 was added to the candidates because a rocking chair is known to have a relaxation effect.<sup>9</sup> Type 4 was added to the candidates as an uncomfortable rocking motion in this comparative study. The parameters of Type 1, Type 2, and Type 4 are shown in Table 1.

In order to produce the motion of a rocking chair shown in Fig. 3, we first measured the motion of an actual rocking chair by using a 3D motion capture system (Motion Analysis) when an adult male was seated in the rocking chair. Type 3 is the rocking motion produced after the experimenter lowered the backrest of the rocking chair and released it. The motion of the rocking chair consists only of rotary motion. We set the amplitude of the rotary motion to as large a value as possible within a range that was comfortable for the subject. Moreover, the rotary angle in the steady state was set to 25 degrees, which is the same as the angle determined from the angle of a comfortable sitting

position reported in Ref. 6. The Type 3 rocking motion is shown in Fig. 4.



Fig. 3. Photograph of rocking chair.

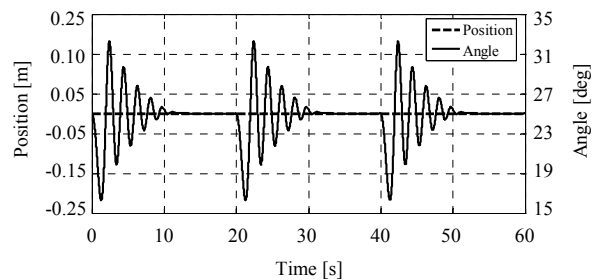


Fig. 4. Rocking motion (Type 3).

The Type 4 rocking motion is represented by Eq. (1). The frequency was determined to be 0.063 Hz, which has been shown to have a high correlation with motion sickness<sup>10</sup>. The amplitude was determined so that the acceleration was almost the same as those of other rocking motions and within the range of acceleration that can be produced by the excitation apparatus. The

Table 1. Parameters of the rocking motions.

Parameter	Type 1	Type 2	Type 4	Type 5	Type 6	Type 7	Type 8	Type 9	Type 10
$A_x$ [m]	0.115	0.098	0.250	0.095	0.100	0.098	0.098	0.060	0
$A_\theta$ [deg]	2.455	2.734	10.0	3.136	2.332	2.734	0	0	2.734
$B_\theta$ [deg]	25	25	25	25	25	25	25	25	25
$f_x$ [Hz]	0.326	0.234	0.063	0.226	0.243	0.234	0.234	0.468	0
$f_\theta$ [Hz]	0.326	0.234x2	0.063	0.226x2	0.243x2	0.234x2	0	0	0.234x2
$\phi$ [rad]	$\pi$	$\pi/2$	$\pi$	$\pi/2$	$\pi/2$	$-\pi/2$	$\pi/2$	$\pi/2$	$\pi/2$

parameters of the Type 4 motion are also shown in Table 1.

#### 4.2. Results in Experiment I

From the results of the paired comparison method, we obtained the frequency distribution matrix shown in Table 2. Table 2 shows the number of subjects who offered the response “The first rocking motion was more effective for inducing sleep than the second rocking motion”. The first and second rocking motions are shown in the rows and columns of Table 2, respectively. The scale values for the sleep-inducing effect of the rocking motions were derived by applying Thurstone’s paired comparison method (Case V) to Table 2. The scale values are shown in Table 3. From Table 3, we can rank the four types of rocking motions based on their sleep-inducing effects as follows:

$$\text{Type 2} > \text{Type 1} > \text{Type 3} > \text{Type 4}.$$

Moreover, we verified the validity of adopting Thurstone’s paired comparison method (Case V) by using Mosteller’s goodness-of-fit test. The goodness-of-fit,  $\chi^2$ , was 3.52, and the flexibility,  $df$ , was 3, meaning that a 5% significance level was not rejected. Therefore, Thurstone’s paired comparison method (Case V) can be adopted for evaluating the sleep-inducing effect.

We examined the significant differences between the four rocking motions by using the method proposed in Ref. 11. The result is shown in Fig. 5. We found that the 95% confidence interval of Type 1 overlapped with that of Type 3. The combination of Type 1 and Type 3 showed no significant difference, whereas the other five combinations showed significant differences. In other words, of the four types of rocking motions, we found

that Type 2 was the most effective for inducing sleep in adults and Type 4 was the least effective.

Table 2. Frequency distribution matrix in Experiment I.

	Type 1	Type 2	Type 3	Type 4
Type 1	—	6	3	2
Type 2	3	—	2	0
Type 3	6	7	—	2
Type 4	7	9	7	—

Table 3. Scale values of different rocking motions in Experiment I.

	Type 1	Type 2	Type 3	Type 4
Scale value	0.19	1.06	-0.11	-1.15

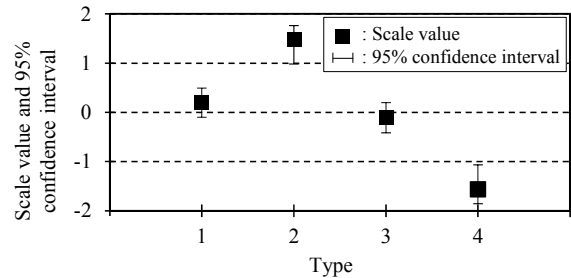


Fig. 5. Scale values and 95% confidence intervals of the four types of rocking motions in Experiment I.

#### 4.3. Rocking motions used in experiment II

We prepared three types of rocking motions, namely Type 5, Type 6 and Type 7, in addition to Type 2. In Fig. 2, R1, R2, R3, and R4 correspond to Type 2, Type 5, Type 6, and Type 7, respectively. Type 5 was a rocking motion based on one given to a 5 kg baby in another study<sup>5</sup>, and Type 6 was a rocking motion based on one

given to a 7 kg baby in the same study. More details of these rocking motions are shown in Ref. 5. Type 7 was the same as Type 2 except for the phase, which differed by 180 deg. These parameters are shown in Table 4.

#### 4.4. Results in Experiment II

Figure 6 shows the scale values and the 95% confidence intervals for the sleep-inducing effect of the rocking motions obtained using Thurstone's paired comparison method (Case V) and the method proposed in Ref. 11. From the scale values in Fig. 6, we can rank the four types of rocking motions based on their sleep-inducing effects as follows:

$$\text{Type 2} > \text{Type 6} > \text{Type 5} > \text{Type 7}.$$

Moreover, the validity of adopting Thurstone's paired comparison method (Case V) for evaluating the sleep-inducing effects was confirmed in the same way as in Experiment I.

In Fig. 6, the combination of Type 2 and Type 7 showed a significant difference, whereas the other five combinations showed no significant differences. We concluded that, of the four types of rocking motions, Type 2 was the most effective for inducing sleep in adults. As for the reason why no significant differences appeared, we considered that the evaluations were uneven because it was difficult for subjects to discriminate the small differences in the frequency and amplitude. In this situation, Type 7 was chosen as the least effective rocking motion. With the Type 7 motion, the subjects reported slight motion sickness.

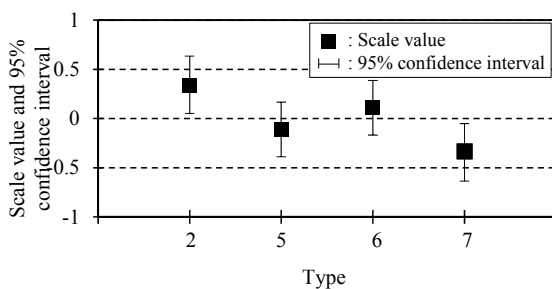


Fig. 6. Scale values and 95% confidence intervals of the four types of rocking motions in Experiment II.

#### 4.5. Rocking motions used in Experiment III

In order to find a more effective rocking motion for inducing sleep, in Experiment III, we focused on the components of the Type 2 motion. We prepared three types of rocking motions, namely, Type 8, Type 9 and Type 10, in addition to Type 2. In Fig. 2, R1, R2, R3, and R4 correspond to Type 2, Type 8, Type 9, and Type 10, respectively. Type 8 was a rocking motion consisting of only the linear motion component of Type 2. Type 9 was also a rocking motion consisting of only linear motion that was reported to be effective for inducing sleep in babies in Ref. 12. Type 10 was a rocking motion consisting of only the rotational motion component of Type 2.

When the frequency of the rocking motion used in Ref. 12 is used instead of the frequency of Type 8, the acceleration is too large. For this reason, the amplitude  $A_x$  was set to a smaller value, and the frequency  $f_x$  was set to a small value, namely, the frequency  $f_\theta$  of the rotary motion component of Type 7. This rocking motion is Type 9. These parameters are shown in Table 1.

#### 4.6. Results in Experiment III

Figure 7 shows the scale values and the 95% confidence intervals for the sleep-inducing effect of the rocking motions obtained by using Thurstone's paired comparison method (Case V) and the method proposed in Ref. 11. From the scale values in Fig. 7, we can rank the four types of rocking motions based on their sleep-inducing effects as follows:

$$\text{Type 8} > \text{Type 10} > \text{Type 2} > \text{Type 9}.$$

Moreover, the validity of adopting Thurstone's paired comparison method (Case V) for evaluating the sleep-inducing effect was confirmed in the same way as in Experiment I.

In Fig. 7, the three combinations including Type 9 (Types 2 and 9, Types 8 and 9, and Types 9 and 10) showed significant differences, whereas the other three combinations showed no significant differences. However, there is a significant difference in the combination of Type 8 and Type 10 if the confidence interval is changed to 80% instead of 95%. Therefore, of the four types of rocking motions, we concluded that

Type 8 is the most effective for inducing sleep in adults. The reason why Type 9 was identified as the least effective rocking motion was that the acceleration of Type 9 is too large, based on the subjects' opinions. We found that the acceleration was related to the effective motion for inducing sleep.

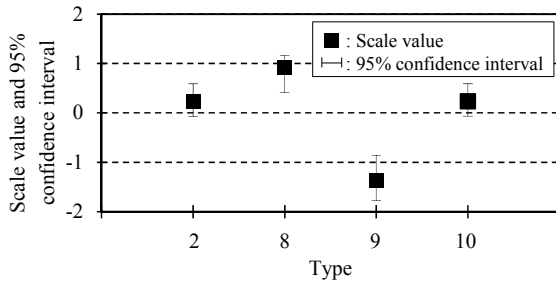


Fig. 7. Scale values and 95% confidence intervals of the four types of rocking motions in Experiment III.

## 5. Conclusion

From subjective experimental results, we found that, of the ten types of rocking motions examined, the linear motion component of a mother's rocking motion (Type 2) was the most effective rocking motion for inducing sleep in adults.

In future work, we plan to confirm that the Type 8 rocking motion, which is the linear motion component of a mother's rocking motion (Type 2), is effective for inducing sleep and reducing stress in adults by using electroencephalogram (EGG) analysis. We will also compare the Type 8 rocking motion and aromatherapy, which is a popular natural way of inducing sleep and bringing about relaxation.

## References

1. Ito, H. and Ishino, Y., Adverse Effects of Sleep Deprivation, *Iho Fuji*, No.124 (2003) (in Japanese), p.1.
2. Mishima, K., Sleep Problems in Dementia, *Proceedings of the Annual Meeting of the Japanese Research Group on Senile Dementia*, Vol.17 (2010) (in Japanese), pp.109-113.
3. RIKEN-TRI Collaboration Center for Human-Interactive Robot Research (RTC), World's first robot that can lift up a human in its arms, RIBA, (online), available from <<http://rtc.nagoya.riken.jp/RIBA/index-e.html>>, (accessed on 13 June, 2014)
4. Yamaguchi, K., Kobayashi, H., Morita, Y. Sakaïda, Y. Ikeura, R. and Yokoyama, K., Motion Analysis of Mother's Embracing and Rocking a Baby and Development of Excitation Apparatus, *Proc. of Int. Conf. on Control, Automation and Systems 2011 (ICCAS2011)* (2011) pp.1792-1796.
5. Morita, Y., Yamaguchi, K., Ashida, K., Ikeura, R. and Yokoyama, K., Verification of Sleep-Inducing Effect by Excitation Apparatus Simulating Mother's Embrace and Rocking Motion, *Proceedings of the 9th International Workshop on Robot Motion and Control (RoMoCo '13)* (2013), pp.80-85.
6. Sasaki, Y., Kawamoto, T. and Ymazaki, N., Development of an Experiment Bed for Searching Comfort Semi-Sitting Position, *Japanese Journal of Ergonomics*, Vol.42, No.6 (2006), pp.373-380.
7. Research Committee of Sensory Evaluation, *Sensory Evaluation Handbook*, JUSE ed., JUSE Press, Ltd., Japan (1973), pp.471-476.
8. Ichikawa, H., A Study of Representing Content for a Special 3D Display (2010) (in Japanese), pp.34-41.
9. Tamakoshi, S., Yamamoto, N., Morimoto, F., Nagae, S., Ichiba, H. and ISO, H., Engineering Psychology on the Relaxation Effects of a Rocking chair, *Behavioral Science Research*, Vol.50, No.2 (2012) (in Japanese), pp.101-105.
10. Siroto, H., Evaluation Method of Motion Sickness in Trains Using Low-frequency Lateral Vibration, *Railway Research Review*, Vol.130 (2006) (in Japanese), pp.38-39.
11. Tabata, Y., Ohga, Y., Kakuta, M., Nakamae, M., Morioka, M., Uto, F., Okunishi, T., Oti, T. and Maeda, K., Confidence Coefficient of Subjective Scale Value in Method of Paired Comparisons (Case V), *Japanese Society of Radiological Technology*, Vol.51, No.4 (1995) (in Japanese), pp.445-449.
12. Fuji, T., Furusawa, T., Takenouchi, T. and Tomotari, M., Development of Electric Bed for Babies for Parenting Support, *Japan Society for Design Engineering* (2006) (in Japanese), pp.19-20.

# Postural Sway Response to Local Vibratory Stimulation in Young, Middle-aged and Elderly People in Standing Position

**Ayaka Yamada, Eishi Nakamura, Noritaka Sato, Yoshifumi Morita**

*Nagoya Institute of Technology  
Gokiso-cho, Showa-ku, Nagoya, Aichi 466-8555, Japan*

**Tadashi Ito, Yoshihito Sakai**

*National Center for Geriatrics and Gerontology  
7-430, Morioka-cho, Obu City, Aichi 474-8511, Japan*

**Kazunori Yamazaki**

*Fujita Health University  
1-98 Dengakugakubo, Kutsukake-cho, Toyoake, Aichi 470-1192, Japan*

*E-mail: a.yamada.067@stn.nitech.ac.jp, e.nakamura.335@stn.nitech.ac.jp, sato.noritaka@nitech.ac.jp, morita@nitech.ac.jp, tada-ito@ncgg.go.jp, jsakai@ncgg.go.jp, ymzkk@fujita-hu.ac.jp*

## Abstract

We investigated the postural sway in response to local vibratory stimulation applied to young, middle-aged and elderly people in the standing position. For this purpose we developed a variable-frequency vibratory stimulation device and measured the postural sway using a gravicorder. As a result, when the vibratory stimulation was applied to the gastrocnemius muscles, the center of pressure moved backward in all subject groups. We found that elderly people with low back pain may perform balance control using their trunks more than their lower legs.

*Keywords:* Vibratory stimulation device, Proprioception, Postural sway, Low back pain, Fall prevention

## 1. Introduction

Falls accidents and low back pain in the elderly are two common problems in modern Japanese society. Up until 2009, over 1800 elderly people died from fall accidents per year.<sup>1</sup> Low back pain is also a serious issue, but the causes are unidentifiable in 85% of patients.<sup>2</sup> One possible factor is the problem of postural control involving voluntary and reflexive muscle responses, as suggested by one study in which it was reported that the elderly and people with low back pain have postural control problems involving deterioration of somatosensory receptors.<sup>3</sup>

To detect the motion of the body and adjust voluntary and reflexive muscle responses, the balance

system uses not only sensory information from visual and vestibular senses but also somatosensory receptors<sup>4</sup> that give superficial sensation and proprioceptive sensation. Moreover, proprioception in the leg and trunk muscles plays an important role in maintaining postural stability.<sup>5</sup> Proprioceptive receptors have eigen response frequencies. Past studies have reported that when vibratory stimulations are applied, the postural sway in the standing position changes.<sup>6</sup> Therefore, from the change of the postural sway during vibratory stimulations with various frequencies, we may be able to determine the cause of low back pain and falls and develop a treatment system for proprioception for recovery to solve these two problems.

On the other hand, other studies have reported that proprioception and vibration sensation in the lower legs decrease with aging.<sup>7</sup> Moreover, postural instability has been observed in elderly people.<sup>8</sup> That study and others, however, examined the postural sway of each age group in response to local vibratory stimulation applied using different vibratory stimulation devices under different experimental conditions.

Against such a background, the final goal of our research is to develop a treatment system for proprioception. To achieve this goal, the procedure involves investigating postural sway in response to local vibratory stimulation applied to human subjects in the standing position, to find the frequency of the vibratory stimulation and the body parts related to low back pain and falls, which will help to determine the causes of low back pain and falls.

In the work described in this paper, we developed a variable-frequency vibratory stimulation device and measured the postural sway response of young, middle-aged, and elderly people to local vibratory stimulation when in the standing position. We focused on low back pain and investigated the frequencies of vibratory stimulation and the body parts related to low back pain.

## 2. Variable-frequency vibratory stimulation device

We developed the variable-frequency vibratory stimulation device shown in Fig. 1. The device consists of a laptop computer, an audio amplifier, four vibrators, and a switch for selecting one of the vibrators. A sine wave signal with an arbitrary frequency generated on the laptop computer is input to the audio amplifier. By regulating the gain of the audio amplifier, the amplitudes of the vibrators can be changed. The range of displacement of the vibrators is 0–0.8 mm, and the frequency range is 30–400 Hz. Each vibrator is fixed to a holder. The four vibrators are attached to the left and right gastrocnemius muscles (GM) and the left and right lumbar multifidus (LM) with rubber belts. The lengths of the rubber belts are adjusted according to the perimeters of the body parts to which they are fixed to keep the pushing forces constant. As a gravicorder, we use a Wii Balance Board (Nintendo Co., Ltd.). The Wii Balance Board has been reported to be reliable enough for medical use.<sup>9</sup>

© The 2015 International Conference on Artificial Life and Robotics (ICAROB 2015), Jan. 10-12, Oita, Japan

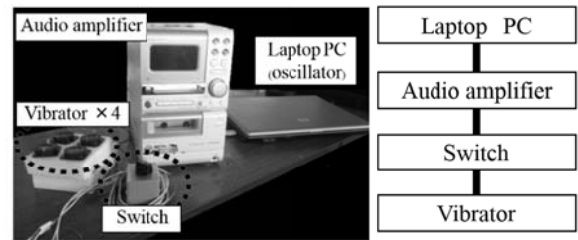


Fig.1. Photograph and block diagram of variable-frequency vibratory stimulation device.



Fig.2. Subject wearing the device.

## 3. Experiment

### 3.1. Purpose

The purpose of the experiment was to investigate the postural sway response to local vibratory stimulation applied to young, middle-aged, and elderly people in the standing position by using the vibratory stimulation device that we developed, together with the Wii Balance Board.

### 3.2. Subjects

The subjects were 25 healthy young people (12 males and 13 females, aged  $21.6 \pm 1.2$ ), 25 healthy middle-aged people (13 males and 12 females, aged  $46.0 \pm 3.0$ ), 46 elderly people with lumbar spondylosis without low back pain (28 males and 18 females, age =  $73.8 \pm 5.3$ ), and 28 elderly people with lumbar spondylosis with low back pain (10 males and 18 females, age =  $75.5 \pm 5.1$ ).

Table 1. Measurement procedure  
(GM: Gastrocnemius muscles, LM: Lumbar multifidus)

	Frequency	Body part where vibratory stimulation is applied
Step 1	30 Hz	GM
Step 2	30 Hz	LM
Step 3	60 Hz	GM
Step 4	60 Hz	LM
Step 5	150 Hz	GM
Step 6	150 Hz	LM
Step 7	240 Hz	GM
Step 8	240 Hz	LM

### 3.3. Method

The center of pressure (CoP) in postural sway while the subject stood still on the Wii Balance Board was measured as shown in Fig. 2. The subject stood barefoot on the Wii Balance Board with his/her feet together and his/her eyes open or closed. The subject was instructed to remain still and relaxed in the standing posture with his/her arms hanging loosely at his/her side.

One measurement for each subject consisted of eight steps for the different vibration frequencies and the different body parts where the vibratory stimulation was applied. The measurement procedure is shown in Table 1. An interval of 60 s was added after every step, during which each subject sat resting in a chair. Figure 3 shows the experimental procedure in one step. The time needed for one step was 75 s. One step consisted of five sections, namely, “EO”, “EC”, “Pre”, “Dur” and “Post”. The time needed for one section was 15 s. In the EO-section, the subject looked at a marker on the wall. In the EC-section and the Pre-section, the eyes were closed. Only in the Dur-section, the vibratory stimulation was applied to the subject with the eyes closed. In the Post-section, the subject's eyes were closed.

The vibratory stimulation was applied alternately to the two muscles (GM and LM). The amplitude of the vibration was set to 0.8 mm. The frequencies were set to 30, 60, 150, and 240 Hz. It is well-known that the eigen response frequencies of Meissner’s corpuscle, muscle spindle, and the corpuscle of Vater-Pacini are 30 Hz, 60 Hz, and 240 Hz, respectively.<sup>10</sup>

### 3.4. Experimental results

We paid attention to the Pre-section and the Dur-section in order to analyze postural sway during local vibratory stimulation in the standing position. For this purpose we used two parameters related to the CoP, namely, the anterior movement of the CoP ( $\Delta MY$ ), and the relative proprioceptive weighting ( $RPW$ ) ratio.  $\Delta MY$  is defined as the difference between the mean values of the

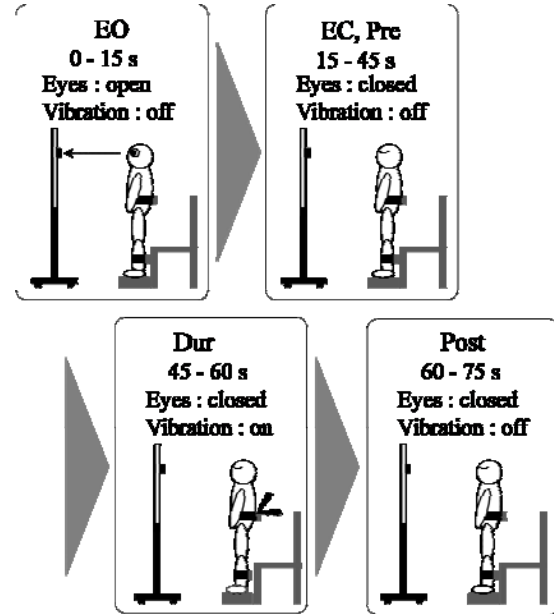


Fig.3. Experimental procedure.

anterior displacement of the CoP in the Pre-section and the Dur-section, which is given by

$$\Delta MY = MY_{Pre} - MY_{Dur}, \quad (1)$$

where

$$MY_{Pre} = \text{Mean}_{Pre} \{Y_{CoP}(k)\}$$

$$MY_{Dur} = \text{Mean}_{Dur} \{Y_{CoP}(k)\}$$

$$Y_{CoP}(k) = y_{CoP}(k) - y_{CoP}(0)$$

Here,  $\text{Mean}_{xx} \{ \cdot \}$  denotes the mean of  $\{ \cdot \}$  during  $xx$ ,  $y_{CoP}(k)$  is the  $y$ -displacement of the CoP,  $k$  represents the sample index, and  $y_{CoP}(0)$  is the value of  $y_{CoP}(k)$  at the start of measurement.  $\Delta MY$  is calculated in each step.  $\Delta MY_{GM}$  and  $\Delta MY_{LM}$  denote the  $\Delta MY$  values for the gastrocnemius muscles and lumbar multifidus, respectively. The  $RPW$  ratio is defined by

$$RPW = \frac{|\Delta MY_{GM}|}{|\Delta MY_{GM}| + |\Delta MY_{LM}|}. \quad (2)$$

As the *RPW* ratio approaches 100%, GM is used more than LM in motor control during quiet standing. This means that a lower leg-steered strategy is used in motor control. As the *RPW* ratio approaches 0%, this means that a trunk-steered strategy is used in motor control.

The experimental results are shown in Fig. 4, which shows the relationship between the frequency and  $\Delta MY$ , and the relationship between the frequency and the *RPW* ratio.

### 3.5. Discussion

Fig. 4(a), (d), (g) and (j) show that when the 60 Hz vibratory stimulation was applied to the GM, the CoP moved backward in all subject groups. This result is similar to the results obtained in previous studies<sup>6,7</sup>. Therefore, the proposed vibratory stimulation device and the experimental method using the developed device were confirmed to be effective in measuring the postural sway during local vibratory stimulation. Moreover, Fig. 4(a), (d), (g) and (j) show that when the vibratory stimulations with the frequencies of 30 Hz, 150 Hz, and 240Hz were applied to the GM, the CoP also moved backward in all subject groups.

On the other hand, Fig. 4(b), (e), (h) and (k) show that when the vibratory stimulations were applied to the LM, the CoP moved backward or forward regardless of the change of frequency. This means that the biological response to vibration is uncertain.

Fig. 4(l) shows that as the frequency increased, the *RPW* ratio decreased. This response is a characteristic seen only in elderly people with low back pain. The same tendency was not seen in the other subject groups, as shown in Fig. 4(c), (f) and (i). This means that the *RPW* ratio does not depend on the frequency. Therefore, the results for the *RPW* ratios suggest that elderly people with low back pain performed balance control using their trunk more than their lower legs when vibratory stimulation with higher vibration frequency was applied.

### 4. Conclusion

In this paper, we investigated the postural sway in response to local vibratory stimulation applied to young, middle-aged, and elderly people in the standing position. For this purpose we developed a variable-frequency

vibratory stimulation device and measured the postural sway according to our experimental method.

As a result, we found that our device and the experimental method were effective in measuring the postural sway during local vibratory stimulation. Moreover, from the result for the *RPW* ratio, we found that elderly people with low back pain used a trunk-steered strategy in motor control.

Future work related to this study will be to analyze the relationship between the postural sway and falls, to determine the causes of low back pain and falls through additional experiments, and to develop a treatment system for proprioception.

### References

1. VITAL STATISTICS, Statistics and Information Department, Minister's Secretariat, Ministry of Health, Labor and Welfare JAPAN, <http://www.mhlw.go.jp/english/database/db-hw/index.html>
2. A. Richard, R. James and L. Daniel, What can the history and physical examination tell us about low back pain? *J. the Am. Med. Assoc.* **268** (1992) 760-765.
3. T. Urushihata and T. Kinugasa, Aging effects on the structure underlying balance abilities tests, *Tairyokukagaku* **56**(6) (2007) 711. (In Japanese)
4. R. Johansson and M. Magnusson, Human postural dynamics *Crit. Rev. Biomed. Eng.* **18** (1991) 413-437.
5. B. Bloem, J. Allum, M. Carpenter and F. Honegger, Is lower leg proprioception essential for triggering human automatic postural responses?, *Experimental Brain Research* **130** (2000) 375-391.
6. B. Simon, C. Paul and V. Sabine, Proprioceptive weighting changes in persons with low back pain and elderly persons during upright standing *Neuroscience Letters.* **366** (2004) 63-66.
7. B. Skinner, L. Barrack and D. Cook, Age-related decline in proprioception *Arch. Phys. Med. Rehabil.* **44** (1963) 645-650.
8. I. Pyykkö, P. Jäntti and H. Aalto, Postural control in elderly subjects, *Age Aging.* **19** (1990), 215-221.
9. A. Clark and L. Bryant, Validity and reliability of the Nintendo Wii Balance Board for assessment of standing balance *Gait & Posture.* **31** (2010) 307-310.
10. T. Ito, Y. Sakai, A. Kubo, K. Yamazaki, Y. Ohno, E. Nakamura, N. Sato, Y. Morita. The relationship between physical function and postural sway during local vibratory stimulation of middle-aged people in the standing position *J. Phys. Ther. Sci.* **26**(10) (2014) 1627-1630.



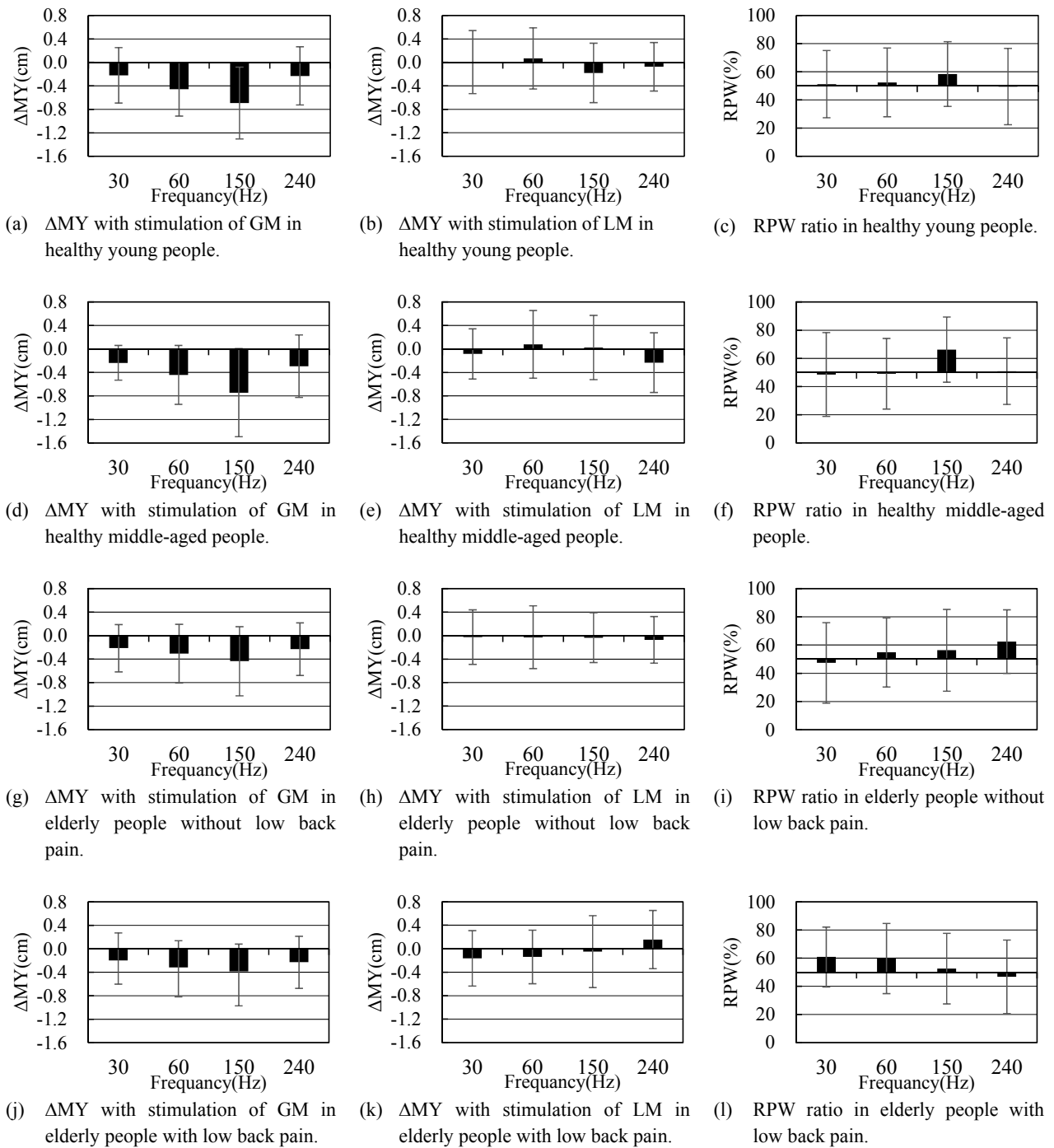


Fig.4. Frequency dependence of  $\Delta MY$  and RPW ratio.

# Development of Unmanned Transport System for Automated Systems

**Hyunhak Cho**

*Department of Interdisciplinary Cooperative Course: Robot, Pusan National University,  
10313, 2, Busandaehak-ro 63beon-gil, Geumjeong-gu, Busan, 609-735, Korea*

**Jungwon Yu, Yeongsang Jeong, Hansoo Lee, Sungshin Kim**

*Department of Electrical and Computer Engineering, Pusan National University,  
10313, 2, Busandaehak-ro 63beon-gil, Geumjeong-gu, Busan, 609-735, Korea  
E-mail: {darkruby1004, garden0312, dalpangi03, hansoo, sskim}@pusan.ac.kr  
www.pusan.ac.kr*

## Abstract

Unmanned transport systems are used in many industries owing to their high efficiency, such as transport of high loads, 24 hour a day use and low cost. Many components of industry are being changed to unmanned transport system. Therefore, this paper introduces application and composition of the unmanned transport systems in industry to the transport, and describes the selected method by the environment conditions. Unmanned transport system is comprised of an Automatic Guidance Vehicle and a Monitoring system. The applied AGV is guided by localization information, which is measured by a laser navigation guidance system with encoders and gyroscope. AGV require a virtual driving path method with map information from conveyor positions and rotation points in an environment, as well as automatic load/unload system for cargo transport, an emergency system for safety, and a communication system with an automatic charger and monitoring system.

*Keywords:* Autonomous guidance system, Localization, Telescope Load/Unload System

## 1. Introduction

Many industries; manufacturing plants, warehouses, port facilities and so on are changing to automatic systems through the development of unmanned robot technology. Automatic production systems in various industrial systems have many components, and the material handling system of components is very important because of its potential to reduce cost. Material handling system means a load /unload/ transport/storage system.

Recently, there has been increasing interest in unmanned transport system to satisfy the flexibility and efficiency of material handling system. The unmanned transport system is an aggregate of various technologies,

such as localization, driving control, load/unload system, path planning, monitoring system, and so on. The technologies of the unmanned transport system are general, and detailed technologies for the LGV are selected according to the conditions of the environment. The AGVs are a changed guidance system; floor state, plant size, maintenance, and so on, wheel type; floor state, oil, and so on, load/unload; conveyor, palette type, and so on system according to the conditions of the environment [1]-[6].

This article introduces the application of the unmanned transport system; AGV and Monitoring system with the combined technology of the mentioned content to the industry field. Among the range of wireless guid-

ance systems available, this study used encoders, a gyroscope and laser navigation. In addition, virtual path planning was used for the wireless guidance system, the driving wheel structure was the differential driving structure, and the controller was an industrial PC. Load/unload system for the cargo used the telescopic type due to the type of palette and conveyor.

Chapter 2 discusses the hardware configuration of the unmanned transport system; load/unload system, body frame of AGV Chapter 3 presents the software configuration of the unmanned transport system; localization, driving controller, virtual path planning. Chapter 4 presents the conclusion.

### 2. Hardware Configuration

In this article, unmanned transport system; AGV, Monitoring system was designed by the present and ATIS (Company in Korea). Fig 1 shows the appearance of the manufactured LGV. Laser navigation, encoders and a gyroscope were used for the localization of LGV. The global position  $(x, y, t)$  of localization information was measured using laser navigation. The local position  $(x, y, t)$  of localization information was calculated by the kinematics with encoders and a gyroscope.

The load/unload system is affected by cargo, conveyor and pallets. Therefore, the telescopic type load/unload system was selected. The system was composed a fixed frame, body frame for moving; left, right and two arms on the body frame for settling the pallet; cargo. The detailed components are the left-right motor for the body frame, up-down motor 2 for the arms.

### 3. Software Configuration

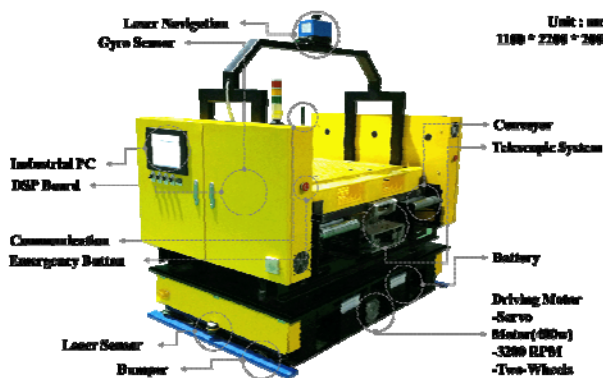


Fig. 1. Autonomous Guidance Vehicle

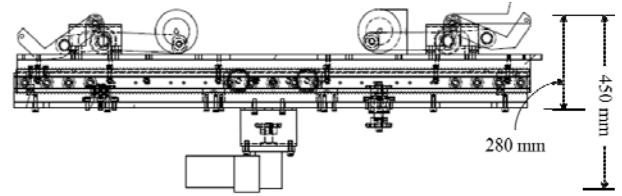


Fig. 2. Telescopic Load/Unload System

The LGV is guided by the laser navigation, encoders and gyroscope of the localization sensors. The laser navigation sensor measured the difference distance and angle between the header of the laser navigation and attached reflectors in the field through a time delay; transmit-receive. The laser navigation calculated the current position of the LGV through a triangulation method using the measured information and saved position information of the reflectors.

AGV with a wireless guidance system is controlled by the error angle. The control system using this method was unstable because of the large increase in the error angle when the distance between the AGV position and destination point was close. Therefore, in this study, the error angle and derailment distance between the current position and driving path was used in equation 1.

$$E = E_d \times a + E_\theta \times (1 - a) \tag{1}$$

The  $a$  in the equation is the ratio, and  $E_d$  and  $E_\theta$  are the derailment distance and error angle. The composition of the equation is the same as shown in Fig 3.

$$E_d = \frac{|aA_x + bA_y + c|}{\sqrt{a^2 + b^2}} \tag{2}$$

$$\begin{aligned} E_\theta &= D_\theta + T_\theta \\ D_\theta &= N_\theta - S_\theta \\ T_\theta &= N_\theta - A_\theta \end{aligned} \tag{3}$$

$D_\theta$  in the equation is the difference between the angles (angle of LGV position Destination position, angle of Virtual Path Destination position).  $T_\theta$  is the angle of the LGV. The voltage difference of the wheels was calculated by  $E$  in Equation 6 with a PD controller, and the

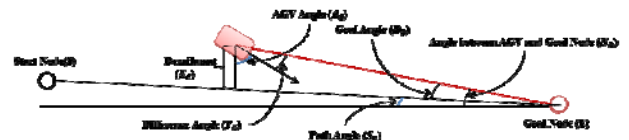


Fig. 3. Error Calculation

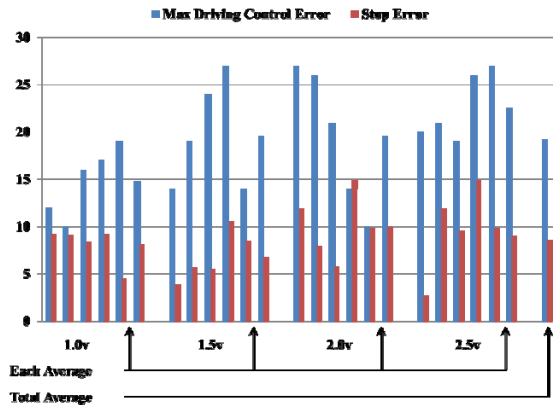


Fig. 4. Result Graph of Localization and Control

LGV was controlled by the difference in voltage.

Fig 4 presents a graph of the experiment results. The driving and stop accuracy of the experiment results are sufficient due to the greater than required accuracy ( $\pm 30$  and  $\pm 15$  mm). When the LGV stops, 0.7v (less 200 mm distance between AGV position and destination point), and 0.4v (less 100 mm), and 0.2v (less than 30 mm) were applied to prevent a collision between the LGV and fixed conveyors.

Virtual Path Planning is a very important configuration in the LGV, and it was used to guide from the start point to the destination point. The configuration form of the conveyor appears like a straight line. In practice, however, the configuration form of the conveyor in the field is a zigzag conformation. In practice, the configuration form of the conveyor in the field is a zigzag conformation. The nodes of virtual path a zigzag path planning to prevent a collision with conveyor, planning are composed of the conveyor position, rotation position, and special position.

Fig 5 shows the configuration of the modified tree structure. The search direction of the virtual path planning method is bidirectional, because the driving direction of the LGV through the Main monitoring system is forward and backward. The modified tree structure is expressed by the adjacent nodes, the node mean conveyor, rotation node, and charger. The link line is the virtual driving path. Whenever searching the virtual path from a new position in map, it should create a tree structure continually. Therefore, a recursive structure was used to solve the previous problem.

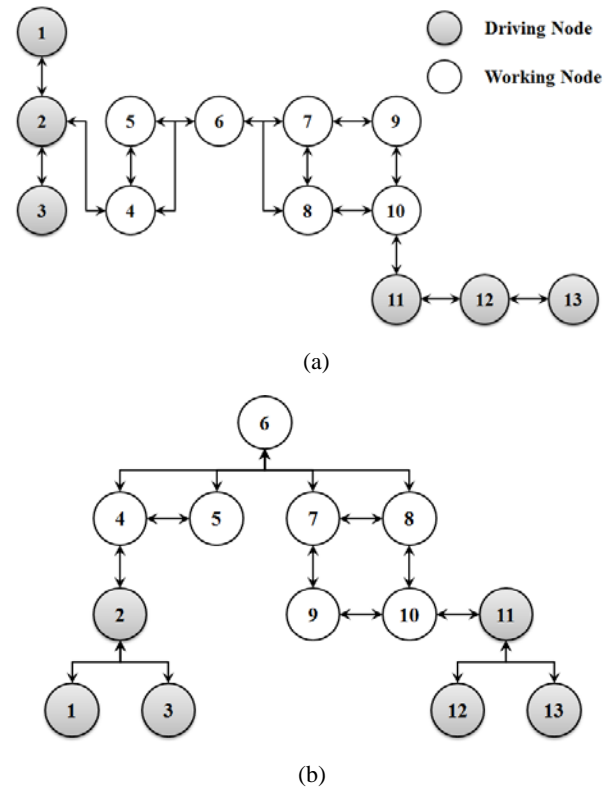


Fig. 5. Result Graph of Localization and Control; (a) Node structure, (b) Tree structure

#### 4. Conclusion

The proposed unmanned transport system is composed of a LGV, conveyor and monitoring system, and the LGV contains a different driving system, a telescopic type (for transporting cargo with a high load) and a communication system. The conveyor type is classified as the A, B and C type through the pallet type or attached equipment. The LGV is guided by the controller using laser navigation but the stability of the system is low. To solve this problem, encoders and a gyroscope are used. The LGV is controlled by the error angle and derailment distance, and LGV is driving through the virtual path from the start node to the destination node.

In the present study, the unmanned transport system, which is an aggregate system of various technologies, such as navigation systems, a driving system, load /unload system, path planning, monitoring system, and emergency system, was examined closely.

## Acknowledgment

This work was supported by BK21PLUS, Creative Human Resource Development Program for IT Convergence and was supported by the MOTIE (Ministry of Trade, Industry & Energy), Korea, under the Industry Convergence Liaison Robotics Creative Graduates Education Program supervised by the KIAT (N0001126).

## References

1. J. L. Crowley, Navigation for an intelligent mobile robot, *IEEE Journal of Robotics and Automation*, 1(1) (1985), pp. 31-41.
2. S. Y. Jung, J. M. Kim and S. S. Kim, Simultaneous localization and mapping of a wheel-based autonomous vehicle with ultrasonic sensors, *Artificial Life and Robotics*, 14(2) (2009), pp. 186-190.
3. M. Gunes and A. F. Baba, Speed and position control of autonomous mobile robot on variable trajectory depending on its curvature, *Journal of Scientific & Industrial Research*, 68(6) (2009), pp. 513-521.
4. J. Lee, S. I. Han and J. M. Lee, Decoupled Dynamic Control for Pitch and Roll Axes of the Unicycle Robot, *IEEE Transactions on Industrial Electronics*, 60(9) (2013), pp. 3814-3822.
5. E. DiGiampaolo and F. Martinelli, A Passive UHF-RFID System for the Localization of an Indoor Autonomous Vehicle, *IEEE Transactions on Industrial Electronics*, 59(10) (2012), pp. 3961-3970.
6. G. Zhao, K. Xuan and D. Taniar, Path kNN Query Processing in Mobile Systems, *IEEE Transactions on Industrial Electronics*, 60(3) (2013), pp. 1099-1107.

# Localization method for AGV using magnetic devices and IMU

**Moonho Park, Eun Kyeong Kim, Yeongsang Jeong, Hansoo Lee, Jungwon Yu, Sunghin Kim**  
*Department of Electrical and Computer Engineering Pusan National University,*  
*Engineering BLDG #10 10313, 2, Busandaehak-ro 63beon-gil, Geumjeong-gu, Busan, 609-735, Korea*  
*E-mail: { 82akakak, kimeunkyeong, dalpangi03, hansoo, garden0312, sskim }@pusan.ac.kr*

## Abstract

This paper is a research of the localization method for AGV (Autonomous Guided Vehicle) with a guidance system using magnetic localization devices. For navigation of AGV, an established magnetic guidance AGV detects a magnetic tape and follows the line. However, there are some weaknesses: disturbance and damage. To make up for the weak points, this paper proposes the localization method using two magnetic localization devices, a gyro sensor and encoders. In order to compensate the global position, AGV's location and angle were compensated for a magnet position and gradient information using two magnetic localization devices. Between spot points, a relative position was calculated by kinematics with the devices. To verify the performance of the proposed method, it was compared with the method using a gyro sensor and encoders. As a result, the proposed method is more efficient than the existing one.

*Keywords:* Autonomous Guided Vehicle, localization method, magnetic device, wireless guidance

## 1. Introduction

An automation system is a sort of automatic process system widely used in design, control, facility management, quality inspection and distribution.<sup>1-2</sup> One of the representative automation systems is AGV. It can reduce personnel expenses and improve productivity.<sup>3</sup> In industrial field, magnetic guidance AGV is often used because of its high accuracy, stability and lower price sensors.<sup>4</sup> However, there are some weaknesses vulnerable to disturbance and damage. To make up for the weak points, the researches into a sensor fusion are continued about magnetic device and the other sensors.<sup>5-7</sup>

This paper proposes the localization method using two magnetic localization devices, a gyro sensor, encoders and magnet spots. The rest of this research paper is as

below. Chapter 2 explains the components of AGV: IMU (Inertial Measurement Unit), magnetic localization devices, a hardware part. Chapter 3 describes the localization system, chapter 4 explains angle compensation, and chapter 5 shows the experimental environment and results. Finally chapter 6 discusses the conclusion.

## 2. AGV

### 2.1. IMU

IMU is used to calculate an object's location or angle using an object's inertial measurement. In this paper, IMU composes one-axis gyro sensor and encoders included a motor of the wheel. The angle needs to calculate by only one-axis in AGV's case. It is why the

one-axis gyro is used in the AGV. Also encoders are substituted for an acceleration sensor.

### 2.2. Magnetic localization devices

With 75mm gap, two magnetic localization devices are attached to front of the AGV. These devices are located at intervals of 20mm in the same level from the floor. Figure 1 is shown magnetic localization devices used in the experiment.<sup>8-10</sup>

### 2.3. Hardware of AGV

AGV is made of frames, two driving wheels and two caster wheels. DSP (Digital Signal Processor) carries out communication with sensors and laptop. The total system configuration of designed AGV is same as Figure 2.

## 3. Localization System

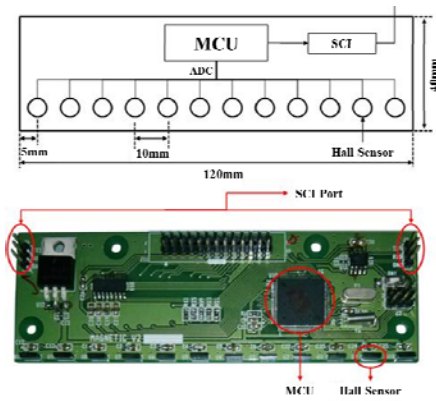


Fig. 1. Magnetic localization devices

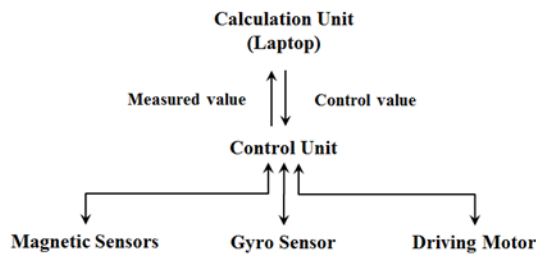


Fig. 2. System configuration

After AGV with a wireless guidance type decides a goal position, it makes a virtual path from the current

position to the next position and follows that line. As AGV follows a virtual path, it finds its position using sensors. In case of the proposed method, the absolute coordinate value is not obtained. Therefore, the coordinate must be updated after an initial position is decided arbitrarily.

### 3.1. Calculation of AGV's position

By encoders' values,  $LWD$  and  $RWD$  are calculated.  $LWD$  is a moving distance of AGV's left wheel. And  $RWD$  is a moving distance of AGV's right wheel.  $L$  is a distance between wheels. An angle  $\theta_{Encoder}$  made by a gap between  $LWD$  and  $RWD$  is obtained by Eq. (1).

$$\theta_{Encoder} \text{ (radian)} = \tan^{-1} \left( \frac{LWD - RWD}{L} \right). \quad (1)$$

As  $\theta_{Encoder}$  is accumulated, we can calculate AGV's body angle. Also X-axis variation and Y-axis variation are obtained by Eq. (2).

$$\theta = \frac{\theta_{Encoder} + \theta_{Gyro}}{2}.$$

$$dv = \frac{(LWD + RWD)}{2}.$$

$$dx = \sin \theta \cdot dv.$$

$$dy = \cos \theta \cdot dv.$$

$\theta_{Gyro}$  is an angle calculated by a gyro output value.  $dv$  is constant needed a coordinate calculation,  $dx$  is X-axis variation,  $dy$  is Y-axis variation. AGV's position is calculated by accumulating X-axis variation and Y-axis variation.

### 3.2. Control with driving error angle

A driving error angle control AGV's direction using the measured values of a gyro sensor, a body angle and a path angle. AGV's path angle is calculated by the current position and the next position. AGV's body angle is calculated by Eq. (3).

$$\alpha = \frac{\theta_{Encoder} + \theta_{Gyro}}{2}.$$

$$\beta = \tan^{-1} \left( \frac{X_2 - X_1}{Y_2 - Y_1} \right).$$

$\alpha$  is a body angle and  $\beta$  is a path angle. Finally, we obtain an error angle  $\theta_{Error}$  by Eq. (4).

$$\theta_{Error} = \beta - \alpha. \quad (4)$$

#### 4. Angle Compensation

Hall sensor measures Gauss of magnet and outputs proportional voltages to measured Gauss.

##### 4.1. Central value calculation

To calculate the central value of magnetic localization devices, an initial reference value is established. A reference value is measured by the experiment. Threshold is used for determining the ON/OFF of each of the hall sensors. To determine the threshold, we make Eq. (5) using heuristic method.

$$Th = M_{NM} + (M_M - M_{NM}) \times \frac{2}{3}. \quad (5)$$

$Th$  is Threshold.  $M_{NM}$  is an average value of each of hall sensors' measured values about 100 times when there is no magnet.  $M_M$  is an average value of each of hall sensors' measured values about 100times when there is a magnet. If a measured value exceeds threshold, it means there is a magnet and hall sensor turns ON. We calculate the central value of magnet by Eq. (6).

$$C = \frac{\sum H_{ONPOS}}{\sum H_{ONCNT}}. \quad (6)$$

$H_{ONPOS}$  is the position value of hall sensor turned ON, and  $H_{ONCNT}$  is the number of hall sensor turned ON. And  $C$  is the central value of magnet.

##### 4.2. Angle calculation

Because of the sensor's accumulative errors, a body angle has always errors. To make up for this weak point, AGV's body angle needs to be compensated and updated. First, we calculate central values of two magnetic localization devices. Second, we calculate a body angle by Eq. (7) when AGV passes through magnet.

$$\alpha = \tan^{-1} \left( \frac{C_2 - C_1}{L} \right) \quad (7)$$

$C_1$  is a central value of first magnet device and  $C_2$  is second one.

##### 4.3. Angle compensation

A point angle is a required angle to change from AGV's current direction to the direction toward next point.

When AGV changes the path, an angle is compensated with a point angle and AGV's angle.

## 5. Experiments & Results

### 5.1. Experiment environment

AGV's size is 760 x 490 x 480mm. A driving path is straight-line section. There are 2 spot points on a driving path. To compensate a driving error angle, there is magnet spot in each point and its size is 80 x 80mm.

### 5.2. Localization using IMU

In the localization experiment using IMU, AGV drives by an angle calculation of encoders and a gyro sensor. If AGV arrives a spot point using a position calculation, a point angle is updated towards next point and AGV starts to drive.

### 5.3. Localization using magnetic devices and IMU

To reduce accumulative errors, a body angle is calculated by magnetic localization devices on each point and angles of encoders and a gyro sensor are updated. For comparison of errors in two experiments, mean error, root mean square error and maximum error are calculated. Table 1 is shown for a comparison of the proposed method with an established IMU.

Table 1. Result of the position measurement

Unit: mm					
IMU			Magnetic device & IMU		
Mean Error	RMSE	Max Error	Mean Error	RMSE	Max Error
226.96	329.74	1089.40	70.24	91.41	186.48

In case of only IMU, error values are immense. On the other hand, error values decrease in case of magnet devices and IMU. Maximum error is six times less. As an angle is compensated using magnetic localization devices, we can measure more accurate position and reduce error value.

## 6. Conclusion

In this paper, we proposed the localization method for AGV with a guidance system using magnetic localization devices and IMU. AGV is designed by us and magnetic localization devices made for advanced



research are attached. Using encoders and a gyro sensor, AGV's position is calculated and a body angle is controlled. When AGV arrives at each point, a body angle is calculated by values of two magnetic localization devices and compensated. As a result, the proposed method is more efficient than an existing one.

### Acknowledgements

This work was supported by BK21PLUS, Creative Human Resource Development Program for IT Convergence and was supported by the MOTIE (Ministry of Trade, Industry & Energy), Korea, under the Industry Convergence Liaison Robotics Creative Graduates Education Program supervised by the KIAT (N0001126).

### References

1. K. Jung, et al, Line Tracking Method of AGV using Sensor Fusion, *Journal of Korean Institute of Intelligent Systems* **20**(1), pp. 54-59, 2010.
2. J. Kim, et al, Fuzzy and Proportional Controls for Driving Control of Forklift AGV, *Journal of Korean Institute of Intelligent Systems* **19**(5), pp. 699-705, 2009.
3. Wu Xing, et al, Design and Control of Material Transport System for Automated Guided Vehicle, *UKACC International Conference on Control*, pp. 765-770, 2012.
4. Pedro Santos, et al, Magnetic vehicle guidance, *Sensor Review* **28**(2), pp. 132-135, 2008.
5. S. Y. Lee, H. W. Yang, Navigation of automated guided vehicles using magnet spot guidance method, *Robotics and Computer-Integrated Manufacturing* **28**(3), pp. 425-436, 2012.
6. H. G. Xu, et al, Extended Kalman Filter Based Magnetic Guidance for Intelligent Vehicles, *Intelligent Vehicles Symposium*, pp. 169-175, 2006.
7. D. Y. Im, et al, Development of Autonomous Vehicle Using Array Magnetic Sensor, in *Proc. 8th International Symposium on Advanced Intelligent Systems*, pp. 914-918, 2007.
8. M. Park, et al, Improvement of Bipolar Magnetic Guidance Sensor Performance using Fuzzy Inference System, *Journal of Korean Institute of Intelligent Systems* **24**(1), pp. 58-63, 2014.
9. M. Park, S. Kim, Magnetic Position Sensor of Analog Type using Optimized Fuzzy Rules, in *Proc. 29th Conf. Institute of Control, Robotics and Systems*, pp. 101-102, 2014.
10. H. Song, et al, Pattern Recognition of Landmark Using Bipolar Magnetic Localization Sensor, in *Proc. 28th Conf. Institute of Control, Robotics and Systems*, pp. 106-107, 2013.

©The 2015 International Conference on Artificial Life and Robotics (ICAROB 2015), Jan. 10-12, Oita, Japan

# On the Effects of Epigenetic Programming on the Efficiency of Incremental Evolution of the Simulated Khepera Robot

**Yasuto Nishiwaki**

*Graduate School of Science and Engineering, Doshisha University, 1-3 Tatara-Miyakotani, Kyotanabe, 610-0321 Kyoto, Japan*

**Ivan Tanev**

*Graduate School of Science and Engineering, Doshisha University, 1-3 Tatara-Miyakotani, Kyotanabe, 610-0321 Kyoto, Japan*

**Katsunori Shimohara**

*Graduate School of Science and Engineering, Doshisha University, 1-3 Tatara-Miyakotani, Kyotanabe, 610-0321 Kyoto, Japan*

*E-mail: {nishiwaki2012, itanev, kshimoha} @sil.doshisha.ac.jp*

## Abstract

We present the results of our work on epigenetic programming (EP) and its application to navigation of mobile cleaning robot. We verify the effect of genetic switch and the feasibility of incorporating histones. The results show individuals applying LEP are better performance and less the number of generations than applying GP but takes costs of calculation. As a result, we believe the histone accelerates efficient evolution of nature.

*Keywords:* Epigenetic Programming, Genetic Programming, Epigenesis, Histone.

## 1. Introduction

The objective of our study is to develop an approach of Epigenetic Programming<sup>1-2</sup> (EP) and to verify the feasibility of incorporating histones (the family of proteins which DNA is wrapped around) in genotype from both the computationally and natural perspectives. Epigenesis refers to a changeable gene expression (and consequently – phenotype) as a result of the interaction of genotype and surrounding environment (food, stress, UV, etc...). We intend to mimic the recent discoveries in molecular biology that suggest that epigenesis plays an important role in evolutionary adaptation of species.

In our previous study<sup>1</sup>, we verified the beneficial effects of histones on the quality of solutions obtained via Genetic Programming (GP). Our approach implied

that the modifications to histones are implemented after the completion of GP, and these modifications were considered as a local search (hill-climbing) around the genotype of the best-evolved individuals. No modifications to histones in due course of evolution were assumed in our previous work.

## 2. Mechanism of EP

### 2.1. The mechanism of modifying the histone switches

We introduce histones as genetic *on* and *off* “switches” that modify the gene expression by activating and deactivating the nodes (and corresponding sub-trees) in the tree representations (i.e., the “genotype”) of the evolved individuals in Genetic

Programming (GP). In canonical GP the abilities of individuals evolve as a result of modifications (via crossover and mutation) to the genes alone. In the proposed EP this genetic modifications are superposed with the modifications of histones to facilitate even better evolutionary adaptation to the environment. Moreover, in some cases the modification to histone alone – i.e., by enabling a disabled code (or vice versa) – would achieve a better performing individual without the need to spend extra time for computationally costly evolution of a new genotype. In this study, we use Lamarckian EP (LEP) as elaborated below.

### 2.2. The mechanism of LEP

LEP is an epigenetic approach in which the modified genetic switches (histones) are stored back in the genotype (i.e., inherited). The Lamarckism implies that the modifications to the histones are inherited back into the genotype of the evolving individuals. LEP evaluates the fitness of individual after applying changes to histones, which, in turn, modifies the state of the genetic *on* and *off* switches. In such a way, by changing the expression of the genes (rather than changing the genes) by these switches, it could be possible to obtain a different phenotype, which eventually features a better fitness value of the evolved individuals. Furthermore, we believe that is possible to evolve better individuals as a result of crossover and mutation operations that operate over the space of genotype superposed by histones.

### 3. System Architecture

In this study, we use the XML-based genetic programming framework<sup>3</sup> (XGP) to maintain the population of evolving individuals and to perform genetic operations (selection, crossover and mutation) on them. The evolved individuals are controllers of a simulated Khepera vacuum cleaning robot. The latter is simulated in a Webots<sup>4</sup> mobile robot simulation environment.

The system architecture is shown in Figure 1.

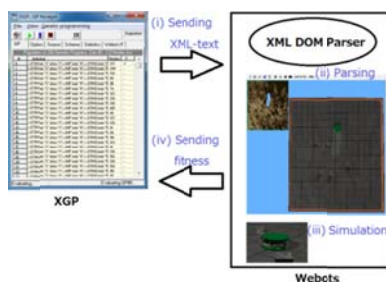


Fig. 1. System architecture

The evaluation of the fitness of evolving controller is accomplished as follows:

- (i) XGP sends the genotype of the individual (as XML-text) for evaluation to Webots via UDP channel,
- (ii) Using XML parser, Webots parses the received individual into a DOM-tree,
- (iii) For each time step of simulation, Webots evaluates the DOM-tree, and based on current perceptions (sensory information) of the simulated bot, decides its current action (e.g., moving forward, moving backward, turning left or turning right). Webots applies the currently issued command on the robot and updates its speed and orientation, which, in turn, defines the position, orientation and the velocity of the bot for the next time step.
- (iv) Upon the completion of simulation, Webots returns (via UDP channel) the fitness value (i.e., the area on the floor that was cleaned by the robot) to the XGP.

The controllers of the robot are evaluated for a number of time steps, given to the robot to clean a room, starting from a given starting position in two consecutive sample 2D scenes – (i) without- and (ii) with obstacles, respectively, as shown in Figure 2.

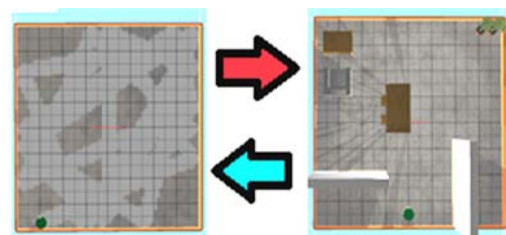


Fig. 2. Experimental setup consisting in two sample scenes: without- (left) and with obstacles (right), respectively. The robot evolves the ability to clean these two rooms consecutively, at two consecutive stages of an incremental evolution.

### 4. Experiments

To verify the feasibility of incorporating histones, we performed two experiments. These two experiments

were intended to allow us to compare the efficiency of evolution via LEP and canonical GP, respectively.

#### 4.1. Exploring evolution characteristic of LEP

In this experiment, we explore how histones influence the efficiency of evolution. The controller of the robot is evolved in the first stage (i.e., room without obstacles) of LEP under the same conditions as GP. We believed that introducing histone would facilitate a faster evolution in that it would require lower computational effort (i.e., would feature a reduced number of evolved generations).

#### 4.2. Two-staged incremental evolution

During the first stage of the incremental evolution, the robot evolves via GP its ability to efficiently clean the room without obstacles. Then, the best controllers are used to seed the second stage of the evolution which involves an evolution (via GP) of the ability to clean the room with obstacles. The same two-staged incremental evolution is used applying LEP with histone-modification at both stages.

After that, the best controllers of second stage are evaluated again in the room without obstacles (i.e., the same environment that is used during the first stage) to investigate their abilities to adapt to the “new” environment. Because of changing environment, the controllers would need to evolve new features in order to perform well in it. We believe that individual used applying LEP can adapt to the new environment by just switching some of their genes *on* and *off* instead of evolving new genotype from scratch.

### 5. Experimental Results

#### 5.1. Result of one-staged evolution

The results of applying LEP or GP on individuals evolved are shown in Figure 3.

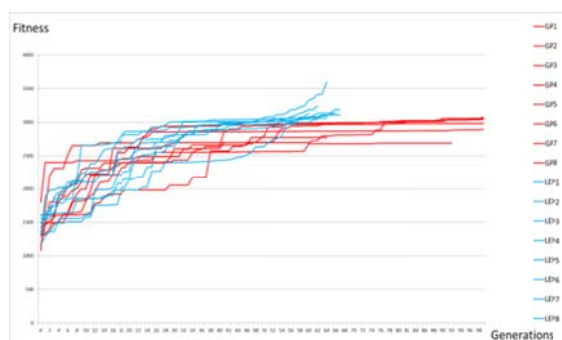


Fig. 3. The results of applying LEP and GP on individuals evolved: transition of fitness LEP (blue line) and GP (red line) Number of population of one generation is 200. Maximum generations are 100. Number of evaluations per one generation of individuals applying LEP is two times as many as GP.

As Figure 3 indicates, the controllers, evolved via LEP have better fitness and evolve faster (with lower number of generations) than canonical GP. On the other hand, the average complexity of genotype (in number of nodes in their DOM-trees) is higher in LEP, which, in turn result in an increased evaluation time of these genotypes. This finding implies that the improvement of computational effort due to the incorporation of histones in LEP comes at the cost of some degradation of computational performance. This degradation, however, is rather negligible, because, in the considered application of LEP, the runtime, needed to simulate the physics of the Khepera robot is much longer than the time spent for evaluating the DOM-tree of the genotype.

#### 5.2. Result of two-staged incremental evolution

In second stage, even if there is no difference in the efficiency of the first stage, performance of controllers applying LEP was better than GP. LEP’s individual tended to live but GP’s individual easy to be weeded out difficult stage. However, some individuals tended to not adapt in first stage when the best individuals in the second stage are returned.

### 6. Discussions

The experimental results suggest that introducing histones as genetic switches facilitates a faster evolution of a simulated Khepera robot. The simulated evolution is relatively fast anyway, and, features about the same runtime overhead as the adaptation via changing of histones. In the real biological world however, the evolution of one generation requires years of time, while the effect of modifications to histones could be observed much sooner. Therefore, we believe that histones incorporated in the genotypes are capable of facilitating the biological evolution.

In addition, in latter experiment, we discovered that some of the controllers could not adapt well to the old “new” environment (room without obstacles), because the parts of their respective genotypes that are responsible for dealing with that environment, was lost during the second stage of evolution (in a room with obstacles). Therefore, it could be interesting to

investigate such a genetic mechanism during the second stage of LEP that could protect the useful features (e.g., ability to move and clean a room without obstacles) evolved at the first stage of evolution, from the destructive effect of crossover and mutation operations. One possibility is to allow the inactivated histones to repel the crossover and mutation operations, in order to preserve the inactivated code from destruction. This code could be deactivated later, when an old “new” environment arises.

## 7. Conclusion

We proposed an approach of LEP and verified the feasibility of incorporating histones. In order to implement histone, we introduced genetic “switches” that modify the gene expression by activating and deactivating the nodes in the tree representations (i.e., the “genotype”) of the evolved individuals in GP. In our approach we propose LEP in that the modified genetic switches are inherited back in the evolving genotypes.

Also, we verified the effect of epigenesis on the efficiency of evolution of controllers of simulated Khepera cleaning robot in two experiments. From the results of the former experiment we concluded that applying LEP facilitates an earlier adaptation compared to canonical GP. The results of the latter experiment - with two-staged incremental evolution - indicate that using LEP contributes to the efficiency of evolution to old “new” environment. We think these results suggest that histones could be seen as a mechanism to “store” dormant abilities once needed to deal with challenging environments. These abilities could be activated again when the organisms face “new” environments that have been already explored in their evolutionary past.

## References

1. Y.Nishiwaki, I.Tanev, and K.Shimohara: Epigenetic Programming and its Application to Mobile Robot, Int. Conf. on Humanized Systems 2013, pp.66-68, September 2013
2. I.Tanev and K.Yuta: Epigenetic programming Genetic programming incorporating epigenetic learning through modification of histones, Information Sciences, p13 (2008)
3. I.Tanev: DOM/XML-based portable genetic representation of the morphology, behavior and communication abilities of evolvable agents, Artificial Life and Robotics, 8:52-56,2004.
4. O.Michel, Webots: Professional mobile robot simulation, Int. J. Adv. Robot. Syst, 1, 39-42 (2004).

# The Effect of Duration of Both Stages of Incremental Genetic Programming on its Efficiency of Evolution of Snakebot

**Naoki Mukosaka**

*Graduate School of Science and Engineering, Doshisha University,  
1-3 Tatara-Miyakotani, Kyotanabe, 610-0321 Kyoto, Japan*

**Ivan Tanev**

*Graduate School of Science and Engineering, Doshisha University,,  
1-3 Tatara-Miyakotani, Kyotanabe, 610-0321 Kyoto, Japan*

**Katsunori Shimohara**

*Graduate School of Science and Engineering, Doshisha University,  
1-3 Tatara-Miyakotani, Kyotanabe, 610-0321 Kyoto, Japan  
E-mail: {mukosaka2012, itanev, kshimoha}@sil.doshisha.ac.jp*

## Abstract

The objective of our work is to investigate the optimal combination of durations of both stages of incremental Genetic Programming (IncGP) on the simulated Snake-like robots (Snakebots). The obtained results suggest that the number of generations cannot be used as criteria for separating the two stages of IncGP. We hypothesized that qualitative criterion, such as the emergence of smooth sidewinding locomotion could be used instead, and conducted additional experiments that proved its worthiness.

*Keywords:* Genetic Programming, Snake-like Robot, Incremental Genetic Programming, Evolution.

## 1. Introduction

Compared to the wheeled and legged vehicles, the wheel-less, limbless Snake-like robots (Snakebots) are more robust and adaptable to both the environmental changes and partial damage. Some of the useful features of Snakebots include smaller size of the cross-sectional area, stability, ability to operate in rugged terrain, good traction, high redundancy, and complete sealing of the internal mechanisms<sup>1</sup>. Due to the morphological complexity of Snakebots, an automated approach of developing their controller via Genetic Programming (GP) is often used<sup>1</sup>.

However, the evolution of Snakebot from scratch via GP is rather inefficient when the bot is situated in a

challenging environment. The main reason for such inefficiency is that the evolution needs to simultaneously discover both (i) the *generic* locomotion traits (that are common for all well-moving bots, regardless of the environment) and (ii) the *specific* traits that are needed to overcome the obstacles in these challenging terrains.

In order to improve the efficiency of such an evolution, in our previous work<sup>2</sup>, we divided the task of evolving the locomotion of simulated Snakebot in challenging terrain into two consecutive, simpler sub-tasks, implemented as two consecutive stages of an incremental Genetic Programming (IncGP): at the first stage we applied GP to evolve a pool of bots that are able to move fast in a smooth, open terrain. Then, during the second stage, we used this pool to seed the

initial population of the bots that are further subjected to evolution in the challenging environment. We demonstrated that the two-staged incremental evolution via IncGP, consisting of two stages of 40 generations each, features a much improved efficiency over the canonical GP<sup>2</sup>.

The *objective* of our current work is to investigate the optimal combination of durations of both stages of incGP. We assume a fixed runtime budget of evolution, corresponding to 80 generations overall. Therefore, our experiments involved evolution of Snakebot via incGP with 7 combinations of durations of both stages of evolution: from 10 generations of the first stage and 70 generations of the second one, to 70 generations of the first and 10 generations of the second one (i.e., 10 and 70, 20 and 60, 30 and 50,..., and, finally, 70 and 10, respectively).

## 2. Simulated Snakebot

In our work we used the Open Dynamics Engine<sup>3</sup> (ODE) physics library to simulate the articulated rigid body dynamics of the Snakebot<sup>2</sup>. ODE allows to account for all forces, resulting from friction, gravity, actuators, and collisions between the segments of the simulated bot, and the environment. The Snakebot is identical to the one as used in our prior work<sup>1, 2, 4, and 5</sup>. It is simulated as 15 identical spherical morphological segments (“vertebrae”). Pairs of nearby segment are linked by universal (Cardano) joints and all joints are powered by two (horizontal and vertical) identical actuators (“muscles”).

In this study we use IncGP to evolve such motion patterns of the segments of the bot that result in fastest speed of locomotion of the bot. Considering the representation of Snakebot, this task could be rephrased as developing the temporal patterns of desired turning angles of horizontal and vertical actuators of each segment, that result in fastest overall locomotion of Snakebot. The proposed representation of Snakebot as a homogeneous system comprising identical morphological segments is intended to significantly reduce the size of the search space of the IncGP (as we need to evolve the functionality of one pairs of actuators only) and to facilitate favorable scalability characteristics of the latter.

## 3. Simulation Setup

We employed IncGP in two consecutive evolutionary stages as follows:

- First, we implemented 30 independent runs of canonical GP to evolve the Snakebot in a smooth terrain for N generations (N=10, 20, 30, ..., 70), and created a pool of 6 best-of-run, fast moving Snakebots for each corresponding value of N.
- In the second stage of IncGP, we conducted additional 30 independent runs, (for 80-N generations) to evolve the bot, situated in a challenging terrain. The initial population of each of these runs is seeded with the 6 fast moving bots, obtained in the first stage of GP, plus additional 194 randomly created bots. For the second stage of IncGP, we considered two cases of challenging environment, and one case of partial damage, as elaborated below.

The considered two cases of challenging terrain include (i) a “pen” of walls (which surrounds the bot from all four sides), and (ii) multiple small immobile (i.e., fixed to the ground) obstacles. In the first case, the height of the wall is automatically increased each time the bot overcomes it. Therefore, the maximum height of the cleared wall (at the end of evolutionary run) could be considered as a measure of the ability of the bot to overcome walls. In the second case, the average speed of the bot (calculated from the travelled center of the gravity of the latter and the time of the trial) is considered as a measure of the ability of bot to overcome obstacles.

In addition, we conducted experiments with IncGP on evolutionary adaptation of the bot to its partial damage to six segments. In this case, we assumed that the damage renders the joint at the tail-side of the affected segment completely immobile.

The main parameters of IncGP are summarized in Table 1. We used our in-house DOM/XML-based implementation of GP<sup>6</sup>.

Table 1. Main parameters of IncGP

Category	Value
<b>Genotype</b>	Patterns of the turning angles of: (i) horizontal actuator, and (ii) Vertical actuator
<b>Population size</b>	200 individuals
<b>Selection</b>	Binary Selection, ratio: 0.1 Reproduction ratio: 0.9
<b>Elitism</b>	Best 4 individuals
<b>Mutation</b>	Random, single point, ratio: 0.01

#### 4. Experimental Results

The experimental results of each of cases are shown in Fig.1, Fig.2, and Fig.3, respectively.

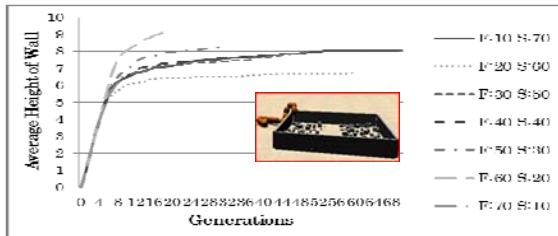


Fig. 1. Dynamics of the height of walls overcome by Snakebot in the second stage of IncGP. Unit on the ordinate corresponds to 1/4<sup>th</sup> of the diameter of the spherical segments of the bot.

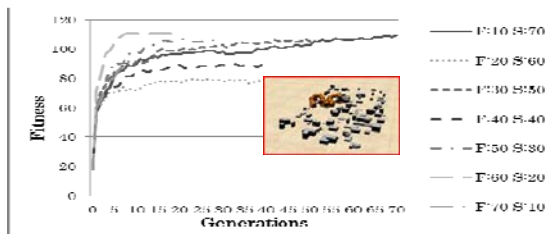


Fig. 2. Fitness convergence of evolving Snakebot in challenging environment with many small obstacles

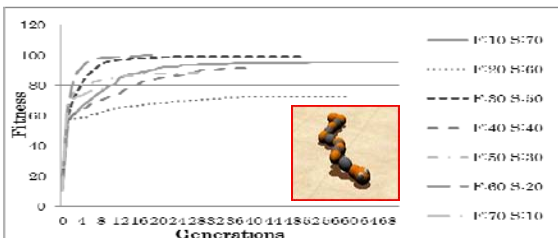


Fig. 3. Fitness convergence of evolving Snakebot with a failure of 6 (out of 15) segments

The statistical results including the complexity of genotype (in number of tree nodes) and fitness value are summarized in Table 2.

#### 5. Discussion

The experimental results suggest that neither the number of generations nor the obtained fitness value at the first stage of IncGP can be used as criteria for optimization of the duration of the two stages of IncGP. Moreover, as the results in Table 2 suggest, there is no correlation between (i) the complexity of the genotype

of the Snakebots (in tree nodes) evolved in the first stage, and (ii) the performance of the best-evolved bot at the second stage of IncGP.

Table. 2. The complexity of genotypes and fitness values in IncGP.  $FN_{avr}$  and  $FF_{avr}$  denote the average number of tree nodes and the average fitness in the first stage of IncGP, respectively.  $HofW_{avr}$  is the height of wall that the bot overcame in the second stage of IncGP.  $FMO_{avr}$  and  $D6F_{avr}$  are the average fitness values in the second stage for the cases of environment with multiple small obstacles and damage to six segments, respectively.

Duration of First (F) and second (S) stages of IncGP	$FN_{avr}$	$FF_{avr}$	$HofW_{avr}$	$FMO_{avr}$	$D6F_{avr}$
<b>F:10 S:70</b>	54.67	87.3	8.067	109	95.17
<b>F:20 S:60</b>	74	89.5	6.7	79.8	72.6
<b>F:30 S:50</b>	82.67	103	7.933	105	99.2
<b>F:40 S:40</b>	95.83	103	7.7	89.3	91.53
<b>F:50 S:30</b>	93.17	107	8.233	106	88.63
<b>F:60 S:20</b>	68	112	9.133	110	100.1
<b>F:70 S:10</b>	77.67	100	6.667	91.4	79.07

Therefore, we hypothesize that the criteria for terminating the first stage of IncGP and initializing the second one might not be necessarily a quantitative one. Rather, an aesthetic, intuitive, subjective, and informal evaluation from the human about the presence of generic locomotion would suffice for the switch between the both stages of IncGP.

In order to verify this hypothesis, conducted additional experiments intended to estimate the importance of human-judged evaluation of the Snakebots as follows:

- First, we implemented 6 independent runs of canonical GP to evolve the Snakebot in a smooth terrain for N generations (N=10, 20, 30, ..., 70), and created a pool of 6 fast moving Snakebots.
- In the second stage of IncGP, we conducted additional 6 independent runs (for 80-N generation) of evolution of the bot, situated in the challenging terrain. For the second stage of IncGP, we only considered the case of “pen” of walls.

We conducted the above mentioned experiments four times for each combination of durations of both stages. We looked at the visual phenotypic traits of the best-of-run, fast moving generic bots obtained at the first stage of IncGP. We noticed that the number of bots



that move smoothly via sidewinding, and feature sinusoidal shape, correlates well with the success at the second stage of IncGP. These results are summarized in Fig.4. As figure illustrates, the quality of the bots (i.e., the height of the wall it overcomes), evolved in the second stage of IncGP, increases with the increase of the number of smooth sidewinders from one to four in the pool of the six bots used for seeding of the second stage of IncGP. Additional increase of the number of smooth sidewinders to five and six is associated with a decrease of the quality in bots evolved at the second stage of IncGP. The reason for such an anomaly is that achieving five or six smooth sidewinding at the first stage usually requires an evolution for too many generations  $N$ , and the remaining budget of the number of generations ( $80-N$ ) for the second stage does not allow enough time for the bot to learn how to overcome tall walls. From another perspective, the non-monotonous nature of the dependency illustrated in Fig.4 suggests that there is an optimal point in configuring the IncGP, and that our consideration of the visual, qualitative phenotypic traits of the evolved Snakebots facilitated the discovery of this point.

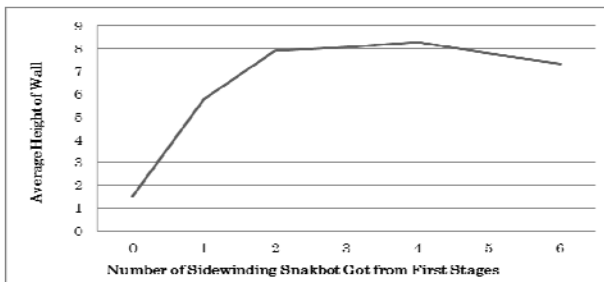


Fig. 4. Height of walls that are overcome by Snakebot in second stage as a function of the number of smooth sidewinding bots evolved in first stage of IncGP.

## 6. Conclusion

In this paper, we investigated the effect of duration of both stages of incremental genetic programming on its efficiency of evolution of Snakebot. We discovered that there the success of the second stage does not depend on the quantitative metrics (e.g., number of generations, fitness value, complexity of genotype, etc.) pertinent to the first stage of evolution of the bot. Consequently, we could conclude that these quantitative metrics could not be used as reliable criteria to decide the switch from the first stage of IncGP to the second one.

We experimentally proved our hypothesis that the smooth sidewinding with an aesthetically well-perceived sinusoidal shape of the bot can be considered as phenotypic traits of the generic locomotion gaits that are very important for the success of the second stage of evolution. Once the evolution discovers these generic gaits, it could terminate the first stage of evolution and switch its efforts to the second stage. During the latter, these generic gaits could be enhanced further by incorporating additional features that are specifically needed to deal with the surrounding challenging terrain. This discovery opens up the opportunity for an original way of incorporating interactive evolution into IncGP in a way that allows a human to subjectively influence the optimal breakdown between the both stages of IncGP. We are planning to investigate this opportunity in our future work.

## Acknowledgement

The first author would like to thank the members of the Laboratory of Socioinformatics at Doshisha University for their support of this study.

## References

1. I. Tanev, T. Ray and A. Buller, Automated Evolutionary Design, Robustness and Adaptation of Sidewinding Locomotion of Simulated Snake-like Robot, IEEE Transactions on Robotics, Vol.21, Number 4, August 2005, pp.632-645
2. N. Mukosaka, I. Tanev, and K. Shimohara, Performance of Incremental Genetic Programming on Adaptability of Snake-like Robot, 17th Asia Pacific Symposium on Intelligent and Evolutionary Systems, IES2013, Volume 24, 2013, pp.152-157
3. R. Smith, Open Dynamics Engine, URL: <http://ode.org/>
4. T. Kuyucu, I. Tanev and K. Shimohara, Incremental Genetic Programming Via Genetic Transpositions For Efficient Coevolution Of Locomotion And Sensing Of Simulated Snake-Like Robot Proceedings of the 20th the European Conference on Artificial Life (ECAL-2011), 8th - 12th August 2011, Paris, France, pp. 439-446
5. I. Tanev, T. Kuyucu, and K. Shimohara, On the Cumulative Effect of Bloat and Genetic Transposition on the Efficiency of Incremental Evolution of Snake-like Robot Genetic and Evolutionary Computation Conference, GECCO-2012, July 7-11, 2012, Philadelphia, USA, pp.161-168
6. I. Tanev. Dom/xml-based Portable Genetic Representation of the Morphology, Behavior and Communication Abilities of Evolvable Agents, Artificial Life and Robotics, 2004, 8:52-56

# Design of a new shoulder joint mechanism for an upper-limb exoskeleton robot.

**Masahito Akiyama**

*Mechanical Engineering, Kyushu University, Fukuoka-shi nishi-ku motooka 744  
Fukuoka, 8190395, Japan*

**Kazuo Kiguchi**

*Kyushu University, System Engineering Laboratory, Fukuoka-shi nishi-ku motooka 744  
Fukuoka, 8190395, Japan*

*E-mail: 2TE1330IT@s.kyushu-u.ac.jp, kiguchi@mech.kyushu-u.ac.jp  
http://zeus.mech.kyushu-u.ac.jp*

## Abstract

This paper proposes an effective shoulder joint mechanism for an upper-limb exoskeleton robot. Human glenohumeral joint moves in 3-dimension in accordance with the movement of the upper-limb such as the shoulder flexion/extension and abduction/adduction motion. In order to reduce the difference between the human glenohumeral joint position and the exoskeleton shoulder joint position, we propose a passive compensation mechanism which consists of links and sliders. This mechanism can imitate the movement of human glenohumeral joint without additional motors.

*Keywords:* exoskeleton robot, shoulder joint, glenohumeral joint

## 1. Introduction

Recently, the progress in robotics and mechatronics technology brings much benefit not only in industries, but also in medicine and welfare. In the medical field, applications of robot supporting operation are spreading such as less invasive surgery, telemedicine services and high precision medical treatment. In the meantime, an exoskeleton power assist robot is expected in the field of welfare. In Japan, especially, researches on exoskeleton robots focus on caregivers support, rehabilitation due to the declining birthrate and aging society.

However, it is not easy to design an exoskeleton power assist robot because the movements of human joints are complex. In an upper limb, a shoulder joint movement is especially complicated. Therefore developed shoulder joints for exoskeleton robots are intricate. IntelliArm<sup>1,2</sup>

and MGA<sup>3</sup> have some additional motors to follow the movement of the human upper limb. Its flexibility and precision are good, but its weight and costs are increased. For simplify the mechanisms, SUEFUL-7<sup>4,5</sup> use links and sliders to follow the movement without adding motors. Its weigh is light, but the following of motion is not perfect. This paper proposes a shoulder joint mechanism for an upper-limb exoskeleton robot with links and sliders.

## 2. The human glenohumeral joint

The human shoulder joint, called a glenohumeral joint, moves in 3-dimension by the movement of the upper-limb such as the shoulder flexion/extension and abduction/adduction motion. Several measurement data about shoulder joints' angles from a medical point of

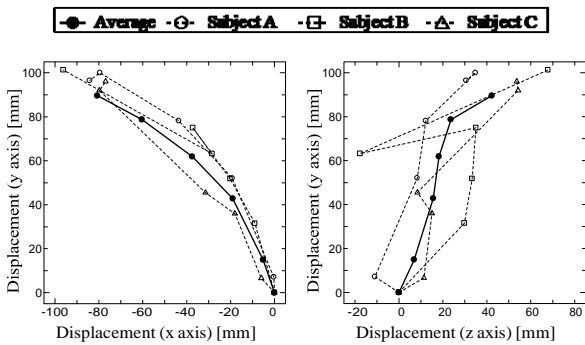


Fig. 1. Measurement results (shoulder abduction motion)

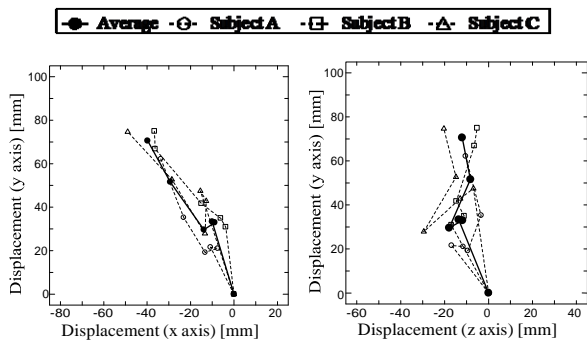


Fig. 2. Measurement results (shoulder flexion motion)

view are reported in Ref. 6. Kiguchi *et.al*<sup>7</sup> measured the coordinate data of glenohumeral joint.

Their measurement data is shown in Figs 1 and 2. In the shoulder abduction motion, the glenohumeral joint moves to inside and high position in x-y plane. In the shoulder flexion motion, the glenohumeral joint moves to high position in z-y plane.

In this paper, a new shoulder joint mechanism for an exoskeleton robot is designed based on the coordinates measured by Kiguchi *et.al*.

### 3. Mechanisms of the robot's shoulder joint

This shoulder joint mechanism use links and sliders to follow the movement and to save its weight. This robot shoulder joint has three DOF (Figure 3) for three DOF of the human shoulder joint. The 1st axis is used for shoulder horizontal abduction/adduction motion. The 2nd axis is used for shoulder flexion/extension motion. The 3rd axis is used for shoulder internal/external rotation motion. Pulleys are rotated by wires around the

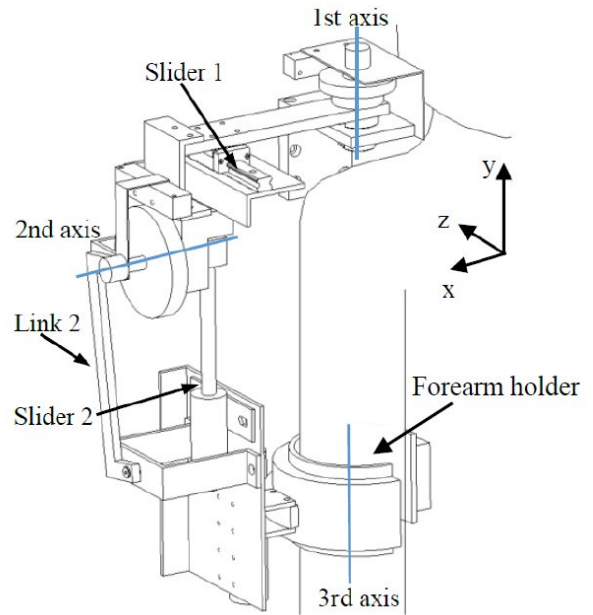


Fig. 3. Proposed shoulder joint

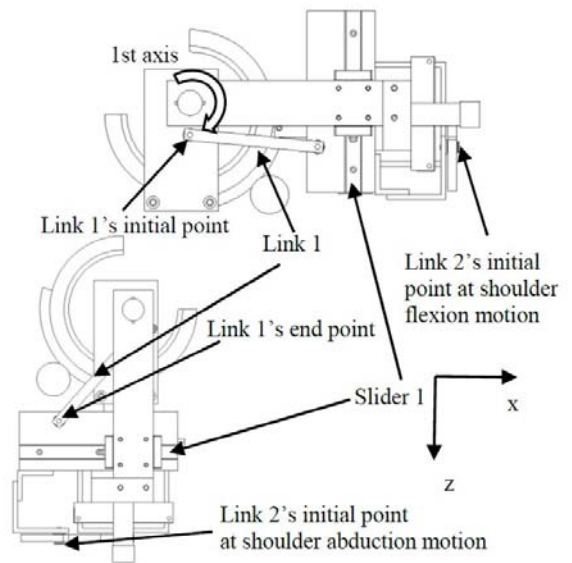


Fig. 4. Top mechanism at shoulder horizontal flexion 0 deg. and 90 deg. (Top view)

1st and 2nd axis. A motor rotates the forearm holder around the 3rd axis.

The angles of the 1st and 2nd axis are limited in 0 deg. to 90 deg. for safety. Two mechanisms linked the 1st and 2nd axis reduce the error between the human

Table 1. The coordinates of the robot

name	axis	value [mm]
Human glenohumeral joint (the origin)	x	0
	y	0
	z	0
1st axis	x	0
	z	0
Link 1 initial point	x	0
	z	28
Link 1 end point	x	112.5
	z	38.6
Length of Link 1		113
2nd axis	y	10
	z	48
Link 2 initial point	y	38
	z	38
Link 2 end point	y	-140
	z	10
Length of Link 2		184

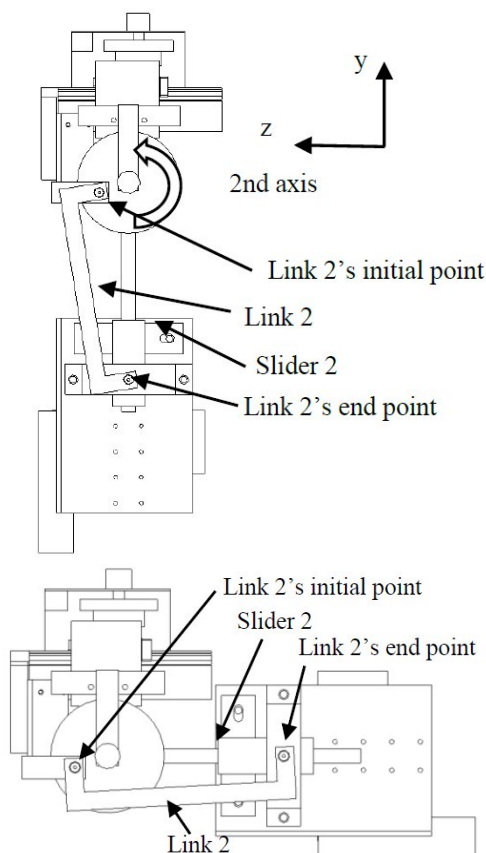


Fig. 5. Side mechanism at shoulder flexion 0 deg. and 90 deg. (Side view)

glenohumeral joint position and the exoskeleton shoulder joint position. Figure 4 shows the top mechanism.

The link 1 and slider 1 change the position of the link 2's initial point. This difference of the positions of link 2's initial point enable this exoskeleton shoulder joint to follow both the human shoulder flexion motion and shoulder abduction motion. The side mechanism is shown in Fig 5. The link 2 changes the length of the slider 2. The slider 2 connect its forearm holder. Shrinking the length of slider 2 means that the center of the exoskeleton robot shoulder joint moves to up or inside.

**4. Simulation in 3D CAD**

This proposed mechanism is evaluated by a simulation in 3D CAD. The coordinates of its points when the angle of horizontal flexion is 0 deg. and the angle of shoulder flexion is 0 deg. show in Table 1. The position of the link

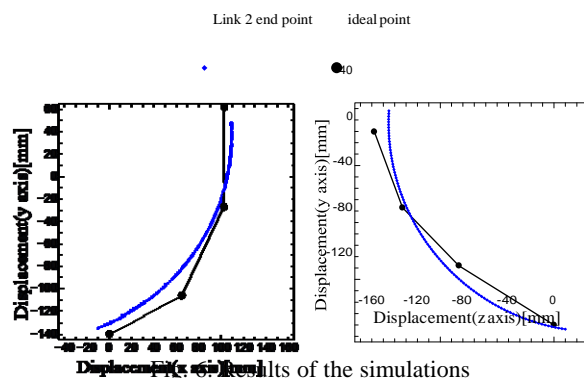


Fig. 6. Results of the simulations (Right: shoulder flexion motion, Left: shoulder abduction motion)

2 initial point is limited. The z value of the point must be bigger than 38mm because of its mechanical interference. The results of the simulation shows in Figure 6. The blue data means the path traced by a moving Link 2 end point. The black data means ideal point calculated from the human measured value. The difference between the position of human glenohumeral joint and the position of the exoskeleton shoulder joint is less than 25 mm.

## 5. Conclusion

In this paper, the simple following exoskeleton shoulder joint for an upper-limb power assist robot is proposed. The proposed shoulder joint mechanism enable the exoskeleton robot to follow the movement of human glenohumeral joint and reduce the difference of these joints. The effectiveness of the proposed mechanism is demonstrated by 3D CAD simulations. We are presently assembling a real robot with this mechanism.

## 6. References

1. Y. Ren, H. -S. Park, L. -Q. Zhang, *Developing a whole-arm exoskeleton robot with hand opening and closing mechanism for upper limb stroke rehabilitation*. In: IEEE international conference on rehabilitation robotics. 2009. p. 761–765.
2. Y. Ren, H. -S. Park, L. -Q. Zhang, *IntelliArm: an exoskeleton for diagnosis and treatment of patients with neurological impairments*. In: Biennial IEEE/RAS-EMBS international conference on biomedical robotics and biomechatronics. 2008. p.109–114.
3. C. Carignan, J. Tang, S. Roderick, *Development of an exoskeleton haptic interface for virtual task training*. In: IEEE/RSJ international conference on intelligent robots and systems. 2009. p. 3697–3702.
4. Gopura RARC, K. Kazuo, Y. Yi, *SUEFUL-7: a 7DOF upper-limb exoskeleton robot with muscle-model-oriented EMG-based control*. In: IEEE/RSJ international conference on intelligent robots and systems. 2009. p. 1126–1131.
5. K. Kazuo, M. H. Rahman, M. Makoto, T. Kenbu, *Development of a 3DOF mobile exoskeleton robot for human upper-limb motion assist*. Robotics and Autonomous Systems 2008; 56:678–691.
6. N. K. Poppen, P. S. Walker, *Normal and abnormal motion of the shoulder*, J Bone Joint Surg Am. 1976;58:195-201.12
7. K. Kazuo, K. Kenryu, H. Yoshiaki, *Design of a 7DOF upper-limb power-assist exoskeleton robot with moving shoulder joint mechanism*. In: Robotics and Biomimetics (ROBIO), 2011 IEEE International Conference on. IEEE, 2011. p. 2937-2942.

# A Machine Learning Approach to a Lateral Continuous Force Estimation for a Walking Biped Robot

**Yeoun-Jae Kim**

*Robotics Program, KAIST, Eu-Seong-Gu Dae-hak-Ro 291 KAIST EE 4231  
Daejeon, 305-701, South Korea*

**Ju-Jang Lee**

*Electrical Engineering, KAIST, Eu-Seong-Gu Dae-hak-Ro 291 KAIST EE 4231  
Daejeon, 305-701, South Korea  
E-mail: lethkim@kaist.ac.kr, jjlee@ee.kaist.ac.kr  
iliad.kaist.ac.kr*

## Abstract

In this paper, a regressor for determining a lateral external continuous force applied upon a walking biped robot is investigated and verified by a numerical simulation. A pre-defined walking gait of a biped robot is constructed by the Tchebyshev method. And a continuous force-action classifier is generated. It determines whether the lateral external force is a continuous force or not. A regressor which estimates a lateral external continuous force acted upon a walking biped robot is constructed by SVR (Support Vector Regressor). The regressor is verified by a numerical simulation. We assumed that only lateral force is applied upon the COG (Center of Gravity) of the walking biped robot.

*Keywords:* walking, biped robot, SVR, regressor, force estimation..

## 1. Introduction

The biped robot (humanoid robot) is the robot which resembles human beings. Not only resembles the appearance, but also resembles its functionality. Compared with other function-specific robots, the humanoid robot is versatile in its functionality. In theorem, it can do almost all the works which humans do. That's why many robot researchers are enthusiastic for making and researching a perfect humanoid robot. The most prominent ones of these humanoid robots are Asimo[1], Petman[2] and Hubo[3]. Other state-of-the-art humanoid robots are found in DARPA (Defense Advanced Research Projects Agency) robotics challenge 2013[4]. The humanoid robot may interact with a human being. For example, it may serve a human being by going and taking a cup of coffee to a human being. And it can sweep the house in which the human and humanoid live together. During interacting with a

human being, the robot can accidentally collide with an object or a human beings. The worse consequence is falling down and gets damage. Many researches are performed to alleviate and avoid this kind of humanoid damages. Fujiwara et.al.[5] made a falling motion control to minimize the falling damage. Morisawa et.al.[6] prevented the collision of a humanoid robot with other objects by incorporating an emergency stop motion planning. Renner and Behnke[7] make use of attitude sensors and reflexes to detect instability and avoid falling down for a humanoid robot. O. Hohn et.al.[8] made a classifier for biped instability. Kim et.al.[9] made a falling detection and avoidance classifier for a biped robot by using SVM(Support Vector Machine). All the above works are about alleviating and avoiding the humanoid damages irrespective of the amount of the external force. If the external force is small, the biped robot can recover from the instability by its inertial. And if the external force is

intermediate and large, KNOWLEDGE ABOUT THE AMOUNT OF THE EXTERNAL FORCE will make the biped robot control more specific and efficient. So, the authors made a SVR based regressor for determining a continuous lateral external force in a walking biped robot. This regressor will be used to determine the lateral continuous external force and control the biped robot not to fall down by the external force. The paper is organized as follows. Section 2 explains the pre-defined walking gait of a biped robot. Section 3 set forth the continuous force-action classifier which determines whether the applied external force is continuous or not. The SVR and SVR based continuous lateral force estimator is explained in Section 4 and 5 and the numerical simulation result is in Section 6. And the conclusion is drawn in Section 7.

Contributions are to be in English. Authors are encouraged to have their contribution checked for grammar. American or British spelling should be used. Abbreviations are allowed but should be spelt out in full when first used. Integers ten and below are to be spelt out. Italicize foreign language phrases (e.g., Latin, French).

## 2. Pre-defined Walking Gait

As pointed out in the abstract, we assumed that the lateral continuous force is applied upon the COG of the walking biped robot. The walking gait of a biped robot is important in making the force-estimating regressor for it changes the lateral dynamics of the biped robot. So, in this section, we explain the pre-defined walking gait of a biped robot. In our previous work [10], an energy-efficient walking gait of a biped robot is constructed by using Tchebyshev method. We adopt the methodology in this paper and made an energy-efficient walking gait. The walking gait is comprised of SSP (Single Support Phase) and DSP (Double Support Phase). However, we only use SSP walking gait for the regressor estimates the lateral continuous force in SSP walking gait. Fig. 1 illustrates the SSP walking gait made by Tchebyshev method. The SSP walking stride is 0.6m and SSP walking time is 1.3sec. The sampling rate of the simulation is 1msec. The walking gaits in Fig. 1 are viewed sagittally.

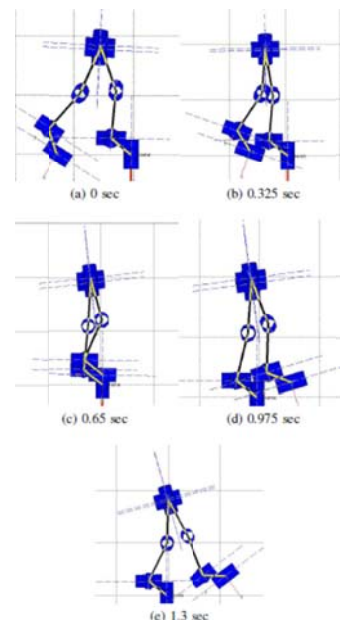


Fig. 1 Walking gait sequence (in sagittal view)

## 3. Continuous Force-Action Classifier

While the biped robot is walking in a pre-defined walking gait, a sudden lateral external force can be applied to the walking biped robot. The biped controller must determine whether some force is applied or not and furthermore if it is, it must also determine whether the applied force is continuous or impulsive. The continuous force-action classifier determines these. Fig. 2 represents the ZMPy graph during walking in the pre-defined gait. The width of the sole is 0.2m, so ZMPy spans  $-0.1 \sim 0.1$ m. The ZMPy graph is a smooth curve within this span, which represents the walking gait is well constructed for the biped robot not to fall down during walking. The sampling rate is 1msec which is previously stated and all the ZMPy points in a SSP walking gait are 1300. The continuous force-action classifier takes 4 points  $ZMPy(t-3)$ ,  $ZMPy(t-2)$ ,  $ZMPy(t-1)$  and  $ZMPy(t)$  from ZMP sensors and compares this 4 ZMP points with the pre-defined ZMPy at the specified walking time and if all the 4 ZMPy points differ, it returns 1 or returns 0. The returned 1 value means that the continuous lateral force is acted upon a biped robot. Algorithm 1 in Fig. 3 represents these working of the continuous force-action classifier.





Fig. 2 ZMPy graph (lateral direction ZMP)

```

Data:  $ZMP_y$ 
Result: 1 or 0
while the biped is walking in SSP do
  read
   $ZMP_y(t-3), ZMP_y(t-2), ZMP_y(t-1), ZMP_y(t);$ 
  if The 4  $ZMP_y$  points not-equals the pre-defined 4
   $ZMP_y$  points then
    | return 1;
  else
    | continue;
  end
end
  
```

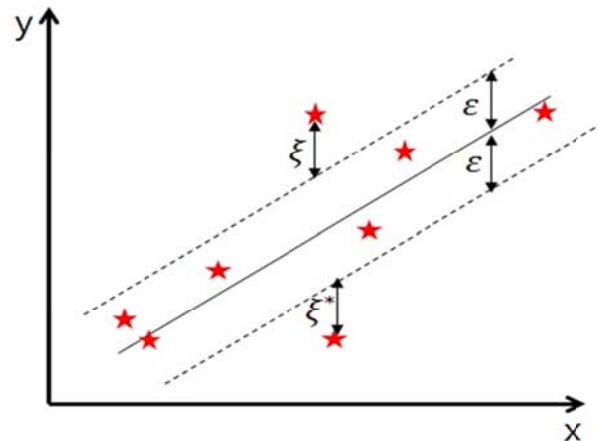
Algorithm 1: Continuous Force-Action Classifier

Fig. 3 Continuous force-action classifier algorithm

#### 4. SVR (Support Vector Regression)

Because the regressor which determines the amount of the lateral continuous force acting upon a walking biped robot makes use of the SVR, we briefly explains what a SVR in this section. SVM (Support Vector Machine)[11] is basically used as a classification problem, however, if it is used as a regressor, it is SVR. The SVR incorporates the same principles as the SVM for classification with only minor differences. In SVM, the constraint is that the distance between the real points and the hyperplane must be larger than  $\epsilon$ (the margin). However in SVR, the constraint is that the distance between the real points and the hyperplane must be smaller than  $\epsilon$ (the margin). In fact, the SVR solution is solving the optimization problem in Fig. 4.

Fig. 4 Support vector regression basic framework



Solution:  $y = wx + b$

Minimize:  $\frac{1}{2} \|w\|^2 + C \sum_{i=1}^N (\xi_i + \xi_i^*)$

Constraints:  $y_i - wx_i - b \leq \epsilon + \xi_i$   
 $w x_i + b - y_i \leq \epsilon + \xi_i^*$   
 $\xi_i, \xi_i^* \geq 0$

#### 5. Lateral Continuous Force Estimator

If the continuous force-action classifier determines that some continuous force is applied, the lateral continuous force estimator is activated to estimate the amount of the continuous force. The whole process of constructing the lateral continuous force estimator is depicted in Fig. 5. In Fig. 5, the SSP gait of a biped robot is depicted. There are 5 consecutive pictures that represent one SSP gait. The walking times are 0, 400, 600, 800 and 1300msec. The biped pictures are viewed sagittally and the inertial coordinate system is represented as X-Y-Z coordinates in right side of the picture. We assumed that the external continuous force is activated laterally in -Y direction to the COG (Center Of Gravity) of the biped robot at any SSP gait sequence.

We divided the SSP walking gait as 5 times (0, 400, 600, 800 and 1300msec) to make it easy to construct a force estimator. At each of this 5 gait times, the lateral continuous force estimator is constructed by utilizing SVR with linear kernel. And if the force is activated at the 4 time intervals (0~400, 400~600, 600~800 and 800~1300msec) the linear interpolation technique is



adopted to decide the amount of the applied continuous force. All this procedure is expressed in Fig. 5.

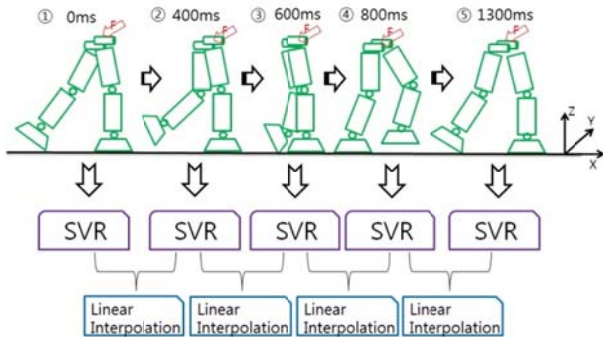


Fig. 5 Lateral continuous force estimator framework

### 6. Simulation Results

In this section, the simulation results are presented. In Fig. 6 the ZMP vs. the applied force graph at half walking time after training is presented. The points are acquired by the numerical simulation of the biped robot

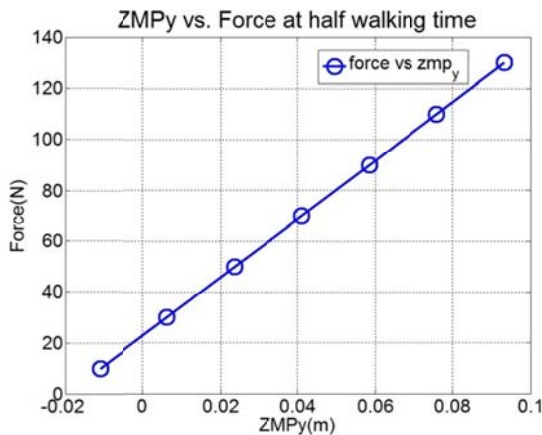


Fig. 6 ZMPy vs. Force at half walking time and the linear line represents a trained linear SVR. The results show that the ZMP-force graph is almost linear and the resulting trained SVR curve is also almost linear. In Fig. 7 there are two graphs represents the performance of the lateral continuous force estimator. The upper graph is when the force is applied at 500msec in the walking time and the latter graph is when the force is applied at 700msec. The ZMPy points are 2.75, 20.22, 37.69, 55.16, 72.13 and 90.1mm at 500msec and 3.91, 13.46, 30.84, 48.22, 65.60 and 82.98mm at 700msec. the blue rectangular points represents the exact applied force from the numerical simulation and

the red triangular points represents the estimated external force. As the two graphs represents, the estimated value is fairly well matches the exact value. The RMS (Root Mean Square) errors at 500msec and 700msec are 0.1838N and 8.3336N. The reason of relatively large RMS error at 700msec compared with

Fig. 6 ZMP-applied force graph at half walking time that at 500msec is the large estimation error at ZMPy value 0 in 700msec graph. This is the limitation of linear SVR and other kernel-based SVR will cope with this estimation error.

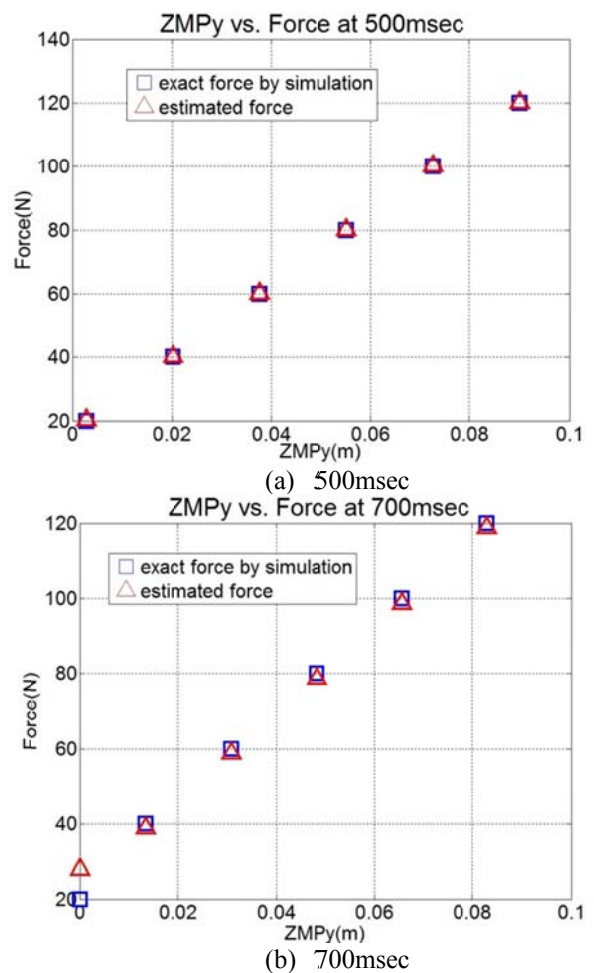


Fig. 7 Lateral continuous force estimator performances

### 7. Conclusion

In this paper, the lateral continuous force estimator is constructed and verified by numerical simulations. The lateral continuous force estimator estimates the externally applied lateral force when a biped is walking.

We assumed that the external continuous force is applied to the COG of the biped laterally. It makes use of linear SVR and linear interpolation technique. The numerical simulation results show that the estimator well predict the external force. Future works are to train the estimator with different kernel to reduce the RMS error and to perform other regression model except SVR.

## 8. Acknowledgement

This research was supported by the MOTIE (The Ministry of Trade, Industry and Energy), Korea, under the Technology Innovation Program supervised by KEIT (Korea Evaluation Institute of Industrial Technology), 10045252, Development of robot task intelligence technology.

## References

References are to be listed in the order cited in the text. Use the style shown in the following examples. For journal names, use the standard abbreviations. Typeset references in 9 pt Times Roman.

1. K. Hirai, M. Hirose, Y. Haikawa and T. Takenaka, *The development of Honda humanoid robot in Proc. of 1998 IEEE Int. Conf. on Robotics and Automation*, pp.421-439.
2. <http://www.bostondynamics.com/>.
3. J. H. Oh, D. Hanson, W. S. Kim, Y. Han, J. Y. Kim and I. W. Park, *Design of Android type Humanoid Robot Albert HUBO in Intelligent Robots and Systems, 2006 IEEE/RSJ Int. Conf. on*, pp.1428-1433.
4. E. Ackerman, *DARPA Robotics Challenge Trials: Final Results* available at <http://spectrum.ieee.org/automaton/robotics/humanoids/darpa-robotics-challenge-trials-results>.
5. K. Fujiwara, F. Kanehiro, F. Kajita, K. Kaneko, K. Yokoi, and H. Hirukawa, *UKEMI: Falling Motion Control to Minimize Damage to Biped Humanoid Robot in Proc. of the 2002 IEEE/RSJ Int. Conf. on Intelligent Robots and Systems*, pp.2521-2526.
6. M. Morisawa, K. Kaneko, F. Kanehiro, S. Kajita, K. Fujiwara, K. Harada, H. Hirukawa, *Motion Planning of Emergency Stop for Humanoid Robot by State Space Approach in Proc. of the 2006 IEEE/RSJ Int. Conf. on Intelligent Robots and Systems*, pp.2986-2992.
7. R. Renner and S. Behnke, *Instability Detection and Fall Avoidance for a Humanoid using Attitude Sensors and Reflexes in Proc. of 2006 IEEE/RSJ Int. Conf. on Intelligent Robots and Systems*, pp.2967-2973.
8. O. Hohn, J. Gacnik and W. Gerth, *Detection and Classification of Posture Instabilities of Bipedal Robots in Climbing and Walking Robots*, pp.409-416.
9. J. J. Kim, Y. J. Kim and J. J. Lee, *A Machine Learning Approach to Falling Detection and Avoidance for Biped Robot in Society of Instrument and Control Engineers Annual conference 2011*, pp.562-567.
10. Y. J. Kim, J. Y. Lee, J. J. Lee, *Bipedal Walking Trajectory Generation Using Tchebychev Method in International Conf. on Mechatronics and Informatics*, pp.265-271.
11. V. Vapnik, S. Golowith and A. Smola, *Support Vector Method for Multivariate Density Estimation in Advances in Neural Information Processing Systems*, vol.12, pp.659-665.

# The Improvement of Robust Robot SLAM Algorithm Based on Sensor Fusion

Jiwu Wang<sup>1</sup>

*School of Mechanical, Electronic and Control Engineering, Beijing Jiaotong University  
Beijing 100044, China<sup>1</sup>*

Shunkai Zheng<sup>1</sup>, Fangbo Liao<sup>1</sup>

*School of Mechanical, Electronic and Control Engineering, Beijing Jiaotong University  
Beijing 100044, China<sup>1</sup>*

Sugisaka Masanori<sup>2</sup>

*Alife Robotics Corporation Ltd, Japan and Open University, United Kingdom<sup>2</sup>  
E-mail: jwwang@bjtu.edu.cn; sugisaka3@mocha.ocn.ne.jp*

## Abstract

The Kinematic model of the robot is a very important part in SLAM, It's error model will influence the positioning accuracy of robot and map building. Generally, the motion model relies simply on the data from encoder feedback. Due to cumulative error, the robot pose accuracy is relatively poor by mileage positioning with encoder. Here a new method is put forward based on data fusion of gyro sensor with the encoder data, and the robot pose accuracy is analyzed and improved. Then we use the optimization Kinematic model on SLAM to verify the robustness.

*Keywords:* sensor fusion; DCM; EKF filtering; SLAM

## 1. Introduction (Basic Measurement Unit)

The idea of pose measurement system based on the fusion is as following: firstly, build motion analysis model; then with the inertial sensor data, give the accurate pose estimation.

Hardware IMU measurement system used in this paper to achieve mini atomization of inertial measurement through the MEMS technology, the IMU module contains ITG3205 gyroscope, ADXL345 accelerometer, HMC5883L electronic compass. The sensor is connected to the microprocessor via a bus, and the

microprocessor reads and writes data correction of sensors.<sup>1</sup>

Gyroscope, accelerometer, compass data from these three sensors output are implemented on an I<sup>2</sup>C bus interface, the sensor run as a slave device, a microprocessor done as the master device.<sup>2</sup> The system structure is shown in Figure 1.

The MEMS sensor with 3 axes digital output angular velocity, each axis is provided with a 16bit A/D converter, built-in low-pass filter with adjustable bandwidth, shown in figure 2.<sup>3</sup> The measuring range is

$\pm 2000^\circ/s$ , and ADC output frequency can be adjust in the range of 8000HZ to 3.9HZ.

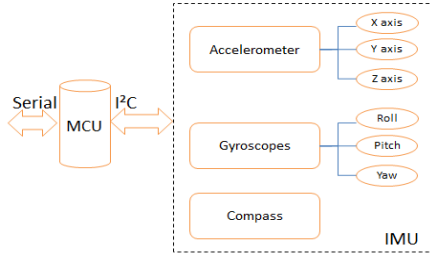


Fig.1. IMU pose measurement system architecture diagram

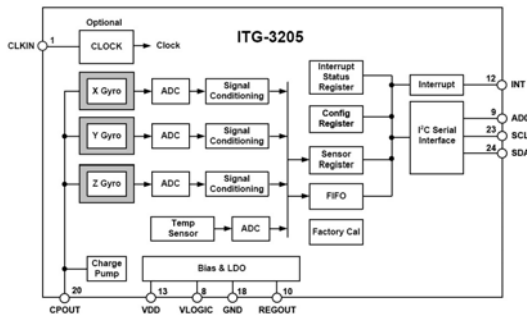


Fig.2. ITG-3205 structure diagram

ADXL345, the three axis acceleration of an ultra-low power design, measurement range of up to  $\pm 16g$ . Moreover, the device also has the knock detection, free fall detection, etc., shown in figure 3.

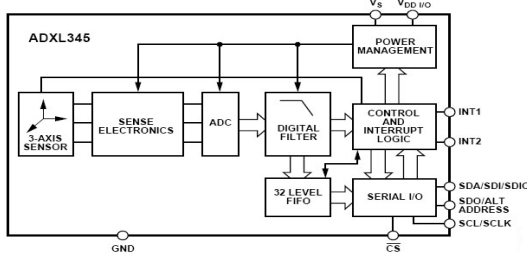


Fig.3. ADXL345 structure diagram

Electronic compass HMC5885, as a low cost electronic compass with a high precision, has a 12 bit ADC conversion accuracy, compass navigation precision can be  $1^\circ$  or  $2^\circ$ .

## 2. Analysis of DCM Algorithm

The DCM algorithm is as followings: a nonlinear correlation gyro measurement data and the direction cosine change rate of difference equations. <sup>4</sup> The flow algorithm in digital system is shown in figure 4.

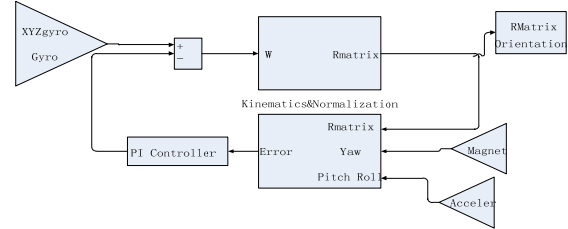


Fig.4. ITG-3205 structure diagram

### 2.1. The Kinematics analysis algorithm

The kinematics equation is:

$$\frac{dr(t)}{dt} = \omega(t) \times r(t) \quad (1)$$

$\omega(t)$  is the angular velocity vector.

With the initial state and rotating vector, it can be:

$$\begin{cases} r(t) = r(0) + \int_0^t d\theta(\tau) \times r(\tau) \\ d\theta(\tau) = \omega(\tau) d\tau \end{cases} \quad (2)$$

Where  $r(0)$  is the initial vector

Further, in the global coordinate system, using the method of approximate matrix, it will be

$$\begin{cases} r_{global}(t+dt) = r_{global}(t) + r_{global}(t) \times d\theta(t) \\ d\theta(t) = \omega(t) dt \end{cases} \quad (3)$$

For error compensation of angular velocity, a modified angular velocity is introduced, which is determined by the angular velocity and its correction.

$$\omega(t) = \omega_{gyro}(t) + \omega_{cor}(t) \quad (4)$$

Formula (5) is the DCM update equation matrix about gyroscope.

$$R(t+dt) = R(t) \begin{bmatrix} 1 & -d\theta_z & d\theta_y \\ d\theta_z & 1 & -d\theta_x \\ -d\theta_y & d\theta_x & 1 \end{bmatrix} \quad (5)$$

Here,  $d\theta_x = \omega_x dt, d\theta_y = \omega_y dt, d\theta_z = \omega_z dt$

### 2.2. Drift compensation

In order to calculate the Roll, Pitch, Yaw for compensation, a feedback PI controller is introduced. The controller error calculation of Roll and Pitch uses the acceleration and the electronic compass Yaw error. In our experiments, the following figure is drawn based on the sensor data by IMU sensor.

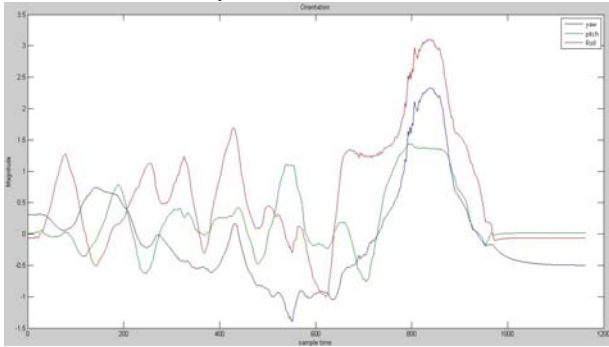


Fig.5. Orientation sampling curve

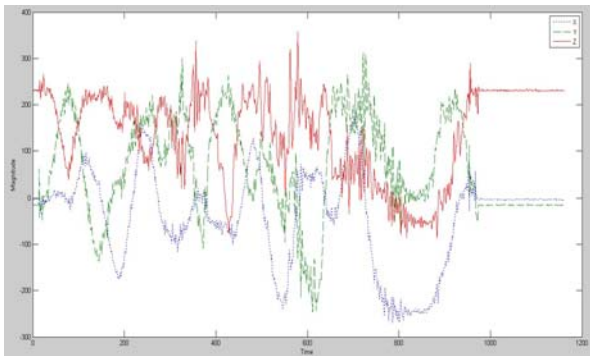


Fig.6. Three axis speed curves

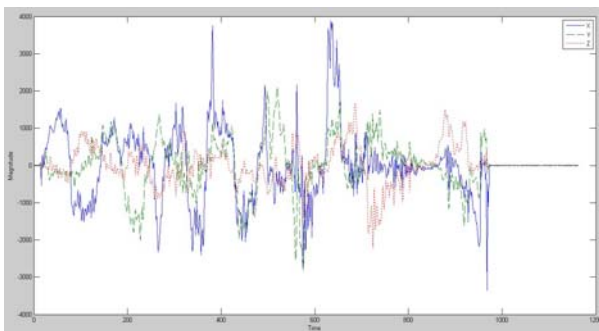


Fig.7. Three axis angle velocity curves

In figure 6, the movement state of three axes are given. Z axis acceleration is caused by the acceleration of gravity. In figure 7, they are three axis angular velocity.

### 3. The Extended Kalman Filter Algorithm

Now the encoder measuring odometry data (Odom) and the inertial measurement data (IMU) can be determined. The full state vector in the space is expressed as

$$x_k = [X_k, Y_k, Z_k, \phi_k, \theta_k, \psi_k, v_k, \omega_k]^T \quad (6)$$

With  $\Delta t$  time, we can get

$$\begin{cases} v_R = \eta \frac{N_L}{\Delta t} \\ v_R = \eta \frac{N_R}{\Delta t} \\ \omega = \frac{v_R - v_L}{L} \\ v = \omega * L \end{cases} \quad (7)$$

Where  $\eta$  is parameter of the wheel diameter and encoder. The pose after  $\Delta t$  will be

$$x_{k+1} = \begin{pmatrix} X_k + v_k \cos(\psi_k) \Delta t \\ Y_k + v_k \sin(\psi_k) \Delta t \\ 0 \\ 0 \\ 0 \\ \psi_k + \omega_k \Delta t \\ v_k \\ \omega_k \end{pmatrix} \quad (8)$$

The EKF data integration system model is given as follows:

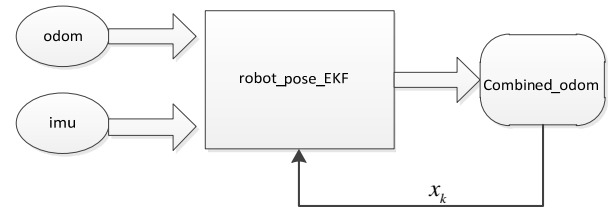


Fig.8. EKF data integration system model

The extended Kalman filter with fusion of encoder and gyroscope data, the system state equation is derived:

$$x_{k+1} = \phi_{k+1|k} x_k + \Gamma_k W_k \quad (9)$$

The measurement model for encoder is

$$y_{odom,k} = C_{odom} x_k = \begin{bmatrix} X_k \\ Y_k \\ \psi_k \\ v_k \\ \omega_k \end{bmatrix} + e_{odom,k}(d) \quad (10)$$

The simplified IMU mathematical model is

$$y_{gyro,k} = C_{gyro} x_k = \begin{bmatrix} \psi_k \\ \omega_k \end{bmatrix} + e_{gyro,k} \quad (11)$$

Error covariance of the matrix is:

$$R(d) = \begin{bmatrix} R_{odom}(d) & 0 \\ 0 & R_{gyro} \end{bmatrix} \quad (12)$$

With above the measurement model and state transition model, using the extended Kalman filtering, the robot pose estimation can be determined.

In order to validate the Kalman filter, with the above data, Matlab simulation is performed.

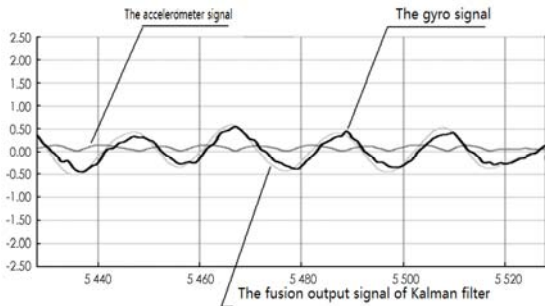


Fig.9. The introduction of Kalman filter wave curve

Figure 9 is the introduction of Kalman filter wave curve. The output curve gets smoothing, and angle estimation accuracy is greatly improved.

#### 4. The Simulation Experiment of SLAM

When we use only the encoder as the sensor, We measured the control noises of mobile robot Kinematics model is:

$$\delta v = 0.4m/s, \delta G = 6radians$$

And when we use the improvement of our new method, the control noises is:

$$\delta v = 0.3m/s, \delta G = 3radians$$

Then we carries on the simulation test of SLAM using the different control noises, the results as below:

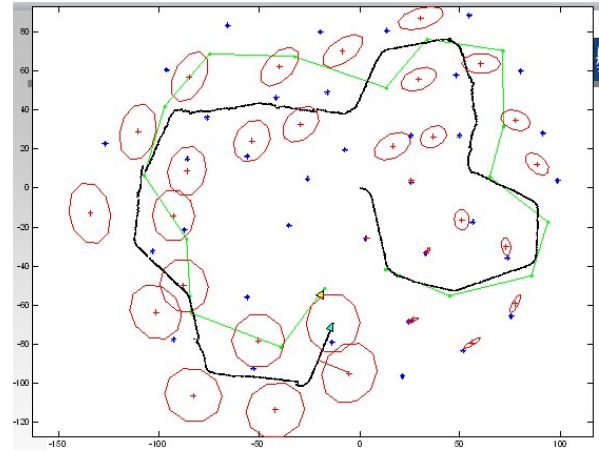


Fig.10.The simulation test of SLAM ( $\delta v=0.4m/s, \delta G=6radians$ )

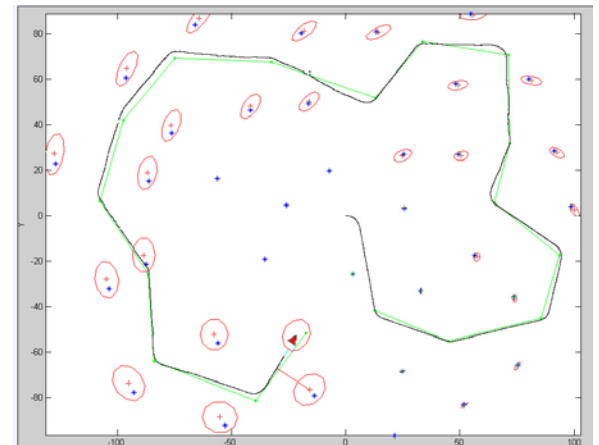


Fig.11.The simulation test of SLAM ( $\delta v=0.3m/s, \delta G=3radians$ )

We can see from the Fig10 and Fig11, after using the new method on SLAM, Robot positioning is more accurate, the robustness is improved obviously.

#### 5. Conclusions

In this paper, the Kalman filtering accelerometer, gyro and the electronic compass fusion method is studied.

Based on dynamic test data, the Kalman filter compensates the sensor drift, noise and other factors caused by the accelerometer, gyroscope and the electronic compass. It reduces the angle measurement error, and improves the operation accuracy. The experiment results show the effectiveness of the proposed method.

## References

1. R. A. Mohammad, Sensor fusion by pseudo information measure: a mobile robot application, *ISA Transactions*, 41 (2002)283-301.
2. A. J. Terrya, M. Z. John, Sensor fusion by a novel algorithm for time delay estimation, *Digital Signal Processing*, 22(2012) 439-452.
3. R. S. Blum, Multisensor image fusion performance limits from an estimation theory perspective, *Information Fusion*, 7(2006) 250-263.
4. A. Weckenmann, X. Jiang, Multisensor data fusion in dimensional metrology, *CIRP Annals-Manufacturing Technology*, 58(2009)701-721.
5. H. Youngjoon, H. Hernsoo, Localization and classification of target surfaces using two pairs of ultrasonic sensors, *Robotics and Autonomous Systems*, 33(2000) 31-41.
6. J. B. Gao, C. J. Harris, Some remarks on Kalman filters for the multisensor fusion, *Information Fusion*, 3(2002)191-201
7. G. Gerasimos, G. Rigatos. Extended kalman and particle filtering for sensor fusion in motion control of mobile robots, *Mathematics and Computers in Simulation*, 81(2010)590-607

# Interactive Musical Editing System to Support Human Errors and Offer Personal Preference for an Automatic Piano

**Kenji Tsunenari**

*Department of Mechanical Information Science and Technology, Kyushu Institute of Technology  
680-4, Kawazu, Iizuka-City, Fukuoka, 820-8502, Japan  
Email: ktsune@mmcs.mse.kyutech.ac.jp*

**Eiji Hayashi**

*Department of Mechanical Information Science and Technology, Kyushu Institute of Technology  
680-4, Kawazu, Iizuka-City, Fukuoka, 820-8502, Japan  
E-mail: haya@mmcs.mse.kyutech.ac.jp*

## Abstract

We have developed a system that allows a piano to perform automatically. In order to play music in the manner of a live pianist, we must add expression to the piano's performance. In the case of music, there are often 1,000 or more notes in the score, requiring that an editor spend a huge amount of time to edit. Therefore, we have developed an interactive musical editing system that utilizes a database to edit music more efficiently.

*Keywords:* Automatic Piano, Knowledge Database, Computer Music, Music Interface

## 1. Introduction

We have developed a system that allows a piano to perform automatically. In this system, 90 actuators have been installed on the keys and pedals of a grand piano. These actuators execute key strokes and pedal movements to govern the piano's performance. (See Fig.1)

In order to develop an automatic piano that plays music in the manner of a live pianist, we have to add expression to the piano's performance. Essentially, variations in tempo, dynamics, and so on are needed in order to arrange the respective tones in a desired way. Moreover, in the case of piano music, there will often be 1000 or more notes in the score of even a short piece of

music, and the editor must spend a huge amount of time to accurately simulate an actual emotionally expressive performance that a highly skilled pianist could give.

Moreover, a highly skilled pianist is able to play an unfamiliar piece of music by sight, even if the performance is not completely in accord with an intended specific musical interpretation. Current computing systems cannot perform a new piece of music by sight, and thus they cannot simulate a human pianist's musical expression. Therefore, we have developed an interactive musical editing system that utilizes a database in order to edit music more efficiently<sup>1</sup>.



In a current research, MIDI data regarding the performances of highly skilled pianists has been analyzed in order to observe the stylistic tendencies of their performances. The results showed that phrases having similar patterns in the same composition were performed in the similar style.

We developed a system that searches for similar phrases throughout a musical score and infers the style of the performance. Here, we proposed a method using Dynamic Programming (DP) matching as a way to search for similar phrases. In our interactive musical editing system, we have created the Score Database which contains information regarding a musical score. This database contains a field called “Note Value,” in which data indicates the type of note--e.g., a quarter note, a triplet, and so on. This system converts notes into character strings using the “Note Value” data.

In addition, the system computes DP matching using the character strings and calculates the degree of disagreement between these strings. It uses an index to judge the resemblance between the strings. For its method of inferring performance expression, it uses the best alignment for DP matching, which enables it to express the best correspondence between notes. In order to edit music more efficiently, we must consider dynamic marking, beat and so on and we created database contains them. We developed an inferring process with regards to similar phrases using the best alignment and database.

In this paper, we describe the results of searching for similar phrases using DP matching and inferring for them using DP matching and database.

## 2. Searching for Similar Phrases

As a result of the analysis, it was found that phrases of the same pattern existing in the same tune are performed in a similar expression<sup>2</sup>. This time, we used DP matching to search for similar phrases.

DP matching is a technique used widely in the field of speech recognition, bioinformatics and so on. It has a feature that can calculate the similarity between two words that are different in a number of characters from each other.

In Fig.2, the route of minimum cost in each point is taken, and the route with the lowest cost is assumed finally to be the optimal path. The cost at that time is



Fig.1. The automatic piano.

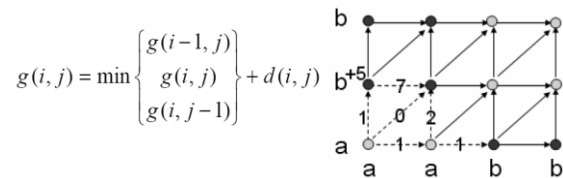


Fig.2. DP Matching

defined as the distance between patterns. In this system, this distance is handled as a threshold to judge whether the phrases are similar to each other.

For example, if the cost moves up or to the right, then it is increased by 1. If it moves to the upper right, then it does not increase. Also, if the characters do not correspond in each point, then the cost is increased by 5.

## 3. Musical Editing Support System

### 3.1. System Architecture

The structure of the system is shown in Fig.3, The

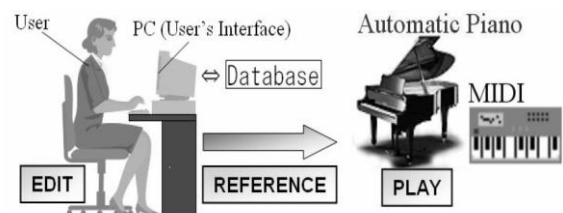


Fig.3. Structure of the editing system

user edits music via the user’s interface on a computer display. The user can also access a database that has musical grammar, the user’s preferences, and so on. As a result, edition work is reduced and efficient editing becomes possible.

**3.2. Format of Performance Information**

The parameters of performance are shown in Tables 1 and 2. The automatic piano that we have developed uses a music data structure that is similar to MIDI. We defined performance information, dividing it into two categories: the notes and the pedals. The note information is comprised of the six parameters involved in producing a tone: “Key” (note), “Velo” (velocity), “Gate”, “Step”, “Bar” and “Time”. “Velo” is the dynamics, given by the value of 1-127. “Gate” is the duration of the note in milliseconds. “Step” is the interval of time between notes, and it also exhibits tempo. “Bar” is the vertical line placed on the staff to divide the music into measures.

The pedal information is comprised of four parameters: “Key” (indicating the kind of pedal: “Damper” or

notation. It is composed of five tables containing “Dynamics marks”, “Articulation marks”, “Symbol of Changing Dynamics or Changing Tempo” (symbol that affects the speed of a note or the increase or decrease of the volume), “Time signature”, and “Tempo marks”. Analyzing a music symbol according to its usage allows efficient information processing by the system.

**3.3.2 Score Database**

This database has symbols including time signatures, notes, rests and so on in standard musical notation. Symbols were pulled together in order of bars, and bar symbols were arranged in a time series. Performance expression in itself is only information such as pitch, strength, and length and concerns only the enumeration of a sound. Because the identification of each sound is difficult, editing of the performance expression is difficult. By adding the Score Database’s information to performance expression, we can connect each note to its enumeration. In doing so, it becomes easy to edit each phrase.

This database consists of three tables, the “Element

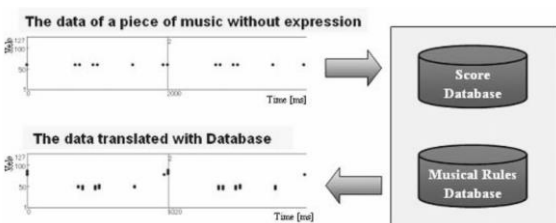


Fig.4. Automatic translation with database

“Shifting”), “Velo” (the pedaling quantity), “Time” (the duration for which the pedal is applied)”, and “Bar”.

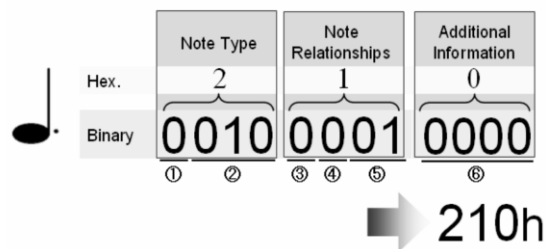
**3.3. Editing Support Process with Database**

Our system can automatically apply a rough performance expression using Musical Rules Database and Score Database. (See Fig.4)

In addition, the system has Preference Database, which stores the editing characteristic of the user.

**3.3.1 Musical Rules Database**

This database contains the architecture of musical grammar necessary to interpret symbols in musical



- ① Note or Rest (0: Note, 1: Rest)
- ② Note Value (000: A whole note, 001: A half note ... etc)
- ③ Tie (If the note has a tie then this number is 1.)
- ④ Ornament  
(If the note has an ornament then this number is 1.)
- ⑤ The number of dots  
(Exceptionally, if it is “11” then the note is tuplet.)
- ⑥ Additional Information  
The number of tuplets. (Triplets: 0011)  
The type of an ornament. (Trill:010) etc...

Fig.5. Note Value

table” (showing the position of the note and the composition of the chord), the “Symbol table” (showing the position of the music symbol) and the “Same table” (showing the position of the repetition of the phrase). The Element table contains the field “Note Value”. Data in this field indicates the type of note, e.g., a quarter note, a triplet, and so on. “Note Value” is expressed by three hexadecimal numbers, which are shown in Fig.5.

### 3.4. Beat Database

We created Beat Database to edit music more efficiently. Beat Database is stored data which is Gerhard Oppitz’s performance of beat expression. Using it, only step is inferred to change tempo.

### 4. Inferring Result

In Fig.6a is an input phrase used to search similar phrase for comparative experiments. Fig.6b is searched similar phrase. It is inferred two methods and results are outputted. First method, similar phrase is inferred, not to use Beat Database. The second method, Beat Database is used. The two results and data that performed by pianist in the similar phrase are compared to confirm improvement of the result.

The results of the experiment are shown Table1 and Fig.7. The results provide three values: the “Existing result” which don’t use Beat Database, the “New result” which use Beat Database and the ”Oppiz data” which is the actual emotional expression in a performance by a Oppitz in the similar phrase. “No.” means note number. “No.1” means the first note in the phrases.

We have consistently found that the emotional expression represented by the “New result” resembles the “Oppitz Data” more than it resembles the “Existing result”



Fig.6. Phrases for inferring

Table 1. Results of inference

StepRate
----------

No.	Existing result	New result	Oppitz data
1	1.0000	0.8962	0.7596
2	1.2115	1.2115	1.2981
3	1.1648	0.9184	0.8240
4	1.0440	0.9144	0.6992
5	1.1500	0.9712	0.6923

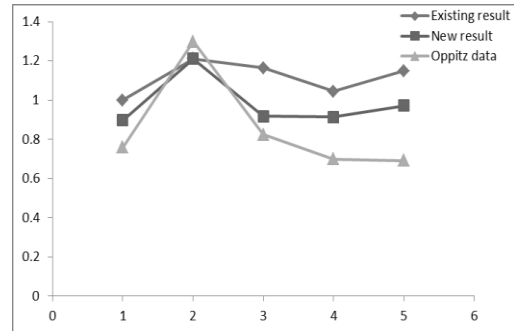


Fig.7. Results of inference

### 5. Conclusion

We developed an interactive musical editing system to edit music more efficiently. This system is composed of a "Searching system of similar-patterned phrases" and an "Inferring system of emotional expression in a performance. The Inferring system infers the emotional expression in a performance of similar phrases by referring to the databases automatically, greatly reducing the time needed for editing. Moreover, the interactive musical editing system provides edited phrases that resemble the "Pianist Data," which are the actual emotional expressions in a performance by a skilled human pianist.

### References

1. E. Hayashi et al, *Behavior of piano-action in a grand piano.I*, Journal of acoustical Society of America, Vol.105, pp.3534-3544, 1999.
2. Y. HIKISAKA and E. Hayashi, *Interactive musical editing system for supporting human error and offering personal preferences for an automatic piano –Method of searching for similar phrases with DP matching and inferring performance expression-*, Proc. Of the 12<sup>th</sup> International Symposium on Artificial Life and Robotics, GS4-3, 2007.

# Modeling of collaboration in design process Based on Channel Theory

**Patchanee Patitad and Hidetsugu Suto**

*Muroran Institute of Technology, 27-1 Mizumoto-cho,*

*Muroran-shi, Hokkaido, 050-8585, Japan*

*Email: info@sdlabo.net*

*www.sdlabo.net*

## Abstract

Collaboration is one of the effective approaches that help us to share knowledge together and exchange ideas within a team member. Sometimes, new helpful knowledge that is not held by the members emerges as a result of the collaboration. Such knowledge often contributes to get prime solutions during collaboration process. However, the way to generate such new knowledge is implicit. In this paper, a method of creating a model, which represents effects of collaboration in design process is proposed. By using this scheme, we can illustrate what new knowledge can be gotten from a collaboration and we can know the effect of the collaboration.

*Keywords:* Collaboration, Channel Theory, design process, synergetic effects

## 1. Introduction

Collaboration is one of the effective approaches that help us to share knowledge together and exchange ideas within a team member. It is a communication process in which two or more people from different disciplines participate in knowledge transfer to achieving a goal of team [1]. During collaboration process, synergetic effects among a team member may contribute to generate novel knowledge. Thus, effective collaborations are expected in a team.

In design area, viewpoints of designers play an important role to bring about a novel design idea [2]. Different experiences and knowledge cause different

viewpoints [3]. Designers can share their viewpoints through collaboration process. Thus, collaboration is a promising method, which assists the designer to create more outstanding design and increase ability to fulfill client's requirement more perfectly. However, the way to generate new knowledge is implicit. Thus, this study aims to represent the process of generating such knowledge by using mathematical model.

As a result of synergetic effects, new knowledge is produced within in collaboration process. To investigate effective collaboration, a representation model of collaboration mechanism is proposed. Channel Theory

© The 2015 International Conference on Artificial Life and Robotics (ICAROB 2015), Jan. 10-12, Oita, Japan

[4] is introduced to create the model. Moreover, Chu space [5], that is a mathematical construction, which represents scheme of infomorphism, is adopted to account for the new knowledge in collaboration system.

## 2. Literature reviews

### 2.1. Related works

There are many researches have applied Channel Theory to study about communication system. For example, Suto et al. have proposed a representation model for communication medium with Channel Theory [6]. This model could describe the semantic information flow, which is corresponding to a kind of medium. Kawakami et al. have proposed a modeling system framework that involves diversity and context dependencies base on Channel Theory [7]. It has the potential to model diversity using the arbitrariness of information flows, Schorlemmer [8] proposed a formalization of knowledge sharing scenarios by using diagram in the Chu category, etc. In this section, Channel Theory and Chu spaces are introduced briefly.

### 2.2. Channel Theory

Channel Theory provides a mathematical framework of qualitative theory of information. The basic concepts of Channel Theory consist of classification, local logic, infomorphism, and information channel.

A classification  $A = \langle tok(A), typ(A), \vDash_A \rangle$  consists of

- (i) a set,  $tok(A)$ , of objects to be classified, called the “tokens of  $A$ ,”
- (ii) a set,  $typ(A)$ , of objects used to classify the tokens, called the “types of  $A$ ,” and
- (iii) a binary relation,  $\vDash_A$ , between  $tok(A)$  and  $typ(A)$ .

A classification is represented with indicating the types to which tokens to be classified.

Given a classification  $A$ , a pair  $\langle \Gamma, \Delta \rangle$  of subsets of  $typ(A)$  is called a “sequent of  $A$ .” A token  $a \in tok(A)$  satisfies  $\langle \Gamma, \Delta \rangle$  if  $a$  is of type  $\alpha$  for  $\forall \alpha \in \Gamma$  then  $a$  is of type  $\beta$  for  $\exists \beta \in \Delta$ . If every token  $a \in A$  satisfies  $\langle \Gamma, \Delta \rangle$ , say  $\Gamma \vDash_A \Delta$ , and  $\langle \Gamma, \Delta \rangle$  is called a “constraint” supported by  $A$ .

A local logic  $\mathcal{L} = \langle A, \vdash_{\mathcal{L}}, N_{\mathcal{L}} \rangle$  consists of a

© The 2015 International Conference on Artificial Life and Robotics (ICAROB 2015), Jan. 10-12, Oita, Japan

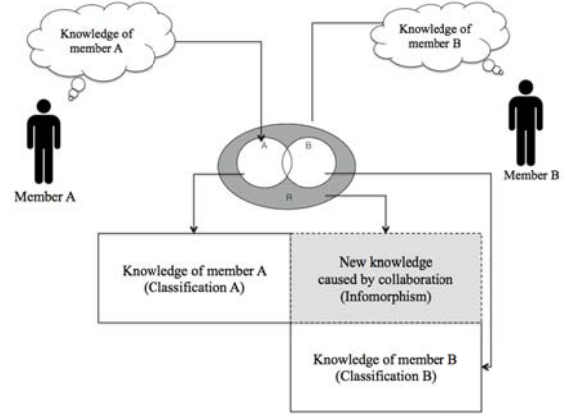


Fig. 1. A framework of collaboration mechanism represented by using Channel Theory

classification  $A$ , a set  $\vdash_{\mathcal{L}}$  of sequents of  $A$  called the constraints of  $\mathcal{L}$ , and a set  $N_{\mathcal{L}} \subseteq tok(A)$  of tokens called the normal token of  $\mathcal{L}$ , which satisfy all the constraints of  $\mathcal{L}$ .

An infomorphism is important relationship between two classifications and provides a way of moving information back and forth between them. Infomorphism  $\langle f^{\wedge}, f^{\vee} \rangle$  is a pair of functions, in which  $f^{\wedge}$  is a function from the types of one of these classifications to the types of the other, and  $f^{\vee}$  is a function from the tokens of one of these classifications to the tokens of the other. Given two classifications,  $A$  and  $B$ , an infomorphism from  $A$  to  $B$  written as  $A \rightleftharpoons B$  satisfies the following Fundamental Property of Infomorphisms:

$$f^{\vee}(b) \vDash_A \alpha \text{ iff } b \vDash_B f^{\wedge}(\alpha) \quad (1)$$

for each token  $b \in tok(B)$  and each type  $\alpha \in typ(A)$ .

An channel  $C$  is an indexed family  $\{f_i: A_i \rightleftharpoons C\}_{i \in I}$  of infomorphisms with a common codomain  $C$ , called the “core of  $C$ .”  $I$  is an index set.

## 3. Proposed model and examples

### 3.1. A model of collaboration mechanism

The framework of proposed model is shown in Fig. 1. Each circle indicates a set of knowledge held by a member. Due to synergetic effects in collaboration, team performance cannot be calculated as simple union of the

abilities of each member. Possibility domain of collaboration can be described as  $R - (A \cup B)$ . This situation can be represented by using classification of Channel Theory as shown below the circles in the figure. Here, we can deduce the knowledge, which can be obtained from synergetic effects by using infomorphism.

By using this scheme, we can demonstrate effective collaboration by representing how new reachable design solution broadens. To verify potential of the proposed framework, example of collaboration in webpage design is used to be a case study.

### 3.2. Example: Layout designer and Color designer

A collaboration between designer A, who is practiced on

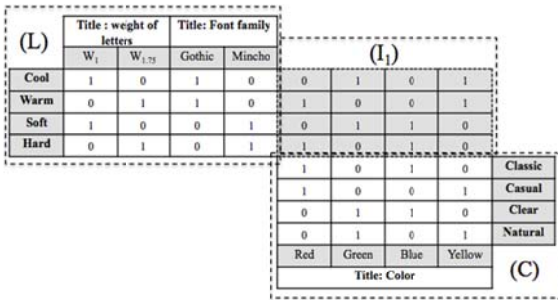


Fig. 2. A model of collaboration in webpage design between layout designer and color design

layout design and designer B, who is proficient on color design is considered as an example. This situation can be represented as matrices shown in Fig. 2 by using the proposed method. In this case, the model consists of three classifications, i.e. L, C, and  $I_1$ .

#### Classification of layout design knowledge (L):

The classification of layout design knowledge is shown in Fig. 3 (L). Here, each token stands for impression and each type stands for layout item, font weight or font style. For example, when font weight is thin and the style is Mincho (Japanese Serif style), it gives cool impression to the observers. Such knowledge can be described as a classification as following:

$$\begin{aligned} tok(L) &= \{Cool, Warm, Soft, Hard\} \\ typ(L) &= \{W_1, W_{1.75}, Gothic, Mincho\} \end{aligned}$$

$$\begin{aligned} Cool \models_L W_1, & \quad Cool \models_L Gothic, & \quad Warm \models_L W_{1.75}, \\ Warm \models_L Gothic, & \quad Soft \models_L W_1, & \quad Soft \models_L Mincho, \\ Hard \models_L W_{1.75}, & \quad Hard \models_L Mincho \end{aligned}$$

Types  $W_1$  and  $W_{1.75}$  mean weights of letters, which define as normal and bold respectively. Types Gothic and Mincho mean font styles of letters in title part, which define as Gothic and Mincho styles respectively.

**Classification of color design knowledge (C):** The classification of color design knowledge is shown in Fig. 3 (C). Here, each token stands for an image and each type stands for color decorating. For example, when webpage is decorated with Red and Blue, it gives classic image to the observers. Such knowledge can be described as a classification as following:

$$\begin{aligned} tok(C) &= \{Classic, Casual, Clear, Natural\} \\ typ(C) &= \{Red, Green, Blue, Yellow\} \end{aligned}$$

$$\begin{aligned} Classic \models_C Red, & \quad Classic \models_C Blue, & \quad Casual \models_C Red \\ Casual \models_C Yellow, & \quad Clear \models_C Green, & \quad Clear \models_C Blue, \\ Natural \models_C Green, & \quad Natural \models_C Yellow \end{aligned}$$

**Infomorphisms from L to C ( $I_1$ ):** Each line in the ( $I_1$ ) means a combination between a token in classification L and a token in classification C. For instance, Cool in (L) is combined with the Natural in (C) because the first line of ( $I_1$ ) has the same element of the fourth line of (C). While, each column in the ( $I_1$ ) means a combination between a type in classification L and a type in classification C. For instance, Red in (C) is combined with  $W_{1.75}$  in (L) because the leftmost column

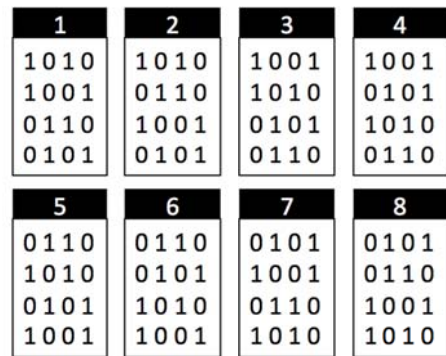


Fig. 3. Infomorphisms from layout design knowledge to color design knowledge

of ( $I_1$ ) has the same element of the second column from the left in (L).

In this case, infomorphisms are established from “classification of layout design knowledge” to “classification of color design knowledge.” Eight infomorphisms have been obtained as shown in Fig. 3. It means there are eight situations that may occur when layout designer and color designer collaborate in a design process. Each situation explains new knowledge, which layout designer and color designer obtained from cooperation in the design process. However, all possible situations are derived with the proposed method. Thus, we cannot say that all situations are proper understanding in the context. For example, in Fig. 3., infomorphism 1 shows that

$$\begin{aligned} f^{\wedge}(\text{Cool}) &= \text{Classic}, & f^{\wedge}(\text{Warm}) &= \text{Casual}, \\ f^{\wedge}(\text{Soft}) &= \text{Clear}, & f^{\wedge}(\text{Hard}) &= \text{Natural} \end{aligned}$$

From this infomorphism, a designer can understand that the design, which has cool imoression, is corresponding with classic image, while warm impression is corresponding with casual image. Moreover, soft impression is corresponding with clear image and hard impression is corresponding with natural image. It can say that this new knowledge is possible to be true because this knowledge is consistent in semantics. Meanwhile, infomorphism 2 shows that

$$\begin{aligned} f^{\wedge}(\text{Cool}) &= \text{Classic}, & f^{\wedge}(\text{Warm}) &= \text{Clear}, \\ f^{\wedge}(\text{Soft}) &= \text{Casual}, & f^{\wedge}(\text{Hard}) &= \text{Natural} \end{aligned}$$

From this infomorphism, cool impression and hard impression can be implied as same as infomorphism 1. But soft impression is corresponding to casual image and warm impression is corresponding to clear image. It must be misunderstanding because warm impression is conflict with clear image according to the theory of science of color [9].

#### 4. Conclusion

A modeling method of collaboration mechanism is proposed based on Channel Theory. An example of webpage design case was shown as case studies. The example is illustrated the situation that two designers who have different knowledge, collaborated in a webpage design process. In the example, designer A is practiced on layout design whereas designer B is proficient on layout design. They could have several possible knowledge as a result of the collaboration.

We can say that the proposed model can explicitly represent the situation, which possible to occur in collaboration in a webpage design process. However, we cannot say that all situations are correct understanding because all possible situations are derived with the proposed method. Nevertheless, with using the proposed model, we can illustrate potential of collaboration by representing how new reachable design solution broadens.

#### Acknowledgement

This work was supported by Grants-in-Aid for Scientific Research from Japan Society for the Promotion of Science (NO.23611025) and Grants-in-Aid for research advancement from Muroran Institute of Technology (2014).

#### References

1. G.W. Dickson and G. DeSanctis, *Information Technology and the Future Enterprise: New Models for Managers*, 1st edn. (Prentice Hall PTR Upper Saddle River, NJ, USA, 2000).
2. H. Suto, P. Patitad and N. Kang, A collaboration Support Tool for Multi-cultural Design Team Based on Extended ADT Model, in *Proc. HCI Conf.* (Crete, Greece, 2014), pp. 548-557.
3. F. DeALtienne, Viewpoints in co-design: a field study in concurrent engineering, *DES STUD.* **26**(3) (2005) 215-241.
4. J. Barwise and J. Seligman, *Information Flow: The Logic of Distributed Systems* (Cambridge Univ. Press, 1997).
5. M. Barr, *-Autonomous Categories*, LECT NOTES MATH **752**. (Springer-Verlag, Berlin, 1979).
6. H. Suto, T. Taniguchi and H. Kawakami, A Study of Communication Scheme for Media Biotope, in *Proc. SICE Annu. Conf.* (Tokyo, Japan, 2011), pp. 206-209.
7. H. Kawakami, T. Hattori, T. Shiose and O. Katai, Modeling of System Diversity Based on Qualitative Information Theory, *WSEAS Trans. Syst.* **10**(5) (2006) 2411-2417.
8. M. Schorlemmer, *Duality in Knowledge Sharing* (The university of Edinburgh, UK, 2002).
9. S. Kobayashi, *A book of colors: matching colors, combining colors, color designing, color decoration*, (Kodansha, USA, 1987).

# **Sterilizing system of ballast water using an arc discharge**

**Jae-cheol Lee, Seung-hwa Baek, Sheng-Xu Piao**

*Department of Electrical Engineering, Pusan National University, Address  
Jangjeon-dong, Geumjung-gu, Korea*

**Hee-Je Kim**

*Department of Electrical Engineering, Pusan National University, Address  
Jangjeon-dong, Geumjung-gu, Korea*

*E-mail: piaoshengxu88@hotmail.com, heeje@pusan.ac.kr*

*[www.pusan.ac.kr](http://www.pusan.ac.kr)*

## **Abstract**

The inadvertent transfer of harmful aquatic organisms and pathogens in the ballast water of ships has been determined to cause a significant adverse impact to all around the world coastal regions. Recently, in order to solve this issue, a number of technologies have been developed and commercialized. Most of the treatment technologies are barely used independently. In addition, there are several combined methods to treat the ballast water. The overall aim of this study is to suggest on of the best way of sterilization of ballast water using DAB Charging and high voltage pulsed arc discharge.

*Keywords:* Sterilization System, Ballast Water, DAB.

## **1. Introduction**

Ballast water from ships has been established as a potential vector for transference of various species around the world. The shifts will have negative impacts on the environment through factors such as competition for food, altered substrate or ambient temperature and light availability [1]. The International Maritime Organization (IMO) has estimated that every year the world's fleet moves ten billion tons of ballast water around the world and that on average more than 3000 species of plants and animals are being transported daily around the world. Once these are introduced to local environment, it is virtually impossible to get rid of them. This could have a permanent effect on the environment,

which could bring catastrophic effect on local fisheries. It is therefore imperative that introduction of harmful aquatic organisms is prevented rather than cured afterwards. In Process of loading and discharging the ballast water, we apply our arc discharge technologies to the object species that is not effectively disinfected chemically or filtered physically.

*©The 2015 International Conference on Artificial Life and Robotics (ICAROB 2015), Jan. 10-12, Oita, Japan*



## 2. The sterilization of ballast water

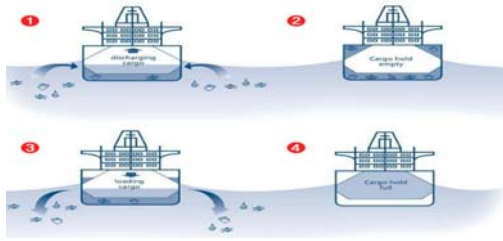
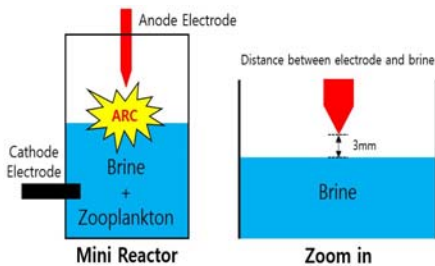


Fig.1 The schematics of ballast water.

As shown in Fig. 1, an introduction of harmful aquatic organisms is prevented rather than cured afterwards. Especially the processes for the balance of the large ship, many kinds of the harmful aquatic organisms are moved to the different ocean by this ballast water. Because of this problem, IMO declared the importance of sterilization. In the processes of loading and unloading the ballast water, it is very important to eliminate many

## 3. Experimental processes

Arc discharge generates under the certain condition like some distance between electrodes or voltages applied. In this study, the distance between the seawater surface and electrode edge was an important factor. To make the constant discharge during the sterilization experiments, we have to keep that distance within 1cm between the seawater surface and the needle electrode



edge.

Fig. 2. The electrode edge and the seawater surface.

However the oxidation and combustion of needle electrode is inevitable during arc discharge. Therefore, the distance between the electrode edge and the seawater surface increased as the electrode edge was worn out, the discharge was not lasted more over. In this process, we want to keep the certain distance between the electrode edge and the seawater surface using a motor control.



Fig. 3. The boosting circuit for 20KVDC arc discharge.

For the first active experiments of sterilizing organisms with high voltage arc discharge treatment system, we have made the high voltage circuit that can cause reasonable arc discharge. The first circuit in this picture can make 2kV with 20kHz from 12VDC Input. A MC34063 for boost topology, IR2153 and 2:340 turn ratio transformer were used for fly-back topology. After that, this output connected to the Cockcroft Walton voltage multiplier circuit that can boost from 2kVAC to more than 20kVDC. To make the active arc discharge, the voltage more than 5kV is needed. But in this case, as the applied arcing voltage between the seawater and the electrode edge is needed more than between metal electrodes.

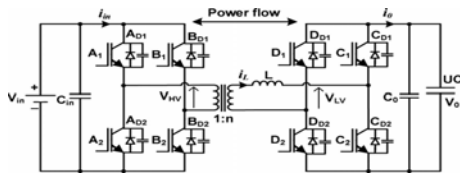


Fig. 4. DAB converter

Shown Fig.4, we use DAB to charge a capacitor. The DAB is a bidirectional converter having characteristic of Phase shift, Buck+Boost bidirection, not needing additional snubber and high efficiency and ZVS.

If use this circuit we can Quicker Charging.

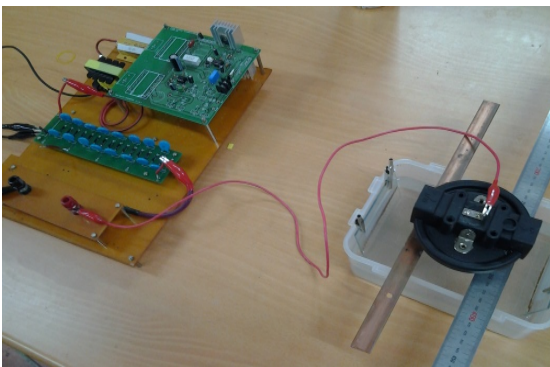


Fig. 5. Arc discharge experiment to Artemia cysts.

To confirm the sterilizing effect of this arc discharge treatment system, we bred artemia cysts that is the kind of brine shrimp causing harmful effects to non-native coastal region. The cysts hatch after 48hours in salt water illuminated light source.

In the arc discharge experiment, the 20kVDC output from the circuit generating high voltage was applied between the seawater surface and the needle electrode. Saltwater same as salinity of seawater of 500ml is used in this experiment to spread the hatched cysts in this salt water.

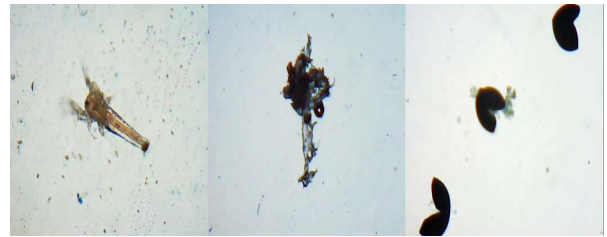


Fig. 6. Artemia cysts and their eggs before and after the experiments.

After arc discharge about 10minutes, most of them were sterilized. They were sterilized and melted by the ozone and OH radical produced from arc discharge. However the fixed needle electrode was shortened by the oxidation and combustion for discharge process. As increasing the distance between needle electrode and saltwater, the discharge processes were stopped. Originally sharpened needle electrode was shortened and flattened after many trials of discharging experiments.

#### 4. Conclusion

Our studies show that arc discharge treatment system is potentially effective to adopt the technology for ballast water management. Species which cannot easily disinfected chemically or filtered physically are subject to sterilized by pulsed power and electrical energy during arc discharge experiment. As the arc phenomenon by the pulsed power, it is more cost effective than the other treatment methods. This study also showed that oxidized and flattened electrodes by the arc discharge need to be controlled by motor control to increase the efficiency of stabilizing processes, the distance between electrode and seawater has to keep the certain distance. In this part, the control system can move automatically to sustain a constant rate by the speed of shortening needle. Further research has to be needed from these basic ideas and active experimental results.

## **Reference**

1. Sutherland T. F, Levings C. D, Petersen S, Hesse W. W., Mortality of Zooplankton and Invertebrate Larvae Exposed to Cyclonic Pre-Treatment and Ultraviolet Radiation., MTS Journal. 37(2) (2001) .
2. Hee-Je Kim et. al, terilization system for ballast water, (patent No. 10-1178382 , korean ,2012).
3. “App Note 500 - Calculating Capacitor Charge Time” , TDK-Lambda, 2009

# The design of medical ruby laser power supply system using LLC resonant converter

**Jaechol Lee**

*Electrical Engineering Department, Pusan National University, Jangjeon 2-dong, Geumjeong-gu  
Busan, Korea*

**Piao Shengxu**

*Electrical Engineering Department, Pusan National University, Jangjeon 2-dong, Geumjeong-gu  
Busan, Korea*

**Zheng Tao**

*Electrical Engineering Department, Pusan National University, Jangjeon 2-dong, Geumjeong-gu  
Busan, Korea*

**Heeje Kim**

*Electrical Engineering Department, Pusan National University, Jangjeon 2-dong, Geumjeong-gu  
Busan, Korea*

*E-mail: [dl7553@naver.com](mailto:dl7553@naver.com), [heeje@pusan.ac.kr](mailto:heeje@pusan.ac.kr)*

*[www.pusan.ac.kr](http://www.pusan.ac.kr)*

## Abstract

Because of its usability, the use of ruby laser for medical therapy has attracted a lot of interest. LLC resonant converter is used to control laser power density in ruby laser power supply. Zero voltage switching(ZVS) is implemented to minimize switching loss by LLC resonant converter. We use DAB(Dual Active Bridge) to charge the capacitor. We obtained maximum laser output of 0.5J. Repetition of laser out is 3Hz.

*Keywords:* Ruby laser, LLC resonant converter, ZVS, DAB

## 1. Introduction

According to development of laser over almost all industrial fields, the application using laser in medical field is also expanding rapidly. Nowadays, as a one of the most convenient and strong clinical devices, the range of laser use is becoming wider more and more in clinical parts such as not only curable disease but also

diagnosis and treatment of disease, and frequency of use is increasing.

Medical ruby laser was used for vascular lesion at the beginning of development but not used now. Recently, laser is used widely in dyspigmentation, for example freckle or blemish, and used in tattoo removal

©The 2015 International Conference on Artificial Life and Robotics (ICAROB 2015), Jan. 10-12, Oita, Japan

using Q-switched pulse increased strength and shortened irradiation time.

This paper aims the development of power supply for laser output of 3Hz\*0.35J. The Power supply was designed using LLC resonance converter in 2kW class.

## 2. Laser power supply

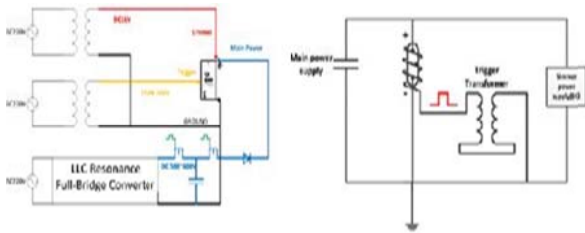


**Figure 1 Laser power supply(left) and Simmer mode triggering circuit(right)**

Solid laser power supply consists of trigger power supply, simmer power supply, and main power supply, as shown Fig.1. Laser is generated by intense visible ray made from Xenon lamp through conducting high current instantaneously to Xenon lamp. For conducting high current lamp, impedance should be low. Lowering lamp impedance is triggering. Through this we can make visible ray in Xenon lamp in condition of relatively low voltage.

In this paper, we use simmer mode triggering circuit like Fig 1. This method enables miniaturization and has large advantage of enabling to secure stability of circuit by separation main power from triggering power supply. Lamp is ionized stably by keeping low current DC voltage in Xenon lamp.



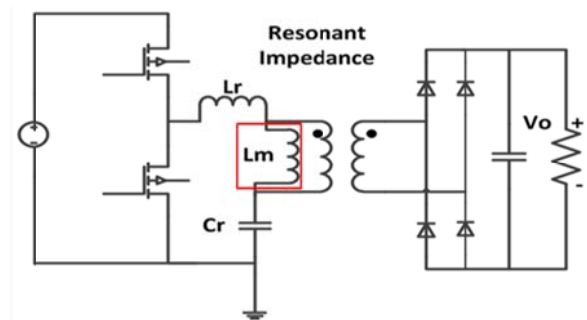
ip

When triggering acts like Fig.2 steamer discharge is generated in Xenon lamp. Then lamp impedance is lowered, so Arc discharge can be made of relatively low voltage.

## 3. LLC resonant converter design.

The main power supply was designed applied LLC resonant converter. The aims of main power supply are charging voltage into high capacity condenser continuously, generating Arc discharge through high current conducted into Xenon lamp when the capacitor discharges.

The converter enables  $L_m$  to be concerned with resonant tank through reducing difference between  $L_r$  and  $L_m$  compared with LC resonant converter. LLC resonant converter can make regulated power over wide range of input voltage and in condition of relatively little frequency fluctuation. Also the efficiency of converter is increased by ZVS(Zero Voltage Switching) that reduces switching losses.



or

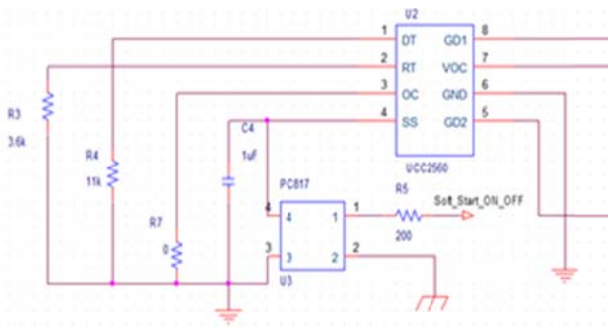
## 4. Soft start applied UCC25600

In laser power supply, excessive inrush current occur because when laser oscillation, the voltage charged in capacitor is discharged so to recharge this. Therefore soft start should be applied to block the inrush current so to assure stability of power supply in addition to beginning parts, whenever laser oscillation occur. This is made by combining photo coupler and SS pin , controlling soft start operation of the chip, of UCC25600

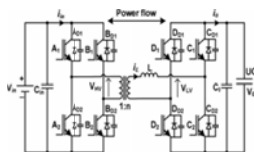
As shown Fig. 4, capacitor is discharged when photo coupler act, and then the capacitor recharged operated soft start.

Table 1. Specification of converter

Maximum input voltage	310V
Minimum input voltage	270V
Average input voltage	290V
Output voltage	600V
Output current	3.5A
Maximum power	2.1kW



5. Dual Active Bridge



erter

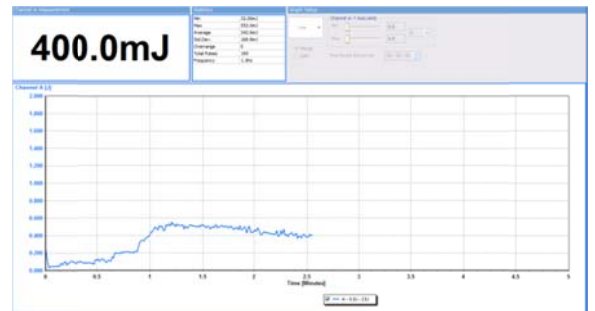
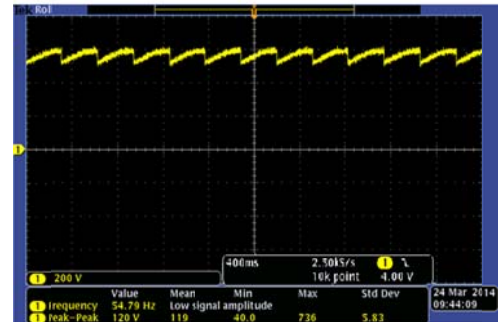
Shown Fig.5, we use DAB to charge a capacitor. The DAB is a bidirectional converter having characteristic of Phase shift, Buck+Boost bidirection, not needing additional snubber and high efficiency and ZVS.

It is appropriate low voltage battery charge system so generally used for robot battery charge system.

We use this circuit just restrictively to test this circuit before design robot battery charge system.

6. Result

In 3Hz experiment, 0.5J of light output is generated with 600V of charging voltage. Depending on increasing charging voltage, laser output increases.



7. Conclusion

Today, a medical laser is the most actively studied field of many laser fields and the optimization of power supply is urgent. In this study we design ruby laser power supply that has 3Hz\*0.35J output and research the change of laser output with regard to charging voltage. When charging voltage increases, light output also increases and 0.5J of light output is generated at 600V, the maximum charging voltage. If we increase repetition to 4Hz, it is expected to 0.25J of light output generated.

8. References

[1] Jin Yun-Sik, Kim Hee-Je, "Fabrication of Compact Ruby

Laser and its Operation Characteristics”, KIEE, 1995.7.

[2] Alex D. McLeod, “Design Consideration for Triggering of Flashlamps”, PerkinElmer, 1998.

[3] “App Note 500 – Calculating Capacitor Charge Time”, TDK-Lambda, 2009.

[4] Sam Abdel-Rahman, “Resonant LLC Converter : Operation and Design”, Infineon, 2012.

[5] UCC25600 Datasheet, Texas Instruments, 2011.

# Online Rule Updating System Using Evolutionary Computation for Managing Distributed Database

Wirarama Wedashwara, Shingo Mabuchi, Masanao Obayashi and Takashi Kuremoto  
Graduate School of Science and Engineering, Yamaguchi University  
Tokiwadai 2-16-1, Ube, Yamaguchi 755-8611, Japan  
E-mail: {t001we, mabuchi, m.obayashi, wu}@yamaguchi-u.ac.jp

## Abstract

This research proposes a decision support system of database cluster optimization using genetic network programming (GNP) with on-line rule based clustering. GNP optimizes cluster quality by reanalyzing weak points of each cluster and maintaining rules stored in each cluster. The maintenance of rules includes : 1) adding new relevant rules, 2) moving rules between clusters and 3) removing irrelevant rules. The simulation focuses on optimizing cluster quality response against several unbalanced data growth to the data-set that is working with storage rules. The simulation results of the proposed method shows better results compared to GNP rule based clustering without on-line optimization.

*Keywords:* Genetic Network Programming, Rule Based Clustering, Cluster Optimization

## 1. Introduction

Nowadays many large scale database systems with very high data growth are being utilized to improve the global human activity, such as communication, social networking, transaction, banking, etc. A distributed database management system becomes a solution to improve data access speed by organizing data in multiple storages for multiple types of user accesses. Problems of distributed database management system are not only how to manage the number of data, but also how to organize data patterns in distributed storages. Clever data organization is one of the best ways to improve the retrieval speed and reduce the number of disk I/Os and thereby reduce the query response time.

In this paper, we propose a decision support system for database cluster optimization using Genetic Network Programming (GNP) with on-line rule based clustering. Main purpose of this research is to provide an on-line

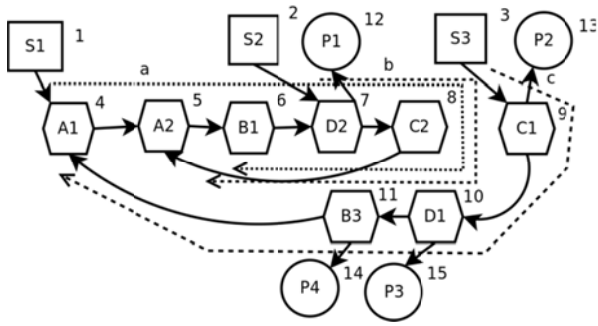
algorithm to maintain the cluster adaptability against several unbalanced data growth. For example, the unbalanced data growth occurs when different kinds of items (data) comparing to the items stored in the current database begin to be stored as the time goes on (the trend of data is changed).

## 2. Review of the Proposed Framework

### 2.1. Rule Based Clustering

Rule based clustering is one of the solutions to provide automatic database clustering and interpretation of data storage patterns. Rule based clustering represents data patterns as rules by analyzing database structures on both of attributes and records<sup>3,4</sup>.





$$s = \frac{b - a}{\max\{a, b\}}$$

$$= \begin{cases} 1 - a/b & \text{if } a < b \\ 0 & \text{if } a = b \\ b/a - 1 & \text{if } a > b \end{cases}$$

Fig. 1. GNP Implementation on Cluster Optimization.

Table 1. Gene Structure of GNP Corresponding to the Program in Fig. 2.

i	NTi	Ai	Ri	Ci
1	1	0	0	4
2	1	0	0	7
3	1	0	0	9
4	2	A	1	5
5	2	A	2	6
6	2	B	1	7
7	2	D	2	8,12
8	2	C	2	5
9	2	C	1	10,13
10	2	D	1	11,15
11	2	B	3	4,14
12	3	1	1	0
13	3	2	3	0
14	3	3	2	0
15	3	4	4	0

**2.2. Genetic Network Programming**

Genetic network programming (GNP) that is an evolutionary optimization technique with directed graph structures is used to provide data classification. GNP has a distinguished representation ability with compact programs, which is derived from the re-usability of nodes that is inherently equipped function of the graph structures. For the purpose of rule based clustering, GNP is useful to handle rule extraction from data-sets by analyzing the records.

**2.3. Silhouette**

Silhouette value is used to evaluate the clustering results. Silhouette provides a succinct graphical representation of how well each object lies within its cluster<sup>5,8</sup>. Silhouette value is calculated by Eq. 1.

s: Silhouette value for a single sample. The Silhouette value for a set of samples is given as the mean of the Silhouette values of each sample, a: mean distance between a sample and all the other points in the same cluster, b: mean distance between a sample and all the other points in the second nearest cluster. A good clustering result will make the silhouette value be close to 1.0 and a bad clustering result will close to -1.0. Silhouette value is used as a threshold in the rule updating process of GNP.

**3. Detail of the Proposed Method**

GNP optimizes the cluster quality by re-analyzing each cluster and updating rules stored in each cluster. The proposed method provides a rule updating mechanism as an additional function to maintain rules as shown in Fig 1. The rule updating mechanism includes: 1) adding new relevant rules; 2) moving rules between clusters and 3) removing irrelevant rules. The rule extraction and rule updating task is executed by the evolutionary optimization technique of GNP to get the best cluster adaptability against several unbalanced data growth.

GNP is used to extract rules from a data-set by analyzing all the records. Phenotype and genotype structures of GNP are described in Fig. 1 and Table 1, respectively. In Fig. 1, each node has its own node number (1–15), and in Table 1, the node information of each node number is described. The program size depends on the number of nodes, which affects the amount of rules created by the program. There are 3 kinds of nodes used in GNP rule extraction for the cluster rule updating. 1) Start node (rectangle) represents the start point of the sequence of judgment nodes which are executed sequentially by their connections. Multiple placements of start nodes will allow one individual to extract a variety of rules, which is shown in Table 1 2) Judgment node (hexagon) represents an attribute of the data-set, which is represented by Ai showing an index of attribute i such as price, stock, etc., and Ri showing a range index of attribute i. For example, Ai=A represents price attribute,

and  $R_i=1$  represents value range  $[0,50]$  and  $R_i=2$  represents value range  $[51,80]$ . 3) Processing node (round) shows the end point of the sequence of judgment nodes and processes the rule updating in a cluster whose cluster number is described in the processing node. For example P1 processes an addition of extracted rules to cluster no 3. Multiple placement of processing nodes will make one individual extract variety of rules, which is shown in Table 2. Sequences of nodes starting from each start node ( $S_1, S_2, S_3$ ) are represented by dotted line a, b and c. A node sequence flows until support for the next combination does not satisfy the threshold. The nodes with the attributes that have already appeared in the sequence will be skipped. Candidate rules extracted by the program of Fig. 1 to the data-set of Table 1 are shown in Table 2. In Table 2, three rules are extracted by the node sequence from each start node.

Fig. 2 shows an example of the Silhouette values of rules with only one attribute. In Fig. 3 threshold is set at 8.5, so only the attributes with Silhouette values under 8.5 will be used for the judgment nodes in GNP for rule extraction. In Fig. 2, attribute of price is not included in the rule extraction of GNP because its silhouette values are never under 8.5 (rule updating is not necessary), but the values of stock and weight for some data are under 8.5, thus those attributes are included in GNP for updating rules. Each cluster has dominant values of attributes which are anchors of cluster quality, which then influence the silhouette values. For example, when 10kg is a dominant value for the attribute of weight in a cluster, farther values from 10kg will have a lower silhouette and should be moved to another cluster to improve the cluster quality.

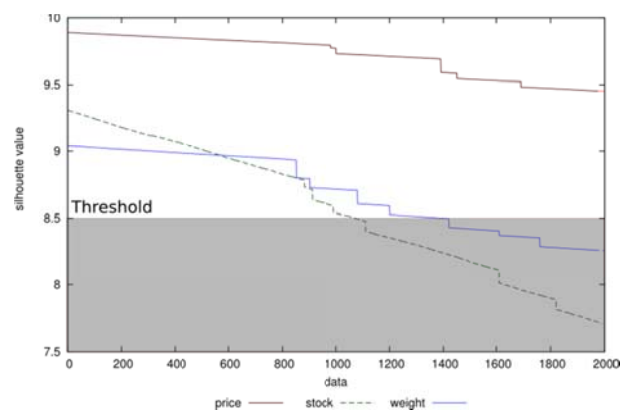


Fig. 2. Example of Silhouette Values

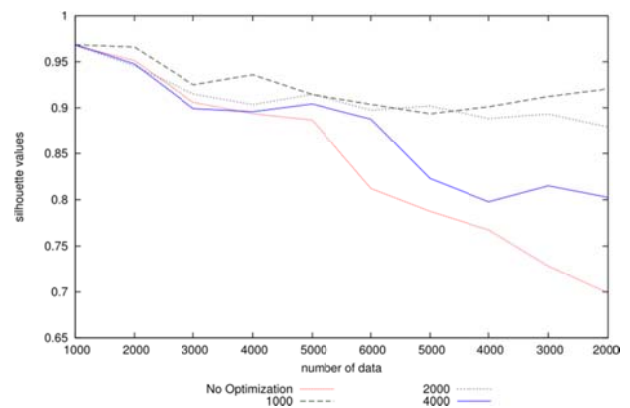


Fig. 3. Graph of Simulation Results of Rule Updating Frequency and Number of Data Comparison.

#### 4. Simulation

The simulation focuses on verifying the cluster adaptability against several unbalanced data growth of the data-set, where cluster adaptability is evaluated by silhouette values. Data-set used in the simulations has 1000 data with 8 attributes. The adaptability is

Table 3. Simulation Result of Rule updating Frequency and Number of Data Comparison.

Step	Number of Data	Increment/Decrements	Rule updating frequency			
			No rule updating	1000	2000	4000
1	1000 (Default)	-	0.967	0.967	0.967	0.967
2	2000	+1000	0.945	0.965*	0.944	0.947
3	3000	+1000	0.902	0.923*	0.915*	0.899
4	4000	+1000	0.892	0.935*	0.902	0.895
5	5000	+1000	0.882	0.912*	0.909*	0.903*
6	6000	+1000	0.812	0.902*	0.897	0.887
7	5000	-1000	0.787	0.892*	0.901*	0.821
8	4000	-1000	0.765	0.901*	0.888	0.797
9	3000	-1000	0.723	0.912*	0.892*	0.815*
10	2000	-1000	0.698	0.909*	0.879	0.802
Average			0.832	0.938	0.923	0.8845

evaluated by the following two points. 1) The number of data in the database is changing as the time goes on. The initial number of data is 1000, then every time step, 1000 new data are added to the database. After the number of data reaches 6000, 1000 data are decreased every time step. 2) The rule updating frequency, where the rule updating is executed when a predefined number of new data are given to the data-set (this predefined number is defined as "rule updating frequency"). For example, if the rule updating frequency is 1000, the rule updating will be processed every increments or decrements of 1000 data. The comparisons of the simulation results are carried out between four methods, i.e., the proposed method with rule updating frequency of 1000, 2000 and 4000, and the clustering method of standard GNP without online rule updating.

The silhouette values obtained by the four methods are shown in Table 3, and Fig. 3. Star marks (\*) on the side of silhouette values show the times when the rule updating is carried out. The rule updating frequency of 4000 shows only a slight difference from no rule updating but shows increment of silhouette values in step 5 and 9, which means that the rule updating is effectively carried out. The best results are obtained by the rule updating frequency of 1000, where silhouette values are stable with relatively high level compared to other frequency parameters. Rule updating frequency of 2000 also shows decrements on step 3, which previous silhouette value are high enough.

## 5. Conclusions

This paper proposed a new rule updating mechanism for distributed database with unbalanced data growth. The simulation results of the proposed method showed the better clustering results comparing to GNP rule-based clustering without on-line adaptation. In the future, we

will apply fuzzy membership functions to attribute judgment to make rules with better clustering ability.

## References

1. Kaoru Shimada, Kotaro Hirasawa, and Jinglu Hu. Genetic network programming with acquisition mechanisms of association rules, *JACIII*. 10(1) (2006) 102-111.
2. Shingo Mabu, Ci Chen, Nannan Lu, Kaoru Shimada, and Kotaro Hirasawa. An intrusion-detection model based on fuzzy class-association-rule mining using genetic network programming Systems, *Man, and Cybernetics, Part C: Applications and Reviews, IEEE Transactions on*. 41(1) (2011) 130-139.
3. Mansoori, E.G., FRBC: A Fuzzy Rule-Based Clustering Algorithm, *Fuzzy Systems, IEEE Transactions*. 19(5) (2011) 960-971.
4. Sinaee, M.; Mansoori, E.G., Fuzzy Rule Based Clustering for Gene Expression Data, *Intelligent Systems Modelling & Simulation (ISMS)*, 4th International Conference (2013) 7-11.
5. Zhao, JiangFei and Huang, TingLei and Pang, Fei and Liu, YuanJie, Genetic algorithm based on greedy strategy in the 0-1 knapsack problem, *Genetic and Evolutionary Computing*, 3rd International Conference on (2009) 105-107.
6. Sylvain Guinepain and Le Gruenwald. Using cluster computing to support automatic and dynamic database clustering, *Cluster Computing IEEE International Conference*, (2008) 394-401.
7. Sylvain Guinepain and Le Gruenwald. Automatic database clustering using data mining. *Database and Expert Systems Applications, DEXA IEEE* 06(17) (2006) 124-128.
8. Yanchi Liu, Zhongmou Li, Hui Xiong, Xuedong Gao, and Junjie Wu. Understanding of internal clustering validation measures, *Data Mining (ICDM) IEEE 10th International Conference*, 10 (2010) 911-916.

# Reinforcement Learning with Symbiotic Relationships for Multiagent Environments

**Shingo Mabu**

*Graduate School of Science and Engineering, Yamaguchi University, Tokiwadai 2-16-1  
Ube, Yamaguchi , 755-8611, Japan*

**Masanao Obayashi**

*Graduate School of Science and Engineering, Yamaguchi University, Tokiwadai 2-16-1  
Ube, Yamaguchi , 755-8611, Japan*

**Takashi Kuremoto**

*Graduate School of Science and Engineering, Yamaguchi University, Tokiwadai 2-16-1  
Ube, Yamaguchi , 755-8611, Japan*  
*E-mail: mabu@yamaguchi-u.ac.jp, m.obayas@yamaguchi-u.ac.jp, wu@yamaguchi-u.ac.jp*

## Abstract

Studies on multiagent systems have been widely studied and realized cooperative behaviors between agents, where many agents work together to achieve their objectives. In this paper, a new reinforcement learning framework considering the concept of “Symbiosis” in order to represent complicated relationships between agents and analyze the emerging behavior. In addition, distributed state-action value tables are also used to efficiently solve the multiagent problems with large number of state-action pairs. From the simulation results, it is clarified that the proposed method shows better performance comparing to the conventional reinforcement learning without considering symbiosis.

*Keywords:* reinforcement learning, symbiosis, multiagent system, cooperative behavior,

## 1. Introduction

There are many situations where interests of some parties are coincided or conflicted<sup>1</sup>, for example, human relationships, cooperation or competition between companies, and even international relationships. Recently, the globalization is rapidly progressing, thus, the relationships between persons and organizations have become very complicated networks. On the other hand, information systems have been intelligent and

working cooperatively with each other, for example, cloud networks, car navigation systems and automation by robots. Research on complex networks began around 1998<sup>2</sup> and have attracted attentions recently as an important research for analyzing phenomena in social systems. Therefore, a model that can predict problems caused by the complex networks and propose the optimal solutions for the problems will be useful for realizing safe and secure social systems. In addition, if

the best relationships between parties can be found, it will contribute to the development of the whole society.

In this paper, a novel reinforcement learning algorithm that introduces a concept of "Symbiosis" in order to build Win-Win relationships between parties even if each party is pursuing the maximization of its own profits. Symbiosis can be defined as a relationship where two or more organisms live in close association with each other<sup>3</sup>, and several computational models based on the symbiosis in the ecosystem have been studied<sup>4-7</sup>.

In the proposed reinforcement learning method, multiagent environments are considered where there are several agents (persons and organizations) that have cooperative, competitive or self-satisfied relationships, and such relationships are defined as "symbiotic vectors". The symbiotic vectors consist of six basic symbiotic relationships, i.e., mutualism, harm, predation, altruism, self-improvement and self-deterioration. The symbiotic vectors are used to calculate rewards given to each agent when updating Q values in reinforcement learning. The symbiotic vectors contain not only the target direction of self-profit, but that of the other agents working in the same environment. Therefore, the proposed method can predict the results under the current symbiotic relationships by implementing simulations.

This paper is organized as follows. In section 2, Q learning algorithm with distributed state-action value table is introduced for efficiently solving the multiagent problems with large number of state-action pairs. Section 3 explains the proposed learning algorithm using symbiotic vectors. Section 4 describes the simulation environments and results. Finally, section 5 is devoted to conclusions.

## 2. Q learning with distributed state-action value tables

In the standard reinforcement learning, the number of state-action pairs increases exponentially as the numbers of inputs, objects to be perceived, and possible actions increase, that is called "The curse of dimensionality"<sup>8</sup>. Therefore, Q learning algorithm with distributed state-action value table (Q table) is introduced in this paper.

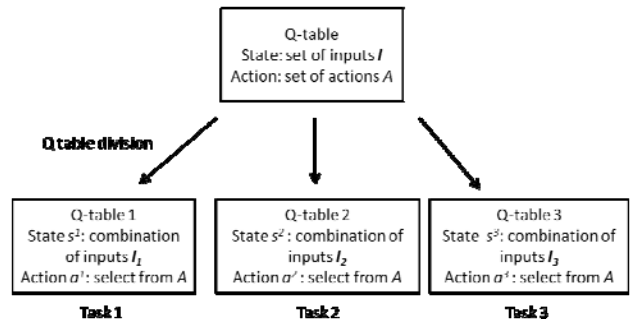


Fig. 1. Q-table division

### 2.1. Representation of distributed Q tables

Suppose that a set of inputs (sensors) of agents is  $I$ , and a set of possible actions is  $A$ . Then  $I$  is manually divided into several subsets, i.e.,  $I_1, I_2, \dots, I_n$  ( $I = \{I_1, I_2, \dots, I_n\}$ ), depending on the problems. For example, in the self-sufficient garbage collecting problem used in the simulations of this paper, there are mainly three tasks which have to be achieved by agents, thus,  $I$  is divided into three subsets, i.e.,  $I_1, I_2, I_3$ . Therefore, three sub-Q-tables are created based on  $I_1, I_2, I_3$ , respectively (Fig. 1).

### 2.2. State transition and learning

In this subsection, the procedure of deciding an action is explained based on an example shown in Fig. 1 (three sub-Q-tables are used).

The procedure of deciding an action is as follows.

- 1) When inputs are given from an environment, each sub-Q-table independently determines the current state  $s^n$  ( $n$  is the sub-Q-table number.  $n \in \{1, 2, 3\}$ ).
- 2) Three actions  $a^n$  are independently selected by each sub-Q-table using greedy policy<sup>9</sup>.
- 3) Compare the three Q-values of  $a^n$ , and the sub-Q-table selecting the action with the maximum Q-value is defined as  $n^{winner}$  (winner-Q-table), and its current state is defined as  $s^{winner}$ .
- 4) The action selected by winner-Q-table is executed with the probability of  $\epsilon$ , or random action is executed with the probability of  $1-\epsilon$ . This executed action is defined as  $a^{winner}$ .

The procedure of Q-learning is as follows.

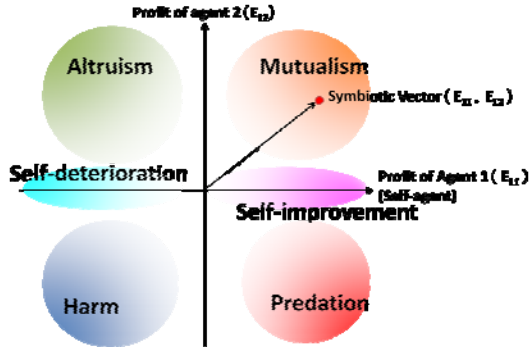


Fig. 2. Symbiotic vector and six symbiotic relationships for agent 1 (An example of two dimensions)

$$Q(n_t^{winner}, s_t^{winner}, a_t^{winner}) \leftarrow Q(n_t^{winner}, s_t^{winner}, a_t^{winner}) + \alpha \left[ r + \gamma \max_{n, a^n} Q(n, s_{t+1}^n, a^n) - Q(n_t^{winner}, s_t^{winner}, a_t^{winner}) \right], \quad (1)$$

where,  $n_t^{winner}$ ,  $s_t^{winner}$  and  $a_t^{winner}$  show the number, state and action of the winner sub-Q-table at time  $t$ , respectively.  $n$  is a sub-Q-table number,  $s_{t+1}^n$  is the state of sub-Q-table  $n$  at time  $t+1$ , and  $a^n$  is a possible action in sub-Q-table  $n$ .  $r$  is a reward,  $\alpha$  is a learning rate, and  $\gamma$  is a discount rate

### 3. Reinforcement Learning with Symbiosis

This section introduces a symbiotic vector and how to apply the symbiotic vector to reinforcement learning.

#### 3.1. Symbiotic vectors

Standard reinforcement learning aims to maximize rewards that the self-agent obtains, however, in the proposed method, not only the rewards for the self-agent, but also the rewards for other agents are considered to execute reinforcement learning. In addition, six symbiotic relationships are considered to build the action strategies, that is, Predation, Mutualism, Altruism, Harm, Self-improvement and Self-deterioration. Fig. 2 shows symbiotic strategy for "agent 1", where one axis shows the weight ( $E_{11}$ ) on the profit of agent 1 (self-agent), the other axis shows the weight ( $E_{12}$ ) on the profits of agent 2. In other words,  $E_{11}$  shows the

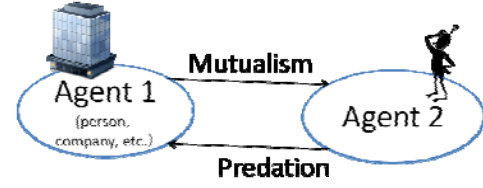


Fig. 3. Symbiotic relationships between two agents

symbiotic strategy of agent 1 for agent 1, and  $E_{12}$  shows the symbiotic strategy of agent 1 for agent 2. Therefore, if agent 1 aims to maximize rewards for both agents, it will take "Mutualism" strategy where symbiotic vector  $\mathbf{v}_I=(E_{11}, E_{12})=(1.0, 1.0)$  ( $-1.0 \leq E_{11}, E_{12} \leq 1.0$ ). Fig. 3 shows a symbiotic relationship between two agents, where one agent takes mutualism strategy and the other agent takes predation strategy. In this case, it can be considered that the symbiotic vector of agent 1 is  $\mathbf{v}_I=(E_{11}, E_{12})=(1.0, 1.0)$ , and that of agent 2 is  $\mathbf{v}_2=(E_{21}, E_{22})=(-1.0, 1.0)$ . Intermediate values between -1.0 and 1.0 can be also used to define a symbiotic relationship. For example, a symbiotic vector  $\mathbf{v}=(1.0, 0.1)$  shows a weak mutualism that considers the other agent's profit a little. Therefore, the symbiotic vector flexibly represents any degree of symbiotic relationships, and moreover, it can be extended to the relationships between many agents.

#### 3.2. Reinforcement learning with Symbiotic vectors

This subsection explains how to update Q values considering a symbiotic vector. Here, suppose there are  $p$  agents (agent #1 – #p), where the symbiotic vector of agent  $k$  ( $1 \leq k \leq p$ ) is  $\mathbf{v}_k=(E_{k1}, E_{k2}, \dots, E_{kp})$ . After agent  $k$  takes an action and finds rewards for all the agents ( $r^1, r^2, \dots, r^p$ ), the modified reward used for updating Q value of agent  $k$  in (1) is calculated as follows.

$$r_k = \sum_{l=1}^p E_{kl} r^l \quad (2)$$

Eq. (2) means that the modified reward  $r_k$  for agent  $k$  is based on all the rewards given to agents #1 – #p and the sum of the weighted rewards is calculated.

### 4. Simulations

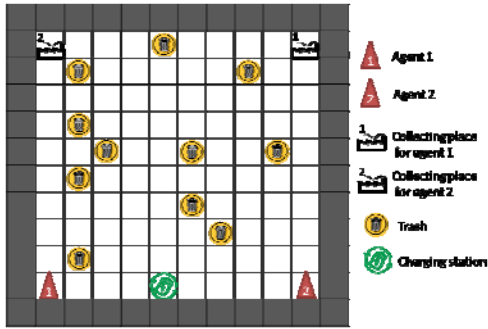


Fig. 4. A simulation environment

### 4.1. A simulation environment

Self-sufficient garbage collecting problem<sup>10</sup> is used for the performance evaluation of the proposed method. Fig. 4 shows the simulation environment used in this paper, where there are two agents, 11 trashes, one charging station, and two trash collecting places. The aim of this problem is to collect many trashes in the environment and take them to the collecting place assigned to each agent, i.e., agent  $k$  has to take trashes to the collecting place for agent  $k$  to obtain reward. In addition, each agent has a limited energy to move, thus the agents should check the remaining energy and go to the charging station before running out of the energy. Table 1 shows the inputs and possible actions that the agents can use. The initial energy is 100 (full charge), and when an agent goes forward, energy is used by three, and when it turns right or left, energy is used by one. The energy can be recharged gradually if the agent stays at the charging station. The total time for one episode is 100 steps. Reward 100 is given when an agent takes one trash to the collecting place for agent  $k$ , 10 is given when it collect a trash, and  $0.1 \times (\text{charged energy})$  is given when it stays at the charging station.

### 4.2. Conditions of Q-learning with Distributed Q-tables

Table 2 shows the setting of distributed Q-tables, where three sub-Q-tables are prepared for dealing with tasks for agent 1's benefit, for agent 2's benefit, and charging energy, respectively. Each agent has its own Q-table (three sub-Q-tables), i.e., the learning of the two agents are carried out independently. The learning parameters are set as learning rate  $\alpha=0.1$ , discount rate  $\gamma=0.9$ , and  $\epsilon=0.05$ .

Table 1. Inputs and actions

#	Input contents	Input value
1	forward cell	nothing, obstacle, collecting place for agent 1, collecting place for agent 2, trash, charging station
2	backward cell	the same as "forward cell"
3	right cell	the same as "forward cell"
4	left cell	the same as "forward cell"
5	direction of nearest trash	forward, backward, right, left
6	direction of charging station	forward, backward, right, left
7	direction of collecting place for agent 1	forward, backward, right, left
8	direction of collecting place for agent 2	forward, backward, right, left
9	the number of holding trashes	0, 1, 2 (max 2)
10	current energy level	low (less than 30), high (more than 70), middle (other values)
Actions		
1	go forward	
2	turn right	
3	turn left	
4	no action	

Table 2. Sub-Q-table setting

table #	Main task	Input # used in each sub-Q-table
1	for agent 1's benefit	1,2,3,4,5,7,9
2	for agent 2's benefit	1,2,3,4,5,8,9
3	Charging energy	1,2,3,4,6,10

### 4.3. Simulation results

In this subsection, in order to confirm the basic effects of the symbiotic relationship, the proposed method with mutualism strategy is compared with the conventional Q-learning, i.e., both agents take Self-improvement strategy.

Fig. 5 shows the number of trashes taken to the collecting places for agent 1 and that for agent 2, respectively, obtained by the conventional method. Each line is the average over 20 independent simulations. As the episode goes on, the number of trashes increases, and in 5000th episode, 1.5 trashes are taken to the collecting place for agent 1 and 2.25 trashes are for agent 2. Fig 6 shows the results of the proposed method, where 2.1 trashes are taken for agent 1 and 3.9 trashes are for agent 2. It should be noted that the number of

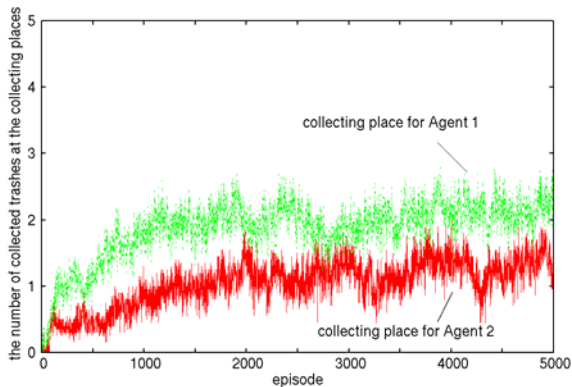


Fig. 5. The number of collected trashes at collecting places for Agent 1 and Agent 2 (Conventional method)

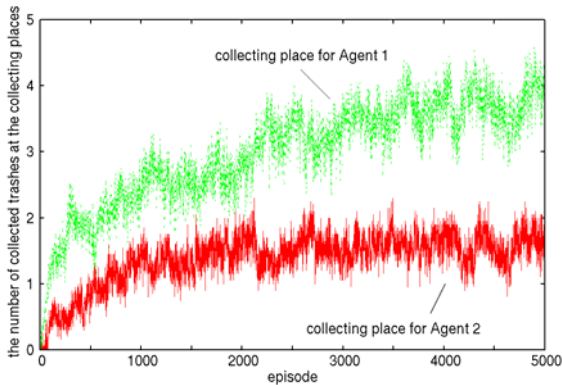


Fig. 6. The number of collected trashes at collecting places for Agent 1 and Agent 2 (Proposed method with Mutualism)

collected trashes for agent 1 increases without decreasing that for agent 2 (even increasing). Therefore, it is clarified that the proposed method with mutualism strategy can obtain cooperation behavior and show better performance than the conventional method.

## 5. Conclusions

In this paper, a novel reinforcement learning algorithm based on symbiotic relationships is proposed, where symbiotic vector is introduced to represent various kinds of relationships. In the simulations, the effectiveness of the proposed method with mutualism strategy has been shown. By considering not only the profits of self-agent, but also those of the other agents, cooperative behaviors emerged. In the future, other combinations of symbiotic relationships are considered to analyze the emerging behaviors, and moreover,

multilateral relationships are also considered to build simulation models dealing with real situations of cooperation or conflict between agents.

## References

1. Ken Binmore, *Game Theory: A Very Short Introduction* (Oxford University Press, 2007)
2. D. J. Watts, S. H. Strogatz, Collective dynamics of small-world networks, *Nature*, **393** (1998) 440-442.
3. L. Margulis, *The Symbiotic Planet*, Contact, (1999).
4. T. Eguchi, K. Hirasawa, J. Hu, and N. Ota, A Study of Evolutionary Multiagent Models Based on Symbiosis, *IEEE Trans. on Systems, Man, and Cybernetics, part B*, **(36)** 1, (2006).
5. J. Y. Goulermas and P. Liatsis, Hybrid symbiotic genetic optimization for robust edge-based stereo correspondence, *Pattern Recognition*, **(34)**, (2001) 2477-2496.
6. J. Y. Goulermas and P. Liatsis, A collective-based adaptive symbiotic model for surface reconstruction in area-based stereo, *IEEE Trans. on Evolutionary Computation*, **(7)** 5, (2003), 482-502.
7. C. P. Pieters, Symbiotic networks, in *Proc. of the IEEE Congress on Evolutionary Computation*, (2003) 921-927.
8. R. E. Bellman, *Dynamic Programming*, (Princeton University Press, 1957).
9. R. S. Sutton, A. G. Barto, *Reinforcement Learning - An Introduction* -, (1998).
10. R. Pfeifer, and C. Scheier. *Understanding intelligence*, (MIT press, 1999).



# Development of a Dividual Model Using a Modular Neural Network for Human-Robot Interaction

Toshiyuki Tanaka<sup>1</sup> and Kunikazu Kobayashi<sup>1\*</sup>

<sup>1</sup> Aichi Prefectural University,  
1522-3 Ibaragabasama,  
Nagakute, Aichi 480-1198, Japan  
\*E-mail: kobayashi@ist.aichi-pu.ac.jp

## Abstract

Currently, in the field of human-robot interaction (HRI), robots have a problem that can only interact the same at all times with humans. In this paper, therefore, we introduce the concept called a dividual and build a model of the dividual to grow through interactions with others. In addition, using a modular neural network and reinforcement learning (actor-critic), we confirmed process to choose an appropriate dividual out of plural dividuals.

*Keywords:* Model of dividual, Human-robot interaction, Robot, Modular neural network, Reinforcement learning

## 1. Introduction

In recent years, many types of robots have been developed and successfully applied to a variety of fields, such as medical care and disaster relief. Currently, in the field of human-robot interaction (HRI), robots have a problem that they can only interact with humans in a stereotypical way. Humans can however change correspondence depending on a human to be interacted, and realize a variety of interactions (communications). On conventional interaction between humans and robots, robots receive unilateral orders by performing prearranged movement and utterance from humans, and perform given tasks<sup>1,2,3,4,5</sup>. This cannot however realize robots which live together and support humans.

As one of researches on HRI, Kojima tried to have a mind like human for building a social relationship and proposed a model of develop-

ment to obtain communication skills through social interactions<sup>6</sup>. Shibata made robots play a role in human society. Then he developed a seal-shaped robot and reported that elderly people get pleasure and spiritual comfort through physical interactions such as touching and petting<sup>7</sup>. Naya et al. also presented a system dealing with haptic interactions between humans and robots<sup>8</sup>.

In the present paper, in the field of HRI, we develop a dividual model to grow through interactions with others. Then, we introduce a concept of dividual that it is formed into a self with respect to another human through repetitive communications with others<sup>9,10</sup>. Individual cannot divide anymore whereas dividual can divide into plural ones. We use two machine learning techniques to construct the dividual model. Then, we confirm a process to choose an appropriate dividual out of plural dividuals when we appropriately prepare an input set for a dividual

model defined by category elements and action ones.

## 2. Dividual

A concept of dividual is proposed by Japanese novelist Keiichiro Hirano to interact properly with another human<sup>9</sup>. Individual cannot divide anymore whereas dividual can divide into plural ones. Based on the concept of dividual, a human can change to another self according to environments and human relations. Dividual is formed into a self with respect to another human through repetitive communications with others. In addition, dividual is strictly divided into three types as shown in Fig.1.



Figure 1: Conceptual diagram of dividual.

The first one is a social dividual. This is a standard dividual to interact with a stranger or an unfamiliar person. The second one is a group-oriented dividual. This corresponds to a dividual for a specific group such as a school class or a tennis club. The third one is an individual-oriented dividual. This is a dividual for a specific person such as family members or a close friend. In the present paper, the last one, i.e. individual-oriented dividual is treated.

## 3. Dividual Model

### 3.1. Design of Dividual Model

We introduce a modular neural network as a general framework of the dividual model<sup>11,12</sup>. One module corresponds to one dividual as shown in Fig.2. Firstly, a dividual model creates a dividual as a module by giving inputs and learning. This corresponds to in-

teraction between humans and robots. Secondly, the model chooses an appropriate dividual out of plural ones according to input information by an output value from each modules. This corresponds to robots could change interaction according to humans.

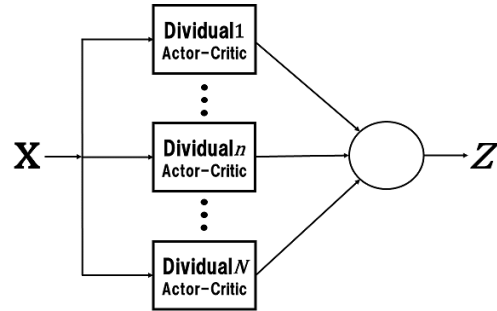


Figure 2: Configuration of a dividual model.

### 3.2. Learning of Dividual Model

We introduce an actor-critic reinforcement learning method to train each modular neural network in Fig.3<sup>13</sup>. Reinforcement learning is a learning framework that acquires the desirable output and time sequence with a trial and error by being maximized value for result of interaction with environment, that is reward of expectation. One of the representative technique is actor-critic. The actor-critic method consist of an actor to select an action and a critic to evaluate its action.

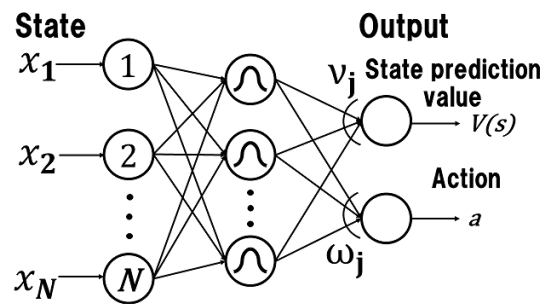


Figure 3: Structure of a neural network based on actor-critic.

The parameters are repeatedly modified as follows.

*TD error:* Critic observes the rewards  $r$  and the next state  $\mathbf{s}' = (x_1, x_2, \dots, x_N)^T$ , and calculate temporal difference error (TD error) as learning index of critic and actor. TD error  $\delta$  at time  $t$  is expressed by Eq.(1).

$$\delta = r + \gamma V(\mathbf{s}') - V(\mathbf{s}), \quad (1)$$

where  $\gamma$  is a discount rate,  $0 \leq \gamma \leq 1$ .

*Learning of middle unit:* The output function of middle unit is assumed as Gaussian function with an average  $\mathbf{c}_j$  and a variance  $\sigma_j^2$  in Eq.(2).

$$y_j = \exp\left(-\frac{\|\mathbf{s} - \mathbf{c}_j\|^2}{2\sigma_j^2}\right), \quad (2)$$

The average  $\mathbf{c}_j$  becomes close to input  $\mathbf{s}$  as Eq.(3).

$$\mathbf{c}_j \leftarrow \mathbf{c}_j + \zeta \delta v_j \frac{\mathbf{s} - \mathbf{c}_j}{\sigma_j^2} y_j, \quad (3)$$

where  $\zeta$  is a learning coefficient,  $0 \leq \zeta \leq 1$ . In the present paper, the variance  $\sigma_j^2$  of Gaussian function is assumed to be fixed.

*Learning of critic:* A weight  $v_j$  is updated by Eq.(4) so that TD error becomes zero.

$$v_j \leftarrow v_j + \eta \delta y_j, \quad (4)$$

where  $\eta$  is a learning coefficient,  $0 \leq \eta \leq 1$ .

*Learning of actor:* A weight  $\omega_j$  is updated so as to take a higher state value  $V(\mathbf{s})$  using Eq.(5).

$$\omega_j \leftarrow \omega_j + \rho \delta, \quad (5)$$

where  $\rho$  is a learning coefficient,  $0 \leq \rho \leq 1$ .

*Selection probability of modules:* We introduce a soft-max technique based on Gibbs distribution in Eq.(6) so as to adjust the selection probability of modules.

$$\pi(\mathbf{s}) = \frac{\exp(p(\mathbf{s}))}{\sum_{\mathbf{s}' \in X} \exp(p(\mathbf{s}'))}, \quad (6)$$

where  $X$  refers to an input set and the parameter  $p(\mathbf{s})$  is updated by Eq.(7).

$$p(\mathbf{s}) \leftarrow p(\mathbf{s}) + \beta \delta, \quad (7)$$

where  $\beta$  is a learning coefficient,  $0 \leq \beta \leq 1$ .

## 4. Computer Simulation

Through computer simulations, we confirm a process to choose an appropriate dividual out of plural dividuals.

### 4.1. Design of Input Information

We prepare an input set for the dividual model in advance. It basically consists of two kinds of information. The first one is category information to identify a person, e.g. name, sex, age, nationality, hobby and etc. The second one is action information to express interactions, e.g. question, answer and etc. For convenience of identifying a person, we should keep the input dimensions of action information as small as possible. Further, we design four patterns for each person whose category elements are identical but action elements are not.

### 4.2. Simulation Results

When the proposed model newly gets an input for an unfamiliar person, it creates a novel dividual module for him/her. We designed that each dividual module gets a positive reward for an input containing good action and a negative reward for the other inputs so as to form an appropriate dividual in a module. The accumulated rewards for three dividual modules is illustrated in Fig.4. This figure shows that each module learns correctly because the accumulated rewards is monotonically increasing.

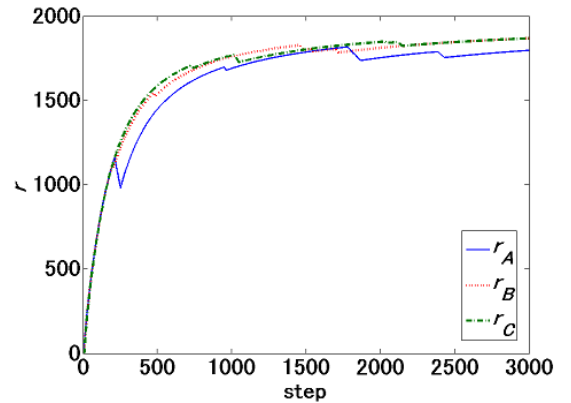


Figure 4: Accumulated reward for three persons.

Figure 5 illustrates the transition of output  $V(\mathbf{s})$ . As shown in this figure, the output of each module takes higher value than other two modules after 3,000 learning steps. We can therefore identify the person by observing  $V(\mathbf{s})$ . Thus, we can confirm the process to choose an appropriate individual out of plural individuals for input information.

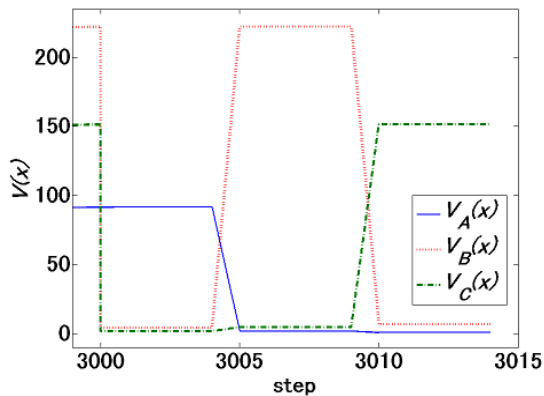


Figure 5: Output value  $V(x)$  from each module.

## 5. Conclusion

In the present paper, in the field of HRI, we developed a dividual model to grow through interactions with others. Through computer simulations, we confirmed a process to form an appropriate individual-oriented dividual.

As a future problem, we should implement social dividual and group-oriented dividual. Then we should verify the validity of a dividual model.

In the near future, when a home robot is introduced to our house, we hope that it should be developed to learn and grow through interactions with family members, and can separately correspond to each family member. In order to realize such a home robot, we must develop a system to enable smooth communication between humans and robots. Once a dividual based human-robot interaction system is developed, robots can take a role in a family member and a doctor and then relationship between humans and robots will be dramatically changed.

## Acknowledgments

This work was partly supported by President's Special Research Fund from Aichi Prefectural University, Japan.

## References

1. T. Fong, I. Nourbakhsh, and K. Dautenhahn, "A Survey of Socially Interactive Robots," *Robotics and Autonomous Systems*, **42**, 143–166 (2003).
2. M. A. Goodrich and A. C. Schultz, "Human-Robot Interaction: A Survey," *Human-Computer Interaction*, **1**(3), 203–275 (2007).
3. T. Kanda, "Research Trends towards Social Robots in HRI," *Journal of the Robotics Society of Japan*, **29**(1), 2–5 (2011) (in Japanese).
4. T. Ono, M. Imai, T. Etani, and R. Nakatsu, "Construction of Relationship between Humans and Robots," *Journal of Information Processing*, **41**(1) 158–166 (2000) (in Japanese).
5. K. Kobayashi and S. Yamada, "Human-Robot Cooperation with Commands Embedded in Actions," *Transactions of the Japanese Society for Artificial Intelligence*, **21**(1), 63–72 (2006) (in Japanese).
6. H. Kozima, "Epigenesis of social intelligence and theory of mind," *IPSJ SIG Notes. ICS, ICS122-3*, 13–18 (2000) (in Japanese).
7. T. Shibata, "Research on Interaction between Human and Seal Robot, PARO," *Journal of the Robotics Society of Japan*, **29**(1), 31–34 (2011) (in Japanese).
8. F. Naya, K. Shinozawa, and K. Kogure, "Human-Robot Tactile Interaction," *IPSJ Magazine*, **44**(12), 1227–1232 (2003) (in Japanese).
9. K. Hirano, "Who am I? : From Individual to Dividual," *Kodansha Shinsho* (2012) (in Japanese).
10. M. Kawamura and K. Kobayashi, "An Action Selection Method Using Degree of Cooperation in a Multi-agent Reinforcement Learning System," *Journal of Robotics, Networking and Artificial Life*, **1**(3), 231–236 (2014).
11. T. Tanaka and K. Kobayashi, "Construction of a Dividual Model Using a Modular Neural Network for Human-Robot Interaction," *Proceedings of Tokai-Section Joint Conference on Electrical and Related Engineering*, N1-6 (2014) (in Japanese).
12. R. Anand, K. Mehrotra, C. K. Mohan, and S. Ranka, "Efficient Classification for Multiclass Problems Using Modular Neural Network," *IEEE Trans. Neural Networks*, **6**(1), 117–124 (1995).
13. R. S. Sutton and A. G. Barto, "Reinforcement Learning: An introduction," MIT press (1998).

# Associative Memory with Class I and II Izhikevich Model

**Yoshika Osawa**

*Department of Electrical Engineering and Information Systems, The University of Tokyo  
7-3-1 Hongo, Bunkyo-ku, Tokyo 113-8656, Japan*

**Takashi Kohno**

*Institute of Industrial Science, University of Tokyo  
4-6-1, Komaba, Meguro-ku, Tokyo, 153-8505, Japan  
E-mail: osawa@sat.t.u-tokyo.ac.jp, kohno@sat.t.u-tokyo.ac.jp  
www.sat.t.u-tokyo.ac.jp/~kohno/*

## Abstract

Spiking neural network is a system that qualitatively reproduce the nervous system. It was shown in previous researches that the performance of associative memory task in all-to-all connected networks is higher when they are composed of Class II neurons than Class I neurons. The Izhikevich model in its Class II mode, however, does not have this performance boost. In this study, we focus on phase resetting curve as an index that reflects neuronal properties related to neuron classes in detail.

*Keywords:* Spiking neural network, associative memory, Izhikevich model, Phase resetting curve, Hodgkin's classification

## 1. Introduction

Nervous system has robust, autonomous, and power-efficient information processing capacity. Neurons generate overshoot of their membrane potential called spike, when sufficiently large stimulus is applied, which travel through their axon and transmit signals to post-synaptic neurons via synapses by transmitter.

There are several approaches in modeling neuronal activities. Conductance-based models that focus on the current through the cell membrane such as the Hodgkin-Huxley model<sup>1</sup> can reproduce those activities precisely. Since this type of models are composed of complex differential equations, large-scale simulation is impractical. The Leaky Integrate-and-Fire (LIF) model<sup>2</sup> represents the spike by resetting of membrane potential. This method yields simple and low-dimensional system

equations. It is very easy to simulate using this model but it reproduces limited aspects of neuronal behaviors. In the meanwhile simplified expression while maintaining the mechanism of the conductance-based models develops the qualitative modeling. One of them, Digital Spiking Silicon Neuron (DSSN) model<sup>3</sup> is composed of two differential equations that expresses the spike generation process without reset of system variables. The Izhikevich (IZH) model<sup>4</sup> captures only the spike decision process qualitatively, and represents the spike by reset of its system variables. It is possible to reproduce a variety of spike patterns.

Neurons are classified by characteristics of the periodic firing in the Hodgkin's classification<sup>5</sup>. Associative memory simulation using the DSSN model built by Li et al.<sup>6</sup> showed that an all-to-all connected network of Class II neurons has higher recall ability than that of

© *International Conference on Artificial Life and Robotics 2015, 01/10-12 (ICAROB 2015)*

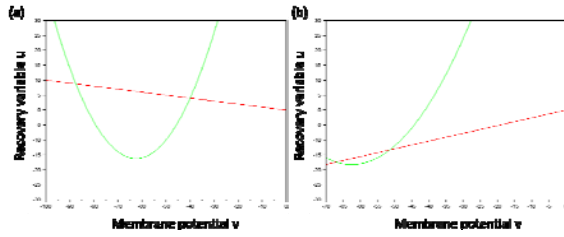


Fig. 1. The phase plane of Izhikevich model in (a) Class I and (b) Class II modes.

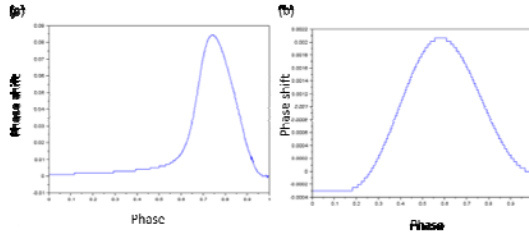


Fig. 2. Phase resetting curve of Izhikevich model in (a) Class I and (b) Class II modes.

Class I neurons. Higher recall ability here means that an original stored pattern is recalled from an associated input pattern with higher error. We configured similar associative memory using the IZH model and evaluated the difference of its performance by focusing on the shape of the phase resetting curve (PRC)<sup>7</sup>.

## 2. Neuron Model and Synapse Model

### 2.1. Izhikevich Model

The IZH model captures the mechanism of spike decision process based on its bifurcation structure. Saddle-node and Hopf bifurcations produce Class I and II properties, respectively. In the IZH model, this mechanism is described by two differential equation (1), and membrane potential  $v$  is reset when it exceeds 30.

$$\begin{aligned}
 \frac{dv}{dt} &= 0.04v^2 + 5v + 140 - u + I \\
 \frac{du}{dt} &= a(bv - u) \\
 \text{If } v > 30 \text{ then} \\
 v &\leftarrow c \\
 u &\leftarrow u + d
 \end{aligned} \tag{1}$$

Here,  $u$  is a variable that represents membrane recovery the parameters  $a$ ,  $b$ ,  $c$ , and  $d$  are constants that specify the model's firing property, and  $I$  represents a stimulus input. The phase portraits of Class I and II neuron modes of this model are described in Fig. 1. Class II

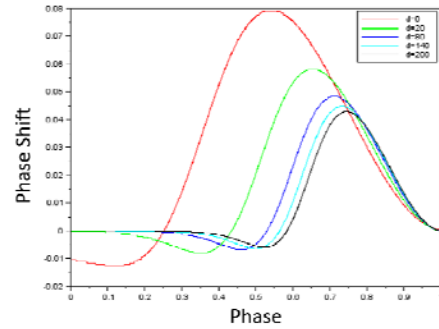


Fig. 3. Change of the shape of the phase resetting curve depending on the resetting parameter  $d$ .

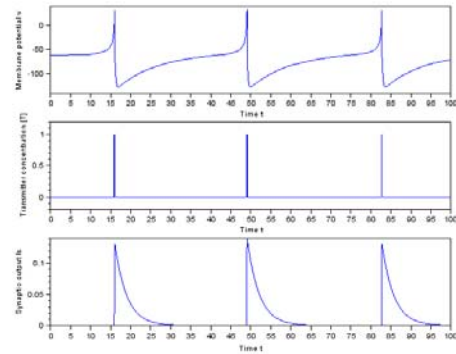


Fig. 4. Time course example of membrane potential, transmitter concentration, and synaptic output.

neuron arise periodic firing before he intersection of the two lines disappear although no occur in Class I. The PRC is a plot of spiking phase shift in a neuron at periodically spiking state induced by sufficiently small pulse stimulus. Its horizontal axis is the phase at which the stimulus is applied. Fig. 2 shows the PRC of the IZH model. There are two types of the shape. The Type 1 is always positive, and Type 2 is biphasic. The PRC of the IZH model is Type 1 and 2 in Class I and II models, respectively. The PRC of Class II has a jump point induced by reset. Its jump is reduced by reset parameter  $d$  (Fig. 3).

### 2.2. Synapse Model

Synapses transmit signals to post-synaptic neurons. Chemical synapses release transmitter when its pre-synaptic neuron fires. In our model, the neurotransmitter is in the same manner as Li et al., approximated to vary in a pulse form while the spike exceeds a threshold. The expression of synaptic output  $I_s$  is shown in Eq. (2)<sup>8</sup>.

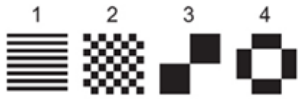


Fig. 5. Stored patterns in our associative memory simulation.



Fig. 6. Examples of input patterns, generated by applying errors to the stored pattern 1.

$$\frac{dv}{dt} = \begin{cases} \alpha(1 - I_s) & ([T] = 1) \\ -\beta I_s & ([T] = 0) \end{cases} \quad (2)$$

Here,  $\alpha$  and  $\beta$  are constants that represent the time constant of rising and phase of synaptic outputs, respectively. The amount of transmitter  $[T]$  is set to 1 when  $v > 0$ , and 0 when  $v < 0$ . Figure 4 represents example of time variation of the membrane potential, neurotransmitter concentration, and the synaptic current.

### 3. Simulation

We examined the performance of the associative memory composed of Class II Izhikevich model varying resetting parameter  $d$ . The associative memory is composed of all-to-all connected networks and outputs a stored pattern similar to the input data. In this work,  $p$  patterns of  $N$  dots which are orthogonal to each other are stored ( $p = 4$ ,  $N = 256$ ). The patterns are listed in Fig. 5. The weight  $W_{ij}$  of the synapses from  $i$ -th to  $j$ -th neuron is calculated by Eq. (3).

$$W_{ij} = \begin{cases} \sum_{k=1}^p x_i^k x_j^k & (i \neq j) \\ 0 & (i = j) \end{cases} \quad (3)$$

Input patterns are generated by applying random errors to a stored pattern (Fig. 6). We made 100 input patterns for every error rate. The error level vary from 5 to 50% with basically 5% steps and 1% in a region where the recall rate starts to decrease rapidly.

Firstly, we apply a pulse stimulus only to the neurons corresponding black dot. Then, stimulus current to all neurons was set to the value that induce periodic firing.

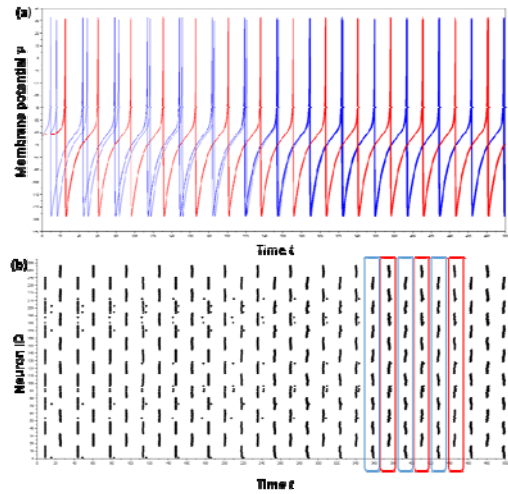


Fig. 7. (a) Waveform example of membrane potential and (b) its raster plot. Input pattern is the upper left in Fig. 6. Blue and red waveforms and squares correspond to the black and white dots of the stored pattern 1 in Fig. 5.

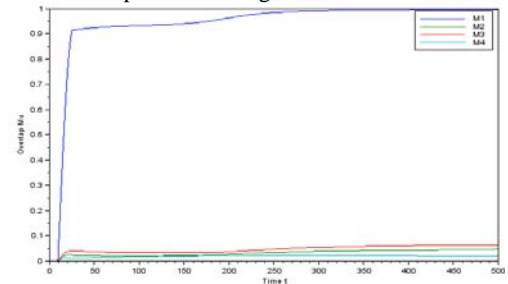

 Fig. 8. Time course of the overlap  $M_u(t)$  that corresponds to Fig. 7(a).

Figure 7(a) is an example of time series data of 256 neuron's membrane potential when the upper left pattern was input. Figure 7(b) shows the raster plot of this example. In this figure, we can see that at early phase of the recall process the neurons fire relatively in an asynchronous manner. The synchronicity increases as the neurons continue firing. And finally the neurons that correspond to black (white) dots fire synchronously. These two synchronously firing neuron groups are antiphase. To assess this quantitatively, we used overlap  $M_u(t)$  that calculates the matching degree of  $u$ -th stored pattern from the phase in the period of each neuron at a time  $t$  (Eq. (4)).

$$\begin{aligned} \phi_j(t) &= 2\pi k + 2\pi \frac{t - t_j^k}{T_j^k - t_j^k} \\ M_u(t) &= \frac{1}{N} \left| \sum_{j=1}^N x_j^u \exp(i\phi_j(t)) \right| \end{aligned} \quad (4)$$



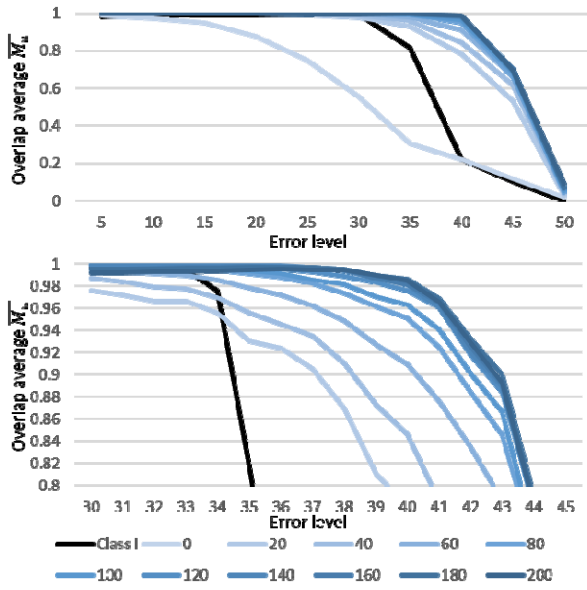


Fig. 9. Overlap average  $\overline{M}_u$  of each error level. (a) From 5% to 50% by 5%. (b) From 30% to 45% by 1%.

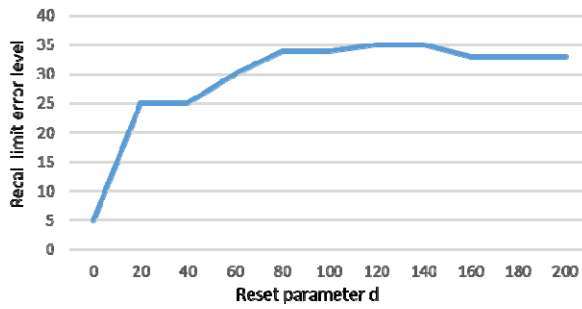


Fig. 10. Maximum input error level with which the recall is correct ( $\overline{M}_u > 0.95$  for all trial).

Here,  $t_k^u$  is the time that  $k$ -th spike is generated.  $\overline{M}_u = 1$  indicates that the  $u$ -th pattern is recalled successfully. The time course of  $\overline{M}_u(t)$  calculated by applying Eq. (4) to the data in Fig.7 is shown in Fig. 8. This result indicates that the stored pattern 1 is recalled correctly. We performed simulation for 100 input patterns for each error level. The reset parameter  $d$  of each neuron was varied from 0 to 200 by 20 in this simulation. Figure 9 shows the overlap average  $\overline{M}_u$  for each error level. Since that the change of  $\overline{M}_u$  is relatively large when input error level is 30-45%, we varied the error level by 1% step. We define that the recall is correct when  $\overline{M}_u > 0.95$  for all trials. Figure 10 plots the maximum input error rate from which our network recalled the correct pattern. As shown in Fig. 10, it got almost saturated in the vicinity of  $d = 120$ . Compared with the shape of

PRC shown in Fig. 3, the balance between the regions of positive and negative value of the phase shift may be important for the performance of associative memory.

#### 4. Conclusion

We have configured the associative memory consisting of 256 neurons of the IZH model. The performance of Class II network was worse than Class I, but the performance of the associative memory is improved by increasing the reset parameter  $d$ , by which the shape of the PRC changes. In the future, the validation by a phase model representing the shape of the quantitative PRC will be performed to quantitatively evaluate how the shape of the PRC contributes to the performance of the associative memory.

#### Acknowledgements

This work was supported by JSPS Grant-in-Aid for scientific Exploratory Research Number 25240045

#### References

1. Hodgkin, A. L, and Huxley, A. F, A quantitative description of membrane current and its application to conduction and excitation in nerve. (*J. Physiol.* 117, 500–544, 1952).
2. Stein R.B, Some models of neuronal variability (*Biophysical Journal*, 7: 37–68, 1967).
3. Kohno, T. and Aihara, K, Digital spiking silicon neuron: concept and behaviors in GJ-coupled network (in *Proceedings of International Symposium on Artificial Life and Robotics*, Beppu, OS3–OS6, 2007).
4. Izhikevich, E. M, *Dynamical Systems in Neuroscience: The Geometry of Excitability and Bursting* (Cambridge: MIT Press, 2006).
5. Hodgkin, A. L, The local electric changes associated with repetitive action in a nonmedullated axon (*J. Physiol.* 107, 165-181, 1948).
6. J. Li, Katori, Y, and Kohno, T, An FPGA-Based Silicon Neuronal Network with Selectable Excitability Silicon Neurons (*Frontiers in neuroscience* 6 183, 2012).
7. Ermentrout B, Type I membranes, phase resetting curves and synchrony (*Neural Computation* 8:979-1001, 1996).
8. Destexhe, A., Mainen, Z. F., and Sejnowski, T. J, *Kinetic models of synaptic transmission*, (in *Methods in Neuronal Modeling*, eds C. Koch and I. Segev Cambridge, FL: MIT Press, 1–25, 1998).



# Medical Image Recognition of Heart Regions by Deep Multi-layered GMDH-type Neural Network Using Principal Component-regression Analysis

**Tadashi Kondo**<sup>†</sup>

*Graduate School of Health Sciences  
3-18-15 Kuramoto-cho Tokushima 770-8509 Japan  
Email: <sup>†</sup>kondo@medsci.tokushima-u.ac.jp*

**Juniji Ueno**

*Graduate School of Health Sciences  
3-18-15 Kuramoto-cho Tokushima 770-8509 Japan*

**Shoichiro Takao**

*Graduate School of Health Sciences  
3-18-15 Kuramoto-cho Tokushima 770-8509 Japan*

## Abstract

In this study, a deep Group Method of Data Handling (GMDH)-type neural network using principal component-regression is applied to the medical image recognition of the heart regions. The deep GMDH-type neural network algorithm can organize the neural network architecture with many hidden layers fitting the complexity of the nonlinear systems so as to minimize the prediction error criterion defined as AIC (Akaike's Information Criterion) or PSS (Prediction Sum of Squares). This algorithm is applied to the medical image recognition of the heart regions and it is shown that this algorithm is useful for the medical image recognition of the heart regions because deep neural network architecture with many hidden layers is automatically organized using the principal component-regression analysis, so as to minimize AIC or PSS criterion.

*Keywords:* Deep neural networks, GMDH, Medical image recognition, Evolutional computation

## 1. Introduction

The deep Group Method of Data Handling (GMDH)-type neural networks and their applications have been proposed in our early works<sup>1,2</sup>. Deep GMDH-type neural networks can automatically organize neural network architecture by heuristic self-organization method<sup>3</sup>, which is a type of evolutional computation. In this study, a deep GMDH-type neural network algorithm using the principal component-regression analysis is applied to the medical image recognition of the heart regions. In this algorithm, optimum neural network architecture is automatically selected from three neural network architectures such as sigmoid function neural

network, radial basis function (RBF) neural network and polynomial neural network so as to minimize the prediction error criterion defined as AIC<sup>4</sup> or PSS<sup>5</sup>. This algorithm is applied to the medical image recognition of the heart regions and results show that the deep GMDH-type neural network algorithm is useful for the medical image recognition of the heart regions and is easy to apply practical complex problem because the deep neural network architecture with many hidden layers is automatically organized so as to minimize AIC or PSS criterion.

## 2. Deep multi-layered GMDH-type neural network

© The 2015 International Conference on Artificial Life and Robotics (ICAROB 2015), Jan. 10-12, Oita, Japan

Fig.1 shows the architecture of the deep multi-layered GMDH-type neural network.

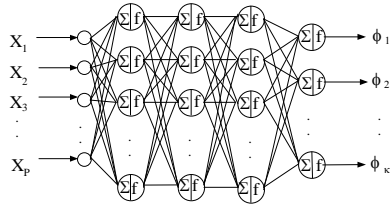


Fig.1 Architecture of the deep GMDH-type neural network

**2.1 The first layer**

$$u_j = x_j \quad (j=1,2,\dots,p) \quad (1)$$

where  $x_j (j=1,2,\dots,p)$  are input variables of the nonlinear system, and  $p$  is the number of input variables.

**2.2 The second layer**

All combinations of  $r$  input variables are generated. For each combination, optimum neuron architectures are automatically selected so as to minimize AIC or PSS. Deep GMDH-type neural network algorithm can select optimum neural network architecture from three neural network architectures such as sigmoid function neural network, RBF neural network and polynomial neural network.

**(1) Sigmoid function neural network**

**1) The first type neuron**

$\Sigma$ : (Nonlinear function)

$$z_k = w_1 u_i + w_2 u_j + w_3 u_i u_j + w_4 u_i^2 + w_5 u_j^2 - w_0 \theta_l \quad (2)$$

$f$ : (Nonlinear function)

$$y_k = \frac{1}{1 + e^{(-z_k)}} \quad (3)$$

**2) The second type neuron**

$\Sigma$ : (Linear function)

$$z_k = w_1 u_1 + w_2 u_2 + w_3 u_3 + \dots + w_r u_r - w_0 \theta_l \quad (r < p) \quad (4)$$

$f$ : (Nonlinear function)

$$y_k = \frac{1}{1 + e^{(-z_k)}} \quad (5)$$

**(2) Radial basis function neural network**

**1) The first type neuron**

$\Sigma$ : (Nonlinear function)

$$z_k = w_1 u_i + w_2 u_j + w_3 u_i u_j + w_4 u_i^2 + w_5 u_j^2 - w_0 \theta_l \quad (6)$$

$f$ : (Nonlinear function)

$$y_k = e^{(-z_k^2)} \quad (7)$$

**2) The second type neuron**

$\Sigma$ : (Linear function)

$$z_k = w_1 u_1 + w_2 u_2 + w_3 u_3 + \dots + w_r u_r - w_0 \theta_l \quad (r < p) \quad (8)$$

$f$ : (Nonlinear function)

$$y_k = e^{(-z_k^2)} \quad (9)$$

**(3) Polynomial neural network**

**1) The first type neuron**

$\Sigma$ : (Nonlinear function)

$$z_k = w_1 u_i + w_2 u_j + w_3 u_i u_j + w_4 u_i^2 + w_5 u_j^2 - w_0 \theta_l \quad (10)$$

$f$ : (Linear function)

$$y_k = z_k \quad (11)$$

**2) The second type neuron**

$\Sigma$ : (Linear function)

$$z_k = w_1 u_1 + w_2 u_2 + w_3 u_3 + \dots + w_r u_r - w_0 \theta_l \quad (r < p) \quad (12)$$

$f$ : (Linear function)

$$y_k = z_k \quad (13)$$

Here,  $\theta_l = 1$  and  $w_i (i=0,1,2,\dots,9)$ . Value of  $r$  is the number of input variables  $u$  in each neuron.  $p$  is the number of input variables  $x_i (i=1,2,\dots,p)$ .

**2.2.1 Estimation procedure of weight  $w_i$**

First, values of  $z_k^{**}$  are calculated for each neural network architecture as follows.

**a) Sigmoid function neural network**

$$z_k^{**} = \log_e \left( \frac{\phi}{1 - \phi} \right) \quad (14)$$

**b) RBF neural network**

$$z_k^{**} = \sqrt{-\log_e \phi'} \quad (15)$$

**c) Polynomial neural network**

$$z_k^{**} = \phi \quad (16)$$

where  $\phi'$  is the normalized output variable. Then the weights  $w_i (i=0,1,2,\dots,5)$  are estimated by using the principal component-regression analysis.

**2.2.2 Principal component-regression analysis**

In the GMDH-type neural network, the multicollinearity is generated in the function  $\Sigma$  of the neurons. In this study, the function  $\Sigma$  is calculated using the principal component-regression analysis.

In the case of Eq.(2), orthogonal vector  $\underline{v}$  is calculated.

$$\underline{v} = C \cdot \underline{u} \quad (17)$$

Here,  $\underline{v} = (v_1, v_2, \dots, v_5)$ ,  $\underline{u} = (u_i, u_j, u_i u_j, u_i^2, u_j^2)$

$\underline{v}$  is orthonormal vectors and  $C$  is orthonormal matrix.  $C$  is calculated using the following eigenvalue equation.

$$R \cdot C = C \cdot A \quad (18)$$

Here,  $R$  is a correlation matrix. Then, variable  $z_k$  is calculated using orthogonal regression analysis.

$$z_k = \underline{w}^T \cdot \underline{v} = w_1 v_1 + w_2 v_2 + \dots + w_5 v_5 \quad (19)$$

Using the principal component-regression analysis, variable  $z_k$  in the function  $\Sigma$  is calculated without multicollinearity. In (19), useful orthogonal variables  $v_i$  ( $i=1,2,\dots,5$ ) are selected using AIC<sup>4</sup> or PSS<sup>5</sup>.

From these generated neurons,  $L$  neurons which minimize AIC or PSS values are selected. The output values ( $y_k$ ) of  $L$  selected neurons are set to the input values of the neurons in the third layer.

**2.3 The third and successive layers**

In the second layer, optimum neural network architecture is selected from three neural network architectures which is sigmoid function neural network or RBF neural network or polynomial network. The same calculation of the second layer is iterated until AIC or PSS values of  $L$  neurons with selected neuron architecture, stop decreasing. When iterative calculation is terminated, neural network architecture is produced by  $L$  selected neurons in each layer.

**3. Application to the medical image recognition of heart regions**

In this study, the heart regions were automatically recognized using the deep GMDH-type neural network and these regions were extracted. Multi-detector row CT (MDCT) images of the heart were used in this study.

**3.1 Results of the medical image recognition by the deep GMDH-type neural network**

The MDCT image shown in Fig.2 was used for organizing the neural network.  $x$  and  $y$  coordinates and the statistics of the image densities in the neighboring regions of the  $N \times N$  pixels at the positions of the learning points are used as the input variables of the neural network. Only five input variables which are the mean, the standard deviation, the variance and  $x$  and  $y$  coordinates were automatically selected as useful input variables. The output value of the neural network is zero or one. When  $N \times N$  pixel region is contained in the heart regions, the neural network set the pixel value at the center of the  $N \times N$  pixel region to one and this pixel is shown as the white point. The neural networks were organized when the values of  $N$  were from 3 to 10. It was determined that when  $N$  was equal to 4, the neural

network architecture had the smallest recognition error. Five useful neurons were selected in each hidden layer. Fig.3 shows the PSS values of the three types of neurons in the second layer. The sigmoid function neural network architecture was selected by the deep GMDH-type neural network algorithm. Fig.4 shows the variation of PSS values. PSS values decreased gradually and very small PSS values were obtained at the tenth layer. The heart region was recognized by using the organized neural network and was extracted automatically. Fig.5 shows the output image of the deep GMDH-type neural network. This output image was processed by the post-processing analysis. In the post-processing, the small isolated regions were eliminated and the outlines of the heart regions were expanded outside by  $N/2$  pixels. Fig.6 shows the output image after this processing. In order to check the matching between the original image and the output image of the neural network, the output image was overlapped on the original image of Fig.2. The overlapped image is shown in Fig.7. From Fig.7, we can see that the output image was very accurate. Fig.8 shows the extracted heart image.

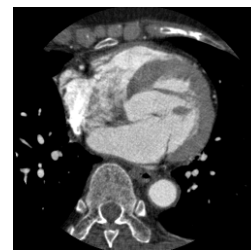


Fig. 2 Original image

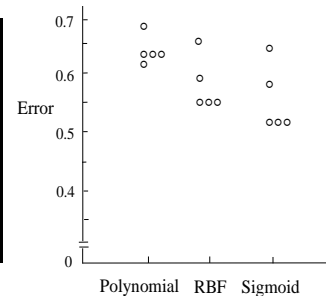


Fig. 3 PSS values of three types of neurons

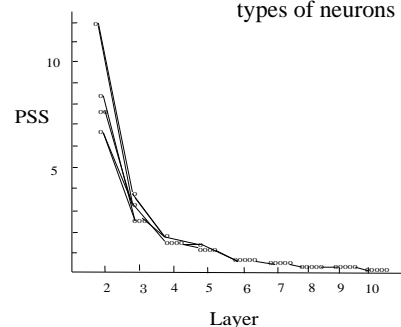


Fig. 4 Variation of PSS in each layer

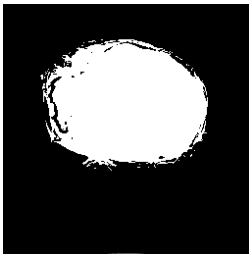


Fig. 5 Output image

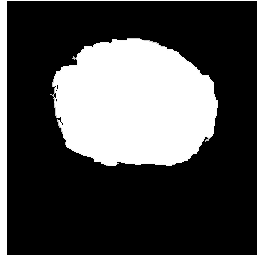


Fig.6 Output image after the post processing



Fig. 7 Overlapped image

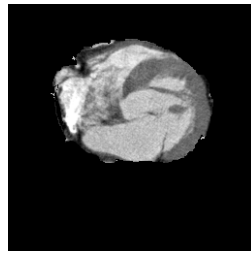
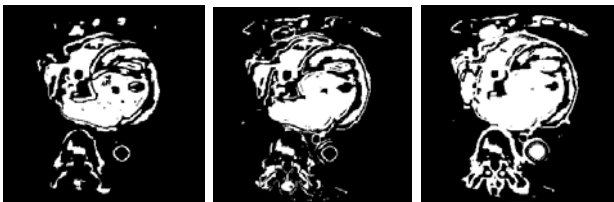


Fig. 8 Extracted image

### 3.2 Extraction by the conventional neural network using sigmoid function.

A conventional neural network trained using the back propagation algorithm was applied to the same recognition problem. The learning calculations of the weights were iterated changing structural parameters such as the number of neurons in the hidden layer and the initial values of the weights. The output images, when the numbers of neurons in the hidden layer ( $m$ ) are 5, 7 and 9, are shown in Fig.9. These images contain more regions which are not part of the heart and the outlines of the heart are not extracted with required clarity compared with the output images obtained using the deep GMDH-type neural network algorithm, which are shown in Fig.5.



(a)  $m=5$  (b)  $m=7$  (c)  $m=9$   
 Fig. 9 Output images of the conventional sigmoid function neural network

## 4. Conclusions

In this paper, the deep multi-layered GMDH-type neural network algorithm was applied to the medical image recognition of heart regions and the results were compared with those of the conventional sigmoid function neural network trained using the back propagation algorithm. It was shown that the deep multi-layered GMDH-type neural network algorithm was a useful method for the medical image recognition of heart regions because the deep neural network architecture with many hidden layers is automatically organized so as to minimize the prediction error criterion defined as AIC or PSS.

### Acknowledgment

This work was supported by (JSPS) KAKENHI 26420421.

### References

1. T. Kondo, J. Ueno and S. Takao, Hybrid multi-layered GMDH-type neural network using principal component regression analysis and its application to medical image diagnosis of liver cancer, *Procedia Computer Science*, **22**, (2013) 172-181.
2. T. Kondo, J. Ueno and S. Takao, Hybrid feedback GMDH-type neural network using principal component-regression analysis and its application to medical image diagnosis of lung cancer, *ICIC Express Letters (ICIC-EX)* **8** (4) (2014) 1053-1060.
3. S. J. Farlow ed., *Self-organizing methods in modeling, GMDH-type algorithm*, New York: Marcel Dekker Inc., 1984.
4. H. Akaike, A new look at the statistical model identification, *IEEE Trans. Automatic Control* **AC-19** (6) (1974) 716-723.
5. H. Tamura, T. Kondo, Heuristics free group method of data handling algorithm of generating optimum partial polynomials with application to air pollution prediction, *Int. J. System Sci.* **11** (9) (1980) 1095-1111.

# Deep Feedback GMDH-Type Neural Network Using Principal Component-Regression Analysis and Its Application to Medical Image Recognition of Abdominal Multi-Organs

**Tadashi Kondo**<sup>†</sup>

*Graduate School of Health Sciences  
3-18-15 Kuramoto-cho Tokushima 770-8509 Japan  
Email: <sup>†</sup>kondo@medsci.tokushima-u.ac.jp*

**Juniji Ueno**

*Graduate School of Health Sciences  
3-18-15 Kuramoto-cho Tokushima 770-8509 Japan*

**Shoichiro Takao**

*Graduate School of Health Sciences  
3-18-15 Kuramoto-cho Tokushima 770-8509 Japan*

## Abstract

The deep feedback Group Method of Data Handling (GMDH)-type neural network is proposed and applied to the medical image recognition of abdominal organs such as the liver and spleen. In this algorithm, the principal component-regression analysis is used for the learning calculation of the neural network, and the accurate and stable predicted values are obtained. The neural network architecture is automatically organized so as to fit the complexity of the medical images using the prediction error criterion defined as Akaike's Information Criterion (AIC) or Prediction Sum of Squares (PSS). The recognition results show that the deep feedback GMDH-type neural network algorithm is useful for the medical image recognition of abdominal organs.

*Keywords:* Deep neural networks, GMDH, Medical image recognition, Evolutional computation

## 1. Introduction

The deep GMDH-type neural network algorithms were proposed in our early works<sup>1</sup> and can automatically organize the neural network architectures by using heuristic self-organization method<sup>2</sup> which is a type of the evolutional computation. In this study, deep feedback GMDH-type neural network algorithm is applied to the medical image recognition of the abdominal organs such as the liver and spleen. The learning calculations of the weights is the principal component-regression analysis and the accurate and stable predicted values are obtained. The deep feedback GMDH-type neural network algorithm is applied to the

medical image recognition of the abdominal organs and the recognition results are compared with those obtained using the conventional neural networks trained using the back propagation algorithm.

## 2. Deep feedback GMDH-type neural network

The architecture of the deep feedback GMDH-type neural network developed in this paper has a feedback loop as shown in Fig.1.

### 2.1 First loop calculation

First, all data are set to the training data. Then the architecture of the input layer is organized.

#### 2.1.1 Input layer

$$u_j = x_j \quad (j=1,2,\dots,p) \quad (1)$$

© The 2015 International Conference on Artificial Life and Robotics (ICAROB 2015), Jan. 10-12, Oita, Japan

where  $x_j$  ( $j=1,2,\dots,p$ ) are the input variables of the system, and  $p$  is the number of input variables.

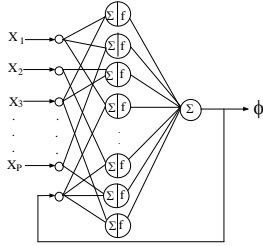


Fig.1 Architecture of the deep feedback GMDH-type neural network

**2.1.2 Hidden layer**

All combinations of the  $r$  input variables are generated. For each combination, three types of neuron architectures which are the sigmoid function neuron, the radial basis function (RBF) neuron and the polynomial neuron, are generated and  $L$  neurons which minimize AIC<sup>3</sup> and PSS<sup>4</sup> value are selected for each type of neuron architectures.

**(1) Sigmoid function neural network**

**1) The first type neuron**

$\Sigma$ : (Nonlinear function)

$$z_k = w_1 u_i + w_2 u_j + w_3 u_i u_j + w_4 u_i^2 + w_5 u_j^2 - w_0 \theta_l \quad (2)$$

$f$ : (Nonlinear function)

$$y_k = \frac{1}{1 + e^{(-z_k)}} \quad (3)$$

**2) The second type neuron**

$\Sigma$ : (Linear function)

$$z_k = w_1 u_1 + w_2 u_2 + w_3 u_3 + \dots + w_r u_r - w_0 \theta_l \quad (r < p) \quad (4)$$

$f$ : (Nonlinear function)

$$y_k = \frac{1}{1 + e^{(-z_k)}} \quad (5)$$

**(2) Radial basis function neural network**

**1) The first type neuron**

$\Sigma$ : (Nonlinear function)

$$z_k = w_1 u_i + w_2 u_j + w_3 u_i u_j + w_4 u_i^2 + w_5 u_j^2 - w_0 \theta_l \quad (6)$$

$f$ : (Nonlinear function)

$$y_k = e^{(-z_k^2)} \quad (7)$$

**2) The second type neuron**

$\Sigma$ : (Linear function)

$$z_k = w_1 u_1 + w_2 u_2 + w_3 u_3 + \dots + w_r u_r - w_0 \theta_l \quad (r < p) \quad (8)$$

$f$ : (Nonlinear function)

$$y_k = e^{(-z_k^2)} \quad (9)$$

**(3) Polynomial neural network**

**1) The first type neuron**

$\Sigma$ : (Nonlinear function)

$$z_k = w_1 u_i + w_2 u_j + w_3 u_i u_j + w_4 u_i^2 + w_5 u_j^2 - w_0 \theta_l \quad (10)$$

$f$ : (Linear function)

$$y_k = z_k \quad (11)$$

**2) The second type neuron**

$\Sigma$ : (Linear function)

$$z_k = w_1 u_1 + w_2 u_2 + w_3 u_3 + \dots + w_r u_r - w_0 \theta_l \quad (r < p) \quad (12)$$

$f$ : (Linear function)

$$y_k = z_k \quad (13)$$

Here,  $\theta_l = 1$  and  $w_i$  ( $i=0,1,2,\dots,5$ ) and  $w_i$  ( $i=0,1,2,\dots,r$ ) are weights between the input and hidden layer. Weights  $w_i$  ( $i=0,1,2,\dots$ ) in each neural network architecture are estimated by the principal component-regression analysis.

**[Estimation procedure of weight  $w_i$ ]**

First, values of  $z_k^{**}$  are calculated for each neural network architecture as follows.

**a) Sigmoid function neural network**

$$z_k^{**} = \log_e \left( \frac{\phi'}{1 - \phi'} \right) \quad (14)$$

**b) RBF neural network**

$$z_k^{**} = \sqrt{-\log_e \phi'} \quad (15)$$

**c) Polynomial neural network**

$$z_k^{**} = \phi \quad (16)$$

where  $\phi$  is an output variable and  $\phi'$  is the normalized output variable whose values are between 0 and 1.

**[Principal component-regression analysis]**

Multi-collinearity is generated in the function  $\Sigma$  of the neurons. In this study, the function  $\Sigma$  is calculated using the principal component-regression analysis.

In the case of Eq.(2), orthogonal vector  $\underline{v}$  is calculated .

$$\underline{v} = C \cdot \underline{u} \quad (17)$$

Here,  $\underline{v} = (v_1, v_2, \dots, v_5)$ ,  $\underline{u} = (u_i, u_j, u_i u_j, u_i^2, u_j^2)$

$\underline{v}$  is orthonormal vectors and  $C$  is orthonormal matrix.  $C$  is calculated using the following eigenvalue equation.

$$R \cdot C = C \cdot A \quad (18)$$

Here,  $R$  is a correlation matrix. Then, variable  $z_k$  is calculated using orthogonal regression analysis.

$$z_k = \underline{w}^T \cdot \underline{v} = w_1 v_1 + w_2 v_2 + \dots + w_5 v_5 \quad (19)$$

Using the principal component-regression analysis, variable  $z_k$  in the function  $\Sigma$  is calculated without multi-

colinearity. In (19), useful orthogonal variables  $v_i(i=1,2,\dots,5)$  are selected using AIC<sup>3</sup> or PSS<sup>4</sup> criterion.

$L$  neurons having the smallest AIC or PSS values are selected for three types of neuron architectures. The output variables  $y_k$  of  $L$  selected neurons for three types of neuron architectures are set to the input variables of the neurons in the output layer.

**2.1.3 Output layer**

For three types of neural network, the outputs  $y_k$  of the neurons in the hidden layer are combined by the following linear function.

$$\phi^* = a_0 + \sum_{k=1}^L a_k y_k \tag{20}$$

Here,  $L$  is the number of combinations of the input variables and  $y_k$  is the intermediate variables. Eq. (20) is calculated for three types of neural network architectures. The neural network architecture which has smallest AIC or PSS value is selected. Then, the estimated output values  $\phi^*$  which is selected in the output layer is used as the feedback value.

**2.2 Second and subsequent loop calculations**

First, the estimated output value  $\phi^*$  is combined with the input variables  $x$  and all combinations between the estimated output value  $\phi^*$  and the input variables  $x$  are generated. The same calculation as the first feedback loop is iterated. When AIC or PSS value of the linear function in (20) is not decreased, the loop calculation is terminated and the complete neural network architecture is organized by the  $L$  selected neurons in each feedback loop.

**3. Application to the medical image recognition of abdominal multi-organs**

In this study, the regions of the liver and spleen in the abdominal regions were recognized and extracted automatically. Multi-detector row CT (MDCT) images of the abdominal regions are used in this study.

**3.1 Extraction of the liver regions**

An abdominal MDCT image shown in Fig.2 was used for organizing the deep feedback GMDH-type neural network. The statistics of the image densities and  $x$  and  $y$  coordinates in the neighboring regions, the  $N \times N$  pixel regions, were used as the image features. The

neural networks were organized when the values of  $N$  were from 3 to 10. When  $N$  was equal to 6, the neural network architecture had the smallest recognition error. Fig.3 shows errors in the first feedback loop. Error of the sigmoid neuron was smallest in the three types of neurons. Fig.4 shows the variation of PSS value in each layer. The PSS values were decreased gradually through the feedback loops and small PSS value was obtained in the fifth feedback loop. The deep feedback GMDH-type neural network output the liver image (Fig.5) and the first post-processing analysis of the output liver image was carried out. Fig.6 shows the output image after the first post-processing. The output image after the first post-processing was overlapped to the original image (Fig.2) as shown in Fig.7. The recognized liver region are very accurate. The liver region was extracted from the original image as shown in Fig.8. A conventional neural network trained using the back propagation algorithm was applied to the same recognition problem. The output images, when the numbers of neurons in the hidden layer ( $m$ ) are 5, 7 and 9, are shown in Fig.9. These images contain more regions which are not part of the liver.



Fig. 2 Original image

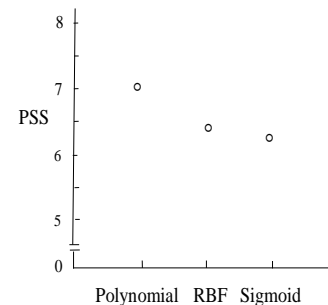


Fig. 3 Errors of three types of neurons (1)

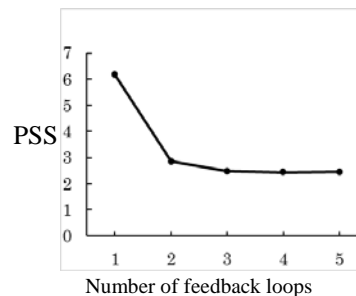


Fig. 4 Variation of PSS (1)



Fig. 5 Output image(1)





# Synchronized Response to Grayscale Image Inputs in the Chaotic Cellular Neural Network

**Masayuki FUJIWARA, Akihiro YAMAGUCHI**

*Department of Information and Systems Engineering, Fukuoka Institute of Technology,  
3-30-1 Wajiro-higashi, Higashi-ku, Fukuoka, 811-0116, JAPAN*

**Masao KUBO**

*Department of Computer Science, National Defense Academy of Japan,  
1-10-20 Hashirimizu, Yokosuka, Kanagawa, 239-8686, JAPAN*

*E-mail: s11c1040@bene.fit.ac.jp, aki@fit.ac.jp, masaok@nda.ac.jp*

## Abstract

In this article, synchronized response in the chaotic cellular neural network for grayscale visual stimulus was studied in the viewpoint of neural coding. Simple gradation patterns were used as visual stimuli and the synchronized response was analyzed by the correlation of spike firing times. As results, synchronized responses were observed for the neurons which have similar input value and they formed chaotic cell assemblies. Each assembly was distinguished from the others in terms of cross-correlation.

*Keywords: chaotic synchronization, neural coding, spike response model, visual segmentation*

## 1. Introduction

Recently, several information coding schemes using synchronized firing of neurons have been proposed<sup>1,2</sup>. As one of such schemes, the correlated firing is also regarded having an important role for information processing in the brain as a binding mechanism of neural information<sup>1</sup>. On the other hand, chaotic system is well-known to produce various complex behaviors by simple equations. When we consider to represent binding information by the correlated firing, the chaotic firing pattern has an advance in its variety compared to the periodic firing pattern. There is some possibility to represent more various information by the chaotic spike sequence than the periodic sequence<sup>3,4</sup>.

Authors have been studied formation of chaotic cell assembly in the chaotic cellular neural network (Chaotic-CNN) that is a two dimensional coupled network of chaotic spike response model (Chaotic-SRM)<sup>5,6</sup>. The Chaotic-SRM is an extended spike response model<sup>7</sup> that exhibits chaotic inter-spike interval by adding the background sinusoidal oscillation<sup>4,8</sup>. One fundamental

goal of this study is to realize visual segmentation using chaotic synchronization.

In our previous study, chaotic cell assemblies is formed in Chaotic-CNN for each localized stimulus when the stimulus is a two-dimensional binary pattern<sup>6</sup>. For the segmentation of real image, it is, however, necessary to analyze the case that the stimulus has analog continuous values. In this study, synchronized chaotic responses of Chaotic-CNN to the grayscale visual stimulus are numerically analyzed.

## 2. Chaotic-SRM

The spike response model (SRM) was introduced by Gerstner and Kistler<sup>7</sup>. In SRM, the dynamics of neuron is directory described by kernel functions and it is not necessary to solve differential equations for its simulation. We proposed the Chaotic-SRM that is extended SRM to exhibit the chaotic inter-spike intervals<sup>5</sup>. The definitions of Chaotic-SRM is as follows. The membrane potential  $u(t)$  of neuron at time  $t$  is defined as

$$u(t) = u_{rest} + \eta(t - t^{(f)}) + \beta, \quad (1)$$

where  $u_{rest}$ ,  $t^{(f)}$  and  $\beta$  denote the resting potential of neurons, the last firing time of this neuron and the external input, respectively. The kernel function  $\eta$  describes the response of membrane potential after firing. The definition of the kernel function  $\eta$  is

$$\eta(t - t^{(f)}) = -\eta_{init} \exp\left(\frac{t - t^{(f)}}{\tau_{\eta_0}}\right) \theta(t - t^{(f)}), \quad (2)$$

where  $\tau_{\eta_0}$  is the time constant of spike response and  $\theta$  is the step function such that  $\theta(s)$  is 1 for  $s \geq 0$  and 0 for the others. In this model, when the membrane potential exceeds the threshold value  $\vartheta$ , this neuron is firing and the membrane potential is reset by the update of the last firing time  $t^{(f)}$ . The term  $-\eta_{init}$  is an initial value of the kernel function  $\eta$  after firing. In the original SRM, this term is constant. Therefore, the original SRM is periodically firing and its period is determined by the external input value  $\beta$ .

We extended the original SRM to exhibits chaotic response by adding background sinusoidal oscillation in the same way of the bifurcating neuron<sup>8</sup> and the chaotic pulse coupled neural network<sup>4</sup>. In the extended SRM, the background oscillation is added to the term  $\eta_{init}$  and its definition is

$$\eta_{init} = \eta_0 - A_{\eta_0} \sin(2\pi\omega_{\eta_0} t^{(f)}), \quad (3)$$

where  $\eta_0$  denotes the constant  $\eta_{init}$  in the original model and,  $A_{\eta_0}$  and  $\omega_{\eta_0}$  denote the amplitude and the frequency of background oscillation. In this article, we call this extended model the Chaotic-SRM. The Chaotic-SRM exhibits various chaotic behavior depending on the parameter values of  $A_{\eta_0}$  and the external input  $\beta$ .

The bifurcation diagram and the Lyapunov exponent for the external input  $\beta$  are obtained by numerical simulation<sup>6</sup> (Fig.1), where the parameter values of Chaotic-SRM are set as follows:  $u_{rest} = -70\text{mV}$ ,  $\theta = -35\text{mV}$ ,  $\eta_0 = 55$ ,  $\tau_{\eta} = 10\text{msec}$ ,  $\omega_{\eta_0} = 0.75/2\pi$  and  $A_{\eta_0} = 10.9$ . In the bifurcation diagram (Fig.1(a)), the period doubling bifurcation that is typical behavior of chaotic system were observed. In Fig. 1(b), several regions where the Lyapunov exponents is positive, are existing and these regions correspond to the chaotic region in the bifurcation diagram.

### 3. Chaotic-CNN

The Chaotic-CNN is defined as a two dimensional coupled system of Chaotic-SRM<sup>6</sup>. In the Chaotic-CNN, each neuron is put on the  $N \times M$  lattice and connected to

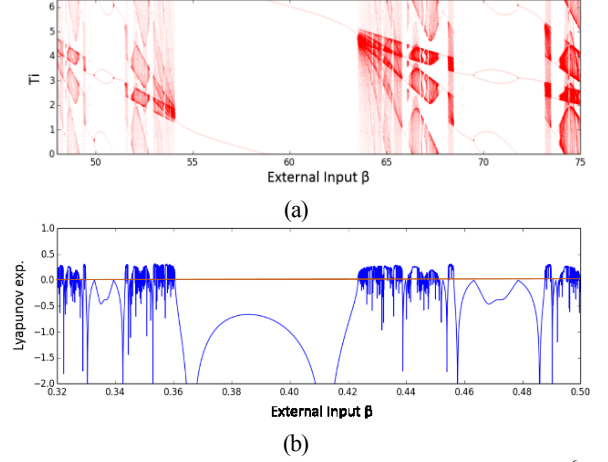


Fig.1. (a) The bifurcating diagram and (b) Lyapunov Exponent<sup>6</sup>.

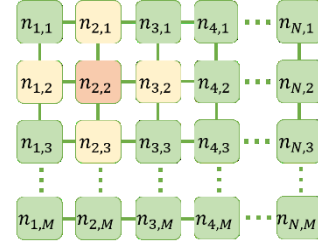


Fig. 2. Chaotic-CNN<sup>6</sup>.

the nearest neighbors in four directions (up, down, left and right) as shown in Fig. 2. Let  $n_{x,y}$  be a neuron that allocated at the location  $(x, y)$ . The membrane potential of  $n_{x,y}$  is denoted by  $u_{x,y}$  and it is defined as

$$u_{x,y}(t) = u_{rest} + \eta(t - t_{x,y}^{(f)}) + \beta_{x,y} + \xi \times [o_{x-1,y}(t) + o_{x+1,y}(t) + o_{x,y-1}(t) + o_{x,y+1}(t)], \quad (4)$$

where  $t_{x,y}^{(f)}$ ,  $\beta_{x,y}$  and  $\xi$  denote the last firing time, the external input of  $n_{x,y}$  and the coupling weight, respectively. The boundary condition is fixed as follows:  $o_{x^*,y}(t) = o_{x,y^*}(t) = 0$  ( $x^* \in \{0, N+1\}$ ,  $y^* \in \{0, M+1\}$ ).

The function  $o_{x',y'}$  is the output from the connected neuron  $n_{x',y'}$  and it is also defined as

$$o_{x',y'}(t) = \sum_{t_{x',y'}^{(f)} < t_{x',y'}^{(k)} < t} \varepsilon(t - t_{x',y'}^{(k)}), \quad (5)$$

where  $t_{x',y'}^{(k)}$  denotes the  $k$ -th firing time of the neuron  $n_{x',y'}$ . The kernel function  $\varepsilon$  describes the response of synaptic connection. The definition of the kernel function  $\varepsilon$  is

$$\varepsilon(s) = \frac{s}{\tau_{\varepsilon}} \exp\left(-\frac{s}{\tau_{\varepsilon}}\right) \theta(s), \quad (6)$$

where  $\tau_{\varepsilon}$  is the time constant of the synaptic connection.

#### 4. Correlation Analysis

In this article, a synchronized response is analyzed by the correlation. As an index of the synchronized response, the cross-correlation between two neurons are analyzed. Let  $S_{x,y}$  be a set of the firing times of the neuron  $n_{x,y}$ . The cross-correlation between  $S_{x,y}$  and  $S_{x',y'}$  with time shift  $\phi$  is defined as

$$CC(S_{x,y}, S_{x',y'}; \phi) = \frac{\#\{t_{x,y}^{(k)} | \exists t_{x',y'}^{(l)} \in S_{x',y'}, |t_{x,y}^{(k)} - t_{x',y'}^{(l)} - \phi| \leq \Delta s\}}{\#(S_{x,y})} \quad (7)$$

where  $\#(X)$  denotes the number of elements of  $X$  and  $\Delta s$  is a time resolution of coincident firing. In this article,  $\Delta s$  is set to 0.5 msec. The auto-correlation is also defined as  $AC(S_{x,y}; \phi) = CC(S_{x,y}, S_{x,y}; \phi)$ . The maximal value of the cross-correlation is defined as

$$CC^*(S_{x,y}, S_{x',y'}) = \max_{\phi} CC(S_{x,y}, S_{x',y'}; \phi). \quad (8)$$

In the case that  $CC^* = CC(S_{x,y}, S_{x',y'}; \phi) \simeq 1$ ,  $S_{x,y}$  and  $S_{x',y'}$  are synchronized with the time shift  $\phi$ . In the case that  $AC^* = AC(S_{x,y}; \phi) \simeq 1$ ,  $S_{x,y}$  is periodic with the period  $\phi$ . When the spike sequence  $S_{x,y}$  is chaotic,  $AC(S_{x,y}; \phi)$  exponentially decays for the time shift  $\phi$ .

#### 5. Numerical Experiments

As numerical experiments, we simulated the Chaotic-CNN for  $20 \times 20$  grayscale image patterns shown in Fig. 4(a) and Fig. 5(a), where the parameters of the single neuron are set as the same values mentioned in the section 2 and the parameters of coupling are set as follows:  $\tau_{\epsilon} = 0.5\text{msec}$  and  $\xi = 4$ . The grayscale pixel value  $g_{x,y} \in \{0, 1, \dots, 255\}$  is mapped to the external input  $\beta_{x,y} \in [\beta_0, \beta_1]$  such that

$$\beta_{x,y} = (\beta_1 - \beta_0) \times \frac{g_{x,y}}{255} + \beta_0. \quad (9)$$

In this simulation, we chose the interval  $[48, 54]$  as  $[\beta_0, \beta_1]$  that includes the chaotic region in the bifurcation diagram (Fig. 1).

The input pattern shown in Fig. 4(a) is a simple gradation pattern from black to white in the direction of x-axis. The neurons aligned in the direction of y-axis have the same input value. A response of the Chaotic-CNN is shown in Fig. 4(b) as a raster plot of firing times, where the abscissa is time and the ordinate is an id of neuron such that  $id = 20x + y$  for the neuron  $n_{x,y}$ . Spike responses are roughly synchronized for each input values. The maximal cross-correlations between the neuron indicated by the arrow and the others were

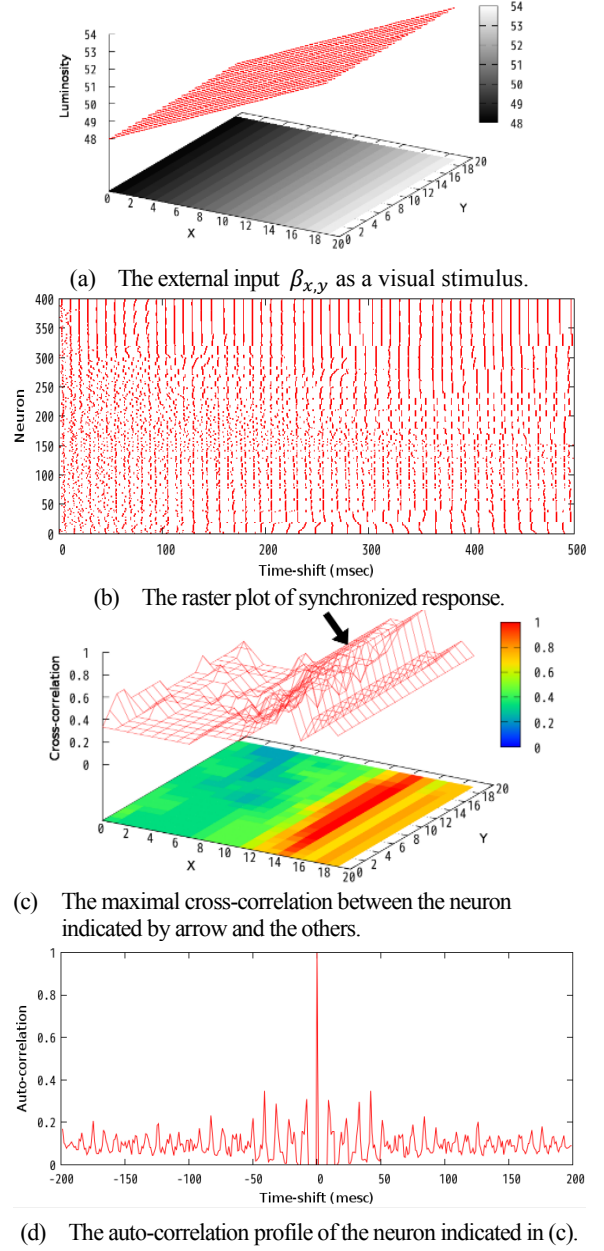
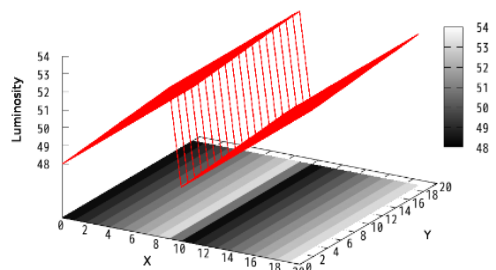
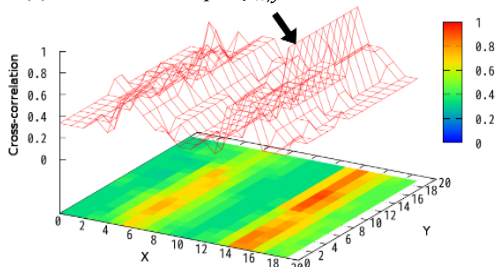


Fig.4. Response to the simple gradation pattern.

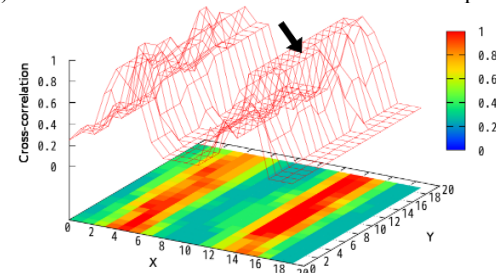
calculated (Fig.4(c)). As shown in Fig.4(c), high correlation is observed for the neurons in the direction of y-axis and relatively lower correlation is observed for the others. The auto-correlation profile was also calculated for the neuron indicated in Fig. 4(c). As a result, exponential decay of auto-correlation is observed as shown in Fig. 4(d). These results support the formation of the chaotic cell assemblies.



(a) The external input  $\beta_{x,y}$  as a visual stimulus.



(b) The maximal cross-correlation for the chaotic response.



(c) The maximal cross-correlation for the periodic response.

Fig.5. Response to the repeated gradation pattern.

In order to demonstrate a difference between the chaotic cell assembly and the periodic one, responses to a twice repeated gradation pattern shown in Fig. 5(a) was analyzed. The maximal cross-correlation for the case of the chaotic spike response is shown in Fig. 5(b) and for the case of the periodic one is shown in Fig. 5(c). For the latter, the amplitude of background oscillation  $A_{\eta_0}$  was set to 0 to generate periodic spike responses. For this case, the neuron indicated by arrow has high correlation with neurons in the two regions where neurons have similar input value (Fig. 5(c)). In terms of correlation, these two regions are not distinguished from each other. On the other hand, for the case of the chaotic spike response, the neuron indicated by arrow has high correlation with neurons in one region included itself and has relatively low correlation with the other neurons. In this case, chaotic cell assemblies invoked by the grayscale input is distinguished from the others even if they have similar input value.

## 6. Conclusions

For grayscale visual stimulus, synchronized response of the Chaotic-CNN was analyzed by the correlation of spike firing times. As results, synchronized responses to the similar input value and a formation of chaotic cell assembly were observed. These results indicate a possibility of visual segmentation using synchronized chaotic response. Analysis for the real image input is one of our future works.

## Acknowledgements

This work was partially supported by JSPS KAKENHI Grant Numbers 24650120.

## References

1. Gray, C.M., Koenig, P., Engel, A.K., & Singer, W., Oscillatory responses in cat visual cortex exhibit inter-columnar synchronization which reflects global stimulus properties, *Nature*, 338, pp.334-337, 1989.
2. Fuji, H., Ito, H., Aihara, K., Ichinose, N., & Tsukada, M., Dynamical cell assembly hypothesis - Theoretical possibility of spatio-temporal coding in the cortex, *Neural Networks*, Vol.9, No.8, pp.1303-1350, 1996.
3. Akihiro Yamaguchi, Naoto Okumura, Hiroyuki Chaki, Mitsuo Wada, Chaotic synchronized cluster in the network of spike response neurons, *IEICE Tech. Rep.*, Vol.99, No.685, NC99-119, pp. 15-20, Mar. 2000 (in Japanese).
4. Yutaka Yamaguchi, Kosei Ishimura, Mitsuo Wada, Chaotic synchronized assembly in Pulse Coupled Neural Networks, *IEICE Tech. Rep.*, Vol.101, No.615, NC2001-98, pp.127-134, Jan. 2002 (in Japanese).
5. Akihiro Yamaguchi, On a chaotic synchronization of one-way coupled two spike response neurons, *Fukuoka Institute of Technology Reports of Computer Science Laboratory*, Vol.24, pp.1-6, 2013 (in Japanese).
6. Akihiro Yamaguchi, On an information coding using localized synchronization in the two dimensional coupled system of chaotic spike response neurons, *Fukuoka Institute of Technology Reports of Computer Science Laboratory*, Vol.25, pp.1-6, 2014 (in Japanese).
7. Gerstner, W., & Kistler, W., Spiking Neuron Models: Single Neurons Populations Plasticity, *Cambridge University Press*, 2002.
8. Lee G., & Farhat, N.H., The Bifurcating Neuron Network 1, *Neural Networks*, Vol. 14, pp.115-131, 2001.

# **Design of Down Scaled Simulator to Apply the Flying Touch Method in Hot Rolling Process**

**Sung Jin Kim**

*School of Interdisciplinary Program in Robotics, Pusan National University,  
San 30 Jangjeon-dong, Geumjeong-gu,  
Busan, 609-735, South Korea*

**Hyun Hee Kim**

*School of Interdisciplinary Program in Robotics, Pusan National University,  
San 30 Jangjeon-dong, Geumjeong-gu,  
Busan, 609-735, South Korea*

**Min Cheol Lee**

*School of Mechanical Engineering, Pusan National University,  
san 30 Jangjeon-dong, Geumjeong-gu,  
Busan, 609-735, South Korea*

*E-mail: [jins2410@naver.com](mailto:jins2410@naver.com), [sleepingjongmo@nate.com](mailto:sleepingjongmo@nate.com), [mcllee@pusan.ac.kr](mailto:mcllee@pusan.ac.kr)  
[www.pusan.ac.kr](http://www.pusan.ac.kr)*

## ***Abstract***

In the hot rolling process, scratches are occurred on the surface of a slab because of its strong friction. One of the methods to solve this scratches problem of slab is proposed which is the Flying Touch hot rolling process. This paper introduces that the simulator for applying Flying Touch Method is manufactured to evaluate a performance of the Flying Touch Method. Furthermore, it is evaluated by the simulator how much Flying Touch hot rolling process can reduce the scratch.

*Keywords* :Flying touch , hot rolling, simulator

## **1. Introduction**

Steel plates, or slabs, used in industries are produced through the following process: Iron making process, the smelting of iron ores into pig iron, Steel manufacture process, the elimination of impurities, and Casting

process, the shaping of molten metal into a plate. The result of this process is slab (Slabs), which can be modified into coils through a process called Rolling process. These coils are then sold after going through processes such as Cold rolling.

© The 2015 International Conference on Artificial Life and Robotics (ICAROB 2015), Jan. 10-12, Oita, Japan

One of the many defects created by hot rolling is called scratch. Scratch is created when the iron plate is in motion. It shows in a long line on the surface of the product and drastically reduces the quality of the product. The flying touch method is one solution to the scratch.

However, this new process is only theoretical and may cause huge financial loss in its application. Therefore it is preferably applied in minimized simulators instead of in actual systems. This paper explains the flying touch method and introduces a simulator of 40:1 ratio, to which this theory can be applied.

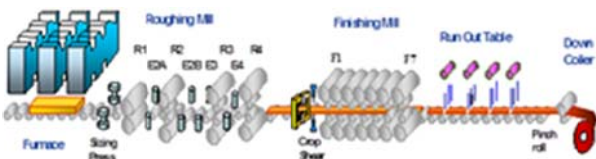


Fig. 1. Hot rolling process

## 2. Flying Touch Method

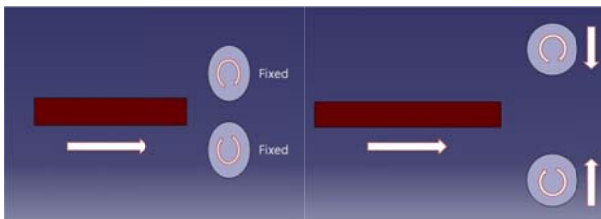


Fig. 2. Previous method and Flying Touch Method

The previous method of rolling process rolled the slab through two stationary rollers as depicted in Fig. 2. (a). As each roller processes only 2-4% of the slab at a time, multiple installed rollers roll slabs. In this process, each installed roller interacts with the slab, and the impact of the last roller creates a scratch at the end of the coil. However, in the flying touch method, as seen in Fig. 2.

(b), friction and impact between the roller and the slab is minimized by synchronizing the movement of the slab with the rotation of the roller and using the Soft touch type, in which the rollers are not fixed, but mobile. The speeds of the slab before being rolled and after being rolled are different because as the slab becomes thinner its amount increases. At this moment, a slip occurs between the slab and the roller, and to decrease this slip, the speed value calculated by forward slip must be applied to the roller. forward slip, the average of the slab's speed before and after being rolled, must be applied in order to synchronize the speed of the roller and the speed of the slab.

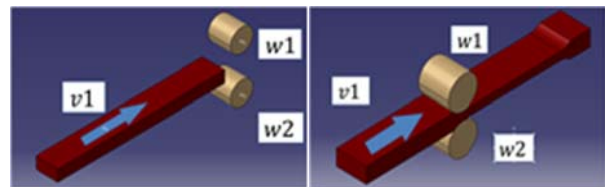


Fig. 3. Flying Touch Method

Fig. 3 depicted the idea of flying touch simply.  $v_1$  is the speed of the slab,  $w_1$  is the angular speed of the upper roller, and  $w_2$  is the angular speed of the lower roller. Because  $w_1$  and  $w_2$  are connected by joints, they have equal speeds. Thus the scratch and impact can be minimized if the speed of the slab and the speed of the rollers are synchronized.

## 3. Design of simulator

The simulator in Fig. 4 was constructed in order to apply the flying touch method and its ratio to an actual rolling mill is 40:1. Fig. 5 is a floor plan of the simulator's modeling picture. Because producing actual iron plates was too difficult for a 40:1 simulator due to the huge torque of the motor, a rubber belt was used.





M1 is a feed motor, and M2, M3 and M4 are position control motor. M3 and M4 are the drive motors of the upper and lower motor. The upper and lower rollers can be controlled by a ball screw. Because the simulator cannot process the 2-4% of the rubber belt as an actual rolling mill would a slab, it is constructed to compress 10% of it, or approximately 1mm.

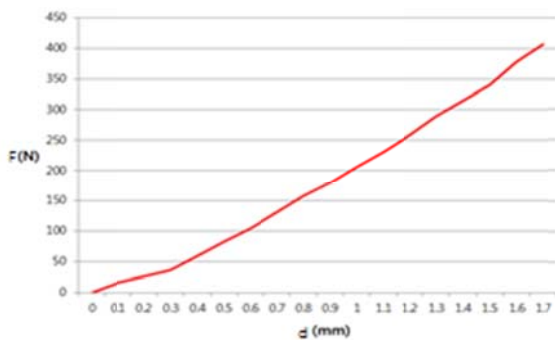


Fig. 6. Rubber belt's deformation-force graph

For getting the rubber belt's elasticity, pressing test has done by deformation processing compressor. The result is represented in Fig. 6. Because the rubber belt's area compressed by the deformation machine is  $300\text{mm}^2$ , the elastic modulus is  $0.7\text{N/mm}^2$  by calculating the slope of deformation-force graph. This elastic modulus is used to select the motors.

The motors' spec is shown in table.1.

Table 1. Motors' specification

	Stall torque	Velocity
M1	6.5N/m	3000rpm
M2	6.5N/m	3000rpm
M3	3.25N/m	3000rpm
M4	3.25N/m	3000rpm

Fig. 7 shows the results of the flying touch control based on the 1/40 downscaled simulator.

The results showed that a speed between simulator roll and assumed steel slab can be synchronized by the designed simulator.

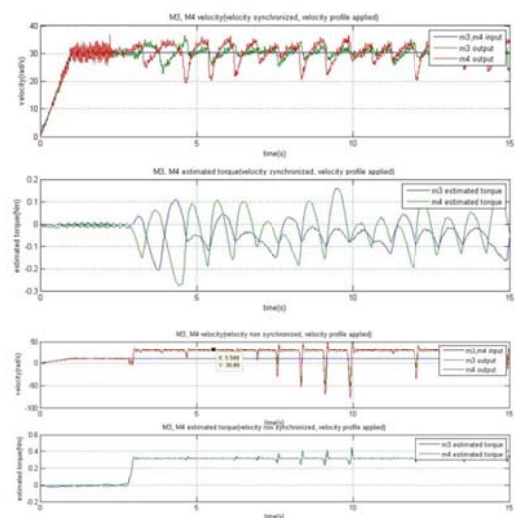


Fig. 7. Simulation graph

#### 4. Conclusion

This research designed the 1/40 downscaled pseudo simulator to apply the flying touch method. The flying touch experiment results showed that the simulator can

synchronize a speed between simulator roll and assumed steel slab.

### **Acknowledgments**

This research was supported by the MOTIE (Ministry of Trade, Industry & Energy), Korea, under the Industry Convergence Liaison Robotics Creative Graduates Education Program supervised by the KIAT (N0001126)."

### **5. References**

1. Choi Y. J and Lee M. C. "PID Sliding Mode Control for Steering of Lateral Moving strip in hot strip Rolling," *International Journal of Control, Automation, and Systems*, pp. 399-407, 2009 7(3):
2. Sansal K. Yildiz, J. Fraser Forbes, Biao Huang, Yale Zhang, Vit Vaculik, Mike Dudzic, "Dynamic modeling and simulation of a hot strip finishing mill, *Applied Mathematical Modeling* 33, pp. 3208-3225, 2009
3. Choi Y.J , Yoo K.S, and Lee M. C, "Development of the strip Off-center Meter Using Line Scan Camera in FM Line ", *Journal of Control, Automation, and Systems, Engineering Col.11, No.6*, 2005
4. Rohde, W. and Rosenthal, D, "High-tech rolling in hot strip mills – theory and practice ", *Metallurgical Plant and Technology*, Vol.1,p.48-55, 1990



# Improving Accuracy of Inertial Measurement Unit using Discrete Wavelet Transform

**Jae-Hoon Jung**

*Dep. of Electronic Eng., Pusan National University, Jangjeon-dong, Geumjeong-gu  
Busan, 609-735, Korea Republic*

**Dong-Hyuk Lee**

*Dep. of Electronic Eng., Pusan National University, Jangjeon-dong, Geumjeong-gu  
Busan, 609-735, Korea Republic*

**Jang-Myung Lee**

*Dep. of Electronic Eng., Pusan National University, Jangjeon-dong, Geumjeong-gu  
Busan, 609-735, Korea Republic*

*E-mail: jaehoon1696@pusan.ac.kr, ldh0917@pusan.ac.kr, jmlee@pusan.ac.kr*

*www.pusan.ac.kr*

## Abstract

In this paper, using discrete wavelet transform in the way of noise removal. wavelet analysis has been used to denoise a digital image corrupted by noise in the acquisition step. Previous studies use Low-pass filter or moving average filter for removing noise. But these filters are corresponded unsuitably for the rapidly changing data. This correspondence cause distortion of the original signal and cause another error for removing noise. In order to compensate for these disadvantages, discrete wavelet transform is applied.

*Keywords:* Discrete Wavelet Transform, Inertial Measurement Unit, Thresholding, Noise Removal .

## 1. Introduction

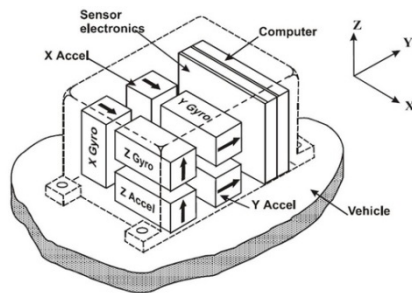


Fig. 1 The structure of Inertial Measurement Unit

Inertial measurement unit is a single of Integrated unit that consist of the accelerometer which can measure the movement of inertia and the gyroscopes which can measure the rotation of inertia, the earth magnetic which can measure the azimuthal.

In order to measure the free movement in three-dimensional space, this unit has each sensor (acceleration, gyroscopes, earth magnetic) that consists of a 3-axis. Here, ARS(Attitude Reference System) measures the attitude with accelerometer and gyroscopes. And AHRS(Attitude Heading Reference System) measures the attitude with accelerometer,

gyroscopes and geomagnetic.

An acceleration sensor is not to measure the moving distance but to use a combined data of acceleration and gyro by calculating the angle with acceleration due to gravity. AHRS is the combined form of fusion of the two sensors and a geomagnetic sensor.

Currently, these inertial measurement units are widely used in localization, attitude control and navigation at water, ground and air. In particular, this unit is applied to an inertial navigation. And this system comes into the spotlight in the field of localization.

But such inertial measurement unit includes instantaneously changing noises and internally generated noises. If these slight noises of data are continued, as time goes fatal cumulative error will be generated in the case of localization

Besides, biasing and misalignment errors generated by the sensor will also affect the antibody, including noise and quantization error, non-aligned mounting error, and the error caused by inaccuracy of the sensor[1]

For this reason, the study for improving the performance with applying to a variety of signal processing algorithms in the inertial navigation system is becoming an issue.

In order to reduce the error when operating localization, attitude control and navigation system, by the wavelet transform which is relatively new signal processing technique, a data of the inertial measurement unit is processed to a more accurate value [2],[3].

Using a characteristic of the wavelet transform, original studies mainly perform a similar role like the low-pass filter or the high-pass filter which remove the data for a specific frequency range [2].

But in this paper, generated errors in the inertial measurement unit more efficiently is reduced with thresholding which is one of the techniques of removing noise.

**2. Wavelet transform**

**2.1. Discrete wavelet transform**

Wavelet transform is a signal conversion technique which is utilized most with FFT (Fast Fourier Transform) and STFT (Short Time Fourier Transform) in the recent signal processing field.

Among them, FFT is often used as a signal processing technique and a solution of the differential equation. But because signal analysis is possible only in frequency domain, this technique has disadvantage that can't know the time information and the frequency information of signal at the same time. To overcome this limitation, STFT which is called the window function and is added the time-dependent weighting function at Fourier building blocks is introduced.

However, because analysis region is always constant for a time-frequency, STFT has disadvantage that can not efficiently analyze non-stationary signal which has the change of stochastic characteristics according to the change of time.

In contrast, the wavelet transform compose a measure using a expansion or contraction of the mother wavelet without the window function. And because functions that occur by a result of moving are used as building blocks, this technique can accomplish time-frequency analysis more efficiently than STFT.

Wavelet transform which is the way to extract partial scale component of the signal with wavelet which can change a size can be defined as Eqs. (1) ~ (2) [4],[5].

$$W_f(b, a) = \int_{-\infty}^{+\infty} f(t)\psi_{b,a}^*(t)dt \tag{1}$$

$$\psi_{a,b}(t) = \frac{1}{\sqrt{a}}\psi\left(\frac{t-b}{a}\right) \tag{2}$$

The function  $\psi$  as the mother wavelet, can be expanded, contracted by the compression coefficient and shifted by the transition coefficient.

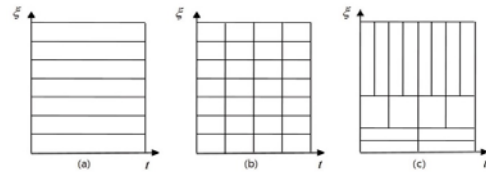


Fig. 2 Time-frequency analysis area by (a) Fourier transform, (b) Local Fourier transform, (c) Wavelet transform

Discrete wavelet transform provide Multi-resolution analysis for the signal. And from a signal processing point of view, this is closely related to reconstruction of each band signal based on the filter bank. Multi-resolution analysis can divide into approximation which is the low-frequency component and detail which is the high-frequency component. This process can be expanded by the concept of two kinds of filter using the low-pass filter and the high pass filter at same time [4],[2],[5].

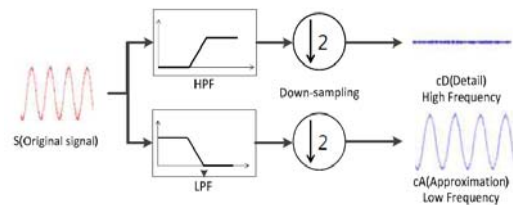


Fig. 3 Multi-resolution analysis of Discrete wavelet transform

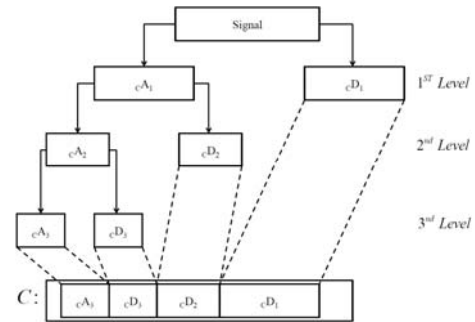


Fig. 4 Multi-resolution decomposition of Discrete wavelet transform

**2.2. Wavelet Thresholding**

The technique to reduce the noise with the wavelet transform is developed in order to remove noise contained in the image. The most common way of noise removal techniques is wavelet shrinkage technique which is represented by thresholding technique [6],[3].

If the wavelet coefficients calculated by performing the wavelet transform do not reach the threshold value, the wavelet thresholding technique makes the wavelet coefficients to zero. This way assumes that the size of the actual signal is greater than the noise level and the noise is mixed by the frequency area. In this case, if the value of the specific frequency component has a

smaller data than the known noise level of the actual signal, its value is made of zero by considering the noise.

Because of the characteristics to remove all frequencies components above a specific frequency, typical low-pass filter bring the actual signal loss. In particular, the accelerometer signal for the signals of the inertial sensor is instantaneously changed when there is the acceleration of a vehicle. And if the accelerometer signal goes through the low-pass filter, this signal is made to be slow by distorting a momentary change of the signal.

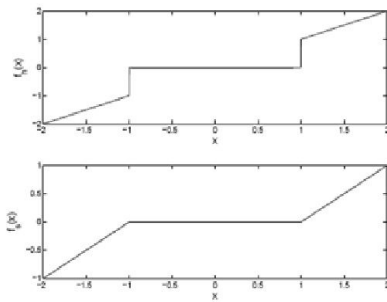


Fig. 5 Hard thresholding function and Soft thresholding function

The thresholding technique is divided into the soft thresholding and the hard thresholding. Ep. (3) is hard thresholding function and Ep. (4) is soft thresholding function.

$$T_{\lambda}^{hard} = \begin{cases} u & \text{if } |u| \geq \lambda \\ 0 & \text{otherwise} \end{cases} \quad (3)$$

$$T_{\lambda}^{soft} = \begin{cases} (u - \text{sign}(u)\lambda) & \text{if } |u| \geq \lambda \\ 0 & \text{otherwise} \end{cases} \quad (4)$$

The value  $u$  which is wavelet coefficients makes the coefficients below the reference value to zero.

For applying the thresholding technique, general way to set the reference value depends on Ep. (5)

$$\lambda = \sqrt{2 \log n \sigma} \quad (5)$$

### 3. Noise removal algorithm in the wavelet

Wavelet analysis is a good tool for denoising, owing to achieving good localization in both space and scale domains, and superior separation of noise and signal contents. Because of the absence of space invariance in the Wavelet, thresholding rather than convolution is the typical technique for denoising with wavelets.[7]

### 4. Experiment

Experiments are performed by the test board is made for processing the wavelet transform in real time.

the acceleration values that most largely include the internal noise of the Inertial measurement unit and the external noise by the external cause are used as a experimental data. And the level 3 is applied to the level of the discrete wavelet.

After receiving the acceleration value, the configured system performs resolution decomposition using discrete wavelet transform. And using the inverse discrete wavelet, this system restores removed noise acceleration data.

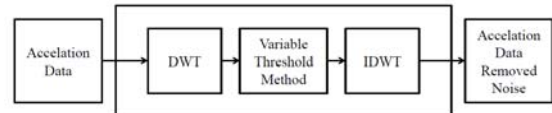


Fig. 6 Filter system block diagram of Discrete wavelet transform

Micro control unit used in the experiment is TMS320F28335. And inertial measurement unit used in the experiment is EBIMU-9DOF.

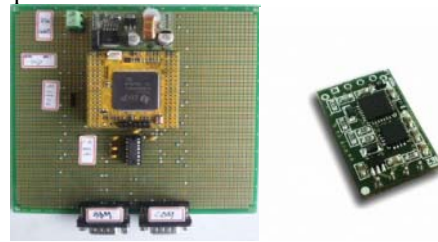


Fig. 7 Test board and inertial measurement unit

The underwater straight running experiment is tested in the 262 (w) × 175 (h) × 50 (d) cm size water tank with AUV.



Fig. 8 The underwater straight line driving experiment

To know degree of internal noise removal, filtering the acceleration data in a stopped state is performed in real-time. Fig. 9 represents that noises of data with the discrete wavelet transform are largely removed than original data.

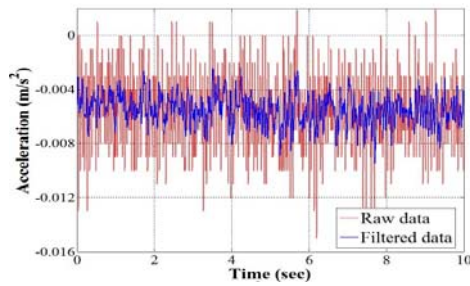


Fig. 9 Comparing original acceleration data and filtered acceleration data in a stopped state

Next experimental data is acceleration data which is measured by straight line driving for 3.5 second. Fig. 10 represents that noises of data with the discrete wavelet transform are largely removed than original data.

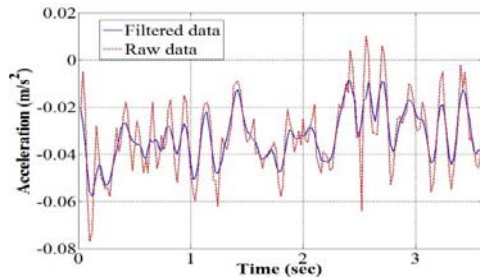


Fig. 10 Comparing original acceleration data and filtered acceleration data in underwater straight line driving

## 5. Conclusion

In this paper, We studied to revise the internal noise and the external noise of the IMU(Inertial Measurement Unit) using the discrete wavelet transform.

By dividing into high frequency component and low frequency component of the noise, removing noises is determined by the threshold value. And the more active filtering effect can be expected unlike the moving average filter or the low pass filter by removing or maintaining the noises.

Finally, we will apply to localization of the actual submarine or mobile robot using the wavelet transform.

In the case of localization, the cumulative error can be reduced when applying effective noise removal. And the robust localization system design will be possible for the disturbance.

## Acknowledgements

This research was supported by the MOTIE (Ministry of Trade, Industry & Energy), Korea, under the Industry Convergence Liaison Robotics Creative Graduates Education Program supervised by the KIAT (N0001126).

## References

1. G. H. Jang, S. B. Chun, E. S. Lee, J. Y. Lee, T. S. Kang and J. R. Kim, "Low Grade IMU Calibration Using Reference Sensor", *KSAS* April.6, pp.772-776, 2014
2. S. P. Kim, E. T. Kim and K. J. Seong, "Sensorz Fusion of GPS/INS/Baroaltimeter Using Wavelet Analysis," *the Journal of Institute of Control, Robotics and Systems*, Vol. 14, No. 12, pp. 1232-1237, 2008
3. Andrew. K. Chan, Cheng Peng, *Wavelets for Sensing Technologies*, Artech House Publishers, 2003
4. B. D. Yoon, H. N. Yoon, S. H. Choi and J. M. Lee, "Estimated Position of Sea-surface Beacon Using DWT/UKF," *the Journal of Institute of Control, Robotics and Systems*, Vol. 19, No. 4, pp. 341-348, 2013
5. S. H. Lee, *Introduction to the Wavelet Transform*, Jinhon M&B,2003
6. C. W. Kang, C. G. Park and N. I. Cho, "Improvement of INS-GPS Integrated Navigation System using Wavelet Thresholding," *the Journal of The Korean Society for Aeronautical and Space Sciences*, Vol. 37, No. 8, pp. 767-773, 2009
7. B. S. Kang, G. S. Shin and M. G. Kang, "Noise Removal Algorithm Using the Wavelet Dependences in the Scale and along the Scale",*Proceedings of ICEIC2006*, June 27-28,2006, Ulaanbaatar,Mongolia

# Outdoor Localization for Quad-rotor using Kalman filter and Path planning \*

**Chen-Hu<sup>†</sup>**

*Department of Electronic Engineering, Pusan National University,  
Jangjeon-2-dong, Geumjeong-gu, Busan 609-735, South Korea<sup>‡</sup>*

**Yo-Seop Hwang**

*Department of Electronic Engineering, Pusan National University,  
Jangjeon-2-dong, Geumjeong-gu, Busan 609-735, South Korea*

**Wang Zhitao**

*Department of Electronic Engineering, Pusan National University,  
Jangjeon-2-dong, Geumjeong-gu, Busan 609-735, South Korea*

**Jang-Myung Lee**

*Department of Electronic Engineering, Pusan National University,  
Jangjeon-2-dong, Geumjeong-gu, Busan 609-735, South Korea*  
E-mail: [chenhu@pusan.ac.kr](mailto:chenhu@pusan.ac.kr), [mmx001@pusan.ac.kr](mailto:mmx001@pusan.ac.kr), [jmlee@pusan.ac.kr](mailto:jmlee@pusan.ac.kr), [zhitao7379@pusan.ac.kr](mailto:zhitao7379@pusan.ac.kr)  
[www.pusan.ac.kr](http://www.pusan.ac.kr)

## Abstract

This paper proposes a new technique that produces the improved local information using low-cost GPS/INS system combined by Kalman filter and Path Planning when a Quad-rotor flies. Throughout the research, the low cost GPS is combined with INS by using the Kalman filter in order to improve local information. However, this system has certain disadvantages as follows. The level of estimation accuracy could get worse when the quad-rotor flies through the air by forming a curve. Also, the level of precision for the position information is influenced by the performance of GPS. In order to deal with such disadvantages, the algorithm based on the path planning can be adopted. When the quad-rotor flies outdoor, it is possible to predict that its moving path is short, since all the short moving paths of the quad-rotor can be assumed to be straight. The path planning is used to make such a short moving path and determine the closest local information of the GPS/INS system. Through the foregoing process, an improved kind of local information can be obtained when the quad-rotor flies. Also, the performance of the proposed system can be verified based on the outdoor experiments.

*Keywords:* Path Planning, Cell Divided Algorithm, Kalman filter, Quad-rotor, GPS, INS

## 1. Introduction

Recently, the level of interest regarding the unmanned aerial vehicle (UAV), which can effectively carry out

various monitoring tasks for disasters, life-saving situations, environmental conditions, traffic congestion and military reconnaissance, has been increased [1]. The low-cost and small-sized quad-rotor can be regarded as



a rotary-blade-type UAV which flies by using four rotors. Since it has various advantages including such functions as vertical takeoff and landing, hovering and omnidirectional movements, the quad-rotor has been widely used in real life for such tasks as serving meals, delivering various objects and supporting various outdoor activities including jogging. Also, researches have been actively carried out in regard to the field. In order to carry out various tasks, the quad-rotor needs to have an autonomous navigation function which is possible only when it can precisely recognize its position. As the quad-rotor carries out its tasks mainly outside, it is necessary to use a precise kind of navigation technology for the estimation of outdoor positions. For such a technology, the recently – executed researches [2][3] have focused on the process of precisely estimating positions based on the combination of the inertial navigation system (INS) and GPS. The INS system is composed of such sensors as the acceleration sensor, the gyro-sensor and the geomagnetic sensor which can be used to estimate both absolute and relative positions simultaneously [4]. It can provide precise information regarding positions within a short time. However, due to the disturbance caused by the property errors of the sensors and the external environment, it is possible to see an accumulation of errors when it is used for a long time. GPS has such a shortcoming as the possibility for having a great position error within a short time. Also, it would be hard to use GPS in the radio-shadow area where the GPS signals can be disconnected [5]. However, it provides a stable kind of information for absolute positions in a long time, since it keeps correcting the position information by continuously receiving signals from the satellite in real time without having any accumulation of errors. In order to establish the GPS/INS fusion position estimation system with the advantages mentioned above, GPS and INS are combined by using the Kalman filter, the extended Kalman filter and the Particle filter, while the properties of each other are compensated through such a process.

This paper is concerned with the process of designing, implementing and experimentally validating the combination of the GPS/INS-fusion position estimation system where the Kalman filter and the path planning algorithm are properly adopted. The Kalman filter is suitable for estimating the states of linear systems with a small amount of computations. However, this Kalman

filter is not enough by itself to overcome the linear errors occurring during the flight of the quad-rotor since it has a low level of accuracy for the state estimation regarding the nonlinear path. Even though the precise GPS/INS fusion system can be implemented by using the Kalman filter, its accuracy is also limited by the accuracy of each sensor. To overcome the sensor capabilities as well as the filtering limits, the path planning information has been utilized for the localization with the direction information captured by the geomagnetic sensor in the INS system. In other words, the estimated path has been mapped onto the nearest path provided by the path planning to improve the localization accuracy overall.

The paper consists of the following sections. In Section II, the configuration of the system is introduced. In Section III, the GPS/INS fusion algorithm is described. After that, in Section IV, the Path planning algorithm is discussed. Then, in Section V the performance of the position estimation process, which is suggested in this paper, is verified through an experiment. Lastly, a conclusion is given.

## 2. System Configuration

In this paper, the configuration of the proposed system is given as shown in Figure 1. The micro-controller unit (MCU), which was used to control the system, is ATMEGA 2560 made by Atmel. Also, MPU-6050, which is a combined form of a tri-axis gyro-sensor and a tri-axis acceleration sensor, HMC-5883, which is a tri-axis geomagnetic sensor, and BMP-085, which is a pressure sensor, were used, while MTK-3329, which is a GPS sensor, was applied for the recognition of positions. In order to generate the thrust of the quad-

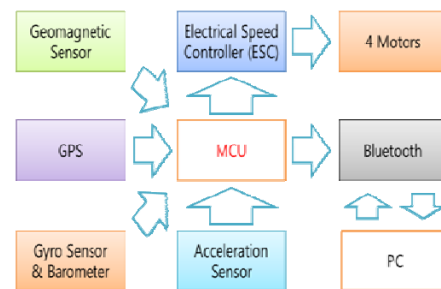


Fig. 1. System Block Diagram

rotor, the electrical speed controller (ESC) and the brushless motor from RoHS were used.

The propellers of the quad-rotor were designed to offset the rotating force of one another and generate a thrust in order to prevent the body from rotating, while RN-42 Bluetooth from RoHS was used to command the robot to move and return. Figure 2 shows the hardware configuration of the system. The GPS receiver was designed to be located on the upper part of the quad-rotor in order to receive the data as accurately as

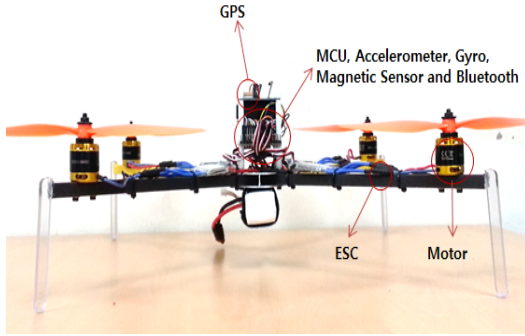


Fig. 2. Total Quad-rotor Configuration

possible, while MCU and IMU sensors were arranged below.

### 3. GPS/INS Fusion

Since INS consecutively provides information regarding the velocity of the body and the change of positions by integrating the acceleration data twice, its dynamic feature could be good, but it is possible to have an accumulation of errors as time goes by. Also, while GPS provides the position information of the body outside, it could create severe errors based on the geographical features. In order to compensate the disadvantages of GPS and INS by combining the data given by each system, the Kalman filter (KF) and the Extended Kalman filter (EKF) can be used. The Kalman filter can be applied to the linear system, while the Extended Kalman filter can be applied to the nonlinear system. The position and state of the quad-rotor in a straight path contains some linear factors. Therefore, in the research, GPS and INS can be combined by using the Kalman filter.

The GPS/INS-fusion algorithm used in this paper is shown in Figure 3.

By using the angular velocity ( $\tilde{\omega}_{ib}^b$ ) obtained from the gyro-sensor, the position expressed in quaternions ( $\hat{q}$ ) can be updated

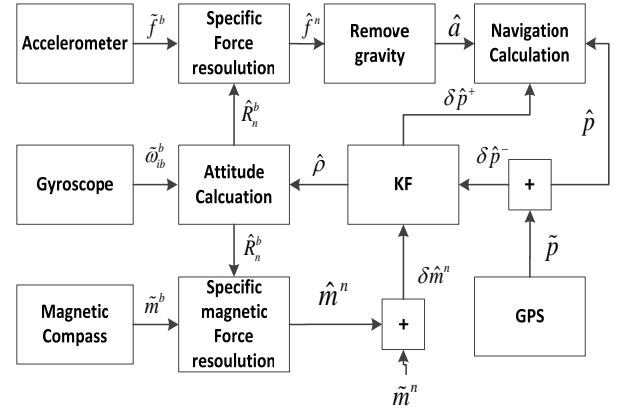


Fig. 3. Fusion algorithm of GPS and INS

$$\hat{q} = \frac{1}{2} q \times (\tilde{\omega}_{ib}^b - \hat{b}_{gyro}) \quad (1)$$

As shown in Equation (1), the position expressed in

$$\hat{R}_n^b = \begin{bmatrix} \hat{q}_1^2 + \hat{q}_2^2 - \hat{q}_3^2 - \hat{q}_4^2 & 2(\hat{q}_2^2 \hat{q}_3^2 - \hat{q}_1^2 \hat{q}_4^2) & 2(\hat{q}_1^2 \hat{q}_3^2 + \hat{q}_2^2 \hat{q}_4^2) \\ 2(\hat{q}_2^2 \hat{q}_3^2 + \hat{q}_1^2 \hat{q}_4^2) & \hat{q}_1^2 - \hat{q}_2^2 + \hat{q}_3^2 - \hat{q}_4^2 & 2(\hat{q}_3^2 \hat{q}_4^2 - \hat{q}_1^2 \hat{q}_2^2) \\ 2(\hat{q}_2^2 \hat{q}_4^2 + \hat{q}_1^2 \hat{q}_3^2) & 2(\hat{q}_1^2 \hat{q}_2^2 + \hat{q}_3^2 \hat{q}_4^2) & \hat{q}_1^2 - \hat{q}_2^2 - \hat{q}_3^2 + \hat{q}_4^2 \end{bmatrix} \quad (2)$$

quaternions can be used to calculate the transformation matrix which transforms the structural coordinates to the navigation coordinates.

The difference between the position ( $\hat{p}$ ) which is obtained by integrating the acceleration ( $\hat{a}$ ) of the navigation coordinates twice and the position ( $\tilde{p}$ ) which is obtained through the reception of GPS can be calculated as shown in the following equation.

$$\delta \hat{p}^- \equiv \tilde{p} - \hat{p} \quad (3)$$

By using the transformation matrix, the measured value ( $\hat{m}^b$ ) of the geomagnetic sensor can be transformed to the value of ( $\hat{m}^n = \hat{R}_n^b \hat{m}^b$ ) in order to measure the value of the magnetic value of the earth. The difference between the actual magnetic value of the earth ( $m^n$ ) and the calculated magnetic value of the earth can be defined as  $\delta \hat{m}^n \equiv \tilde{m}^n - \hat{m}^n$ . By using  $\delta \hat{p}^-$  and  $\delta \hat{m}^n$  as the measured values of KF, the following state space equation can be designed to estimate the position error ( $\hat{p}$ ) and the location error ( $\delta \hat{p}^+$ ). Based on the calculated error, the position and the location can be updated in order to obtain corrected values.

$$\delta \mathbf{x}_k = f_k(\delta \mathbf{x}_{k-1}) + \omega_k, \delta \mathbf{y}_k = h_k(\delta \mathbf{x}_k) + v_k \quad (4)$$

The estimated value of  $k$  can be given as  $\hat{k}$ , while the measured value can be defined as  $\tilde{k}$ .  $f_k$  is the state propagation function and  $h_k$  is the measurement equation, while  $\omega_k$  is the system error and  $v_k$  is the measurement error.  $\delta y_k$  is the measured value. KF can be considered to have 15 states with such random variables as the 3-dimensional location errors ( $\delta p$ ), the velocity errors ( $\delta v$ ), the position errors ( $\rho$ ) and the bias errors given by the acceleration sensor ( $\delta b_{acc}$ ) and the gyro-sensor ( $\delta b_{gyro}$ ).

$$qx = [\delta p^T \quad \delta v^T \quad \rho^T \quad \delta b_{acc}^T \quad \delta b_{gyro}^T] \quad (5)$$

Here, the equation of  $\delta k \equiv k - \hat{k}$  can be given, while the factors of each random variable can be defined as follows.

$$\begin{aligned} p &\equiv [x \quad y \quad z]^T \\ v &\equiv [v_x \quad v_y \quad v_z]^T \\ \rho &\equiv [\varepsilon_N \quad rl \quad \varepsilon_D]^T \end{aligned} \quad (6)$$

Here,  $\varepsilon_N$  is a tilt error, while  $\varepsilon_D$  is a heading error.

#### 4. Path Planning Algorithm

The path planning process is carried out by using the cell divide algorithm and the geomagnetic information. The cell divide algorithm is one of the methods used to plan the path of a moving object, which could also be used to divide free space into various cells where such a path can be easily planned in order to plan the entire moving path. By making a graph which connects the neighboring cells based on the divided ones, an optimal path can be traced. In such a case, it is possible to divide the process into the approximate-cell division and the complete-cell division based on the way of dividing cells. In case of the complete-cell division, the divided cells need to become the original free space when they are united [6][7]. Unlike any robot moving on the ground, the flying quad-rotor is not subject to any limitation regarding an obstacle. Therefore, in this paper, the complete-cell division was used.

The order for the determination of positions through the cell divide algorithm proposed in this paper is shown in Figure 4.

A 10m straight route from the current position obtained from the GPS sensor is planned in advance,

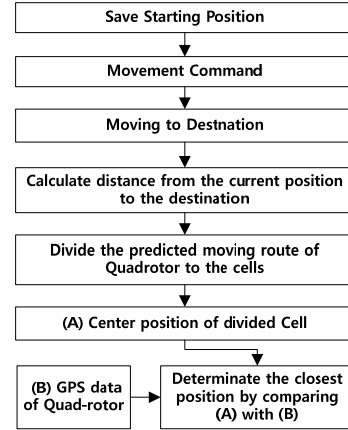


Fig. 4. Block diagram of cell divide algorithm

while the planned route is transformed into approximate longitude and latitude values through an equation before being divided into cells [8]. When the quad-rotor flies along a curve, the route is subject to the rotational transformation process based on the directional values given by the geomagnetic sensor. As a result, it is possible to carry out the path planning process even when the quad-rotor moves along a curve. The center coordinates of the divided cells can be compared with

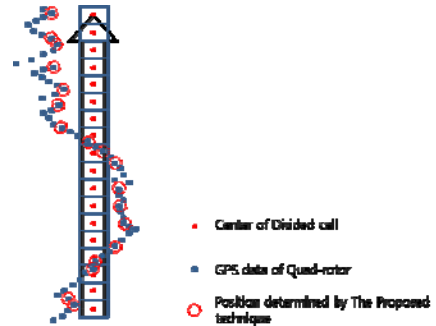


Fig. 5. Position determined by cell divide algorithm

the GPS/INS-fusion position information in order to choose the position information which is the closest to the actual position. Figure 5 shows how the closest position is selected.

#### 5. Experiment

In this paper, the low-cost GPS position information having a relatively great error and the INS position information having an accumulation of errors were combined by using the Kalman filter in order to estimate the outdoor positions of the quad-rotor.



However, since the performance of the Kalman filter tends to be poor in terms of the estimation on a curve which shows a high level of nonlinearity and the GPS/INS-fusion system is greatly influenced by the performance of GPS, the system, which can be used to improve the performance of the position estimation process by applying the path planning algorithm, is proposed to compensate such a problem. In order to evaluate the performance of the proposed system, we carried out an experiment for the position estimation



Fig. 6. The experimental environment

process by flying the quad-rotor over 150m in the playground of our school. The position information of the moving quad-rotor was received in real time by using the Bluetooth communication technology.

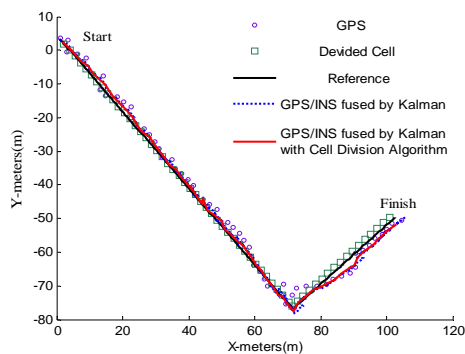


Fig. 7. The experimental result

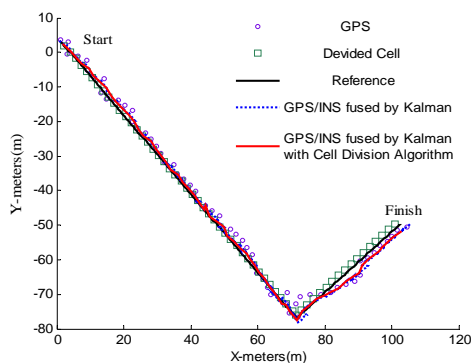


Fig. 8. Partial magnification image of the experimental result

Fig. 7 compares the performance of the position estimation process carried out by the proposed system with the performance of the process carried out by the GPS-INS-fusion system using the Kalman filter.

Table 1. The caption should be placed before the table.

Sort	Average Local Error(m)
GPS	2.8955
GPS/INS	1.8953
Path planning+GPS/INS system	1.612

As shown in Fig. 7 and 8, it is possible to see that the level of precision for the estimation of positions is improved more as the information which is close to the actual positions is chosen out of the position information given by the GPS/INS-fusion system which is combined by using the Kalman filter based on the path planning algorithm. Table 1 show the resulting average position errors.

## 6. Conclusion

In conclusion, the experimental results reveal that the proposed system, using the Kalman filter and Path planning, is more accurate than a single low cost GPS or GPS/INS system fused by Kalman filter. The results also suggest that when tracking location outdoors, the proposed system is a good alternative to DGPS and RTK-GPS. This is because the proposed system is more cost efficient and similarly as accurate as the other localization systems. After this research, it will be configured that position estimation system which is capable of estimating the mobile robot's position as it travels an outdoor curved path.

## Acknowledgements

This research was supported by the MOTIE (Ministry of Trade, Industry & Energy), Korea, under the Industry Convergence Liaison Robotics Creative Graduates Education Program supervised by the KIAT (N0001126).

## References

1. M.G.Kim, Y.D.Kim, "Multiple UAVs Nonlinear Guidance Laws for Stationary Target Observation with Waypoint Incidence Angle Constraint", *Int'l J. of Aeronautical & Space Sci*, Vol.14, No.1, pp 67-74, 2013
2. S. Kim, C. Roh, S. Kang, and M. Park, "Outdoor navigation of a mobile robot using differential GPS and curb detection", *Proceeding of IEEE International Conference on Robotics and Automation*, pp 3414-3419, Roma, April 10-14, 2007
3. G. T. Schmidt, "INS/GPS Technology Trends", *NATO Research and Technology Organization*, May 2009
4. J.H. Seung, D.J. Lee, J.Y.Ryu, "Precise Positioning Algorithm Development for Quadrotor Flying Robots Using Dual Extended Kalman Filter", *Journal of Institute of Control, Robotics and System*, Vol.19, No.2, pp 183-163, 2013
5. K.W.Chiang, Y.W.Huang, "An intelligent navigator for seamless INS/GPS integrated land vehicle navigation applications", *Appied Coft Computing*, Vol 8, No 1, pp 722-733, 2008
6. J.T.Kim, D.J.Kim, "New Path Planning Com bining Visibility Graph and Adaptive Cell Decomposition", *Journal of KIISE : Computer Systems and Theory*, Vol. 36, No. 1, pp 357-361, 2009
7. J.W.Kang, S.J.Kim, "Path Planning for Complete and Efficient Coverage Operation of Mobile Robots", *International Conference on Mechatronics and Automation*, pp 2126-2131, Harbin, China, August 5-8, 2007
8. M.Rengarajan, G. Anitha "Algorithm Development And Testing Of Low Cost Way Point Navigation System", *Engineering Science and Technology: An International Journal*, Vol 3, No. 2, pp 411-414, April 2013

# Distributed Terminal Backstepping control for Multi-Agent Euler-Lagrange Systems

**Seong-Ik Han**

Dep. of Electronic Eng., Pusan National University, Jangjeon-dong, Geumjeong-gu  
Busan, 609-735, Korea Republic

**Yun-Ki Kim**

Dep. of Electronic Eng., Pusan National University, Jangjeon-dong, Geumjeong-gu  
Busan, 609-735, Korea Republic

**Hoang Nhat Minh**

*Dep. of Electronic Eng., Pusan National University, Jangjeon-dong, Geumjeong-gu  
Busan, 609-735, Korea Republic*

**Jang-Myung Lee**

*Dep. of Electronic Eng., Pusan National University, Jangjeon-dong, Geumjeong-gu  
Busan, 609-735, Korea Republic*

*E-mail: skhan@pusan.ac.kr, mecha8404@pusan.ac.kr, nhatminh1696@pusan.ac.kr, jmlee@pusan.ac.kr  
www.pusan.ac.kr*

## Abstract

This paper presents a distributed terminal (finite-time) backstepping consensus control for multi-agent Euler-Lagrange systems. Terminal virtual error surfaces and virtual controls are proposed to guarantee the finite-time error consensus and formation convergence of a group of one-leader and multi-follower cooperative tracking Euler-Lagrange system. Finite-time stability including infinite-time stability was proved by the finite-time Lyapunov candidate function. Simulation example shows the effectiveness of the proposed finite-time backstepping coordinated tracking controller.

*Keywords:* Euler-Lagrange multi-agent system, backstepping control, Terminal virtual error surface.

## 1. Introduction

In recent years, there has been a great interest for researches of multi-agent systems, whose applications include spacecraft, mobile robots, sensor networks, etc. Interesting research directions are containment control, consensus, formation, and flocking control [1]. These problems focus on two cases, namely, the case that there does not exist a leader and the case where there exists a leader. The coordinate tracking problems to track a single leader have been investigated for followers with single-integrator, double-integrator, high-order dynamics, nonlinear or Euler-Lagrange dynamics [2-5]. Linear control theory and variable structure control methods in most researches are used. On the other hand, there are few examples that use the backstepping control technique [6] for nonlinear or Euler-Lagrange multi-agent system. In this method, the problem of unmatched uncertainty and neglecting the efficient nonlinearities is overcome via adopting step-by-step recursive process.

However, although a controller designed using this theorem guarantees the infinite-time stability of a closed-loop system, it has drawbacks such as a slow convergence rate and reduced robustness to uncertainty. On the other hand, systems with finite-time settling-time design possess attractive features such as improved robustness and disturbance rejection properties [7]. In this paper, terminal backstepping control based multi-agent consensus control for Euler-Lagrange system with one-leader and multi-followers is developed.

## 2. Background and Preliminaries

### 2.1. Concept of Graph Theory

In this paper, multi-agent robot Euler-Lagrange systems consisting of one leader and  $n$  followers are considered. Graph theory is introduced to solve the coordination problem and model information exchange between agents. The communication topology is a directed graph,  $\mathcal{G} = \{\mathcal{V}, \mathcal{E}\}$ , where  $\mathcal{V} = \{0, 1, 2, \dots, n\}$  is the set of nodes, node  $i$  represents the  $i$ th agent,  $\mathcal{E}$  is the set of

edges, and an edge in  $\mathcal{G}$  is denoted by an ordered pair  $(i, j)$ .  $(i, j) \in \mathcal{E}$  if and only if the  $i$ th agent can send information to  $j$ th agent directly, but not necessarily vice versa. A directed tree is a directed graph, where every node has exactly one parent except for the root, and the root has directed paths to every other node. A directed graph,  $\mathcal{G} = \{\mathcal{V}, \mathcal{E}\}$ , has a directed spanning tree if and only if  $\{\mathcal{V}, \mathcal{E}\}$  has at least one node with a directed path to all other nodes.  $A = [a_{ij}] \in R^{(n+1) \times (n+1)}$  is called the weighted adjacency matrix of  $\mathcal{G}$ , where  $a_{ii} = 0$  and  $a_{ij} \geq 0$  with  $a_{ij} > 0$  if there is an edge between the  $i$ th agent and  $j$ th. The Laplacian of the weighted graph can be defined as  $L = D - A \in R^{(n+1) \times (n+1)}$ , where  $D = \text{diag}(d_0, d_1, \dots, d_n) \in R^{(n+1) \times (n+1)}$  is the degree matrix and  $d_i = \sum_{j=0}^n a_{ij}$  for  $i = 0, 1, \dots, n$ . For simplicity, it is assumed that  $a_{ij} = 1$  if  $(i, j) \in \mathcal{E}$  and 0 otherwise. The connection weight between agent  $i$  and the leader is denoted by  $b_i$  such that  $b_i = 1$  if agent  $i$  connected to the leader and 0 otherwise.

## 2.2. Multi-Agent Euler-Lagrange Systems

The nonlinear dynamics of a group of  $n+1$  fully actuated Euler-Lagrange systems are described as follows:

$$M_i(q_i)\ddot{q}_i + C_i(q_i, \dot{q}_i)\dot{q}_i + G_i(q_i) + \tau_{di} = \tau_i, \quad i = 1, \dots, n+1, \quad (1)$$

where  $M_i(q_i)$  is a symmetric and positive definite inertia matrix;  $C_i(q_i, \dot{q}_i)$  is a velocity-dependent centripetal and Coriolis forces matrix;  $G_i(q_i)$  is a gravitational vector;  $\tau_{di}$  is a bounded unknown disturbance including unmodelled dynamics and exogenous disturbance; and  $\tau_i$  is an input torque. The simple dynamic equation can be expressed as the following state space model:

$$\begin{aligned} \dot{x}_{i,1} &= x_{i,2}, \\ \dot{x}_{i,2} &= f_i(\bar{x}_2) + g_i(\bar{x}_2)u_i, \\ y_i &= x_{i,1}, \quad i = 1, \dots, n+1, \end{aligned} \quad (2)$$

where  $x_{i,1} = q_i$ ,  $x_{i,2} = \dot{q}_i$ ,  $\bar{x}_2 = [x_{i,1}, x_{i,2}]^T$ ,  $f_i(\bar{x}_2) = -M_i^{-1}C_i(\bar{x}_{i,2})x_{i,2} - M_i^{-1}G_i(x_{i,1}) - M_i^{-1}\tau_{di}$ ,  $g_i = M_i^{-1}$ , and  $u_i = \tau_i$ .

**Assumption 1.**  $\|M_i^{-1}\tau_{di}\| \leq \delta_{di}$ ,  $\|K_i^C - M_i^{-1}C_i(\bar{x}_{i,2})\| \leq \delta_{ci}$ ,  $\|K_i^G x_{i,1} - M_i^{-1}G_i(x_{i,1})\| \leq \delta_{gi}$ , and  $\delta_{ci} + \delta_{gi} + \delta_{di} \leq \delta_{hi}$ , where  $K_i^C$  and  $K_i^G$  are positive definite diagonal matrices and vectors, respectively, and  $\delta_{hi} > 0$  are upper bounds.

## 3. Distributed Terminal backstepping Controller Design and Stability Analysis

### 3.1. Controller Design

The tracking errors and virtual error surfaces are defined as follows:

$$z_{i,1} = \sum_{j=1}^n a_{ij}(y_i - y_j) + b_i(y_i - x_0), \quad (3)$$

$$z_{i,2} = x_{i,2} + c_{i,1} \text{sig}(z_{i,1})^{\gamma_{i,1}} - \alpha_{i,1}, \quad i = 1, \dots, n, \quad (4)$$

where  $x_0$  is the position of the leader,  $\alpha_{i,1}$  are the virtual controls,  $\text{sig}(z_{i,1}) = \|z_{i,1}\|^{\gamma_{i,1}} \text{sgn}(z_{i,1})$ ,  $c_{i,1} > 0$  are constants, and  $\gamma_{i,1} = \xi_{i,1} / \zeta_{i,1}$ ,  $\xi_{i,1}$  and  $\zeta_{i,1}$  are positive odd numbers,  $\xi_{i,1} < \zeta_{i,1} < 2\xi_{i,1}$ ,  $\text{sgn}(z_{i,1})$  is a sign function. (3) can be changed for the formation control case as follows:

$$z_{i,1} = \sum_{j=1}^n a_{ij}(y_i + \Delta_i - y_j - \Delta_j) + b_i(y_i + \Delta_i - x_0 - \Delta_0) \quad (5)$$

The time derivative of the first error surfaces  $z_{i,1}$  along (2) is

$$\begin{aligned} \dot{z}_{i,1} &= (d_i + b_i)(z_{i,2} - c_{i,1} \text{sig}(z_{i,1})^{\gamma_{i,1}} + \alpha_{i,1}) \\ &\quad - \sum_{j=1}^n a_{ij} \dot{x}_{i,2} - b_i \dot{x}_0. \end{aligned} \quad (6)$$

The Lyapunov function candidate  $V_{i,1} = z_{i,1}^T z_{i,1} / 2$  to design the distributed virtual controller. Differentiating  $V_{i,1}$  yields

$$\begin{aligned} \dot{V}_{i,1} &= z_{i,1}^T [(d_i + b_i)(z_{i,2} - c_{i,1} \text{sig}(z_{i,1})^{\gamma_{i,1}} + \alpha_{i,1}) \\ &\quad - \sum_{j=1}^n a_{ij} \dot{x}_{i,2} - b_i \dot{x}_0]. \end{aligned} \quad (7)$$

Choosing the distributed virtual control as

$$\alpha_{i,1} = \frac{1}{d_i + b_i} \left( -k_{i,1} z_{i,1} + \sum_{i=1}^n a_{ij} \dot{x}_{i,2} + b_i \dot{x}_0 \right), \quad (8)$$

(7) becomes

$$\dot{V}_{i,1} = -k_{i,1} z_{i,1}^T z_{i,1} - (d_i + b_i) c_{i,1} \|z_{i,1}\|^{\gamma_{i,1}+1} + (d_i + b_i) z_{i,1}^T z_{i,2}, \quad (9)$$

where  $k_{i,1} > 0$  are constants. Differentiating the Lyapunov function,  $V_{i,2} = V_{i,1} + z_{i,2}^T z_{i,2} / 2 + \tilde{\delta}_{hi}^2 / 2\eta_i$ , along (2) and (4),

$$\begin{aligned} \dot{V}_{i,2} &= -k_{i,1} z_{i,1}^T z_{i,1} - (d_i + b_i) c_{i,1} \|z_{i,1}\|^{\gamma_{i,1}+1} + (d_i + b_i) z_{i,1}^T z_{i,2} \\ &\quad + z_{i,2}^T [f_i(\bar{x}_2) + g_i(\bar{x}_2)u_i + c_{i,1} \gamma_{i,1} \|z_{i,1}\|^{\gamma_{i,1}-1} \dot{z}_{i,1} - \dot{\alpha}_{i,1}] \\ &\quad - \tilde{\delta}_{hi} \hat{\delta}_{hi} / \eta_i. \end{aligned} \quad (10)$$

Choosing the control inputs and adaptive laws as

$$\begin{aligned} u_i &= g_i^{-1} [-k_{i,2} z_{i,2} - (d_i + b_i) z_{i,1}^T + K_i^C x_{i,2} + K_i^G x_{i,1} \\ &\quad - c_{i,1} \gamma_{i,1} \|z_{i,1}\|^{\gamma_{i,1}-1} \dot{z}_{i,1} - c_{i,2} \text{sig}(z_{i,2})^{\gamma_{i,2}} \\ &\quad + \frac{\hat{\delta}_{hi} z_{i,2}}{\|z_{i,2}\| + \kappa_{i,2}} + \dot{\alpha}_{i,1}], \end{aligned} \quad (11)$$

$$\dot{\hat{\delta}}_{hi} = \eta_i \left( \|z_{i,2}\|^2 / (\|z_{i,2}\| + \kappa_{i,2}) - \eta_i' \hat{\delta}_{hi} \right), \quad (12)$$

where  $k_{i,2} > 0$ ,  $\eta_i > 0$ ,  $\eta'_i > 0$ ,  $c_{i,2} > 0$ , and  $0.5 < \gamma_{i,2} < 1$  are constants,  $\tilde{\delta}_{hi} = \delta_{hi} - \hat{\delta}_{hi}$ ,  $\hat{\delta}_{hi}$  are estimates of  $\delta_{hi}$ , we obtain the following expression:

$$\begin{aligned} \dot{V}_{i,2} &\leq -\sum_{k=1}^2 k_{i,1} z_{i,k}^T z_{i,k} - (d_i + b_i) c_{i,1} \|z_{i,1}\|^{\gamma_{i,1}+1} - c_{i,2} \|z_{i,2}\|^{\gamma_{i,2}+1} \\ &\quad + \tilde{\delta}_{hi} (z_{i,2}^T - \hat{\delta}_{hi} / \eta_i) \\ &\leq -\sum_{k=1}^2 k_{i,1} z_{i,k}^T z_{i,k} - \frac{\eta'_i \tilde{\delta}_i^2}{2} - \sum_{k=1}^2 \beta_{i,k} \|z_{i,k}\|^{\gamma_{i,k}+1} + \eta'_i \tilde{\delta}_i^2 / 2 \\ &\leq -\left( \sum_{k=1}^2 k_{i,1} z_{i,k}^T z_{i,k} + \frac{\eta'_i \tilde{\delta}_i^2}{2} \right) - \left( \sum_{k=1}^2 \beta_{i,k} z_{i,k}^T z_{i,k} + \frac{\eta'_i \tilde{\delta}_i^2}{2} \right)^{\frac{\gamma_{i,k}+1}{2}} \\ &\quad + \mu_i \\ &\leq -a V_{i,2} - b \frac{\gamma_{i,k}+1}{2} V_{i,2}^{\frac{\gamma_{i,k}+1}{2}} + \mu_i, \end{aligned} \quad (13)$$

where  $\beta_{i,k} = \min[(d_i + b_i) c_{i,1}, c_{i,2}]$ ,  $a = \min[2k_{i,1}, 2k_{i,2}, \eta'_i]$ ,

$$b = \min[2\beta_{i,1}, 2\beta_{i,2}, \eta'_i], \mu_i = \eta'_i \|z_{i,k} \tilde{\delta}_i\|^2 + \left( \frac{\eta'_i \tilde{\delta}_i^2}{2} \right) + \frac{\eta'_i \tilde{\delta}_i^2}{2}$$

### 3.2. Finite-Time Stability Analysis

((13) can be rewritten the following two forms:

$$\begin{aligned} \dot{V}_{i,2} &\leq -a V_{i,2} - \left( b \frac{\gamma_{i,k}+1}{2} - \frac{\mu_i}{V_{i,2}^{\frac{\gamma_{i,k}+1}{2}}} \right) V_{i,2}^{\frac{\gamma_{i,k}+1}{2}} \\ &= -a' V_{i,2} - b' V_{i,2}^{\gamma'}, \end{aligned} \quad (14)$$

where  $a' = a - \mu_i / V_{i,2}$ ,  $b' = b \frac{\gamma_{i,k}+1}{2} - \mu_i / V_{i,2}^{\frac{\gamma_{i,k}+1}{2}}$ , and  $\gamma' = \frac{\gamma_{i,k}+1}{2}$ . From (14), if  $a$  and  $b$  is selected such

that  $a > \mu_i / V_{i,2}$  and  $b > \mu_i^{\frac{2}{\gamma_{i,k}+1}} / V_{i,2}$ , respectively. Then, from the definition of finite-time stability [7], the equilibrium point  $x=0$  is globally finite-time stable and the settling time  $t_s$  can be given by

$$t_s \leq \frac{1}{a(1-\gamma')} \ln \frac{aV_{i,2}^{1-\gamma'}(x_0) + b'}{b'}. \quad (15)$$

## 4. Simulation Example

To validate the proposed control scheme, the following group of one leader indexed by 0 and four followers indexed by 1, 2, 3, and 4, respectively as shown in Fig. 1. The strict feedback state equations of each agent are expressed as

$$\begin{aligned} \dot{x}_{i,1} &= x_{i,2}, \\ \dot{x}_{i,2} &= f_{i,2}(x_{i,1}) + g_{i,2} u_i, \end{aligned} \quad (16)$$

where  $f_{i,2} = -[G_i(q_i) + \tau_{di}] / J_i$ ,  $g_i = 1 / J_i$ ,  $u_i = \tau_i$ ,  $J_i = m_i L_i^2 / 3$ ,  $G_i(q_i) = m_i L_i \cos q_i$ , the mass of the link  $m_i = 1 \text{ kg}$ , and the length of link  $L_i = 0.25 \text{ m}$ . Let the initial condition of four followers be  $x_{1,1} = 1, x_{1,2} = 0$ ,  $x_{2,1} = 1.2, x_{2,2} = 0$ ,  $x_{3,1} = 2, x_{3,2} = 0$ ,  $x_{4,1} = -1.2, x_{4,2} = 0$ . The Laplacian can be written as

$$L = \begin{bmatrix} 0 & 0 & 0 & 0 & 0 \\ 0 & 3 & -1 & -1 & -1 \\ 0 & 0 & 1 & -1 & 0 \\ -1 & 0 & -1 & 1 & 0 \\ -1 & 0 & 0 & 0 & 0 \end{bmatrix}, b_3 = 1, b_4 = 1.$$

Simulation results are obtained with the time-varying control input to the leader being designed as  $u_0 = -\sin(x_{0,1}) / (1 + e^{-t})$ ,  $x_{0,1} = \pi / 2$ , and  $x_{0,2} = 0$ .

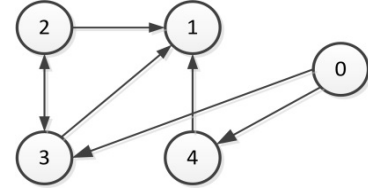
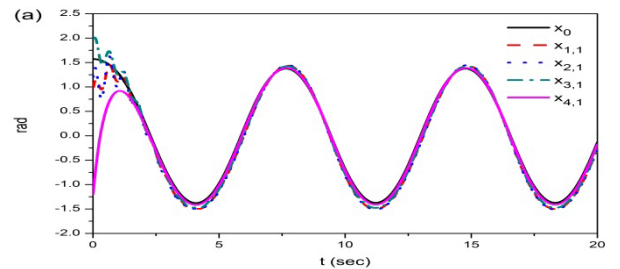


Fig. 1. Directed graph of the manipulator group  
The error functions for the illustration of the formation control are changed into (5), where  $\Delta_1 = -1$ ,  $\Delta_2 = -2$ ,  $\Delta_3 = -3$ , and  $\Delta_4 = -4$ . Simulation results are presented in Fig. 2 (consensus control) and Fig. 3 (formation control), where the settling time of the proposed TBSC system is 31% faster than that of the BSC system. In addition, the steady state errors of the TBSC system are smaller compared to the BSC system.

## 5. Conclusion

A terminal backstepping control scheme to guarantee the fast error convergence and small tracking error performance for a multi-agent Euler-Lagrange system is developed in this paper. A virtual finite-time error surface is defined to design a virtual control. The finite-time convergence is proved by the finite-time stability analysis of Lyapunov function. Simulation for one-link manipulator agents confirms the theoretical proposal.



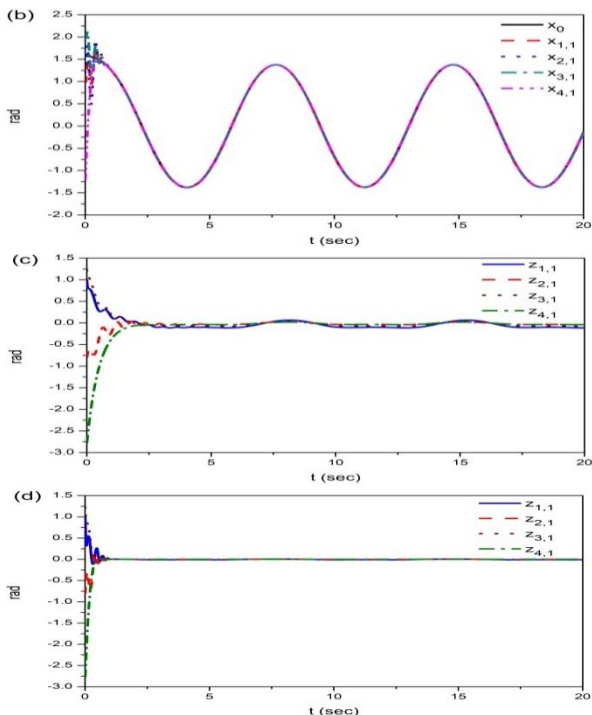


Fig. 2. Consensus control simulation results. (a) Tracking outputs of BSC system. (b) Tracking outputs of TBSC system. (c)  $z_{1,1}$  of BSC. (d)  $z_{1,1}$  of TBSC.

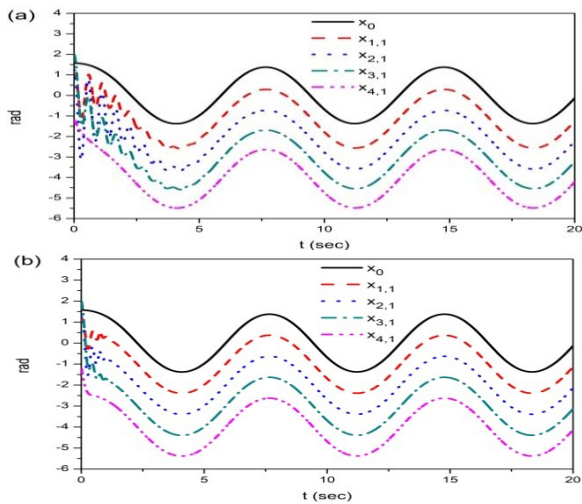


Table 1. Settling time (sec) of BSC and TBSC systems

	Consensus		Formation	
	BSC	TBSC	BSC	TBSC
$z_{1,1} \leq 0.01$	2.03 s	0.77 s	2.23 s	0.83 s
$z_{2,1} \leq 0.05$	2.20 s	0.67 s	2.63 s	0.91 s
$z_{3,1} \leq 0.01$	2.07 s	0.76 s	2.83 s	0.86 s
$z_{4,1} \leq 0.05$	2.15 s	0.42 s	1.46 s	0.29 s
Mean (%)	100%	32%	100%	31%

**Acknowledgements**

This research was supported by the MOTIE (Ministry of Trade, Industry & Energy), Korea, under the Industry Convergence Liaison Robotics Creative

Graduates Education Program supervised by the KIAT (N0001126).

**References**

1. W. Ren, *Distributed consensus in multi-vehicle cooperative control* (Springer-Verlag, London, 2008).
2. H. Arcaç, and M. Wen, Adaptive motion coordination: using relative velocity feedback to track a reference velocity, *Automatica*, **45**(2) (2009) 1020-1025.
3. H. Su, G. Chen, and Z. Lin, Adaptive second-order consensus of networked mobile agents with nonlinear dynamics, *Automatica*, **47**(2) (2011) 368-375
4. H. Zhang, and F. L. Lewis, Adaptive cooperative tracking control of high-order nonlinear systems with unknown dynamics, *Automatica*, **48** (2012) 1432-1439.
5. S. Chung, and J. J. Slotine, Cooperative robot control and concurrent synchronization of Lagrangian systems, *IEEE Tran. Robotics*, **25**(3) (2012) 686-700.
6. K. Krstic, I. Kanellakopoulos, and P. V. Kokotovic, *Nonlinear and adaptive control design* (Wiley, New York, 1995).
7. S. Yu, X. Yu, B. Shirinzadeh, and Z. Man, Continuous finite-time control for robotic manipulators with terminal sliding mode, *Automatica*, **41** (2005) 1975-1964.

# Vision-Based Grasp Planning and Experiments of a Mobile Manipulator

**Yi-Fu Chiu**

*Institute of Electrical Control Engineering, National Chiao Tung University  
1001 Ta Hsueh Road, Hsinchu 30010, Taiwan*

**Kai-Tai Song**

*Institute of Electrical Control Engineering, National Chiao Tung University  
1001 Ta Hsueh Road, Hsinchu 30010, Taiwan  
E-mail: ivan790721.ece01g@nctu.edu.tw, ktsong@mail.nctu.edu.tw*

## *Abstract*

In this paper, a motion planner is designed and implemented for of a mobile manipulator to travel to a spot for grasping of an object. In this work, the probability of successful grasping inside the workspace of the robot arm is used for grasping planning. A vision SLAM system is combined with reachability calculation to figure out the grasping position. Using a laboratory dual-arm robot, we conducted experiments in different conditions to verify the effectiveness of the developed system.

*Keywords:* Mobile manipulation, visual servoing, visual navigation, robot grasping.

## **1. Introduction**

Mobile manipulation technologies have been developed rapidly in recent years. It has been expected that various robots will come into our everyday life for living aids. In order to help people with housework, a robot needs to be equipped with many abilities such as communication, navigation, grasping and object recognition. Therefore, developing a mobile manipulator which is able to move and handle objects such that it can support people in a home setting deserves urgent attention.

Cosero<sup>1</sup> has achieved notable success in RoboCup@Home contests for its mobile manipulation performance. It localizes objects and plans path based on a 2D occupancy grid map constructed from multiple 3D scans of the environment<sup>2</sup>. Collision with obstacles can be avoid using the map, even though it cannot perceive an obstacle with current sensor's view. PR2<sup>3</sup> processes sensory data from 3D visual sensors in point clouds. Multilayered 2D costmaps and a layered

representation of the robot body are used to reduce the possibility of collision<sup>4</sup>. In the work of Stulp et al.<sup>5</sup>, through experience-based learning, the robot first learns a so-called generalized success model which distinguishes among positions from which manipulation may succeed or fail. The model is used to compute a probability distribution that maps positions to a predicted probability of successful manipulation, taking into account the uncertainty of the robot and object's positions.

A key factor of mobile manipulation design is that a suitable pose of the mobile robot needs to be obtained through navigation in order to conduct object manipulation. One possibility is simply to travel from the current position to a position such that the target object is reachable, as depicted in Fig.1. As shown in Fig 1(a), the object is placed in front of the table, where an obstacle exists to influence the grasping. In this case, the object might not be successfully grasped due to the limited workspace of the robot arm. However, if the

mobile robot travels to the side of the table as shown in Fig. 1(b), the object can be easily grasped. It is therefore desirable to develop a method to plan a pose for the robot such that the target object is easy-to-reach.

Attamimi et al.<sup>6</sup> proposed a method to use perception maps that express the robot arm reachability and robot platform navigation reachability to a target object. The authors also show that by integrating these two maps, a proper position that has maximum probability of successful grasping is determined. In this study, we developed a motion planning system for determining the proper pose for grasping objects. The robot position is determined based on the arm's reach and ease of movement. We adopted the design of Attamimi et al.<sup>6</sup> to describe the limitations of robot workspace, the situation of environment and target object position. By constructing the reachability map that represents the ease of robot mobile platform motion and the graspability map that describes the success rate of grasping of robot arms in workspace, robot is able to determine the proper position to move toward and increase the success rate of mobile manipulation task. Visual EFK-SLAM and visual servo technics are integrated into the design for vision-based grasping of the object.

## 2. The Dual Arm Robot

A dual-arm robot is designed and constructed for mobile manipulation experiments. The 6-DOF dual-arm design allows the robot to grasp various objects in the environment. A Kinect RGBD camera is installed on top of the robot for visual servo control. The forward and inverse kinematics of two robot arms are derived and implemented on the robot controller. Two laser

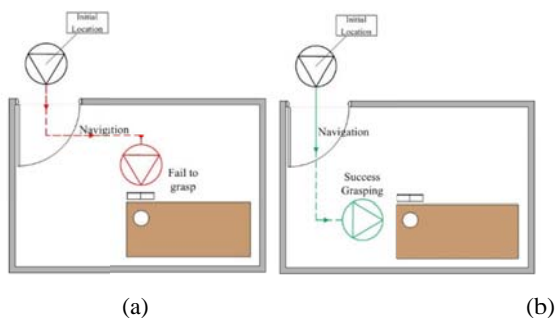


Fig.1 An example of mobile manipulation is influenced by an obstacle in front of the target.

range finders are equipped on the mobile platform in forward and backward directions for obstacles detection. An on-board industrial PC (IPC) is used for data processing and motion control of the robot. The steer-and-drive mechanism allows the robot to move in omnidirection<sup>7</sup>. The implemented EKF-SLAM<sup>8</sup> allows the robot to navigate and localize itself in the environment. The visual servo system<sup>9</sup> allows the robot to move and fetch an object without collisions.

### A. Visual EKF-SLAM

A visual SLAM system has been developed for the omnidirectional mobile robot<sup>8</sup>. There are three main steps of the EKF-SLAM: a measurement step to acquire the location vector of robot relative to the feature in the environment, a prediction step to predict the location of robot using motion model and an update step to calculate Kalman gain and update robot state according to above two steps. Then, the updated robot state is delivered to prediction step to calculate the next moment state of robot. These steps repeat to achieve the real time localization and mapping.

### B. Visual servo grasping

By using the depth data from Kinect, the input image is segmented into several planes. In this method<sup>9</sup>, the plane that the target object locates is first labeled. The labeled plane is featured by SURF algorithm and is matched with data base to find where the target object is. Except for the target object, the other objects in the environment are obstacle for robot manipulation. Potential field is then combined gravity and repulsion with these indices for safe path planning of robot arms. According to this, the robot is able to move its arms in the workspace without collisions and to grasp the targeted object.

## 3. Grasp Planning

The proposed system architecture is shown in Fig. 2. For representation of the environment, we utilize EKF-SLAM algorithm and Kinect sensor to construct a feature map of the environment. For grasping planning, we adopted the method of Attamimi et al.<sup>6</sup> in this design. The feature map is used as input to the mobile platform to calculate the easiness of traveling to the reachable



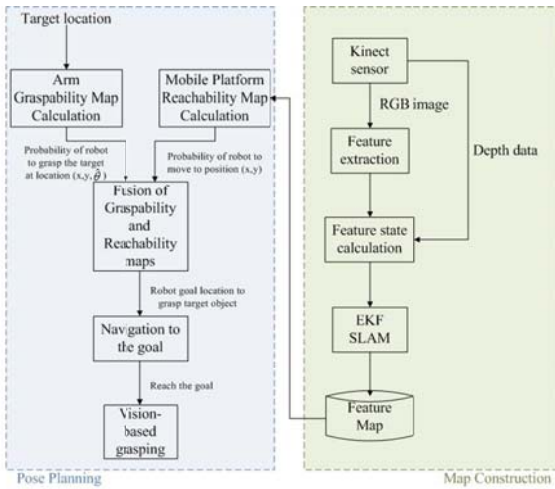


Fig.2 System architecture

region of the robot. On the other hand, the target location is inputted to arm graspability calculation to represent the extent of graspable region of robot arms. We fuse the two representations to decide the goal location for robot to grasp the target object. This work uses EKF-SLAM algorithm for robot navigation control. First, we extract SURF features that represent the configuration of the environment. Then, EKF is utilized to improve the localization error and to correct the coordinates of features. For grasping, we use Kinect for environment detection so that the robot is able to detect not only the target object but also the obstacle in the environment and to guide its arms to fetch the target. The inverse kinematics solution map suggested in the work of Attamimi et al.<sup>6</sup> is adopted to calculate reachable/unreachable points. Then a probability distribution is given to all reachable points for later decision making of the grasping position. To include the description of robot navigation in the motion planning of grasping, we have to consider the navigation control of the mobile robot in an environment. Obstacles in the environment influence the motion planning of the robot. In this work, a feature map is built to express the environment by using EKF-SLAM algorithm. We adopted the method proposed by Attamimi et al.<sup>6</sup> to construct a reachability map for motion planning. The closer to obstacles, the less probability is given for the robot to reach. The motion planning of the robot is then determined for the robot to

move to the maximum probability of the integrated representation of the navigation and arm motion<sup>6</sup>.

#### 4. Experiments and discussion

Three interesting experiments have been carried out for grasp planning to verify the effectiveness of the proposed system. We first verify that different locations of target object in the same environment will result in different robot navigation behavior. Then we add an obstacle around the target area to verify the adaptation of the robot.

##### A. Target object in different locations

Fig. 3 shows the environment of this experiment, Condition A and Condition B are termed to distinguish two locations of the object on the table. We first utilize EKF-SLAM to construct the feature map of the environment. Then we replace the features with the size of robot. Fig. 4(a) shows the planning result of condition A. It is noted that the planned grasping position is in front of the table, which is depicted in dotted line. For condition B, the planned grasp position is at the side of the table, as shown in Fig. 4(b). Fig. 5 shows the experiment by real robot in Condition A and Fig. 6 shows the experiment in Condition B.

##### B. Grasping planning affected by obstacles

The purpose of this experiment is to verify the proposed method is able to judge the proper grasp position under the obstacle situation. Fig. 7 (a) shows the setup of this experiment, termed Condition C. The target object is at the same position as Condition A but is behind the obstacle. The planning result is shown in Fig. 7(b). The graspable region moves to the side of the table because

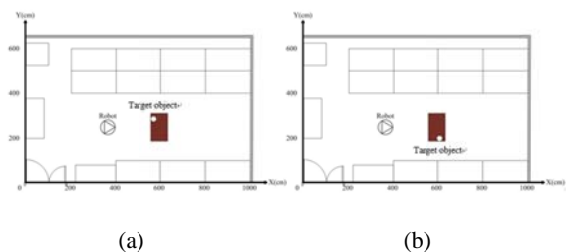


Fig. 3 Environment setup for experiments (a) Condition A, target in the front of the front of the table, (b) Condition B, target on the side of the table.

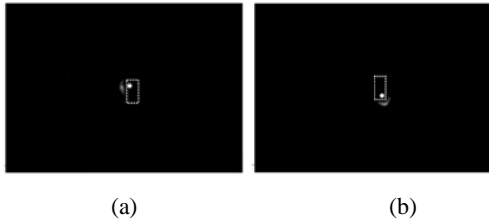


Fig. 4 (a) The planning result of Condition A, (b) the planning result of Condition B.

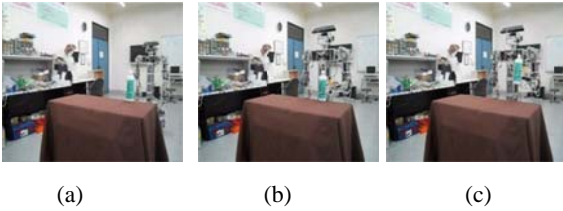


Fig. 5 Task execution of Condition A on real robot

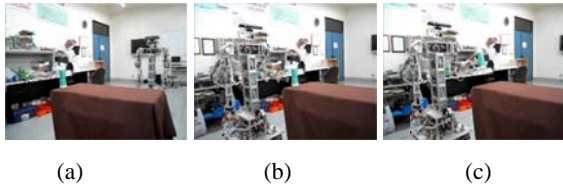


Fig. 6 Task execution of Condition B on real robot

of the graspability affected by the obstacle changes. Compare with Condition A, the difference is the obstacle effect that causes the different planning from proposed method.

## 5. Conclusions and Future Work

A dual-arm robotic system has been designed and implemented for mobile manipulation tasks in an unstructured environment. A grasp planning system is developed based on visual SLAM and visual servoing of the robot. The proposed system has been verified in three different conditions. The experimental results show that the robot can adapt to the variation of environment and find a suitable place to grasp the object. In the future, object fetching in more extensive environments will be studied.

## Acknowledgements

This work was partly supported by Ministry of Science and Technology of Taiwan, under grant NSC 102-2221-E-009-140.

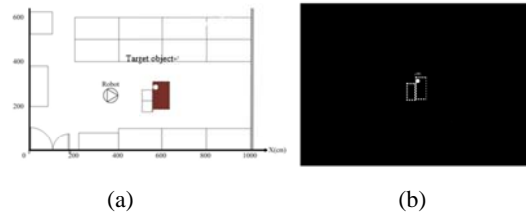


Fig. 7 (a) Environment setup of Condition C (b) the planning result of Condition C.

## References

1. Jorg Stuckler and Sven Behnke, "Benchmarking Mobile Manipulation in Everyday Environments," in *Proc. of 2012 IEEE Workshop on Advanced Robotics and its Social Impacts (ARSO)*, (Munich, Germany, 2012), pp. 1-6.
2. J. Klaess, J. Stuckler and S. Behnke, "Efficient Mobile Robot Navigation Using 3D Surfel Grid Maps," in *Proc. of 7th German Conf. on Robotics (ROBOTIK)*, (Munich, Germany, 2012), pp. 1-4.
3. Sachin Chitta, E. Gil Jones, Matei Ciocarlie and Kaijen Hsiao, "Mobile Manipulation in Unstructured Environments: Perception, Planning, and Execution," in *IEEE Robotics & Automation Magazine*, 19(2012), 58-71.
4. Hornung, A., Phillips, M., Jones, E.G., Bennewitz, M., Likhachev, M. and Chitta, S., "Navigation in Three-Dimensional Cluttered Environments for Mobile Manipulation," in *Proc. of 2012 IEEE International Conference on Robotics and Automation*, (Minnesota, USA, 2012), pp. 423-429.
5. Freek Stulp, Andreas Fedrizzi and Michael Beetz, "Action-Related Place-Based Mobile Manipulation," in *Proc. International Conference on Intelligent Robots and Systems*, (St. Louis, MO, USA, 2009), pp. 3115-3120.
6. Muhammad Attamimi, Keisuke Ito, Tomoaki Nakamura and Takayuki Nagai, "A Planning Method for Efficient Mobile Manipulation Considering Ambiguity," in *Proc. International Conference on Intelligent Robots and Systems*, (Vilamoura-Algarve, Portugal, 2012), pp. 965-972.
7. Kai-Tai Song, Sin-Yi Jiang and Chia-Chang Wu, "Pose Control of a Four-Wheel Drive Omni-Directional Mobile Robot," in *Proc. of 2012 CACS International Automatic Control Conference*, (Yunlin, Taiwan, 2012).
8. Chien-Hung Liu and Kai-Tai Song, "A New Approach to Map Joining for Depth-Augmented Visual SLAM," in *Proc. of ASCC 2013*, (Istanbul, Turkey, 2013).
9. Kai-Tai Song and Shih-Cheng Tsai, "Vision-Based Adaptive Grasping of a Humanoid Robot Arm," in *Proc. of IEEE ICAL 2012*, (Zhengzhou, China, 2012), pp.160-165.

# Combining playware exergaming with a mobile fitness app

Emmanouil Giannidakis    Henrik Hautop Lund

Centre for Playware, Technical University of Denmark, 2800 Kgs. Lyngby, Denmark

[hhl@playware.dtu.dk](mailto:hhl@playware.dtu.dk)  
[www.playware.dk](http://www.playware.dk)

**Abstract:** We propose a novel playware as a merge between exergames and mobile fitness apps to engage the users in physical exercises, not only as competitive play, but also in the form of cooperative play. The concept connects modular interactive tiles with radio communication to Android tablets and smart phones, which can connect to the Internet. This allows the players to monitor their playware exergaming performance on the smart device(s). A test was set up over 8 days allowing two school classes to compete with each other on which class was going to collect the most points playing on the modular tiles during the test. The test subjects were from 6th and 7th grade (12-13 years old children). As a social playware, we investigated how the playware mediated cooperative and competitive play amongst the users. It was found that the majority of game play involved social interaction between players, and that 8 out of 10 pupils on the top-10 were girls. The playware seemed to motivate the girls to become physically active.

**Keywords:** Playware, Exergaming, Mobile App, Modular Technology, Cooperative Play, Gender, Social Playware.

## I. INTRODUCTION

Exergaming has been a popular area of research and development in recent year, for instance resulting in games for health. Exergaming ("exercise" and "gaming") is fitness gaming where video games provide exercise, and it may often rely on technology that tracks body movement or reaction. Some exergames results from the research field of playware [1, 2], which has a core technology research activity focusing on research into modular playware technology and its supporting fundamental research areas of modern AI, adaptivity, modular robotics, and tangible interfaces. This is combined with a deep knowledge of play and play culture to create exergames that are fun, playful and motivating for the users to engage with out of their own free will and desire to play.

With the work presented here, we propose a novel playware as a merge between the exergames and mobile fitness apps to engage the users not only in competitive play, but also in cooperative play. We try to incorporate both competitive and cooperative play, since we hypothesize that this may attract both genders, especially also girls, to become physically active. Hence, we build a simple mobile app for smart devices on top of a playware tool (modular interactive tiles) – see Fig. 1 – with well-known health benefits [3], and make a qualitative study

of the effect of the competitive and cooperative social play that the mobile app adds to the playware tool.



Figure 1: The concept connects modular interactive tiles with radio via a board with XBee and Bluetooth to Android tablets and smart phones, which can connect to the Internet (e.g. for storing database). Players can choose games and player IDs on the smart device(s) and monitor their performance on the smart device(s).

A system of modular robotic tiles was developed [4, 5] and used extensively in physiotherapy and rehabilitation using this platform as a form of exergaming, e.g. [6]. The way the system works is that in the tiles different games can be programmed and the patients are performing physiotherapy exercises by playing these physical interactive games. A challenge for a system like the modular interactive tiles and other exergaming systems is

how they can motivate the users to keep playing. Therefore we conducted a user testing in a school where pupils from two classes acted as testers in order to see if competition between the users, cooperation between the users, seeing the score from a game and seeing the score from the other players affected the motivation of the pupils to play.

## II. MOBILE APP FOR SMART DEVICES

We developed a simple app to run on top of the modular interactive tiles to provide feedback to the users on a tablet (in a shared form) or a smart phone (privately). When a user is playing a game on the modular interactive tiles, the system can monitor different variables such as points, time, level, etc. These variables are provided to the mobile app, which can provide feedback to the user after the end of a game. The feedback provided to the user consists of the following attributes:

1. The **points** that the user got
2. The **duration** of the game
3. The number of **misses**
4. The **level** of difficulty
5. The **winner** of the game
6. The **number of tiles** that were used

Not all the attributes are relevant to every game. For example the winner attribute is not being used in one player games.

To simplify the setup of the experiment presented here, we used an Arduino Uno board to facilitate the communication between the tiles, which communicate with XBee, and the mobile device(s), which communicate with Bluetooth. To the Arduino Uno board, we attached a Bees shield with an Xbee radio module and a Bluetooth Bee module (see Fig. 2). The way we achieve communication is that the master tile communicates with the Xbee radio module of the Arduino board and the mobile device is connected with Bluetooth communication with the Bluetooth Bee (see Fig. 1). The Arduino Uno is responsible of receiving the messages from one radio module and properly forward and modify the received message to the other radio module. The tablet application sends messages that contain request for the tiles to change the game to another one, while the tiles send messages that contain the feedback of the game.



Figure 2. Arduino Uno with beeshielded Bluetooth and Xbee.

The mobile app was developed to run on Android devices. It was developed to be able to run on both Android tablets and Android smart phones. This application supports user creation, group creation and competition creation. In addition, it is connected with the modular interactive tiles so that the user can choose the game that the user wants to play and to receive and store the score from the game. With the tablet, more than one user can play a game, and in that case the score is divided by the number of users. The received score is being saved in a local database. Finally, the users have access to their current total score, the high score they have achieved for each game as well as the current total score and the high scores of the other players.

## III. USER TESTING SETUP

A test was set up over 8 days in the Oesterbro international school in Copenhagen, Denmark. The premise of the test was that two classes were going to compete with each other on which class was going to collect the most points during the test. For this purpose 6th and 7th grade (12-13 years old children) was chosen and they would compete with each other.

We provided the school with a set of 10 modular tiles (1 master and 9 normal), a tablet with the tablet application and the Arduino board with the Bees shield.

The pupils had the chance to play with the tiles during the breaks. The school had two break sessions: one from 09:35-09:55, and one from 11:45-12:05, i.e. two times 20 minutes per day. During those periods whoever of the participants who wanted to play could come, choose the desired game and the other participants that they wanted to play with (if they wanted to play with other people), and they would start playing. Hence, in total the pupils could play for  $8 \text{ days} * 2 * 20 \text{ minutes/day}$ .



## IV. RESULTS

Of the 33 active participants, 14 were male and 19 were female (i.e. 42.5% were male and 57.5% were female). On average, each of the 33 participants played 29.2 times and for 2.9 days. On average, each player played for 1171 seconds during the testing with the most active player to have played 4057 seconds. Out of the total 401 games that were played, 222 were played by groups of people. The groups that were formed were consisting of students of the same class. Table 1 shows the top 10 players of the high score list at the end of the test. It is noteworthy that from the ten players with the highest total score 8 were female and 2 were males (the number one player being male).

Table 1. The top 10 players at the end of the experiment. 80% of the top 10 players were female.

Player id	Total score	Total duration	Number of games	Gender
42	3934	2630	49	Female
53	4645	3679	117	Female
19	5016	2423	38	Male
8	5112	2519	49	Female
39	5403	2680	85	Female
37	5419	3414	91	Female
9	5589	2178	38	Female
48	5989	2120	64	Female
27	6087	4057	91	Female
55	7520	3201	94	Male

When looking more detailed at the play of the boys and the girls, there are some significant differences. Most notably, on average each participating girl played for a total of 1464 seconds, while each participating boy, on average, played for a total of 774 seconds. Hence, each girl would play almost double as much as each boy. Since the participants were free to come to the room to play whenever they wanted during the breaks during the 8 experiment days, it indicates that the girls were attracted more to the playware game than the boys.

As a qualitative evaluation of the test, a research assistant made observations during the intervention and made notes of these observations. Three cases were representative of the observations that were made during the experiment: the pupils would engage in

- *Social, competitive play*: groups would cooperate to achieve a higher group score than another group
- *Social play to support individual competitive play*: a group would form to help one individual to gain a higher score
- *Individual competitive play*: an individual would compete against herself or another individual on getting a higher score or reaching a specific goal

## V. DISCUSSION

Even if the collection and display of scores may seem to promote competitive play with focus on getting a higher score, the results showed that more than 55% of the use (222 out of 401 games played) was group play with social interaction between the players, and girls participated in 90% of these group plays. Even if the players tried to get a higher score, they did so in a cooperative manner in the majority of cases. This may be a contributing factor in explaining the relative high success amongst the girls (the girls were twice as active as the boys, and 8 out of 10 pupils on the top-10 were girls), who may possibly enjoy the social, cooperative play. It is interesting that this playware motivated the girls to become so physically active.

We may speculate that the relative high success of this playware with the girls may be attributed partly to the facilitation of *social, cooperative play* in the competitive game scenario. The modularity of the modular interactive tiles facilitates social interaction by the physical layout of the modules, and the games are designed so that players can cooperate in the physical play. For instance, as more tiles are added to a platform of tiles, the more players can participate at the same time and cooperate to succeed in the game. One example is the Final Countdown game in which the user(s) has to keep the platform 'alive'. Each tile is counting down its LEDs, but all LEDs on the tile shine up again if the tile is being stepped on. If one tile in the whole platform goes to zero LEDs on, then the game is lost. The game can be played by one player, who will rush around on the tiles platform to keep all tiles alive, but a group of players soon discovers that they can help each other by each being in control of keeping a few of the tiles alive. So they distribute amongst each other the task of keeping the whole platform alive. Other games are designed in a similar fashion to allow social interaction and cooperation amongst the players.

Research in play, toys, computer games, and robotic games show that girls often tend to prefer cooperative play and boys tend to prefer competitive play, e.g. [7, 8, 9, 10]. It is therefore also interesting, that with the physical interactive games, we can observe here that the facilitation of social, cooperative play within a competitive game scenario seem to attract the girls to engage in the play and to become physically active.

It suggests that the playware in this experiment becomes a mediator for playful social interaction. Indeed, *social playware* has been defined as playware which aims at creating playful social interaction between several users [11], see also [12]. With social playware, the starting point for the research and development becomes the social interaction mediated by the technology rather than the individual interaction mediated by the technology. In the present case, the results suggest that users – boys and girls – become physically active in a social way with social playware like the one which was carefully designed for the present experiment in the form of modular interactive tiles with a mobile app for both cooperative and competitive play.

## ACKNOWLEDGEMENT

The author would like to thank colleagues from the Center for Playware, DTU for collaboration, help and discussions related to the experiment presented here. Also, the authors would like to thank the participating children and teachers at Oesterbro International School, Denmark.

## REFERENCES

- [1] H. H. Lund, T. Klitbo, and C. Jessen, C. “Playware Technology for Physically Activating Play”, *Artificial Life and Robotics Journal*, 9:4, 165-174, 2005.
- [2] H. H. Lund, and P. Marti. “Designing Modular Robotic Playware”. In *Proc. of 18th IEEE Int. Symposium on Robot and Human Interactive Communication (Ro-Man 2009)*, IEEE Press, 115-121, 2009.
- [3] Lund, H. H., and Jessen, J. Effects of Short-Term Training of Community-Dwelling Elderly with Modular Interactive Tiles, *Games for Health Journal*, 3:5, 2014.
- [4] Lund, H. H. “Modular Robotics for Playful Physiotherapy”. In *Proceedings of IEEE International Conference on Rehabilitation Robotics*, IEEE Press, 571-575, 2009.
- [5] US Patent No: 8,241,183. “Modular robotic tiles for physical interaction”, 2012.
- [6] Nielsen, C. B. and Lund, H. H. “Adapting Playware to Rehabilitation Practices”. *International Journal of Computer Science in Sport*, 11:1, 2012.
- [7] Leaper, C. “Gender, affiliation, assertion, and the interactive context of parent-child play”. *Developmental Psychology*, 36, 381-393, 2000.
- [8] Dawson, C., Cragg, A., Taylor, C., and Toombs, B. “Video games: research to improve understanding of what players enjoy about video games, and to explain their preferences for particular games”. British Board of Film Classification, 2007.
- [9] Lund, H. H. and L. Pagliarini, L. “LEGO Mindstorms Robot Soccer”. In *Proceedings of RoboCup’98, LNAI 1604*, Springer-Verlag, Heidelberg, 1999.
- [10] Lund, H. H. “Adaptive Robotics in Entertainment”. *Applied Soft Computing*, 1:1, 2001.
- [11] Lund, H. H. and T. Thorsteinsson, T. “Social playware for mediating teleplay interaction over distance”. *International Journal Artificial Life and Robotics*, 16:4, 435-440, 2012.
- [12] Suzuki, K. “Social Playware: Device-mediated social interaction for therapeutic activities.” *Robot and Human Interactive Communication, 2014 RO-MAN: The 23rd IEEE International Symposium on*. IEEE, 2014.

# Parallel Relational Universes – experiments in modularity

Luigi Pagliarini<sup>1,2</sup> Henrik Hautop Lund<sup>1</sup>

Centre for Playware, Technical University of Denmark, 2800 Kgs. Lyngby, Denmark

<sup>2</sup>Academy of Fine Arts of Macerata, Via Berardi, 6, 405111 Macerata, Italy

[luigipagliarini@gmail.com](mailto:luigipagliarini@gmail.com)

[www.playware.dk](http://www.playware.dk)

**Abstract:** We here describe Parallel Relational Universes, an artistic method used for the psychological analysis of group dynamics. The design of the artistic system, which mediates group dynamics, emerges from our studies of modular playware and remixing playware. Inspired from remixing modular playware, where users remix samples in the form of physical and functional modules, we created an artistic instantiation of such a concept with the Parallel Relational Universes, allowing arts alumni to remix artistic expressions. Here, we report the data emerged from a first pre-test, run with gymnasium's alumni. We then report both the artistic and the psychological findings. We discuss possible variations of such an instrument. Between an art piece and a psychological test, at a first cognitive analysis, it seems to be a promising research tool.

**Keywords:** Art, Playware, Modular Technology, Remixing Playware, Social Art.

## I. INTRODUCTION

Parallel Relational Universes (URP) is an attempt, both artistic and scientific, to conceive a method to investigate the small groups psycho-dynamics expressed throughout a Relational Modularity logic into a graphical modality.

The project is located in between an artistic conception and a psychological need of a new method for small groups' analysis, since it aspires at catching the "essence" of a group by materializing and framing the social interaction into a unique graphical expression resulting from a collective action. All of that, to look for tangible artefacts that might be "witnesses" of small groups' dynamics readable throughout a Psychology of Shape analysis. In other words, the basic assumption is that the emerging shape might reveal the psychological structure of the related group.

URP was inspired by different artistic, psychological and informatics sources as the Cadavre exquis [1], the Pittura Stocastica [2], the Tree Testing Tool [3], Modular Tiles [4], Remixing Playware [5].

Such playware is defined as intelligent hardware and software that creates play and playful experiences for users of all ages [6, 7], and R&D in playware has led to numerous applications in various areas such as rehabilitation [4, 8], playgrounds [7], education [9], art

[10], and sport [11]. In all such cases, users interact with the playware as a free and voluntary activity that they engage in for the pleasure of play, even if the activity may be shown to have collateral effects e.g. in terms of health and skills. It has been proposed that *modular playware* is of particular interest to develop solutions for such varied areas of application, since modularity may facilitate easy assembly and adaptation of the playware to different interaction modalities [12]. We can view the modular playware as enabling the user to *remix* with modules to combine and construct new playware solutions.

Indeed, the proposed design of the artistic system, which mediates group dynamics, emerges from our studies of modular playware [12] and remixing playware [5]. Inspired from remixing modular playware, where users remix samples in the form of physical and functional modules, we created an artistic instantiation of such a concept with the Parallel Relational Universes, allowing arts alumni to remix artistic expressions.

Remixing playware has been defined [6, 7] to allow sampling and remixing of both physical and functional aspects of a system. Such remixing playware has a number of distinguished features which include: *user-configurable modularity*, which allows the users to interact and manipulate with samples; *user-guided behavior-based system*, which allows compositions to

emerge from the way performers interact with the “instruments” that provide the primitive behaviours; *intelligent sampling* as the ability of creating samples that allow anybody to remix with the samples ensuring an engaging outcome.

When created in the right manner, *playware can mediate social creativity*, as exemplified with the MusicTiles MagicCubes, which allow anybody in an easy and intuitive way to remix music samples according to their individual taste [5, 13]. Designing and developing the samples in large, soft forms as 1m3 cubes pushes the users into social interaction, since a user will only be able to control one instrument (sample set) himself, and will have to coordinate actions with other people to create/perform a remix. As a social playware, such a system explores the cooperative creativity: the MagicCubes seamless push the users into social play dynamics resulting in the users interacting and cooperating in their play to create and perform their collective new hit song versions.

The first pilot study of Parallel Relational Universes [14] was run with an analogical method and conducted with the alumni of an Italian art school, and its output has been exhibited to the public as an art piece while, below, we describe an automated ALife version of the same concept that allows the widening of the method to larger and more heterogeneous audiences.

## II. DESCRIPTION AND PROCEDURE

The first, analogical, version of URP was conceived to be an “art game” with as simple as possible procedure so that it might consent to any people of any age to be involved in the building of the art piece. Indeed, we only used a dichromatic scale (black and white) and we gave users very easy instructions/suggestions/rules. In particular 3 of them: A. a strict rule; B. an elastic demand; C. a suggestion (that we then defined as almost-a-rule).

The procedure itself was the following one. Once individualized and chosen a specific group, it was summoned in a room and given to each component (i.e. in our first experiment art gymnasium alumni) an expressive module (i.e. in this case a canvas). Later we imparted the group of participants with a general disposition (B. elastic demand) to freely locate themselves in the physical space so to get close to each other. We moved from the in part prejudicial idea that the group elements would convey to spatial subgroups based

on a continuum of interpersonal relational, emotional and affective forces.

After that, we asked participants to paint the canvases in two specific colours, black (or white) as background and white (or black) as foreground. We strongly, but not strictly, suggested (C. almost-a-rule) to cover 50% of the space with the foreground colour leaving the resting 50% for the background.

Finally, we introduced the unique must (A. rule) which is the continuity of the sign (or gesture/geometry) on each and every side of the module-borders where a module collide with other modules (see Figure 1). In other words, each canvas border has to shape a continuous drawing with the neighbourhood and each and every executor has to negotiate such drawing with all of its neighbours. There must be a perfect continuity in each direction, north, east, west, south, south-west, etc.



Figure 1.

Tiles' borders must be continuous.

The A rule has been introduced both for aesthetical purposes and, mainly, to push people interactivity which is necessary to highlight the pre-existing and emerging conflicts. (Those, indeed, are very descriptive of the specific group dynamic).

Besides those described above, two more rules/possibilities emerged from the interaction with the alumni: D. the Good Neighborhood; E. the Teleport. Shortly, the first one (i.e. D) is a negotiation, which allows one painter to penetrate (i.e. in a more or less reciprocal way) into others' painters canvases. The second one (i.e. E) is a negotiation, which allows the executor to engrave a far canvas with his/her sign. Both the emerging behaviours were kept because useful for both the aesthetic aspects and the psychological analysis of the behaviours.

## III. HYPOTHESIS AND RESULTS

Paintings realized with the URP method will tend to



structure around an unpredictable shape. On the contrary, they will be largely descriptive (i.e. in terms of shape) of most of the group dynamics, while poorly suffering for the interfering chaotic and occasional intervening factors. The supervisor can, as well, decide if the painting is to be a unity or can be spontaneously subdivided in islands (i.e. emerging subgroups).

The theoretical hypothesis serving the entire model is that the group dynamics will force the execution towards a specific result, which can be interpreted both under the morphological and the graphical point of view. The two elements, besides all the aesthetical aspects, will be able to depict many of the group, such as cohesion, collaboration, competition, harmony, conflicts, etc. , as well as to describe most of the group members' personality as, for example, dominant or gregarious, weak or strong, aggressive or myths, timid or extrovert, etc.

The URP method discloses and reports, through the signs, the innumerable groups' dynamics. It camouflages with the pictorial context those behavioural rules and regulations that could result heavy, bulky or frustrating in other circumstances. Such an influence will bring to a semiotic drift the whole system, transforming the experience in a highly descriptive expression of a particular group in a particular historical moment of its existence.

The administration of our relational painting game has produced appreciable results in, at least, three domains of knowledge: Education-Pedagogy; Psychology-Sociology; Art. Although, for this very first trial we have made no measurements, all the teachers and professors involved in the experiment agreed on the extreme efficiency of the method under the motivational point of view. In particular, it has been underlined that, educationally, it pushes in a quite gentle way the young students at dealing with "abstract representations", a pretty difficult theme to communicate in normal classes. At the very same time, pedagogically speaking, it impresses and forces the classes into a cooperative and collaborative modality that is both practical (i.e. alumni have to do) and theoretical (i.e. alumni have to understand). This last consideration drives us directly to the most important aspect of the game, the extremely strong interactive modality the game carries along with itself. Indeed, under a psychological and sociological light, the URP method plays with the concept of *individuality* as counterweighted to the idea of *sociality*. The students ego – defined as peripersonal and interpersonal space – is

solicited both in terms of virtual and physical boundaries. More than that, the playful and pitoric spirit of the game makes it so that even the weakest personalities can easily deal with the concept of borders and improve their capacity in mediating social actions without getting scared. Therefore, it has to be noticed that, URP for the very same reasons kind of stimulate the self-consciousness of both aggressive and remissive personalities. This makes of it a good candidate has method to be used in art-therapy.



Figure 2.  
Aesthetical results.

Under the artistic point of view, URP instantiates a new approach to modularity that allows users to play with the shape (i.e. intended as painting and painting content) in a deep and articulated way. In other words, it proposes an escape from canonical painting shape (see Figure 2), opening up to a number of geometrical solutions, which can be perceived as unlimited.

#### IV. DISCUSSION

As a matter of facts, the URP method idea is to build a projective test that can measure groups' dynamics (i.e. cooperation, collaboration, etc.) – psychodynamics of groups is reported in [15]. Such a method, indeed, could catch particular structures of groups' cohesion (i.e. opening, esteem, trust, etc.) and desegregation (i.e. closing, mistrust, depreciation, etc.) returning them both in the form of geometry and in the form of inter-relational aesthetical contents. That is why, besides any possible aesthetical consideration, the authors' interest was focused on building an instrument able to measure and predict psychological aspects of groups, and under this point of view this first attempt can be considered a great success. The hope is that in future we will be able to reiterate such an experiment with different groups of different ages so to properly measure, analyse and define

unknown clusters of behaviour that can be found in small groups.

Indeed, the encouraging results obtained with the analogical instantiation of the URP method has driven us to move on to an automation of it, which could facilitate and speed up the testing.

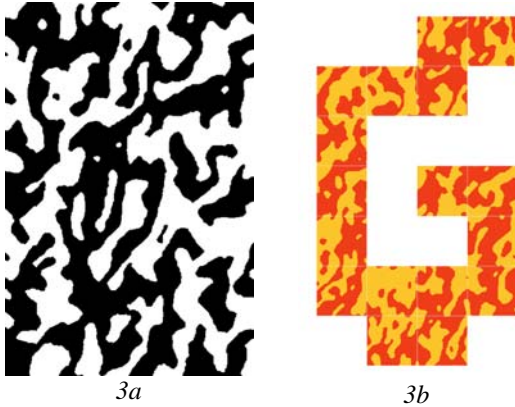


Figure 3a and 3b.  
Two e-URP screenshots

At the moment a first instantiation of such algorithm, called e-URP has taken its first steps, as shown in Figure 3a and 3b.

## ACKNOWLEDGEMENT

The author would like to thank Antonello Tolve, Parallelo 42°, the teachers Pierpaolo Serini, Amalia Ricci, Maria Valori, Silvia Volpe, and students of the Istituto Statale d'Arte "Bellisario-Misticoni" of Pescara, Italy.

## REFERENCES

- [1] Alastair B.; Gooding M. Surrealist Games. London: Redstone Press. pp. 143-144. (1991).
- [2] Lombardo S., Interpretazioni e preferenze di strutture casuali. Rivista di Psicologia dell'Arte anno XV, nn. 3-4-5, 1994, (1994)
- [3] Crotti E., E tu che albero sei? Come interpretare la personalità attraverso il disegno dell'albero, Mondadori Ed. (2006).
- [4] H. H. Lund. Modular Robotics for Playful Physiotherapy, in Proceedings of IEEE Int. Conference on Rehabilitation Robotics, IEEE Press, 571-575, 2009.
- [5] Lund, H. H., Marti, P., & Tittarelli, M. (2014, August). Remixing playware. In Robot and Human Interactive Communication, 2014 RO-MAN: The 23rd IEEE International Symposium on (pp. 49-55). IEEE..
- [6] H. H. Lund, and C. Jessen, "Playware - Intelligent technology for children's play." Technical Report TR-2005-1, June, Maersk Institute, University of Southern Denmark, 2005.
- [7] H. H. Lund, T. Klitbo, and C. Jessen, "Playware Technology for Physically Activating Play," Artificial Life and Robotics Journal, 9:4, 2005, pp. 165-174.
- [8] H. H. Lund, "Modular Playware as a Playful Diagnosis Tool for Autistic Children." In Proceedings of IEEE International Conference on Rehabilitation Robotics, IEEE Press, 2009, pp. 899-904.
- [9] H. H. Lund, P. Marti, "Physical and Conceptual Constructions in Advanced Learning Environments," Interaction Studies 5:2, 2004, pp. 269-299.
- [10] H. H. Lund, M. Ottesen, "RoboMusic - A Behavior-Based Approach," Artificial Life and Robotics Journal, 12: 1-2, 2008, pp. 18-23.
- [11] H. H. Lund, T. Thorsteinsson, "Social playware for mediating teleplay interaction over distance." International Journal Artificial Life and Robotics, 16:4, 2012, pp. 435-440.
- [12] H. H. Lund, P. Marti, "Designing Modular Robotic Playware." In 18th IEEE International Symposium on Robot and Human Interactive Communication (Ro-Man 2009), IEEE Press, 2009, pp. 115-121.
- [13] Pagliarini, L., & Lund, H. H. (2012). MagicTiles. ALife for Real and Virtual RoboMusic. In Proc. of 17th International Symposium on Artificial Life and Robotics, ISAROB, Japan.
- [14] Pagliarini L. Universi Relazionali Paralleli, Rivista di Psicologia dell'Arte, N.25 in stampa (2014).
- [15] Di Maria F., Lo Verso G.. La psicodinamica dei gruppi. Teorie e tecniche. Cortina Raffaello Ed. (1995)

## Identifying humanoid and human physical parameters

**Jovic Jovana**\*

*CNRS-AIST JRL (Joint Robotics Laboratory), UMI3218/CRT  
Tsukuba, 305-8568, Japan*

**Adrien Escande**\*

*CNRS-AIST JRL (Joint Robotics Laboratory), UMI3218/CRT  
Tsukuba, 305-8568, Japan*

**Gentiane Venture**†

*Tokyo University of Agriculture and Technology  
Tokyo, 183-8538, Japan*

**Ko Ayusawa**\*

*CNRS-AIST JRL (Joint Robotics Laboratory), UMI3218/CRT  
Tsukuba, 305-8568, Japan*

**Eiichi Yoshida**\*

*CNRS-AIST JRL (Joint Robotics Laboratory), UMI3218/CRT  
Tsukuba, 305-8568, Japan*

*E-mail: [jovic.jovana@aist.go.jp](mailto:jovic.jovana@aist.go.jp), [adrien.escande@gmail.com](mailto:adrien.escande@gmail.com), [venture@cc.tuat.ac.jp](mailto:venture@cc.tuat.ac.jp), [k.ayusawa@aist.go.jp](mailto:k.ayusawa@aist.go.jp),  
[e.yoshida@aist.go.jp](mailto:e.yoshida@aist.go.jp)*

[www.aist.go.jp](http://www.aist.go.jp)

[www.tuat.ac.jp](http://www.tuat.ac.jp)

### Abstract

Dynamical and kinematic analysis of humanoid and human movements require accurate estimation of segment mass parameters (mass, center of mass, and inertia matrix), and their misinterpretation can lead to significant variation in estimated joint kinematics. In the field of robotics, several methods have been developed for estimation of mass parameters of humanoid robots, as well as human subjects, based on linear properties of dynamic equation of bipedal systems with respect to the set of mass parameters. This talk will focus on those methods addressing the state-of-the-art research in the topic. Examples of both human and humanoid robots mass parameters estimation

---

\* 1-1-1 Umezono, Tsukuba, Ibaraki 305-8568 Japan.

† 3-8-1 Harumi-cho, Fuchu-shi, Tokyo 183-8538

© The 2015 International Conference on Artificial Life and Robotics (ICAROB 2015), Jan. 10-12, Oita, Japan

will be given. Identified mass parameters improve output of human dynamic analysis and humanoid simulation and model-based control.

**Keywords:** Inertia parameters, Identification, Optimization, Dynamics.

## 1. Introduction

Body segment inertia parameters (BSIPs) are important variables in biomechanical analyzes. In case of human inertia parameters are usually estimated using scaling equations provide in anthropometric tables based on data collected from young subjects [1]. Extrapolating those data to the different population or different age subjects is restrictive due to different body morphologies.

In case of humanoid robots, BSIPs given by robot manufacturers are estimated using CAD software. Those parameters are rough estimation of true inertia parameters and they often do not take into account wiring materials.

Hence, in this study we propose a method for estimation of subject specific whole body segment mass parameters. The method applies is based on use of Hierarchical Quadratic Programming (HQP) [2] optimization approach and linear properties of rigid bipedal body dynamics with respect to the BSIPs.

## 2. Method

The dynamic equations of dynamics of bipedal multi body systems is expressed by the following equation [3]:

$$\begin{bmatrix} H11 & H12 \\ H21 & H22 \end{bmatrix} \begin{bmatrix} \ddot{q}_1 \\ \ddot{q}_2 \end{bmatrix} + \begin{bmatrix} b1 \\ b2 \end{bmatrix} = \begin{bmatrix} 0 \\ \tau \end{bmatrix} + \sum_{k=1}^{N_c} \begin{bmatrix} J1k^T \\ J2k^T \end{bmatrix} f_k \quad (1)$$

Where:

- $q_1$  represents position and orientation of base link, and  $q_2$  is vector of joint angles of the body segments;
- $H_{1j}$  and  $H_{2j}$  ( $j = 1,2$ ) are the inertia matrix of the base link and body segments, respectively;
- vectors  $b_1$  and  $b_2$  are the bias force vectors including centrifugal, Coriolis, and gravity forces of the base link and body segments, respectively;
- $\tau$  is the vector of joint torques of the body segments;

- $f_k$  is the vector of the external forces at contact  $k$ .  $N_c$  is the number of contact points with the environment;
- $J_1$  and  $J_2$  are Jacobian matrices at contact  $k$  that map external forces to the joint space of the base link and body segments, respectively.

From equation (1) the following equation of motions of base link can be written in its linear form with respect to the set of BSIPs [4]:

$$Y\varphi = F \quad (2)$$

where:

- $Y$  is the regressor matrix which is a function of  $q_1$ ,  $q_2$  and their derivatives;
- $F$  is the vector of external forces applied to the link;
- $\varphi$  is a vector of BSIPs to estimate.

For each body segment  $i$ , vector  $\varphi_i$  is composed of 10 parameters:

- the mass of the segment  $m_i$  ;
- the Center of Mass (CoM) of the segment  $i$ ;
- the components of the inertia matrix  $I_i$  expressed in the segment frame;

The equation (2) can be solved by formulating a four level optimization problem that we solve with an HQP solver [2]:

$$(l1 \leq A1\varphi \leq u1) \prec (l2 \leq A2\varphi \leq u2) \prec (Y\varphi = F) \prec (\varphi = \varphi^{ref}) \quad (3)$$

where vector  $\varphi^{ref}$  is a vector of BSIPs parameters found in Dumas Anthropometric Tables (AT) [5] in case of human BSIPs identification, or extracted from CAD data in case of humanoid robot BSIPs identification. The notation is taken from [2]. The first level inequality constraints is chosen to enforce the solution to be physically plausible. The second level inequality constraints is chosen to enforce symmetry between the BSIPs of the left side of the body.

### 3. Experimental validation

#### 3.1. Experiments with human subject

Motions of one healthy adult volunteer (male, 70kg, 1.82m) were measured using a stereophotogrammetric system and force plates. The participant performed optimal motion defined in [4] that excites the dynamics of the considered system. In order to test the ability of the algorithm to detect segment mass changes, the participant was asked to perform validation trial executing the same motion and wearing a weighted belt located at the lower trunk level.

Joint angles were estimated from marker positions using Cortex Motion Analysis software.

#### 3.2. Experiments with humanoid robot

The exciting trajectories [6] were executed into humanoid robot. Examples of exciting trajectories are shown in Fig. 1. The robot is 1.54m height, with the CAD mass of 56kg. It is composed of 31 segment links, and has 30 degrees of freedom. The robot is equipped with sensors measuring the joint angles, force sensors under the feet and hands, accelerometer and gyroscope sensors. Due to the maintenance of the robot some parts were replaced.

The robot modifications resulted in changes of its segment inertial properties.

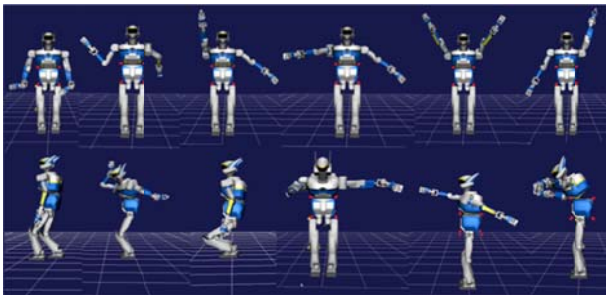


Fig. 1. Examples of exciting trajectories performed by humanoid robot.

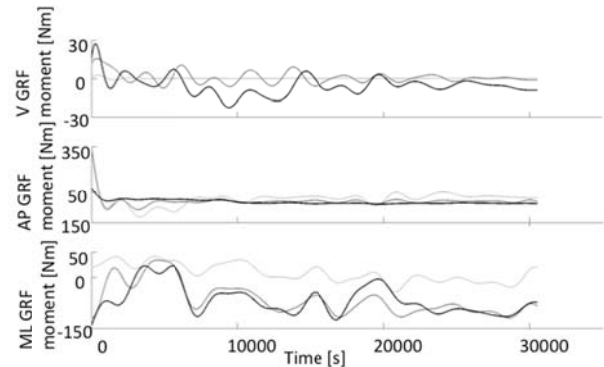


Fig. 2. GRF moments in vertical (V), anterior- posterior (AP), and medio-lateral (ML) directions reconstructed using identified BSIPs (dark gray line), BSIPs from AT (light gray line), obtained using forceplates measurements during the experiment with the human subject (black line).

### 4. Results

Example of Ground Reaction Force (GRF) moments reconstructed using proposed method, method based on use of AT, and those obtained using the force plates measurement during the experiment with human subject is shown in the Fig. 2. Figure 3 illustrates increase of identified segments masses of human subject model and those computed using AT based method during the validation trial when the volunteer was carrying weighted belt located at lower trunk level. The mass of each segment link of humanoid robot obtained using our method and the ones given by CAD software are presented in Fig. 4.

### 5. Conclusion

We presented a method, based on use of HQP optimization technique, for identification of segment inertia parameters. We compared results obtained using our method with the results obtained using BSIPs computed from Dumas AT [5] in case of human BSIPs identification and extracted from CAD data in case of identification of BSIPs of humanoid robot. The method proposed in this study showed better performances in estimation of the atypical asymmetric segment weights of human subject, and was able to estimate mass properties of modified segments of humanoid robot.

Moreover, the proposed method was able to reconstruct the ground reaction forces and respective force moments more accurately compared with methods based on use of anthropometric tables or CAD data.

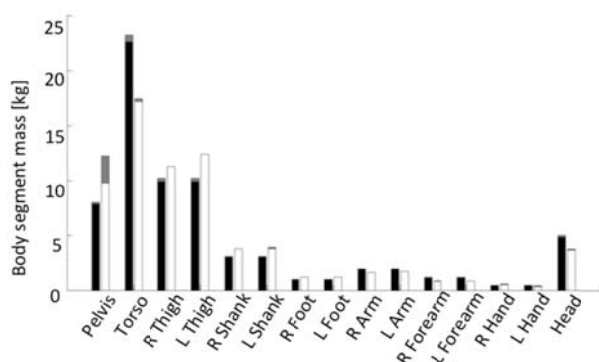


Fig. 3. Segment mass increase (gray) of identified body segment masses (white) and body segment masses from AT (black) for the human subject for validation trial. Right and left sides of the human body are abbreviated with R and L, respectively.

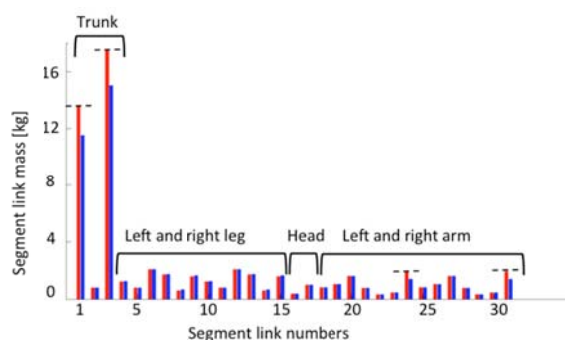


Fig. 4. Segments masses of humanoid robot identified using proposed method (red) and extracted from CAD data (blue). Dotted lines show expected segment mass based on the knowledge of replaced components.

### Acknowledgements

This study has been partially supported by Japanese Society for Promotion of Science.

### References

1. "Human Body Properties Database", Available: <https://www.dh.aist.go.jp/database/properties/index-e.html>.
2. A. Escande et al., "Hierarchical Quadratic Programming: Fast Online Humanoid-Robot Motion Generation", *The Int. J. of Robotics Research*, vol. 33, no. 7, pp 1006-1028, 2014.
3. W. Khalil, E. Dombre, "Modeling, Identification and Control of Robots", Taylor & Francis, Inc., Bristol, PA, 2002.
4. G. Venture et al., "A Numerical Method For Choosing Motions With Optimal Excitation Properties For Identification Of Biped Dynamics - An Application to Human", *IEEE/RAS-Proc.*, 2009.
5. R. Dumas et al., "Adjustments to McConville et al. and Young et al. body segment inertial parameters", *J Biomech.*, vol. 40, no. 3, pp. 543-53, 2006.
6. Jovic. F. Philipp, A. Escande, K. Ayusawa. E. Yoshida, A. Kheddar. G. Venture, "Identification of dynamics of humanoids: systematic exciting motion generation ", submitted to *Proc. IEEE Int. Conf. on Robotics and Automation*, Washington, USA, 2015.

# Construction of Evaluation Index System for Graduate Course

**Ai Dongmei**\*

*Mathematics Laboratory, University of Science and Technology Beijing, China*

**Wen Jiawei**

*Department of Mathematics and Physics, University of Science and Technology Beijing, China*

**Ning Xiaojun**

*Graduate School, University of Science and Technology Beijing, China*

*E-mail: first\_aidongmei@ustb.edu.cn*

## Abstract

*Abstract:* Establishing the index system is the key to carry out the student assessment, evaluation of teaching quality largely depends on scientific index system. The related factors influencing the reliability and feasibility of teaching evaluation is analyzed in this article, and fair and scientific evaluation index system is established. Based on the summary of domestic and foreign existing evaluation index system, a set of new evaluation index system with a school teaching characteristics is established. The analytical hierarchy process is used to set up corresponding weights for each indicator, which makes the evaluation index system more complete and accurate.

*Keywords:* Curriculum evaluation; Indicator system; Analytic hierarchy process

## 1. Factors Affecting the Students' Evaluation of Teaching

The key which achieves the desired purpose of the assessment work lies in if the specific indexes can objectively and scientifically reflect the actual situation about the teaching work and teaching effect. Therefore, it is necessary to carefully study all the elements that may impact the fairness and scientificity of evaluations before establishing high quality index system, such as the differences between students and teachers, individual and group, as well as the nature of courses, etc.

## 2. Principles in Establishing Scientific Index System

The following principles should be abided by when we build an index system: people-oriented, comprehensive, coordinated[1], scientific and feasible[2]. The following details combining with the specific teaching situation should also be noted:

- i) Choose and establish indicators from the standpoint of students.
- ii) Besides the quantitative questions, open questions should also be included in the evaluation index system.
- iii) The indicators should be measurable so that we can get quantitative results.

---

This paper is supported by the postgraduate education and development grant of University of Science & Technology Beijing

© The 2015 International Conference on Artificial Life and Robotics (ICAROB 2015), Jan. 10-12, Oita, Japan



iv) Weight distribution should be reasonable and strong basis is needed[3].

### 3. Establishment of Reasonable and Scientific Evaluation Index System

The establishment of evaluation index system is to refine the teaching activity process and form different levels to reflect the real teaching process and teaching effect. Some evaluation indicators used by universities both at home and abroad are selected and all these indicators can reflect actual teaching situation and effect from some certain aspects, as shown in table 1.

Table1. Evaluation indicators used by universities both at home and abroad

The first level indicators	The secondary level indicators
Curriculum design	Explicit teaching goal
	Detailed teaching plan
Curriculum	Moderate difficulty
	Reasonable schedule
Inspection and test	Fair and justice
	Reasonable content
Teaching materials and supplementary materials	Teaching materials are easy to understand
	Supplementary materials are useful
Teaching	Express clearly and fluently, Full of passion
	Teachers can timely find problems and solve difficulties for students
	Explain new terms, concepts and principles clearly
Student feedback	Understand the main content of this course
	Develop an interest in this course

Based on the summary of domestic and foreign existing teaching evaluation index system, combined with the actual situation of the school for many years to carry out the assessment activities, we designed a new evaluation index system involved four primary indicators: teaching attitude, teaching contents, teaching methods and teaching effect, which are consistent with the method

used by most universities. Specific indicators are shown in table 2.

Table2. Index system in teaching evaluation of our school

The first level indicators	The secondary level indicators
Teaching attitude	Serious and fully prepared
	Express clearly and fluently
Content of courses	Well organized, Highlight keys and difficulties
	Enrich content properly
Teaching method	Use multimedia correctly
	Clean and tidy blackboard writing
Teaching efficiency	Pay attention to the interaction with students, Inspire students' learning enthusiasm effectively
	Cultivate the ability of independent thinking
	Combine scientific research with production practice

### 4. Analytic Hierarchy Process (APH)

The analytic hierarchy process[4] (AHP) is a system analysis method put forward by Saaty (T.L.S Saaty), a professor at university of Pittsburgh, in the mid-1970s. In this way, the qualitative thinking process can be turned into a standard quantitative output which can be measured and also to keep the consistency of the thinking process and the decision making process.

#### 4.1. Concrete implementation steps of analytic hierarchy process

##### 4.1.1. Establishment of the hierarchy relationships

The top layer of hierarchical structure is the target, that is, the evaluation activities we want to carry out. The middle layer or criterion layer is the first level indicators. The bottom layer is the evaluation objects corresponded to the secondary level indicators.



4.1.2. Construction of judgment matrix

Given the influence degree to the target layer is different, we thus compare different indicators within the same level of N and the results of the comparison constitute the judgment matrix. Elements of judgment matrix represent the relatively importance degree related to the upper layer.

Table3. Assignment standard for the elements of judgment matrix

Assignment t	Illustration
1	Indicators $T_i$ and $T_j$ are equally important
3	Indicator $T_i$ is a little important than $T_j$
5	Indicator $T_i$ is obviously important than $T_j$
7	Indicator $T_i$ is more important than $T_j$
9	Indicator $T_i$ is much more important than $T_j$
else	Between the above judgment value

$T_i$  and  $T_j$  represent any two different evaluation indexes within the same level,  $a_{ij}$  and  $a_{ji}$  respectively represent the judgment value acquired from comparing  $T_i$  and  $T_j$  as well as  $T_j$  and  $T_i$ , we make the definition:  $a_{ij} = 1 / a_{ji}$ .

Get the n-order judgment matrix as follows:

$$A = \begin{pmatrix} 1 & a_{12} & \dots & a_{1n} \\ a_{21} & 1 & \dots & a_{2n} \\ \vdots & \vdots & \ddots & \vdots \\ a_{n1} & a_{n2} & \dots & 1 \end{pmatrix} = \begin{pmatrix} 1 & a_{12} & \dots & a_{1n} \\ \frac{1}{a_{12}} & 1 & \dots & a_{2n} \\ \vdots & \vdots & \ddots & \vdots \\ \frac{1}{a_{1n}} & \frac{1}{a_{2n}} & \dots & 1 \end{pmatrix}$$

4.1.3. Method of weight calculation

There are many methods of weight calculation, such as eigenvalue method, least squares method, sum method etc. We use the way of sum one.

The first step: Normalize the column elements of A,

we get the matrix  $\bar{A} = (\bar{a}_{ij})$

$$\bar{a}_{ij} = \frac{a_{ij}}{\sum_{i=1}^n a_{ij}}$$

The second step : Add up the row elements of  $\bar{A}$ ,

we get matrix  $\bar{W} = [\bar{w}_{ij}, \bar{w}_{ij}, \dots, \bar{w}_{ij}]^T$

$$\bar{w}_i = \sum_{i=1}^n \bar{a}_{ij}$$

The third step : Normalize the matrix  $\bar{W}$ , we can get matrix

$$W = [w_{ij}, w_{ij}, \dots, w_{ij}]^T$$

$$w_i = \frac{\bar{w}_i}{\sum_{i=1}^n \bar{w}_i}$$

4.2. The application of analytic hierarchy process – Take a certain university as an example

4.2.1. Construction of judgment matrix A

According to the relative importance among nine indicators provided by the graduate school, we get the judgment matrix A

$$A = \begin{pmatrix} 1 & 5 & 1 & 3 & 7 & 7 & 3 & 3 & 5 \\ 1/5 & 1 & 1/5 & 1/3 & 3 & 3 & 1/3 & 1/3 & 1 \\ 1 & 5 & 1 & 3 & 7 & 7 & 3 & 3 & 5 \\ 1/3 & 3 & 1/3 & 1 & 5 & 5 & 1 & 1 & 3 \\ 1/7 & 1/3 & 1/7 & 1/5 & 1 & 1 & 1/5 & 1/5 & 1/3 \\ 1/7 & 1/3 & 1/7 & 1/5 & 1 & 1 & 1/5 & 1/5 & 1/3 \\ 1/3 & 3 & 1/3 & 1 & 5 & 5 & 1 & 1 & 3 \\ 1/3 & 3 & 1/3 & 1 & 5 & 5 & 1 & 1 & 3 \\ 1/5 & 1 & 1/5 & 1/3 & 3 & 3 & 1/3 & 1/3 & 1 \end{pmatrix}$$

4.2.2. The sum method is used to get the matrix  $\bar{A}$

$$\bar{A} = \begin{pmatrix} 0.2713 & 0.2308 & 0.2713 & 0.2908 & 0.1892 & 0.1892 & 0.2908 & 0.2908 & 0.2308 \\ 0.0543 & 0.0462 & 0.0543 & 0.0331 & 0.0811 & 0.0811 & 0.0331 & 0.0331 & 0.0462 \\ 0.2713 & 0.2308 & 0.2713 & 0.2908 & 0.1892 & 0.1892 & 0.2908 & 0.2908 & 0.2308 \\ 0.0904 & 0.1385 & 0.0904 & 0.0993 & 0.1351 & 0.1351 & 0.0993 & 0.0993 & 0.1385 \\ 0.0388 & 0.0154 & 0.0388 & 0.0199 & 0.0270 & 0.0270 & 0.0199 & 0.0199 & 0.0154 \\ 0.0388 & 0.0154 & 0.0388 & 0.0199 & 0.0270 & 0.0270 & 0.0199 & 0.0199 & 0.0154 \\ 0.0904 & 0.1385 & 0.0904 & 0.0993 & 0.1351 & 0.1351 & 0.0993 & 0.0993 & 0.1385 \\ 0.0904 & 0.1385 & 0.0904 & 0.0993 & 0.1351 & 0.1351 & 0.0993 & 0.0993 & 0.1385 \\ 0.0543 & 0.0462 & 0.0543 & 0.0331 & 0.0811 & 0.0811 & 0.0331 & 0.0331 & 0.0462 \end{pmatrix}$$

4.2.3. Add up the row elements of  $\bar{A}$

$$\bar{W} = (2.2550 \ 0.4625 \ 2.2550 \ 1.0259 \ 0.2221 \ 0.2221 \ 1.0259 \ 1.0259 \ 0.4625)^T$$

4.2.4. Normalize the matrix  $\bar{W}$

$$W = (0.2518 \ 0.0516 \ 0.2518 \ 0.1145 \ 0.0248 \ 0.0248 \ 0.1145 \ 0.1145 \ 0.0516)^T$$

Table4. Evaluation index system with the weight

Evaluation indicators	Weight
Serious and fully prepared	0.2518
Express clearly and fluently	0.0516
Well organized, Highlight keys and difficulties	0.2518
Enrich content properly	0.1145
Use multimedia correctly	0.0248
Clean and tidy blackboard writing	0.0248
Pay attention to the interaction with students, Inspire students' learning enthusiasm effectively	0.1145
Cultivate the ability of independent thinking	0.1145
Combine scientific research with production practice	0.0516

5. Conclusions

With the development of Chinese higher education, differences exist in colleges and universities in aspects like the level of academic, quality of faculties and students, etc. In the process of designing index system, we did not solely comply with the index system of

others, instead, a number of additional factors such as the actual teaching situation, students' learning style and the school culture were all taken into consideration. A set of new evaluation index system was established so that teachers can be more freely to play their own unique teaching style, at the same time students can focus fully on the evaluation to reduce factors affecting the authenticity and credibility of assessment process.

However, the evaluation index system is not able to adapt to different course categories and we only consider for students, the corresponding teacher mutual evaluations and expert assessments were ignored.

As for evaluation questionnaire itself, there are also some inevitable defects. It is difficult to get comprehensive and detailed information because of the limitation of indicator quantity. It's not enough to persuade us purely by evaluation scores, other effective ways must be combined with, for instance, communications and symposiums[5].

Acknowledgements

This paper is supported by the postgraduate education and development grant of University of Science & Technology Beijing and National and Natural Science Foundation of China (61370131).

References

1. Gu Yao, Establishment of the Evaluation Index System for the Construction of Discipline in Colleges and Universities[J]. *Academic Degrees & Graduate Education*, 2007(5), 56-57.
2. Xu Ci-ning, and GuoBao-xing, Establishment of Reasonable Evaluation System of Teaching Quality in Higher Education[J]. *Theoretical Front in Higher Education*, 2002(11), 44-45.
3. Chang Xue-qin, and Xing Xi-zhe, Establishment & Practice of Evaluation System of Classroom Teaching Quality[J]. *Theory and Practice of Education*, 2004, 24 (7), 51-52.
4. Wang Jian-dong, A Survey on the Integrative Quantitative Evaluation Methodology of the Classroom Teaching Quality in the Chinese Higher Education Institutions[J]. *Journal of Hubei University (Philosophy and Social Science)*, 2007, 34(7), 113-115.
5. Liu En-yun and Yang Cheng-de, Reflection & Construction of Evaluation System of Teaching Quality

in Higher Education[J]. *Jiangsu Higher Education*,  
2004(1), 85-87.

# Extracting Pattern of Arm Movements based on EMG Signal for Stroke Therapy

**Khairunizam Wan, Rashidah Suhaimi and Aswad A.R**

*Advanced Intelligent Computing and Sustainability Research  
School of Mechatronic, Universiti Malaysia Perlis, MALAYSIA  
khairunizam@unimap.edu.my*

**D. Hazry, Zuradzman M. Razlan and Shahrman AB**

*Centre of Excellence for Unmanned Aerial Systems (COEUAS)  
Universiti Malaysia Perlis, MALAYSIA*

**Mohd Asri Ariffin and Haslina M**

*School of Health Science,  
Kampus Kesihatan Universiti Sains Malaysia, MALAYSIA*

khairunizam@unimap.edu.my

**Abstract:** This paper presents the investigation pattern of arm movements for the purpose of the rehabilitation for a stroke patient in the virtual reality (VR) environments. The investigation results are used to design the virtual objects in the virtual environments. The muscle activities are analyzed by using electromyography (EMG). Six EMG channel are attached to the right arm of the subject, which is at the location of deltoid anterior fibres, deltoid middle fibres, bicep, triceps, flexor and extensor while performing arm movements. The electrical signals acquired from EMG are analyzed to extract the signal's pattern by using signal processing technique. In the studies, several fundamental arm movements are performed by the subject and the acquired patterns of EMG signals are defined as muscle activities. The experimental results show that deltoid, bicep and triceps move with a significant value compared with flexor and extensor and are used to investigate the muscle activities, which is suitable to the stroke therapy.

**Keywords:** Stroke Therapy, Arm movement, Signal pattern

## 1 INTRODUCTION

Stroke rehabilitation is based on the continuous movement of the stroke patient affected limb to stimulate the brain function that has been deteriorated. The brain damage effects not only cognition impairment but also a motor impairment [1]. The motor impairment can be treated by intense use of active movement in repetitive tasks and task-orientated activities which will result in improving motor skills and muscular strength. The treatment done by first introducing the external movement to the patient to develop their muscle activity but the amount of movement done is crucial whereas to not stress the patient to much or cause movement to little that will slow the treatment [2]. Repetitive rehabilitation exercises is one of the method used in the treatment by slowly developed the muscle and motor function, but without knowing which fundamental arm movement that will affect the muscle first can halted the course of treatment. The amount of muscle activity is to be slowly increased for steady muscle development and treat the motor impairment [3].

Virtual Reality (VR) is a digital environment which can be manipulated by the respective party. VR has its various function in today's development in various applications which most have been used by the medical doctor for

surgery simulation and psychological therapy for the mind [4-8].

This research paper organized as subsequent; Section 2 encompasses literature review of the related research and approach toward VR based stroke therapy. Section 3 presents the methodologies of applied procedures. Section 4 is divided into 2 sections, first section states about experiment setup where second section demonstrates the results of experiments. Finally section 5 expresses the conclusions over current research.

## 2 LITERATURE REVIEW

Stroke is the second leading cause of death worldwide, with fatality of 4.4 million of the total of more than 50 million deaths each year and only 10 percent recover almost completely while some other survivor have to live with few disability or impairment [1]. Thus this stroke patient needs special care and rehabilitation to gain back their body function. Obesity, high blood pressure and many other factors could be taken to considerations of early stroke [9]. Stroke is when there is a blood clot block the flow in a vessel or artery interrupting the blood flow to an area of the brain which causes the brain cells to die [10].

Kate Laver et. al [11] mentioned that virtual reality and interactive video gaming have emerged as new treatment

approaches in stroke rehabilitation. These approaches may be advantageous because they provide the opportunity to practice activities that are not or cannot be practiced within the clinical environment. Furthermore, virtual reality programs are often designed to be more interesting and enjoyable than traditional therapy tasks, thereby encouraging higher numbers of repetitions. Various applications of the VR which have make rise to the development of interfacing devices such as dataglove, head-mounted display (HMD) and mechanical suit [12]. The application has various usages in the rehabilitation therapy for the stroke patient. Recently many types of equipment have been developed based on VR applications.

### 3 METHODOLOGIES

**Fig. 1** shows the flow chart of the proposed works. In the experiments, a subject performs 22 fundamental movements. Six EMG channels are attached at to the upper and lower arms. The acquired EMG signals are analyzed by using signal processing techniques. The signal patterns are extracted and the investigation of the motion sequences are conducted based on the extracted signal patterns.

#### 3.1 Hemiparesis Stroke

Hemiparesis stroke attacks when blood flow to the brain stopped. The oxygen and blood that supply to the brain will stop which result in the damage of the brain which can affect the important body parts that control daily activities. Hemiparesis sufferer will experience one side of weakness. They often experience balance impairments which cause difficulties to perform movements such as grabbing objects, drinking from a glass, eating and using bathroom.

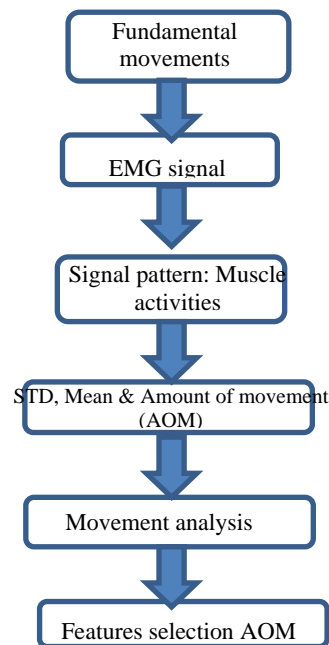


**Fig. 1.** Flow chart of the proposed works

#### 3.2 Fundamental Movements in Stroke Rehab

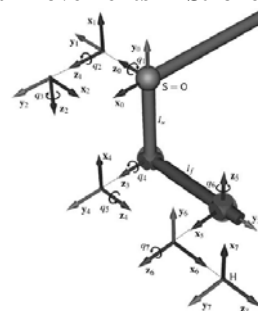


**Fig. 2.** Kinematics of human arm

Human arm consists of seven degree of freedom, which is shoulder, elbow and wrist as shown in **Fig. 2**. In rehabilitation for disability and hemiparesis stroke patient it is important to first assess their movement and limitation. The human arm can be model by the shoulder with 3 degree of freedom, elbow 2 degree of freedom and wrist with two degree of freedom. In the shoulder deltoid muscle involves in elevation, depression, shoulder flexion, shoulder extension, abduction, adduction, horizontal abduction, horizontal adduction, external rotation and internal rotation. Biceps and triceps muscles involve in the movement associate with elbow flexion, elbow extension, elbow supination and elbow pronation. The wrist uses movement as extension, flexion, ulnar deviation and radial deviation. All these movements are being used as reference of fundamental arm movement.

### 3.3 Processing EMG signal

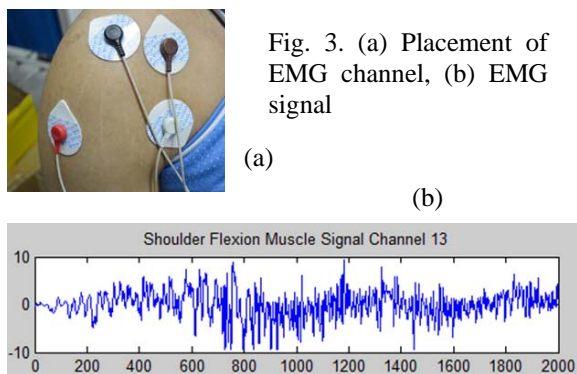


Fig. 3. (a) Placement of EMG channel, (b) EMG signal

EMG is used to record the electrical activity produced by the skeletal muscle. **Fig. 3** shows EMG signal of the deltoid muscle recorded when the subject performed the arm movements. The sampling rate is 1000 Hz/s. Butterworth low pass digital filter is used to remove noises in the signal which the cut off frequency of 10 Hz and 0.001 normalization value.

### 3.4 Signal patterns

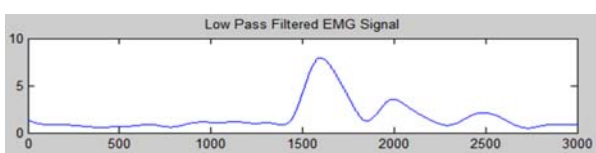


Fig. 4. EMG signal after preprocessing

Fig. 4 shows the EMG signal after processing by using signal processing technique. Then, means, standard deviation and amount of movement (AOM) of the filtered signal are extracted and are defined as features or muscle activity [13].

## 4 EXPERIMENTS

### 4.1 Experimental setup

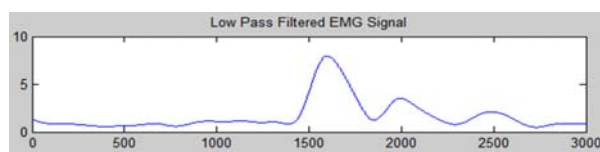


Fig. 4. Placement of EMG channel

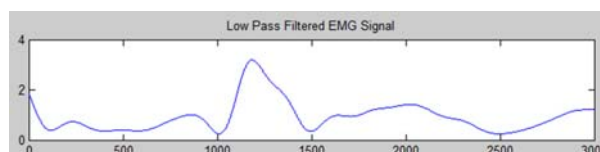
**Fig. 4** shows the locations of the electrode placement where the main muscle can be detected which were deltoid, biceps, triceps, extensor and flexor. The shoulder was to

detect the deltoid muscle as for every movement that involves the shoulder for example elevation, depression, shoulder flexion, shoulder extension, abduction, adduction, horizontal abduction, horizontal adduction, external rotation and internal rotation. The second part of the arm was the elbow, the movement associated with the elbows were elbow flexion, elbow extension, elbow supination and elbow pronation. All these movements were used as references of fundamental arm movements

### 4.2 Experimental results

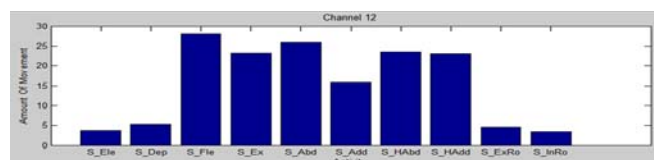


(a)

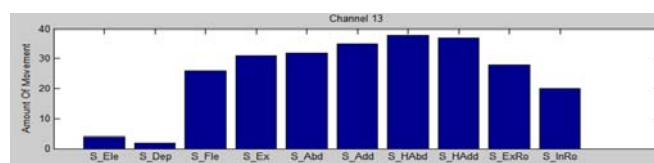


(b)

Fig. 5. (a) Elbow Flexion Signal, (b) Shoulder Flexion Signal



(a)



(b)

Fig. 6. AOM (a) Biceps (b) Triceps

**Fig. 5** (a) and (b) show EMG signals of elbow and shoulder flexion after preprocessing step. The results show that the noise was removed from the signal. The motion features, which were mean, standard deviation and amount of movement (AOM) were measured from this signal. **Fig. 6** (a) and (b) show the AOM from the selected fundamental movements and it could be used to represent movement patterns of the arm. From the experiments, it was decided to use locations for EMG measurement, which were deltoid, biceps and triceps. **Fig. 7** shows the AOM for deltoid, triceps, biceps, extensor and flexor as denoted by (a), (b), (c), (d) and (e), respectively. The graphs show that the

deltoid, triceps and biceps had a significant value of AOM. In the future research for the investigation of movement sequence deltoid, triceps and biceps will be used for the electrode placements. Fig. 8 shows the placement of the electrode at the human arm.

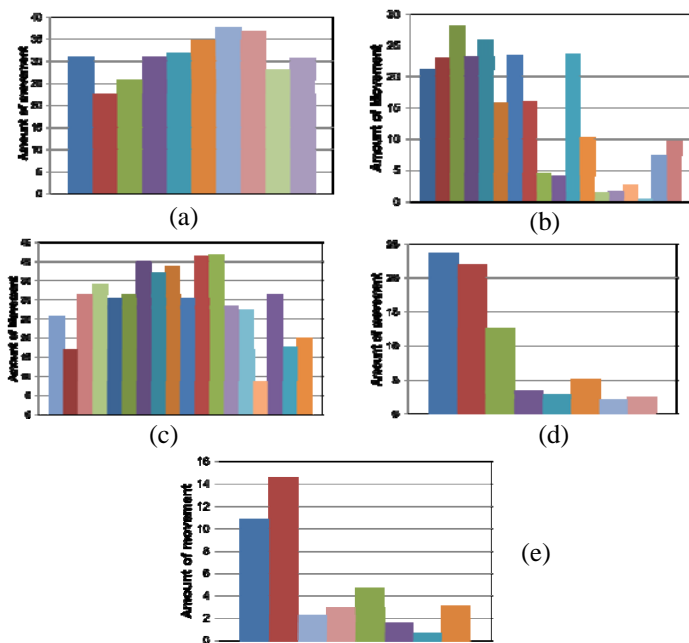


Fig. 7. Amount of movement (a) Deltoid (b) Biceps (c) Triceps (d) Extensor (e) Flexor

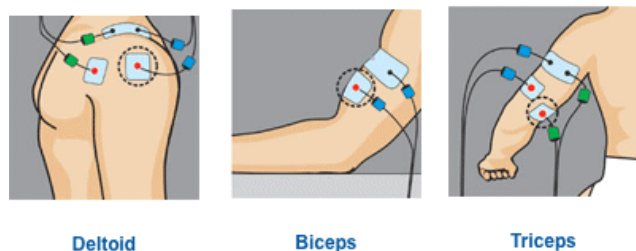


Fig. 8. (a) Elbow Flexion Signal, (b) Shoulder Flexion Signal

## 5 CONCLUSIONS

The paper discusses the analysis of arm movements by using EMG device. The signal processing technique is proposed to remove noises and to smoothen the acquired EMG signal. Then, the signal pattern is extracted, which is mean, standard deviation and amount of movement (AOM). The experimental results show that AOM is the best pattern to represent arm movements. In the future three electrode placement is chosen which is deltoid, triceps and biceps.

## REFERENCES

[1] Tasuku Miyoshi and T. Komeda (2008), "Antiphasic Electromyographic Activities between Biarticular Arm

Muscles Reflects Improved Two Joint Arm Movement Performances In Stroke Patients," IEEE International Conference on Systems, Man and Cybernetics (SMC 2008), pp. 1350-1354.

[2] A. Phinyomark (), "Evaluation of EMG Feature Extraction for Hand Movement Recognition Based on Euclidean Distance and Standard Deviation," Department of Electrical Engineering, Faculty of Engineering, Prince of Songkla University, Thailand.

[3] Y. M. Aung and A. Al-Jumaily (2011), "Rehabilitation Exercise with Real-Time Muscle Simulation based EMG and AR," 11th International Conference on Hybrid Intelligent Systems (HIS), pp. 641-646.

[4] Holden M (), "Virtual Environments for Motor Rehabilitation: Review," Cyber Psychology and Behavior Vol. 8, No. 3, pp. 187-211.

[5] Forducey P. et al. (), "Tele-Rehabilitation using the Rutgers Master II glove following Carpal Tunnel Release surgery," IEEE Trans Neural Syst Rehabil Eng., Vol. 15, No. 1, 43-49.

[6] Deutsch J., Latonio J. and Burdea G (2001), "Rehabilitation of Musculoskeletal Injury Using the Rutgers Ankle Haptic Interface: Three Case Reports," Eurohaptics'01, pp. 11-16.

[7] Sveistrup H., McComas J. and Thornton M. (), "Experimental Studies of Virtual Reality-Delivered Compared to Conventional Exercise Programs for Rehabilitation," CyberPsychology & Behavior, Vol. 6, No. 3, pp. 245-249.

[9] Aswad A.R, Khairunizam Wan, Nazrul H. ADNAN, Shahrman A.B, D. Hazry, Zuradzman M. Razlan, Nabilah H.E and M. Hazwan ALI (2014), "Glove Based Virtual Reality (VR) Interaction for the Purpose of Rehabilitation," Australian Journal of Basic and Applied Sciences, Vol. 8, No.4, pp. 170-175.

[9] H. Kim (2013), "Kinematic Data Analysis for Post-Stroke Patients," Transaction on Neural Systems and Rehabilitation Engineering, Vol. 21, No. 2, pp. 153-164.

[10] R.Sanchez (2004), "Monitoring Functional Arm Movement for Home-Based Therapy after Stroke," Proceedings of the 26th Annual International Conference of the IEEE EMBS, USA.

[11] Kate Laver, Stacey George, Susie Thomas, Judith E. Deutsch and Maria Crotty (2014), "Virtual Reality for Stroke Rehabilitation," Journal of the American Heart Association, Print ISSN: 0039-2499. Online ISSN: 1524-4628.

[12] Nazrul H. ADNAN et al., "Principal Component Analysis For The Classification Of Fingers Movement Data Using DataGlove "GloveMAP", " International Journal of Computer Engineering & Technology (IJCET), 4(2): pp. 79-93.

[13] Rashidah Suhaimi and Khairunizam WAN (2014), "Analysis of EMG-based Muscles Activity for Stroke Rehabilitation, ". ICED 2014.



# Cascade Controller Design For Steering Control Of Nonholonomic Autonomous Mobile Robot Vehicle

<sup>1</sup>S. Faiz Ahmed, D. Hazry, <sup>2</sup>F. Azim

<sup>1</sup>Centre of Excellence For Unmanned Aerial Systems (COEUAS) Universiti Malaysia Perlis (UniMAP),  
Seriab, 01000, Kangar, Perlis, Malaysia.

<sup>2</sup>Hamdard University, Karachi Pakistan  
[hazry@unimap.edu.my](mailto:hazry@unimap.edu.my)

**Abstract-** In this research article a cascade control system is presented for steering control of control of nonholonomic autonomous mobile robot vehicle. The propose system consist of a master controller and two slave controllers. The master controller is based on Fuzzy Logic Controller (FLC) which computes the required speed and angular speed needed by the two motors to drives the robot. Fuzzy logic is used to generate target trajectory movement. The two slave controllers are Proportional+Integral+Derivative (PID) controllers which ensured the desired speeds that needed for the both DC motors. PID controller parameters were tuned according to four ranges of speeds using model based tuning method. In addition, the control law is offered to select a suitable rule base for fuzzy controller in order to ensure the system is stable. The proposed cascaded controller is implemented on a nonholonomic mobile robot and the results have shown that, the proposed controller achieved the desired turning angle and the mobile robot tracks the target efficiently.

**Keywords:**nonholonomic autonomous mobile robot vehicl, Fuzzy Logic Controller, PID controller

## I. INTRODUCTION

Autonomous navigation is the most important topic of artificial intelligence, various approaches have been tried to solve navigation problems [1]. The researchers have done studies to both holonomic and nonholonomic mobile robots [2-3]. Autonomous navigation is the ability of a mobile robot to move in an environment that is available to achieve a goal, without interacting with humans. In recent years, various new approaches to steering mobile robots have been developed. In 2004 Marichal , designed and present a fuzzy logic control system to decide how a mobile robot steer the wheel to achieve the desired orientation [4]. So, the desired target can be achieved simply by tuning the steering wheel towards the target. Besides that PID feedback controller is employed in the system to improve the performance of the system [5]. The purposed cascade fuzzy -PID controller is implemented on the mobile robot and the results showed the proposed method can achieve the desired turn angle to ensure that the autonomous mobile robot can reach the target set.

## II. KINEMATIC MODEL OF THE NONHOLONOMIC MOBILE ROBOT

### A. Differential Steering System

In the differential steering system to prevent slippage and achieve pure rolling motion, the mobile robot rotates around a point on the same axis in the two-wheel drive. This point is called the instantaneous center of rotation (ICR). By changing the drive speeds of two wheels move, the ICR will also be moved and will be followed by

different trajectories [6]. Figure 1 shows the differential steering system of mobile robot.

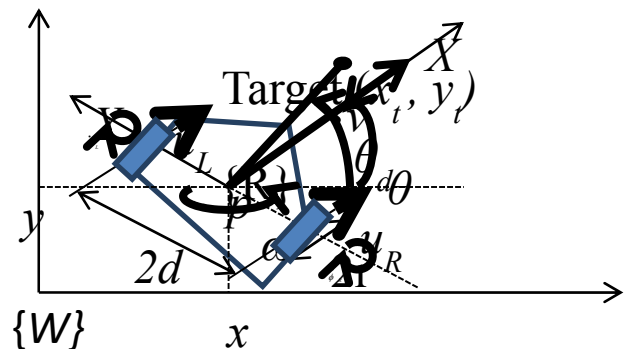


Fig 1: Differential steering system of the mobile robot

In this figure  $(x, y)$  is reference frame,  $(X, Y)$  is robot coordinates fame,  $R$  is the position of robot in  $(x, y)$ ,  $\theta$  represents orientation angle of robot,  $r$  is wheel radius,  $2d$ : distance between two wheels,  $u_R/L$  are the speed of right and left wheels respectively,  $u, \omega$  are the speed and angular speed of robot and  $\dot{\phi}_R$  and  $\dot{\phi}_L$  : angular speed of right and left wheels respectively

The speed of the center of mass of the robot is orthogonal to the axis of the wheel. It is also assumed that the mass of wheels and wheel inertias is neglected. Meanwhile, center of mass of the mobile robot is located in the middle of the axis connecting the drive wheels.

$p$  defines the origin of robot coordinate system with coordinate  $(x, y)$ .  $\theta_d$  is the angle between X-axis of



world coordinate system denoted by {W} and the X-axis of robot coordinate system denoted by {R}.

The speed relative to the ground of the right wheel and the left wheel can be expressed as follows, respectively.

$$u_R = r\dot{\phi}_R = r \times \frac{\Delta\phi_R}{\Delta t} \tag{1}$$

$$u_L = r\dot{\phi}_L = r \times \frac{\Delta\phi_L}{\Delta t} \tag{2}$$

With,  $\phi_{R,L}$  can be calculated by using following equation:

$$\phi_{R,L} = \frac{x_{R,L}}{N_{R,L} \times 60} \tag{3}$$

where, NR,L are numbers of encoder per revolution of right and left wheel respectively,  $x_{R,L}$  are the number of encoder pulses obtained from the encoders for the right wheel and the left wheel, respectively.

Therefore speed and the angular speed of a mobile robot related to the wheel speeds can be expressed as follows:

$$u = \frac{(u_R + u_L)}{2} = \frac{r}{2\Delta t} (\Delta\phi_R + \Delta\phi_L) \tag{4}$$

$$\omega = \frac{1}{2d} (u_R - u_L) = \frac{r}{2d\Delta t} (\Delta\phi_R - \Delta\phi_L). \tag{5}$$

Where in Equation (5),  $u_R > u_L$  and 2d is the width of the mobile robot from the center of the right wheel to the center of the left wheel.

### III. Proposed Control technique for Mobile Robot

A cascade control system has been implemented to control the movement of the robot that consist a Fuzzy logic based master controller and two PID based slave controller for each DC motors as shown in Figure 2. Fuzzy logic is applied to generate target trajectory movement with the information extracted from vision system such

as the distance of target and the orientation of target. We take the speed of mobile robot, for the robot speed could be fast, medium or slow. Using fuzzy logic terms, speed is a linguistic variable that takes the fuzzy sets: fast, medium or slow. The two slave Proportional+Integral+Derivative (PID) controllers are used to control the speed of each wheel as per desire value.

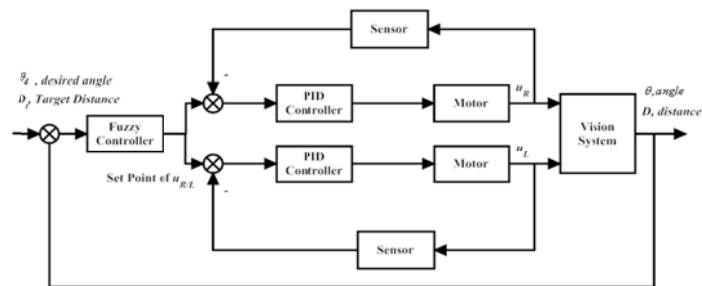


Figure 2: A cascade control system

### IV. The Fuzzy Controller

A block diagram of the fuzzy controller is shown in Figure 3. The desired command signal  $\theta_d$  and  $D_t$  are transmitted from the vision system to the fuzzy controller inside the PC. The error between the command signal and the actual position, as well as the change in error of signal are calculated and fed into the fuzzy controller embedded in the DAQ. From the Equation (5), it can be seen that the different between the speed of the right and left wheels determines the turn speed. The fuzzy controller is designed to output PWM signal corresponding to  $u_R$  and  $u_L$  to the right motor and left motor respectively to control the mobile robot turn angle  $\theta$  to the desired angle  $\theta_d$  and target distance  $D_t$ .

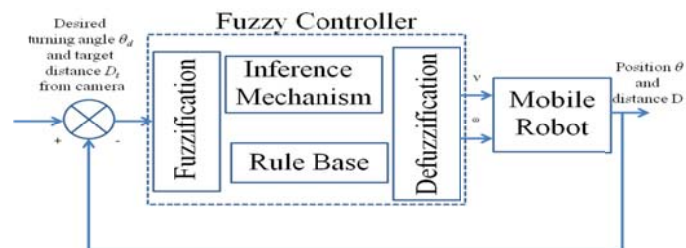


Figure 4: Block diagram of the fuzzy logic controller

The fuzzification procedure maps the crisp input values to the membership values between 0 and 1. Here we use three membership functions for target distance  $D_t$  and five membership functions desired angle  $\theta_d$ . Figure 4 and Figure 5 illustrate the input membership functions for  $D_t$  and  $\theta_d$  respectively.



Figure 4: Input membership functions for target distance  $D_t$

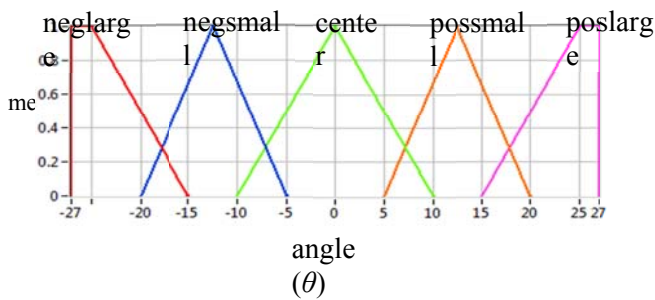


Figure 5: Input membership functions for desired angle  $\theta$

The control rules are designed based on expert knowledge and testing. Furthermore, the control rules also meet the trajectory requirements derived from PI control. For example, if  $\theta_d$  is “poslarge” and is  $D_t$  “far”, then the left motor should be much than the right motor, i.e.,  $u_L - u_R$  should be “more left” and speed  $u_L + u_R$  should be “fast”. Based on knowledge, we can obtain 15 rules. Table 1 represents conclusion understanding that the expert has about how to control the turn angle given the angle and distance as inputs. The input and output linguistic variables are shown in the table.

Table 1: Rules table for the steering system

		Angle of target ( $\theta$ )				
		Neg-large	Neg-small	center	Pos-small	Pos-large
Distance of target ( $D$ )	far	more left, fast	left, fast	zero, fast	right, fast	more right, fast
	close	more left, medium	left, medium	zero, medium	right, medium	more right, medium
	too close	more left, slow	left, slow	zero, slow	right, slow	more right, slow

The de-fuzzification procedure maps the fuzzy output from the inference mechanism to a crisp signal. We use the “center of area” (COA) de-fuzzification method for combining the recommendations represented by the implied fuzzy sets from all the rules. The fuzzy logic controller then uses the Equation (6) to calculate the geometric center of this area.  $x$  donate the value for  $v$  or  $\omega$ . Let  $\int f(x)$  denote the area under the membership function  $f(x)$ . The COA method computes the crisp value to be

$$COA = \frac{\int_{x_{min}}^{x_{max}} f(x) \cdot x dx}{\int_{x_{min}}^{x_{max}} f(x) dx} \tag{6}$$

where COA is the center of area,  $x$  is the value of the linguistic variable, and  $x_{min}$  and  $x_{max}$  represent the range of the linguistic variable. Figure 6 and Figure 7 show the output membership functions. Note that the output PWM signals should be selected to meet the convergence requirements.

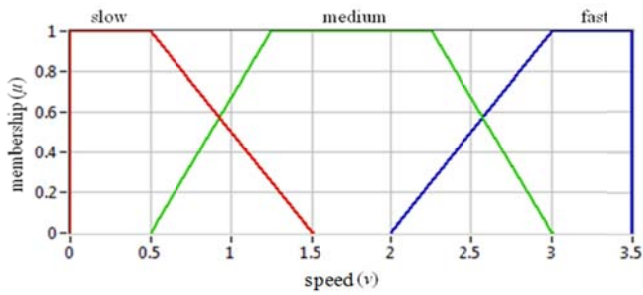


Figure 6: Output membership functions for the speed

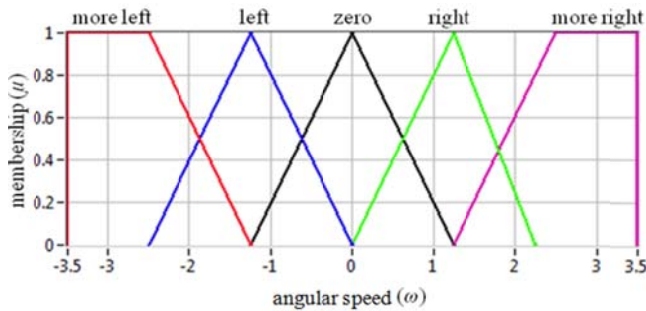


Figure 7: Output membership functions for the angular speed

### V. The PID Controller

In the nonlinear control of mobile robots, the problems to achieve the desired speed for right wheel  $u_R$  and left wheel  $u_L$  are often caused by such factors as actuator constraint, time delay and other disturbances. One simple way to control the speed is to use a Pulse Width Modulation (PWM) pulse generator with PID feedback controller which can be used to improve the performance of the system.

The PID controller transfer function in Z Domain as shown below :

$$PID = \frac{g + g_1 z^{-1} + g_2 z^{-2}}{1 - z^{-1}} \quad (7)$$

Tuning of the PID controllers can be done using Model Based Method

### VI. Model Based Method

In the Model based method the transfer function is derived from calculation of model parameters from a step experiment response. The Second

order transfer functions are obtained for various segmentations of speed and PID parameters are calculated using classical controller design. This design method is known as pole assignment or pole shifting method.

The transfer function of a DC motor in discrete-time model is described as second order system by [7] as:

$$\frac{y(t)}{u(t)} = \frac{b_1 z^{-1}}{1 + a_1 z^{-1} + a_2 z^{-2}}$$

#### a. Design with Classical Method and PID Control

During designing parameters for the PID controller, consider the feedback control system as shown in Figure 8.

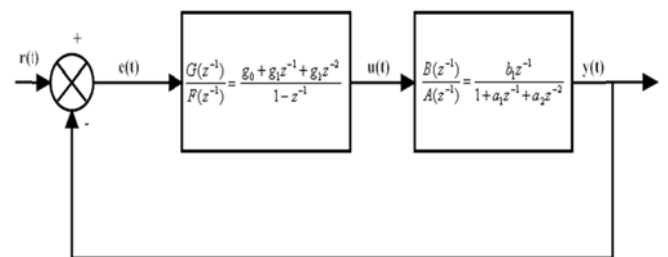


Figure 8: Feedback control system

The Close loop transfer function for this system can be write as :

$$\frac{y(t)}{r(t)} = \frac{b_1 z^{-1} (g_0 + g_1 z^{-1} + g_2 z^{-2})}{(1 - z^{-1})(1 + a_1 z^{-1} + a_2 z^{-2}) + b_1 z^{-1} (g_0 + g_1 z^{-1} + g_2 z^{-2})} \quad (8)$$

Using pole assignment method defined in [9], we compare characteristic equations with desired second order polynomial as:

$$(1 - z^{-1})(1 + a_1 z^{-1} + a_2 z^{-2}) + b_1 z^{-1} (g_0 + g_1 z^{-1} + g_2 z^{-2}) = 1 + t_1 z^{-1} + t_2 z^{-2} \quad (9)$$

with

$$t_1 = -2e^{-\xi\omega_n T_s} \cos T_s \omega_n \sqrt{1 - \xi^2} \quad (10)$$

$$\text{and } t_2 = e^{-2\xi\omega_n t} \quad (11)$$

Thus, the Parameters of PID controller can be calculated by comparing the coefficients form (9). The PID parameters results for four different speeds of right wheel and left wheel are shown in Table 2.

Table 2: The result of the PID model based tuning for right wheel and left wheel

Right Wheel PID Tuning				
PID	0-1.0 RPS	1.0-2.5 RPS	2.5-3.0 RPS	3.0-3.5 RPS
Kp	2.2769	25.248	41.079	176.7889
Ki	4.6592	16.6431	17.1421	152.4726
Kd	16.7932	210.1562	39.5797	431.8131

**VII. Results & Simulation**  
**a) Discussions**

The speed and angular speed of mobile robot was determined by the number of encoder pulses for the right wheel and the left wheel. The PID controller is used to produce the same speed of the right wheel and left wheel in order to make the mobile robot move in straight line.

The robot system provides a stable speed property after implementing an onboard PID controller on free wheels time response experiments. Figure 9, 10, 11, 12, 13, 14, 15 and 16 show eight examples of the speeds time response with different speeds for left wheel and right wheel. The rising time increase when the desired speed is higher. The range of oscillations gets smaller for higher speeds. Through the experiences, the PID controller is also available for low speed such as 0.5 RPS except model based tuning method controller, but the

oscillation is more drastic. The fast tuning PID controller shows the best result for free wheel time response experiments.

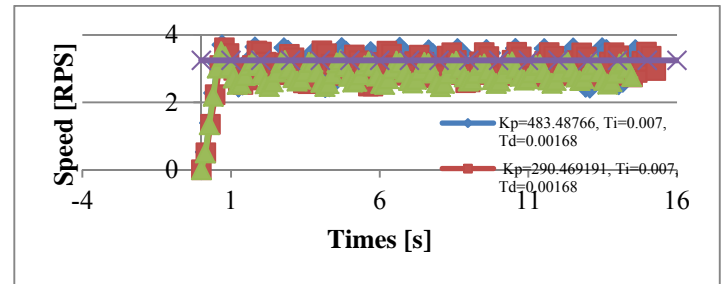


Figure 9: Time response of left wheel speed with 3.25 [RPS] step input, Fast Tuning blue, Normal Tuning red, Model Based Tuning green

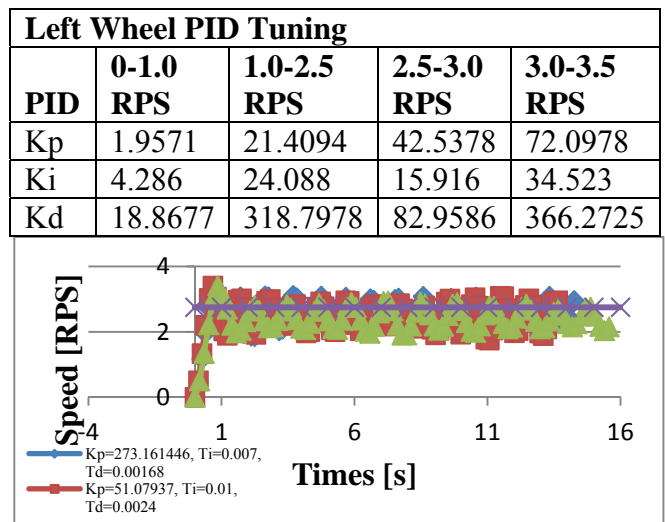


Figure 10: Time response of left wheel speed with 2.75 [RPS] step input, Fast Tuning blue, Normal Tuning red, Model Based Tuning green

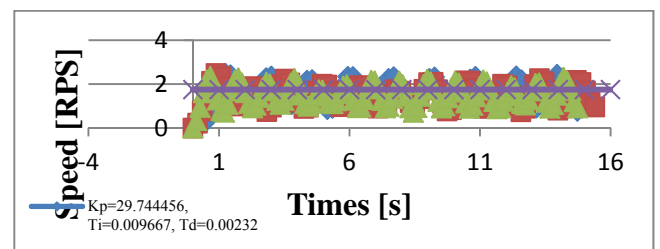


Figure 11: Time response of left wheel speed with 1.75 [RPS] step input, Fast Tuning blue, Normal Tuning red, Model Based Tuning green

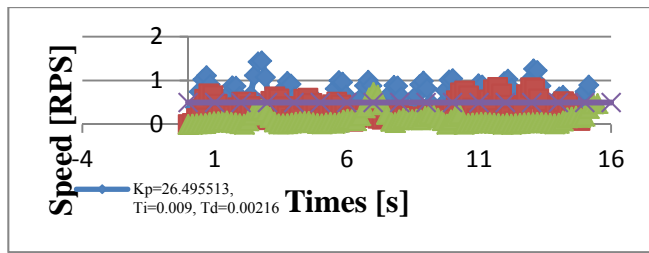


Figure 12: Time response of left wheel speed with 0.5 [RPS] step input, Fast Tuning blue, Normal Tuning red, Model Based Tuning green

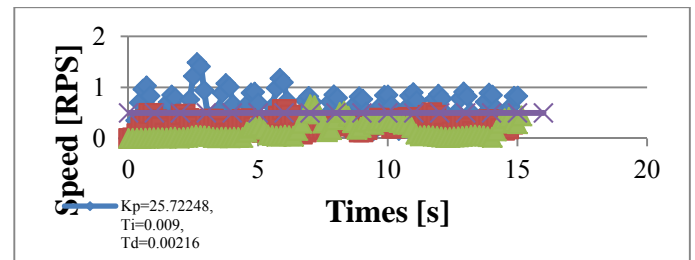


Figure 16: Time response of right wheel speed with 0.5 [RPS] step input, Fast Tuning blue, Normal Tuning red, Model Based Tuning green

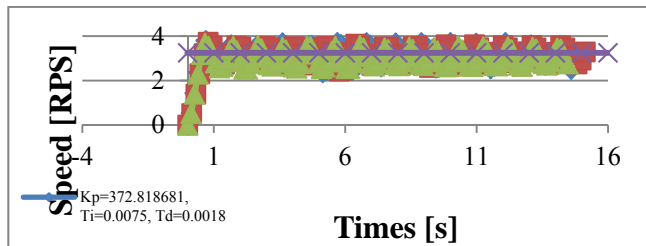


Figure 13: Time response of right wheel speed with 3.25 [RPS] step input, Fast Tuning blue, Normal Tuning red, Model Based Tuning green

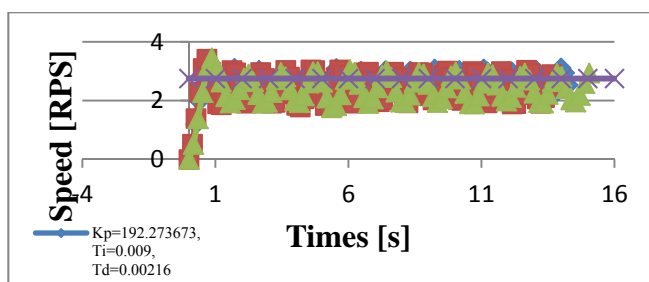


Figure 14: Time response of right wheel speed with 2.75 [RPS] step input, Fast Tuning blue, Normal Tuning red, Model Based Tuning green

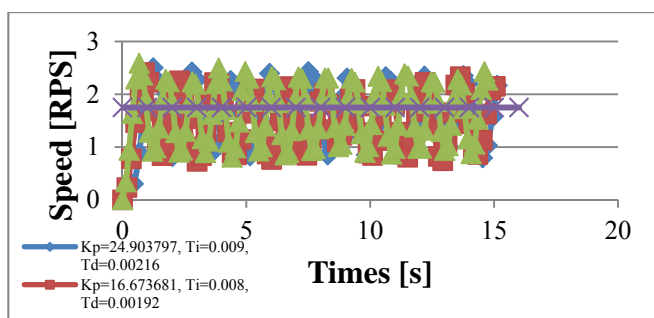


Figure 15: Time response of right wheel speed with 1.75 [RPS] step input, Fast Tuning blue, Normal Tuning red, Model Based Tuning green

Experiments were conducted to make a comparison of the test results between four ranges of speeds using Fast Tuning PID controller parameters in Table 2. The results are presented in Figures 17, 18, 19 and 20.

In the Figures, the horizontal axis is the traveling distance of mobile robot in centimeters and the vertical axis is the speeds of the wheel rotations defined by Equation (5.7) and Equation (5.8). The data plotted in the Figure 19 and 20 provide evidence that the speeds in wheel rotations of the Fast Tuning PID controller for the right wheel and the left wheel are in unstable condition at lower desired speed. The mobile robot shows high speeds from beginning of moving distance and does not move ahead to the target point in straight line tracking. In Figure 18 and Figure 19, we deduce that the small differences between the right wheel of speeds and the left wheel of speeds. Therefore, the mobile robot will move stably in tracking straight line.

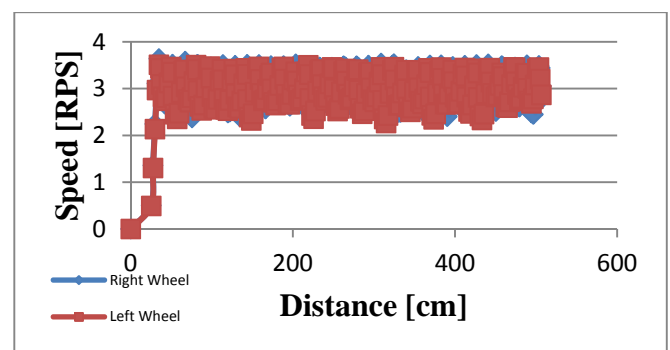


Figure 17: Comparison of the speeds in wheel rotations in straight line tracking at 3.25 [RPS] desired speed



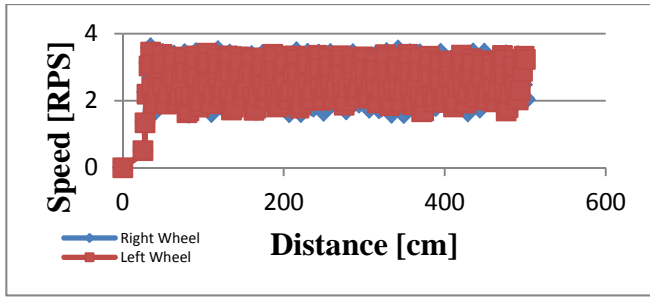


Figure 18: Comparison of the speeds in wheel rotations in straight line tracking at 2.75 [RPS] desired speed

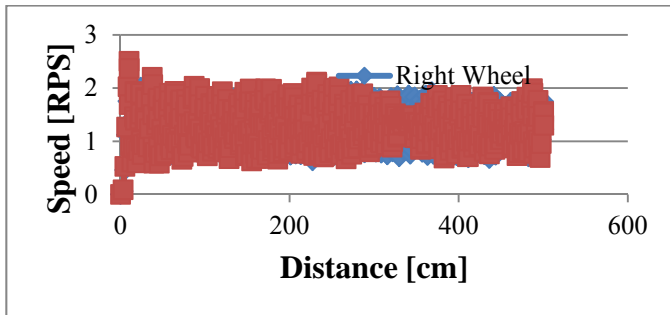


Figure 19: Comparison of the speeds in wheel rotations in straight line tracking at 1.75 RPS desired speed

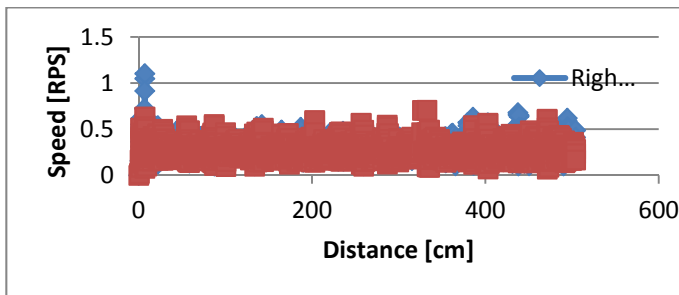
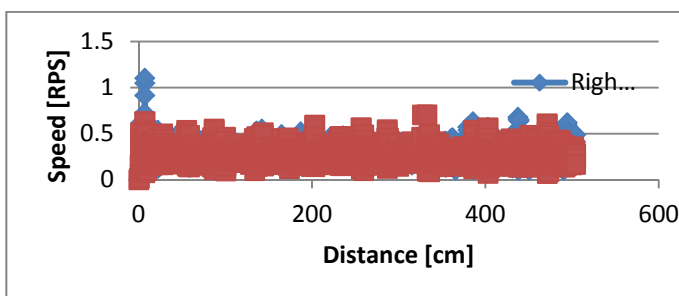


Figure 20: Comparison of the speeds in wheel rotations in straight line tracking at 0.5 RPS desired speed



From the experimental result studies, the mobile robot shows a stable movement in straight line tracking after using Fast Tuning PID controller for the right wheel and the left wheel for high desired speed as shown in Figure 17 and Figure 18 respectively. These PID control parameter

were determined by performing fine tuning experiment explained. The system of two wheels of the mobile robot works concurrently with different PID controller parameter to perform a stable movement in straight line tracking for high desired speed.

### VIII. Conclusion

In this article, an analysis and design of fuzzy control law for steering control of the developed nonholonomic mobile robot are presented. PID controller method is exploited to guarantee the stability of the straight line and turning trajectory. The proposed fuzzy controller with PID controller is implemented on the developed mobile robot. The system has performed well and satisfactory results are obtained which show that the proposed fuzzy controller and PID controller achieved the desired turn angle thus it can make the autonomous mobile robot moving to the target successfully. A system for two wheels of a mobile robot moves simultaneously with different parameters of PID controller to ensure the stability of movement in a straight line.

### References

- [1]. Rimon, E. ; Dept. of Electr. Eng., Yale Univ., New Haven, CT, Exact robot navigation using artificial potential functions, IEEE Transactions on Robotics and Automation, Vol.8, Issue: 5, Oct 1992, pp: 501 - 518
- [2]. Qing Yu and I-Ming Chen, A General Approach to the Dynamics of Nonholonomic Mobile Manipulator Systems, *J. Dyn. Sys., Meas., Control* 124(4), Dec, 2002, pp: 512-521

- [3]. Dongjun Lee, Semi-Autonomous Teleoperation of Multiple Wheeled Mobile Robots Over the Internet, Conference Sponsors: Dynamic Systems and Control Division, October 20–22, 2008, pp. 147-154
- [4]. Yang, Simon X , An embedded fuzzy controller for a behavior-based mobile robot with guaranteed performance, IEEE Transactions on Fuzzy Systems, Vol:12 (4) August 2004, pp: 436 – 446
- [5]. Hongfu Zhou, DC Servo Motor PID Control in Mobile Robots with Embedded DSP, International Conference on Intelligent Computation Technology and Automation (ICICTA), 2008 Vol: 1
- [6]. MohdSaifizi Saidonr#1, HazryDesa, RudzuanMd Noor, A Differential Steering Control with Proportional Controller for An Autonomous Mobile Robot, IEEE 7th International Colloquium on Signal Processing and its Applications, 2011 pp: 90-94
- [7]. Sudjana, O. , Trajectory control of analog servo motor with limited state information using estimated discrete time model, IEEE International Conference on Robotics, Biomimetics, and Intelligent Computational Systems (ROBIONETICS), 2013 pp: 73 - 76

# Research on Iris Recognition Based on the BP Neural Network

Fengzhi Dai, Li Fan, Chunyu Yu, Bo Liu

College of Electronic Information and Automation, Tianjin University of Science and Technology,  
80 MailBox, 1038 Daguananlu Road, Hexi District, Tianjin 300222, China

E-mail: daifz@tust.edu.cn, fanli0476@126.com

www.tust.edu.cn

## Abstract

Iris recognition is the high confidence personal identification technology among the other biometrics recognition. This is not only because the iris's unique feature, but also due to its stability that the iris is immune to age and environment. In this paper, we design a feed forward neural network and use the back propagation algorithm to explore an elementary iris recognition system model. 10 iris samples are used as the recognition objects. The experiment demonstrates that though the recognition model is simply constructed, it has a high recognition rate and the recognition speed is reasonable. The proposed methodology provides a convenient way for iris recognition.

*Keywords:* iris recognition, artificial neural network, back propagation algorithm, image processing

## 1. Introduction

At present, iris recognition is used in various fields due to its significant advantages: (1) Iris is human's internal organization which is covered with a transparent membrane (cornea). For this reason, it is hard to be changed. However, fingerprint is apt to be blurred after a few years manual labor and can be forged by fingerprint paster. (2) Iris is quite smooth as its geometry shape is only controlled by two cooperative muscles (sphincter pupillae and dilator pupillae). Therefore, the shape of iris is easier to be predicted. (3) Like the texture of fingerprint, the texture of iris is random determined in the period of gestation. Many factors can influence the formation of iris so the error probability of matching is quite low even though it is not testified technically that the iris's texture is absolutely unique<sup>1,2</sup>. (4) Iris scanning is as simply as taking photograph. It can be processed from 10cm to several meters. Thus, the measured object needs not to touch the scanner.

Many applications of iris recognition are used. For instance, Canada Border Services Agency introduces CANPass program<sup>3</sup>. Netherlands, Arab, Britain and Germany also apply the iris recognition technology into

immigration clearance. Meanwhile, many scientists have devoted to relevant study<sup>4</sup>. Boles and Boashash built a 1D representation of the gray level signature of the iris and applied it to zero-crossing of the dyadic wavelet<sup>5</sup>. Ma, Wang, and Tan used a bank of Gabor filters to capture the iris profile<sup>6</sup>. Poursaberi generated a binary code representation of the iris and used a minimum Euclidian distance for matching<sup>7</sup>.

In this paper, an algorithm that simplifies the procedure of recognition is proposed. Our approach is characterized by: (1) Image pre-processing is used so as to avoid using complex mathematical algorithms. (2) The BP neural network is adopted. (3) Use grayscale value of each pixel for learning and recognition.

The paper is organized as follows: Section 2 discusses the reason of using iris as object and the status quo of iris recognition technology. In section 3, the related and background of artificial neural network is reviewed. Section 4 presents the pre-processing of 10 iris samples, the design of the BP neural network, the application of the entire recognition system model and the experiment results. Finally, section 5 draws some conclusions.



## 2. Iris Recognition

### 2.1. Biological characteristics of iris

The iris is the colored, thin, circular structured muscle within the eye, which regulates the size of the pupil and thus controls the amount of light that enter the eye. The iris begins to form as soon as the third month of gestation. By the eighth month, the structures that creating the iris patterns are largely completed. However, pigment accretion can continue during the first postnatal years. Because the iris patterns are formed randomly, even genetically identical twins will not have the same iris patterns<sup>8</sup>. Fig.1 shows the iris image and its position in the eye.

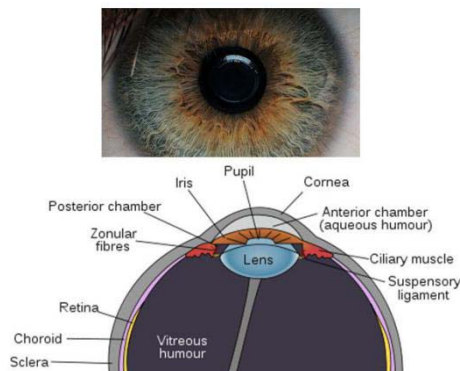


Fig. 1. Iris and its position in the eye

### 2.2. The history of the iris identification

The French ophthalmologist Alphonse Bertillon (1885) is considered to be the first for iris identification based on its color<sup>9</sup>. In 1985, ophthalmologists Leonard Flom and Aran Safir proposed that no two irises are exactly the same, and they got the patent application in 1987<sup>10</sup>. Then they cooperated with Dr. John Daugman<sup>11</sup>, a computer scientist of the University of Cambridge, UK, and developed an algorithm to automatically identify the human iris. In 1993, the Defense Nuclear Agency began to test and deliver a prototype unit, which was successfully completed by 1995 due to the combined efforts of Flom, Safi and Daugman.

After that, many scientists have devoted themselves to the relevant study, such as R.Wildes<sup>12</sup>, W.Boles<sup>13</sup> and R.Sanchez-Reillo<sup>14</sup> proposed different algorithms. In 1995, the first commercial products became available<sup>15</sup>. Many companies began to develop their own iris recognition algorithm. For example, L-1 Identity Solution which was established in 2006 provides all service and solution concerning human identification. Oki also provides a variety of security system based on iris identification.

## 3. Neural Network

### 3.1. Biological neuron

Neuron is the basic unit of structure and function of the nervous system, Fig. 2 shows a typical neuron structure.

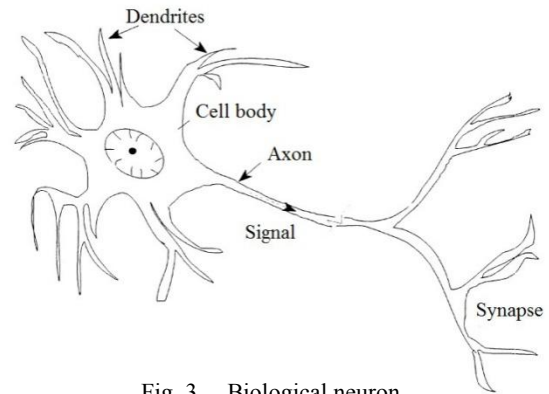


Fig. 3. Biological neuron

When a neuron is stimulated and excited, exciting will be converted into a signal and be conveyed to synapse through axon. After the rapid diffusion of chemical molecules defused by the synapse in the synaptic space, the neighboring neurons generate new impulses and pass them to the next neurons in the same way.

This simplified mechanism of signal transfer constituted the fundamental step of early neurocomputing development<sup>16</sup>.

### 3.2. Artificial neuron

Artificial neuron simulates the nonlinear characteristics of biological neuron (multiple input and single output). In 1943, McCulloch and Pitts proposed the McCulloch-Pitts neuron model (shown in Fig. 3). The mathematical expression is:

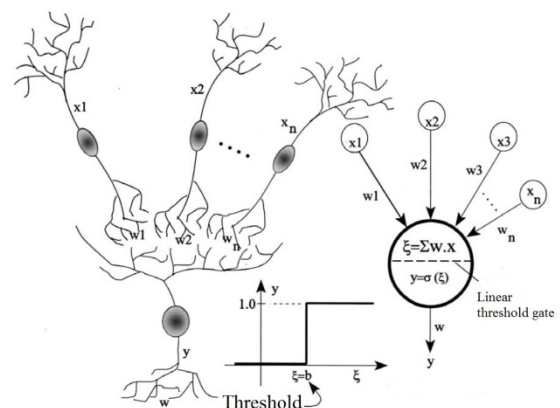


Fig. 2. Artificial neuron model

$$y = \sigma(\xi) \tag{1}$$

$$\xi = \sum_{i=1}^n w_i x_i - b \tag{2}$$

$x_i$  ( $i=1,2,\dots,n$ ) is the input signal from other neurons;  $w_i$  ( $i=1,2,\dots,n$ ) presents the weight between two neuron;  $b$  is the threshold of the neuron<sup>17</sup>,  $y$  is the output of the neuron;  $\sigma(\cdot)$  is the activate function. The output  $y$  is 0 or 1, which presents suppression or exciting respectively.

$$y = \sigma(\xi) = \begin{cases} 1, & \xi \geq 0 \\ 0, & \xi < 0 \end{cases} \tag{3}$$

### 3.3. Multilayer feedforward neural network

In 1985, Rumelhart and McClelland research group proposed the multilayer feedforward theory and the error back propagation algorithm base on parallel distributed information processing. The BP neural network may contain one or several hidden layers (Fig.4).

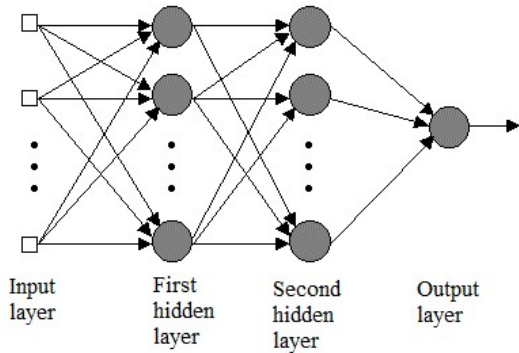


Fig. 5. Multilayer neural network

## 4. Application on Iris Recognition

### 4.1. Pre-processing of raw images

Ten different colored iris images are selected to be pre-processed<sup>18-20</sup> to grayscale images (shown in Fig.5)

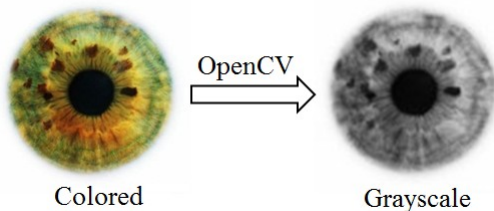


Fig. 6. Image processing

and extracted the grayscale pixel features as the inputs to the neural network. All the iris images are processed by OpenCV, and converted the size to 100×100 pixels.

### 4.2. Neural network design

First, get the input and target samples of the neural network. We treat the processed image as a 100×100 matrix, each element stores the grayscale pixel value as shown in Eq. (4). After that, the matrix is converted into a 10000×1 column vector that is treated as the input vector of the neural network (Fig. 6).

$$\begin{bmatrix} v001001 & v001002 & \dots & v001099 & v001100 \\ v002001 & v002002 & \dots & v002099 & v002100 \\ \vdots & \vdots & \ddots & \vdots & \vdots \\ v099001 & v099002 & \dots & v099099 & v099100 \\ v100001 & v100002 & \dots & v100099 & v100100 \end{bmatrix} \tag{4}$$

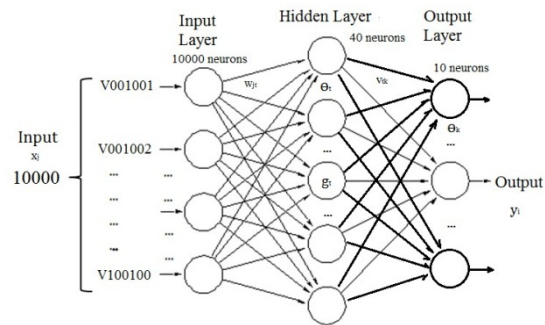


Fig. 4. The input of network

Thus, the input layer of neural network has 10000 neurons. Learning assumes that each input vector is paired with a target vector representing the desired output; together they are called a learning pair<sup>21</sup>. In this study, 10 learning pairs would be required, so the output layer neurons is 10. Output results are restored in a 10×1 column vector.

For the number of hidden layer neurons, we refer to the empirical formula Eq.(5). After that, we delete the hidden neurons whose influence is little and then set the final hidden layer neurons number as 40.

$$n_2 = \sqrt{n_1 + n_3} + c \tag{5}$$

Here,  $n_1$ ,  $n_2$  and  $n_3$  are the numbers for the input, hidden and output layer neurons.

### 4.3. Neural network learning

The learning rate  $\eta$  and learning times are 0.4 and 5000 respectively. All the weights ( $w_{jk}, v_{jk}$ ) and threshold values ( $\theta_j, \theta_k$ ) must be initialized to small random

decimals before starting the learning process.

Training the BP neural network follows the five steps:

- (1) Select the learning pair  $(X^p, Y^p)$  from the 10 pairs.

$$X^p = (x_1, x_2, \dots, x_m)^T \quad (6)$$

$$Y^p = (Y_1, Y_2, \dots, Y_n) \quad (7)$$

- (2) Calculate the hidden and output vector of the neural network by Eq.(8) and Eq.(9) respectively.

$$g_t = f(\sum_{j=1}^m w_{jt}x_j - \theta_t) \quad (t = 1, 2, \dots, a) \quad (8)$$

$$y_k = f(\sum_{t=1}^a v_{tk}g_t - \theta_k) \quad (k = 1, 2, \dots, n) \quad (9)$$

- (3) Calculate the general errors of each layer of neural network,  $\delta_k^p$  and  $\delta_t^p$ .

- (4) Adjust the weights of the network.

$$v_{tk}(n+1) = v_{tk}(n) + \eta \cdot \sum_{p=1}^P \delta_k^p \cdot g_t^p \quad (10)$$

$$w_{jt}(n+1) = w_{jt}(n) + \eta \cdot \sum_{p=1}^P \delta_t^p \cdot g_j^p \quad (11)$$

$$\theta_k(n+1) = \theta_k(n) + \eta \cdot \sum_{p=1}^P \delta_k^p \quad (12)$$

$$\theta_t(n+1) = \theta_t(n) + \eta \cdot \sum_{p=1}^P \delta_t^p \quad (13)$$

- (5) Repeat steps 1 through 4 for the 10 pairs until the sum squared error in Eq.(14) for the entire set is acceptable low.

$$E = \sum_{p=1}^P \sum_{k=1}^n (y_k^p - \hat{y}_k^p)^2 / 2 \quad (14)$$

The result of the neural network learning is illustrated in Fig. 7. After 3000 times training, the sum squared error is acceptable low.

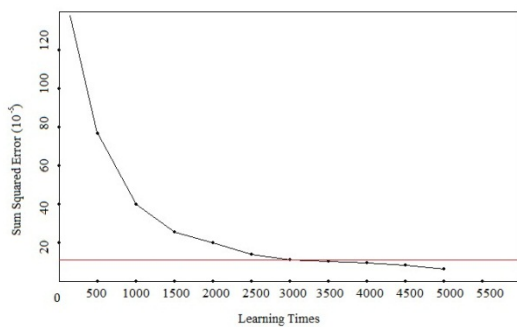


Fig. 7. Sum squared error for 5000 times learning

#### 4.4. Recognition and results

Recognition requires the steps<sup>22</sup>: in Fig. 8, (1) Click the menu 'File' on the left top corner, to load the original

grayscale iris images. The 10 images are displayed. (2) Select the region of iris model (as the 100×100 region) from the 10 iris images then generates the model. After this step, 10 iris models will be converted to 10 matrixes and displayed below the original images (circled in Fig. 8).

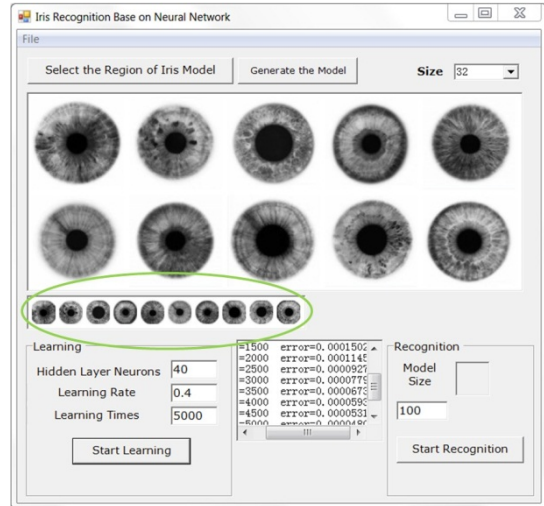


Fig.8. Neural network learning

- (3) Train the neural network by clicking the button "Start Learning", and the training procedure is also shown in Fig.8. (4) Click the button "Start Recognition" to recognize whether the selected iris is one of those 10 irises or not.

The recognition procedure is shown in Fig.9 and the recognized object is marked by the square. The experiment result shows the match rate is 99.946% for the selected object.

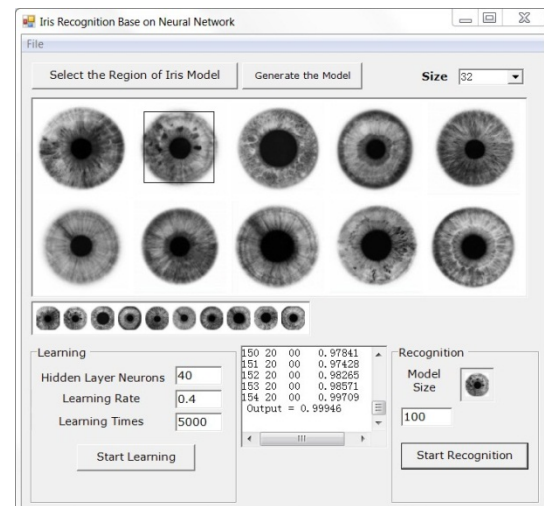


Fig.9. Recognition results

## 5. Conclusion

In this paper, we design a neural network and used the back propagation algorithm to develop an elementary iris recognition system. The experiment demonstrates that the system has an ideal identification rate. With the development of the demand of identity recognition, this system can be applied in many fields such as security check and entrance guard.

In this study, the extraction of the basic features of the iris mainly utilize image processing, future research will use more shape and structural characteristics of the iris itself as the feature values.

## Acknowledgment

The research is partly supported by the Scientific Research Foundation of Tianjin University of Science and Technology (20130123), and the Open Foundation (YF11700102) of Key Laboratory for Water Environment and Resources, Tianjin Normal University.

## References

1. P. C. Kronfeld, The gross anatomy and embryology of the eye, *The Eye*, Vol. 1,(1968) pp. 1–66.
2. I. Mann, *The Development of the Human Eye*, (1950)
3. <http://www.cbsa-asfc.gc.ca/media/facts-faits/009-eng.html>, 04/07/2012
4. F.N. Sibai, Iris recognition using artificial neural networks, *Expert Systems with Applications* Vol.38, (2011) 5940–5946.
5. Boles. W. and Boashash. B., A human identification technique using images of the Iris and wavelet transform, *IEEE Trans. Signal Processing*, Vol. 46, No. 4 (1998) 1185–1188.
6. Ma. L., Wang. Y. and Tan. T., Iris recognition using circular symmetric filters, In *Proc. 16th Int. Conf. Pattern Recognition*, Vol. 2, (2002) 414–417.
7. Poursaberi. A. and Araabi. B., A novel iris recognition system using morphological edge detector and wavelet phase features, *ICGST-GVIP Journal*, Vol. 5, No.6 (2005).
8. F. H. Adler, *Physiology of the Eye*, St. Louis, MO: Mosby (1965)
9. A.Bertillon, *La couleur de l'iris*, Revue scientifique, France, (1885)
10. L. Flom and A. Safir, Iris recognition system, *U.S. Patent 4 641 349*, 1987.
11. J. Daugman, High confidence personal identification by rapid video analysis of iris texture, the *IEEE Int. Carnahan conf. on security technology*, (1992)
12. R.P.Wildes, J.C. Asmuth, G.L. Green and S.C. Hsu, A system for automated iris recognition, *IEEE paper*, (1994)
13. W.W.Boles, A security system based on human iris identification using wavelet transform, in *1<sup>st</sup> Int. Conf. Knowledge-based intelligent electronic systems*, Adelaide, Australia. Ed, 21-23 May 1997.
14. R.Sanchez-Reillo, C.Sanchez-Avila and J-A.Martin-Pereda, Minimal template size for iris recognition, in *Proc. BMES/EMBS Conf., IEEE Publication, Atlanta*, October 1999.
15. Irisian Technologies, Historical Timeline, (2003)
16. I.A. Basheera and M. Hajmeerb, Artificial neural networks: fundamentals, computing, design, and Application, *J. Microbiological Methods*, Vol.43 (2000) 3–31.
17. Jain. A.K., Mao. J. and Mohiuddin. K.M., Artificial neural networks: a tutorial, *Comput. IEEE* March, (1996) 31–44.
18. Daugman. J., How iris recognition works. In *Proc. Int. Conf. Image Processing*, Vol. 1, (2002).
19. Wildes. R. et al., A system for automated iris recognition, In *Proc. 2nd IEEE workshop on applications of computer vision*, pp.121–128
20. Lim, S., Lee, K., Byeon, O. and Kim, T., Efficient Iris recognition through improvement of feature vector and classifier, *ETRI Journal*, Vol.23, No.2, (2001) pp.1–2.
21. P. D. Wasserman, *Neural computing: theory and practice*, Van Nostrand Reinhold Co. New York, NY, USA (1989)
22. Sakai Kouichi, *Foundation and Application of digital image processing by Visual C#.NET and Visual Basic.NET* (in Japanese), CQ Press (2006)

© The 2015 International Conference on Artificial Life and Robotics (ICAROB 2015), Jan. 10-12, Oita, Japan

# Synchronization Control of a Four-wing Fractional-Order Chaotic System and Its Analog Circuit Design

**Hongyan Jia**

*Department of Automation , Tianjin University of Science and Technology,  
1038 Daguananlu Road, Hexi District, Tianjin 300222, PR China*

**Qian Tao**

*Department of Automation , Tianjin University of Science and Technology,  
1038 Daguananlu Road, Hexi District, Tianjin300222, PR China*

**Jinfang Li**

*Department of Automation , Tianjin University of Science and Technology,  
1038 Daguananlu Road, Hexi District, Tianjin300222, PR China*

**Wei Xue**

*Department of Automation , Tianjin University of Science and Technology,  
1038 Daguananlu Road, Hexi District, Tianjin 300222, PR China  
E-mail: jiahy@tust.edu.cn, susantaoqian@sina.com  
www.tust.edu.cn*

## **Abstract**

The four-wing fractional-order chaotic system is firstly introduced in this paper, Then, its synchronization control is also discussed, and the results from numerical analysis show the chaotic synchronization control is simple and practical. An last, an analog circuit is designed to implement it, and the results are in agreement with numerical analysis, which probably provide an practical technology for application of fractional-order chaos , such as secure communication and image encryption.

*Keywords:* Fractional-order, chaotic system, synchronization control, analog circuit

## **1. Introduction**

Although Fractional calculus has a history of more than 300 hundred years,<sup>1-2</sup> it hasn't attracted more and more attention until many systems are found to show fractional-order dynamics, such as the fractional-order Chua's circuit,<sup>3</sup> the fractional-order Lorenz system,<sup>4</sup> the fractional-order Chen system,<sup>5-6</sup> the fractional-order Rössler system,<sup>7</sup> and so on.<sup>8-10</sup> Recently, some study on synchronization and control of fractional-order chaotic systems are attracting more and more attention from an application point of view, such as secure communication, image encryption and control processing.<sup>11-17</sup> It was firstly reported in Pecora and Carroll's paper in 1990 that two chaotic trajectories with different initial

conditions can be synchronized.<sup>18</sup> Subsequently, some other methods of synchronization have been represented and researched, such as the PC method, the PAD method, the one-way method and the bidirectional coupled method.<sup>19-25</sup>

In 2008, Chen et al. reported a integer-order four-wing chaotic system.<sup>26</sup> Some interesting phenomenon are found, for example, the system shows four-wing chaotic attractors, three-wing chaotic attractors, and periodic attractors in different periods when selecting different system parameters. In 2011, Jia et al. further analyzed its dynamic behaviors by computer-aid topological horseshoe analysis and analog circuit experiments.<sup>27</sup> In 2014, based on the theory of fractional calculus and the method of frequency domain

approximation, Jia et al. study the fractional form of the integer-order four-wing system, and found that chaotic characteristic exist in it.<sup>28</sup>All these work show the dynamics of the four-wing chaotic system are very complex, it may be more interesting to make some application study by utilizing the system.

In this paper, the fractional-order four-wing chaotic system is firstly reported. Then, a synchronization method is discussed, and the simulation results have confirmed the effectiveness of the synchronization method. At last, an analog circuit is designed to realize the chaotic synchronization, and all of results show the synchronization method is rather simple and convenient.

### 2. The Four-Wing Fractional-Order Chaotic System

The four-wing fractional-order system in Ref.28 is described by

$$\begin{cases} \frac{d^\alpha x}{dt^\alpha} = ax + ky - yz \\ \frac{d^\alpha y}{dt^\alpha} = -by - z + xz \\ \frac{d^\alpha z}{dt^\alpha} = -x - cz + xy \end{cases} \quad (1)$$

Where  $a, b, c, k \in R; 0 < \alpha < 1$ .

Based on frequency domain approximate method, the fractional operator of order “ $\alpha$ ” can be finished by the transfer function  $1/s^\alpha$  in the frequency domain. Then

the transfer function  $1/s^\alpha$  can be represented by an approximated integer-order transfer function with errors of approximately 2 dB according to Ref.29, and thus the approximation adopted in this paper is

$$\frac{1}{s^{0.9}} \approx \frac{1.766s^2 + 38.27s + 4.914}{s^3 + 36.15s^2 + 7.789s + 0.01} \quad (2)$$

When  $\alpha = 0.9$ ,  $(a, b, c, k) = (5, 12, 5, 1)$ , the four-wing fractional -order system is chaotic as shown in Fig. 1. Its corresponding chaotic characteristics analysis has been given in the Ref..28 one can see it for the details.

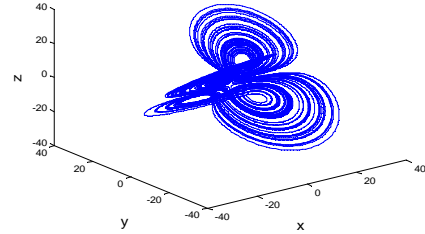


Fig. 1. Phase plots of the fractional-order system

### 3. Synchronization of the Four-Wing Fractional-Order Chaotic System

In this paper, based on master-slave configuration method with linear coupling, a chaotic synchronization control is briefly discussed between the two four-wing fractional-order systems whose structure are same. Here, the master four-wing fractional-order chaotic system can be written as system(1), and the coupled slave four-wing fractional-order system has the following form.

$$\begin{cases} \frac{d^\alpha x'}{dt^\alpha} = ax' + ky' - y'z' + k_1(x - x') \\ \frac{d^\alpha y'}{dt^\alpha} = -by' - z' + x'z' + k_2(y - y') \\ \frac{d^\alpha z'}{dt^\alpha} = -x' - cz' + x'y' + k_3(z - z') \end{cases} \quad (3)$$

The constant parameters  $k_1, k_2, k_3$  are coupling strength. Now let the coupling strength  $k_1 > 0, k_2 = 0, k_3 = 0$ , by continuously increasing the coupling strength  $k_1$  from zero, in step 1, a value of  $k_1$  is obtained to make the two four-wing fractional-order systems synchronized. That is, When  $k_1 = 4$ , the two coupled chaotic systems can be synchronized. Simulation results are shown in Fig.2 and Fig.3, which are the time response and the phase synchronization, respectively.

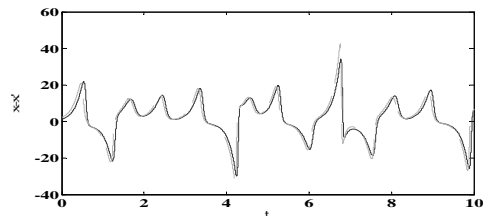


Fig. 2. time response of  $x$  (-) and  $x'$  (--);



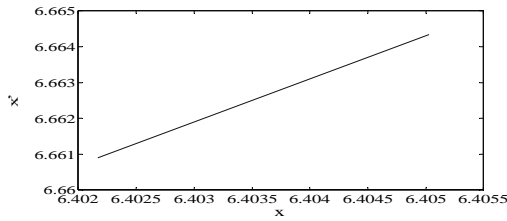


Fig. 3. Phase synchronization of  $x$  and  $x'$

#### 4. Analog Circuit for Synchronization of the Four-Wing Fractional-Order Chaotic System

Finally, we designed an analog circuit to realize the synchronization control for the four-wing fractional-order system by using the basic devices such as Ad633, LF347, resistors, and capacitors, as shown in Fig. 4 and Fig. 5. Fig. 4 is an analog approximate circuit for fractional-order  $\frac{1}{s^\alpha}$ , and Fig. 5 is an analog circuit for the synchronization control. Resistors and capacitors in the circuit are  $R_3 = R_3' = R_4 = R_4' = R_6 = R_6' = R_7 = R_7' = R_{10} = R_{10}' = R_{11} = R_{11}' = R_{13} = R_{13}' = R_{14} = R_{14}' = R_{17} = R_{17}' = R_{18} = R_{18}' = R_{20} = R_{20}' = R_{21} = R_{21}' = 10k\Omega$ ,  $R_2 = R_2' = R_9 = R_9' = R_{15} = R_{15}' = 100k\Omega$ ,  $R_8 = R_8' = 8.3k\Omega$ ,  $R_{16} = R_{16}' = 20k\Omega$ ,  $R_5 = R_5' = R_{12} = R_{12}' = R_{19} = R_{19}' = 1k\Omega$ ,  $R_a = 1.55M\Omega$ ,  $R_b = 61.54M\Omega$ ,  $R_c = 2.5k\Omega$ ,  $C_1 = 730nF$ ,  $C_2 = 520nF$ ,  $C_3 = 1.\mu F$ , respectively. In addition, The resistors  $R_1$ ,  $R_1'$ , and  $R_{22}$  are adjustable according to the system parameters  $a$  and  $k_1$ . When selecting  $R_1 = 20k\Omega$ ,  $R_1' = 100k\Omega$ ,  $R_{22} = 25k\Omega$ , the two coupled chaotic systems are synchronized, and the simulation results are shown in Fig. 6.

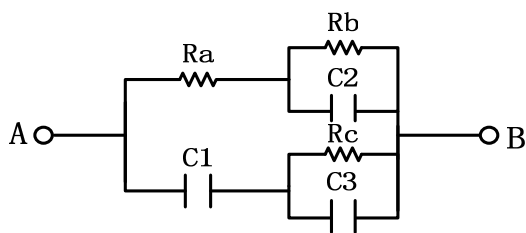


Fig. 4. Approximate Circuit for  $\frac{1}{s^\alpha}$

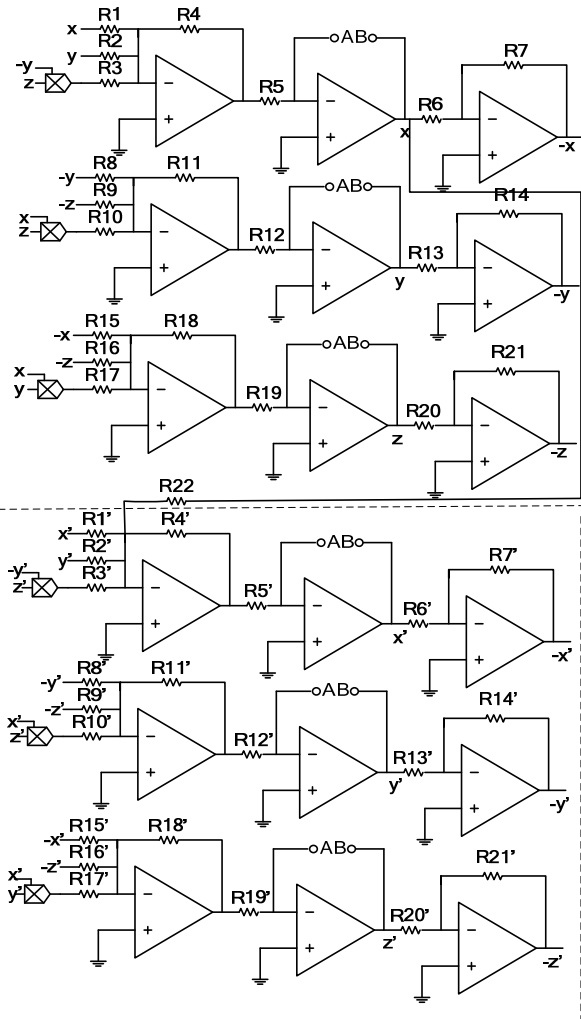
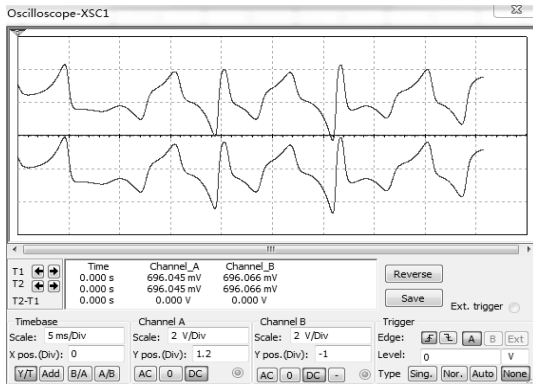


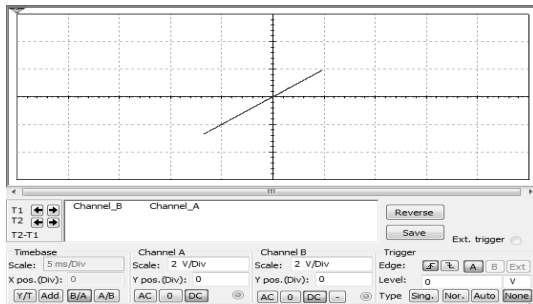
Fig. 5. Analog circuit of synchronization between system (1) and system (3).

#### 5. Conclusion

In this paper, by linear coupling and frequency domain approximation, a synchronization control method for a four-wing fractional-order chaotic system is studied, and the simulation results have confirmed the feasibility and effectiveness of this synchronization method. In addition, An analog circuit is also designed to implement the synchronization control. Numerical simulations and circuit experiments are given to verify the effectiveness of the proposed synchronization scheme, and it is rather simple and convenient for the synchronization scheme to be realized. Some work in this paper probably provide an practical technology for application of fractional-order chaos, such as secure communication and image encryption.



(a) Time response of  $x - x'$



(b) Phase synchronization of  $x$  and  $x'$

Fig. 6. Circuit simulation observations of synchronization

### Acknowledgements

This work was supported in part by the Young Scientists Fund of the National Natural Science Foundation of China (Grant No. 11202148), the Natural Science Foundation of China(Grant No. 61174094).

### References

1. I. Podlubny, *Fractional Differential Equations*, (Academic Press, New York, 1999).
2. R. Hilfer (Ed.), *Applications of Fractional Calculus in Physics*, (World Scientific, New Jersey, 2001).
3. T.T. Hartley, C.F. Lorenzo, *Nonlinear Dyn.* 29 (2002) 201.
4. I Grigorenko, E Grigorenko. Chaotic dynamics of the fractional Lorenz system. *Phys. Rev. Lett.*, 2003, 91: 034101.
5. C.P. Li, G.J. Peng, Chaos in Chen's system with a fractional order , *Chaos Solitons Fractals* 22 (2004) 443-450.
6. J.G. Lu, G.R. Chen, A note on the fractional-order Chen system. *Chaos Solitons Fractals* 27 (2006) 685-688.
7. C.G. Li, G. Chen, *Phys. A* 341 (2004) 55.

8. W. Deng, C.P. Li, *Physica A* 353 (2005) 61.
9. Qi G Y, Chen G R, Du S Z, Chen Z Q, Yuan Z Z 2005 *Physica A* 352 295.
10. Z.M. Ge, A.R. Zhang, *Chaos Solitons Fractals* 32 (2007) 1791.
11. C.G. Li, X.X. Liao, J.B. Yu, *Phys. Rev. E* 68 (2003) 067203.
12. T.S. Zhou, C.P. Li, *Phys. D* 212 (2005) 111.
13. X. Gao, J.B. Yu, *Chaos Solitons Fractals* 26 (2005) 141.
14. J.G. Lu, *Chaos Solitons Fractals* 26 (2005) 1125.
15. J.P. Yan, C.P. Li, *Chaos Solitons Fractals* 32 (2007) 725.
16. G. Peng, Y. Jiang, F. Chen, *Phys. A* 387 (2008) 3738.
17. G. Peng, Y. Jiang, *Phys. Lett. A* 372 (2008) 3963.
18. Pecora, L.M., Carroll, T.L.: Synchronization in chaotic systems. *Phys. Rev. Lett.* 64, 821–824 (1990).
19. Pecora LM, Carroll TL. Synchronization in chaotic systems. *Phys Rev Lett* 1990;64:821–4.
20. Sira-Ramirez H, Cruz-Hernandez C. Synchronization of chaotic systems: a generalized Hamiltonian systems approach. *Int J Bifurcat Chaos* 2001;11(5):1381–95.
21. Petras I. Control of fractional-order Chua's system. *J Electr Eng* 2002;53(7–8):219–22.
22. Lu JG. Chaotic dynamics and synchronization of fractional-order Chua's circuits with a piecewise-linear nonlinearity. *Int J Modern Phys B* 2005;19(20):3249–59.
23. Li CP, Deng WH, Xu D. Chaos synchronization of the Chua system with a fractional order. *Physica A* 2006;360:171–85.
24. Junwei Wang, Xiaohua Xiong, Yanbin Zhang. Extending synchronization scheme to chaotic fractional-order Chen systems. *Physica A* 2006;370:279–85.
25. Changpin Li, Jianping Yan. The synchronization of fractional differential systems. *Chaos, Solitons & Fractals* 2007, 32:751–7.
26. Z.Q. Chen, Y. Yang, Z.Z. Yuan, A single three-wing or four-wing chaotic attractor generated from a three-dimensional smooth quadratic autonomous system, *Chaos, Solitons & Fractals*, 38 (2008) 1187-1196
27. H.Y. Jia, Z.Q. Chen, Q. Y. Qi, Topological horseshoe analysis and the circuit implementation for a four-wing chaotic attractor, *Nonlinear Dynamics*, 65 (2011) 131-140.
28. H.Y. Jia, Z.Q. Chen, Q. Y. Qi, Chaotic characteristics analysis and circuit implementation for a fractional-order system, *IEEE TRANS. CIUCUITS & SYSTEMS -I: REGULAR PAPERS*, 61(3) (2014) 845-853.
29. Tom T. Hartley, Carl F. Lorenzo, and Helen Killory Qammer, Chaos in a Fractional Order Chua's System, *IEEE TRANS. CIRCUITS & SYSTEMS*, 42 (8) (1995) 485-449.

© The 2015 International Conference on Artificial Life and Robotics (ICAROB 2015), Jan. 10-12, Oita, Japan



# A fractional-order hyper-chaotic system and its circuit implementation

**Wei Xue**

*Department of Automation , Tianjin University of Science and Technology,  
1038 Daguananlu Road, Hexi Distric, Tianjin 300222, PR China*

**Hui Xiao**

*Department of Automation , Tianjin University of Science and Technology,  
1038 Daguananlu Road, Hexi Distric, Tianjin 300222, PR China*

**Jinkang Xu**

*Department of Automation , Tianjin University of Science and Technology,  
1038 Daguananlu Road, Hexi Distric, Tianjin 300222, PR China*

**Hongyan Jia**

*Department of Automation , Tianjin University of Science and Technology,  
1038 Daguananlu Road, Hexi Distric, Tianjin 300222, PR China  
E-mail:xuwei@tust.edu.cn, xiaohuiJC@126.com  
www.tust.edu.cn*

## Abstract

In this paper, the commensurate 3.6-order Qi hyper-chaotic system is investigated. Based on the predictor-corrector method, we obtain phase portraits, bifurcation diagrams, Lyapunov exponent spectra of this system, and find that the system can present a four-wing hyperchaotic attractor. In addition, a circuit is designed for the fractional-order hyperchaotic system and the circuit implementation result show the existence of the four-wing hyperchaotic attractor, which verifies the correct of the theoretic analysis and provides the technical support for its application in engineering.

*Keywords:* Fractional-order; Qi hyper-chaotic system; Lyapunov exponent; Circuit design; Implementation.

## 1. Introduction

Since Lorenz discovered the famous Lorenz chaotic attractor in 1963,<sup>1</sup> a great deal of new chaotic systems have been proposed, such as Chen system,<sup>2</sup> Lü system,<sup>3</sup> and so on.<sup>4-5</sup> which have made very significant influences in the research on nonlinear science. Recently, the research on the chaotic dynamics are gradually expanding to the engineering applications on the basis of mathematical theory and physical theory, such as secure communication,<sup>6</sup> image encryption,<sup>7</sup> and other fields.<sup>8-9</sup>

There also are some specific characteristics in the fractional-order system, that is, the fractional-order chaotic system not only can enhance the nonlinear and

complexity of the systems, but also possess a very strong historical memory to reflect historical information of the system. Therefore, The fractional-order equation could describe the physical phenomenon more accurately,<sup>10</sup> in recent years, the fractional differential operator was introduced into the integer-order chaotic system to construct the fractional-order chaotic system.<sup>11-13</sup> It is also been verified that the fractional-order chaotic systems have more complex dynamics characteristics than integer-order chaotic systems. And thus the research on the fractional-order chaotic system has attracted more and more focus from application point of view. In addition, as the fractional-order hyper-chaotic system has two positive Lyapunov exponent , it could be more

© The 2015 International Conference on Artificial Life and Robotics (ICAROB 2015), Jan. 10-12, Oita, Japan

suitable for the application in secure communication and image encryption.

Therefore, it is necessary to investigate the analog circuit design and implementation of the fractional-order hyper-chaotic systems, which provides the technical basis for its further applications in engineering. In this paper, the commensurate fractional-order Qi hyper-chaotic system is investigated and an analog circuit is designed to implement the hyper-chaotic system.

## 2. Numerical analysis of fractional-order Qi hyper-chaotic system

Qi hyper-chaotic system has been proposed in Ref. [14], and it is constructed by adding a linear feedback control to the chaotic system in Ref.[5]. On this basis , we will analyze the commensurate fractional-order Qi hyper-chaotic system which is described as follow:

$$\begin{cases} \frac{d^q x}{dt^q} = a(y - x) + eyz, \\ \frac{d^q y}{dt^q} = cx + dy - xz - w \\ \frac{d^q z}{dt^q} = -bz + xy \\ \frac{d^q w}{dt^q} = fy \end{cases} \quad (1)$$

Where  $0 < q < 1, a, b, c, d, e, f \in R$ , and when  $q = 0.9, a = 15, b = 40, c = -5, d = 20, e = 5, f = 50$ , system(1) is 3.6-order system, and it is chaotic .

### 2.1. Phase portraits

When  $q = 0.9, a = 15, b = 40, c = -5, d = 20, e = 5, f = 50$ , the phase portraits of 3.6-order Qi hyper-chaotic system is shown in Fig.1, It can be seen that this system presents four-wing chaotic attractor.

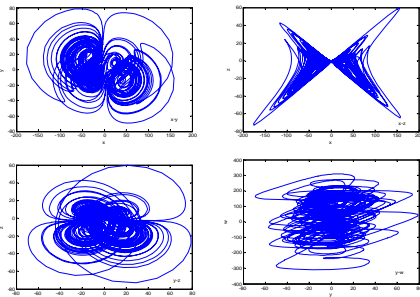


Fig.1 (color online) Phase portraits of system (1)

### 2.2. Lyapunov exponent & bifurcation diagrams

The characteristics of some system motion can be characterize by its Lyapunov exponent, and for a hyper chaotic system, there must have at least two positive Lyapunov exponents. Here, through numerical simulations, the effect on the Lyapunov exponent and the bifurcation of system(1) are analyzed when system parameter  $a$  changes. The Lyapunov exponent spectra and bifurcation diagrams of system(1) with  $a \in [0, 60]$  are shown in Fig.2 and Fig.3, respectively.

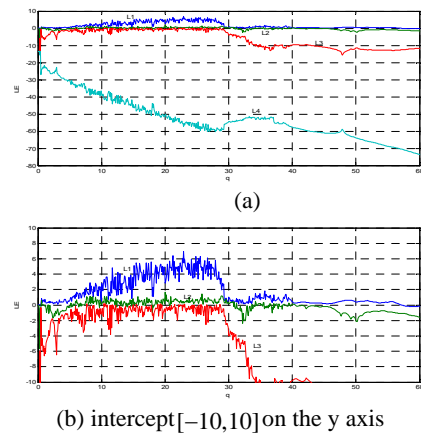


Fig.2 (color online) Lyapunov exponent diagrams of system (1)

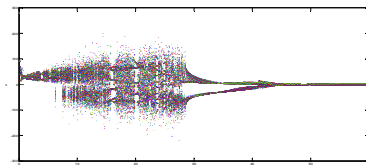


Fig.3 (color online) Bifurcation diagram of system (1) on x axis

In Fig. 2 and Fig. 3, it can be seen that the Lyapunov exponent on the parameter  $a$  is in agreement with the bifurcation diagram. As  $L_4$  always less than  $-10$  in Fig.2, in order to observe the other three exponent expediently, so we intercept  $[-10, 10]$  on the y axis as shown in Fig.2(b). When  $a = 15$ , four Lyapunov exponents of system (1) are  $L_1 = 2.199, L_2 = 0.4077, L_3 = 0, L_4 = -44.64$  respectively. It can be seen that this system is hyper-chaotic.

### 3. Circuit implementation of fractional-order Qi hyper-chaotic system

Through carrying out a series of numerical simulation and analysis of system (1), further for circuit simulation

and realization of the system. Based on the method of approximation conversion from time domain to frequency domain, we utilize the approximation of  $1/s^{0.9}$  with discrepancy 2dBto design the analog circuit, the circuit unit of  $1/s^{0.9}$  is shown in Fig.4. Where  $R_1 = 62.84M\Omega, R_2 = 250K\Omega, R_3 = 2.5K\Omega$   $C1 = 1.232\mu F, C2 = 1.84\mu F, C3 = 1.1\mu F$ .

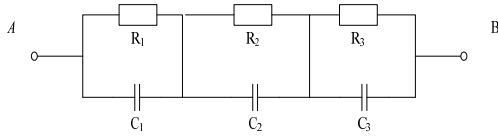


Fig. 4 Unit circuit of  $1/s^{0.9}$

The fractional-order hyper-chaotic circuit is designed. In this circuit, LF353P is selected to be the amplifier and AD633JN (the output gain is 0.1) is selected to be the multiplier. In order to make the change range of state variables can work in the voltage range of the operational amplifier, The parameters are scaled according to the phase portraits of the system, let  $x=50x', y=25y', z=25z', w=100w'$ , the system(1) is modified for circuit implementation, which is described as follow:

$$\begin{cases} \frac{d^q x'}{dt^q} = -ax' + 0.5ay' + 12.5 ey'z', \\ \frac{d^q y'}{dt^q} = 2cx' + dy' - 50 x'z' - 4w' \\ \frac{d^q z'}{dt^q} = -bz' + 50 x'y' \\ \frac{d^q w'}{dt^q} = 0.25 fy' \end{cases} \quad (2)$$

Then the time scale is amplified by letting  $t = \tau_0\tau, \tau_0 = 200$ . Thus the circuit design is shown in Fig.5. Where the module of  $f^{0.9}$  is the circuit unit of  $1/s^{0.9}$  as shown in Fig.4.

According to the circuit diagram in Fig.5, the actual circuit is built to implement the fractional-order hyper-chaotic system(1), and the circuit experimental results are shown in Fig.6 through the TDS2014B digital oscilloscope, which is consistent with the numerical simulation result as shown in Fig.1, which verifies the existence of hyper-chaotic attractor of the fractional-order hyper-chaotic system on the physical level.

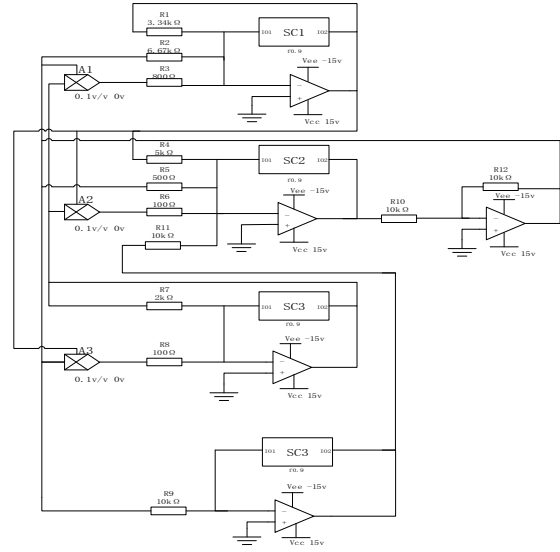


Fig. 5 Circuit diagram of system(1)

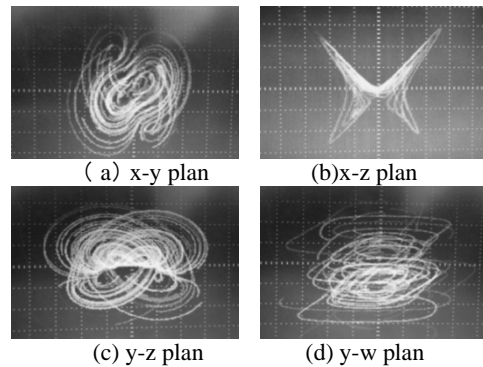


Fig.6 Phase portraits of hyper-chaotic system(1) through the oscilloscope TDS2014B

#### 4. Conclusion

In this paper, the fractional-order Qi hyper-chaotic system is investigated. By analyzing phase portraits, bifurcation diagrams, Lyapunov exponent spectra of fractional-order Qi hyper-chaotic system, it is found that the system has four-wing hyper-chaotic attractors in certain range of parameters. Based on the numerical simulation of the fractional-order hyper-chaotic system. An analog circuit is designed to implement the fractional-order chaotic system, and circuit experiment results are coincide with the numerical simulation results, which provides technical basis and support for the further application of the fractional-order hyper-chaotic system in engineering.

## Acknowledgements

This work is supported by the Young Scientists Fund of the National Natural Science Foundation of China (Grant No.11202148).

## References

1. Lorenz E N. Deterministic Non - periodic Follow. *Atoms. Sci.* 1963, 20: 130-141.
2. Chen G R, Ueta T., Yet another chaotic attractor, *Int. J. Bifurcation and Chaos*. 1999, 9(7): 1465-1466.
3. Lü J H, Chen G R. A new chaotic attractor coined. *Int. J. Bifurcation and Chaos*, 2002, 12(3): 659-661.
4. Liu C X, Liu L, Liu T, et al., A new butterfly-shaped attractor of Lorenz - like system. *Chaos, Solitons and Fractals*. 2006, 28(5): 1196-1203.
5. Qi G Y, Chen G R, van Wyk M A, van Wyk B J and Zhang Y, A four-wing chaotic attractor generated from a new 3-D quadratic autonomous system. *Chaos, Solitons & Fractals*. 2008, 38(3): 705-721.
6. Li W, Hao J H, Qi B, An encryption approach to chaos synchronization communications by using CPRNG. *Acta. Phys. Sin.* 2008, 57(3): 1398-1403.
7. Peng Z P, Wang Ch H, Lin Y, Luo X W, A novel four-dimensional multi-wing hyper-chaotic attractor and its application in image encryption. *Acta. Phys. Sin.* 2014, 63(24): 240506.
8. Yu Ch Y, Zhu J L, Guo J Y, Four-dimensional hyper-chaotic system and application research in signal encryption. *Electric Machines and Control*. 2012, (03): 96-100.
9. Sheng Q W, Jiang B, Chaotic encryption algorithm in the network security technology research and application. *Network Security Technology & Application*, 2014, (8): 51.
10. Hifer R, *Applications of Fractional Calculus in Physics*. New Jersey: World Scientific, 2001.
11. Jia H Y, Chen Z Q, Xue W, Analysis and circuit implementation for the fractional-order Lorenz system. *Acta. Phys. Sin.* 2013, 62(14): 140503.
12. Huang L L, Xin F, Wang L Y, Circuit implementation and control of a new fractional-order hyper-chaotic system. *Acta. Phys. Sin.* 2011, 60(1): 010505.
13. Min F H, Yu Y, Ge C J, Circuit implementation and tracking control of the fractional-order hyper-chaotic Lü system. *Acta. Phys. Sin.* 2009, 58(3): 1456-1461.
14. Xue W, Qi G Y, Mu J J, Jia H Y, Guo Y L, Hopf bifurcation analysis and circuit implementation for a novel four-wing hyper-chaotic system. *Chin. Phys. B*. 2013, 22(8): 080504.

# Research on Early Crop Monitoring Using Photosynthetic Production Index in China

Fengzhi Dai<sup>1</sup>, Li Fan<sup>1</sup>, Daijiro Kaneko<sup>2</sup>, Nozomu Hirose<sup>3</sup>, Chunyu Yu<sup>1</sup>

<sup>1</sup> College of Electronic Information and Automation, Tianjin University of Science and Technology, 80 MailBox, 1038 Daguananlu Road, Hexi District, Tianjin 300222, China

<sup>2</sup> Remote Sensing Environmental Monitor, Inc., Japan

<sup>3</sup> Department of Civil and Environmental Engineering, Matsue College of Technology, Japan  
E-mail: daifz@tust.edu.cn, fanli0476@126.com

www.tust.edu.cn

## Abstract

For monitoring the early stage of crop growth in China, this paper presents a photosynthesis-based monitoring model for grain production. Not only the normalized difference vegetation index and elements such as the growing degree day are considered, the factors of sunshine and the cost of water resource are also considered in the model.

*Keywords:* Crop Monitoring, Photosynthesis, Remote sensing, Water resource

## 1. Introduction

In China, huge population and the shortage of water resource becomes the main contradiction between supply and demand of grain. But Chinese grain production is very important because of its huge consumption.

The World Bank, the Worldwatch Institute<sup>1</sup> and the World Water Council<sup>2</sup> have warned about the present unsustainable use of water resources for irrigation in China, India, and the U.S., which have significant influence on the total quantity of grain production.

On the condition that both the crop yield and water resource are needed, it is required to monitor the grain production and irrigation water synchronously<sup>3,4</sup>.

Early crop monitoring method is mainly based on the meteorological data such as temperature and precipitation. By the application of satellite, remote sensing data are considered gradually<sup>5</sup>. Thus both the remote sensing and the meteorological data are used in the paper<sup>6</sup>.

## 2. Monitoring Crop Production

Conventional crop studies have correlated grain quantity with the growth index of growing degree day (GDD).

$$GDD = \frac{T_{\max} + T_{\min}}{2} - T_b \quad (1)$$

where,  $T_{\max}$  and  $T_{\min}$  are the maximum and minimum daily air temperature.  $T_b$  is the threshold of temperature for the crop, below which the plant physical activity is inhibited and  $T_b$  is always set equal to 10°C.

Rasmussen presented the net primary production (NPP) according to Eq. (2)<sup>7</sup>:

$$NPP = \varepsilon \int_0^t ((aNDVI + b) \cdot PAR) dt \quad (2)$$

where  $\varepsilon$  is the efficiency coefficient,  $t$  is the time,  $a$  and  $b$  are regression coefficients, and  $PAR$  is the photosynthetically active radiation ( $\text{MJ m}^{-2}$ ).  $NDVI$  is the normalized difference vegetation index.

NPP is calculated by the accumulation of NDVI. And the value NDVI can be measured and calculated by satellite remote sensing. Although NPP in Eq.(2) is the photosynthesis-based model, it does not consider the influence of the temperature.

The former photosynthesis-type crop production index (CPI) is defined in Eq.(3) that is concerning the period

from the seeding time  $t_s$  to the harvest time  $t_h$ . PSN is the photosynthesis velocity ( $\text{g m}^{-2} \text{day}^{-1}$ ).

$$\text{CPI} = \int_{t_s}^{t_h} \text{PSN} \, dt \quad (3)$$

But during the grain growth, low-temperature sterility and high-temperature injury to the grain should be considered<sup>8, 9</sup>. The present research also develops the photosynthesis-type monitoring method by measuring the water stress so as to improve Eq.(2). The final form of the photosynthesis rate is defined in Eq.(4)<sup>10</sup>, which considered the solar radiation, air temperature, stomatal opening, and vegetation biomass.

$$\text{PSN} = \frac{a \cdot \text{APAR}}{b + \text{APAR}} \cdot f_{\text{Syn}}(T_c) \cdot \beta_s \cdot e\text{LAI} \quad (4)$$

$a$  and  $b$  are Michaelis -Menten constants,  $\text{APAR}$  is the absorbed photosynthetically active radiation,  $T_c$  is the canopy temperature,  $\beta_s$  is the stomatal opening,  $e\text{LAI}$  is the effective leaf area index, and  $f_{\text{Syn}}$  is the temperature response function of photosynthesis.

Define  $K_{Lster}$  and  $K_{Hster}$  as the coefficients of low-temperature and high-temperature that affect the crop growth.  $T_{Lster}$  and  $T_{Hster}$  are the minimum and maximum temperatures for the crop sterility.  $F_{ster}$  in Eq.(5) is the temperature response function for the crop sterility due to both the low and high temperatures:

$$F_{ster}(T_c) = \int_{t_f}^{t_r} f_{ster}(T_c) \, dt = F_{Lster}(T_c) \cdot F_{Hster}(T_c) \quad (5)$$

where  $F_{Lster}(T_c) = 1 - \exp[k_{Lster}(T_{Lster} - T_c)]$ ,

$F_{Hster}(T_c) = 1 - \exp[k_{Hster}(T_c - T_{Hster})]$ ,  $t_f$  and  $t_r$  are the times of flowering and ripening.

Eq.(5) is obtained from Fig.1(a) and Fig.1(b), and the result is shown in Fig.2(a)<sup>9</sup>. Here  $K_{Lster}=0.8$ ,  $K_{Hster}=0.4$ . Thus CPI is revised from Eq.(3) to Eq.(6):

$$\text{CPI} = \int_{t_s}^{t_h} \text{PSN} \cdot F_{ster}(T_c) \cdot dt \quad (6)$$

### 3. Data Used in The Model

Many researchers have presented crop simulation models that involve growth of crops and incorporate remote sensing data<sup>11</sup>. By measuring growth of crop vegetation using remote sensing instead of simulation, the present paper estimates the photosynthesis rate by treating the growth of crop as a known variable.

Estimation of the photosynthesis rate needs daily weather data of solar radiation and air temperature, so that the daily meteorological data must be taken. The world weather data is most suitable for the index CPI because daily regular data are currently observed as weather reports in real time. The CPI requires the NDVI at the positions of the world weather sites using a database derived from NOAA AVHRR<sup>12</sup>.

### 4. Result of iNDVI

Fig.3 shows the distribution of NDVI data in Southeast Asia<sup>13</sup>. And Fig.4 is the integrated NDVI (iNDVI) of the monitoring points in China. If there is neither water stress nor low temperature sterility around the time of flowering, the crop quantity of production should be high in crop areas where the iNDVI is large.

Therefore the large values of the integrated vegetation index at Jinan and Yichan in Fig.4 suggest a good harvest in those areas. The iNDVI is a vegetation growing index, which measures the crop plant density. However, the iNDVI cannot express the effect of a lack of sunshine, or the influence of low-temperature sterility during flowering and filling.

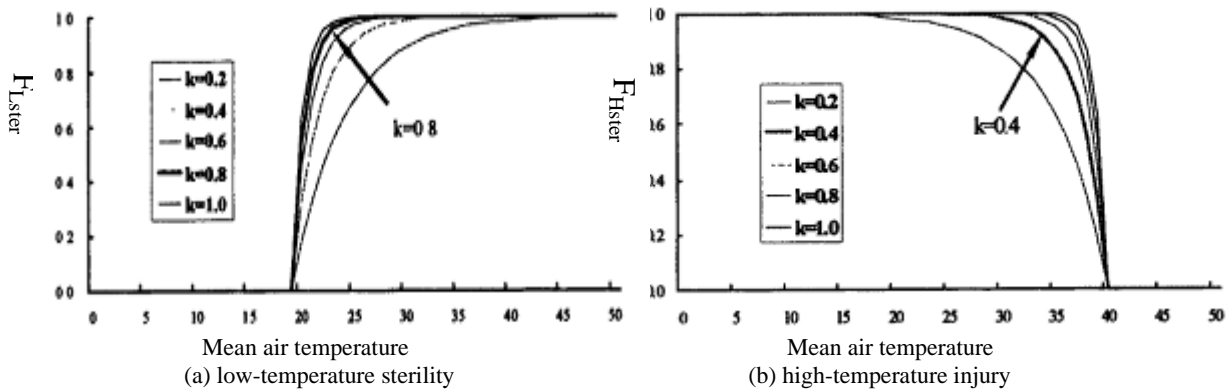
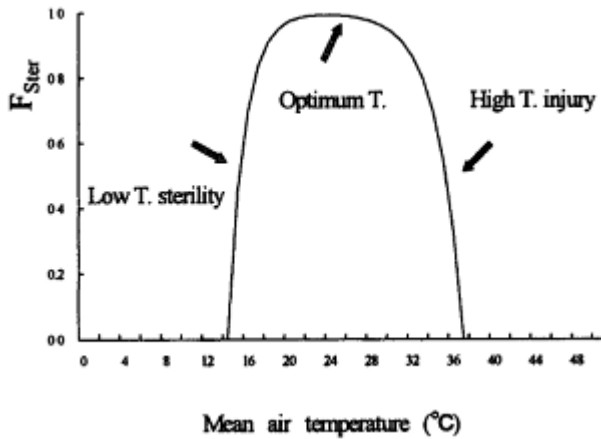
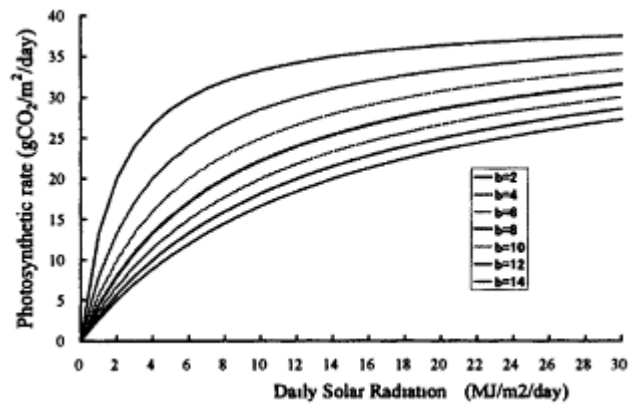


Fig.1 Relationship between  $F_{Lster}$  and  $F_{Hster}$  to air temperature



(a) Temperature response function



(b) Michaelis –Menten type photosynthetic rate

Fig.2 Function and coefficients in temperature response function for the crop sterility

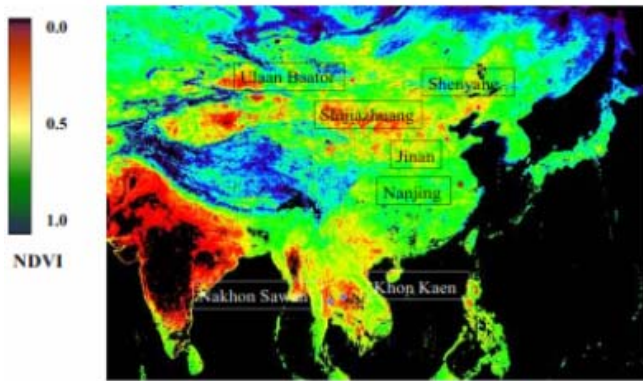


Fig.3 Distribution of NDVI in Southeast Asia

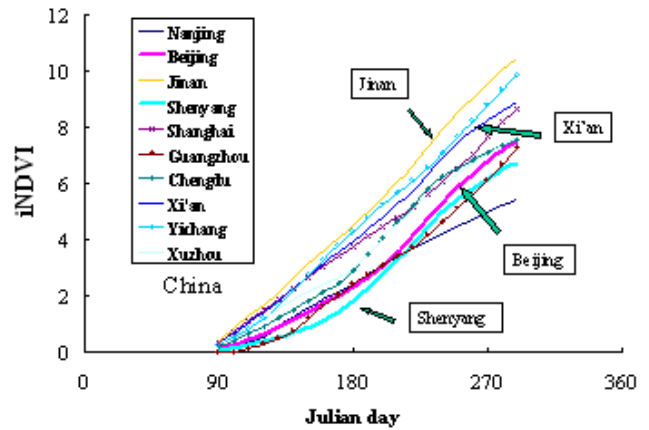


Fig.4. Integrated NDVI (iNDVI) of paddy rice fields in China as a growth index for crop production

### 5. Experiment on Water Stress

For containing the element of water resource into CPI, the effect of water stress to crop growth is experimented. As we know, the reflectance spectrum of plant leaves changes with the different water stress situation. The paper tests the influence of water stress on rice plant by MODIS and Aster<sup>14</sup>. Rice plants are firstly given the appropriate amount of irrigation, and then the watering is stopped to strengthen water stress to the rice plants. The results of NDVI and NDWI (normalized difference water index) are shown in Fig.5 and Fig.6 respectively<sup>3</sup>.

The relationship between NDVI and NDWI is shown in Fig.7 (Four regions are selected: Matsue, Jinan, Hikawa and Thailand). As we know, if the value NDVI is small, it means that the vegetation amount is small. And for the same value of NDVI, the smaller the value NDWI is, the higher the water stress strength is. The distribution of

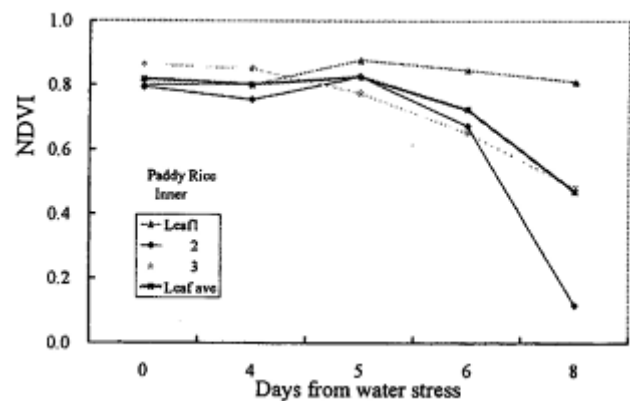


Fig.5 NDVI data in water stress experiment

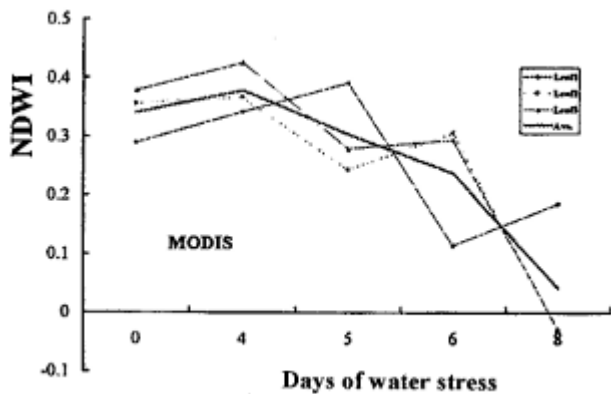


Fig.6 NDWI data in water stress experiment

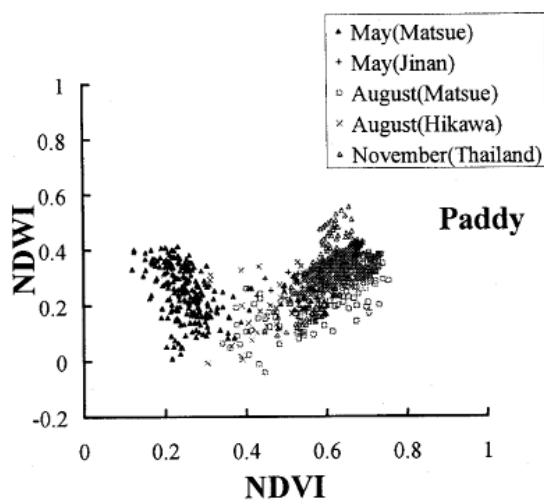


Fig.7 Relationship between NDVI and NDWI

NDVI and NDWI in Fig.7 shows a linear relationship, from which the parameter  $\beta_s$  (the stomatal opening) in CPI can be defined.

## 6. Conclusion

The paper aims to develop a method of early monitoring the crop quantity in production that would be useful in the present era.

Organization of crop monitoring using the model that is based on daily meteorological and satellite data should be established for China to solve the problem with crop growth<sup>15</sup>. Strategies for crisis management should be available in advance. Technical collaboration and information supply for early warning by the monitoring method proposed in this paper would be useful in guiding agricultural policies of Asian countries.

The proposed photosynthesis-based crop production index CPI considers the factors such as solar radiation, air

temperature, vegetation biomass, and stomatal opening using satellite data and world weather data.

## Acknowledgements

The research is partly supported by the Open Foundation (YF11700102) of Key Laboratory for Water Environment and Resources, Tianjin Normal University; and the Scientific Research Foundation of Tianjin University of Science and Technology (20130123).

## References

1. Postel S. *Pillar of sand – Can the irrigation miracle last?*, W. W. Norton & Company, Inc., New York, U.S.A. with the Worldwatch Institute, U.S.A. 1999.
2. World Water Council. The 3rd World water forum, *Thematic/Regional statements Ministerial declaration*, 2003, 105.
3. Daijiro Kaneko. Application of crop production index (CPI) on the Japanese paddy rice and Chinese wheat. *Annual Research Report of Chiba University*, from NII-Electronic Library Service, 2005, pp. 28-33.
4. Kaneko D, Onishi M, and Ishiyama T. Proposal of early monitoring method for crop production in China and India in the recent era of water resources restriction. *Environmental Systems Research*, Japan Society of Civil Engineering, 31(2003): 235-244.
5. Food and Agriculture Organization of the United Nations. *(FAO FAOSTAT Database, 2003)*.
6. Kaneko D. Estimation of global solar radiation using world weather data for early monitoring of crop production by satellites, in *Proc. 6th symp. water resources*, 2002, 677-682.
7. Rasmussen MS. Developing simple, operational, consistent NDVI-vegetation models by applying environmental and climatic information: Part II. Crop yield assessment. *Int. J. Remote Sensing*, 19(1)(1998): 119-137.
8. Matsui T, Namuco OS, Ziska LH and Horie T. Effects of high temperature and CO<sub>2</sub> concentration on spikelet sterility in indica rice. *Field Crops Research*, 51(1997): 213-219.
9. D. Kaneko, M. Ohnishi. Modeling on indices for monitoring crop production using meteorological data and Vegetation Index NDVI. *Japanese J. Crop Science*. 72(2) (2003): 92-93.
10. D. Kaneko, T. Itohara, M. Ohnishi, T. Ishiyama. Early warning method for rice production using remote sensing and meteorological data: Photosynthetic crop production index. *WIT Trans. Ecology and the Environment*, Vol.84 (2005): 815-824.
11. Monteith J L. The quest for balance in crop modeling. *Agronomy J.*, 88(1996): 695-697.
12. Tateishi R. Twenty-year global 4-minute AVHRR NDVI dataset, (CEReS. Chiba University, 2001).



13. Daijiro Kaneko, Masao Ohnishi, Takashi Ishiyama, Ryutaro Tateishi. Proposal for Early Crop Monitoring Using a Photosynthetic Production Index and Remotely Sensed Data, in *Proc. 4th Int. Crop Science Congress*, 2004. Available from [http://www.cropscience.org.au/icsc2004/poster/2/8/252\\_daijir.htm#TopOfPage](http://www.cropsscience.org.au/icsc2004/poster/2/8/252_daijir.htm#TopOfPage)
14. Li Jun, Dai Fengzhi, Li Yuan, Yu Chunyu, Hirose Nozomu, Analysis the vegetation and soil moisture in Beijing-Tianjin area to prevent desertification by long-term satellite remote sensing. *Applied Mechanics and Materials*, Vol. 385-386 (2013): 388-391.
15. Elenita Dano, Elpidio Peria. Emergency or expediency? A study of emergency rice reserve schemes in Asia. *A joint publication of AFA and AsiaDHRRRA*, 2006. Available from <http://asiadhrra.org/wordpress/wp-content/uploads/2008/05/rice%20reserve%20scheme.pdf> or <http://asiadhrra.org/wordpress/2007/12/16/emergency-or-expediency-a-study-of-emergency-rice-reserve-schemes-in-asia/>

# Design and Implementation of Motor Test System based on Virtual Instrument

Yulong Xia<sup>\*</sup>, Huailin Zhao

*School of Electrical & Electronic Engineering, Shanghai Institute of Technology, Shanghai, 201418, China*

Jihong Zhu, Yang He

*Department of Computer Science & Technology, Tsinghua University, Beijing, 100084, China*

*zhao\_huailin@yahoo.com*

## Abstract

Because of using Windows Multimedia Clock, most of existing test system based on General Computer has problems of inaccurate timing and poor real-time capacity. A motor test system is developed for improving above problems and testing more motors simultaneously by serial communication with high baud rate. The test system software uses LabVIEW development platform and is developed with the idea of software engineering, which is used to make each module functionally independent and to improve reliability of the system. Simultaneously the test system uses the characteristic of LabVIEW to complete relatively accurate timing tasks and has excellent portability. In communications, it is used that professional serial port board supporting high baud rate and bus connections. After using the system, it shows that the system is not only reliable, easy to operate, high availability and reduces test costs, but also it is able to meet the needs of the actual test.

Key words: Virtual Instrument; Motor Test System; Timing Tasks; High baud rate; Bus connections

## 1. Introduction

Virtual instrument, which integrates computer hardware resources with instrument hardware resources by software, is a computer-based automated test equipment system. Compared with traditional instruments, Virtual Instrument stresses that software is the core of instruments.

In the development of software, this system needs to collect and transfer data, storage and do other work. Software design is not only the most important and complex part of the entire test system, but the core of the test system. Therefore, choosing the right software development tools can play a multiplier effect. Because of easy to use and convenient, LabVIEW is more fit to this system<sup>1</sup>.

LabVIEW (Laboratory Virtual Instrument Engineering Workbench) is an innovative software product of

National Instruments (referred to as NI). LabVIEW is a graphical programming language, known as the "G" language. G refers Graphical Programming Language. Compared with traditional software development language, graphical programming approach can save more than 85 percent of program development time and the speed of developed program is not affected. This doesn't only reflect a high level of efficiency, but also brings convenience from the LabVIEW controls. Coupled with LabVIEW's outstanding performance at data acquisition, analysis, chart displays and other aspects, LabVIEW program language has become a first alternative to this system<sup>2</sup>.

In the aspect of communication, because of higher baud rates in the system, common serial port devices do not meet the requirement and devices' reliability is not well, so professional MOXA serial port board is selected. The bus is selected as the connection of communication link. Through broadcasts the command is sent to the next

---

<sup>\*</sup> 201418, No.100, Haiquan Rd., Shanghai, China

© *The 2015 International Conference on Artificial Life and Robotics (ICAROB 2015), Jan. 10-12, Oita, Japan*

crew. At the same time there is only one answer audience-bit machine, so data interference on the link can be reduced greatly.

## 2. The Structure of Motor Test System

In Fig.1, it shows that the entire test system is made of a PC and four next crews, each of which is made of controller, Drive and sensor. Based on internal communication protocol, the PC communicates with each controller via RS-422 at bus link. Through graphic user interface, PC encapsulates the command that comes from the test staff into 9 bytes data frame with header, device code, command data, the checksum. Because PC connects with the next crew by bus connections, after PC sends the data, all the controller can receive this data. After receiving the data frame from PC, firstly, controller determines whether the device code field of data frame matches device equipment receiving this frame data. If not match, this frame data is discarded. Otherwise controller will calculate the checksum to verify the accuracy of the frame data. If controller confirms the correct frame, decapsulates the frame date to get command data, then send command data to the drive. After getting command from the controller, the drive makes motor work as testers' intention. Voltage, current, speed and other parameters of the motor running captured by the sensor and forming an analog signal sent to the A / D converter. A / D converter analog signal coming from the sensor is converted into a digital signal, and then sent to the controller. According to internal communication protocol, controller encapsulates data into 21-byte frames, sent to the host computer by serial devices through RS422 bus. After receiving the data frame, the same as controller, PC also verify the checksum to ensure the correct frame data, analyze the frame to get voltage, current, speed and other information from tested motor, and displayed in the interface<sup>3</sup>.

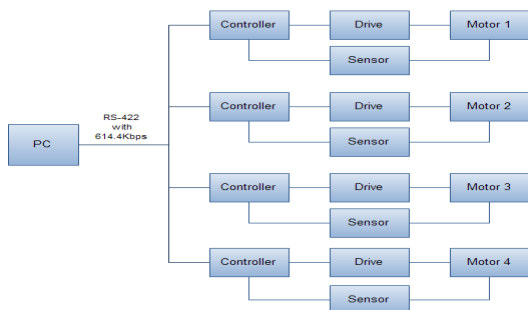


Fig. 1 The diagram of Motor Test System's structure

## 3. Software Design of Motor Test System

### 3.1. Requirement Analysis

Fig.2 is a diagram of Each module of Motor Test System.

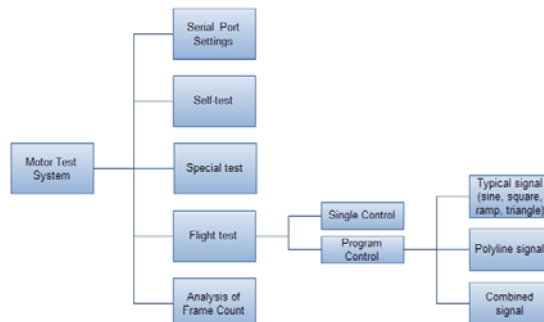


Fig. 2 Each module of Motor Test System

Serial port settings module provides many functions, which are setting number, baud rate and other serial interface attributes. Because the requirements of this system is that the baud rate 614.4Kbps, while common serial port device does not yet support such a high baud rate, so this system selected MOXA serial port board.

This system is divided into three test modules: self test, special tests and flight tests.

In the self test, the main task is to test the state of communication link. Defined test state is divided into checking, normal and abnormality. Firstly, after turning low-voltage power on, the PC sends self test commands to the four devices in round robin way and maintains a counter for each device. Secondly, if only the PC receives the next crew feedback information that indicates that this equipment is normal, the PC will make the counter of the equipment plus one. Finally, if only there are three continuous data frame that indicates the state is normal, self test will be passed.

In the special test, the main task is to test the state of the single specified motor at low speed. Firstly, after turning high voltage power on, the next crew receives from the PC's special test execution command and the motor runs 5 seconds at low speed. And the next crew timely feedback to the PC with information that indicates that the motor has begun to run and could send status query command. Then the PC send "status query command" every 10ms, the PC displays feedback that come from the controller. Finally, testers will find whether the next crew and the motor are normal or not.

In the flight test, the control can be divided into single control and program control. Single control can be controlled by modifying the interface control value; in program control, after configuring the timing command in the timing configuration module for single or

multiple motor, then start program control. The PC sends these preconfigured programmed commands at one command in 2ms intervals. For each motor, it will receive one command at each 8ms. After receiving command data, the next crew will follow the commands to complete control and feedback status information to the PC.

After the test, the PC can save data and do further analysis offline. The PC supports to analysis for frame count in order to count the number of loss frames, heavy frames frame, frame loss rate, and heavy frame rate<sup>4</sup>.

### 3.2. Design of Main Modules

#### 3.2.1 Flight Test Module

Round robin mode has a clear structure, clear program flow, fast response. But if a single control does not occur, the round robin mode will still check the flag variable, which will be a great waste of CPU. On the contrary, the event structure is not only to reduce the CPU load, but has a timely response. More importantly, it uses queue to store time of the trigger mode, thus which avoids missing any events. Different from a single control, once program control is launched, it will be necessary to send one command in 2ms interval. There are two schemes could be used. One is to generate a command and to send it to controller immediately, the benefits of which is to need less memory space but requires CPU to read and write memory operations. The other is to generate all the commands before sending the data and to store the commands into disk file. Once the program control is start, the commands will be read into memory one time from disk file and be sent one by one, the benefits of which can greatly reduce CPU's load during transmission greatly, which is because the commands has been read in contiguous memory space. It guarantees the timing requirements of 2ms. At the same time, because the data stored in the hard disk file, you can also reuse the same program control. In comparison, the second solution is clearly better.

By using one or more queues, multiple threads issue is solved in elegant and safe way. Producer thread insert elements to the queue, the consumer thread and remove them. Using the queue can safely pass data from one thread to another thread. Blocking queue can not only accomplish this task, but if elements are tried to add to the full queue, or to remove from the empty queue, thread will both be blocked. This will further improve the utilization of the CPU. Fortunately, LabVIEW has integrated producer consumer model based on blocking queue into its own development environment. This is producer-consumer recycling based on data or event<sup>5</sup>.

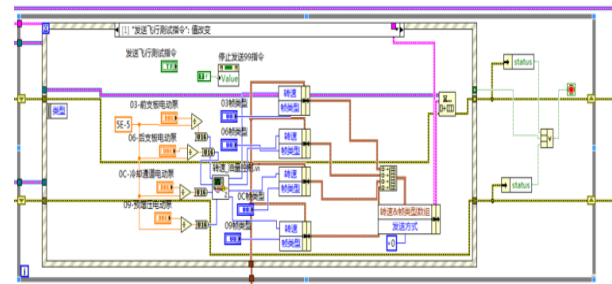


Fig. 3 The producer loop based event

As shown in Fig.3, the outermost layer is a while loop, whose inside is the event structure. Event structure in a while loop can handle a mouse click, keyboard pressing and many other events until the end of the loop. After a single control event and the program control event occurs, the system will both place commands in the queue. And each consumer loop fetches command from the queue and sends it to controller. The flag variable should be set in the respective event branch, which make that consumer loops will not affect each other.

#### 3.2.2 Analysis frame count module

This system uses serial communication at 614.4Kbps baud rate and bus connections. High-voltage power affecting for baud rate and seizing bus are likely to be the weak part that affects for the stability of the system. Therefore, it is necessary to detect and analyze the frame count. In internal communication protocol of the system, frame count field is an 8-bit unsigned integer type, ranging from 0 to 255. Under normal circumstances, due to data overflow will become 0 and then continue to accumulate the feedback information in the next crew; the frame count field will accumulate from 0 to 255, and then continue to accumulate. Therefore, the quantity of loss frames can be got by the following formula:

$$m = \begin{cases} n_2 - n_1 + 1 & , n_2 > n_1 \\ 255 + n_2 - n_1 & , n_2 < n_1 \end{cases} \quad (1.1)$$

$n_2$  represents current frame count,  $n_1$  represents previous frame count.

As shown in Fig.4 and Fig.5, it is single motor/ multiple motors frame count analysis under the high-power supply. In anyone of these charts, the vertical axis is the difference between the current frame count and frame count of the previous frame. Normally, if the overflow does not occur, the difference will be 1; if the overflow occurs, the difference will be -255.

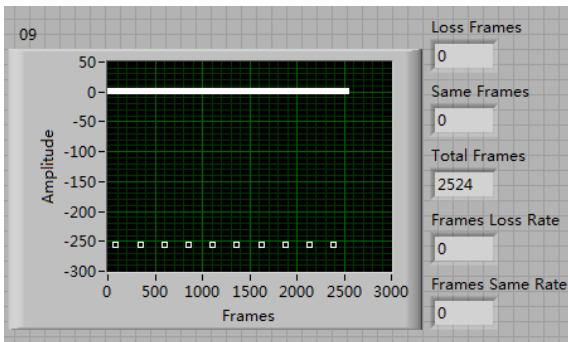


Fig. 4 Frame count analysis for single motor

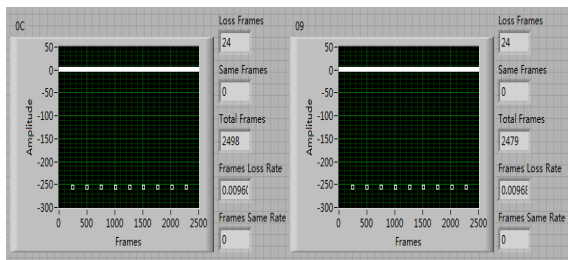


Fig. 5 Frame count analysis for two motors

As shown in Table 1, when there is only one running motor, even if in the case of high baud rate, communication would not have dropped any frame. When multiple motors are running simultaneously, because of bus connection, the data will seize the bus to result in dropped frames. However, frame loss rate is less than 1%, so communication is very reliable.

Table. 1 The analysis of frame count

Type	Motor_ id	The total number of frames	The number of loss frames	Frame loss rate
Single	09	2524	0	0.00%
Multiple	0C	2498	24	0.960%
	09	2479	24	0.968%

### 3.2.3 Timing Transfer Modul

Programmers rack their brains to pursue the goal that is to control precisely for timing. Regrettably, because of the absence of a hardware timer cases, The highest timing accuracy under Windows operating system is 1ms. And the 1ms talking about here refers to the computer system time maintained by a battery. After LabVIEW 7.x version, there is emerging a new timing structure - timing loop, which is available as a Windows operating system to improve the accuracy of the program effective means of time control. However, the timing loop will take up more system resources<sup>6</sup>.

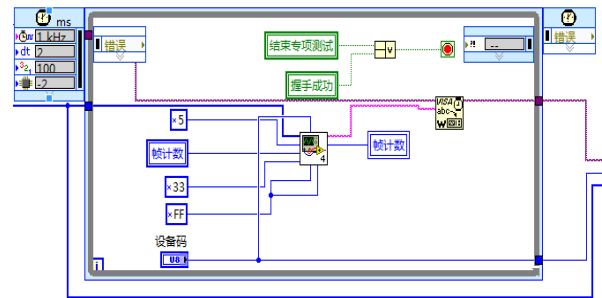


Fig. 6 Timing loop

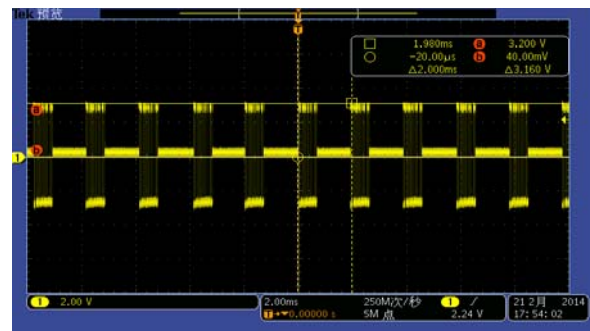


Fig. 7 Sending interval measured by oscilloscope

As shown in Fig.6, the main task in the timing loop is to send data through the serial port every 2ms. As shown in Fig.7, in the actual testing, the time measured by oscilloscope to send data through the serial port is 2ms, and no frame loss.

## 4. Conclusion

This test system uses LabVIEW as a development platform. The code is clear, easy to be maintained, reused and expanded. This system has achieved the serial communication, motor control, data acquisition, preservation and analysis for frame count. In addition, the motor control module of the system is able to execute more precise time control on top of the operating system. Testers can not only enjoy the convenience of the operating system, but can use the system to complete high precision timing test tasks. Test system described here provides a solution for coping with high real-time and high baud rate serial communications, and can provide certain references to the college labs or enterprises in building up testing systems based on virtual instrument.

## 5. References

1. T.H. Lu, J. Wang, Design of Real-time Monitoring-survey System for Motor Power Consumption Based on LabVIEW, Computer Measurement & Control 2012,20 (3) : 580-582, 609.

2. R. Bitter, T. Mohiuddin, M. Nawrocki, LabVIEW: Advanced Programming Techniques, 2nd ed., CRC Press, Boca Raton, 2007.
3. J.P. Chen, S.Z. Wang, W.Y. Wu, Implementing method of serial communication data checksum based on LabVIEW, Process Automation Instrumentation 29 (2008) 32-34.
4. J. Huang, J.H. Zhu and X.M. Yuan, Software Engineering in the Application of Virtual Instrument-Based Dynamics Testing System for UAV, Journal of Communication and Computer 10 (2013) 926-932.
5. Y. Yang, M.G. Wang, Y.L. Zhao, Design of test system for flight control computer based on LabVIEW, The Electronic Measurement Technology 32 (2009) 96-99
6. LabVIEW User Manual, National Instrument Corporation. April, 2007.

# Consensus Problem of Distributed Multi-agent Systems\*

Huailin Zhao<sup>†</sup>

*School of Electrical & Electronic Engineering, Shanghai Institute of Technology, Shanghai, 201418, China*

Wei Ren

*Department of Electrical Engineering, UCR, CA92521, USA*

Jian Jiang

*School of Mechanical Engineering, Shanghai Institute of Technology, Shanghai, 201418, China*

Masanori Sugisaka

*Alife Robotics Corporation LTD, Oita, Japan*

*zhao\_huailin@yahoo.com*

## Abstract

The paper focuses on the consensus problem of distributed control systems. It's the basic research subject related with the distributed coordination of multiple robots such as the unmanned robots which has been a very active research one studied widely by the control researchers. The paper mainly discusses the most typical topics which have made large progress in distributed multi-agent coordination in recent years including the system dynamics, the time delay effect, the network topology, the convergence, and so on.

*Keywords:* multi-agent system, consensus, distributed coordination, network topology, convergence

## 1. The general description

Consensus refers to the typical group behavior of the multi-agent system that all the agents reach asymptotically a certain common agreement based on a local distributed protocol, with or without predefined common speed and orientation.

To the distributed control of a group of autonomous robots, the main objective is typically to have the whole group of robots working in a cooperative way base on a distributed protocol. The cooperative refers to a close

relationship among all robots in the group where information sharing plays a key role. The distributed method has many advantages in achieving cooperative group performances, especially with low operational costs, less system requirements, high robustness, strong adaptivity, and flexible scalability, therefore has been widely interested and recognized<sup>[1-2]</sup>

Let's express the typical consensus problem based on which we discuss the consensus problem. Consider a group of  $n$  agents, each with single-integrator kinematics described by

---

\* 201418, No.100, Haiquan Rd., Shanghai, China

$$\dot{x}_i = u_i(t); i=1, 2, \dots, n \quad (1)$$

where  $\dot{x}_i$  and  $u_i(t)$  are, respectively, the state and the control input of the  $i$ th agent. A typical consensus control algorithm is designed as

$$u_i(t) = \sum_{j=1}^n a_{ij}(t)[x_j(t) - x_i(t)] \quad (2)$$

where  $a_{ij}(t)$  is the  $(i, j)$ th entry of the corresponding adjacency matrix at time  $t$ . The main idea with formula (2) is that each agent moves towards the weighted average of the states of its neighbors. Given the switching network pattern due to the continuous motions of the dynamic agents, coupling coefficients  $a_{ij}(t)$  in formula (2), so the graph topologies, are generally time-varying. There is the conclusion that consensus is achieved if the underlying directed graph has a directed spanning tree in some jointly fashion in terms of a union of its time-varying graph topologies [1-4].

Consensus does as a fundamental principle for the design of distributed multi-agent coordination algorithms. Therefore, investigating consensus has been a main research direction in the study of distributed multi-agent coordination. To establish the relationship between the study of consensus algorithms and many physical properties inherited in practical systems, it is necessary and meaningful to study consensus by considering many practical factors such as actuation, control, communication, computation, robot dynamics, and so on, which characterize some important features of practical systems [1-6].

Please make sure that shared information is a necessary condition for coordination. Information necessary for cooperation may be shared in various ways. For example, relative position sensors may enable robots to construct state information for other robots [7], knowledge may be communicated among robots using a wireless network [8], or joint knowledge might be preprogrammed into the robots before a mission begins [9]. Based on this concept, information exchange becomes a key problem in coordination control.

## 2. The system dynamics

Consensus is concerned with the behavior of a group of robots, so it is natural to consider the system dynamics for practical robots in the study of the consensus problem. Although the study of consensus under various system dynamics is due to the existence of complex dynamics in practical systems, it is also interesting to observe that system dynamics play an important role in determining the final consensus state. For example, the well studied consensus of multi-agent systems with single-integrator kinematics often converges to a constant final value. However, consensus for double-integrator dynamics might admit a dynamic final value. These important problems make the study of consensus under various system dynamics become hot.

As a direct extension of the study of the consensus problem for systems with simple dynamics, for example, with single-integrator kinematics or double-integrator dynamics, consensus with general linear dynamics was also studied [10-12], where research is mainly devoted to finding feedback control laws such that consensus (with the output states) can be achieved for general linear systems.

$$\dot{x}_i = Ax_i + Bu_i, \quad y_i = Cx_i \quad (3)$$

where  $A$ ,  $B$ , and  $C$  are constant matrices with compatible sizes. Apparently, the well studied single-integrator kinematics and double-integrator dynamics are special cases of system (3) for properly choosing  $A$ ,  $B$ , and  $C$ .

Consensus for complex systems has been extensively studied too. Here, the term consensus for complex systems is used for the study of consensus problem when the system dynamics are nonlinear or with nonlinear consensus algorithms [13-17].

Although the complex system dynamics are different from the well studied single-integrator kinematics and double-integrator dynamics, the main research problem is same, namely, to drive all agents to some common states through local interactions among agents. Similarly to the consensus algorithms proposed for systems with simple dynamics, the consensus algorithms used for these complex models are also



based on a weighted average of the state differences, with some additional terms if necessary. Main research work has been conducted to design proper control algorithms and derive necessary or sufficient conditions such that consensus can be achieved ultimately.

### 3. The time delay

Time delay exists in almost all practical systems due to several reasons such as limited communication speed, extra time required by the sensor to get the measurement information, computation time required for generating the control inputs and execution time required for the inputs being acted. Generally, time delay reflects an important property inherited in practical systems due to actuation, control, communication, and computation.

Knowing that time delay might degrade the system performance or even destroy the system stability, studies have been conducted to investigate its effect on system performance and stability. A well studied consensus algorithm for system (1) is given in formula (2), where it is now assumed that time delay exists. Two types of time delays, communication delay and input delay, have been considered in some research. Communication delay accounts for the time for transmitting information from source to destination. More precisely, if it takes time  $T_{ij}$  for agent  $i$  to receive information from agent  $j$ , the closed-loop system of (1) with (2) under a fixed network topology becomes

$$\dot{x}_i(t) = \sum_{j=1}^n a_{ij}(t)[x_j(t - T_{ij}) - x_i(t)] \quad (4)$$

An explanation of (4) is that at time  $t$ , agent  $i$  receives information from agent  $j$  and uses data  $x_j(t - T_{ij})$  instead of  $x_j(t)$  due to the time delay. Please note that agent  $i$  can get its own information instantly, therefore, input delay can be considered as the sum of computation time and execution time. More precisely, if the input delay for agent  $i$  is given by  $T_i^p$ , then the closed-loop system of (1) with (2) becomes

$$\dot{x}_i(t) = \sum_{j=1}^n a_{ij}(t)[x_j(t - T_i^p) - x_i(t - T_i^p)] \quad (5)$$

Clearly, (4) refers to the case when only communication delay is considered while (5) refers to the case when only input delay is considered. It should be emphasized that both communication delay and input delay might be time-varying and they might co-exist at the same time.

The main problem involved in consensus with time delay is to study the effects of time delay on the convergence and performance of consensus [18]. The existing study of consensus with time delay mainly focuses on analyzing the stability of consensus algorithms with time delay for various types of system dynamics, including linear and nonlinear dynamics. Generally, consensus with time delay for systems with nonlinear dynamics is more challenging. For most consensus algorithms with time delays, the main research topics is to determine an upper bound of the time delay under which time delay does not affect the consensusability. For communication delay, it is possible to achieve consensus under a relatively large time delay threshold. A notable phenomenon in this case is that the final consensus state is constant. Considering both linear and nonlinear system dynamics in consensus, the main tools for stability analysis of the closed-loop systems include matrix theory [19], Lyapunov functions [20], frequency-domain method [21], passivity [22], and the contraction principle [23].

### 4. The Network Topology

In multi-agent systems, the network topology among all robots plays a very important role in determining consensus. The objective here is to explicitly identify necessary or sufficient conditions on the network topology such that consensus can be achieved under properly designed algorithms.

It is often reasonable to consider the case when the network topology is deterministic under ideal communication channels. Accordingly, main research on the consensus problem was conducted under a deterministic fixed or switching network topology. That is, the adjacency matrix  $A(t)$  is deterministic. In some other times, when considering random communication

failures, random packet drops, and communication channel instabilities inherited in physical communication channels, it is necessary and important to study consensus problem in the stochastic setting where a network topology evolves according to some random distributions. That is, the adjacency matrix  $A(t)$  is stochastic. By now the current study on consensus over stochastic network topologies has shown some interesting results regarding that how to determine the probability of reaching consensus almost surely and when the network topology itself is stochastic as well as what are the advantages and disadvantages of the stochastic network topology regarding such as robustness and convergence rate when compared with the deterministic network topology.

As is well known, disturbances and uncertainties often exist in networked systems such as channel noise, communication noise, uncertainties in network parameters, etc. In addition to the stochastic network topologies mentioned above, the effect of stochastic disturbances and uncertainties on the consensus problem also needs investigation [24-25]. Study has been mainly devoted to analyzing the performance of consensus algorithms subject to disturbances and to presenting conditions on the uncertainties such that consensus can be achieved. Besides, another interesting direction in dealing with disturbances and uncertainties is to design distributed local filtering algorithms so as to save energy and improve computational efficiency. Distributed local filtering algorithms play an important role and seems more effective than traditional centralized filtering algorithms for multi-agent systems [26-27].

## 5. The convergence analysis

To the control system, the convergence problem is always an important topic. Of course it is one of the key performance measure for consensus algorithms too.

The existing study mainly focuses on the analysis of the convergence speed under various network topologies and optimization of the convergence speed for certain

given network topologies. Considering the fact that consensus under different network topologies may behave different convergence speeds, a natural topic is how to design an optimal network topology with proper adjacency matrix such that optimal convergence speed can be achieved [28-29].

The study of convergence speed for the consensus problem, finite-time consensus, reaching consensus in a finite time, has also been studied. Compared with most existing research on the consensus problem, finite time consensus behaves a disturbance rejection property and robustness against uncertainties. In addition, due to the finite-time convergence, it is often possible to decouple the consensus problem from other control objectives when they are considered simultaneously [30-31].

Please note that the existing research on finite-time consensus mainly focuses on systems with simple dynamics, such as single-integrator kinematics and double-integrator dynamics, in the continuous-time field. Because many practical systems are better and more proper to be described by general linear or nonlinear dynamics, it is natural to study finite-time consensus for systems with general linear or nonlinear dynamics further. Besides, it is meaningful to study finite-time consensus in the discrete-time field. Some research on this topic can be found in [32-33], where the objective is to compute the final consensus value for all agents in a finite number of steps.

## 6. The conclusion

The consensus problem is the basic and very important topic in coordination control of the multi-agent system. It mainly refers to some basic concepts including the system dynamics, the time delay and the system network topology. The convergence is also an very important concept. But the paper doesn't introduce the consensus and the convergence related with the subjects such as asynchronous effects, sampled-data framework, quantization, and so on. The existing research on the consensus problem has covered a number of physical

properties for practical systems and control performance analysis. However, the study of the consensus problem covering multiple physical properties or control performance analysis has been largely ignored. Therefore more problems discussed in the above need to be taken into consideration simultaneously when studying the consensus problem in the future.

## 7. References:

1. W. Ren and R. W. Beard, *Distributed Consensus in Multi-vehicle Cooperative Control*, ser. Communications and Control Engineering. London: Springer-Verlag, 2008.
2. Yongcan C., Wenwu, Y., Wei R., Guanrong C.. "An overview of recent progress in the study of distributed multi-agent coordination", *IEEE Transactions on Industrial Informatics*, Vol. 9, No. 1, Feb., 2013, p427-348
3. W. Ren and R. W. Beard, "Consensus seeking in multiagent systems under dynamically changing interaction topologies," *IEEE Transactions on Automatic Control*, vol. 50, no. 5, pp. 655–661, May 2005.
4. L. Moreau, "Stability of multi-agent systems with time-dependent communication links," *IEEE Transactions on Automatic Control*, vol. 50, no. 2, pp. 169–182, February 2005.
5. W. Ren, R. W. Beard, and E. M. Atkins, "Information consensus in multivehicle cooperative control: Collective group behavior through local interaction," *IEEE Control Systems Magazine*, vol. 27, no. 2, pp.71–82.
6. W. Ren and Y. Cao, *Distributed Coordination of Multi-agent Networks: Emergent Problems, Models, and Issues*, ser. Communications and Control Engineering. London: Springer-Verlag, 2011.
7. A. G. Dimakis, S. Kar, J. M. F. Moura, M. G. Rabbat, and A. Scaglione, "Gossip algorithms for distributed signal processing," *Proceedings of the IEEE*, vol. 98, no. 11, pp. 1847–1864, 2010.
8. P. P. Menon and C. Edwards, "Decentralised static output feedback stabilisation and synchronisation of networks," *Automatica*, vol. 45, no. 12, pp. 2910–2916, 2009.
9. C. W. Wu, *Synchronization in Complex Networks of Nonlinear Dynamical Systems*. World Scientific, 2007.
10. J. H. Seo, H. Shim, and J. Back, "Consensus of high-order linear systems using dynamic output feedback compensator: Low gain approach," *Automatica*, vol. 45, no. 11, pp. 2659–2664, 2009.
11. Z. Li, Z. Duan, G. Chen, and L. Huang, "Consensus of multiagent systems and synchronization of complex networks: A unified viewpoint," *IEEE Transactions on Circuits And Systems-I: Regular Papers*, vol. 57, no. 1, pp. 213–224, 2010.
12. T. Yang, S. Roy, Y. Wan, and A. Saberi, "Constructing consensus controllers for networks with identical general linear agents," *International Journal of Robust and Nonlinear Control*, vol. 21, no. 11, pp. 1237–1256, 2011.
13. J. Lu and D. W. C. Ho, "Globally exponential synchronization and synchronizability for general dynamical networks," *IEEE Transactions on Systems, Man, and Cybernetics, Part B: Cybernetics*, vol. 40, no. 2, pp. 350–361, April 2010.
14. L. Wang and X. Wang, "New conditions for synchronization in dynamical communication networks," *Systems and Control Letters*, vol. 60, no. 4, pp. 219–225, 2011.
15. W. Ren, "Distributed leaderless consensus algorithms for networked EulerLagrange systems," *International Journal of Control*, vol. 82, no. 11, pp. 2137–2149, 2009.
16. Q. Hui, W. M. Haddad, and S. P. Bhat, "Finite-time semistability and consensus for nonlinear dynamical networks," *IEEE Transactions on Automatic Control*, vol. 53, no. 8, pp. 1887–1890, 2008.
17. Q. Hui and W. M. Haddad, "Distributed nonlinear control algorithms for network consensus," *Automatica*, vol. 44, no. 9, pp. 2375–2381, 2008.
18. C.-Q. Ma and J.-F. Zhang, "Necessary and sufficient conditions for consensusability of linear multi-agent

- systems,” *IEEE Transactions on Automatic Control*, vol. 55, no. 5, pp. 1263–1268, 2010.
19. F. Xiao and L. Wang, “Consensus protocols for discrete-time multiagent systems with time-varying delays,” *Automatica*, vol. 44, no. 10, pp. 2577–2582, 2008.
  20. J. Cao, G. Chen, and P. Li, “Global synchronization in an array of delayed neural networks with hybrid coupling,” *IEEE Transactions on Systems, Man, and Cybernetics, Part B: Cybernetics*, vol. 38, no. 2, pp. 488–498, April 2008.
  21. Y.-P. Tian and C.-L. Liu, “Consensus of multi-agent systems with diverse input and communication delays,” *IEEE Transactions on Automatic Control*, vol. 53, no. 9, pp. 2122–2128, 2008.
  22. J. Yao, H. O. Wang, Z.-H. Guan, and W. Xu, “Passive stability and synchronization of complex spatio-temporal switching networks with time delays,” *Automatica*, vol. 45, no. 7, pp. 1721–1728, 2009.
  23. W. Wang and J.-J. Slotine, “Contraction analysis of time-delayed communications and group cooperation,” *IEEE Transactions on Automatic Control*, vol. 51, no. 4, pp. 712–717, 2006.
  24. Z. Li, Z. Duan, and G. Chen, “On H1 and H2 performance regions of multi-agent systems,” *Automatica*, vol. 47, no. 4, pp. 797–803, 2011.
  25. H. Kim, H. Shim, and J. H. Seo, “Output consensus of heterogeneous uncertain linear multi-agent systems,” *IEEE Transactions on Automatic Control*, vol. 56, no. 1, pp. 200–206, 2011.
  26. W. Yu, G. Chen, Z. Wang, and W. Yang, “Distributed consensus filtering in sensor networks,” *IEEE Transactions on Systems, Man, and Cybernetics, Part B: Cybernetics*, vol. 39, no. 6, pp. 1568–1577, 2009.
  27. L. Shi, M. Epstein, and R. M. Murray, “Kalman filtering over a packetdropping network: a probabilistic perspective,” *IEEE Transactions on Automatic Control*, vol. 55, no. 3, pp. 594–604, 2010.
  28. J. Zhou and Q. Wang, “Convergence speed in distributed consensus over dynamically switching random networks,” *Automatica*, vol. 45, no. 6, pp. 1455–1461, 2009.
  29. F. Xiao, L. Wang, J. Chen, and Y. Gao, “Finite-time formation control for multi-agent systems,” *Automatica*, vol. 45, no. 11, pp. 2605–2611, 2009.
  30. Y. Cao, W. Ren, and Z. Meng, “Decentralized finite-time sliding mode estimators and their applications in decentralized finite-time formation tracking,” *Systems and Control Letters*, vol. 59, no. 9, pp. 522–529, 2010.
  31. L. Wang and F. Xiao, “Finite-time consensus problems for networks of dynamic agents,” *IEEE Transactions on Automatic Control*, vol. 55, no. 4, pp. 950–955, 2010.
  32. S. Sundaram and C. N. Hadjicostis, “Finite-time distributed consensus in graphs with time-invariant topologies,” in *Proceedings of the American Control Conference*, New York City, NY, July 2007, pp. 711–716.
  33. Y. Yuan, G.-B. Stan, M. Barahona, L. Shi, and J. Gonçalves, “Decentralised minimal-time consensus,” in *Proceedings of the IEEE Conference on Decision and Control*, Orlando, FL, December 2011, pp. 4282–4289.

# Dingle's Model-based EEG Peak Detection using a Rule-based Classifier

Asrul Adam<sup>1</sup>, Norrima Mokhtar, Marizan Mubin

Applied Control and Robotics (ACR) Laboratory, Department of Electrical Engineering, Faculty of Engineering, University of Malaya, 50603 Kuala Lumpur, Malaysia

Zuwairie Ibrahim

Faculty of Electrical and Electronic Engineering, Universiti Malaysia Pahang, 26600 Pekan, Pahang, Malaysia

Mohd Ibrahim Shapiai

Malaysia-Japan International Institute of Technology Universiti Teknologi Malaysia, 81310 Johor Bahru, Malaysia

E-mail: asrul.adam@siswa.um.edu.my, zuwairie@ump.edu.my, norrimamokhtar@um.edu.my, md\_ibrahim83@.utm.my, and marizan@um.edu.my

www.um.edu.my, www.ump.edu.my, www.mjit.utm.my

## Abstract

The employment of peak detection algorithm is prominent in several clinical applications such as diagnosis and treatment of epilepsy patients, assisting to determine patient syndrome, and guiding paralyzed patients to manage some devices. In this study, the performances of four different peak models of time domain approach which are Dumpala's, Acir's, Liu's, and Dingle's peak models are evaluated for electroencephalogram (EEG) signal peak detection algorithm. The algorithm is developed into three stages: peak candidate detection, feature extraction, and classification. Rule-based classifier with an estimation technique based on particle swarm optimization (PSO) is employed in the classification stage. The evaluation result shows that the best peak model is Dingle's peak model with the highest test performance is 88.78%.

*Keywords:* Electroencephalogram (EEG) signal, Peak detection, Rule-based classifier, Particle swarm optimization (PSO), Biomedical applications.

## 1. Introduction

Electroencephalogram (EEG) signal is a microvolt electrical brain signal that is used for recording the brain activity of human behaviors. The most traceable signal pattern exists in the EEG signal is a peak point which signifies the brain activity on particular events or stimulus. The known peak point through the response of the brain can be translated into commands, for example, wheelchair movement.

Peak detection algorithm can be categorized based on four approaches which are time [1], frequency [2], time-frequency [3], and nonlinear [4] domains. In the time domain approach, the peaks are analyzed with respect to time. In frequency domain approach, the peaks are analyzed with respect to frequency. In time-frequency

domain approach, the peaks are analyzed in both time and frequency domain. In nonlinear approach, some statistical parameters of the peaks are analyzed.

Several algorithms [1, 3, 5, 6] are designed by considering different peak models in the time domain approach which are Dumpala's [5], Acir's [6], Liu's [3], and Dingle's [1] peak models. Therefore, this study focuses on the employment on the different peak models into the proposed peak detection algorithm. The performances on the different peak models are evaluated and the best peak model is presented.

## 2. Methodology

Figure 1 shows the algorithm of the EEG signal peak detection using rule-based classifier. In the first stage, the detection of peak candidates is performed to differentiate

---

<sup>1</sup>Applied Control and Robotics Laboratory (ACR), Department of Electrical Engineering, Faculty of Engineering, University of Malaya, Malaysia.

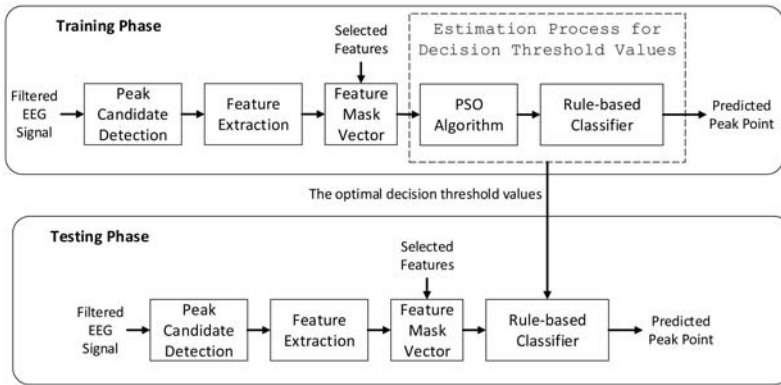


Fig. 1. The EEG signal peak detection algorithm

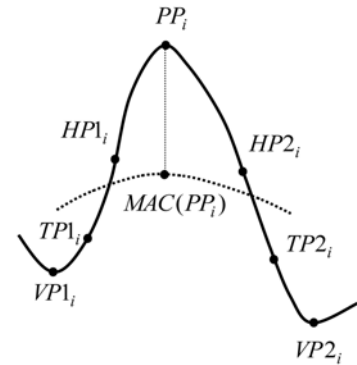


Fig. 2. Peak model parameters

Table 1. List of Different Peak Models and Sets of Feature

Peak Model	Set of Feature	Number of Features
Dumpala <i>et al.</i>	$f_1, f_6, f_{11}, f_{12}$	4
Acir <i>et al.</i>	$f_1, f_2, f_7, f_8, f_{13}, f_{14}$	6
Liu <i>et al.</i>	$f_1, f_2, f_3, f_4, f_6, f_9, f_{10}, f_{11}, f_{12}, f_{13}, f_{14}$	11
Dingle <i>et al.</i>	$f_3, f_6, f_{11}, f_{12}$	4

between a peak candidate and a non-peak point. The second stage is the extraction of peak candidate features. The selected features of all peak candidates based on different peak models are extracted in this stage. Then, the selected peak features of peak candidates act as input to the rule-based classifier. During the training, the decision threshold values are estimated to find the optimal value. The estimation process is done by using PSO algorithm. The optimal decision threshold values are then used during the testing phase. The final output of the training and testing phases is the predicted peak points and non-peak points of the identified peak candidates.

### 2.1. Peak Candidate Detection

A discrete-time signal,  $x(I)$ , of  $L$  points is considered in this stage. Next, the  $i$ th candidate peak point,  $PP_i$ , are identified using three-points sliding window method. Those three-points are denoted as,  $x(I-1)$ ,  $x(I)$ , and  $x(I+1)$  for  $I=1,2,3,\dots,L$ . A candidate peak point is identified when  $x(PP_i - 1) < x(PP_i) > x(PP_i + 1)$  and two associated valley points,  $VP1_i$  and  $VP2_i$ , are in between as shown in Fig. 2. Both valley points exist when  $x(VP1_i - 1) > x(VP1_i) < x(VP1_i + 1)$  and  $x(VP2_i - 1) > x(VP2_i) < x(VP2_i + 1)$ . Another parameters of the  $i$ th peak location are a half point at first half wave ( $HP1_i$ ), a half point at second half wave ( $HP2_i$ ), a turning

point at first half wave ( $TP1_i$ ), a turning point at second half wave ( $TP2_i$ ), and a moving average curve ( $MAC(PP_i)$ ).

### 2.2. Feature Extraction

The peak features are calculated based on the eight parameters as shown in Fig. 2. The total peak features obtained from the existing peak models are 14 [7]. Those features are peak-to peak amplitude at the first half wave,  $f_1$ , peak-to peak amplitude at the second half wave,  $f_2$ , turning point amplitude at the first half wave,  $f_3$ , turning point amplitude at the second half wave,  $f_4$ , moving average amplitude,  $f_5$ , peak width,  $f_6$ , first half wave width,  $f_7$ , second half wave width,  $f_8$ , turning point width,  $f_9$ , half point width,  $f_{10}$ , peak slope at the first half wave,  $f_{11}$ , peak slope at the second half wave,  $f_{12}$ , turning point slope at the first half wave,  $f_{13}$ , and turning point slope at the second half wave,  $f_{14}$ . The list of peak models with their feature set is tabulated in Table 1.

### 2.3. Rule-based Classifier

A rule-based classifier is employed to distinguish either the candidate peak is a true peak or true non-peak from the extracted features. Each feature has a corresponding threshold value in the classification process. Given a set of features, a true peak only can be identified if all the feature values are greater or equal than the decision threshold values. The form of the rule is,

IF  $f_1 \geq th_1$  AND  $f_2 \geq th_2$  AND ... AND  $f_M \geq th_M$  THEN Candidate Peak is a True Peak where  $f_i$  is denoted as selected peak features,  $th_i$  is the corresponding decision threshold value of  $f_i$ ,  $M$  is total number of selected peak features, and true peak is predicted peak point.

Algorithm 1. PSO Algorithm	
1:	Initialization
2:	while <i>not stopping criteria</i> do
3:	for each <i>ith particle in a population</i> do
4:	calculate fitness function
5:	update <i>pbest</i> and <i>gbest</i>
6:	end for
7:	for each <i>particle in a population</i> do
8:	update the <i>ith</i> particle's velocity and
9:	update the <i>ith</i> particle's position
10:	end for
11:	end while

Table 2. Representation of Particle Position

Particle	Decision Thresholds			
	1	2	...	F
$s_i^k$	$x_{i,1}^k$	$x_{i,2}^k$	...	$x_{i,d}^k$

#### 2.4. Parameters Estimation using Particle Swarm Optimization

Fundamentally, the PSO algorithm follows several steps as described in Algorithm 1.

In PSO, particles search for the best solution and update the position information among each other iteration to iteration. Each particle in the population consists of a vector position and vector velocity in  $d$  dimension. The position of particle  $i$  at iteration  $k$  is denoted as  $s_i^k = \{x_{i,1}^k, x_{i,2}^k, x_{i,3}^k, \dots, x_{i,d}^k\}$ . To obtain the updated position of a particle,  $s_i^{k+1}$ , each particle changes its velocity as the following:

$$v_i^{k+1} = \omega v_i^k + c_1 r_1 (p_i^k - x_i^k) + c_2 r_2 (p_g^k - x_i^k) \quad (1)$$

where  $c_1$  is a cognitive coefficient,  $c_2$  is a social coefficient,  $r_1$  and  $r_2$  are random values [0,1], and  $\omega$  is a decrease inertial weight calculated as follows:

$$\omega = \omega_{\max} - \left( \frac{\omega_{\max} - \omega_{\min}}{k_{\max}} \right) \times k \quad (2)$$

where  $\omega_{\max}$  and  $\omega_{\min}$  denote the maximum and minimum values of inertia weight, respectively, and  $k_{\max}$  is the maximum iteration. Then, the particle's position is updated based on Eq. (3).

$$s_i^{k+1} = s_i^k + v_i^{k+1} \quad (3)$$

Table 2 illustrates the representation of particle position. The  $i$ th particle at iteration  $k$ ,  $x_i(k)$ , in represents continuous type of dimension,  $s_i^k = \{x_{i,1}^k, x_{i,2}^k, x_{i,3}^k, \dots, x_{i,d}^k\}$ . The  $d=1,2,3,\dots,F$  is a  $d$ th dimension.  $F$  is the total number of decision thresholds. The total number of decision thresholds is equal of the total number of peak features.

Table 3. Parameters Setting of PSO Algorithm

Parameters	Value
Decrease inertia weight, $\omega$	0.9 ~ 0.4
Cognitive component, $c_1$	2
Social component, $c_2$	2
Random value, $r_1$ and $r_2$	Random [0,1]
Velocity vector for each particle	0
Initial pbest score for each particle	0
Initial gbest score	0
Range of search space for $F=1$ to $F=5$	[0 30]
Range of search space for $F=6$ to $F=10$	[0 781.25]
Range of search space for $F=11$ to $F=14$	[0 24.16]

### 3. Experimental Setup

The experiment for each peak model is conducted in 10 independent runs. In PSO, 30 particles are used. For each particle, the total number of dimensions is depending on the number of features in a feature set. The maximum iteration was set to 1000. The parameters setting of PSO algorithm are tabulated in Table 3. The fitness function used in this study is geometric mean (*Gmean*).

#### 3.1. Experimental Protocols

The EEG signal recording was conducted using the g.MOBILab portable signal acquisition system. The EEG signal was recorded from C4 channel. The EEG signal of channel CZ was used as a reference. The ground electrode was located on the forehead. The electrode was placed using the 10-20 international electrode placement system. The sampling frequency was set to 256-Hz.

The filtered EEG signal is shown in Figure 3. The total length of EEG recording is 40-second. 40 locations of true peak points are highlighted in the red circle. The next process is to prepare the training and testing data.

From the data collection, 40 true peak points have been identified. In 40-second signal there are 10280 sampling points,  $x(I)$ . There are only 40 peak points and the remaining of 10240 sampling points are the non-peak points. For preparing the training and testing signal, the training signal is selected from 1 to 5140 sampling points while the remaining EEG signal is used for testing signal.

### 4. Results and Discussions

Four peak models are employed for evaluating those peak model performances in the proposed algorithm. The training and testing performance based on those four different measures for each model is shown in Table 4.

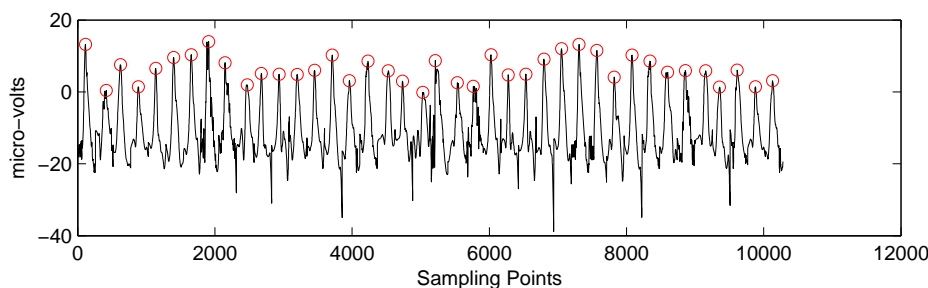


Fig. 3. Filtered EEG Signal

The testing performance for average, maximum, minimum, and STD is 81.22%, 91.83%, 74.15%, 9.13 for Dumpala *et al.*'s peak model; 68.59%, 77.43%, 54.77%, 6.97 for Acir *et al.*'s peak model; and 88.78%, 94.75%, 77.44%, 7.98 for Dingle *et al.*'s peak model, respectively. Compared to the test average performance of the peak models, the highest performance is obtained by Dingle *et al.*'s peak model, which is 88.78%.

For the Liu *et al.*'s peak model, will give 0% performance for training and testing phase. This result indicates that the limitation of rule-based classifier when dealing with this feature sets. During the training process on this feature sets, the particles in the PSO algorithm does not meet the optimum decision threshold values and the particles might also be trapped at local optima. Based on the preceding rule, a true peak only can be identified if all the feature values are greater or equal than the decision threshold values. So, if one of the feature values do not satisfy the decision threshold value, the classifier will decide the peak candidate as a non-peak point. When this happens to all peak candidates, *Gmean* will give 0% performance.

## 5. Conclusions

In this study, a rule-based classifier with PSO-based estimation technique was employed in the proposed algorithm of EEG signal peak detection. The four different peak models that consist of different feature sets are used in the feature extraction stage. The best peak model is Dingle *et al.*'s peak model with highest performance obtained is 88.78%.

## Acknowledgement

This project is funded by the Ministry of Education Malaysia (UM.C/HIR/MOHE/ENG/16 Account code: D000016-16001). The first author would like to thank the Ministry of Education Malaysia for awarded him MyPhD scholarship.

Table 4. Training and Testing Performance of Peak Detection for each Peak Model

Peak Model	Training (%)				Testing (%)			
	Avg	Max	Min	STD	Avg	Max	Min	STD
Dumpala <i>et al.</i>	84.01	89.15	80.58	4.43	81.22	91.83	74.15	9.13
Acir <i>et al.</i>	74.4	80.59	67.08	3.71	68.59	77.43	54.77	6.97
Liu <i>et al.</i>	0	0	0	0	0	0	0	0
Dingle <i>et al.</i>	90.98	94.76	83.66	5.1	88.78	94.75	77.44	7.98

## References

1. A. A. Dingle, R. D. Jones, G. J. Carroll, and W. R. Fright, A Multistage System to Detect Epileptiform Activity in the EEG, *IEEE Transactions on Biomedical Engineering* **40** (1993) 1260-1268.
2. A. Juozapavi, G. Bacevi, D. Bugelskis, and R. Samaitien, EEG analysis – automatic spike detection, *Journal of Nonlinear Analysis: Modelling and Control* **16** (2011) 375-386.
3. H. S. Liu, T. Zhang, and F. S. Yang, A Multistage, Multimethod Approach for Automatic Detection and Classification of Epileptiform EEG, *IEEE Transaction on Biomedical Engineering* **49** (2002) 1557-1566.
4. M. Putignano, A. Intermite, and C. P. Welsch, A non-linear algorithm for current signal filtering and peak detection in SiPM, *Journal of Instrumentation* **7** (2012) 1-19.
5. S. R. Dumpala, S. N. Reddy, and S. K. Sarna, An algorithm for the detection of peaks in biological signals, *Computer Programs in Biomedicine* **14** (1982) 249-256.
6. N. Acir, I. O. Kuntalp, B. Baklan, and C. Güzelis, Automatic Detection of Epileptiform Events in EEG by a Three-Stage Procedure Based on Artificial Neural Networks, *IEEE Transactions on Biomedical Engineering* **52** (2005) 30-40.
7. A. Adam, M. I. Shapiai, M. Z. Mohd Tumari, M. S. Mohamad, and M. Mubin, Feature Selection and Classifier Parameters Estimation for EEG Signals Peak Detection Using Particle Swarm Optimization, *The Scientific World Journal* (2014).



# Different Learning Functions for Weighted Kernel Regression in Solving Small Sample Problem with Noise

Zuwairie Ibrahim, Nurul Wahidah Arshad

Faculty of Electrical and Electronic Engineering, Universiti Malaysia Pahang, 26600 Pekan, Pahang, Malaysia

Mohd Ibrahim Shapiai

Malaysia-Japan International Institute of Technology Universiti Teknologi Malaysia, 81310 Johor Bahru, Malaysia

Norrima Mokhtar

Applied Control and Robotics (ACR) Laboratory, Department of Electrical Engineering, Faculty of Engineering, University of Malaya, 50603 Kuala Lumpur, Malaysia

E-mail: zuwairie@ump.edu.my

## Abstract

Previously, weighted kernel regression (WKR) for solving small samples problem has been reported. In the original WKR, the simple iterative learning technique and the formulated learning function in estimating weight parameters are designed only to solve non-noisy and small training samples problem. In this study, an extension of WKR in solving noisy and small training samples is investigated. The objective of the investigation is to extend the capability and effectiveness of WKR when solving various problems. Therefore, four new learning functions are proposed for estimating weight parameters. In general, the formulated learning functions are added with a regularization term instead of error term only as in the existing WKR. However, one free parameter associated to the regularization term has firstly to be predefined. Hence, a simple cross-validation technique is introduced to estimate this free parameter value. The improvement, in terms of the prediction accuracy as compared to existing WKR is presented through a series of experiments.

*Keywords:* Learning functions, Small sample problem, Regression.

## 1. Introduction

In general, the kernel based regression aims at regressing the unknown function based on the available training samples. In real world applications, to obtain sufficient training samples is too expensive as when dangerous real measurements have to be performed [1]. There are numerous techniques in machine learning for regression. However, all the available techniques mainly focus in solving sufficient training samples problem. As most existing techniques perform well under sufficiently large training samples, the performance of those techniques degrades as the size of samples decreases.

Weighted Kernel Regression (WKR) [2] has proved to solve small sample problems with high accuracy by assuming all the available training samples are free from error. An example of regression using WKR is shown in Fig. 1. To design a WKR, one must estimate the weight parameters,  $W$ , before it can be used to predict unseen

samples. The estimation of the weight parameters depends on the learning functions and learning techniques.

In general, the ability of WKR is only restricted to solve non-noisy training samples. Hence, the formulated learning function and simple iterative learning technique in WKR may fail in estimating weight parameters if the observed training samples are corrupted by noise. An example of regression using WKR in the presence of noise is shown in Fig. 2. Therefore, in this study, four learning functions are considered to particularly solve small and noisy samples problems.

## 2. Weighted Kernel Regression

Given training samples,  $\{x_i, y_i\}_{i=1}^n$ , where  $n$  is the number of training samples, input is denoted as  $x_i \in \mathcal{R}^d$ , and  $y_i \in \mathcal{R}$  is the target output. WKR is the technique to regress the output space by mapping the input space  $\mathcal{R}^d$  to  $\mathcal{R}$ . In general, WKR is a modified Nadaraya-Watson kernel regression (NWKR) [3] by expressing the weight based on the observed samples through a kernel function.

The existing WKR relies on the Gaussian kernel function as given in Eq. (1).

$$K(X, X_i) = \frac{1}{\sqrt{2\pi}} \exp\left(\frac{-\|X - X_i\|^2}{h}\right) \quad (1)$$

where  $h$  is the smoothing parameter. As in NWKR, the selection of smoothing parameter,  $h$ , is important to compromise between smoothness and fitness. As in existing WKR, Eq. (2) is employed to determine the value of  $h$ .

$$h = \max\left(\|X_{k+1}\|^2 - \|X_k\|^2\right) \quad (2)$$

where  $1 < k < n-1$  and  $\|X_{k+1}\|^2 > \|X_k\|^2$ .

The kernel matrix  $K = [K_{ij}]$ , where  $i = j = 1, \dots, n$ , with a generalised kernel matrix based on the Gaussian kernel, is given in Eq. (3). The matrix  $K$  transforms the linear observed samples to non-linear problems by mapping the data into a higher dimensional feature space.

$$K_{ij} = \begin{cases} \frac{\prod_{p=1}^d K(X_i^p, X_j^p)}{\sum_{l=1}^n \left[ \prod_{p=1}^d K(X_{i \setminus l}^p, X_j^p) \right]} & i \neq j \\ \frac{1}{\sum_{l=1}^n \left[ \prod_{p=1}^d K(X_{i \setminus l}^p, X_j^p) \right]} & i = j \end{cases} \quad (3)$$

In WKR, the most popular function for regression problems is used which to minimize the RSS to estimate the weight parameters,  $W$ .

$$\min f(W) \Leftrightarrow \min \|Kw - y\|^2 \quad (4)$$

Once the optimum weight is estimated, the model is ready to predict any unseen samples (test samples). The test samples can be predicted by using Eq. (5).

$$\hat{y}(X, \hat{W}) = \frac{\sum_{i=1}^n \hat{w}_i \left( \prod_{p=1}^d K(X^p, X_i^p) \right)}{\sum_{i=1}^n \left( \prod_{p=1}^d K(X^p, X_i^p) \right)} \quad (5)$$

### 3. Extension of Weighted Kernel Regression

In general, minimizing the error term only may lead to numerical instabilities and bad generalization performance. The instability yields a high variance model which potentially produces large differences of weight parameter values given different training samples, even minor perturbation of the same training samples. In general, this instability can be addressed by restricting the class of permissible solution by introducing the

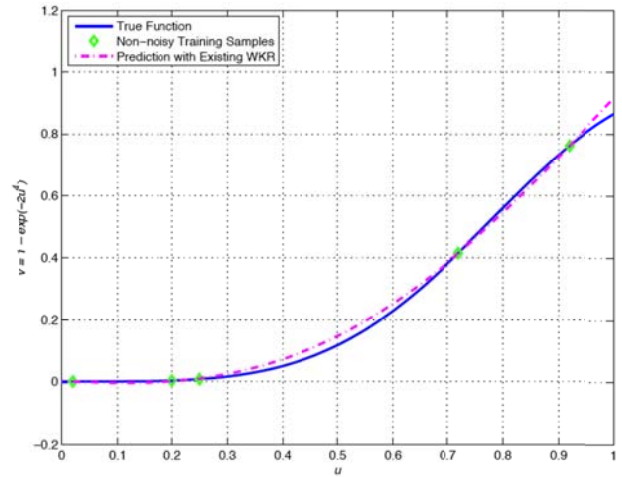


Fig 1. Regression using WKR

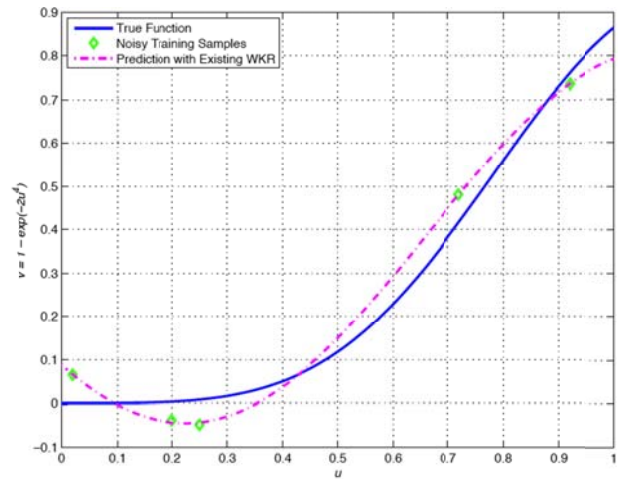


Fig 2. Regression using WKR in the presence of noise

regularization term to the formulated learning function. The regularization term is usually of the form of a penalty term for complexity, such as restrictions for smoothness.

Therefore, all the investigated learning functions will comprise not only the error term but also the regularization term as given in Eq. (6).

$$f_{learning} = f_e + f_r \quad (6)$$

where  $f_e$  refers to error term and  $f_r$  refers to regularization term.

The addition of regularization term is to avoid the magnitude of estimated weight parameters to be very large which may lead to over-fitting problem. Hence, the addition of regularization term gives advantages to the regression quality. In general, the error term and regularization term can be formulated either with  $L_1$  norm or  $L_2$  norm function. Therefore, the four learning functions are formulated with combination of  $L_1$  and  $L_2$  as error term and regularization term based on the WKR concept are proposed in this study.

Table 1. Parameter setting of GA

Generation	300
Population size	100
Probability of cross-over	0.7
Probability of mutation	0.001

The error term with  $L_2$  norm is a popular choice and most widely used for linear model but it is less robust. Meanwhile, error term in  $L_1$  norm form is not sensitive and produces robust estimation as compared to  $L_2$  norm but  $L_1$  norm function is not differentiable. For regularization term, the  $L_2$  norm offers lower variances model by shrinking the estimated weight parameter values as compared to learning function without regularization term. The  $L_2$  norm regularization term is also known as Tikhonov regularization [4] or Ridge regularization [5] for solving matrix inverse problem to learning problems with good generalization.  $L_1$  norm regularization not only offers lower variances model but also produces sparseness solution which offers a better generalization. The sparseness solution forces some estimated weight parameter value equals to zero. Also,  $L_1$  norm regularization term creates accurate predictive models that also have interpretable or parsimonious representations. The proposed formulated learning functions, which are based on learning function in the existing WKR, are given in Eq. (7) to Eq. (10).

$$f_{L_2R_2}(W) = \underset{W}{\operatorname{argmin}} (\|KW - Y\|^2 + \lambda \|W\|^2) \quad (7)$$

$$f_{L_2R_1}(W) = \underset{W}{\operatorname{argmin}} (\|KW - Y\|^2 + \lambda \|W\|_1) \quad (8)$$

$$f_{L_1R_2}(W) = \underset{W}{\operatorname{argmin}} (\|KW - Y\|_1 + \lambda \|W\|^2) \quad (9)$$

$$f_{L_1R_1}(W) = \underset{W}{\operatorname{argmin}} (\|KW - Y\|_1 + \lambda \|W\|_1) \quad (10)$$

where  $K$  is kernel matrix,  $W$  is weight parameter to be estimated,  $Y$  is observed output domain values,  $\|\cdot\|_1$  is  $L_1$  norm function,  $\|\cdot\|^2$  is  $L_2$  norm function, and  $\lambda$  is a free parameter that control the generalization of the regressed function.

In general, the formulated learning functions can be categorized into two types; closed form solution function and non-closed form solution function. Closed form solution function can be derived analytically as compared to non-closed form solution function when estimating the weight parameters. For non-closed form function, there is no analytical solution can be obtained as the function is nondifferentiable. As evolutionary computing offers an effective way to optimize i.e. estimate the weight parameters for non-differentiable function, hence, Genetic Algorithm (GA) is introduced as a learning technique. The formulated learning function with  $L_1$  norm term either as error term or regularization term is considered as non-closed form solution function.

Prior to estimating the weight parameters based on new formulated learning functions, an associated  $\lambda$  value has firstly to be estimated. Cross-validation is a technique to evaluate model in order to generalize the predictive performance when predicting unseen samples. The need of cross-validation is important in model selection as some models parameters, such as  $\lambda$  value has to be estimated. In general, cross-validation separates the available training samples into two sets, called the training set and validation set. Training set is used to build the model and validation set is used to evaluate the model based on the selected models parameter with respect to the cross-validation error. Typically, the cross-validation error is measured based on MSE performance criterion. The model with the lowest cross-validation error is then used as a final model which possibly offers a better generalization performance.

There are various cross-validation techniques available in literatures such as hold-out method, K-fold cross-validation, and leave-one-out cross-validation (LOOCV). In general, LOOCV is very expensive to compute but it is able to retrieve a lot of information from the available training samples. As the focus of the study is to solve small and limited training samples problem, LOOCV is found to offer several advantages in terms of information retrieval and computational time.

In general, LOOCV separates the available  $n$  training samples into a training set of size  $n-1$  and a validation of size 1. For every selected models parameter, there are  $n$  different combinations of training and validation set. The lowest cross-validation on the validation set is used as an indicator to select the final model.

#### 4. Experiment, Result, and Discussion

Since the learning function which possesses  $L_1$  norm term is considered as non-closed form solution function, an analytic form solution cannot be obtained when minimizing the corresponding learning function in estimating the weight parameter. This drawback has led to the use of GA. The parameter settings of GA are summarised in Table 1. A specific function is employed with three different Gaussian noise distributions,  $N\sim(0,0.1)$ ,  $N\sim(0,0.3)$ , and  $N\sim(0,0.5)$ .

The quality of prediction for every learning function for three different problems is tabulated in Table 2, Table 3, and Table 4. In general, the learning function with  $L_2$  norm of error term offers a better generalization as compared to the learning function with  $L_1$  norm of error term.

Table 2. Results of 100 experiments to predict  $1 - \exp(-2u)^4$  with  $n = 5$  and contaminated by Gaussian noise,  $N\sim(0,0.1)$  with various learning functions

Learning Function	Average MSE	Standard Deviation	Min MSE	Max MSE
$L_2R_2$	0.00707	0.00517	0.00184	0.01834
$L_2R_1$	0.00704	0.00474	0.00221	0.01831
$L_1R_2$	0.01201	0.00926	0.00199	0.02916
$L_2R_1$	0.00930	0.00681	0.00181	0.02440

Table 3. Results of 100 experiments to predict  $1 - \exp(-2u)^4$  with  $n = 5$  and contaminated by Gaussian noise,  $N\sim(0,0.3)$  with various learning functions

Learning Function	Average MSE	Standard Deviation	Min MSE	Max MSE
$L_2R_2$	0.04832	0.04122	0.01180	0.16416
$L_2R_1$	0.05048	0.04831	0.00630	0.17170
$L_1R_2$	0.06403	0.05314	0.00871	0.19740
$L_2R_1$	0.05940	0.05353	0.00862	0.19563

Table 4. Results of 100 experiments to predict  $1 - \exp(-2u)^4$  with  $n = 5$  and contaminated by Gaussian noise,  $N\sim(0,0.5)$  with various learning functions

Learning Function	Average MSE	Standard Deviation	Min MSE	Max MSE
$L_2R_2$	0.11101	0.10993	0.03022	0.4474
$L_2R_1$	0.10767	0.11666	0.00402	0.45964
$L_1R_2$	0.14788	0.14201	0.02225	0.56058
$L_2R_1$	0.13753	0.13729	0.02376	0.56251

### 5. Conclusions

An extension of WKR is investigated to address regression problem with noisy training samples. The investigation emphasized on formulation of learning functions. Prior to these two investigations, the free parameter,  $\lambda$  value has firstly to be estimated. The

improvement, in terms of quality of prediction is experimented and presented. In general, the selection of learning technique must be based on the formulated learning function, which implies the dependency of problem being solved. Also, the quality of prediction is mainly determined by the selection of  $L_2$  norm as error term regardless of norm type of regularization term. Hence, the inclusion of regularization term is a must in formulating the learning function.

### Acknowledgement

This work is financially supported by the RAGS Grant Scheme (RDU131416) awarded by the Ministry of Higher Education (MOHE) to Universiti Malaysia Pahang (UMP).

### References

1. C. Huang and C. Moraga, A diffusion-neural-network for learning from small samples, *International Journal of Approximate Reasoning* **35**(2) (2004) 137-161.
2. M. I. Shapiai, Z. Ibrahim, M. Khalid, L. W. Jau, and V. Pavlovic, Enhanced Nadaraya Watson Kernel Regression: Surface Approximation for Extremely Small Samples, *The 5th Asia Modeling Symposium* (2011) 7-12.
3. E. A. Nadaraya, On Estimating Regression, *Theory of Probability and its Applications* **9**(1) (1964) 141-142.
4. A. Tikhonov and V. Arsenin, *Solutions of Ill-posed Problems* (1977).
5. A. E. Hoerl and R. W. Kennard, Ridge Regression: Biased Estimation for Nonorthogonal Problems, *Technometrics* **12**(1) (1970) 55-67.

# Simultaneous Computation of Model Order and Parameter Estimation of a Heating System Based on Particle Swarm Optimization for Autoregressive with Exogenous Model : An Analysis

**Teoh Shin Yee, Zuwairie Ibrahim, Kamil Zakwan Mohd Azmi**  
*Faculty of Electrical and Electronic Engineering, Universiti Malaysia Pahang*  
*26600 Pekan, Pahang, Malaysia*  
*E-mail: zuwairie@ump.edu.my*  
*www.ump.edu.my*

**Norrima Mokhtar**  
*Applied Control and Robotics (ACR) Laboratory, Department of Electrical Engineering, Faculty of Engineering*  
*University of Malaya, 50603 Kuala Lumpur, Malaysia*

## Abstract

System identification is one of the method for solving a mathematical model of a system by performing on analysis only at its input and output behaviour. In system identification, the procedure of modelling the system is separated into four main parts. The first part is constructing an experiment to collect the input and output data of the system. Then, with some criteria, the model order and structure are selected. The next part is to estimate the parameters of the model. For the final part, the mathematical model is verified. Model order selection and parameter estimation are two important parts of finding the mathematical model for system identification. Previously, a technique called simultaneous model order and parameter estimation (SMOPE), which is based on Particle Swarm Optimisation (PSO) and ARX model, has been introduced to combine these two parts simultaneously. This technique, however, exclude the error term of ARX model. In this study, an analysis is shown to prove that the performance of SMOPE based on PSO and ARX model degraded as the magnitude of error increases.

*Keywords:* ARX, Particle swarm optimization (PSO), System identification.

## 1. Introduction

System identification is a method to find the mathematical model of a dynamic system which uses statistical methods to build mathematical models from measured data. Two types of models are common in the field of system identification: grey-box model and black-box model. Grey-box model refers to the model where some information is partially known from first principle while the rest of the information is obtained from experiment. On the other hand, a black-box model uses no priori physical knowledge of the system. A number of model structures have been proposed in the

area of black-box identification system. The most common models are autoregressive model with exogenous inputs (ARX) [1], autoregressive moving average with exogenous inputs (ARMAX) [2], and Box-Jenkins (BJ) model [3].

Autoregressive with exogenous (ARX) model is the simplest model in linear black box identification. In solving the linear black box identification problem of the ARX model, the model order selection and parameter estimation part is solved as separate process. Previously, a technique called simultaneous model order and parameter estimation (SMOPE), which is based on Particle Swarm Optimisation (PSO) and ARX model,

has been introduced to combine these two parts simultaneously [4]. This technique, however, exclude the error term of ARX model. In this study, an analysis is conducted to investigate the performance of SMOPE based on PSO and ARX model with error term included.

### 2. Simultaneous Model Order and Parameter Estimation

In ARX model, AR refers to the autoregressive part and X refers to the exogenous input. The single-input single-output (SISO) ARX mathematical model can be defined as:

$$y(t) = \frac{B(q)}{A(q)}u(t) + \frac{1}{d} \varepsilon(t) \quad (1)$$

where  $u(t)$  and  $y(t)$  are input and output variables, respectively,  $\varepsilon[t]$  is a Gaussian white noise process,  $A(q)$  and  $B(q)$  are polynomials in the backward shift operator. In ARX, a mathematical model of a system can be represented as:

$$G(z) = \frac{Y(z)}{U(z)} = \frac{b_0 + b_1z^{-1} + \dots + b_mz^{-m}}{1 + a_1z^{-1} + \dots + a_nz^{-n}} \quad (2)$$

In SMOPE, however, the error term  $\varepsilon[t]$  is ignored and the maximum order of 9<sup>th</sup> is considered. To decide the parameter 'a' and 'b', the constraint  $n \geq m$  is taken into account. This is due to the transfer function form which the order value of poles ( $n$  value) must be the same or less than the order of zeroes ( $m$  value).

The purpose of PSO algorithm [5], as shown in Fig. 1, is to search for the best mathematical model. The combination of model order and parameter for ARX equation are considered in particle representation, which is shown in Table 1. For example, if the model order is 2, then 'n' value is 2 and all possible mathematical models are subjected to fitness calculation. Specifically, the calculations involve two mathematical models, which are  $\frac{b_1z^{-1}}{1 + a_1z^{-1} + a_2z^{-2}}$  and  $\frac{b_1z^{-1} + b_2z^{-2}}{1 + a_1z^{-1} + a_2z^{-2}}$ .

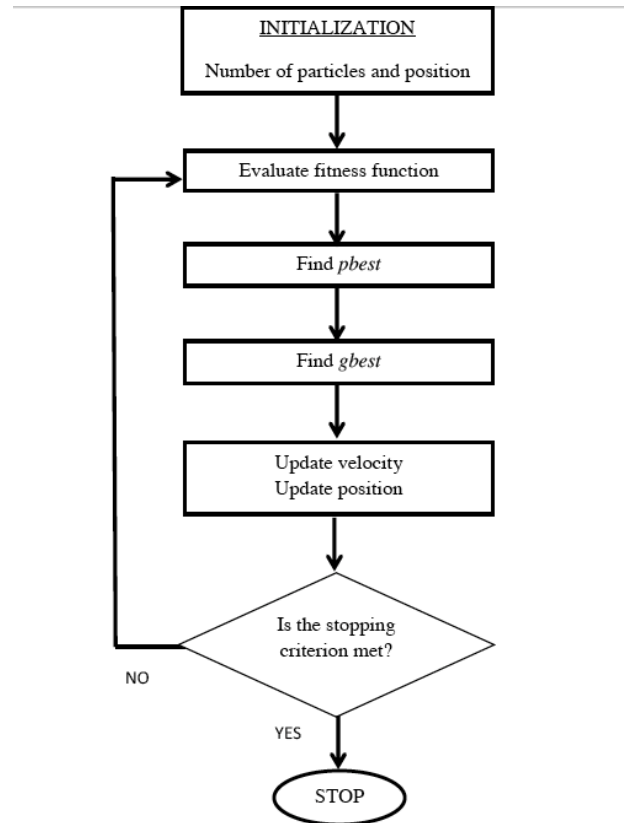


Fig. 1. The flowchart of PSO algorithm.

In the earlier stage of PSO algorithm, some parameters are initialized. The PSO parameter values used in this study is shown in Table 2. The PSO parameter includes the number of particles, the inertia weight, cognitive component,  $c_1$ , social component,  $c_2$ , and the maximum number of iterations,  $k$ . The initial position and velocity of particle is randomly located in a search space. After the initialization stage is done, the fitness function is calculated as follows:

$$best\ fit = 100 \left[ 1 - \frac{\text{norm}(P_{best\_current} - J^*)}{\text{norm}(y - \hat{y})} \right] \% \quad (3)$$

The personal best or  $pbest$  is the best solution found by each particle and  $gbest$  is defined as the best  $pbest$ . Both  $pbest$  and  $gbest$  are updated at every iteration. The velocity of a particle is updated using Eq. (4):

$$v_i^{k+1} = \omega v_i^k + c_1 \text{rand}() (p_{best} - s_i^k) + c_2 \text{rand}() (g_{best} - s_i^k) \quad (4)$$



Table 1. Particle representation.

Dimension	1	2	3	4	5	6	7	8	9	10	11	12	13	14	15	16	17	18	19
Variable in ARX	Order, $n$	$a_1$	$a_2$	$a_3$	$a_4$	$a_5$	$a_6$	$a_7$	$a_8$	$a_9$	$b_1$	$b_2$	$b_3$	$b_4$	$b_5$	$b_6$	$b_7$	$b_8$	$b_9$

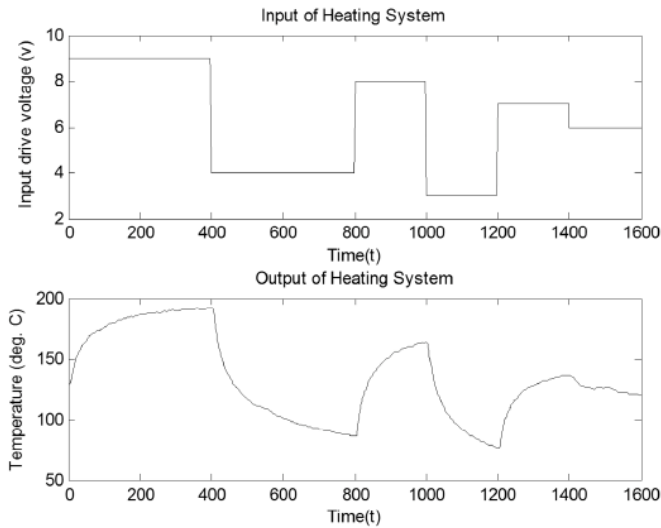


Fig. 2. Input and output behavior of heating system.

Table 2. PSO parameters.

Parameters	Value
Maximum number of particles, $i$	10
Decrease inertia weight, $\omega$	0.9~0.4
Cognitive Component, $c_1$	2
Social Component, $c_2$	2
Random value, $rand$	[0,1]
Maximum iterations, $k$	150
Number of run	100

where  $v_i^k$  is the velocity particle  $j$  at iteration  $k$ ,  $rand$  is random numbers [0,1],  $\omega$  is inertia weight, and  $c_1$  and  $c_2$  denote the cognitive and social coefficients, respectively. The particle's new velocity is then used to update the particle's position using Eq. (5).

$$v_i^{k+1} = \omega v_i^k + c_1 r_1 (p_{best} - s_i^k) + c_2 r_2 (p_{best} - s_i^k) \quad (5)$$

where  $s_i^k$  is the position of particle  $i$  at iteration  $k$ . In this study, the linear dynamic inertia weight is used and calculated according to Eq. (6) as follows:

$$\omega = \omega_{max} - \frac{\omega_{max} - \omega_{min}}{k_{max}} \times k \quad (6)$$

where  $\omega_{max}$  and  $\omega_{min}$  denote the maximum and minimum values of inertia weight, respectively, and  $k_{max}$  is the maximum iteration.

Note that the PSO will assign floating values to every dimension of a particle even though the value of model

order is discrete. Hence, for the first dimension, the floating value is converted to discrete data by rounding its value. If the value is not in range, the previous value is used instead. Then, the particle refers to other parameters for the calculation of fitness.

### 3. The Heating System

In heating system, the input drives a 300 Watt Halogen lamp, suspended several inches above a thin steel plate. The output is a thermocouple measurement taken from the back of the plate. The input and output of the experiment is shown in Fig. 2, which is taken from <http://www.esat.kuleuven.ac.be/sista/daisy>. The data collect from the system is halfly separated for estimation and validation. This estimation data is used to calculate the model order and parameter of the ARX while the validation data is used to validate the model.

### 4. Experiment, Result, and Discussion

Using MATLAB for simulation and based on the PSO parameter shown in Table 2, an example of a convergence curve is shown in Fig. 3. The minimum and maximum value of best fit obtained in estimation is 99.0018% and 99.3211%, respectively. Average value of best fit is 99.2242%. In validation, the minimum, maximum, and average best fit are 92.6557%, 98.7011%, and 98.0763%, respectively. This experiment gives model order value as 3 and mathematical model as follows:

$$G_{HD}(z) = \frac{0.0024z^{-1} + 0.0020z^{-2} + 0.0720z^{-3}}{1 - 1.6169z^{-1} + 0.7306z^{-2} - 0.0833z^{-3} - 0.0321z^{-4}} \quad (7)$$

where the model order,  $n = 4$ , parameter value  $b_1 = 0.0024$ ,  $b_2 = 0.0020$ ,  $b_3 = 0.0720$ ,  $a_1 = -1.6169$ ,  $a_2 = 0.7306$ ,  $a_3 = 0.0833$ , and  $a_4 = -0.0321$ .

An analysis has been conducted to investigate the performance of SMOPE based on PSO and ARX model with error term,  $\varepsilon[\tau]$ , included. The complete ARX model shown in Eq. (1) and the same PSO parameters have been used. The error term is a white noise, which can be generated in MATLAB using `rand` command.

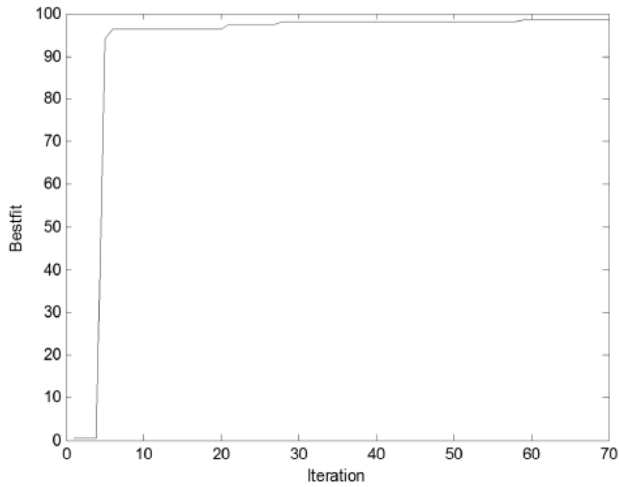


Fig. 3. An example of convergence curve.

The average best fit obtained is 98%, which is very much similar to the result of the previous experiment. Additional experiments with different magnitude of noise have been done and the result is shown in Fig. 4. Note that only 10 runs are considered. This analysis shows that the best fit decreases as the magnitude of error increases.

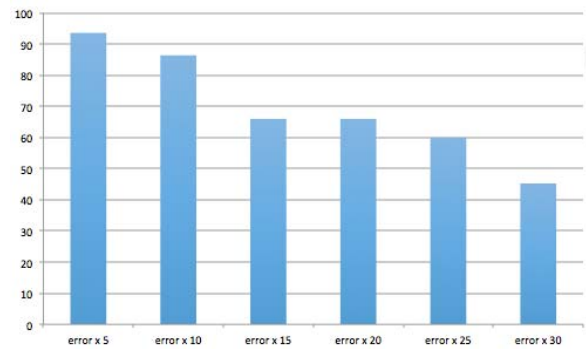
## 5. Conclusion

In the previous study, a system identification results from a heating system case study has been presented to investigate the performance of simultaneous model order and parameter estimation technique based on PSO and ARX model. However, the error term is excluded from the previous experiment. In this paper, with different magnitude of white noise are considered and included in the experiment. Based on the 10 runs and different magnitude of white noise up to 30, this study proved that the performance of SMOPE based on PSO and ARX model degraded as the magnitude of error increased.

## Acknowledgements

This work is financially supported by the Exploratory Research Grant Scheme (RDU130605) awarded by the Ministry of Higher Education (MOHE) to Universiti Malaysia Pahang (UMP).

Fig. 4. Best fit decreases as the magnitude of error increases.



## References

1. L. Ljung, *System Identification Theory for the User*, 2nd ed., Prentice Hall, CA: Linkoping University Sweden, 1999.
2. S. M. Moore, J. C. S. Lai, K. Shankar, ARMAX modal parameter identification in the presence of unmeasured excitation—I: Theoretical background, *Mechanical Systems and Signal Processing* **21** (2007) 1601-1615.
3. R. Pintelon, Y. Rolain, J. Schoukens, Box-Jenkins identification revisited—Part II: Applications, *Automatica* **42** (2006) 77-84.
4. J. Kennedy, Particle Swarm Optimization, *Encyclopedia of Machine Learning* (2010) 760-766.
5. Z. Ibrahim, S. W. Nawawi, S. Razali, B. Muhammad, K. Z. Mohd Azmi, Z. Aspar, N. A. Ab. Aziz, Simultaneous Computation of Model Order and Parameter Estimation of a Heating System Based on Particle Swarm Optimization for Autoregressive with Exogenous Model, *ICIC Express Letters*, **9** (2015) 1159-1165.



# Maximum Probability Algorithm for Fault Diagnosis

Fengzhi Dai, Li Fa, Bo Liu

College of Electronic Information and Automation, Tianjin University of Science and Technology,  
80 MailBox, 1038 Daguananlu Road, Hexi District, Tianjin 300222, China

E-mail: [dai fz@tust.edu.cn](mailto:dai fz@tust.edu.cn), [fanli0476@126.com](mailto:fanli0476@126.com)

[www.tust.edu.cn](http://www.tust.edu.cn)

## Abstract

This paper considers the fault diagnosis by outside fault phenomena. The method only depends on experience and statistical data to set up the fuzzy query relationship between the outside phenomena (fault characters) and the fault sources (fault patterns). From this relationship, the most probable fault sources can be located, and the standard fuzzy relationship matrix is stored as database.

*Keywords:* maximum probability algorithm; fault diagnosis; fault phenomena-sources tree; servo system

## 1. Introduction

It is difficult to detect and diagnose the faults for non-linear systems, because it is difficult to obtain its accurate state description<sup>1</sup>. And if there is no particular technique is adopted<sup>2</sup>, it is always difficult to set up a complicated detection device based on the state description for this kind of systems.

In an actual control system, it is often difficult to find out where the faults are if only based on the outside fault phenomena (fault characters), but what we often obtain are these phenomena. This paper will discuss how to use these fault characters and some points' measurement to locate the fault sources.

The maximum probability algorithm is based on the theory of fuzzy recognition, has the effect of the expert system. It is to find the position of the most probable fault source that has the maximum fault probability. When the fault occurs, according to the outside phenomena and some points' measurement, all possible

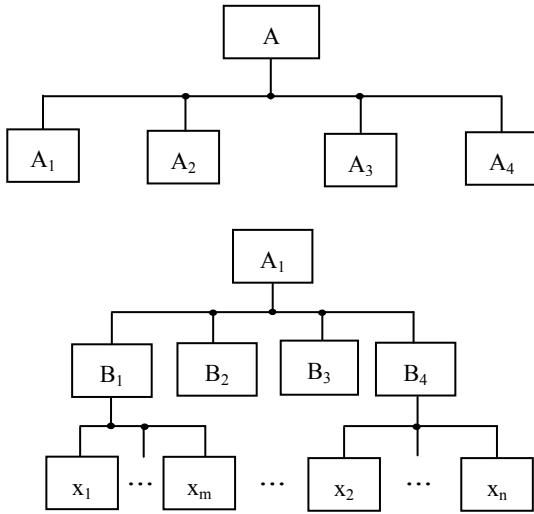
fault sources are listed, and they can be examined based on their fault probabilities that are from large to small.

## 2. Fault phenomena-sources Tree

In an actual control system, there are strong logic bonds between the fault phenomena and the fault sources. The fault tree that describes the system can be built up by verifying the truth and the integrity of this relationship. When the system's fault tree is completed, from which the system's fault phenomena- sources tree (Fig.1) can be obtained.

In Fig.1,  $A$  is the top event (the whole system);  $A_i$ ,  $B_j$  are the second and third level events; and  $x_k$  are the bottom events (components or the sub-systems).

From the system's fault phenomena-sources tree, the relationship between the system's fault sources and all kinds of fault characters (Table 1.) can be obtained and analyzed. In the paper, there are 14 sensors are mounted on the servo system at the experiment stage<sup>3</sup>.



- A : system abnormality
- A<sub>1</sub>: controller cannot rotate
- A<sub>2</sub>: system oscillation
- A<sub>3</sub>: abnormal noise
- A<sub>4</sub>: unsatisfied dynamics

Fig.1 System's fault phenomena-sources tree

### 3. Fault Diagnosis Approach

When faults occurs, there will be all kinds of fault phenomena, such as  $x_1, x_2, \dots$ . The purpose is to diagnose the faults from these outside fault phenomena and some points' measurement results.

#### 3.1. Fault diagnosis theory

When one fault state  $A_i$  (a sub-system or a component) occurs, it may result in many fault phenomena, such as  $x_j$ , designated by  $x_j=1$ , otherwise  $x_j=0$ .

On the other hand, if a series of fault phenomena  $X_j = \{x_1, x_2, \dots\}$ , then an array composed of 0,1 for the faulty state of  $A_i$  can be achieved.

We want to know, when the fault phenomena  $X_j = \{x_1, x_2, \dots\}$  occur, how much is the probability that it is the fault state  $A_i$  causing these phenomena.

The maximum of this probability  $\mu_{A_i}(X_j)$  – the probability that  $A_i$  causes these phenomena  $X_j = \{x_1, x_2, \dots\}$  should be obtained

$$\max_{A_i} \mu_{A_i}(X_j) \quad i = 1, 2, \dots, n \quad (1)$$

$n$  is the number of fault states.

Thus the maximum value of  $\mu_{A_i}(X_j)$  ( $i=1, 2, \dots, n$ ) is the maximum probability of the probable fault state.

#### 3.2. $\mu_{A_i}(X_j)$

First, set up a typical fault state  $A_i$ , based on the system's fault tree, the corresponding standard fault phenomena (fault characters)  $X_0^i = \{x_{i1}, x_{i2}, \dots, x_{ip}\}$ , give each fault character  $x_{ir}$  a weight  $\omega_{ir}$ , then the characteristic parameter that symbols  $X_0^i$  results from  $A_i$  is

$$P_{A_i}^0 = \sum_{r=1}^p \omega_{ir} x_{ir} \quad (2)$$

where  $x_{ir} = 1$  ( $i=1, 2, \dots, p$ ),  $p$  is the number of fault phenomena that can cause the fault state of  $A_i$  ( $A_i$  can be obtained from the system's fault tree),  $\omega_{ir}$  is the weight of  $x_{ir}$  in the fault state  $A_i$ .

Second, according to a series of fault characters  $X_j = \{x_1, x_2, \dots, x_q\}$ , define the parameter that symbols  $X_j$  results from  $A_i$  is

$$P_{A_i} = \sum_{r=1}^q \omega_r x_r \quad (3)$$

If  $x_r$  ( $r=1, 2, \dots, q$ ) is in the  $X_0^i = \{x_{i1}, x_{i2}, \dots, x_{ip}\}$ , then

$x_r = 1, \omega_r = \omega_{ir}$ , otherwise  $\omega_r = 0$ .

Then for the obtained fault characters  $X_j = \{x_1, x_2, \dots, x_q\}$ , the probability of all these fault characters result from fault  $A_i$  is:

$$\mu_{A_i}(X_j) = \frac{P_{A_i}}{P_{A_i}^0} \quad (4)$$

### 3.3. Steps

From the analysis above, the steps of fault diagnosis can be obtained by the following three steps:

(i) Finding: The first step is to analyze and obtain the system's fault sources and all kinds of fault characters.

(ii) Inspection: Obtain the system's fault tree and set up the standard fuzzy relationship matrix of  $X_0^i - A_i$  (Table 1.) off-line.

Table 1. Standard fuzzy relationship matrix ( $X_0^i - A_i$ ).

$\omega_{ir}$	$X_0^i$			
	$X_{i1}$	$X_{i2}$	...	$X_{ip}$
$A_1$	$\omega_{11}$	$\omega_{12}$	...	$\omega_{1p}$
$A_2$	$\omega_{21}$	$\omega_{22}$	...	$\omega_{2p}$
$\vdots$	$\vdots$	$\vdots$	$\vdots$	$\vdots$
$A_i$	$\omega_{i1}$	$\omega_{i2}$	...	$\omega_{ip}$
$\vdots$	$\vdots$	$\vdots$	$\vdots$	$\vdots$
$A_n$	$\omega_{n1}$	$\omega_{n2}$	...	$\omega_{np}$

When faults occur, they are identified by using the sampled data. After removing noise signals, the faults can be found according to the maximum probability algorithm by analyzing the fault tree and the fault information on-line.

(iii) Detection, diagnosis and precaution: Give the alarm and the results of the fault diagnosis.

### 3.4. The algorithm diagram

Fig.2 gives the flow chart of the algorithm. And the fault searching steps are as follows:

For the certain relationship between fault phenomena and fault sources, once the phenomena occur, the fault components can be found easily.

For the relationship with fuzzy characters, they are queried based on the method presented in the paper.

All the probable fault sources, which have non-zero fault probabilities, are listed from large to small.

For the unsolved faults, a method for isolating faults is presented.

## 4. Experiment

Based on the above approach, the software is developed using C language. The standard fuzzy relationship matrix

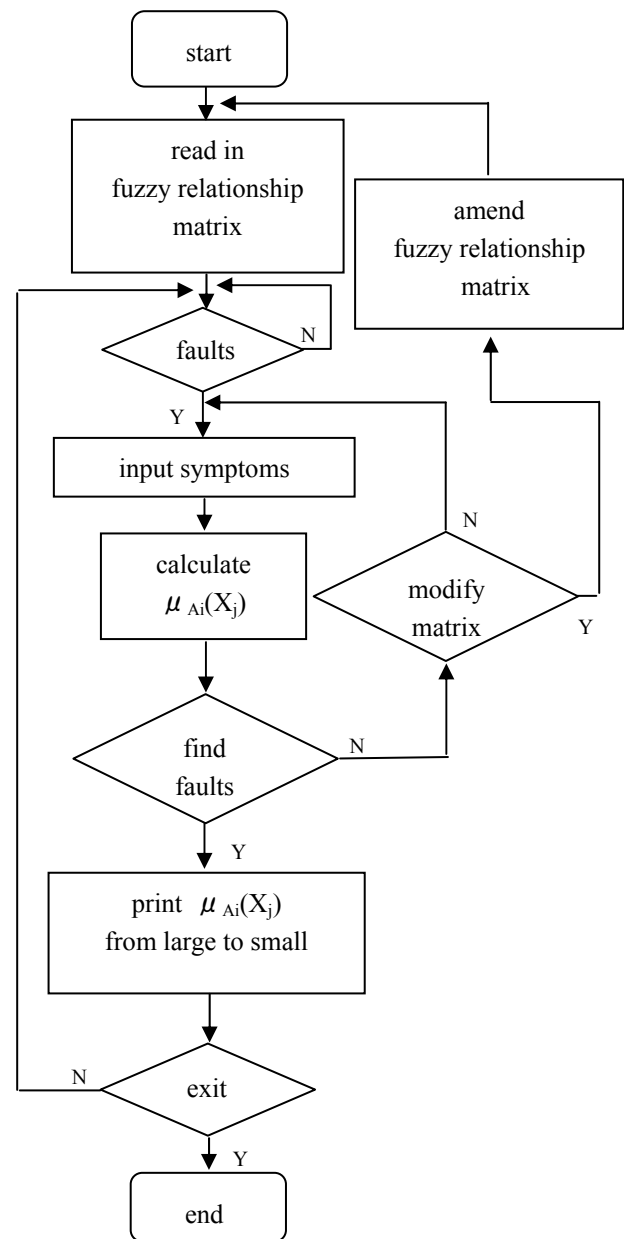


Fig.2 The algorithm diagram

is imported to the computer as a system database.

Some faults have been set intentionally, and they all can be detected. The detailed analysis is given by Ref. 4.

For the purpose of detailed explanation, an example is given in Table 2.

Table 2. An example.

$\omega_{ir}$	$X_1$	$X_2$	$X_3$	$X_4$	$X_5$	$X_6$	$X_7$	$X_8$
---------------	-------	-------	-------	-------	-------	-------	-------	-------

A <sub>1</sub>	1	0	15	5	100	0	2	10
A <sub>2</sub>	5	10	100	0	0	2	4	7
...	...	...	...	...	...	...	...	...

If there are symptoms of x<sub>2</sub>, x<sub>3</sub>, x<sub>4</sub>, that is X<sub>j</sub>={x<sub>2</sub>, x<sub>3</sub>, x<sub>4</sub>}, then

$$\mu_{A_1}(X_j) = \frac{0 + 15 + 5}{1 + 0 + 15 + 5 + 100 + 0 + 2 + 10} = 0.15,$$

$$\mu_{A_2}(X_j) = \frac{10 + 100 + 0}{5 + 10 + 100 + 0 + 0 + 2 + 4 + 7} = 0.86.$$

Then from symptoms of x<sub>2</sub>, x<sub>3</sub>, x<sub>4</sub>, the probability that the fault state is A<sub>2</sub> is larger than A<sub>1</sub>. Because the weight of x<sub>3</sub> in A<sub>2</sub> is very large, if symptom x<sub>3</sub> happens, the most probable fault state is A<sub>2</sub>. Of course this is a simple example, but the principle is the same.

### 5. Conclusion

Based on experience and statistical data, accurate fuzzy relationship matrix between the outside fault phenomena and fault sources can be identified after a series of training. This relationship can be stored in the computer as a database, and the important parameters can be on-line sampled and analyzed. When faults occur, the faults can be found, alarm is given<sup>5</sup>.

One thing worthy of mention is that this method does not provide the exact fault positions, but the maximum probability of fault sources. To detect and diagnose the faults quickly and accurately, the key work is to optimize the X<sub>0</sub><sup>i</sup>-A<sub>i</sub> standard fuzzy relationship matrix and obtain

the perfect weight  $\omega_{ir}$ .

### Acknowledgements

The research is partly supported by the Open Foundation (YF11700102) of Key Laboratory for Water Environment and Resources, Tianjin Normal University; and the Scientific Research Foundation of Tianjin University of Science and Technology (20130123).

### References

1. Frank PM, Fault diagnosis in dynamic systems using analytical and knowledge-based redundancy – a survey, *Automation*, 26 (1990) : 459 - 474.
2. Zhou DH, Frank PM., Sensor fault tolerant control of non-linear system: A unified approach. In *Proc. TEMPUS*

*Workshop on Advanced Control Systems in System Modeling, Fault Diagnosis and Fuzzy Logic*, (Sydney, 1996), pp. 69-79.

3. F. Dai, The research of fault diagnosis on the servo system. (*Beijing Institute of Technology*, 1998).
4. D. MA, Y. HU, F. DAI, Application of Maximum Probability Approach to The Fault Diagnosis of a Serve System. *Journal of Beijing Institute of Technology*, 11(1), (2002):29-32.
5. LP. Khoo, SB. Tor, JR. Li, A Rough Set Approach to the Ordering of Basic Events in a Fault Tree for Fault Diagnosis, *Int. J. Advanced Manufacturing Technology*, 17(10) (2001):769-774.

# The Fractional Order Hyperchaotic Generalized Augmented Lü System and its Circuit Implementation

**Xue Wei**

*Department of Automation , Tianjin University of Science and Technology,  
1038 Daguanlu Road, Hexi Distric, Tianjin 300222, PR China*

**Jinkang Xu**

*Department of Automation , Tianjin University of Science and Technology,  
1038 Daguanlu Road, Hexi Distric, Tianjin 300222, PR China*

**Hongyan Jia**

*Department of Automation , Tianjin University of Science and Technology,  
1038 Daguanlu Road, Hexi Distric, Tianjin 300222, PR China  
E-mail:xuewei@tust.edu.cn, xiaohuiJC@126.com  
www.tust.edu.cn*

## Abstract

In this paper, a commensurate fractional-order hyperchaotic generalized augmented Lü system is investigated. we analyze its chaotic characteristics by drawing phase portraits, Poincaré maps, Lyapunov exponent spectra and power spectrum, and find that the system can present a four-wing hyperchaotic attractor. In addition, a circuit is designed for this system and the circuit implementation result show the existence of the four-wing hyperchaotic attractor, which verifies the correct of the theoretic analysis and provides the support for its application in engineering.

*Keywords:* Fractional-order; Generalized augmented Lü system; Hyperchaos; Numerical simulation; Circuit design.

## 1. Introduction

Since Lorenz found the first chaotic attractor in 1963,<sup>1</sup> the study of chaotic phenomenon have received great attention during the past forty years and many chaotic systems have been proposed to research<sup>2-5</sup>. Due to its complex characteristics such as extremely sensitive to initial conditions, inherent randomness, continuous broadband spectrum and so forth, chaotic system can be widely applied in engineering like secure communication, image encryption and so on<sup>6-8</sup>. While hyperchaos is characterized as at least two positive Lyapunov exponents, which is more complex than chaos, so it is more suitable for the engineering application.

Fractional order calculus is a kind of calculus with an arbitrary order, which has become a hot spot during the past decades for its application in engineering. It is found that the fractional-order system could reflect the

physical phenomenon more accurately and fractional-order chaotic systems have more complex dynamics characteristics than integer-order chaotic systems<sup>9</sup>.

In this paper, a new fractional order hyperchaotic system is proposed and we analyze its chaotic characteristics through Matlab numerical simulations. Furthermore, an analog circuit is designed to realized the proposed fractional order hyperchaotic system ,and the circuit experiment results agree with the theoretic analysis.

## 2. System Analysis

According to the generalized augmented Lü system<sup>10</sup>, by introducing linear state feedback controllers into its second and third equation, Xue et al<sup>11</sup> adopt chaos anti-control to construct the hyperchaotic generalized augmented Lü system. On this basis, we will investigate the commensurate fractional

order hyperchaotic generalized augmented Lü system which is described as follow:

$$\begin{cases} \frac{d^q x_1}{dt^q} = -\frac{ab}{a+b}x_1 - x_2x_3, \\ \frac{d^q x_2}{dt^q} = ax_2 + x_1x_3 + x_4, \\ \frac{d^q x_3}{dt^q} = bx_3 + x_1x_2 + cx_1 + x_1x_4, \\ \frac{d^q x_4}{dt^q} = dx_2, \end{cases} \quad (1)$$

Where  $0 < q < 1$ ,  $a, b, d < 0$  and  $c \in R$ . Here when  $q=0.9$ , system(1) is characterized as a 3.6 order system(1).

### 3. Phase Portraits and Poincaré Maps

When  $q=0.9, a=-9, b=-14, c=1, d=-1$ , the phase portraits of system(1) is shown in Fig.1. It can be seen that the fractional-order system presents four-wing chaotic attractor.

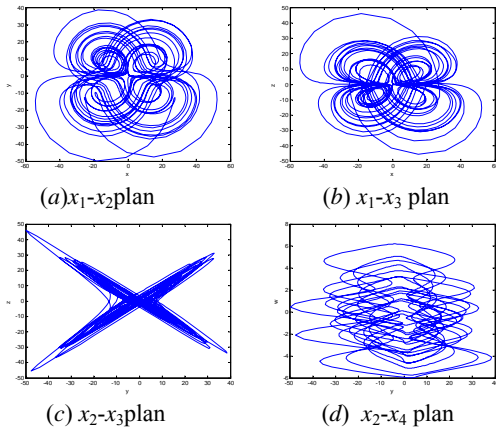


Fig.1 Phase portraits of system (1)

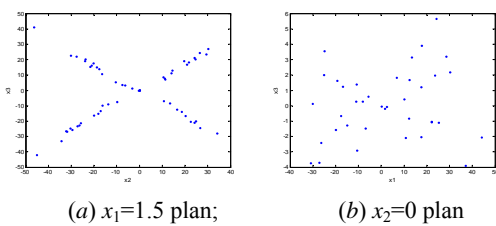


Fig.2 Poincaré maps of system (1)

Poincaré map is known as an intuitive way to determine whether a system is chaotic. From Fig. 2, we can see that Poincaré maps of system(1) are formed by points in confusion, which indicates system(1) is in chaos state. Furthermore, by calculating the Lyapunov exponents of system(1) when  $q=0.9, a=-9, b=-14, c=1, d=-1$ , we get  $L_1=1.6987, L_2=0.6500, L_3=-0.2817, L_4=-19.5887$ . For it has two positive Lyapunov

exponents, system(1) presents hyperchaos and we get the dimension of system(1) as

$$\begin{aligned} D_L &= j + \frac{1}{|LE_{(j+1)}|} \sum_{i=1}^j LE_i = 2 + \frac{LE_1 + LE_2}{|LE_3 + LE_4|} \\ &= 2 + \frac{1.6987 + 0.6500}{|-0.2817 - 19.5887|} = 2.118 \end{aligned}$$

indicating that hyperchaotic system(1) has a fractional dimension with a fractal feather.

### 4. Lyapunov Exponent

In order to analyze the chaotic characteristics of system(1) as system parameters change, we draw the Lyapunov exponent spectra of system(1) as shown in Fig. 3 (As  $L_4$  is always less than -10, so we only give curves of  $L_1, L_2, L_3$ ) when parameter  $a, b$  change in a certain range. From Fig. 3, we can observe that as  $a, b$  vary in a larger range, system(1) has two positive Lyapunov exponents, which shows that system(1) presents hyperchaotic in a large range as parameters change.

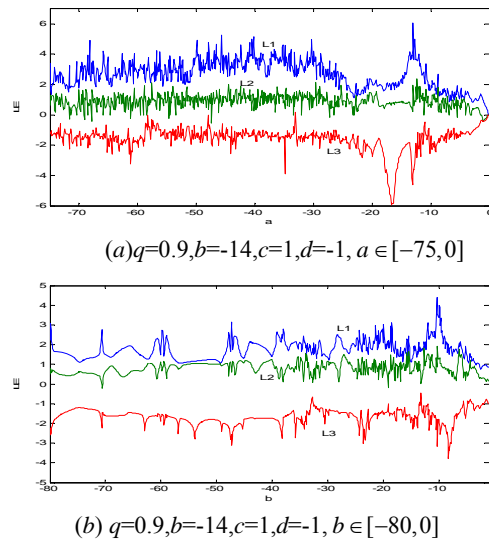


Fig.3 Lyapunov exponent spectra of system (1)

### 5. Power Spectrum

In addition, the power spectrum of system(1) is shown in Fig. 4 when  $q=0.9, a=-9, b=-14, c=1, d=-1$ . It can be seen that the power spectrum of system(1) is a continuous decreasing curve with noise background and wide band.

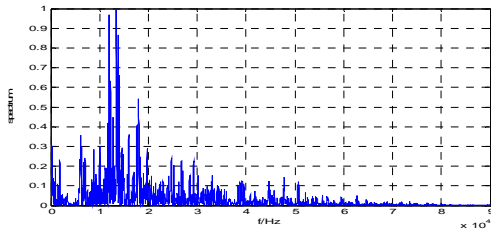


Fig.4 Power spectrum of system(1)

**6. Circuit Implementation**

we usually adopt the method of the approximation conversion from time domain to frequency domain to design a chaotic circuit. Here we utilize the approximation of  $1/s^{0.9}$  with discrepancy 2dB to design the analog circuit of 3.6 order hyperchaotic system(1). According to Ref. [12], we can get

$$\frac{1}{s^{0.9}} \approx \frac{2.2675(s+1.292)(s+215.4)}{(s+0.01292)(s+215.4)(s+359.4)}$$

In Ref.[13], a circuit unit is proposed to realize the  $1/s^{0.9}$  as shown in Fig.5. Where  $R_1=62.84M\Omega, R_2=250K\Omega; R_3=2.5K\Omega; C_1=1.232\mu F, C_2=1.84\mu F, C_3=1.1\mu F$ .

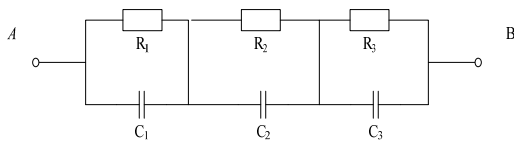


Fig. 5 Circuit unit of  $1/s^{0.9}$

Here LF347N is selected as the amplifier and AD633JN (the output gain is 0.1) as the multiplier to design the hyperchaotic circuit. In order to restrict the change of state variables to the operating voltage of the analog circuit, the state variables are decreased by 10 times, namely  $(x_1, x_2, x_3, x_4) \rightarrow (20x_1, 20x_2, 20x_3, 20x_4)$ . The analog circuit design of 3.6 order hyperchaotic system(1) when  $a=-9, b=-14, c=1, d=-1$  is shown in Fig. 6, where F09 represents the circuit unit of  $1/s^{0.9}$  and  $R_1=1.825K\Omega, R_3=1.111K\Omega, R_4=10K\Omega, R_6=0.714K\Omega, R_7=R_{10}=10K\Omega, R_2=R_5=R_8=R_9=50\Omega$ . If we choose  $R_4$  as a reference resistance, we can change the value of  $a, b, c, d$ , by changing the ratio of  $R_3, R_6, R_7, R_{10}$  to  $R_4$  respectively.

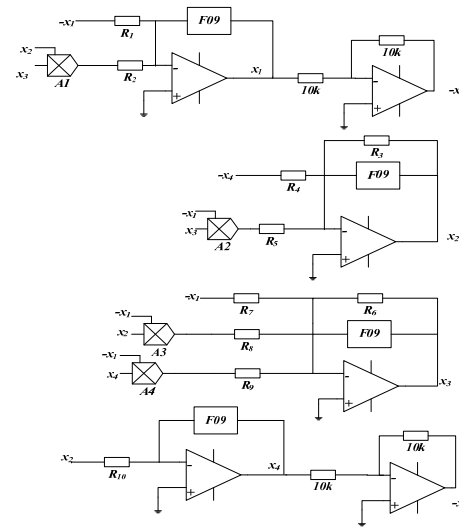


Fig. 6 Circuit diagram of 3.6 order system(1)

Based on the circuit diagram in Fig.6, we conduct the circuit experiment and the result is observed through the YB4365 analog oscilloscope as shown in the Fig.7, which agrees with the numerical simulation result, verifying the existence of hyperchaotic attractor in 3.6 order system(1).

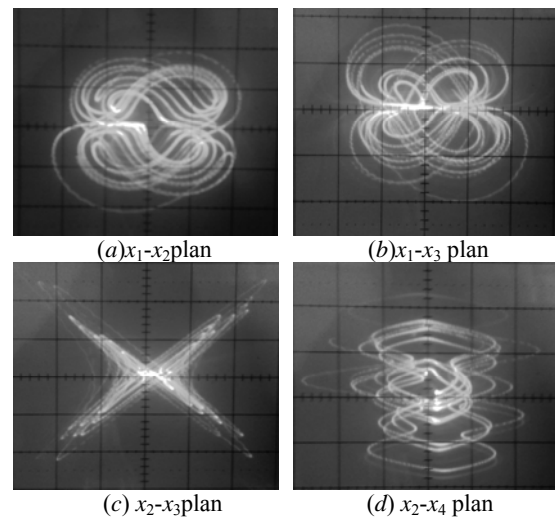


Fig.7 Phase portraits of 3.6 order hyperchaotic system(1) through the oscilloscope YB4365

**7. Conclusion**

In this paper, the fractional order hyperchaotic generalized augmented Lü system is investigated. By analyzing phase portraits, Poincaré maps, Lyapunov exponent spectra and power spectrum of the fractional order system, it is found that there exists four-wing

hyperchaotic attractors in the system and the system is hyperchaos with a fractional dimension in a large range of parameters. Moreover, take 3.6 order system for example, an analog circuit is designed to implement the fractional order hyperchaotic system and circuit experiment results agree with the numerical analysis, providing technical basis for its further application in engineering.

### Acknowledgements

This work is supported by the Young Scientists Fund of the National Natural Science Foundation of China (Grant No.11202148).

### References

1. Lorenz E N. Deterministic Non-periodic Follow. *Atoms. Sci.* 1963, 20:130-141.
2. Liu C X, Liu L, Liu T, et al. A new butterfly-shaped attractor of Lorenz-like system. *Chaos, Solitons and Fractals.* 2006, 28(5) 1196-1203.
3. Lü J H, Chen G R. A new chaotic attractor coined. *Int. J. Bifurcation and Chaos.* 2002, 12(3) 659-661.
4. Chen G R, Ueta T. Yet another chaotic attractor. *Int. J. Bifurcation and Chaos.* 1999, 9(7):1465-1466.
5. Qi GY, Chen GR, van Wyk MA, van Wyk BJ and Zhang Y. A four-wing chaotic attractor generated from a new 3-D quadratic autonomous system. *Chaos, Solitons & Fractals.* 2008, 38(3): 705–721.
6. Han Q, Liu C X, Sun L Zhu D R. A fractional order hyperchaotic system derived from a Liu system and its circuit realization. *Chin. Phys. B* 2013, 22(2) 020502.
7. Peng Z P, Wang C H, Lin Y, Luo X W. A novel four-dimensional multi-wing hyper-chaotic attractor and its application in image encryption. *Acta. Phys. Sin.* 2014, 63(24):240506.
8. Sheng Q W, Jiang B. Chaotic encryption algorithm in the network security technology research and application. *Network Security Tech. & Appl.* 2014, (8):51-51.
9. Hifer R. *Applications of Fractional Calculus in Physics.* (New Jersey: World Scientific, 2001).
10. Qiao X H, Bao B C. Three-dimensional four-wing generalized augmented Lü system, *Acta. Phys. Sin.* 2009, 58(12) 8152-8159.
11. Xue W, Fang Y F, Li Q. A novel four-wing hyper-chaotic system and its circuit implementation, *Procedia Engineering*, 2012, 29:1264-1269.
12. Ahlnad W M, Sprott J C. Chaos in fractional-order autonomous nonlinear systems. *Chaos, Solitons and Fractals*, 2003, 16(2) 339-351.
13. Wang F Q, Liu C X. Study on the critical chaotic system with fractional order and circuit experiment, *Acta Phys. Sin.* 2006, 55: 3922-392



# Selecting Words and Notation Using Literary Data in the Integrated Narrative Generation System

**Jumpei Ono<sup>†</sup>**

*Department of Software Information Science, Iwate Prefectural University  
152-52 Sugo, Takizawa, Iwate Science, 020-0693, Japan*

**Takashi Ogata<sup>‡</sup>**

*Department of Software Information, Iwate Prefectural University  
152-52 Sugo, Takizawa, Iwate, 020-0693, Japan  
E-mail: <sup>†</sup>g236m001@s.iwate-pu.ac.jp, <sup>‡</sup>t-ogata@s.iwate-pu.ac.jp*

## Abstract

This paper presents a way for selecting noun concepts based on the analysis of appearance frequency of noun words in the data of modern Japanese novels (“Aozora Bunko”). The proposed method is incorporated into some mechanisms in our integrated narrative generation system (INGS). We also show an overview of INGS, in particular the mechanism relating the proposed method in this paper. Additionally, we introduce a preliminary experiment to confirm and discuss the effectiveness.

*Keywords:* Integrated Narrative Generation System, Word Frequency, Conceptual Dictionary, Noun Concepts, Word Notation, Aozora Bunko.

## 1. Introduction

Language generation controlled by a story or as a narrative is an important communication ability in robotics and artificial life. We have been developing a narrative generation system called “Integrated Narrative Generation System: INGS” [1,2]. In intelligent informatics such as natural language processing and artificial intelligence, narrative generation or story generation is an important and challenging topic in the following scientific and applicable points: an interdisciplinary approach of informatics and literary theories including narratology, generating consistent discourse structures, creating advanced contents technologies, etc. INGS is a synthesis of our various previous researches of narrative generation.

INGS generates narrative events and the sentences using the generation techniques and knowledge

elements including conceptual dictionaries [3] and language notation dictionary [4]. Though we will give the mechanism in the next section, overview, INGS selects the noun concepts (terminal nodes in the hierarchical structure) in an event to be generated in the limited range (the lower range of one or more intermediate noun concepts) in the noun conceptual dictionary. But, the selection is randomly processed. As the lower range of an intermediate noun concept includes various types of noun concepts, for example difficult/easy, new/old, etc., various types noun concepts are mixed in the generated events in many cases. In the mechanism of INGS, noun concepts are basically defined by the level of words and noun concepts are transformed to words with each actual letter representation (notation) using a language notation dictionary. So selecting the concepts directly has an influence on the quality of generated sentences. Our

© The 2015 International Conference on Artificial Life and Robotics (ICAROB 2015), Jan. 10-12, Oita, Japan

goal to solve it is implementing more strategic mechanisms for concepts (and notations) selection and this paper will present a simple method based on the frequency analysis of words' appearance as the first step.

In particular, we automatically analyze frequency information of noun words from novels stored in "Aozora Bunko", which is a digital library that includes a variety of texts of modern Japanese novels mainly, to select noun concepts in events to be generated according to the acquired frequency information. For example, if we use noun concepts according to high-frequency noun words, the output text will be more readable.

There are studies of word familiarity relating to the theme of this paper. [5] considered the readability of a sentence based on the relationship between word familiarity and word frequency and sorted sentences based on readability according to the idea that high-frequency words are high-familiarity words.

In the large framework, our goal is not necessarily only readable story generation. Readable story generation based on high appearance frequency, namely concepts and words selection easy to read, is one of the strategic choices. In contrast, we will be able to make more difficult or strange sentences intentionally using low-frequency words and concepts. Additionally, for the processing relating to the final words notation in INGS, for instance, we will be able to concentrate on analyzing specific authors to simulate or imitate words representation in each style of authors. Though it is not the theme of this paper, we will mention the attempt.

## 2. An Overview of INGS and Noun Concept Selection Mechanism

This section will give an overview of INGS architecture to show the noun concepts selection mechanism. The architecture of INGS has two types of macro level parts (Fig. 1.): "generation mechanism" and "knowledge mechanism". The former part has three main elements of "story generation mechanism", "discourse mechanism", and "surface generation mechanism (including language, music, and image)". The main elements of the latter "knowledge mechanism" are "conceptual dictionaries (for noun concepts and verb concepts chiefly)", "language notation (letter notation) dictionary", "state-event transformation knowledge base", and so on.

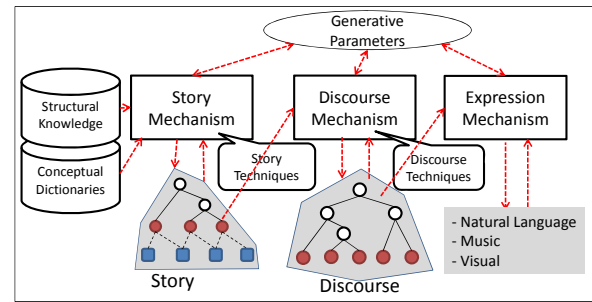


Fig. 1. The architecture of INGS

### 2.1. Generation Mechanisms

In story generation, "story" means the content of a narrative or a temporal sequence of events. In narrative generation process, a story is described as a tree structure in which the basic elements are an event that is described by conceptual representation and a relation for combining among events or sub-structures. Additionally, an event is principally combined with a preceding state and a subsequent state. The major functions are holding the knowledge about a story world and managing the coherency of the flow of events. A story structure including events and relations is generated using one or more story techniques and states associating with the events are made according to another mechanism.

In the next discourse mechanism, "discourse" means how to form a narrative, which is a sequence or a structure of events to be narrated actually. A discourse is corresponded to the structure as the transformation of a story's structure and various discourse techniques process the structural transformation. We use the narrative discourse theory by Genette [6] for the categorization of discourse techniques. In the expression mechanism, "expression" means the part for representing the above conceptual representations with surface media including mainly natural language, such image or visual media as animated movie, and music.

The first two phases are conceptual generation parts in a process. Both of story and discourse structures are commonly represented by each structure to be operated respectively using various types of techniques. As stated above, we call the structural operation techniques "story techniques" and "discourse techniques".

### 2.2. Conceptual Dictionaries

An event is constructed with the instantiation of conceptual materials stored in conceptual dictionaries for noun concepts and verb ones. Each dictionary has a hierarchical structure from higher concepts to lower ones. The noun dictionary currently contains 115765 terminal concepts and 5809 intermediate ones. Each intermediate concept has (1) a list of hyponymy concepts, (2) the number of depth in the hierarchy, (3) the serial number of the super-ordinate concepts, and (4) the range of serial numbers of the hyponymy concepts (Fig. 2.). Fig. 3 shows the description of a noun concept.

```
(<intermediate concept>
(hierarchy
(depth <number>)
(hype <intermediate concept>)
(hypo <intermediate concept>)
(terminal <terminal concept>)))
```

Fig. 2. Description form of an intermediate concept

```
(男[Man]
(hierarchy
(depth 8)
(hype 人間<男女>[Human<Gender>])
(hypo 男[接辞][Man[Affix]])
(terminal 男[Man] 父[Father] 少年[Boy]...))
```

Fig. 3. The description of the noun concepts, "Man"

On the other hand, the verb concepts hierarchy has 11951 terminal concepts and 36 intermediate categories. Each terminal verb concept describes the following three elements: (1) a "sentence-pattern" to show a pattern for a sentence including the verb, (2) one or more "case-frame(s)" to show the types of required noun cases, and (3) one or more "constraint(s)" to define the range in the noun conceptual dictionary in which each noun concept in the above case-frame(s) requires. For example, Fig. 4. is the description of the verb concept, "eat". When INGS materializes the framework of a case-frame, it selects concepts in the noun conceptual dictionary. The objective of the paper is revising the selecting method.

```
((name 食べる 2 [eat])
(sentence-pattern "N1 が N2 を食べる"[N1 eat N2])
(case-cons-set
((case-frame ((agent N1) (object N2) ...))
(constraint ((人[human] -死人[corpse]
-人間<人称[person]> -準人間[semi-human])
(食料[food] -調味料[flavoring]
-飲物[drink]・たばこ[cigarette])) ...)))
```

Fig. 4. The description of a verb concept

### 2.3. Concept Selection in Story Generation

First, we show a story structure to be generated in the story generation mechanism in INGS to explain a story generation process (Fig. 5.). As indicated in the above figure, the hierarchical structure of a story is constructed with three elements: (1) an "event" consists of a verb concept and some noun concepts (as stated above), (2) a "state" is the attribute information to position before and behind of the events (an event changes a state to the next state), and (3) a "relation" connects the lower structure semantically.

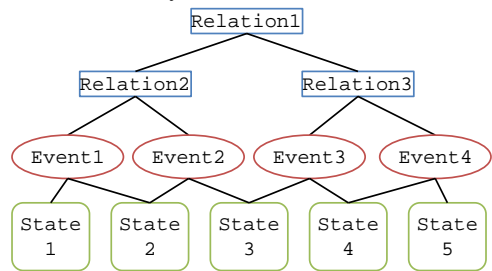


Fig. 5. The form of a story structure

A story generation process is equal to expanding or transforming a story structure. In particular, under some parameters ("macro-structure", "length", etc.) given in the first step, a story technique makes a new event or a sub-structure including one or more new events using a variety of story contents knowledge to integrate them into the original structure using various relations. According to a generated new event, new states are also generated. When an event is generated, the above story contents knowledge gives the basic form based on the description of a case-frame in Fig. 4. Each constraint indicates the range in the noun conceptual dictionary to decide a noun concept. Actually, each noun concept in an event is transformed into an instance using attribute information if necessary. Finally, each generated event is transformed into a natural language sentence using specific word representation. Fig. 6 shows the process.

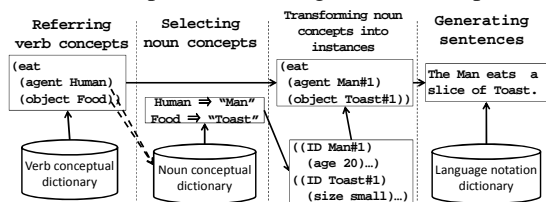


Fig. 6. The process of generating an event

As mentioned above, in applying constraints to choose noun concepts, terminal concepts under an intermediate node in the noun conceptual dictionary are not fully organized. In the following sections, we will present a method using words' appearance frequency instead of revising the organization or structure.

### 3. Concept Selection Based on Word Frequency

We will describe the method to analyze word frequency and show some generation examples using the result.

#### 3.1. The Method of Word Frequency Analysis

We have analyzed word frequency in 4980 texts (mainly novels) in Aozora Bunko from 1872 through 1963 to use it for noun concept selection in story generation. The image of the processing is shown in Fig. 7. KH Coder [7] is used in the analysis in the first step to account the word frequency. And the mechanism links acquired frequency information to the corresponded noun concepts in the noun conceptual dictionary.

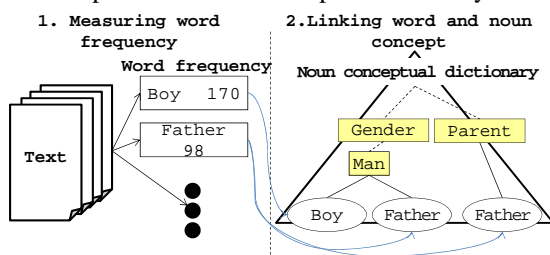


Fig. 7. An image to use frequency

We describe the method in detail. Firstly, in the texts (corpus) to be used, we have accounted the word frequency for “general nouns”, “nominalized adjectives”, and “nouns as stems of adjectival verbs”.

On the other hand, in the noun conceptual dictionary to give frequency, for such 3549 noun concepts that become a concept by the combination with another concepts as “～学校 [～school]”, we do not give frequency. Additionally, terminal noun concepts that have a same name sometimes exist under different intermediate concepts. For example, two intermediate concepts, “君主 [王](monarch)” and “貴人 [君主](nobleman)”, respectively include a terminal concept, “王 (king)”. The number of this type of terminal concepts was 28421. When such overlapped terminal noun concepts appear in analyzing a text, the

mechanism adds frequency 1 to all the concepts. We count the overlapped noun concepts as one concept, so the above 28421 are equal to the number of sets of overlapped concepts and 36187 concepts that the 28421 are eliminated from all the overlapped concepts are not included in the range of the noun conceptual dictionary to add frequency. Considering the above conditions, the number of terminal noun concepts to which appearance frequency should be added is 76029 (for 115765 terminal concepts in the noun conceptual dictionary).

According to the conditions, the mechanism analyzes the word appearance frequency in the target texts by morphological analysis. As stated above, the mechanism accounts the frequency of “general nouns”, “nominalized adjectives”, and “nouns as stems of adjectival verbs”. Next, the proposed mechanism relates the above nouns with frequency to terminal noun concepts in the noun conceptual dictionary by simple matching. Though each description of noun concepts is theoretically a kind of label and the linguistic notation is proposed by the language notation dictionary, a general notation is actually used for each of the description.

As a result, we have acquired word frequency for 57131 nouns in the target texts and linked the frequency to 44332 terminal noun concepts. 44332 concepts are equal to 58% for all terminal noun concepts in the noun conceptual dictionary in INGS.

#### 3.2. Concept Selection Based on Frequency

Fig. 8. is an example of story generation using noun concepts with the highest frequency. Actually, it is the result transformed by “sentence generation mechanism” in INGS. An event in a story is simply transformed into a sentence based on the sentence pattern. Additionally, the future version of INGS is necessary to change some noun representations in each sentence to another nouns using attributes for each noun concept. For instance, “child” will be changed to an actual name such as “Taro”. The mechanism will enable to represent a noun concept by a noun phrase, such as “Taro in a forest”.

### 4. Preliminary Evaluation and Discussion

We conducted a survey to find out the effectiveness of selecting noun concepts in stories generated based on the acquired frequency. The subjects were 4 students.

子が「子が煙草を摘む」ために出かける。蛇が毒素を薬に混入する。蛇が薬を女に与える。女が眠る。蛇が名人に対して「名人が女を樽に詰める」と命令する。名人が女を樽に詰める。蛇が名人に「名人が樽を海へ投げる」と命令する。名人が樽を海へ投げる。勇士が土から国まで来る。殿が勇士に助けを求める。殿が勇士を送り出す。勇士が冒険に備える。勇士は国から帝国へ出国する。婆が「勇士が屑を食べる」ことを勇士に命じる。勇士が命に従う。勇士が屑を食べる。婆が百姓を勇士に紹介する。勇士が百姓に会う。百姓が杖を勇士に譲渡する。杖が勇士を庭に運れる。勇士が蛇と戦う。蛇が時計を奥より下に落とす。勇士が時計を拾う。蛇が勇士に敗れる。勇士が女を発見する。勇士が森を飛び出す。勇士が女を捕らえる。勇士が女を方向に運れる。勇士が帝国から脱出する。勇士が帝国より国へ到着する。男が言い張る。男が礼を殿に要求する。殿が勇士と会う。勇士が時計を持参する。勇士が時計を女に返す。女が現実を知る。女が現実を殿に伝える。殿が現実を知る。殿が「男が殿に「男が女を助ける」と嘘を言う」ことに気付く。男の夢が露見する。勇士が公に昇格する。殿が蛇を容赦する。殿が男を容赦する。勇士が女と結婚する。<<<A child goes out to cull tobacco. A snake mixes a toxin in medicine. The snake gives a woman the medicine. The woman sleeps. The snake orders a master to pack the woman in a barrel. The master packs the woman in a barrel. The snake orders the master to throw the barrel into the sea. The master throws the barrel into the sea. A warrior comes from a ground to a nation. A lord asks for helping the warrior. The lord sends away the warrior. The warrior provides against an adventure. The warrior departs from the nation to an empire. An old maid orders eating rubbish to the warrior. The warrior obeys the old maid. The warrior eats the rubbish. The old maid introduces a farmer to the warrior. The warrior meets the farmer. The farmer transfers a staff to the warrior. The staff takes the warrior to a garden. The warrior fights the snake. The snake drops a clock from the inside to the bottom. The warrior picks up the clock. The warrior is defeated by the snake. The warrior discovers the woman. The warrior rushes out of forest. The warrior catches the woman. The warrior takes the woman to the direction. The warrior escapes from the empire. The warrior arrives at the nation from the empire. A man insists to help the woman. The man demands a reward from the lord. The warrior meets the lord. The warrior brings the clock with the warrior. The warrior returns the clock to the woman. The woman knows the actuality. The woman conveys the actuality to the lord. The lord knows the actuality. The lord realized “the man lies “the man helps the woman”. The man’s dream discovers. The warrior is promoted to a duke. The lord pardons the snake. The lord pardons the man. The warrior marries the woman.>>>

Fig. 8. The result of a story generation based on the frequency (Japanese: the original sentences, English: the translation)

For the survey, we prepared five stories including the above example based on the following frequency: [Random] when the mechanism selects a noun concept in an event, it randomly selects a concept from the range of intermediate concepts, [Max] the mechanism selects a concept with the highest frequency, [Middle] it selects a concept with the middle frequency, [Min] it selects a concept with the lowest frequency, [Zero] it selects a concept with no description of frequency. In all cases, if there are two or more candidates, the mechanism randomly selects one concept.

The procedure of the experiment is as follows. The subjects read each story and select one of the evaluation values for pointed nouns: (1) no strange, (2) a few strange, and (3) very strange. Additionally, we set a

time limit (5 minutes) for a story. And we prescribed to not change the already described values and not necessary to confirm previous values.

Table 1. shows the result. The values indicates that the nearer 1, the smaller the sense of strange. This result was same with previous survey [8] which had been conducted for 8 subjects in the halfway stage of the analysis of Aozora Bunko. An interesting point was as follows. As we did the experiments using generated sentences directly, the subjects were sometimes had an effect on contextual information within a sentence or between sentences. It indicates that contextual conditions were also considered in selecting concepts. Considering the problem will be a future issue. On the other hand, in the “average” in this experiment, differences between [Max] and the others were relatively small. This indicates that controlling extremely unreadable word representation is difficult in this way. It will be also an important future topic.

Table 1. The evaluation result

Subject	Random	Max	Middle	Min	Zero
A	1.79	1.04	1.48	1.63	1.85
B	1.40	1.00	1.46	1.45	1.23
C	2.39	1.69	2.25	2.77	2.79
D	1.06	1.06	1.11	1.26	1.04
Average	1.66	1.20	1.57	1.78	1.73

The result of the frequency analysis, there were 12799 words which did not exist in the noun conceptual dictionary. Table 2. shows the two types. “No existing words” (7928) will be able to add to the noun conceptual dictionary. This category includes many complex words. And, in many cases, as the parts are stored in the current version of the noun conceptual dictionary, we would like to address the way for using the knowledge to add the concepts.

In the type of “the problem of notation”, a similar noun concept with a word exists in many cases. The number of such words was 4871. In Table 3., we show concepts to be corresponded to such words. We will be able to connect such words to elements in the language notation dictionary as mentioned above. The language notation dictionary is a writing system which stores letter representations for all concepts using Kanji, Hiragana, Katakana, etc. The extracted words from Aozora Bunko which does not match with concepts directly sometimes are found out in the language

notation dictionary. We will be able to use the mechanism for such words and concepts.

Table 2. Types of words which did not exist

Types		Example
The problem of notation		ネジ[Screw]
		ボランティア[Volunteer]
		食欲[Appetite]
No existing words	Complex words	駅前通り[Street in front of station]
	Others	カフェ[Cafe]

Table 3. Extracted words and the similar concepts

Words	Corresponding concepts
ネジ[Screw]	螺子[Screw]
ボランティア[Volunteer]	ボランテア[Volunteer]
食欲[Appetite]	食欲[Appetite]

### 5. Connecting to Word Representation

As described above, we have been developing a language notation dictionary to give some notation or word (letter) representation for each noun concept (and verb concept). In the part of sentence generation in INGS in which transforms concepts to actual word representation, we have been trying to simulate the characteristics in various authors' novels [9]. In particular, for a novel or a part of a novel, we statistically analyzed the percentage of Kanji, Hiragana, Katakana, etc. for main word classes. In Fig. 9. and Fig. 10., we apply the above method to sentences generated by the proposed method in this paper (Fig. 8.).

子が「子が煙草を摘む」ために出かける。蛇が毒素を薬に混入する。蛇が薬を女に与える。女が眠る。蛇が名人に「名人が女を樽へ詰める」と命令する。名人が女を樽に詰める。蛇が名人に対して「名人が樽を海に投げる」と命令する。名人が樽を海へ投げる。勇士が土から邦に来る。<The rest is omitted>

Fig. 9. Sentences represented according to the notation analysis of 「蜘蛛の糸 (The Spider's Thread)」

子が「子が煙草を摘む」ことにてかける。蛇が毒素を薬にこんにゆうする。蛇から薬を女へあたえる。女がねぶる。蛇が名人に対して「名人が女を樽へ詰める」とことめいれいする。名人が女を樽へ詰める。蛇が名人に「名人が樽を海へ投げる」とことめいれいする。名人が樽を海へなげる。<omission> 勇士ガトケイをヒラウ。ヘビガ勇士にヤブレル。ユウシガ女ヲハツケンスル。勇士ガモリをトビダス。ユウシガ女ヲトラエル。勇士ガ女ヲホウコウヘツラネル。ユウシガ帝国よりダッシュツスル。<The rest is omitted>

Fig. 10. Sentences represented according to the notation analysis of 「みずから我が涙をぬぐいたまう日 (The Day He Himself Shall Wipe My Tears Away)」

### 6. Conclusion

In this paper, we have proposed a way for selecting

noun concepts based on the frequency analysis of the data of Japanese modern novels. We have incorporated the proposed method into our integrated narrative generation system (INGS), in particular the story generation sub-system and the noun conceptual dictionary. And, we have confirmed the effectiveness through the preliminary experiments. Our future plan includes the following immediate and technological topics: the processing of complex words, expanding the noun conceptual dictionary using the result of the analysis, increasing the matching using the language notation dictionary. Additionally, the strategic control of the readability (including un-readability) of texts to be generated is more theoretical issues to be addressed.

### References

- [1] T. Ogata and A. Kanai, *An Introduction to Informatics of Narratology* (Gakubunsha, Tokyo, 2010).
- [2] T. Akimoto and T. Ogata, An Information Design of Narratology: The Use of Three Literary Theories in a Narrative Generation System, *The International Journal of Visual Design* 7(3) (2014) 31-61.
- [3] K. Oishi, Y. Kurisawa, M. Kamada, I. Fukuda, T. Akimoto and T. Ogata, Building Conceptual Dictionary for Providing Common Knowledge in the Integrated Narrative Generation System, *Proc. of 34th Annual Conference of the CogSci* (2012) 2126-2131.
- [4] S. Kumagai, S. Funakoshi, T. Akimoto and T. Ogata, Development of a Language Dictionary and a Simple Narrative Sentence Generation Mechanism, *Proc. of the 26th Annual Conference of The Japanese Society for Artificial Intelligence* (2010) 1J1-OS2-8.
- [5] K. Tanaka-Ishii, S. Tezuka and H. Terada, Sorting Texts by Readability, *Journal Computational Linguistics* 33(2) (2010) 203-227.
- [6] G. Genette, J. E. Lewin (trans.), *Narrative Discourse: An Essay in Method* (Cornell University Press, NY, 1980). (G. Genette, *Discours du récit, essai de méthode, Figures III* (Seuil, Paris, 1972).)
- [7] K. Higuchi, Quantitative Analysis of Textual Data: Differentiation and Coordination of Two Approaches, *Sociological Theory and Methods* 19(1) (2004) 101-115.
- [8] J. Ono and T. Ogata, Selecting Noun Concept Based on Quantitative Data: As a Mechanism in the Integrated Narrative Generation System, *IEICE Technical Report*. (2015. in printing)
- [9] M. Kamata and T. Ogata, Analysis and Imitation of the Japanese Letter Notation in Narrative Texts, *Proc. of the 27th Annual Conference of the Japanese Society for Artificial Intelligence* (2013) 214-5in.

# Evaluation of a Narrative Discourse Generation System Based on the Concept of “Norm and Deviation”

**Taisuke Akimoto**

*Graduate School of Informatics and Engineering, the University of Electro-Communications, 1-5-1 Chofugaoka  
Chofu, Tokyo 182-8585, Japan*

**Takashi Ogata**

*Faculty of Software and Information Science, Iwate Prefectural University, 152-52 Sugo  
Takizawa, Iwate 020-0693, Japan  
E-mail: t8akimo@yahoo.co.jp, t-ogata@iwate-pu.ac.jp*

## Abstract

This paper deals with the verification of the narrative discourse system that automatically produces a variety of “discourse” structures from an inputted “story” structure through an iterative mutual action between a “narrator” mechanism and a “narratee” mechanism. In particular, we analyze a series of 10000 generated discourse structures according to their structural feature values by focusing on the diachronic alternation of “norm”, the narratee’s expectation in receiving discourses. Based on the results, we discuss the achievement and issues to be addressed.

*Keywords:* narrative generation system, automatic analyses, narrative discourse, norm and deviation, Jauss.

## 1. Introduction

Automatic narrative generation is a challenging topic in the field of artificial intelligence. In this topic, methodology for evaluating systems is a difficult issue and has addressed by several researchers. Rowe et al.<sup>1</sup> and Zhu<sup>2</sup> argued for the need to combine the multiple aspects including the authorial process, generated texts, and reading process in the evaluation of narrative generation systems. Pérez y Pérez<sup>3</sup> and Peinado et al.<sup>4</sup> tried to formalize such evaluation criteria as coherence, interestingness, and novelty in generated narratives.

We have been addressing the development of the “Integrated Narrative Generation System” (INGS) based on an “expanded literary theory”, an interdisciplinary approach to narrative generation mechanism in INGS across informatics and literary theories.<sup>5, 6</sup> This paper deals with the verification of the narrative discourse

system that we have developed as a practice of the expanded literary theory.<sup>7, 8</sup>

The system automatically produces a series of “discourse” structures from an inputted “story” structure through an iterative mutual action between a “narrator” mechanism, which generates discourse structures, and a “narratee” mechanism, which receives the generated discourses. This cyclic generation model continuously produces discourse structures through the diachronic alternations of “norm”, the narratee’s “expectation” in receiving discourse structures, via its “deviation” by the narrator. The term “norm” means a fixed frame at the time of generating discourse structures and “deviation” means an action to try to produce a new type of discourse structure by breaking the norm.

This paper objectively consider the behavior of the implemented system for identifying its achievements, limitations, and issues to be addressed. We use

quantitative analyzing methods based on a conceptual framework of “norm and deviation”.

## 2. An Outline of the Narrative Discourse System

The narrative discourse system was implemented with Common Lisp. It automatically produces a series of discourse structures from an input story structure. The details of the mechanism and the generation examples were shown in our previous papers.<sup>7,8</sup>

### 2.1. The discourse structure generation

The generation of a discourse structure in the system means a transformation from a story structure into a discourse structure. A story is a content of a narrative or a temporal sequence of events. In contrast, a discourse means a structure of how the story is narrated. Each of a story and a discourse is represented with a tree structure. The main element of the tree structure is “event”, a character’s action, at each terminal node. Each internal node is a “relation” among the child nodes.

The structural transformation is done by using “discourse techniques” which define transformational operations of a part of the structure. The techniques are defined by referring a part of the discourse categories by Genette.<sup>9</sup> 13 types of discourse techniques including temporal ordering, repetition, and so on are implemented in the system. Different discourse structures are generated according to what techniques are used and where the techniques are applied in the tree structure. The techniques to be used are determined based on the narrator’s “generative goal” which we will describe latter. On the other hand, since the target of each technique is decided at random with several conditions, the output structures by a same generative goal have relatively small differences.

### 2.2. The generation cycle

The output discourse structures gradually change through the mutual action between the narrator and the narratee, called “generation cycle”. In each step, the narrator generates a discourse structure from a story structure according to a set of parameters as “generative goal” or targeting structural features. On the other hand, the narratee feeds back an evaluation of the generated discourse according to a set of parameters as “expectation” or desiring structural features. The ten parameters corresponding to structural features relevant

to the 13 discourse techniques are commonly used in the generative goal and the expectation: supplement, complexity, suspense, length, hiding, descriptiveness, repetition, diffuseness, implication, and temporal-independency. Each parameter takes a value of 1 (small), 2 (medium), or 3 (large).

The diachronic change of output discourses is arisen from the change of parameters’ values in both the generative goal and expectation. This mechanism is modeled based on our original reinterpretation of a part of the literary history model by Jauss<sup>10</sup>. The narrator basically sets the generative parameters to fit the narratee’s expectation and generates discourse structures iteratively. The narratee increases his satisfaction by receiving the fitted discourses to the expectation. The process, however, eventually reaches a point where the narratee gets tired or his satisfaction begins to fall. The turning point of the satisfaction is arbitrary set by the variable  $n_p$ . When this happens, “deviation” occurs and the narrator abandons a portion of the old generative parameters and moves to a new cycle of discourse grounded on the newly found strategy. The narratee’s expectations change according to the reconstruction. In this generation model, the role of the narratee’s expectation is to hold a “norm” for discourse generation.

## 3. The Framework of the Analyses

This section describes the framework of the analyses for a series of discourses produced by the system.

### 3.1. The structure of a series of discourses

A series of discourses can be structured as Fig. 1. Each allow beside “generative goal” and “expectation” in the figure means the duration of same parameters’ values. A “shift in norm” means a change of a parameter’s value in the expectation. We use a subscript number to indicate a specific norm like “norm<sub>i</sub>”. We call a discourse generated by the generative goal equal to the expectation “normative discourse” and a discourse by a generative goal not equal to the expectation “deviated discourse”. The processing of “deviation” is to change a parameter’s value in the generative goal at random and it causes a “shift in norm” in the next step. By segmenting the series with each “shift in norm”, the tale discourse in each segment is the “deviated discourse” and the others are “normative discourses”.



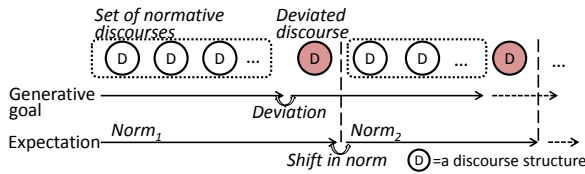


Fig. 1. The structure of a series of discourses.

### 3.2. Four aspects of the analyses

The basic idea of the analyses is to treat each discourse structure as a set of numerical values which represent structural features corresponding to the ten parameters. We call the values “discourse feature values” (DFVs). Each DFV is automatically calculated from a generated discourse. For example, “length” and “complexity” are respectively calculated based on the number of terminal nodes in a discourse structure and the number of relations needed for defining temporal order transformation. A set of discourse structures can be specially treated based on their DFVs. The degree of deviation is calculated as the distance between a space of normative discourses and the deviated discourse. The difference between two norms is also calculated as the difference of their spaces.

Based on the above method, we programed the analyses which consists of following four aspects.

- (i) *Local generation space*: The role of the norm is to restrict the generation space into a certain range. For confirming the behavior of norm-based generation, it analyzes the characteristics of the set of normative discourses in each norm.
- (ii) *Degree of deviation*: The deviation is a process to transcend the generation from the local generation space at the time. For clarify the actual action of the deviation, it calculates the distance of the deviated discourse from the local generation space.

(iii) *Degree of shift in norm*: For clarifying the manner of actual changes in local generation spaces, it calculates the magnitude of the difference of each norm from the last norm.

(iv) *Novelty of norm*: If local generation spaces are always different with all the past local spaces, the system can produce novel norms and discourses continuously. This analysis calculates the magnitude of the difference of each norm from the most similar norm in all the past norms.

## 4. Results and Discussions

We executed the system 10000 steps. The input story was same with the story in Ref. 8: A warrior rescues a princess who was abducted by a snake, the plot consisting of 16 total events. The value of  $n_p$ , the turning point of the narratee’s satisfaction, was 200.

The DFVs of each discourse were automatically calculated. The program preliminary analyzed the range (minimum and maximum), average, and standard deviation of each DFV in all the discourses (Table 1). In addition, 8982 patterns of discourse structures based on DFVs were counted from all the outputs.

Next, the series of discourses was divided into 271 segments, namely norms. The average of segment length (number of discourses) was 36.90 and the minimum and the maximum were 17 and 113.

### 4.1. Local generation space

The analysis (i) analyzed the normative discourses in each norm by the same manner with the above analysis. Table 2 shows two examples of the results. The ranges of DFVs were restricted from the entire set and each norm has different characteristics.

As an issue to be considered, although each local

Table 1. Ranges, averages, and standard deviations of DFVs in all the discourses.

	supplement	complexity	suspense	length	hiding	descriptiveness	repetition	diffuseness	implication	temporal-independency
minimum	0	0	0	11	0	0	0	-9	0	0
maximum	4	50	8	52	10	8	24	20	6	2
average	2.74	8.07	0.69	28.97	3.86	3.44	6.78	2.92	1.90	1.22
SD	1.32	4.48	0.99	6.16	2.34	2.17	3.67	4.21	1.29	0.71

Table 2. The local generation spaces in norm<sub>1</sub> and norm<sub>181</sub>.

Norm <sub>1</sub> (cycles 1-113)										
	supplement	complexity	suspense	length	hiding	descriptiveness	repetition	diffuseness	implication	temporal-independency
minimum	0	0	0	11	3	0	0	-5	0	0
maximum	0	0	0	13	5	0	0	-3	0	0
average	0.00	0.00	0.00	12.30	3.70	0.00	0.00	-3.70	0.00	0.00
SD	0.00	0.00	0.00	0.65	0.65	0.00	0.00	0.65	0.00	0.00
Norm <sub>181</sub> (cycles 6674-6710)										
	supplement	complexity	suspense	length	hiding	descriptiveness	repetition	diffuseness	implication	temporal-independency
minimum	4	8	0	19	5	1	3	-5	1	0
maximum	4	40	5	32	8	3	14	6	3	0
average	4.00	14.94	1.97	25.67	6.72	2.42	6.50	-0.22	2.61	0.00
SD	0.00	7.20	1.26	3.24	0.90	0.72	2.75	2.69	0.54	0.00

© The 2015 International Conference on Artificial Life and Robotics (ICAROB 2015), Jan. 10-12, Oita, Japan

generation space had different characteristics, the timing in which the narratee's expectation is saturated is arbitrary defined by the value of  $n_p$ . On one hand a lot of overlapped discourses with others were appeared in generation spaces which have small ranges like  $norm_1$ . On the other hand, large generation spaces like  $norm_{181}$  were moved to the next norm before the space was not filled sufficiently. A solution is to redefine the saturation as the filling of the local generation space. This calculation will be embedded into the narratee side.

#### 4.2. Degree of deviation

The analysis (ii) calculated the degree of deviation in each norm based on the distance between the local generation space and the deviated discourse. As the result, on one hand about 66% of deviated discourses were positioned outside of the space at the time. On the other hand, about 34% of deviated discourses were included in the space (i.e., the deviation was failed in a practical sense). Such failures occurred due to the partial overlapping between the current local generation space and the deviated (subsequent) space. A solution is to use this analyzing method in the narratee mechanism for judging the success or failure of the deviation.

#### 4.3. Degree of shift in norm

The analysis (iii) calculated the degree of shift in each norm based on the difference of each local generation space from the last space. We confirmed that the local generation spaces were gradually shifted. It means that the holistic diversity of generated discourses was arisen through the restriction of generation space based on the norm and the accumulation of small shifts in the norm.

#### 4.4. Novelty of norm

The analysis (iv) calculated the novelty of each norm based on the difference of each local generation space from the most similar norm in the past. We clarified that the novelty was gradually decreased through the generation cycle. The reason is that there is a limitation of the possible combinations of the parameters' values in the generative goal and expectation.

### 5. Conclusion

In this paper, we analyzed a series of discourse structures produced by the narrative discourse system. We used an analyzing program based on a conceptual framework of "norm and deviation". The results

quantitatively showed that the diverse discourse structures were arisen through the restriction of generation space based on the norm and the accumulation of small shifts in the norm.

In addition, mainly two issues in the mechanism were clarified: the saturation of the narratee's expectation is arbitrary defined regardless the actual reception of generated discourses, and the narrator fails the deviation often in a practical sense. A solution is to embed the analyzing program into the narratee mechanism for controlling the generation cycle based on the actually generated discourses.

The diversity of generable narratives will an important ability for narrative generation systems. The idea of analyzing method proposed in this paper will be applied to other narrative generation systems for clarifying the holistic generation ability.

### References

1. J. P. Rowe, S. W. McQuiggan, J. L. Robison, D. R. Marcey, and J. C. Lester, STORYEVAL: An empirical evaluation framework for narrative generation, in *Papers from the 2009 AAI Spring Symposium, TR SS-09-06* (2009), pp. 103–110.
2. J. Zhu, Towards a mixed evaluation approach for computational narrative systems, in *Proc. 3rd Int. Conf. Computational Creativity* (2012), pp. 150–154.
3. R. Pérez y Pérez, The three layers evaluation model for computer-generated plots, in *Proc. 5th Int. Conf. Computational Creativity* (2014).
4. F. Peinado, V. Francisco, R. Hervás, and P. Gervás, Assessing the novelty of computer-generated narratives using empirical metrics, *Minds & Machines*, **20**(4) (2010) 565–588.
5. T. Ogata, Expanded literary theory for automatic narrative generation, in *Proc. Joint 7th Int. Conf. Soft Computing and Intelligent Systems and 15th Int. Symp. Advanced Intelligent Systems* (2014), pp. 1558–1563.
6. T. Akimoto and T. Ogata, An information design of narratology: The use of three literary theories in a narrative generation system, *The International Journal of Visual Design*, **7**(3) (2014) 31–61.
7. T. Akimoto and T. Ogata, A narratological approach for narrative discourse: Implementation and evaluation of the system based on Genette and Jauss, in *Proc. 34th Annual Conf. the Cognitive Science Society* (2012), pp. 1272–1277.
8. T. Akimoto and T. Ogata, Towards a discourse mechanism in narrative generation system: Proposal of a system introducing narrative discourse theory and reception theory, *Cognitive Studies*, **20**(4) (2013) 396–420.
9. G. Genette, *Narrative discourse: An essay in method*, transl. J. E. Lewin, (Cornell University Press, NY, 1980).
10. H. R. Jauss, Literary history as a challenge to literary theory, in *Toward an Aesthetic of Reception*, transl. T. Bahti, (University of Minnesota Press, MN, 1982), pp. 3–45.

# An aggregating approach of target enclosure of robot swarm

Masao KUBO

Dep. of Computer Science National Defense Academy of Japan  
Yokosuka, Kanagawa, 239-8686, Japan Email: masaok@nda.ac.jp

Hiroshi Sato

Dep. of Computer Science National Defense Academy of Japan  
Yokosuka, Kanagawa, 239-8686, Japan Email: hsato@nda.ac.jp

Akihiro Yamaguchi

Department of Information and Systems Engineering  
Fukuoka Institute of Technology Fukuoka, 811-0295, Japan Email: aki@fit.ac.jp

**Abstract**—This paper presents a robot swarm model to enclose a target. The robots use information of the target and their each neighbors. Every robots have a own but same torch like signal emitter and they can observe the sum of the intensity of their torches. In this paper, the robot uses a direction with strongest intensity of the emitter as direction of its nearest neighbor. We expect that this new approach makes the robot swarm more simple and scalable. We confirm this model by computer simulations.

## I. INTRODUCTION

In this paper, a new implementation of a robot swarm for enclosing a target is examined. The swarm employs a same limited transmission range signal emitter. We suppose that this communication system makes a large swarm be built more easier.

Target enclosure task, which is useful for monitoring disaster sites and unknown vehicles, has recently become an important goal for multiple robots. Robots can operate in dangerous circumstances, replacing human presence.

These sites are usually far from where its operator is. It happens that the group of robots notices the fact of the exact number of sites to be observed and their location. Therefore, it is desirable that the larger number of robots than the necessary size is employed. At least, it will accept the large number of targets than their expectation.

We focused on the study of Takayama et al.[?]. In this model, each robot needs information of directions to one neighbor and to its target. As in other studies, this model also requires the Hamiltonian cycle constraint[?][?].

Recently, research[?] uses hybrid system theory[?][?] and shows robots controlled by Takayama's work referencing nearest neighbors can also enclose a target. The robot swarm with this new reference model can enclose targets while the size of group is changing[?].

Scalability is one of important properties of a robotic swarm. Although this target enclosing algorithm has this ability, the accurate observation of the neighborhood usually becomes difficult as the number of robot increases.

For example, ways to know who is a nearest neighboring robot can be enumerated as follows. (1) every robot has its unique signal emitter. and a receiver measures the power of the incoming signals. (2) each robot observes its neighborhood visually and measures the size of robots. These 2 methods are based on relative distance among robots. (3) each robot calculates own location on a common reference frame. The information of the robot's location are exchanged by broadcasting. The first method is stable but the number of robot is limited. The second method is reasonable but the visibility is strongly influenced by environment condition. The third method is the best way when we can use GPS and a wireless communication network.

We focus on a system with limited range homogeneous signal emitter. We call it torch system. For example, Kilobot[?] has a same small LED emitter as a communication device and a flock of 1000 kilobots can form a large shape. However, the transmission range of their LED light is about 6 robot length. Swarmbot[?] proposes that the robot having a homogeneous light can collect the sufficient number of robots to solve a task. Each robot has same color lights around its body. The intensity of light becomes strong as robots increase. If the intensity of light is too strong a robot will not join the group.

Advantage of this torch system is its high procurability. The very limited transmission range provides less interference of communication. Therefore, emitters which use same signal band can be installed into many robots. Also, its small energy consumption is also an advantage. The more smaller range communication only needs smaller energy consumption.

In this paper, we examine an robotic swarm with torch system for the target enclosing task. We adopt Takayama's work for the control scheme of robot but the referencing robot is different to this work. We propose that a most powerful signal direction is used as the direction of the referencing robot. We call this direction "MOPS" direction. In this paper, we show the proposed robotic swarm can enclose a target successfully by computer simulation.

This paper is composed as follows. Firstly, Takayama's work is introduced. Next, the proposed method based on

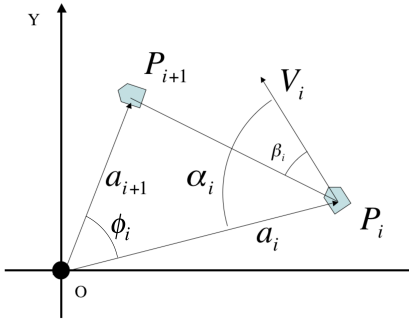


Fig. 1. Model of Takyama's enclosing a target algorithm:  $\alpha, \beta$ .

MOPS is shown. In the third section, communication protocols are proposed. In this section, we show one of the protocols has reasonable scalability for this robotic swarm. Then, by the computer simulations, we show the ability of the target enclosing task of the proposed system.

## II. TAKAYAMA'S TARGET ENCLOSING MODEL

Firstly, Takayama's target enclosing model is explained.

We assume that all robots choose the same target. We assume that on a two-dimensional (2D) plane, there is only one target  $O$  at the origin and  $n$  robots. Robots are numbered counterclockwise as  $P_1, \dots, P_n$ , and  $r_i$  is the position vector of the robot  $P_i$ .

To achieve this task, Takayama et al.[?] proposed the following model. Each robot determines its control input, speed  $v_i$ , and angular velocity  $\omega_i$  using two aspects of angular information: relative angles with respect to the target and an anterior neighboring robot, denoted as  $\alpha_i$  and  $\beta_i$ , respectively. As a result, rotational movement occurs with a central focus on the target.

$$v_i = f\beta_i \quad (1)$$

$$\omega_i = v_i/\bar{r} - k \cos \alpha_i \quad (2)$$

where the parameters  $\bar{r}, k$ , and  $f > 0$  specified beforehand.  $P_{i+1}$  is the robot to which  $P_i$  refers, and  $\bar{r}$  is the expected distance to the target. In Takayama et al.'s model, the  $i$ -th robot refers to the  $i + 1$ -th robot, and the  $n$ -th robot refers to the first robot  $P_1$ . That is, if the relationship between a robot and its reference robot is considered as a link in graph theory, the graph of the group of robots must be a Hamiltonian cycle. The authors proved the convergence to the goal state of the target enclosing task under this constraint.

### A. Nearest neighboring robot as the reference

[?] examined a new reference robot scheme in which each robot considers its nearest neighboring robot as its reference robot. Each robot controls itself as described in equations ?? and ??, but it chooses its nearest neighbor as its reference robot. This system has higher scalability because individual robots need not be identified to observe the nearest robot.

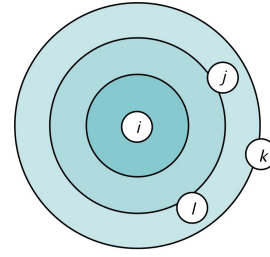


Fig. 2. Diffusion of light of torch

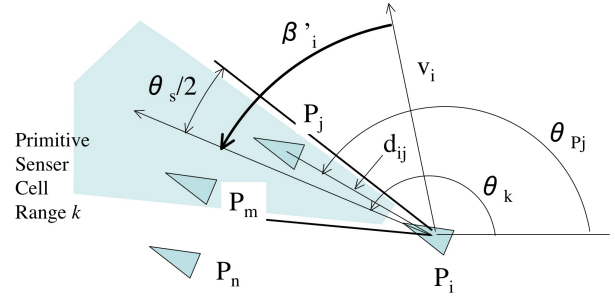


Fig. 3. The most powerful signal(MOPS) direction

## III. THE PROPOSED REFERENCE MODEL: THE MOST POWERFUL SIGNAL DIRECTION REFERENCE MODEL, MOPS MODEL

We propose a new robotic swarm for the target enclosure task. Each robot has its own but same specification torch. Additionally we propose a most powerful direction of their signal is used as the direction of the referencing robot. First, we explain the torch which the robot has.

### A. Torch

Every agent has a same torch and it can turn on/off its torch. The maximum intensity of all the torch is same and known beforehand. We suppose that the speed of propagation of the signal of the torch is so fast that an agent can observe the signal immediately. As shown in Fig.??, during the flight of the signal, the power of the signal is attenuated. The signal propagation function  $p(d)$  is described as follows.

$$p(d) = \begin{cases} \frac{\gamma^{(d/L)}}{(d/L)^2} & d > L \\ 1 & (\text{otherwise}) \end{cases} \quad (3)$$

where  $d$  is the distance from the emitter,  $L$  is the length of an agent,  $\gamma$  is the attenuation coefficient per  $L$ . The equation ?? represents the spherical diffusion of a light. An agent closer to an emitter receives more stronger signal.

### B. target enclosing model with MOPS direction reference model

We explain procedure of receiving signal of the proposed method. Agent  $P_i$  uses the most powerful signal direction

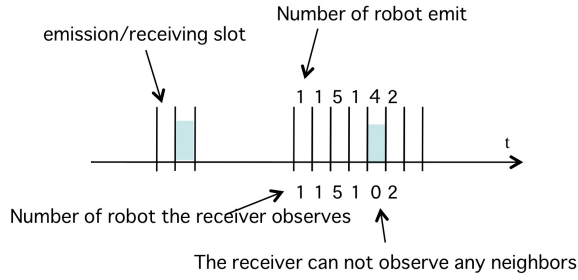


Fig. 4. The number of signal which a robot can receive

instead of the angle from  $P_i$  to  $P_j (= \beta_i)$ . Also, we call the angle  $\beta'_i$ . Fig.?? shows this angle. Now, we suppose agent  $P_i$  has several signal receivers. We call it *sensor primitive*. The direction of  $k$ -th sensor primitive  $sp_k$  is  $\theta_k$ . If  $|\theta_k - \theta_{ij}| \leq \theta_s/2$ , the sensor primitive  $sp_k$  can sense the signal of  $P_j$ . We call  $\theta_s$  a visible range of sensor primitive.

The power of sensor primitive  $sp_k$ ,  $s_k$  is

$$s_k = \sum_{P_m \in \text{visible}} p(d_{i,m}) \quad (4)$$

where  $d_{i,m}$  is the distance between  $P_m$  and  $P_i$  and  $p$  is the signal propagation function in eq.?.  $\beta'_i$  is the substitution of  $\beta_i$ .

$$\beta'_i = \angle v_i O \theta_{\arg - \max_k s_k} \quad (5)$$

#### IV. TORCH FLASHING SIGNAL STRATEGY

In this section, we propose several torch flashing strategies and evaluate them by computer simulation. We show the high performance of protocol B which can collect sufficient information about neighbor agents.

Generally, an agent cannot observe its neighborhood when its torch is turned on because the power of own torch is too strong. This is a kind of dilemma. An agent should turn its torch on to notify other agents its existence. However, an agent should turn its torch off to know existence of other agents. Therefore, some reasonable torch flashing signal strategies are required.

We examine the following 5 strategies. (A) turn on with probability  $r$  and stop after the lapse of a fixed predetermined seconds (we call this strategy random\_start+fixed\_output\_span). (B) turn on when someone starts and stop with probability  $r$  (reactive+random\_stop)[?]. (C) turn on when someone starts and stop after the lapse of a fixed predetermined seconds (reactive+minimum\_span). (D) turn its torch on always and take a break with fixed timing (greedy\_fixed\_output\_span). (E) turn its torch on always and take a break with probability  $r$  (greedy\_random\_stop).

The criteria of the performance of protocol is the average of the number of signals recognized per interval on which an agent emits. We call this interval *slot*. Fig.?? illustrates an example of emission and signal receiving process of an agent. All agents turn their own torches on or off according to the slot. The numbers above the line represent the number

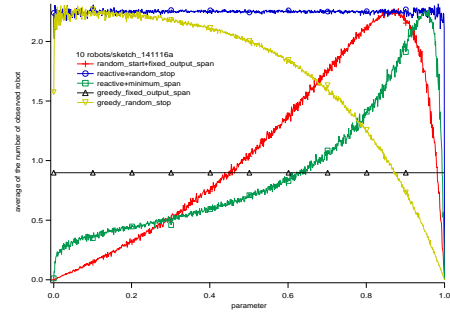


Fig. 5. The performance of the 5 proposed strategies (10 agents)

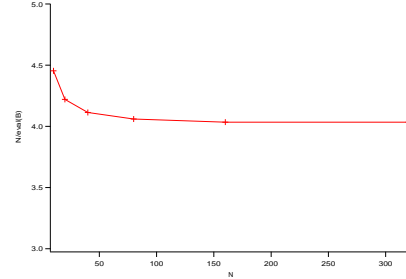


Fig. 6. The performance of strategy B according with the number of agents.

of agents which turn their torch on at each slot. If an agent turns its torch off, the agent can collect correct information of these agents. The number of information of agents which the agent can collect is shown below the line. The performance of protocol  $x$ ,  $eval_x$  is the average of these, namely,

$$eval_x = \frac{\sum_{i \in N} \frac{\sum_{s \in S} receive(s,i)}{|S|}}{|N|} \quad (6)$$

$$receive(s,i) = \begin{cases} 0 & i \in Emit(s) \\ |Emit(s)| & (\text{otherwise}) \end{cases} \quad (7)$$

where  $Emit(s)$  is a set of agents who their torches are on during slot  $s$ .

Fig.?? shows the performance of the 5 strategies in the case of a group of 10 agents by computer simulation. The  $x$  axis indicates the parameter  $r$  and the  $y$  axis shows  $eval_x$ . Strategy B is better than other. This strategy can provide average 2.24 agents' information. This suggests that an agent with strategy B can collect information of all agents during 5 slots  $> 10/2.24$ .

Fig.?? shows  $|N|/eval(B)$  of strategy B.  $|N|/eval(B)$  is the average number of slots which a robot required to collect information of all agents. As this graph indicates,  $|N|/eval(B)$  is almost flat and it shows the agent can collect all members' information during the fixed time span despite of swarm size  $|N|$ .

The above experiment, the agent with strategy B can collect sufficient information to do the target enclosing task in a constant time span. In the next section, we show the result of target enclosing by computer simulation.



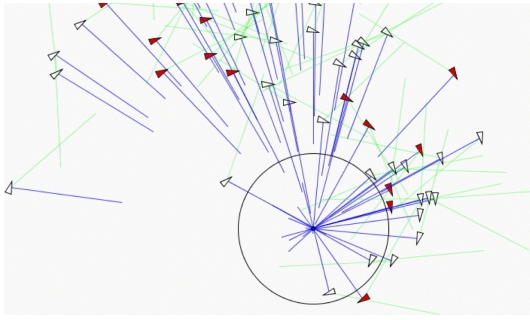


Fig. 7. An example of initial state of target enclosure with 60 agents

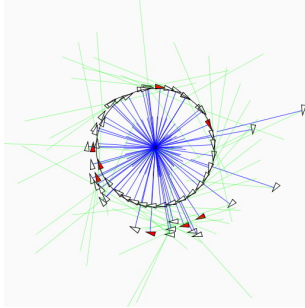


Fig. 8. An example of near completion of target enclosure with 60 agents

### V. COMPUTER SIMULATION

In this section, the result of computer simulation of enclosing a target by a robot swarm with the proposed MOPS direction reference model (eq.??) is shown.

The setting of experiment is explained. There is 1 target at the origin. There are  $|N|$  agent which are deployed at random far from the origin. We suppose that the agents use strategy  $B$  and every agent can receive signal of torch of all agents.

Examples of process of enclosing the target are shown by Fig.??,??. In this case, we set that  $|N| = 60$  and the attenuation coefficient  $\gamma = 0.99999$ . The circle indicates the orbit on which agents enclose the target. A triangle indicates an agent. The 2 lines from each triangle represent its target and the direction  $\beta'_i -$ . If the gap between  $\beta'_i -$  and the direction to

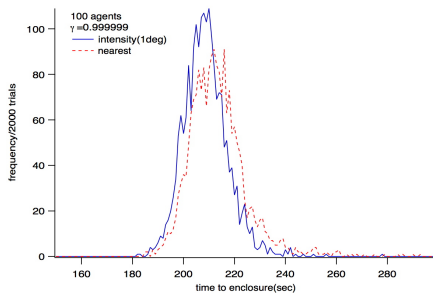


Fig. 9. Histogram of time to enclose a target by 100 agents.2000 trials are examined.

its nearest neighbor agent is large, namely  $(|\beta'_i - \beta_i| > \theta_s)$ , the triangle is filled. As you see In Fig.??, the agents can enclose the target and according with the increase of the number of the agents on this orbit, the number of the filled triangle becomes small.

We repeated 2000 times this attempt to enclose the target. The group size  $|N|$  is 100. At every attempt the agents started from different positions. All the attempts succeeded. Fig.?? shows the histogram of time to enclose the target.

### VI. CONCLUSION

In this paper, a new implementation of a robot swarm for enclosing a target is examined. The swarm employs a same limited transmission range signal emitter. Every robots have a own but same specification torch and they can observe the sum of the intensity of light of their torches. The robot uses the direction with strongest intensity of the light which is an alternative to direction to its nearest neighbor agent. We proposed the scalable torch flashing strategy and the performance of them was evaluated. By the computer simulation, we confirmed that the proposed system can enclose a target.

### REFERENCES

- [1] E.Atlee Jackson, Perspectives of Nonlinear Dynamics 1,Cambridge University Press(1995)
- [2] Tae-Hyoung Kim, Toshiharu Sugie:Cooperative control for target capturing task based on a cyclic pursuit strategy, Automatica 43,1426-1431(2007)
- [3] Kobayashi Y., Otsubo K. , Hosoe S., Autonomous Decentralized Control of Capturing Behavior by Multiple Mobile Robots,Transactions of the Society of Instrument and Control Engineers, 43(8), 663-671(2007)
- [4] Masao Kubo, Tatsuro Yoshimura, Akihiro Yamaguchi, Hiroshi Sato, Takashi Matsubara, Analysis of Angular Information based Target Enclosure Model with Nearest Neighbor Topology,Journal of Japan Society for Fuzzy Theory and Intelligent Informatics 24(3), 778-790, 2012
- [5] Masao Kubo, Hiroshi Sato, Tatsuro Yoshimura, Akihiro Yamaguchi, Takahiro Tanaka, Multiple targets enclosure by robotic swarm, Robotics and Autonomous Systems 62,pp1294-1304,2014
- [6] Joshua A Marshall,Mireille E.Brouvke and Bruce A Francis:Formations of Vehicles in Cyclic Pursuit;IEEE Transactions on Automatic Control, vol49,no11 (2004)
- [7] Masubuchi I., Zhai G.,Control of Hybrid Systems-V : Analysis and Control of Switched Systems,Systems, Control and Information,52(1), 25-31(2008)
- [8] Michael Rubenstein Christian Ahler, Nick Hoff, Adrian Cabrera, Radhika Nagpal, Kilobot: A low cost robot with scalable operations designed for collective behaviors,AAMAS 2013.
- [9] Takayama Y., Yamamoto S., Takimoto T., Distributed Formation Control of a Nonholonomic Multi-agent System for Target-enclosing Operations, Proceedings of 9th SICE System Integration Division Annual Conference (2008)
- [10] Xuping Xu; Guisheng Zhai,Some Results on Practical Asymptotic Stabilizability of Switched Systems,44th IEEE Conference on Decision and Control, 2005 and 2005 European Control Conference. CDC-ECC '05,3998 - 4003(2005)
- [11] Yamaguchi H., A Cooperative Hunting Behavior by Nonholonomic Mobile Robot Troops,Transactions of the Japan Society of Mechanical Engineers. C, 69(688), 3285-3292(2003)
- [12] F. Ducatelle, A. Förster, G. D. Caro, and L. Gambardella, New task allocation methods for robotic swarms, in 9th IEEE/RAS Conference on Autonomous Robot Systems and Competitions, May 2009.

# Probability of mixing up a nearest neighbor robot under target enclosure by robot swarm

Masao KUBO

Dep. of Computer Science National Defense Academy of Japan  
Yokosuka, Kanagawa, 239-8686, Japan Email: masaok@nda.ac.jp

Hiroshi Sato

Dep. of Computer Science National Defense Academy of Japan  
Yokosuka, Kanagawa, 239-8686, Japan Email: hsato@nda.ac.jp

Akihiro Yamaguchi

Department of Information and Systems Engineering  
Fukuoka Institute of Technology Fukuoka, 811-0295, Japan Email: aki@fit.ac.jp

**Abstract**—This paper presents a robot swarm model to enclose a target. The robots use information of the target and their each neighbors. Every robots have a own but same torch like signal emitter and they can observe the sum of the intensity of their torches. In this paper, the robot uses a direction with strongest intensity of the emitter as direction of its nearest neighbor. We expect that this new approach makes the robot swarm more simple and scalable. We confirm this model by computer simulations.

## I. INTRODUCTION

In this paper, a new implementation of a robot swarm for enclosing a target is examined. The swarm employs a same limited transmission range signal emitter. We suppose that this communication system makes a large swarm be built more easier.

Target enclosure task, which is useful for monitoring disaster sites and unknown vehicles, has recently become an important goal for multiple robots. Robots can operate in dangerous circumstances, replacing human presence. These sites are usually far from where its operator is. It happens that the group of robots notices the fact of the exact number of sites to be observed and their location. Therefore, it is desirable that the larger number of robots than the necessary size is employed. At least, it will accept the large number of targets than their expectation.

We focused on the study of Takayama et al.[6]. In this model, each robot needs information of directions to one neighbor and to its target. As in other studies, this model also requires the Hamiltonian cycle constraint[6][3]. Recently, research[1] uses hybrid system theory[7][4] and shows robots controlled by Takayama's work referencing nearest neighbors can also enclose a target. The robot swarm with this new reference model can enclose targets while the size of group is changing[2].

We focus on a system with limited range homogeneous signal emitter. We call it torch system. For example, Kilobot[5] has a same small LED emitter as a communication device and a flock of 1000 kilobots can form a large shape. However, the

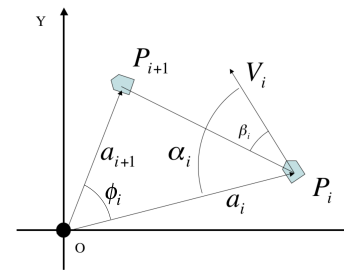


Fig. 1. Model of Takayama's enclosing a target algorithm:  $\alpha, \beta$ .

transmission range of their LED light is about 6 robot length. Swarmlab[8] proposes that the robot having a homogeneous light can collect the sufficient number of robots to solve a task. Each robot has same color lights around its body. The intensity of light becomes strong as robots increase. If the intensity of light is too strong a robot will not join the group.

Advantage of this torch system is its high procurability. The very limited transmission range provides less interference of communication. Therefore, emitters which use same signal band can be installed into many robots. Also, its small energy consumption is also an advantage. The more smaller range communication only needs smaller energy consumption.

In this paper, we examine a robotic swarm with torch system for the target enclosing task. We adopt Takayama's work for the control scheme of robot but the referencing robot is different to this work. We propose that a most powerful signal direction is used as the direction of the referencing robot. We call this direction "MOPS" direction. In this paper, we show the proposed robotic swarm can enclose a target successfully by computer simulation. We discuss the probability of mixing up a nearest neighbor robot under the target enclosure task by robot swarm.

## II. TAKAYAMA'S TARGET ENCLOSING MODEL

Firstly, Takayama's target enclosing model is explained.

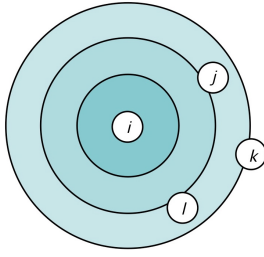


Fig. 2. Diffusion of light of torch

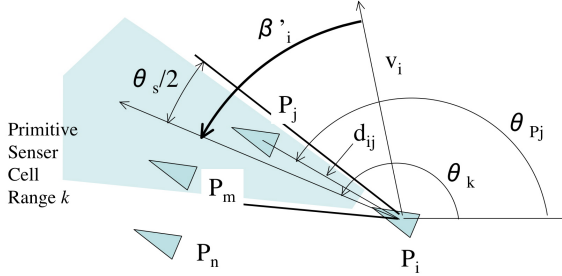


Fig. 3. The most powerful signal(MOPS) direction

We assume that all robots choose the same target. We assume that on a two-dimensional (2D) plane, there is only one target  $O$  at the origin and  $n$  robots. Robots are numbered counterclockwise as  $P_1, \dots, P_n$ , and  $r_i$  is the position vector of the robot  $P_i$ .

To achieve this task, Takayama et al.[6] proposed the following model. Each robot determines its control input, speed  $v_i$ , and angular velocity  $\omega_i$  using two aspects of angular information: relative angles with respect to the target and an anterior neighboring robot, denoted as  $\alpha_i$  and  $\beta_i$ , respectively. As a result, rotational movement occurs with a central focus on the target.

$$v_i = f\beta_i \quad (1)$$

$$\omega_i = v_i/\bar{r} - k \cos \alpha_i \quad (2)$$

where the parameters  $\bar{r}$ ,  $k$ , and  $f > 0$  specified beforehand.  $P_{i+1}$  is the robot to which  $P_i$  refers, and  $\bar{r}$  is the expected distance to the target. In Takayama et al.'s model, the  $i$ -th robot refers to the  $i + 1$ -th robot, and the  $n$ -th robot refers to the first robot  $P_1$ .

#### A. Nearest neighboring robot as the reference

[2] examined a new reference robot scheme in which each robot considers its nearest neighboring robot as its reference robot. Each robot controls itself as described in equations 1 and 2, but it chooses its nearest neighbor as its reference robot. This system has higher scalability because individual robots need not be identified to observe the nearest robot.

### III. THE PROPOSED REFERENCE MODEL: THE MOST POWERFUL SIGNAL DIRECTION REFERENCE MODEL, MOPS MODEL

We propose a new robotic swarm for the target enclosure task. Each robot has the own but same specification torch. Additionally we propose a most powerful direction of their signal is used as the direction of the referencing robot. First, we explain the torch which the robot has.

#### A. Torch

Every agent has a same torch and it can turn on/off its torch. The maximum intensity of all the torch is same and known beforehand. We suppose that the speed of propagation of the signal of the torch is so fast that an agent can observe the signal immediately. As shown in Fig.2, during the flight of the signal, the power of the signal is attenuated. The signal propagation function  $p(d)$  is described as follows.

$$p(d) = \begin{cases} \frac{\gamma^{(d/L)}}{(d/L)^2} & d > L \\ 1 & (\text{otherwise}) \end{cases} \quad (3)$$

where  $d$  is the distance from the emitter,  $L$  is the length of an agent,  $\gamma$  is the attenuation coefficient per  $L$ . The equation 3 represents the spherical diffusion of a light. An agent closer to an emitter receives more stronger signal.

#### B. target enclosing model with MOPS direction reference model

We explain procedure of receiving signal of the proposed method.

Agent  $P_i$  uses the most powerful signal direction instead of the angle from  $P_i$  to  $P_j (= \beta_i)$ . Also, we call the angle  $\beta'_i$ .

Fig.3 shows this angle. Now, we suppose agent  $P_i$  has several signal receivers. We call it *sensor primitive*. The direction of  $k$ -th sensor primitive  $sp_k$  is  $\theta_k$ . If  $|\theta_k - \theta_{ij}| \leq \theta_s/2$ , the sensor primitive  $sp_k$  can sense the signal of  $P_j$ . We call  $\theta_s$  a visible range of sensor primitive.

The power of sensor primitive  $sp_k$ ,  $s_k$  is

$$s_k = \sum_{P_m \in \text{visible}} p(d_{i,m}) \quad (4)$$

where  $d_{i,m}$  is the distance between  $P_m$  and  $P_i$  and  $p$  is the signal propagation function in eq.3.  $\beta'_i$  is the substitution of  $\beta_i$ .

$$\beta'_i = L v_i O \theta_{\arg - \max_k s_k} \quad (5)$$

### IV. COMPUTER SIMULATION

The setting of experiment is explained. There is 1 target at the origin. There are  $|N|$  agent which are deployed at random far from the origin. We suppose that the agents use strategy  $B$  and every agent can receive signal of torch of all agents.

Example of process of enclosing the target are shown by Fig.4. In this case, we set that  $|N| = 60$  and the attenuation coefficient  $\gamma = 0.9999$ . The circle indicates the orbit on which agents enclose the target. A triangle indicates an agent. As you see In Fig.4, the agents can enclose the target.

[dvipdfmx]graphicx amsmath fancyhdr



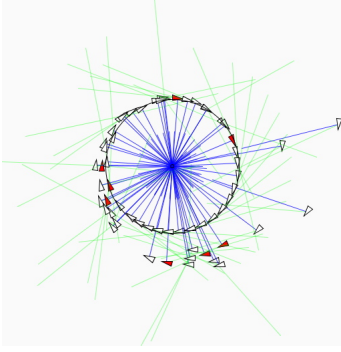


Fig. 4. An example of near completion of target enclosure with 60 agents

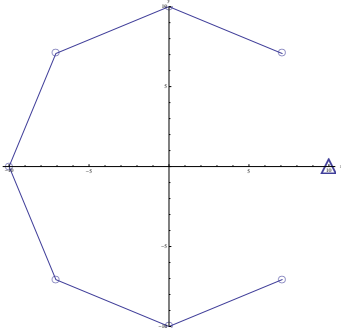


Fig. 5. The location of agents when they enclose the target completely ( $|N| = 8$ ). The target is at the origin  $O$  and  $\Delta$  indicates the reference agent and  $\circ$  means its neighbor agents.

## V. ANALYSIS OF THE PROPOSED DIRECTION REFERENCE MODEL

In this section, we describe the result of analysis of the proposed MOPS reference model. [6] proved that an agent for any reference model converges to the circle having a radius of  $\bar{r}$ . [2] proved that a group of 3 and 4 agents with the nearest neighbor agent reference model can achieve a uniform deployment on the circle. In this section, we clarify that it is possible for a set of adequate sensor primitives to detect the nearest neighbor agent direction if the variance of location of robot is small.

### A. Definition of this target enclosing task

The following 2 conditions for successful enclosing a target are required. For any agent  $P_i$ , the first condition is that the distance between  $P_i$  and the target at  $O$  is equal to  $\bar{r}$ . The second condition is that for any agent  $P_i$  angle  $\angle P_i O P_j = 2\pi/|N|$  where  $P_j$  is the nearest neighbor agent of  $P_i$ .

Now, we suppose that an agent,  $i = 0$  is at  $(r_i, \theta_i) = (\bar{r}, 0)$ . We call the agent with  $i = 0$  the reference agent. Also other agents,  $i = 1, \dots, |N| - 1$  are called neighbor agent. When they enclose the target successfully, the location of the neighbor agent are  $(r_i, \theta_i) = (\bar{r}, iC_\theta)$ ,  $C_\theta = 2\pi/|N|$ ,  $i = 1, \dots, |N| - 1$ . We call this location regular position. Even if the reference agent moves while they keep enclosing a target

successfully, the relative position to the other agents is same. The distance to a neighbor agent  $i$ ,  $i = 1, \dots, |N| - 1$  is

$$d_i = \sqrt{2\bar{r}^2(1 - \cos(iC_\theta))}. \quad (6)$$

Therefore,

$$d_{i=1} = d_{i=|N|-1} < d_{i \neq 0, 1, |N|-1} \quad (7)$$

There are 2 nearest neighbor agents for the reference agent when they enclose the target.

### B. Fluctuation of power of signal caused by displacement of neighbor agents

The power of signal of neighbor agent  $i$  at the reference agent can be approximated by Taylor expansion. It is described as follows.

$$S_i = A_i + K_i \Delta_i, A_i = \frac{\gamma^{\frac{d_i}{L}} L^2}{d_i^2}, K_i = [k_{i,r} k_{i,\theta}] \quad (8)$$

$$k_{i,r} = \frac{L\gamma^{\frac{d_i}{L}} \bar{r} (1 - \cos(iC_\theta)) (2\bar{r}^2 \log(\gamma) \cos(iC_\theta) - 2\bar{r}^2 \log(\gamma) + 2Ld_i)}{d_i^5} \quad (9)$$

$$k_{i,\theta} = \frac{L\gamma^{\frac{d_i}{L}} \bar{r}^2 \sin(iC_\theta) (2\bar{r}^2 \log(\gamma) \cos(iC_\theta) - 2\bar{r}^2 \log(\gamma) + 2Ld_i)}{d_i^5} \quad (10)$$

where  $\Delta_i = [\Delta r_i \Delta \theta_i]^T$ .  $\Delta r_i$  is a displacement along the target direction from its regular position,  $\Delta \theta_i$  is a circumferential displacement from its regular position. We assume that the displacement  $\Delta r_i, \Delta \theta_i$  follows the normal distributions having average 0 and variance  $\sigma_{r_i}^2, \sigma_{\theta_i}^2$  respectively. Also, we assume that the fluctuation of power of signal at the reference agent follows a normal distribution having  $\sigma_i$ . In this case, the average of power of the signal at the reference agent is  $A_i$ , and its distribution  $\sigma_i^2$  is

$$\sigma_i^2 = K_i \Sigma_i K_i^T = k_{i,r}^2 \sigma_{r_i}^2 + k_{i,\theta}^2 \sigma_{\theta_i}^2 \quad (11)$$

where  $\Sigma_i = \text{diag}(\sigma_{r_i}^2, \sigma_{\theta_i}^2)$ .

The deviation of the signal at the reference agent can be calculated if  $|N|$  and  $\sigma_{r_i}, \sigma_{\theta_i}$  are known. We suppose that  $I_s$  means the set of agents which are in visible range of sensor primitive  $s$ . The average  $\bar{p}_s$  and the standard deviation  $M_s$  of signal at the reference agent are described as follows.

$$\bar{p}_s = \sum_{j \in I_s} A_j, M_s = \sqrt{\sum_{j \in I_s} \sigma_j^2} \quad (12)$$

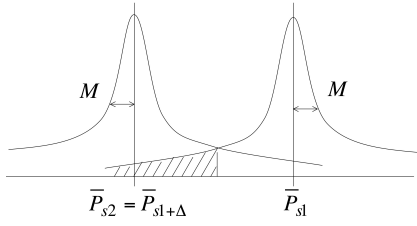


Fig. 6. The probability with which a farther neighbor is recognized as a closer neighbor.

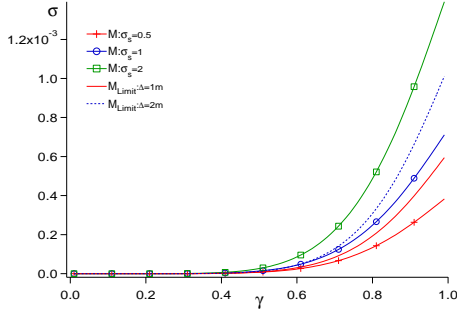


Fig. 7. Limit of variance of signal under which an agent can detect the nearest neighbor agents

*C. Limit of variance of signal under which an agent can detect the nearest neighbor agents*

We assume that there are 2 sensor primitives  $s_1, s_2$  of the reference agent. Each sensor primitive observes one of the nearest neighbor agents in eq.7. Also visible ranges of  $s_1$  and  $s_2$  are so narrow that it receives signal from only one of the nearest neighbor agents. Namely,  $|I_{s1}| = |I_{s2}| = 1$ .

Now, we suppose that a small displacement at the nearest neighbor agents occurs while all of the agents move. We assume that the difference of distance between the 2 nearest neighbor agents is  $\Delta$ . In this case, it can be deduced by using the 3- $\sigma$  rule the condition for the reference agent to choose a sensor primitive correctly which observes the closer agent.

$$\bar{p}_{s1} - kM > \frac{\bar{p}_{s1} + \bar{p}_{s2}}{2} \quad (13)$$

where  $\bar{p}_{s1} \geq \bar{p}_{s2}$  and  $k$  is a positive constant. Here  $k=3$  in the rest of this paper.

Therefore, if the standard deviation of the sensor primitive  $M$  is smaller than  $M_{Limit} = \frac{p(d_1) - p(d_1 + \Delta)}{2k}$ , the reference agent can almost certainly select the correct sensor primitive.  $M_{Limit}$  is described as follows.

$$M \leq \frac{p(d_1) - p(d_1 + \Delta)}{2k} = M_{Limit} \quad (14)$$

$M_{Limit}$  is changed by signal's attenuation coefficient  $\gamma$ . Fig.7 illustrates  $M$  and  $M_{Limit}$  while  $\gamma$  changes.  $M$  with  $\sigma_{\theta_i} = 0.5, 1, 2$  degree are illustrated by line with marker  $+, o,$  and respectively.  $|N| = 8, \bar{r} = 10m, \sigma_{r_i} = 0.1m$ .

The variance of power of signal at reference agent becomes smaller as the  $\sigma_{\theta_i}$  becomes small.

The solid and dashed line represent  $M_{Limit}$  with  $\Delta=1m$  and  $2m$  respectively.

In order to detect the difference in distance of  $\Delta m$  between the nearest agents almost certainly, the variation of the received signal  $M$  must be smaller than  $M_{Limit}$  lines. For example, this figure shows that even if the nearest neighbor agent's location is distributed  $\sigma_{\theta_i} = 0.5$  degree, the reference agent can detect 1m difference between the 2 nearest for any  $\gamma$ . On the other hand, the reference agent cannot detect it if the nearest neighbor agent's location is distributed  $\sigma_{\theta_i} = 1$  and 2 degree.

By this experiment, we expect that if the  $\sigma_{\theta_i}$  is sufficient small, the reference agent can select a correct sensor primitive which observes the nearest neighbor agent that is  $\Delta$  closer than 2nd nearest neighbor agent.

VI. CONCLUSION

In this paper, a new implementation of a robot swarm for enclosing a target is examined. Every robots have a own but same specification torch and they can observe the sum of the intensity of light of their torches. The robot uses the direction with strongest intensity of the light which is an alternative to direction to its nearest neighbor agent.

We analyzed the relation between the most powerful signal direction and the direction of the nearest neighbor. We can expect that if the fluctuation of agent is sufficient small and a gap of distance  $\Delta$  between the nearest neighbor agent and the second nearest neighbor agent is given, the agent can select a correct sensor primitive which observes the nearest neighbor agent.

REFERENCES

- [1] Masao Kubo, Tatsuro Yoshimura, Akihiro Yamaguchi, Hiroshi Sato, Takashi Matsubara, Analysis of Angular Information based Target Enclosure Model with Nearest Neighbor Topology, Journal of Japan Society for Fuzzy Theory and Intelligent Informatics 24(3), 778-790, 2012
- [2] Masao Kubo, Hiroshi Sato, Tatsuro Yoshimura, Akihiro Yamaguchi, Takahiro Tanaka, Multiple targets enclosure by robotic swarm, Robotics and Autonomous Systems 62, pp1294-1304, 2014
- [3] Joshua A Marshall, Mireille E. Broucke and Bruce A Francis: Formations of Vehicles in Cyclic Pursuit; IEEE Transactions on Automatic Control, vol49, no11 (2004)
- [4] Masubuchi I., Zhai G., Control of Hybrid Systems-V : Analysis and Control of Switched Systems, Systems, Control and Information, 52(1), 25-31(2008)
- [5] Michael Rubenstein Christian Ahler, Nick Hoff, Adrian Cabrera, Radhika Nagpal, Kilobot: A low cost robot with scalable operations designed for collective behaviors, AAMAS 2013.
- [6] Takayama Y., Yamamoto S., Takimoto T., Distributed Formation Control of a Nonholonomic Multi-agent System for Target-enclosing Operations, Proceedings of 9th SICE System Integration Division Annual Conference (2008)
- [7] Xuping Xu; Guisheng Zhai, Some Results on Practical Asymptotic Stabilizability of Switched Systems, 44th IEEE Conference on Decision and Control, 2005 and 2005 European Control Conference. CDC-ECC '05, 3998 - 4003(2005)
- [8] F. Ducatelle, A. Förster, G. D. Caro, and L. Gambardella, New task allocation methods for robotic swarms, in 9th IEEE/RAS Conference on Autonomous Robot Systems and Competitions, May 2009.

# Adaptive Multiple-Model Control of A Class of Nonlinear Systems

Chao Yang

*The Seventh Research Division and the Department of Systems and Control, Beihang University (BUAA),  
Beijing 100191, China*

Yingmin Jia

*The Seventh Research Division and the Department of Systems and Control, Beihang University (BUAA),  
Beijing 100191, China*

*E-mails: yangchao\_buaa@163.com; ymjia@buaa.edu.cn*

## Abstract

In this paper, an adaptive multiple-model controller is developed for nonlinear systems in parametric-strict-feedback form. Unlike the previous results, a switching scheme is not required here to switch the most appropriate model into the controller design. The new scheme reduces the number of identification models and uses information provided by all the models more efficiently than previous results by using the convex combination of estimates of parameters. The method guarantees parameter convergence and global asymptotic stability of the closed-loop system. The global boundedness of closed-loop signals and asymptotic convergence to zero of tracking error are proved. A simulation example is included to demonstrate the effectiveness of the obtained results.

*Keywords:* adaptive control, multiple-model design, nonlinear systems, asymptotic tracking

## 1. INTRODUCTION

In recent years, adaptive control has been well investigated<sup>1-5</sup>. It is proposed to cope with the problem of parametric uncertainties in systems larger than traditional method can handle. The typical idea of adaptive control is estimating unknown parameters on-line and designing controller with the estimates as the real ones<sup>2</sup>. Plenty of different stable adaptive controllers have been designed for linear or nonlinear uncertain systems<sup>7-9</sup>. A distinguished problem for adaptive control is that transient performance of the system may include unacceptable large peaks, especially when there exist large initial estimation errors. To overcome this drawback and enhance the transient performance, adaptive control using multiple models for linear systems was proposed in Refs.7, 8, 10 and 11. The basic idea of Ref.10 was running in parallel multiple models, and design an index of performance based on identification errors, so that model closest to the real plant can be selected by switching quickly and transient response can be improved. Latter, the method was extended to switching and tuning in Refs.12 and 13. Numerous of simulations and applications have

demonstrated adaptive multiple-model control can enhance transient performance significantly.

However, the methods are mainly concentrated on linear systems. Adaptive multiple-model control for nonlinear systems is initially considered in Ref.14. Then, adaptive multiple-model control method for nonlinear requiring persistence of excitation is proposed in Ref.15, where the unknown parameters can be calculated in the first place.

In Ref.16, a sufficient condition concerning the parameter convergence is given by constructing a global, explicit strong Lyapunov function. Inspired by this, we develop a novel multiple model adaptive controller for a class of nonlinear system in parametric-strict-feedback form. Unlike the usual hypothesis, the restrictive matching conditions are not required, but the persistency of excitation condition is assumed. The control scheme employs adaptive identification models based on adaptive parameters from a known compact parameter set and a virtual identification model, of which the estimation parameter is both adaptive and resettable. The algorithm reduces the number of identification models by using convex combination method to estimate parameter even as the system is in

operation. Also, global asymptotic stability of the closed-loop system is proved.

This paper is organized as follows. The problem formulation and assumptions are given in Section 2. In Section 3, backstepping adaptive method and the new adaptive multiple-model method are introduced. In Section 4, the closed-loop system dynamics is analyzed including stability and parameter convergence. Section 5 presents a simulation which compares the proposed method with single model adaptive control.

## 2. Problem formulation

Consider the following nonlinear systems in parametric-strict-feedback form <sup>[2]</sup>:

$$\begin{aligned} \dot{x}_1 &= x_2 + f_1^T(x_1)\theta \\ &\vdots \\ \dot{x}_i &= x_{i+1} + f_i^T(x_1, x_2, \dots, x_i)\theta, \quad i = 1, 2, \dots, n-1 \\ \dot{x}_n &= u + f_n^T(\bar{x}_n)\theta \\ y &= x_1 \end{aligned} \quad (1)$$

Where  $x_i \in R, i = 1, 2, \dots, n$  is the state of system,  $u \in R$  is the control input,  $\theta \in R^p$  is a n unknown parameter vector belonging to a known compact set  $S \in R^p$  and  $y \in R$  is the output. The functions  $f_i, i = 1, 2, \dots, i$  are known smooth functions.  $y_r \in R$  is the reference signal to be tracked. We suppose th at the full system states are available. The object is to improve transient performance in the presence of large parametric uncertainties, and meanwhile, ensure th e stability of the closed-loop system.

It should be noted that in the classical backstepping adaptive control design, transient performance can be improved by choosing sufficiently large high-gain parameters<sup>2</sup>. However, a possible shortcoming of such method is that the resulting control efforts may be very large. Another way to improve transient performance is using multiple identifications models.

Before the design of adaptive multiple-model controller, we need necessary assumptions which are useful in the following analysis.

**Assumption 1(A1)** There is a known positive real-valued constant B satisfying

$$\max\{|y_r(t)|_\infty, |\dot{y}_r(t)|_\infty\} \leq B \quad (2)$$

**Assumption 2(A2)**  $f_1(y_r(t))$  satisfies the classical persistent excitation condition, that is, for all  $t \in R$ , there exist positive real-valued constants  $\mu$  and  $T$  such that

$$\mu I \leq \int_{t-T}^t f_1(y_r(l)) \square f_1(y_r(l))^T dl \quad (3)$$

## 3. Design of adaptive multiple model controller

### 3.1 Introduction of backstepping adaptive control<sup>[2]</sup>

The standard backstepping adaptive control and adaptation law for parametric-strict-feedback system are given by

$$u = \alpha_n(x, \hat{\theta}, \bar{y}_r^{(n)}) \quad (4)$$

$$\dot{\hat{\theta}} = \Gamma \tau_n = \Gamma WZ \quad (5)$$

where

$$\theta = [\theta_1, \theta_2, \dots, \theta_p]^T, \bar{\theta} = \hat{\theta} - \theta \quad (6)$$

$$Z = [z_1, z_2, \dots, z_n]^T \quad (7)$$

$$z_1 = y - y_r, z_i = x_i - \alpha_{i-1}, 2 \leq i \leq n, \quad (7)$$

$$W = [\omega_1, \omega_2, \dots, \omega_n] \quad (8)$$

$$\omega_1 = f_1, \omega_i = f_i - \sum_{k=1}^{i-1} \frac{\partial \alpha_{i-1}}{\partial x_k} f_k, \quad (8)$$

$$\tau_1 = \omega_1 z_1, \tau_i = \tau_{i-1} + \omega_i z_i, \quad (9)$$

$$\alpha_i = -c_i z_i - \hat{\theta}^T f_i(x_i) + \dot{y}_r(t), \quad (9)$$

$$\begin{aligned} \alpha_i &= -z_i - c_i z_i - \hat{\theta}^T \omega_i + \frac{\partial \alpha_{i-1}}{\partial \theta} \Gamma \tau_i \\ &+ \sum_{k=1}^{i-1} \left( \frac{\partial \alpha_{i-1}}{\partial x_k} x_{k+1} + \frac{\partial \alpha_{i-1}}{\partial x_k} x_{k+1} + \frac{\partial \alpha_{i-1}}{\partial y_r^{(k-1)}} y_r^{(k)} \right) \\ &+ \sum_{k=2}^{i-1} \left( \frac{\partial \alpha_{k-1}}{\partial \theta} \right) \Gamma \omega_i z_k + \dot{y}_r(t), \quad 2 \leq i \leq n \end{aligned} \quad (10)$$

where  $\Gamma = \Gamma^T > 0$  is the adaptation gain matrix,  $y_r$  is the reference signal to be tracked and  $c_i > 0, 1 \leq i \leq n$  are constants to be designed. The above control design is based on the Lyapunov function

$$V_n(z_1, z_2, \dots, z_n, \bar{\theta}) = \frac{1}{2} \sum_{i=1}^n z_i^2 + \frac{1}{2} (\hat{\theta} - \theta)^T \Gamma^{-1} (\hat{\theta} - \theta)$$

The time derivative of  $V_n$ , computed with (5)-(10) is

$$\dot{V}_n(z_1, z_2, \dots, z_n, \bar{\theta}) \leq -\sum_{i=1}^n c_i z_i^2. \text{ This implies the}$$

boundness of the state  $z_i, 1 \leq i \leq n$  and  $\hat{\theta}$ , which in turn indicates the boundness of system state  $x_i, 1 \leq i \leq n$  and control  $u$ . Under the standard arguments of adaptive control theory, it follows that  $z_i(t), 1 \leq i \leq n$  tend to zero asymptotically, and thus  $\lim_{t \rightarrow \infty} z_1(t) = \lim_{t \rightarrow \infty} (y(t) - y_r(t)) = 0$ . Then asymptotic tracking can be achieved.

**Remark:** In addition to the boundness of the parameter estimation, there are seldom results about parameter convergence. Ref.6 provides sufficient condition for parameter estimates convergence, but the condition is difficult to verify. With assumptions (2) and (3), Ref.16 constructs an explicit, global, strong

Lyapunov function, and proves parameter estimation convergence. See Ref.16 for more details.

### 3.2 Design of adaptive multiple-model controller

We will run in parallel (p+2) models. N (N=p+1) models are in the same structure but different initial parameter values  $\theta_j(0), j = 1, 2, \dots, N$ . The initial values of  $\theta_j(0), j = 1, 2, \dots, N$  are known and the region of uncertainty S of the plant parameter vector  $\theta$  lies in their convex hull K (i.e.  $S \subset K$ ). The other one model called ‘virtual model’ is designed with adaptive and resetting mechanism. The N models will run parallel and parameter estimates are evaluated online by a criterion function  $J(t)$ . Define

$$J_j(t) = \alpha e_j^2(t) + \beta \int_0^t e_j^2(\tau) d\tau \quad (11)$$

as the criterion function for the  $j$ -th adaptive model, where  $\alpha > 0, \beta > 0$  are constants to be designed.  $J_c$  is the criterion function for virtual model. At each resetting time  $t_r$ , if  $J_c > \gamma \cdot \min\{J_1, \dots, J_N\}$ , where  $\gamma \in (0, 1)$  is a constant to be designed, reset the estimate parameter vector  $\theta_c(t)$  of virtual model by

$$\theta_c(t) = \sum_{i=1}^N \gamma_i \theta_i \quad (12)$$

where

$$\gamma_i = \frac{1}{J_i(t)} \bigg/ \sum_{j=1}^N \frac{1}{J_j(t)}, i = 1, 2, \dots, N \quad (13)$$

Otherwise, the estimate parameters remain unchanged and the process repeats. An obvious problem is that whether the resetting is finite or infinite. In the following section, we will prove that only a finite number of resetting can occur.

### 4. Stability analysis

**Theorem** Suppose assumptions (2),(3) hold, and the adaptive multiple-model controller (4) and adaption law (5) in the paper are applied to system (1). Then, for all initial conditions only a finite number of resetting can occur, all closed-loop states and  $\bar{\theta}_j, j = 1, 2, \dots, n$  are bounded, furthermore asymptotic tracking is achieved, i.e.,  $\lim_{t \rightarrow \infty} (y(t) - y_r(t)) = 0$  as  $t \rightarrow \infty$ .

**Proof.** First, we will prove that the number of resetting is finite. After the above analysis, we have  $\bar{\theta}_j(t) \in L_\infty[0, \infty), j = 1, 2, \dots, n$ , for  $i = 1, 2, \dots, n, \forall \epsilon > 0, \exists t_i \in [0, \infty)$ , such that  $|\bar{\theta}_i(t)| < \epsilon, \forall t > t_i$ . Let  $t_{\max} = \max\{t_1, t_2, \dots, t_n\}$ . For  $t > t_{\max}, |\bar{\theta}_i(t)| < \epsilon, i = 1, 2, \dots, N$ . Based on the resetting mechanism,  $|\bar{\theta}_i(t)| = \left| \sum_{j=1}^n \gamma_j \bar{\theta}_j(t) \right| \leq \max\{|\bar{\theta}_j(t)|, j = 1, 2, \dots, N\} < \epsilon$ . Then the resetting adaptive model will estimate parameters with zero error. So, in the worst situation, the amount of resetting  $N_r = \lceil \frac{t_{\max}}{T} \rceil$ , where  $T$  is the resetting interval, and

$\lfloor \cdot \rfloor$  means the floor function. Thus finite number of resetting is proved. Further, after every resetting time  $t_r$ , all adaptive models and the resetting model operate under respective control input and adaptation law, then all closed-loop state is bounded. Once  $t > t_{\max}$ , the system will operate under the classical backstepping scheme, so we can further point out that  $\lim_{t \rightarrow \infty} (y(t) - y_r(t)) = 0$ . This completes the whole proof.  $\square$

### 5. Simulation result

The nonlinear system in parametric-strict-feedback form is as follows:

$$\begin{aligned} \dot{x}_1 &= x_2 + \theta x_1 \\ \dot{x}_2 &= u + \theta \cos(x_1 x_2) \\ y &= x_1 \end{aligned}$$

where  $\theta \in [0.1, 5.5]$  is an unknown parameter. The output  $y = x_1$  is to asymptotically track the reference signal  $y_r = \sin t$ .

In simulation, the controller and adaptation law is developed as (4), (5). For all constant  $B > 1$ , (2) holds.

For any  $\mu_0 \in (0, \pi)$ ,  $\int_{t-2\pi}^t y_r^2(l) dl \geq \mu_0$  follows for all  $t \in \mathbb{R}$ , then let  $\mu = \mu_0, T = 2\pi$ , and (3) holds. The unknown parameter is  $\theta = 1, c_1 = 1.2, c_2 = 1$ , the adaptive gain  $\gamma = 1$ , initial state  $x_1(0) = x_2(0) = 0$ , and the initial estimates of parameter for classical adaptive control and adaptive multiple-mode control are  $\theta_1(0) = 2.8, \theta_2(0) = 0.1, \theta_3(0) = 5.5, \theta(0) = 2.8$

As seen from Figure 1, the state  $x_1$  of the system is bounded, and asymptotic tracking is achieved. Adaptive multiple-model control (d) performs better than single model (a-c) especially when initial parameter estimation error is large (b and c). In Figure 2, all parameter estimations of  $\theta$  asymptotically converge to its true value while the estimation in adaptive multiple-model control (d) is the fastest. Figure 3 illustrates the control input  $u$  is bounded in the two different control schemes. Thus the scheme proposed in this paper is feasible and effective.

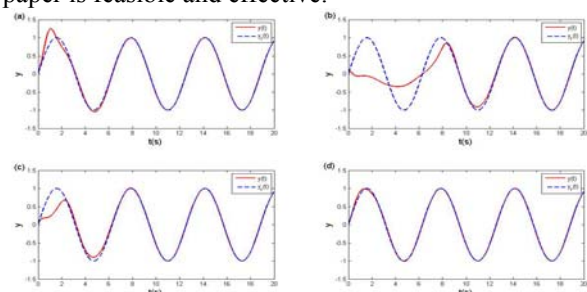


Fig.1. Output and reference signal: (a), (b), (c) single model with  $\theta(0) = 0.1, 5.5, 2.8$  respectively, and (d) resetting model with  $\theta(0) = 2.8$

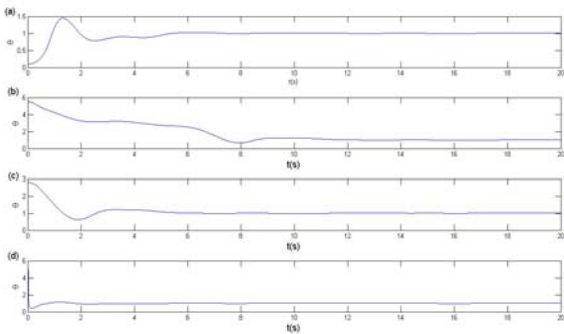


Fig.2. Parameter estimation: (a), (b), (c) single model with  $\theta(0) = 0.1, 5.5, 2.8$ . (d) retting model with  $\theta(0) = 2.8$

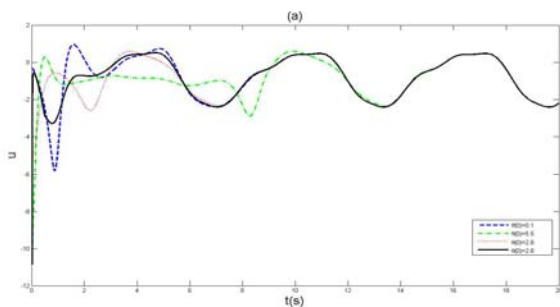


Fig.3. control input  $u$ : dashed line, dash-dot line and dotted line for single model with  $\theta(0) = 0.1, 5.5, 2.8$ , solid line for virtual model with  $\theta(0) = 2.8$

## 6. Conclusion

In this paper, an adaptive multiple-model controller is developed for a class of nonlinear systems in parametric-strict-feedback form. Unlike previous results, a switching scheme is not necessary to guarantee the model closest to the real plant to be switched into the controller design. Global asymptotic stability of the closed-loop system, globally uniformly bounded of all the closed-loop signals and convergence of parameter estimates are proved. The simulation results illustrate the feasibility and effectiveness of the proposed method.

## Acknowledgements

This work was supported by the National Basic Research Program of China (973 Program: 2012CB821200, 2012CB821201) and the NSFC (61134005, 60921001, 61327807).

## References

[1] Narendra KS, Annaswamy AM (1989), Stable Adaptive Systems. Prentice Hall Inc.: Englewood Cliffs, NJ  
 [2] Krstic M, Kanellakopoulos I, Kokotovic PV (1995), Nonlinear and adaptive control design. Wiley, New York  
 [3] Tao G (2003), Adaptive Control Design and Analysis. John Wiley & Sons

[4] Ioannou PA, Sun J (1996), Robust Adaptive Control. Prentice Hall: Englewood Cliffs, NJ  
 [5] Middleton RH, Goodwin G C, Hill D J, Mayne D Q (1988), Design issues in adaptive control. IEEE Trans. Automat. Control 33:50-58.  
 [6] Lin JS, Kanellakopoulos I (1999) Nonlinear enhance parameter convergence in strict feedback systems. IEEE Trans. Automat. Control 44:89-94  
 [7] Morse AS (1996), Supervisory control of families of linear set-point controller, part 1: Exact matching, IEEE Trans. Automat. Control 41:1413-1431.  
 [8] Anderson BDO, Brinsmead T S, Bruyne FD, et al. (2000), Multiple model adaptive control, part 1: Finite controller coverings. Int. J. Robust Nonlinear Control 10:909-929  
 [9] Morse AS (1997), Supervisory control of families of linear set-point controller. 2. Robustness. IEEE Trans. Automat. Control 42:1500-1515  
 [10] Narendra KS, Balakrishnan J (1994), Improving transient response of adaptive control systems using multiple models and switchings. IEEE Trans. Automat. Control 39:1861-1866  
 [11] Narendra KS, Balakrishnan J (1997), Adaptive control using multiple models. IEEE Trans. Automat. Control 42:71-187  
 [12] Han Z, Narendra K S (2010), Multiple adaptive models for control. Proceedings of the 49th IEEE conference on decision and control, Atlanta, Georgia, 60-65  
 [13] Narendra KS, Han Z (2011). The changing face of adaptive control: the use of multiple models. Annual reviews in control 35:1-12  
 [14] Narendra KS, George K (2002), Adaptive control of simple nonlinear systems using multiple models. Proceedings of American Control Conference: 1779-1784  
 [15] Ciliz MK, Cezayirli A (2006), Increased transient performance for the adaptive control of feedback linearizable systems using multiple models, Int. J. Control 79:205-1215  
 [16] He B L, Li J M (2011), Systematic method of parameter convergence in strict-feedback nonlinear systems (in Chinese). J.Sys.Sci.Math.Scis.31(5):501-511



# Attitude Reorientation of Spacecraft with Attitude Forbidden Zones

**Xuhui Lu**

*The Seventh Research Division and the Department of Systems and Control, Beihang University (BUAA), 37 XueYuan Road, Beijing, 100191, P.R. China*

**Yingmin Jia**

*The Seventh Research Division and the Department of Systems and Control, Beihang University (BUAA), 37 XueYuan Road, Beijing, 100191, P.R. China*

*E-mail: luxuhuiluxuhui@163.com, ymjia@buaa.edu.cn  
www.buaa.edu.cn*

## Abstract

This paper investigates an attitude reorientation control scheme of spacecraft, considering attitude forbidden zone and external disturbances. A novel potential barrier function is proposed with an attitude constraint term and a dynamical scaling term. Here the dynamical scaling term is synthesized with a backstepping-based control scheme to accommodate both the avoidance of attitude forbidden zones and disturbance attenuation. Simulation results are given to verify the effectiveness of the proposed method.

*Keywords:* attitude stabilization, attitude constraints, backstepping, dynamic scaling

## 1. Introduction

The attitude reorientation of spacecraft has been extensively studied in the past decades. However, during large-angle attitude maneuvering of spacecraft, some sensitive on-board instruments such as infrared telescopes and interferometers should avoid direct exposure of bright objects like the sun. Therefore, the spacecraft reorientation with the attitude forbidden zones, or the constrained attitude control problem (CAC), is a topic of great interest in applications. In the early work,<sup>1</sup> via implicit magnitude constraint of quaternion, the non-convex attitude constraints can be transformed into linear matrix inequalities (LMIs) and this constrained optimization problem can be analyzed in the semi-definite programming framework. Then, this

convex parameterization can be even used in the construction of logarithmic barrier function to derive controller.<sup>2</sup> Other methods, such as invariant set,<sup>3</sup> randomized algorithm (RA),<sup>4</sup> etc., have also been applied to solve the problem.

However the spacecraft is not free from disturbances, which are not considered in the above methods. Those disturbances are from, e.g., the external environment like atmosphere drag, and the attitude reorientation property would be reduced and even the avoidance of attitude constraint zone is not ensured if disturbances are neglected. Thus a fault-tolerant sliding-mode control scheme is derived in Ref. 5 to accommodate disturbances and actuator fault, where exact upper bound of uncertain inertia matrix can be online estimated. Besides, a finite-time output feedback control

scheme is derived in Ref. 6 for spacecraft stabilization with bounded disturbances.

The aim of the paper is to provide a controller to deal with spacecraft repointing problem in the presence of attitude forbidden zone and disturbances. The main contributions of this paper, compared with the previous results, is the construction of a novel attitude barrier potential function, where the unwanted term in the backstepping controller design is compensated by a scaling factor. Therefore both the avoidance of attitude forbidden zones and disturbance attenuation are achieved.

The remainder of the paper is organized as follows. Section 2 lists the preliminaries including the modeling of spacecraft, attitude forbidden zones and control objective. Controller design with the corresponding proof is given in Section 3. Simulation results and conclusions are offered in Section 4&5.

## 2. Preliminaries

The dynamics of spacecraft is listed below [6]

$$\dot{q} = L(q)w \quad (1)$$

$$J\dot{w} + S(w)Jw = u + d \quad (2)$$

where, for vectors in (1)(2),  $q = [q_0; q_v] \in R^4$  is quaternion with  $q^T q = 1$ ,  $w \in R^3$  angular velocity of spacecraft in the body-attached frame,  $u \in R^3$  control torque from actuators of spacecraft, and  $d \in R^3$  external disturbances. Moreover, for the matrices in (1) and (2)  $L(q) = [-q_v; q_0 I_3 + S(q_v)]$  where  $S(a) = [0, -a_3, a_2; a_3, 0, -a_1; -a_2, a_1, 0]$  with  $a \in R^3$ , and  $J \in R^{3 \times 3}$  is inertia matrix with  $J > 0$ .

In practice, when spacecraft is rotated towards specific orientation, some sensitive on-board instruments like interferometer should circumvent direct exposure of bright celestial objects such as the sun. These unwanted orientations are considered as attitude forbidden zones, and it can be described as<sup>2</sup>

$$x^T R y < \cos\theta$$

where  $R = (q_0^2 - q_v^T q_v) I_3 + 2q_v q_v^T + 2q_0 S(q_v)$  is rotation matrix of spacecraft from body-attached frame to inertia frame,  $x$  is the direction of bright and celestial object in the inertia frame,  $y$  is the instrument's bore-sight vector in the body-attached frame,  $Ry$  is the counterpart in the inertia frame,  $\beta$  is the angle between  $x$  and  $Ry$ , and  $\theta \in (0, \pi)$  is the minimum angle allowed for  $\beta$ . Note that  $x$  and  $y$  are constant.

Furthermore the above constraint can be transformed into<sup>2</sup>

$$q^T M(x, y, \theta) q < 0 \quad (3)$$

where  $M(x, y, \theta) = [A, b; b^T, d]$  with  $A = xy^T + yx^T - (x^T y + \cos\theta) I_3$ ,  $b = x \times y$ ,  $d = x^T y - \cos\theta$ . Moreover, the inequality (3) can be written in more accurate form  $-1 - \cos\theta \leq q^T M(x, y, \theta) q < 0$ .

It is noted that  $q^T M q \rightarrow 0$  if  $\beta \rightarrow \theta$ . The property facilitates the construction of barrier potential function. For simplicity, only one bore-sight vector and one attitude forbidden zone are considered here.

The control objective is to render the spacecraft rotate towards the prescribed attitude  $q_d$  or  $-q_d$ , both of which is equivalent in the physical meaning, from any permissible initial value of attitude  $q(0)$  and angular velocity  $w(0)$ . During the process the spacecraft circumvent the attitude forbidden zones  $\Xi_q = \{q \in S^3 \mid q^T M q < 0\}$  in the presence of external disturbances. It is obvious that  $q_d, q(0)$  are outside attitude forbidden zone, i.e.  $q_d, q(0) \cdot \Xi_q$ . Moreover in the design, there exist  $J_{min} > 0, J_{max} > 0$  such that  $J_{min} I_3 < J < J_{max} I_3$ , and disturbances  $d(t)$  are bounded.

## 3. Controller Design

Compared with the barrier potential function in Ref. 1 and 2, the barrier function of quaternion here is modified to accommodate external disturbances.

First consider quaternion dynamics (1). The corresponding Lyapunov-like barrier function is derived to be  $V_q = (k_1 / r_q + k_2 \ln(-2 / q^T M q)) \|q - q_d\|^2$  where the positive variable  $r_q$  is a scaling factor that would be defined later, and  $k_1 > 0, k_2 > 0$ . Here the virtual control  $w_c$  for  $w$  is set as  $w_c = k_3 L^T(q) q_d$  with  $k_3 = \bar{k}_3 / r_q$  and  $\bar{k}_3 > 0$ , and the dynamics of  $r_q$  is

$$\begin{aligned} \dot{r}_q = & -\frac{k_2 \bar{k}_3}{8k_1} (r_q - r_{qc}) \ln\left(-\frac{2}{q^T M q}\right) (1 + q_d^T q) \\ & + \text{Proj}_{r_q} \left( \frac{2k_2 \bar{k}_3 r_q}{k_1 q^T M q} q^T M L(q) L^T(q) q_d \right) \end{aligned} \quad (4)$$



where  $\text{Proj}_q(\cdot)$  here is defined in Ref 7, with  $r_{qc} > 0$ . Thus after a lengthy calculation, the derivative of  $V_q$  is simplified as

$$\begin{aligned} \dot{V}_q \leq & -\left(\frac{k_1}{r_q} - k_2 \ln\left(-\frac{q^T M q}{2}\right)\right) 2q_d^T L(q) w_r \\ & - \frac{4k_2(1 - q_d^T q)}{q^T M q} q^T M L(q) w_r \\ & - \frac{k_3}{2} \left(\frac{k_1}{r_q} - \frac{k_2}{2} \ln\left(-\frac{q^T M q}{2}\right)\right) (1 - (q_d^T q)^2) \end{aligned}$$

with  $\|q - q_d\|^2 = 2(1 - q_d^T q)$ ,  $q_d^T L(q) L^T(q) q_d = \frac{1}{4}(1 - (q_d^T q)^2)$  used. Here it should be also noted that  $r_q \geq r_{qc}$  given  $r_q(0) \geq r_{qc}$ .

Besides the dynamics of  $w$  is considered. Take the derivative of  $w_r$  and we get

$$J\dot{w}_r = -S(w)Jw + u + d - J\dot{w}_c \quad (5)$$

with  $\dot{w}_c = -k_3 L^T(q_d) L(q) w + k_3 (\dot{r}_q / r_q) L^T(q_d) q$ . Let  $V_{w_r} = w_r^T J w_r / 2$  and accordingly  $u = S(w_c) J w + J_0 \dot{w}_c + u_1$ , thus the derivative of  $V_{w_r}$  is

$$\dot{V}_{w_r} = w_r^T \{u_1 + d\} \quad (6)$$

Then  $V_q$  and  $V_{w_r}$  is combined together and  $V_c = k_4 V_q + V_{w_r}$  with  $k_4 > 0$ . If  $u_1$  is set as

$$\begin{aligned} u_1 = & 2k_4 \left(\frac{k_1}{r_q} - k_2 \ln\left(-\frac{q^T M q}{2}\right)\right) L^T(q) q_d \\ & + \frac{4k_2 k_4}{q^T M q} (1 - q_d^T q) L^T(q) M q - (k_5 + k_6) w_r, \end{aligned} \quad (7)$$

with  $k_5 > 0, k_6 > 0$ , the derivative of  $V_c$  can be scaled as

$$\dot{V}_c \leq -\Pi_2 + \Theta_1 \quad (8)$$

where

$$\Pi_2 = \frac{k_3 k_4}{2} \left(k_2 - \frac{1}{2r_q} \ln\left(-\frac{q^T M q}{2}\right)\right) (1 - (q_d^T q)^2) + k_6 w_r^T w_r$$

and  $\Theta_1 = \bar{d}^T \bar{d} / 4k_5$ , and young inequality is used here.

Here the total control torque  $u$  is summarized as

$$\begin{aligned} u = & S(w_c) J w + 2k_4 \left(\frac{k_1}{r_q} - k_2 \ln\left(-\frac{q^T M q}{2}\right)\right) L^T(q) q_d \\ & + J_0 \dot{w}_c + \frac{4k_2 k_4}{q^T M q} (1 - q_d^T q) L^T(q) M q - (k_5 + k_6) w_r \end{aligned} \quad (9)$$

Before the main result is preceded, it should be noted that both the stability of the variables in Lyapunov

© The 2015 International Conference on Artificial Life and Robotics (ICAROB 2015), Jan. 10-12, Oita, Japan

function  $V_r$  and the boundedness of  $r_q$  should be considered, both of which lead to Theorem 1.

**Theorem 1.** Consider system (1)(2) and controller (4) (9). For  $\forall q(0)$  with  $q^T(0)q(0) = 1, q(0) \cdot \Xi_q, \forall w(0)$ , and  $r_q(0) \geq r_{qc}$ , the following properties hold:

- (i). The variables  $q, w$  are bounded for  $\forall t \geq 0$ , and  $q^T(t)Mq(t) < 0$ , meaning that spacecraft would not rotate into attitude forbidden zone all the time.
- (ii). The variables  $q, w$  would be within a small neighbor of desired Equivalent points  $(\pm q_d, 0_3)$ .
- (iii). The scaling factor  $r_q(t)$  is bounded all the time with the appropriate parameters in the controller and a switching strategy of desired quaternion from  $q_d$  to  $-q_d$  when  $q_d^T q \leq -1 + \varepsilon$  where  $\varepsilon \in (0, 1]$ .

**Proof.** First from (8), it is concluded that  $V_r$  is bounded all the time, and besides  $q^T M q < 0$  all the time.

For the second property,  $\Theta_2$  can be set as sufficiently small as possible via  $k_5, k_6, \Gamma_\theta$ . Thus like<sup>[6]</sup>,  $V_r$  would converge into a neighbor of origin, as sufficient close as possible, in finite time and property 2 is ensured. Moreover, based on properties 1 and 2, there exist  $\varphi > 0$  such that  $q^T M q < -\varphi$ , leading to forward completeness of  $r_q$ .

As for the third property, via appropriate parameters, there exists  $\bar{M} > 0$  for  $r_q$  such that  $\|(2k_2 \bar{k}_3 r_q) / (k_1 q^T M q) q^T M L(q)\| < \bar{M} r_q$ . Besides,  $(k_2 \bar{k}_3) / (8k_1) \ln(-2 / q^T M q) (1 + q_d^T q) \geq \bar{k}_q \square (k_2 \bar{k}_3) / (8k_1) \ln(2 / (1 + \cos \theta)) \varepsilon$  based on  $-1 - \cos \theta \leq q^T M q$  and switching strategy of desired quaternion  $q_d$ . Thus  $\dot{r}_q \leq -\bar{k}_q (r_q - r_{qc}) + \bar{M} \|L^T(q) q_d\| r_q$ . Moreover based on property 2, there exist  $\star_1 > 0$ , where  $\star_1 \leq \bar{k}_q / (2\bar{M})$ , and the corresponding  $T_1 > 0$  such that  $\|L^T(q) q_d\| < \star_1, \forall t \geq T_1$ . Therefore it is concluded that  $\dot{r}_q \leq 0$  when  $r_q \geq 2r_{qc}, t \geq T_1$ , which means  $r_q$  is bounded when  $t \geq T_1$ . Besides  $r_q$  is also bounded when  $0 \leq t \leq T$  due to boundedness of  $q$  and  $q^T M q < -\varphi$ . In all,  $r_q$  is bounded all the time and the proof is complete.  $\square$

#### 4. Simulation Results

The controller scheme is simulated to verify its effectiveness. In the simulation,  $J = [350, 3, 4; 3, 270, 10; 4, 10, 190]$  with  $J_{\max} = 600, J_{\min} = 100$ . As for

attitude forbidden zone,  $x = [0.35; 0.24; 0.9055]$ ,  $y = [1; 0; 0]$ ,  $\theta = 60^\circ$ . Moreover initial values are set as  $q(0) = [0.5, -0.5, -0.5, -0.5]^T$ ,  $w(0) = [0.1, -0.2, 0.12]^T$ ,  $r_q(0) = 1$ , and control parameters are  $k_1 = 2, k_2 = 4, k_3 = 0.6, k_4 = 4, k_5 = 0.4, k_6 = 25, r_{qc} = 0.5$ . Moreover in the simulation, the control torque  $u$  is bounded, i.e.,  $|u_i| < 10N \cdot m, i = 1, 2, 3$ , and external disturbances are set as  $d = [0.5 \sin(0.2t - 45^\circ); 0.6 \sin(0.2t + 30^\circ); 0.3 \cos(0.2t)]$ .

It can be seen from Fig. 1 that the spacecraft is initially located where the bore-sight vector is close to the attitude forbidden zone. Here the controller renders spacecraft circumvent the attitude forbidden zone, and eventually stop at the desired attitude, where the bore-sight vector is also in proximity to attitude forbidden

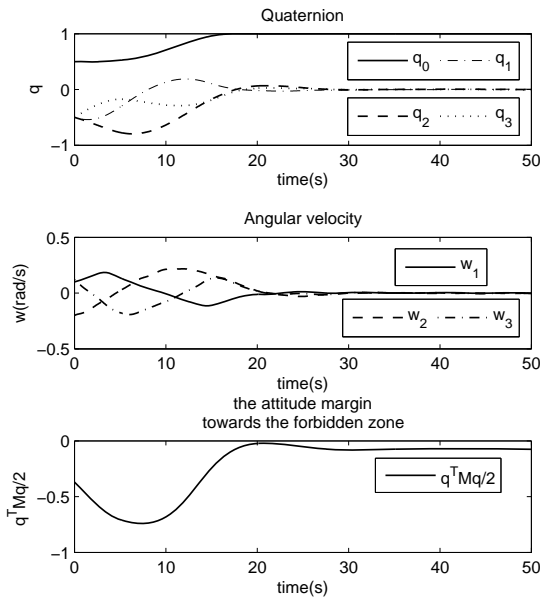


Fig.1, simulation of result of the proposed controller. Besides disturbances are attenuated during the process.

### 5. Conclusion

A Lyapunov-based control scheme for attitude

constrained reorientation of spacecraft with disturbances is derived. A novel attitude potential function with a scaling factor is derived, and a corresponding controller is designed to accomplish the avoidance of attitude forbidden zone and disturbance attenuation. Future work would focus on the constrained attitude control law without measurements of angular velocity.

### Acknowledgements

This work is supported by the National Basic Re-search Program of China (973 Program: 2012CB821200, 2012CB821201) and the NSFC (61134005, 60921001, 61327807).

### References

1. Y. Kim, M. Mesbahi (2004), Quadratically constrained attitude control via semidefinite programming, IEEE Transaction on Automatic Control, 49(5) :731-735.
2. U. Lee, M. Mesbahi (2012), "Spacecraft Reorientation in Presence of Attitude Constraints via Logarithmic Barrier Potentials", in Proceedings of American Control Conference, San Francisco, CA, 450-455.
3. A. Weiss, F. Leve, M. Baldwin, et al., (2014), "Spacecraft Constrained Attitude Control using Positively Invariant Constraint Admissible Sets on  $SO(3) \times R_3$ ", in Proceeding of American Control Conference, Portland, Oregon, 4955-4960.
4. P. Y. Cui, W. G. Zhong, H. T. Cui (2007), "Onboard spacecraft slew-planning by heuristic state spacecraft search and optimization", in Preceding of the 2007 IEEE International Conference on Mechatronics and Automation, Harbin, China, 2115-2119.
5. Q. L. Hu (2010), Robust adaptive sliding-mode fault-tolerant control with  $L_2$ -gain performance for flexible spacecraft using redundant reaction wheels, IET Control Theory and Applications, 4(6): 1055-1070.
6. A. M. Zou (2009), Finite-time output feedback attitude tracking control for rigid spacecraft, American Control Conference, IEEE Transactions on Control System Technology, 22(1), 338-345.
7. Ø. N. Starnes, O. M. Aamo, G. O. Kaasa (2011), A constructive speed observer design for general Euler-Lagrange systems, Automatica, 47(10), pp. 2233-2238.

# Weighted Multiple Model Adaptive Control of Slowly Time-Varying Systems

Weicun Zhang, Qing Li

School of Automation and Electrical Engineering, University of Science and Technology Beijing  
Beijing 100083, China

E-mails: weicunzhang@ustb.edu.cn; qingli@ies.ustb.edu.cn

## Abstract

Weighted multiple model adaptive control is a combination of off-line design and on-line decision, which combines a finite number of simple controllers by weighting algorithm. This paper presents an improved weighting algorithm of slowly time-varying systems and a new method to partition model uncertainty using v-Gap metric. The effectiveness of the proposed methods is verified through Matlab simulations.

Keywords: MMAC; v-Gap; Weighting Algorithm; Time-Varying System

## 1. INTRODUCTION

Weighted multiple model adaptive control (WMMAC) and weighted multiple model adaptive estimation (WMMAE) appeared around 1960's to 1970's, which consists mainly of three components, i.e., the model-set, local controller/estimator design, and weighting algorithm. Multiple Kalman filter is the basis of classical MMAC or MMAE. The purpose of using multiple models is to improve the accuracy of state estimation or control problems with parameter uncertainties<sup>1, 2</sup>. This was followed in later years by several practical applications. In recent years, a new type of WMMAC, i.e., robust multiple model adaptive control (RMMAC) was put forward with convincing experiment results<sup>3,4</sup>, which arouses once again the enthusiasm of researchers in the field of adaptive control in recent years.

Some results are made on MMAC of time-invariant systems. MMAC is proved to be a useful control method to deal with time-invariant system whose parameter is not quite certain.

As previous weighting algorithm could not easily change weight once sub-model's weight converged to 0, it is not suitable for time-varying system. This paper comes up with an improved weighting algorithm to solve this problem. With the help of improved algorithm, the changes of system parameters can be detected and then sub-models' weights can be recalculated. In this way, WMMAC can be used to slow-varying systems.

For WMMAC, weighting algorithm is one of the core contents, it will directly affect whether the weighting algorithm could choose the sub-model from model-set

which is the nearest to the actual control system accurately and rapidly.

The corresponding WMMAC system is shown in Fig. 1 and Fig. 2.

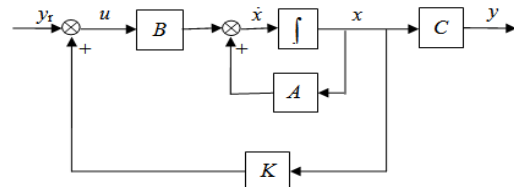


Fig.1 Block diagram of a general control system

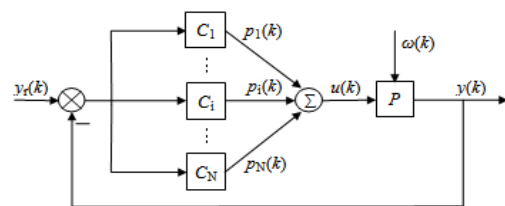


Fig. 2 Block diagram of WMMAC

Consider the following time-varying plant:

$$\dot{x}(t) = A(t)x(t) + E(t)u(t)$$

$$y(t) = Q(t)x(t)$$

## 2. Weighting algorithm

The traditional weighted multi-model adaptive control use maximum a posteriori probability method to calculate the weights of each controller. In the process of calculation, traditional method is quite complex and its calculation is huge.

When one sub-model of model-set is very close to the actual system, its weight should be close to 1. That's

the core concept of weighted multi-model adaptive control method<sup>5</sup>. As the change of weight is smooth rather than mutations, so we could achieve the purpose of model soft switching by using weighted multiple model adaptive control method.

As the actual controlled system and sub-model of model-set is not necessarily the same, the output error  $e_i(k)$  is exist between actual system output  $y(k)$  and each sub-model's output  $y_i(k)$ .

Model's similar degree is evaluated by the magnitude of output error  $e_i(k)$ . If one of the sub-model's output error is the smallest when system became stable, then we can say this sub-model is the nearest to the actual system and its weight should finally converge to 1

Based on the above concept, designing the following weighting algorithm:

- 1) Initialize weights.
- 2) Calculation of error performance metrics.
- 3) Compare the error performance metrics, find the minimum error performance metrics.
- 4) Calculation of weight metrics.
- 5) Calculation of sub-models' weights based on weight metrics.
- 6) Calculation of control law.

The advantage of this method is smooth switching process and stabilized system output. This could decrease the damage to actual system when system parameter changed, as a result this method is quite suitable for industrial.

The weight metrics and sub-models' weights of weighting algorithm are designed as follows:

$$l_i(k) = \frac{l_{\min}^i(k)}{l_i^i(k)} l_i(k-1)$$

Once sub-model's weight  $p_i(k)$  has converged to 0, its weight metric  $l_i(k)$  is also converged to 0. It is not difficult to find that no matter how error performance metrics changes, this sub-model's weights could not become 1. In other word, weighting algorithm could not adapt to the change of actual system parameters.

In order to solve this problem, this paper comes up with an improved weighting algorithm that could make weights recalculate to adapt to system parameter changes.

Compare the output error of each sub-model at every sample instance. Mark the sub-model's number  $i$  which output error  $e_i(k)$  is the smallest. When system parameter has changed, Remark the sub-model which output error is the smallest as  $M_{e_{\min}}(k)$ . If the sub-model marked at current sample instance is different from the one marked at previous sample instance:

$$M_{e_{\min}}(k) \neq M_{e_{\min}}(k-1) \text{ and } M_{e_{\min}}(k-1) = M_{e_{\min}}(k-2) = M_{e_{\min}}(k-3)$$

Initialize the weight of each sub-model. In this way, we can recalculate each sub-model's weight and reselect the best sub-model's controller to control the actual system when system parameter is changed.

### 3. Partition the Model-set Using v-Gap Metric

#### 3.1 v-Gap metric basic concepts and definitions

In order to measure the distance between two nominal plants from a closed-loop perspective, we need a measure to quantify the closeness of closed-loop behavior of two open-loop plants. For this reason, the v-Gap metric introduced by Vinnicombe in is used throughout this paper<sup>[6]</sup>.

The v-Gap metric is defined as:

$$d_v(P_1, P_2) = \left\| \begin{array}{c} \frac{|P_1(e^{jw}) - P_2(e^{jw})|}{\sqrt{1 + |P_1(e^{jw})|^2} \sqrt{1 + |P_2(e^{jw})|^2}} \\ \vdots \\ 1 \end{array} \right\|$$

subject to

$$\det(1 + P_1^* P_2)(e^{jw}) \neq 0, \forall w \text{ And } \text{wind}(1 + P_1^* P_2) + H(P_2) - H(P_1) = 0$$

Where,  $w$  denotes the winding number evaluated on the standard Nyquist contour indented around any imaginary axis poles of  $P_1$  and  $P_2$ .

When  $\delta_v(P_1, P_2)$  is small enough, then we can consider that the controller stabilizing system  $P_1$  could also make system  $P_2$  stable.

#### 3.2 Partitioning the parameter set

As v-Gap can be used to measure the distance of two systems, we use v-Gap to partition the model-set.

For the system with only one uncertain parameter, we can choose a certain value  $r$  as v-Gap metrics ( $0 < r < 1$ ), in order to find sub-models' parameter and partition the model-set into N sub-models.

If actual system's parameter as follows:

$$A = \begin{array}{c} \text{0} \\ \vdots \\ 1 \end{array} \quad \begin{array}{c} 1 \\ \vdots \\ -4 \end{array}, B = \begin{array}{c} \text{0} \\ \vdots \\ 0 \end{array} \quad \begin{array}{c} 1 \\ \vdots \\ 1 \end{array}, C = \begin{array}{c} \text{0} \\ \vdots \\ 2 \end{array} \quad \begin{array}{c} -2 \\ \vdots \\ 1 \end{array}, \\ l \in (-103, -50]$$

System transfer function is calculated as  $G = Q(sI - A)^{-1}B$ , Assume two sub-models:



reference input. What's more, the weight converged much more slowly than usual. However, weighting algorithm still finally identified the nearest sub-model from model-set, and uses its controller to control actual system.

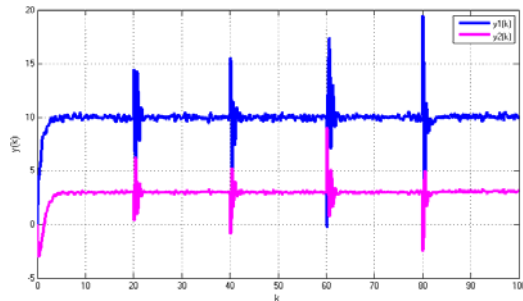


Fig. 7 Slowly time-varying system

From Fig. 7, we can see that even system is disturbed by white-noise signal, WMMAC using weighting algorithm presented in this paper can still control system well. No matter how system parameter changed, weighting algorithm can accurately choose the sub-model which is the nearest to the actual system from model-set (parameter set), and finally stabilized system output.

## 6. Conclusion

Weighted multiple model adaptive control is a useful control method to deal with large uncertainty of system parameters.

V-Gap metric is an important metric of two systems distance, through simulation we can draw a conclusion, though v-Gaps between each two sub-model are the same, sub-model parameter selection are not uniform. v-Gap can be used as the basis of the division of model-set.

To the slowly time-varying system, an improved weighting algorithm mentioned in this paper could make weights recalculate to adapt to system parameter changes. Through simulation, when system parameter

changes, weighting algorithm can quickly realized this change and initialized each weight. If the real model of system to be controlled is included in the model set, WMMAC can quickly find the right model and the corresponding controller.

## Acknowledgements

This work is partially supported by National Basic Research Program of China (973 Program) (No. 2012CB821200), National High Technology Research and Development Program of China (863 Program) (No. 2011AA060408), Beijing Higher Education Young Elite Teacher Project (No. YETP0362), National Key Technology Research and Development Program of China (No. 2013BAB02B07).

## References

1. Magill D.T. Optimal adaptive estimation of sampled stochastic processes. *IEEE Transactions on Automatic Control*. 1965, 10:434-439
2. Lainiotis, D.G. Optimal adaptive estimation structure and parameter adaption, *IEEE Transactions on Automatic Control*, 1972, 16:160-170
3. M. Athans, S. Fekri, and A. Pascoal, Issues on robust adaptive feedback control, in *Preprints 16th IFAC World Congress*, pp. 9-39, Prague, Czech Republic, July 2005
4. Sajjad Fekri, Michael Athans, and Antonio Pascoal, Issues, progress and new results in robust adaptive control, *International Journal of Adaptive Control and Signal Processing*, Vol. 20(10):519-579, 2006
5. Zhang Weicun. Stable Weighted Multiple Model Adaptive Control [J]. *International Journal of Adaptive Control and Signal Processing*, Vol. 27(7):562-581, 2013
6. Hessam Mahdianfar, Sadjaad Ozgoli, Hamid Reza Momeni. Robust multiple model adaptive control: Modified using v-GAP metric. *International Journal of Robust and Nonlinear Control*, 2011, 21:2027-2063

# A Reduced-Complexity Interacting Multiple Model Algorithm for Location Tracking in Heterogeneous Observation

**Xiaoyan Fu**

*The Beijing Engineering Research Center of High Reliable Embedded System, Capital Normal University  
Beijing, 100191, P.R. China*

**Yuanyuan Shang**

*The Beijing Key Laboratory of Electronic System Reliability Technology, Capital Normal University  
Beijing, 100191, P.R. China  
E-mail: fuxiaosg@163.com, syy@bao.ac.cn  
www.cnu.edu*

## Abstract

This paper is devoted to the problem of state estimate of discrete-time stochastic systems. A low-complexity and high accuracy algorithm is presented to reduce the computational load of the traditional interacting multiple model algorithm with heterogeneous observations for location tracking. By decoupling the x and y dimensions to simplify the implementation of location, updated information is iteratively passed based on an adaptive fusion decision. Simulations show that the algorithm is more computationally attractive than existing multiple model methods.

*Keywords:* data fusion, interacting multiple model algorithm, location tracking, wireless sensor networks.

## 1. Introduction

Data fusion deals with the problem of how to extract and utilize useful information contained in multiple sets of data in order to estimate unknown parameters or processes<sup>1</sup>, which has been widely applied in military and civilian fields, e.g., target tracking and localization, air traffic control, guidance and navigation, fault diagnosis, surveillance and monitoring. Estimation fusion is one of the important applications involving wireless sensor networks (WSNs), but the WSNs have very limited sensing range and communication bandwidth which restrict the application of the centralized signal processing method. In other words, not only are accurate positioning algorithms essential to useful location-estimation systems, but also to reduce

energy consumption is worth developing low-complexity schemes for WSNs<sup>2</sup>.

State estimate problem of discrete-time Markovian jump linear system (MJLS) is always the focus of interest in the community of maneuvering target tracking. Multiple-model (MM) algorithms (such as generalized pseudo-Bayesian (GPB), interacting multiple model (IMM), variable-structure MM (SVMM)) are generally considered as mainstream approach to address this problem. Among them, IMM algorithm proposed by Blom<sup>3</sup> is most prevalent.

Nevertheless, the high accurate location estimation for maneuvering target based on the traditional IMM algorithm requires models interacting and inverse operations. The location data fusion algorithm with an IMM technique has high computational complexity, and direct implementation of the IMM algorithm may be too

complex for practical systems. Moreover, local stations in WSNs may not be able to afford IMM estimation due to limited computational power<sup>4</sup>. Consequently, it would be useful to reduce the computational complexity of the IMM algorithm.

Our idea to deal with reduced-complexity state estimation is to reconstruct the IMM algorithm. In contrast to the existing reduced-complexity approach including: alpha-beta filtering, Kalman filtering, our proposed methods is based on a factor graph (FG) by decoupling the  $x$  and  $y$  dimensions to simplify the implementation of location and adaptive data decision for state estimation of a MJLS.

## 2. Background

### 2.1. Model

Consider the dynamic system of tracked target described with the state space form. The mathematical models on the target can be taken by the following Markov jump linear system:

$$x(k+1) = F_j x(k) + \Gamma_j \omega_j(k) \quad (1)$$

$$z(k) = H_j x(k) + v_j(k) \quad (2)$$

where the state  $x(k)$  is an  $n$ -dimensional vector, the observation  $z(k)$  is an  $m$ -dimensional vector, and the subscript  $j \in \mathcal{S} = \{1, 2, \dots, s\}$  denotes the model. The matrix functions  $F_j(\cdot)$ ,  $\Gamma_j(\cdot)$  and  $H_j(\cdot)$  are known. The model-dependent process noise and measurement noise are assumed to be a Gaussian random process.

Let  $M_j^k$  denotes the flight model  $j$  at time  $k$ . The model dynamics are modeled as a finite Markov chain with known model-transitions probabilities from model  $i$  at time  $k-1$  to model  $j$  at time  $k$ .

$$\pi_{ij} = \Pr ob[M_j^k | M_i^{k-1}] = P\{M_j^k | M_i^{k-1}\} \quad (3)$$

### 2.2. Operations of Factor Graphs

In terms of the operations of FG operations, one advantage of multiplications is the distributive law. For example,  $a \times b + a \times c = a \times (b + c)$ , where the left-hand side involves three arithmetic operations, and the right-hand side involves only two operations. Furthermore, according to the inherent distributed feature of the belief propagation algorithm to make the decomposition in accordance with prediction-correction recursion, the messages of the reliable information are processed and

passed among the prediction phases and correction phases with the error propagation law<sup>5</sup>.

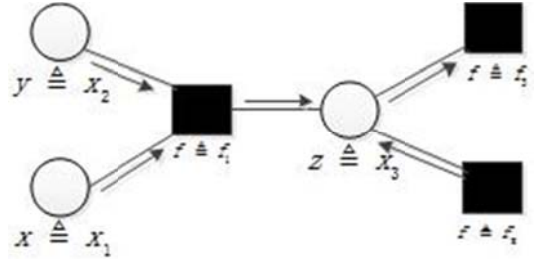


Fig. 1. Message passing from node to node

#### 1) Message from Variable Nodes to Factor Nodes:

Assume that each message in the FG flows is a Gaussian PDF. A message from a variable node to a factor node is the product of incoming messages. For example, a variable node with two incoming messages is illustrated in Fig. 1, where a variable node is represented by a circle; a factor node is represented by a solid square. In fact, the message from a variable node to a factor node can be taken as the correction step in Bayesian filtering, where the mean is the estimated result based on data reliability for location estimation and tracking.

#### 2) Message from Factor Nodes to Variable Nodes:

For two continuous variables  $x$  and  $y$ , the marginal density function of  $y$  is obtained by integrating the joint distribution over variable  $x$ . This operation can be taken as the prediction step using the Bayesian filtering approach for location estimation and tracking.

## 3. Proposed Location Tracking Algorithm

This article focuses on location tracking approaches in terms of the  $X$  and  $Y$  groups individually, and the  $X$  and  $Y$  results of the state and the covariance equations are decoupled as individual input. Moreover, others heterogeneous observations can be viewed as individual input, and corresponding state estimation can be obtained individually. All estimations combined with data fusion algorithm, which can improve the accuracy of location estimation and tracking.

Given the computationally attractive feature of FGs<sup>6</sup>, this article proposes a location tracking scheme based on the FG approach and the error for location and speed estimations to implement the recursive Bayesian estimation and to reduce the computational load of the



traditional IMM algorithm. Furthermore, decoupling the  $X$  and  $Y$  dimensions for different tracking groups also can reduce the computational complexity. Therefore, the 2-D problem is reduced to two 1-D problems. The 2-D problem can be represented by two independent main groups, the  $X$ -coordinate and the  $Y$ -coordinate groups.

According to the concept of undirected graph model<sup>7</sup>, the representation related to estimate speed and location of the  $X$ -coordinate group is illustrated as the black color diagram in Fig. 2, where a correction node is illustrated by a circle; a prediction node is illustrated by a solid square.

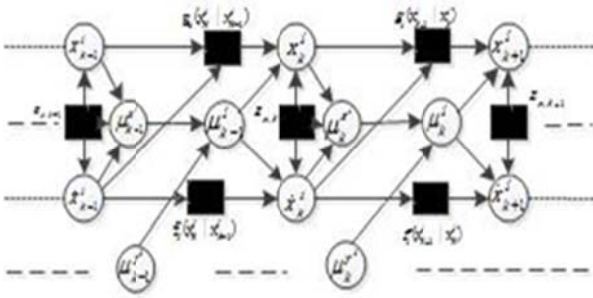


Fig. 2. Graph model of the data-fusion location estimation for  $X$ -coordinate group from the  $k$ th to  $(k+1)$ th.

The measurement model based on IMM algorithm is the situation that the error propagation law can be applied to the linear dynamical system, and then the proposed IMM algorithm based on factor graphs (IMM-FG) for location estimation and tracking are illustrated in the following part.

Step 1: Calculate the mixed initial probability for the filter m-matched to model  $M_j^k (j \in S)$

$$\begin{aligned} \mu_{ij}(k|k) &\square \mathbb{P}\{M_i^{k-1} | M_j^k, z_{0:k-1}\} \\ &= \frac{\mathbb{P}\{M_j^k | M_i^{k-1}, z_{0:k-1}\} \cdot \mathbb{P}\{M_i^{k-1} | z_{0:k-1}\}}{\mathbb{P}\{M_j^k | z_{0:k-1}\}} \\ &= \frac{\pi_{ij} \mu_i^{k-1}}{\bar{c}_j} \quad i, j \in S \end{aligned} \quad (3)$$

where  $\bar{c}_j$  is the normalization constant.

Step 2: Calculate the mixed initial state and corresponding covariance for the filter matched to model

$$x_{0j}^k (j \in S) \square \sum_{i=1}^s \mu_{ij}(k|k) N(x_i^{k-1}; \widehat{S}_{x_{k-1}}, \widehat{V}_{x_{k-1}}) \quad (5)$$

$$\dot{x}_{0j}(k|k) \square \sum_{i=1}^s \mu_{ij}(k|k) N(\dot{x}_i^{k-1}; \widehat{S}_{\dot{x}_{k-1}}, \widehat{V}_{\dot{x}_{k-1}}) \quad (6)$$

© The 2015 International Conference on Artificial Life and Robotics (ICAROB 2015), Jan. 10-12, Oita, Japan

Step3: Filtering ( $j \in S$ )

Prediction state

$$x_j(k|k-1) \sim N_{oper3}(x_j(k|k-1); \widehat{S}_{x_{0j}(k|k)}, \widehat{V}_{x_{0j}(k|k)}) \quad (7)$$

$$\dot{x}_j(k|k-1) \sim N_{oper2}(\dot{x}_j(k|k-1); \widehat{S}_{\dot{x}_{0j}(k|k)}, \widehat{V}_{\dot{x}_{0j}(k|k)}) \quad (8)$$

Correction state

$$x_j^k \square N_{oper1}(x_j^k; \widehat{S}_{x_j(k|k-1)}, \widehat{V}_{x_j(k|k-1)}) \quad (9)$$

$$\dot{x}_j^k \square N_{oper1}(\dot{x}_j^k; \widehat{S}_{\dot{x}_j(k|k-1)}, \widehat{V}_{\dot{x}_j(k|k-1)}) \quad (10)$$

Step4: Combine the state estimates and corresponding covariance according to the updated weights

$$x_j(k) \square \sum_{j=1}^s \mu_j^k N(x_j^k; \widehat{S}_{x_k}, \widehat{V}_{x_k}) \quad (11)$$

$$\dot{x}_j(k) \square \sum_{j=1}^s \mu_j^k N(\dot{x}_j^k; \widehat{S}_{\dot{x}_k}, \widehat{V}_{\dot{x}_k}) \quad (12)$$

Updated weight of model  $M_j^k$  is

$$\begin{aligned} &\mu_j^k \\ &\square \mathbb{P}\{M_j^k | Z^k\} \\ &= \text{decision}[\mathbb{P}\{M_j^k | z_{1,k}, s_{1,k}\}, \mathbb{P}\{M_j^k | z_{2,k}, s_{2,k}\}, \mathbb{P}\{M_j^k | s_{e,k}\}] \\ &= \text{decision}[\mu_{x,j}^k, \mu_{y,j}^k, \mu_{e,j}^k] \end{aligned} \quad (13)$$

where

$$\begin{aligned} \mu_{x,j}^k &= \frac{\mathbb{P}\{z_{x,k} | M_j^k, z_{0:k-1}\} \cdot \mathbb{P}\{M_j^k | z_{0:k-1}\}}{c} \\ &= \frac{N[z_{x,k}; \widehat{S}_{x_{0j}(k|k)}, \widehat{V}_{x_{0j}(k|k)}] \cdot \bar{c}_j}{c} \end{aligned} \quad (14)$$

It's worth mentioning that *decision* [.] refers to a decision-making or data fusion process, for example, *mean*[.], *max*[.], *min*[.] or more intelligent decision, different location and tracking problems can adopt different data fusion for better tracking accuracy.

#### 4. Simulation Results

In this section, we evaluate the performance of IMM-FG algorithm, and the classical IMM algorithm using the target tracking example. The results are obtained from 100 Monte Carlo runs. The  $X$  position and velocity RMSE are shown in Fig.3 and Fig.4, respectively. The  $Y$  position and velocity RMSE are omitted due to limited space. It can be found that accuracy estimate of the IMM algorithm as nearly as the proposed IMM-FG algorithm in almost time. Although IMM-FG algorithm

has a higher position estimate error than IMM algorithm during the second maneuvering (time samples 61-66), the

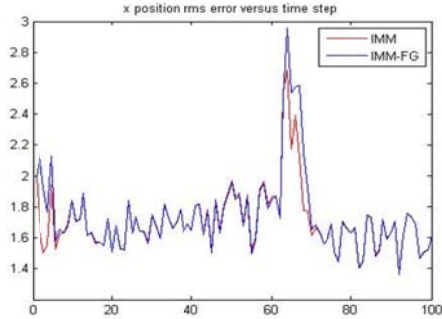


Fig. 3. X position RMSE versus time step.

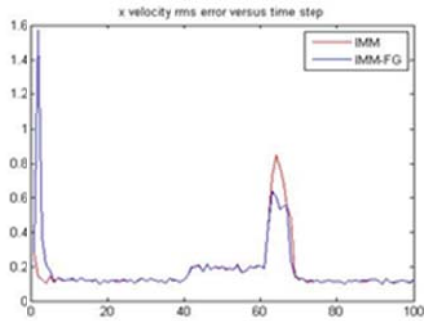


Fig. 4. X speed RMSE versus time step

estimate error converges to zero within a short time. The occurrence of this phenomenon maybe due to that IMM-FG algorithm pays more attention to the rapid change of the velocity during the high maneuvering. On the whole, the estimation accuracy of the IMM-FG algorithm is almost the same with the classical IMM algorithm, but the computing time is short. It can be verified through the comparison computing time between IMM and IMM-FG given in Table 1.

Table1. Computing time between IMM and IMM-FG

	IMM	IMM-FG
50 Monte Carlo runs	1.3767	1.1228
100 Monte Carlo runs	2.4825	2.1691

## 5. Conclusion

The conclusion comes here. In the paper, IMM-FG algorithm is presented for maneuvering target tracking.

It is principally similar to the popular IMM algorithm. The difference lies in the use of filtering. To avoid the inverse of covariance matrix and reducing the complexity of tracking algorithm, the FG algorithm and the idea of decoupling the X and Y dimensions to simplify the implementation of location estimation and tracking is induced to construction of IMM algorithm. Computer simulations indicate that the IMM-FG algorithm has almost the same tracking accuracy with the IMM algorithm.

## Acknowledgements

This work was supported by the NSFC (11178017, 61373090, 61303104, 61203238) and the BNSFC (4132014).

## References

1. D.Jeon, E. Yeonju and K. Hyounkyoung, "Estimation fusion with radar and ADS-B for air traffic surveillance", Information Fusion, 16th International Conference on, 2013, pp. 1328-1335
2. C.L.Wang, Y.S.Chiou and F.Tsai,"Reduced-complexity tracking scheme based on adaptive weighting for location estimation ", IET communications, 2012, pp. 673-684.
3. Blom, H.A.P., Bar-Shalom, Y.,"The interacting multiple model algorithm for systems with Markovian switching coefficients", IEEE Transactions on Automatic Control, 1988, 33, (8), pp. 780-783.
4. Y.X. Gao, X.R. Li and Z.S. Duan, "Estimation Fusion for Markovian Jump Linear System via Data Transformation", IEEE Transactions on Aerospace and Electronic Systems, vol. 50, no. 1, pp. 240-253, Jan.2014
5. Y.S. Chiou and F. Tsai, "A Reduced-Complexity Data-Fusion Algorithm Using Belief Propagation for Location Tracking in Heterogeneous Observations", IEEE Transactions on Cybernetics, vol. 44, no.6, pp. 922-935, Jun. 2014
6. C.L. Wang, Y.S. Chiou, and F. Tsai, "Reduced-complexity tracking scheme based on adaptive weighting for location estimation", IET Communication,vol. 7, no. 7, pp. 673C684, May. 2013
7. Y.-S. Chiou, F. Tsai, C.-L. Wang, and C.-T. Huang, 'A reduced-complexity scheme using message passing for location tracking,'EURASIP J. Adv. Signal Process ., vol. 2012, Jun. 2012.
8. Ho, T.J., Farooq, M.: 'Comparing an interacting multiple model algorithm and a multiple-process soft switching algorithm'. Information Fusion, 2000. pp. 17-24.

---

# Single Image Dehazing on Mobile Device Based on GPU Rendering Technology

**Yuanyuan Shang**

*College of Information Engineering, Capital Normal University, 56 Xisanhuanbei Road  
Beijing, 100048, P.R. China*

**Yue Meng**

*College of Information Engineering, Capital Normal University, 56 Xisanhuanbei Road  
Beijing, 100048, P.R. China*

*Email: syy@bao.ac.cn, mengyue19890119@outlook.com*

*www.cnu.edu.cn*

## Abstract

Image dehazing utilizes a very complex algorithm that requires intensive filtering and floating-point arithmetic operations. Consequently, processing speed is the most significant bottleneck in its application in some vision tasks such as mobile platforms. In this paper, we propose an optimized single image parallel processing dehazing algorithm for mobile platforms and implement it on a Windows Phone device based on GPU rendering technology.

*Keywords:* Fog degradation model, GPU rendering, Image Dehazing, Parallel processing, Windows Phone.

## 1. Introduction

A variety of approaches to image dehazing has been proposed in the literature. They include titles such as Fast visibility restoration from a single color or gray level image, by Tarel and Nautiere<sup>1</sup>; Visibility restoration in bad weather from a single image, by Tan<sup>2</sup>; Single image dehazing, by Fattal; and Single image haze removal using dark channel prior, by He<sup>3</sup>.

With the continuous improvements in image dehazing, the result of haze removal is getting increasingly better. However, processing speed is the most significant bottleneck to the application of dehazing in some vision tasks, especially on mobile platforms.

Graphic processing unit (GPU) rendering technology is widely used in image processing applications to speed up image processing algorithms. In this paper, we propose an optimized single image parallel processing dehazing algorithm for mobile platforms (based on J.P. Tarel's method), and implement it on a Windows Phone device based on GPU rendering technology. The DirectX programming interface, a powerful tool for accessing GPU resources, can be used on the Windows Phone platform. Thus, we chose it to implement and test the algorithm on the Windows Phone device.

## 2. Algorithm Overview

The fundamental concept underlying this fast visibility

restoration algorithm, which was proposed by Tarel, is the fog degradation model. Koshimider proposed the fog degradation model, and Tarel summarized it as in Equation (1):

$$I(x, y) = R(x, y) \left(1 - \frac{V(x, y)}{I_s}\right) + V(x, y) \quad (1)$$

The restored image can thus be obtained by calculating  $R(x, y)$ .

$V(x, y)$  in Equation (1) can then be estimated by following the four steps below:

- (1) Calculate the minimum value of RGB components  $W(x, y)$  in the original image:

$$W(x, y) = \min_{c \in \{R, G, B\}} (I^c(x, y))$$

where  $I(x, y)$  is the original input image.

- (2) Find the median of  $W(x, y)$ :

$$A(x, y) = \text{median}_{S_v}(w(x, y))$$

where  $S_v$  is the template size of the median filter.

- (3) Calculate the difference between  $W$  and  $A$ ,

then calculate the absolute value of the difference:

$$B(x, y) = A - \text{median}_{S_v}(\text{abs}(W - A))(x, y)$$

where  $S_v$  is the template size of the median filter.

- (4) Find the maximum value of the minimum:

$$V(x, y) = p \max(\min(B(x, y), W(x, y)), 0)$$

On obtaining a value for  $V(x, y)$ , the restored image  $R(x, y)$  can then be calculated using Equation (2), which is derived from Equation (1):<sup>5</sup>

$$R(x, y) = \frac{I(x, y) - V(x, y)}{1 - \frac{V(x, y)}{I_s}} \quad (2)$$

where factor  $p$  is used to control the intensity of haze removal, and can be adjusted for different images.

### 3. Algorithm Parallelization

Some parts of the algorithm cannot be applied to the GPU, in which case the CPU is used. A reasonable division of work between CPU and GPU is the key factor that determines the efficiency of the process.

In this paper, we divide the algorithm into three main parts: white balance, restoration core processing, and tone mapping. Some actions cannot be accomplished in GPU because of its structure. Therefore, we have to transfer these parts of the process to CPU. Accordingly, the white balance algorithm described by Tarel<sup>8</sup> and tone mapping have to be divided into several parts, as depicted in Figs.

1 and 2, in order to conveniently implement these parts separately in CPU and GPU.

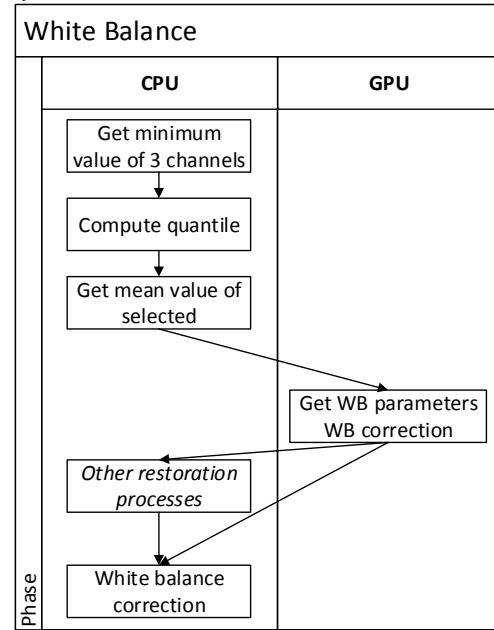


Fig. 1. Division of white balance algorithm between CPU and GPU

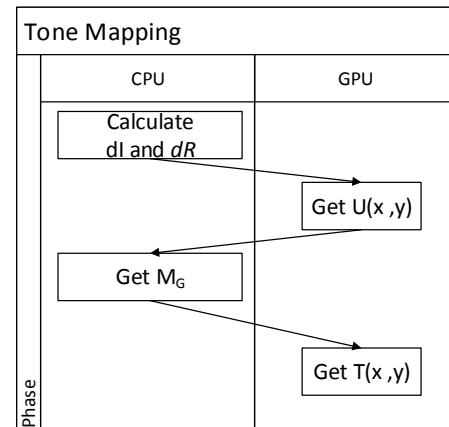


Fig. 2. Division of tone mapping algorithm between CPU and GPU

All processes in the core processing section, which obtains  $V(x, y)$  in four steps and  $R(x, y)$  in the final step, can be carried out in GPU; thus, none of this work needs to be transferred to CPU. This is very beneficial for rapid processing. However, because we need to get the process results for neighboring pixels when performing the second median filter to obtain  $B(x, y)$ , the process has to be split into the two parts: calculating  $A$  and calculating  $R$ ,

as previously discussed. In this process, the final step of the white balance process is combined with the first step of the restoration core processing process, thereby reducing the cost of reassembly.

#### 4. Implementation on Windows Phone

As mentioned before, the GPU processor contains a set of shaders, one of which, pixel shader, has to be programmed in order to implement the image dehazing method. In the DirectX programming interface, a language called high-level shader language (HLSL) is used to program the shaders.<sup>9</sup> A piece of HLSL code corresponds to only a single pixel, not the whole image. All the pixels being processed by the same piece of HLSL program are processed in parallel, rather than sequentially.

Fig. 3. is the workflow chart of the whole algorithm optimized to implement on the GPU, where all textures and parameters have the same name as in the Equation given before. The details of each transfer step were discussed in the previous section.

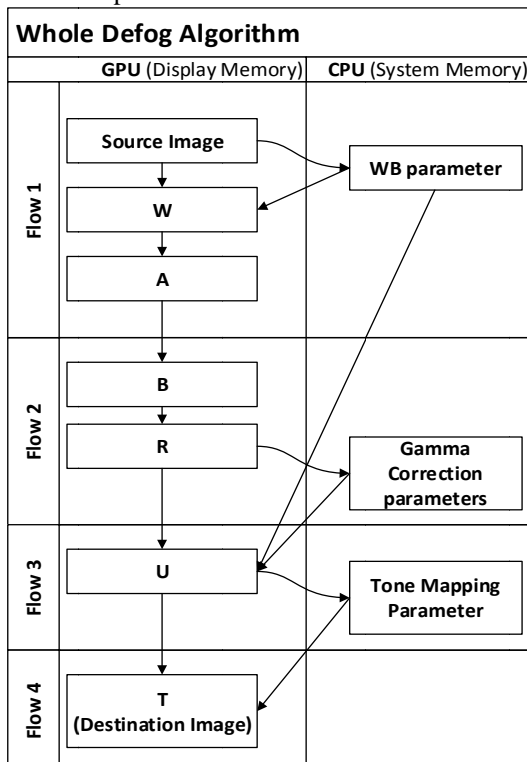


Fig. 3. Workflow of the overall algorithm optimized for G

#### GPU implementation

Note that in the flows across CPU and GPU, curved arrows represent data copies while straight arrows represent parameter transmissions. These are two key techniques in DirectX programming. Data copy refers to the movement of data from display memory to system memory, in order to get access to these data via the usual methods. Parameter transmission is more complex. A class containing the parameters to be transmitted and an ID3D11Buffer to store the parameters in the display memory have to be created. Subsequently, the Context->PSSetConstantBuffer() function has to be used to transmit the parameters to the shader, with the start slot set by this function the same as the register index set in the pixel shader. This is the only interaction between the HLSL and C++ codes.

#### 5. Comparisons and Analyses

Fig. 4 shows the process results. Fig.s 4(a) and 4(d) are the original images, 4(b) and 4(e) are the defog results using GPU, and 4(c) and 4(f) are the defog results using the original algorithm.

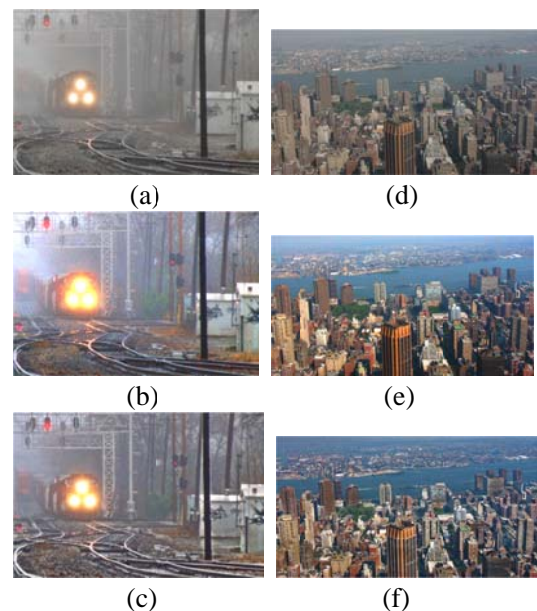


Fig. 4. Experimental results on hazy images

As can be seen in Fig. 4, the process result of GPU

processing is very close to that of the original algorithm. In Fig. 2(b), which has more intricate details, the details of the processed image are not as clear as the original algorithm because of changes in the filtering method; however, they are still within the acceptable range. During the implementation, process, we adjusted the intensity of the tone mapping, such that the restored image is more vivid than the image restored by the original algorithm; the color of the image is more realistic.

The focus of our research is improvement of the processing speed. Table 1. shows the processing time of the original algorithm running in CPU and our optimized algorithm running in CPU and GPU. All the tests were conducted on a Windows Phone device with Snapdragon MSM8260A CPU and 1 GB RAM.

Resolution	CPU	CPU+GPU
<b>640 × 480</b>	11.122 s	0.463 s
<b>800 × 600</b>	18.814 s	0.680 s
<b>1024 × 768</b>	33.382 s	1.127 s
<b>1920 × 1080</b>	105.50 s	3.227 s

Table 1. Time cost of CPU only versus CPU+GPU algorithms

In the above chart, it can clearly be seen that there is an improvement in the processing speed when using GPU technology; in the case of the large image, the speed increased as much as 3,000%. This is because we have taken advantage of parallel computing and the floating-point arithmetic of GPU. The most time-consuming part of the original algorithm is bilateral filtering, which becomes a virtual real-time process when running in GPU. Furthermore, other simple operations have also been accelerated in GPU to various degrees. Accelerations of these parts significantly reduced the overall process time of the whole algorithm.

## 6. Conclusion

With increasing use of image dehazing methods, defogging results are improving significantly. However, the efficiency of the algorithms used in these methods is still very low. GPU technology has developed rapidly in recent years, to the point where general-purpose computing for GPU can be exploited to speed up the

image dehazing process. Following parallelization and optimization, we implemented our proposed optimized single image parallel processing dehazing algorithm on a Windows Phone device. Comparisons and analyses show that the efficiency of the algorithm is significantly improved and the defog effect excellent. The algorithm, implemented in GPU, is written as a Windows Phone application and will be published in the Windows Phone app store. In summary, in terms of effectiveness and efficiency, this design has achieved the expected goals.

## Acknowledgement

This work is supported by National Natural Science Foundation of China (11178017, 61373090, 61303104, 61203238 ), Beijing Natural Science Foundation (4132014) , The Project of Construction of Innovative Teams and Teacher Career Development for Universities and Colleges Under Beijing Municipality, and Beijing Center for Mathematics and Information Interdisciplinary Sciences.

## References

1. J. Tarel and N. Hautière, Fast Visibility Restoration from a Single Color or Gray Level Image. ICCV, 2009, pp: 2201–2208
2. R. Tan, Visibility in bad weather from a single image. CVPR, 2008, pp: 1–8.
3. K. He, J. Sun, and X. Tang, Single image haze removal using dark channel prior. CVPR, 2009, pp: 1956–1963.
4. J. Tarel and N. Hautière, Fast Visibility Restoration from a Single Color or Gray Level Image. ICCV, 2009, pp: 2201–2208.
5. Yue Meng and Yuanyuan Shang, Design of Real-time Haze Image Restoration System Based on FPGA Technology. Information Technology Journal, 2013, pp: 7481–7488.
6. J. Tarel and N. Hautière, Fast Visibility Restoration from a Single Color or Gray Level Image. ICCV, 2009, pp: 2201–2208.
7. P. Shirley, J. Ferwerda, E. Reinhard, and M. Stark. Photographic tone reproduction for digital images. In ACM SIGGRAPH' 02, 2002, pp:267–276.
8. J. Tarel and N. Hautière, Fast Visibility Restoration from a Single Color or Gray Level Image. ICCV, 2009, pp: 2201–2208.
9. HLSL and Pixel Shader for XAML Developers, Walt Ritscher. O'reilly Media, 1st edition July 2012

# Investigation of Feature Quantity in Sound Signal and Feeling Impression Using PCA

**Yusuke Kawakami\***, Tetsuo Hattori

*Graduate School of Engineering, Kagawa University, 2217-20, Hayashi-Cho  
Takamatsu, Kagawa 761-0396, Japan*

**Hikomichi Kawano**

*NTT Advanced Technology Corporation, 19-18, Nakamachi  
Musashino, Tokyo 180-0006, Japan*

**Tetsuya Izumi**

*Micro-Technica Co., Ltd., 3-12-2, Higashi-Ikebukuro  
Toshima, Tokyo 170-0013, Japan*

*E-mail: s11d621@stmail.eng.kagawa-u.ac.jp, hattori@eng.kagawa-u.ac.jp,  
hiromichi.kawano@ntt-at.co.jp, t-izumi@microtechnica.co.jp  
www.kagawa-u.ac.jp*

## Abstract

This paper investigates the relationship between feature quantity of sound signal and feeling impression using PCA. As the feature quantity, we use Fluctuation value and sum of squared errors (Residual) which is calculated by regression analysis of sound signal, in the same way as our previous paper. In order to investigate the feeling impression and effect from sound signal, we have used a questionnaire survey method. As a result, we have found that the feeling response of examinees can be classified into three groups by a clustering analysis. And also we have obtained the results of PCA for the feeling effects depending on each group of examinees and four kinds of frequency zone of sound signal. we also discuss the analysis results on the Kansei (or feeling) effect.

*Keywords:* Signal processing, Fluctuation, Intercept, Sum of squared errors, Feeling impression, PCA

## 1. Introduction

Recently,  $1/f$  fluctuation in various fields of signal has been actively researched, and it brings about an effect of such healing as a human being psychologically feels at ease, if there is a  $1/f$  relation between the power spectrum of the signal and the frequency  $f$ <sup>1-7</sup>. However, we focused that the power spectrum have same fluctuation but the distribution are different. And we doubted the strong influence of the emotional impression factors other than fluctuation value.<sup>8</sup> Therefore, in the previous research, we have defined three kinds of parameters such as fluctuation value (or Fluctuation), intercept (or Intercept), and sum of squared errors (or Residual) as feature quantity in sound

signal obtained from the calculation of the signals' fluctuation degree. And we have investigated the relation between feeling impression and those parameters, by using multiple regression analysis<sup>8</sup>. And we eliminate "Intercept" from the analysis, because this quantity (or parameter) is substantially equal to the volume of sound<sup>8</sup>.

Moreover we had considered possibility of the effect of feeling impression from frequency domains. So we divided into three frequency domains (Low Frequency (LF); 0~300Hz, Middle Frequency (MF); 300~1000Hz, High Frequency (HF); 1000~22050Hz) and analyzed each domain<sup>10, 11, 16</sup>.

As the results, we have understood that feeling impression have an impact on Residual more than

---

\* Graduate School of Engineering, Kagawa University, 2217-20, Hayashi-Cho, Takamatsu, Kagawa, 761-0396, Japan hattori@eng.kagawa-u.ac.jp  
© The 2015 International Conference on Artificial Life and Robotics (ICAROB 2015), Jan. 10-12, Oita, Japan



Fluctuation, especially high frequency. In the regression analysis, we can be seen the impact of the sound features for the evaluation value of individual sensibility adjective items (for example, bright, fast, etc.). Although, it is difficult to capture the main factors on the relation between feature quantity of sound which presented to examinees, and feeling impression of examinees.

In this paper we analyze the affect of the feeling impression, from the music's Fluctuation and Residual, by use of principle component analysis. At first, we investigate the feeling impression of the music by using questionnaire survey. Then, from result we separate the examinees into the groups using clustering analysis.

After that, we perform the PCA by the feeling impression or feature quantity of sound signal each frequency domains. Furthermore we analyze relationship between feeling impression, and Fluctuation or Residual through the correspondence relationship of principal component axis.

## 2. Investigation between 3 Parameters Accompanying on the Calculation Fluctuation value (3PACF) and Feeling Impression

### 2.1. Fluctuation and 3PACF

Among fluctuations, the well-known  $1/f$  fluctuation means that the power spectrum (PS) of a signal is proportional to the  $1/f$  of frequency. Moreover, it is pointed out that there is an effect that a human being feels pleasantness<sup>1-6</sup>. Fig. 1 (a) is shown the conceptual image of PS. Let  $Y(f)$  and  $\varepsilon(f)$  be the power of PS and its error, respectively. And we define the PS which is shown in Fig. 1(a) as Eq. (1).

$$Y(f) = \frac{k}{f^a} + \varepsilon(f) \quad (1)$$

Taking the logarithm of both sides,

$$\begin{aligned} \log Y(f) &= \log \left( \frac{k}{f^a} + \varepsilon(f) \right) = \log \left\{ \frac{k}{f^a} (1 + \tilde{\varepsilon}(f)) \right\} \\ &= \log \left( \frac{k}{f^a} \right) + \log(1 + \tilde{\varepsilon}(f)) \\ \log Y(f) &= -a \log f + \log k + \log(1 + \tilde{\varepsilon}(f)) \end{aligned} \quad (2)$$

$\hat{\varepsilon}(f)$  and  $y(f)$  define  $\hat{\varepsilon}(f) \equiv \log(1 + \tilde{\varepsilon}(f))$  and  $y(f) \equiv \log Y(f)$  respectively, we derive Eq. (3).

© The 2015 International Conference on Artificial Life and Robotics (ICAROB 2015), Jan. 10-12, Oita, Japan

$$\begin{aligned} y(f) &= -a \log f + \log k + \hat{\varepsilon}(f) \\ &\cong -a \log f + b + \hat{\varepsilon}(f) \end{aligned} \quad (3)$$

Fig. 1 (b) shows the regression line of Eq. 3. The vertical axis and the horizontal axis are logarithm of PS and logarithm of frequency  $f$ , respectively. In this paper, we define the absolute-degree of the regression line a "Fluctuation". Then, we define the intercept of the regression line ("Intercept") as  $b$ , and we also define the error from the line as  $e^{\delta}$ . Furthermore, we define the sum of squared errors ("Residual") as Eq. (4). In Eq. (4),  $y$  and  $Y$  mean the actual measurement value and the theoretical value, respectively<sup>8</sup>.

$$s = \sum_i e_i^2 = \sum_i (y_i - Y_i)^2 \quad (4)$$

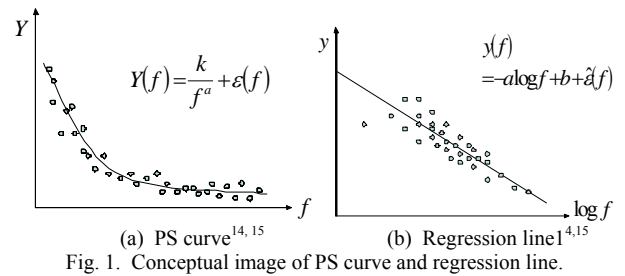


Fig. 1. Conceptual image of PS curve and regression line.

### 2.2. Evaluation of feeling impression

Next, we have used questionnaire survey in order to investigate the relation between 3PACF and feeling impression of music. The examinees are 34 students in the age of early twenties. The list of music used in this survey is shown in Table 1.

These sampling frequency and file format are 44.1 kHz and 16 bit wav, respectively. For every piece of the music, we have taken 20 seconds to play it. The examinees evaluated the 4 items as shown in Table 2, by scoring from one to four. Also they have judged the preference for each of music by scoring from one to ten.

### 2.3. Clustering analysis

Subsequently, we have conducted clustering analysis to divide into examinees groups who was similar feeling impression, by using the results of questionnaire survey. As preprocessing, we convert the evaluation (Item1 ~Item4) and Preference as follows;

- {Item1 ~ Item4} ≥ 3 → 1
- {Item1 ~ Item4} ≤ 2 → 0
- Preference ≥ 6 → 1



- Preference  $\leq 5 \rightarrow 0$

Therefore, the data of whole examinees are consist from 34 set of 50 dimensional ((Item1 ~ Item4, and Preference)  $\times$  10songs) data. That is, this clustering analysis is performed in the 50-dimensional space. And we adopt Ward method<sup>9</sup> as the analysis.

And then, we perform Wilk's Lambda test as the statistical test<sup>9</sup>. It is a test of the difference between the mean values of the vector comprising a plurality of variables. The null hypothesis  $H_0$  and alternative hypothesis  $H_1$  are as follows;

$H_0$ : Difference of all mean vectors are equal.

$H_1$ : Difference of all mean vectors are not equal.

Whenever each time of clustering has finished, we apply Wilk's Lambda Test repeatedly. In this test, we set significance to 1%. And then, if it will not come into effect significance of 1% on next-time test, the clustering is quit<sup>10, 15, 16</sup>.

Table 1. Music list of wave files.<sup>14</sup>

No	Title (.wav)	Genre
1	Another Sky	Easy Listening
2	Londonderry Air	Classic
3	Blieve you	Easy Listening
4	Drafting	Easy Listening
5	Down by the Riverside	Jazz
6	Space Odessey3 Revelation	Easy Listening
7	TOMORROW	Pops
8	Old French Song	Classic
9	Freedom	Pops
10	Red River Valley (brass)	Jazz

Table 2. Evaluation items of the questionnaire survey.

Item1	Slow	1 $\leftrightarrow$ 4	Quick
Item2	Heavy	1 $\leftrightarrow$ 4	Light
Item3	Natural	1 $\leftrightarrow$ 4	Artificial
Item4	Negative	1 $\leftrightarrow$ 4	Positive
Preference	Dislike	1 $\leftrightarrow$ 10	Like

Table 3. Fluctuation and Residual

No.	Title (*.wav)	AF		LF		MF		HF	
		Fl.	Re.	Fl.	Re.	Fl.	Re.	Fl.	Re.
1	Another Sky	1.715	0.414	0.454	0.487	1.713	0.674	1.777	0.394
2	Londonderry Air	1.627	0.399	1.023	0.489	1.873	0.906	1.706	0.369
3	Blieve you	2.111	0.466	0.457	0.503	0.527	0.844	2.472	0.409
4	Drafting	1.593	0.431	0.917	0.474	1.296	1.006	1.706	0.404
5	Down by the Riverside	1.724	0.448	0.553	0.502	0.470	0.679	2.115	0.406
6	Space Odessey3 Revelation	0.990	0.323	1.614	0.195	1.522	0.470	1.004	0.316
7	Tomorrow	2.268	0.555	0.129	0.619	0.721	0.545	2.903	0.463
8	Old French Song	1.398	0.433	1.509	0.275	1.633	1.255	1.515	0.399
9	Freedom	2.173	0.589	-0.259	0.535	-0.047	0.575	2.705	0.517
10	Red River Valley (brass)	1.520	0.526	0.499	0.653	0.723	0.733	1.658	0.507

Fl.: Fluctuation, Re.: Residual

## 2.4. Principal Component Analysis (PCA)

In this section, we describe the PCA<sup>12, 13</sup> performing space and the set of vectors. However, we decide to eliminate Intercept because it substantially equal to the volume of sound.

First, we define Physical Quantity Space (PQS) that is two-dimensional space which axis is the fluctuation value and Residual. The subject of PCA is a set of 10 pieces of music vectors (Table 3), and also we perform PCA in each frequency domain (AF, LF, MF, and HF). The other hand, we define Feeling Adjective Space (FAS) that is five-dimensional space which axis is the feeling impression of the examinees. The subject of PCA is a set of 10 pieces of music's Feeling Impression Vectors (FIVs).

### 2.4.1. Feeling Impression Vector (FIV)

This subsection, we describe the FIVs.

First, we define the evaluation  $S_{(i,k)}$  of examinee  $k$  as Eq. (5).  $i$  and  $e_1, \dots, e_5$  are the music number and the evaluation of Item1 ~ Preference, respectively.

$$S_{(i,k)} = (e_1, \dots, e_5) \quad (5)$$

Then, we convert the evaluation (Item1 ~ Item4) and Preference as same as Section 2.2. And we define the converting processed vector, as Eq. (6).  $a_1, \dots, a_5$  are zero or one in Eq. (6). That is;

$$\tilde{S}_{(i,k)} = (a_1, \dots, a_5) \quad (6)$$

Hence, the vector  $S_i^*$  of the sum of evaluation  $r$  people is FIV which is defined by Eq. (7).  $Z_1, \dots, Z_5$  are the sum of evaluation Item1 ~ Preference of  $r$  people, respectively.

$$S_i^* = (Z_1, \dots, Z_5) = \sum_{k=1}^r \tilde{S}_{(i,k)} \quad (7)$$

That is, we apply Eq. (5) ~ Eq. (7) to each group, which is divided by using clustering analysis, and we perform PCA of the each group. Subsequent sections, we define  $u_n$  ( $n=1, 2$ ) and  $v_m$  ( $m=1, \dots, 5$ ) in the principal component axis of set of vectors on PQS and FAS, respectively. Additionally, we define  $f_i$  and  $x_i$  in the vectors of music number  $i$  ( $i=1, \dots, 10$ ) on PQS and FAS, respectively. So we can express  $f_i$  and  $x_i$  on the coordinate axes  $u_n$  and  $v_m$  respectively as Eq. (8).

$$(\langle \mathbf{f}_i | \mathbf{u}_1 \rangle, \langle \mathbf{f}_i | \mathbf{u}_2 \rangle), (\langle \mathbf{x}_i | \mathbf{v}_1 \rangle, \dots, \langle \mathbf{x}_i | \mathbf{v}_5 \rangle) \quad (8)$$

### 2.5. Correlation of the principal component axis

Subsequently, we investigate the correspondence of principal component axes of PQS and principal component axes of FAS. Let  $C_u$  and  $C_v$  be the coefficient matrix which is calculated by PCA of PQS and the coefficient matrix which is calculated by PCA of FAS, respectively. And we can describe the basis vectors  $\mathbf{u}_n$  and  $\mathbf{v}_m$  by using  $\mathbf{p}_n$  (the basis vectors on PQS) and  $\mathbf{i}_m$  (the basis vectors on FAS), as shown in Eq. (9) and (10).

$$\mathbf{u}_n \equiv C_u \mathbf{p}_n = \begin{bmatrix} C_{u11} & C_{u12} \\ C_{u21} & C_{u22} \end{bmatrix} \begin{bmatrix} \delta_{n1} \\ \delta_{n2} \end{bmatrix}, \delta_{nk} = \begin{cases} (n=k)1 \\ (n \neq k)0 \end{cases} \quad (9)$$

$$\mathbf{v}_m \equiv C_v \mathbf{i}_m = \begin{bmatrix} C_{v11} & \dots & C_{v15} \\ \vdots & \ddots & \vdots \\ C_{v51} & \dots & C_{v55} \end{bmatrix} \begin{bmatrix} \delta_{m1} \\ \vdots \\ \delta_{m5} \end{bmatrix}, \delta_{mk} = \begin{cases} (m=k)1 \\ (m \neq k)0 \end{cases} \quad (10)$$

From Eq. (8) ~ (10), correspondence between  $\mathbf{u}_n$  and  $\mathbf{v}_m$  can be judged by the correlation coefficient  $R$  between  $\langle \mathbf{f}_i | \mathbf{u}_n \rangle$  and  $\langle \mathbf{x}_i | \mathbf{v}_m \rangle$ .  $R$  is defined by Eq. (11).

$$R = \frac{\sum \langle \mathbf{f}_i | \mathbf{u}_n \rangle \langle \mathbf{x}_i | \mathbf{v}_m \rangle}{\sqrt{\sum \langle \mathbf{f}_i | \mathbf{u}_n \rangle^2} \sqrt{\sum \langle \mathbf{x}_i | \mathbf{v}_m \rangle^2}} \quad (11)$$

## 3. Results of Feeling Impression and Discussion

### 3.1. Clustering analysis

Fig. 2 shows the result of clustering analysis and its statistical test. As shown in Fig. 2, 34-person examinees are divided 3 groups. The names of groups (G1, G2, and G3) are given in descending order of head-count. Examinees belonging to A, B, and C are 19 person (55.9% of total), 8 person (23.5% of total), and 7 person (20.6% of total), respectively. Table 4 also shows the results of the aggregate of evaluation items that is preprocessed describing in Section 2.3.

### 3.2. PCA

Fig. 3 shows the results of PCA on PQS (Physical Quantity Space). The plotted marks in Fig. 3 indicate endpoints of the vectors from origin. From Fig. 3, we

consider that the music that is used in the investigation of this paper, the weight of Fluctuation and the Residual are same degree. Because the components of the Fluctuation and Residual are contained in  $\mathbf{u}_1$  and  $\mathbf{u}_2$  approximately equal proportions. The other hand, Fig. 4 shows the results of PCA on FAS (Feeling Adjective Space). In the space, we do not consider principal component  $\mathbf{v}_3$ , because the cumulative contribution ratio of principal component  $\mathbf{v}_1$  and  $\mathbf{v}_2$  are about 94.7% in minimum of each groups.

From Fig. 4, in group G1,  $\mathbf{v}_2$  is Preference, and the

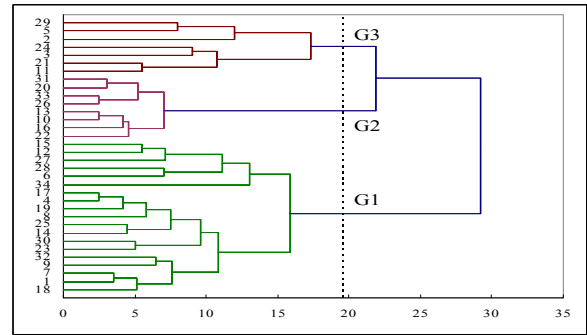


Fig. 2. Dendrogram of clustering result by using questionnaire results of examinees.

Table 4. Results of feeling impression questionnaire

(a) Group G1						
Music#	*.wav	Item1 (Quick)	Item2 (L.Light)	Item3 (Artificial)	Item4 (Positive)	Preference
1	Another Sky	3	14	17	15	7
2	Londonderry Air	1	6	3	8	9
3	Blieve you	3	5	2	18	10
4	Drafting	0	3	3	0	7
5	Down by the Riverside	18	18	15	19	5
6	Space Odessey3 Revelation	1	11	6	1	5
7	Tomorrow	12	12	18	19	13
8	Old French Song	1	7	7	1	3
9	Freedom	19	15	15	18	8
10	Red River Valley (brass)	9	17	15	18	6

(b) Group G2						
Music#	*.wav	Item1 (Quick)	Item2 (L.Light)	Item3 (Artificial)	Item4 (Positive)	Preference
1	Another Sky	1	4	5	8	8
2	Londonderry Air	0	0	0	4	7
3	Blieve you	0	2	0	8	8
4	Drafting	0	0	2	0	7
5	Down by the Riverside	6	7	6	8	7
6	Space Odessey3 Revelation	0	2	1	0	8
7	Tomorrow	7	6	8	8	8
8	Old French Song	0	0	2	0	8
9	Freedom	8	7	5	8	7
10	Red River Valley (brass)	4	8	7	8	8

(c) Group G3						
Music#	*.wav	Item1 (Quick)	Item2 (L.Light)	Item3 (Artificial)	Item4 (Positive)	Preference
1	Another Sky	0	5	4	7	7
2	Londonderry Air	0	1	4	3	6
3	Blieve you	0	3	4	4	5
4	Drafting	2	2	4	2	6
5	Down by the Riverside	1	4	5	6	6
6	Space Odessey3 Revelation	1	4	4	2	4
7	Tomorrow	2	1	4	4	7
8	Old French Song	5	4	5	3	4
9	Freedom	4	3	5	5	3
10	Red River Valley (brass)	5	5	6	6	5

correspondence between  $v_1$  and Item2 (Light) or Item3 (Artificial) are also strong. In group G2 and G3, the correspondence between  $v_1$  and Item4,  $v_2$  and Item1 are strong respectively.

That is, 56% of examinees (G1) prefer brightly and artificial music in which have used this paper. However tendency of music to suit the taste of the remaining of examinees (G2 and G3) are not clear, because there are individual differences. From Fig. 4(a), we consider that examinees of group G1 prefer “Believe\_you”.

### 3.3. Correlation of the principal component axis

We have calculated the correlation coefficient between principal component axes of PQS ( $u_n$ ) and FAS ( $v_m$ ) based on the results of PCA on each space, in each frequency domains (AF, LF, MF, and HF).

Table 5 shows the results of correlation coefficient in each group (G1, G2, and G3). The colored portion of Table 5 indicates that the absolute value of the correlation coefficient is 0.700 or higher.

#### 3.3.1. Group G1

From Table 5 (a), the correlation coefficient on AF and HF between  $u_1$  and  $v_1$  are 0.926 and 0.931 respectively, so they have strong positive correlation.

We refer Fig. 3(a) and (d), increase in Fluctuation and Residual are tendency in response to increase of  $u_1$ . Also from Fig. 4(a), increase in Item2 (Light) and Item3 (Artificial) are tendency in response to increase of  $v_1$ .

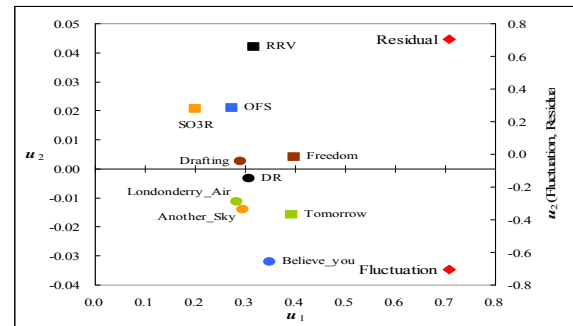
Similarly, the correlation coefficient on LF and MF between  $u_1$  and  $v_1$  are 0.774 and 0.704 respectively, so they have positive correlation.

We refer Fig. 3(a) ~ (c), Fluctuation and Residual on LF of all music are lower than AF. And the music which Fluctuation and Residual are small on AF, there are tendency they increase on MF.

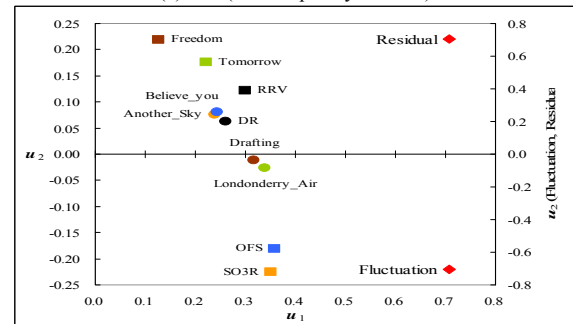
Therefore, we consider the music become brightly and artificial impression by increasing Fluctuation and Residual, on AF, MF, and HF.

#### 3.3.2. Group G2

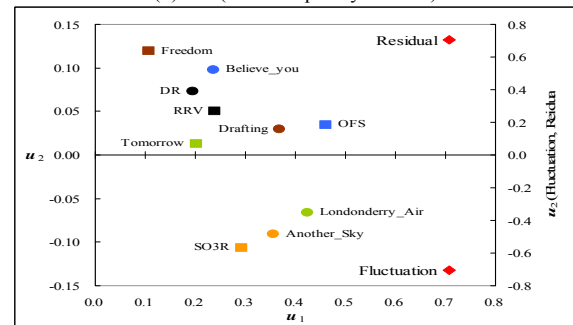
From Table 5 (b), we understand that G2 have tendency same as G1. And, the correlation coefficient of each domain between  $u_1$  and  $v_1$  are higher than 0.761, so they have positive correlation. Besides, we refer Fig. 4(b),



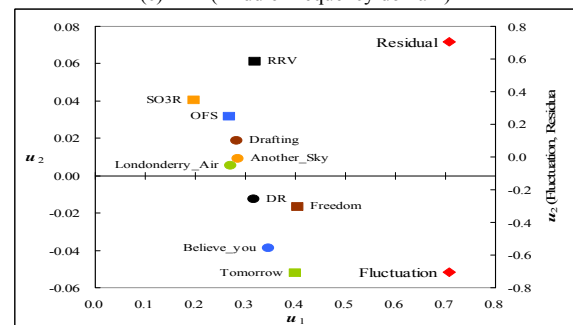
(a) AF (All Frequency domain)



(b) LF (Low Frequency domain)

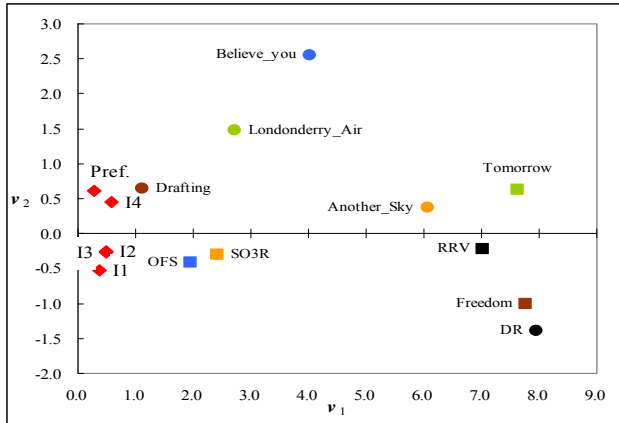


(c) MF (Middle Frequency domain)

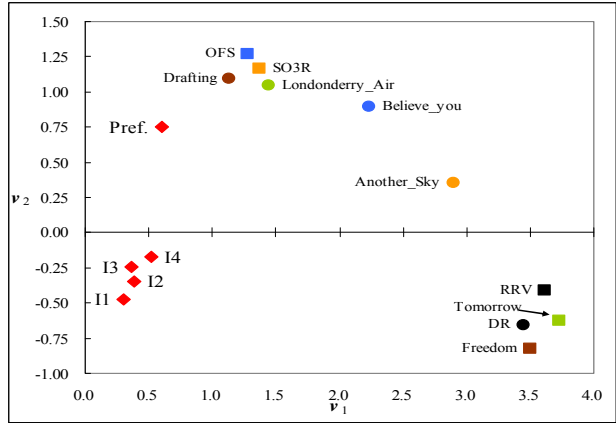


(d) HF (High Frequency domain)

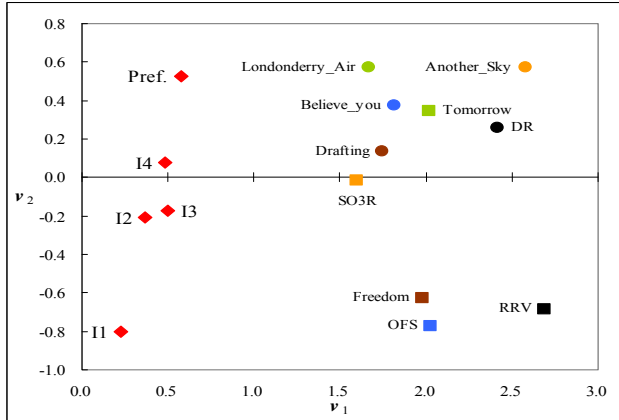
Fig. 3. PCA results on Physical Quantity Space. DR: Down\_by\_the\_Riverside, SO3R: Space\_Odessey3\_Reveration, OFS: Old\_French\_Song, RRV: Red\_River\_Valley (brass)



(a) Group G1



(b) Group G2



(c) Group G3

Fig. 4. PCA results on Feeling Adjective Space.

DR: Down\_by\_the\_Riverside, SO3R: Space\_Odessey3\_Reveration, OFS: Old\_French\_Song, RRV: Red\_River\_Valley (brass), I1: Item1 (Quick), I2: Item2 (Light), I3: Item3 (Artificial), I4: Item4 (Positive), Pref.: Preference (Like)

Table 5. Correlation coefficient between principal axes.

(a) Group G1								
Principal axis	AF		LF		MF		HF	
	$u_1$	$u_2$	$u_1$	$u_2$	$u_1$	$u_2$	$u_1$	$u_2$
$v_1$	0.926	0.028	0.774	0.547	0.704	0.351	0.931	-0.059
$v_2$	0.216	-0.579	0.230	0.068	0.288	-0.080	0.203	-0.294

(b) Group G2								
Principal axis	AF		LF		MF		HF	
	$u_1$	$u_2$	$u_1$	$u_2$	$u_1$	$u_2$	$u_1$	$u_2$
$v_1$	0.956	0.049	0.827	0.506	0.761	0.341	0.960	-0.015
$v_2$	0.251	0.000	0.528	-0.660	0.611	-0.351	0.233	0.371

(c) Group G3								
Principal axis	AF		LF		MF		HF	
	$u_1$	$u_2$	$u_1$	$u_2$	$u_1$	$u_2$	$u_1$	$u_2$
$v_1$	0.976	0.115	0.945	0.280	0.911	0.226	0.975	0.166
$v_2$	0.024	-0.784	0.031	0.083	0.075	-0.425	0.016	-0.482

increase in Item4 (Positive) is tendency in response to increase of  $v_1$ .

Therefore, we consider the music become positive impression by increasing Fluctuation and Residual.

### 3.3.3. Group G3

From Table 5 (c), we understand that the correlation coefficient of each domain of G3 between  $u_1$  and  $v_1$  are higher than 0.911, so they have strong positive correlation. Especially the correlation coefficient of AF between  $u_2$  and  $v_2$  is -0.784, so they have negative correlation. We refer Fig. 4(c), increase in Item4 (Positive) is tendency in response to increase of  $v_1$ . And from Fig 3 (a) ~ (d), increase in Fluctuation and Residual are tendency in response to increase of  $u_1$ . Furthermore, decreasing Fluctuation and increasing Residual are tendency in response to decrease of  $v_2$ . Therefore, we consider the music become positive impression by increasing Fluctuation and Residual. Especially, by increasing Fluctuation and Residual on AF, the music becomes fast impression.

## 4. Conclusion

In this paper, we have investigated the effects between feature quantity of sound signal and feeling impression using PCA. As feature quantity, we have used Fluctuation and Residual. As for the feeling impression questionnaire, we have presented 10 piece of music to examinees and they evaluated 5 items, i.e. quickness, brightness, artificial, positiveness, and preference (like or dislike). Then, we performed clustering analysis based on the evaluation results, the examinees feeling impression could be divided into 3 groups.

Next, we have performed PCA in the Physical Quantity Spaces of the each frequency domain (AF, LF, MF, and HF) and performed PCA in the Feeling Adjective Spaces of each group. Furthermore, we also investigated correlation between the principal component axes.

As the results, we have understood that 56% of examinees feel brightly and artificial impression from the music which both of Fluctuation and Residual were high. And we have also found that they preferred such music. Then, 44% examinees were not seen such correlativity, but they felt positive impression from the music which both of Fluctuation and Residual were high. Moreover, we have found that high frequency feature quantity of sound have the strongest impact to feeling impression.

## References

1. T. Musha, *Reason why person feels pleasantness and unpleasantness --sound, image, and sense of touch-- that approaches to the mystery of "pleasantness"* (Kawade Shobo Shinsya (KAWADE dream new book), 1999) (in Japanese).
2. T. Musha, *The world of fluctuation -Mystery of 1/f fluctuations of the world-* (Kodansha Bluebacks. Kodansha, 1980) (in Japanese).
3. H. Akaike and T. Wada, *Fluctuation and rhythm of living body* (Kodansha Scientific, 1997) (in Japanese).
4. S. Horiuchi, *Mystery of fluctuation* (Shinano Mainichi Newspapers Co. 1997) (in Japanese).
5. E. Teramoto, R. Hirota, T. Musha, and M. Yamaguchi, *Infinity, chaos, and fluctuation* (Bifukan, 1985) (in Japanese).
6. T. Musha, *Conception of fluctuation that approaches to the mystery of 1/f fluctuation* (NHK Books, 1998) (in Japanese).
7. T. Musha, *Science of fluctuation*, Vol.1~10 (Morikita Publication, 1991-1999) (in Japanese).
8. Y. Kawakami, T. Hattori, T. Yamamatsu, T. Izumi, and H. Kawano, Experimental Investigation of the Relation between Feeling Impression and Quantities Accompanying Fluctuation Calculation in Sound Signal, *Transactions of Japan Society of Kansei Engineering* **10**(3), ISSN: 1884-5258 (2011) 365-374 (in Japanese).
9. B. S. Everitt, *The Cambridge Dictionary of Statistics*, 2nd edn. (Cambridge University Press, 2002).
10. Y. Kawakami, T. Hattori, H. Kawano, T. Izumi, Statistical Investigation on Correlation between Feeling Impression and Feature Quantity of Sound Signal, in *Proc. First International Symposium on Affective Engineering 2013*, ISSN: 2187-669X (Kita-Kyushu, Fukuoka, 2013), pp.297-302.
11. T. Kado, *Basic knowledge of descriptive audio* (Ohmsha, 2001) (in Japanese).
12. S. Muto, *Statistical Analysis Handbook* (Asakura Shoten, 1995) (in Japanese).
13. H. Yanai, *Multivariate data analysis - Theory and Applications* (Asakura Shoten, 1994) (in Japanese).
14. Y. Kawakami, T. Hattori, T. Yamamatsu, T. Izumi, and H. Kawano, Investigation of Feeling Effect by Feature Quantity Including Fluctuation in Sound Signal, in *Proc. The Institute of Electrical Engineers of Japan C (CD)* (Kitami, Hokkaido, 2013), pp. 1490-1495 (in Japanese).
15. Y. Kawakami, T. Hattori, H. Kawano, and T. Izumi, Statistical Investigation on Relation between Feeling Impression and Feature Parameters of Sound Signal, *International Journal of Affective Engineering* **13**(1), ISSN: 2187-5413 (2014) 71-80.
16. Y. Kawakami, *Research on Correlation between Feature Quantity of Sound Signal and Kansei Impression*, Doctoral dissertation, Kagawa University, Graduate School of Engineering (2014) (in printing, in Japanese).

© The 2015 International Conference on Artificial Life and Robotics (ICAROB 2015), Jan. 10-12, Oita, Japan

# Automated Color Image Arrangement Method Using Curvature Computation in Histogram Matching

**Yusuke Kawakami\***, Tetsuo Hattori, Yoshiro Imai, Haruna Matsushita  
*Graduate School of Engineering, Kagawa University, 2217-20, Hayashi-cho  
Takamatsu, Kagawa 761-0396, Japan*

**Hikomichi Kawano**  
*NTT Advanced Technology Corporation, 19-18, Nakamachi  
Musashino, Tokyo 180-0006, Japan*

**R. P. C. Janaka Rajapakse**  
*Tainan National City of the Arts, 66, Daci  
Guantian, Tainan 72045, Taiwan*  
*E-mail: s11d621@stmail.eng.kagawa-u.ac.jp, {hattori, imai, haruna}@eng.kagawa-u.ac.jp  
hiromichi.kawano@ntt-at.co.jp, janakaraja@gmail.com  
www.kagawa-u.ac.jp*

## Abstract

This paper proposes improvement color image arrangement method by using curvature computation. The previous paper, we have presented the principle of our method using Histogram Matching based on Gaussian Distribution (HMGD), and how to detect input color image peakedness in its histogram. In this paper, we describe about Variance Estimated HMGD (VE-HMGD) as improvement HMGD. We also show how to estimate the histogram variance of original image based on the curvature computation. Moreover we compare processing results between VE-HMGD and HMGD through some experimentation. As the result, we show that VE-HMGD is natural color than HMGD.

*Keywords:* Automated color arrangement, histogram matching, HMGD, curvature variance estimation

## 1. Introduction

Automated image processing for enhancement and/or arrangement of color images has been more familiar to us according to the spreading of Digital Camera, Smart Phone, DVD, etc.<sup>1-3</sup>. However, we consider that the research on the automated arrangement method that brings about good sensibility effect (or Kansei effect) is still on the way to practical use.

In the previous papers, we have proposed a novel color image automated arrangement method using an elastic transform (ET)<sup>4,5</sup>. And we have proposed a principle of Histogram Matching based on Gaussian Distribution (HMGD) on brightness axis as one of the ET method based on histogram and/or histogram matching. Then we also described how to detect input color image peakedness in its histogram by using curvature computation for automated HMGD processing.

---

\* Graduate School of Engineering, Kagawa University, 2217-20, Hayashi-Cho, Takamatsu, Kagawa, 761-0396, Japan hattori@eng.kagawa-u.ac.jp  
© The 2015 International Conference on Artificial Life and Robotics (ICAROB 2015), Jan. 10-12, Oita, Japan

Furthermore, through experiments, we found that HMGD processing is improved the image of Kansei impression if applied to single-peakedness image. In this paper, first, we explain the principle of HMGD. Second, we explain the method of histogram variance estimation to optimize the shape of the HMGD-reference histogram by using curvature computation. And then, we illustrate the results of improved HMGD (Variance Estimated HMGD; VE-HMGD) processing which is working better than previous HMGD processing, through some experiments.

## 2. Principle of HMGD

In this chapter, we describe the principle of HMGD based elastic transform. Let  $f(x)$  and  $g(y)$  be two probabilistic density functions on real variables  $x$  and  $y$ , respectively. The probabilistic density function (PDF) is corresponding to histogram of image brightness level which is discretely defined. In addition, let  $y=\phi(x)$  be a continuous and monotonous increase function between variables  $x$  and  $y$  as shown in Fig.1<sup>7-9</sup>.

In addition let value of  $x$  be the range from 0 to  $L$ , therefore, variable  $y$  is ranges from 0 to  $\phi(L)$ . And let  $P$  mean the probability. From above definition and Fig. 1, we can derive (1) ~ (3).

$$P(0 \leq x \leq L) = \int_{x=0}^{x=L} f(x)dx = 1 \quad (1)$$

$$P(0 \leq y \leq \phi(L)) = \int_{y=0}^{y=\phi(L)} g(y)dy = 1 \quad (2)$$

$$\begin{aligned} f(x)dx &= P(x_0 \leq x \leq x_0 + dx) \\ &= P(\phi(x_0) \leq y \leq \phi(x_0 + dx)) \\ &= P(y_0 \leq y \leq y_0 + dy) = g(y)dy \end{aligned} \quad (3)$$

From (3), we obtain (4) and (5) because  $y_0 = \phi(x_0)$  and  $y_0 + dy = \phi(x_0 + dx)$ .

$$f(x)dx = g(y)dy = g(y)\phi'(x)dx \quad (4)$$

$$f(x) = g(y)\phi'(x) \quad (5)$$

Thus, if we know  $y=\phi(x)$  and  $g(y)$ , then we have  $f(x)$ . Using the above equations, we derive the principle of HMGD.

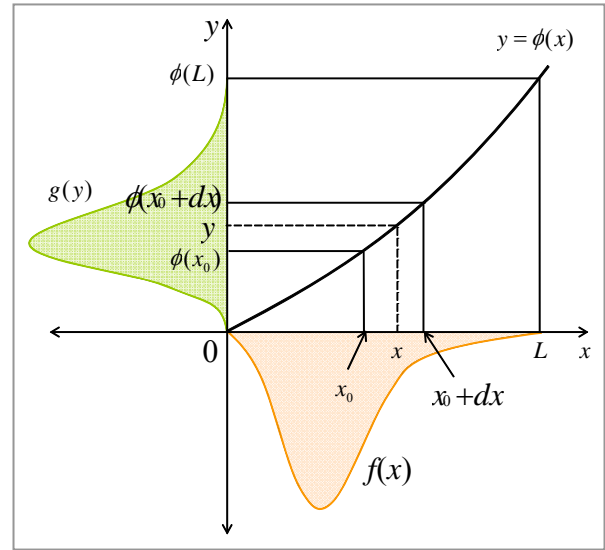


Fig.1. Continuous and monotonous increase function  $y=\phi(x)$  and probabilistic density functions  $f(x)$  and  $g(y)$ <sup>7-9</sup>.

HMGD processing converts the original image histogram into the Gaussian image histogram as shown in Fig. 2. First, because we aim to match Gaussian distribution image histogram, we have to expand brightness level of original image, due to convert into uniform distribution histogram. Let  $\phi(x)$  be defined by (6).

$$y = \phi(x) = L \int_0^x f(x)dx \quad (6)$$

Since  $\phi'(x) = Lf(x)$ , according to (5) and Fig. 2., we derive (7).

$$f(x) = h(y)\phi'(x) = h(y)Lf(x) \quad (7)$$

Therefore, we can derive (8)

$$h(y)L = 1, \quad h(y) = 1/L \quad (8)$$

From (8), we understand that original image histogram  $f(x)$  becomes uniform distribution histogram  $h(y)$  and expands brightness level.

Similarly, let  $Gauss(z)$  and  $\gamma(z)$  be defined by (9) and (10), respectively.

$$Gauss(z) = \frac{1}{\sqrt{2\pi\sigma^2}} \exp\left(-\frac{(z-\mu)^2}{2\sigma^2}\right) \quad (9)$$

$$\gamma(z) = L \int_0^z \text{Gauss}(z) dz = \frac{L}{\sigma\sqrt{2\pi}} \int_0^z \exp\left(-\frac{(z-\mu)^2}{2\sigma^2}\right) dz \quad (10)$$

Then, we obtain (11) because  $\phi(x) = \gamma(z)$  from Fig. 2.

$$L \int_0^x f(x) dx = \frac{L}{\sigma\sqrt{2\pi}} \int_0^z \exp\left(-\frac{(z-\mu)^2}{2\sigma^2}\right) dz \quad (11)$$

And, we can derive (12) from (6) and (10) by differentiating both sides of (11).

$$\begin{aligned} \frac{d}{dx} L \int_0^x f(x) dx &= \frac{d}{dz} \frac{L}{\sigma\sqrt{2\pi}} \int_0^z \exp\left(-\frac{(z-\mu)^2}{2\sigma^2}\right) dz \\ L\phi'(x) &= L\gamma'(z) \quad f(x) = \text{Gauss}(z) \end{aligned} \quad (12)$$

Therefore, we understand that if we take the transform function as (6) and (10),  $f(x)$  becomes Gaussian distribution. It corresponds to the HMGD processing, which means that function defined by cumulative histogram transforms the original histogram into the Gaussian histogram.

### 3. Variance Estimated HMGD (VE-HMGD)

#### 3.1. Approximate of Curvature Computation

In this section, we describe how to calculate the curvature approximation using for variance estimation. Let  $y$  be a function with respect to  $x$ , the definition of the curvature  $R$  is given by (13).

$$R = \frac{\left(\frac{d^2y}{dx^2}\right)}{\left\{1 + \left(\frac{dy}{dx}\right)^2\right\}^{\frac{3}{2}}} \quad (13)$$

$$g(x) = \frac{K}{\sigma\sqrt{2\pi}} \exp\left(-\frac{(x-a)^2}{2\sigma^2}\right) \quad (14)$$

In (14),  $K$  means a coefficient that satisfies (15).

$$\frac{K}{\sigma\sqrt{2\pi}} \int_0^L \exp\left(-\frac{(u-a)^2}{2\sigma^2}\right) du = 1 \quad (15)$$

Then, let  $y=f(x)$  be a function representing the cumulative histogram. So  $f(x)$  can be represented (16).

Since  $y = f(x) = \int_0^x g(u) du$ ,  $g(x)$  can be described as (17).

$$f(x) = \int_0^x g(u) du = \frac{K}{\sigma\sqrt{2\pi}} \int_0^x \exp\left(-\frac{(u-a)^2}{2\sigma^2}\right) du \quad (16)$$

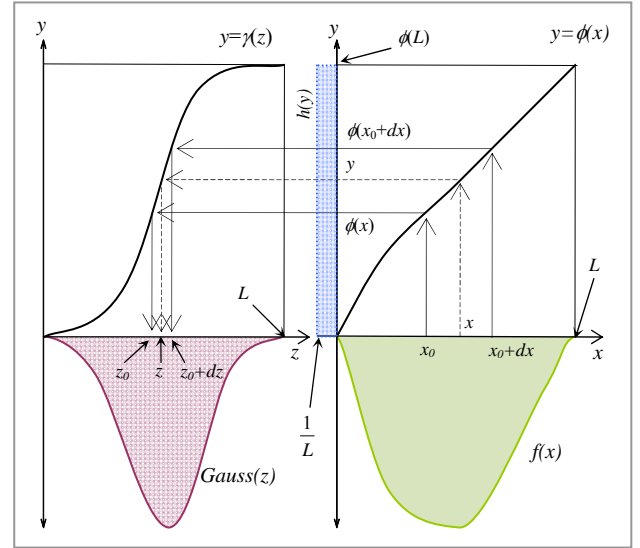


Fig. 2. Conceptual image of HMGD.

$$\frac{dy}{dx} = g(x) = \frac{K}{\sigma\sqrt{2\pi}} \exp\left(-\frac{(x-a)^2}{2\sigma^2}\right) \quad (17)$$

By the same way,

$$\begin{aligned} \frac{d^2y}{dx^2} &= \frac{dg(x)}{dx} = \frac{K}{\sigma\sqrt{2\pi}} \cdot e^{-\frac{(x-a)^2}{2\sigma^2}} \cdot \left(-\frac{1}{\sigma^2}\right) \{2(x-a)\} \\ &= \left(\frac{K}{\sigma\sqrt{2\pi}} \cdot e^{-\frac{(x-a)^2}{2\sigma^2}}\right) \cdot \left(-\frac{(x-a)}{\sigma^2}\right) = g(x) \cdot \left(\frac{(a-x)}{\sigma^2}\right) \end{aligned} \quad (18)$$

Hence, we obtain the following (19) and we can approximate to (13).

$$R = \frac{\frac{(a-x)}{\sigma^2} g(x)}{\left\{1 + g(x)^2\right\}^{\frac{3}{2}}} \cong \frac{(a-x)}{\sigma^2} g(x) \quad (19)$$

The curvature  $R$  varies the sign according to the value of  $x$ ;

- $x < a \rightarrow R > 0$
- $x = a \rightarrow R = 0$
- $x > a \rightarrow R < 0$ .

#### 3.2. Variance Estimation of image histogram

In this section, we describe how to estimate the histogram variance  $\sigma^2$  of the original image by using



curvature computation optimize the shape of the reference histogram, which is used in the VE-HMGD processing. Fig. 3 and Fig. 4 shows a conceptual image of the original histogram and cumulative histogram of variance  $\sigma^2$  and average  $a$ , respectively.

Let  $g(a)$  be a Gauss density function with variance  $\sigma^2$  at average  $a$ . From (14),

$$g(a) = \frac{K}{\sigma\sqrt{2\pi}} \exp\left(-\frac{(a-a)^2}{2\sigma^2}\right) = \frac{K}{\sigma\sqrt{2\pi}} \quad (20)$$

Thus, we can describe  $g(a \pm \sqrt{2}\sigma)$  as follows.

$$g(a \pm \sqrt{2}\sigma) = \frac{K}{\sigma\sqrt{2\pi}} \exp\left(-\frac{(a \pm \sqrt{2}\sigma - a)^2}{2\sigma^2}\right) = g(x)e^{\mp 1} \quad (21)$$

Let  $R(a \pm \sqrt{2}\sigma)$  be curvatures at  $a \pm \sqrt{2}\sigma$ . From (19), we describe these curvatures in (22).

$$R(a \pm \sqrt{2}\sigma) = \frac{(a - (a \pm \sqrt{2}\sigma))g(x)}{\sigma^2 \left\{1 + g(a \pm \sqrt{2}\sigma)^2\right\}^{\frac{3}{2}}} \quad (22)$$

From (21),

$$\begin{aligned} R(a \pm \sqrt{2}\sigma) &= \frac{\left(\mp \frac{\sqrt{2}}{\sigma}\right)g(a \pm \sqrt{2}\sigma)}{\left\{1 + g(a \pm \sqrt{2}\sigma)^2\right\}^{\frac{3}{2}}} \\ &= \left(\mp \frac{\sqrt{2}}{\sigma}\right) \frac{g(a)e^{-1}}{\left\{1 + (g(a)e^{-1})^2\right\}^{\frac{3}{2}}} \equiv \left(\mp \frac{\sqrt{2}}{\sigma}\right)H \quad (23) \end{aligned}$$

In (23),  $H$  is a constant that means following (24).

$$H = \frac{g(a)}{e} \left/ \left\{1 + \left(\frac{g(a)}{e}\right)^2\right\}^{\frac{3}{2}}\right. \quad (24)$$

Hence, we can obtain reference histogram variance  $\sigma^2$  by using (23). In the below equation  $v = \sqrt{2}\sigma$ , and  $v$  means distance from average  $a$ .

$$R(a-v) - R(a+v) = \frac{2\sqrt{2}}{\sigma}H = \left(\frac{4}{v}\right)H \quad \sigma^2 = \frac{v^2}{2} \quad (25)$$

### 3.3. Process of Variance Estimated HMGD

In the previous section, we have described the method to estimate the optimum variance in reference histogram

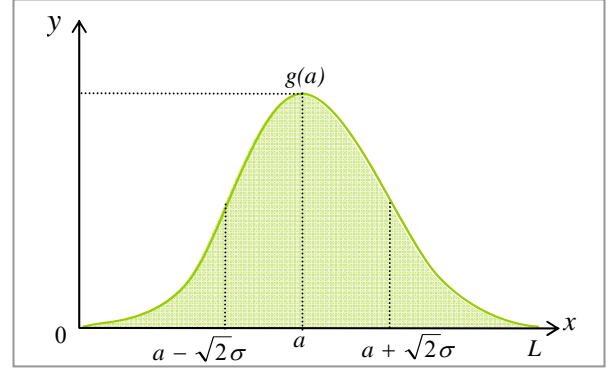


Fig. 3. Conceptual image of the original image histogram of variance  $\sigma^2$  and average  $a$ .

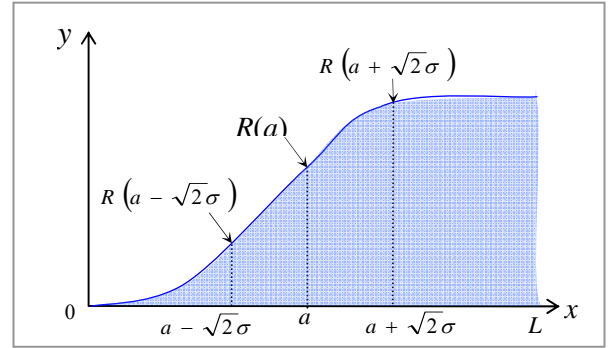


Fig. 4. Conceptual image of the original image cumulative histogram of variance  $\sigma^2$  and average  $a$ .

of HMGD from the histogram of the image, by using curvature computation. In this section, we describe the process of Variance Estimated HMGD (VE-HMGD).

- [Step 1] Proceed to Step 3 if input image has single peakedness histogram after performing curvature calculation. Otherwise go to Step 2.
- [Step 2] Abort VE-HMGD, and outputting inputted image in Step 1.
- [Step 3] Detect the peakedness brightness value of the histogram  $a$ . Proceed to Step 5 if the curvature  $R(a)$  is obtained. Otherwise go to Step 4.
- [Step 4] Set  $\sigma=50$  (default value), and perform HPA-HMGD<sup>7,8</sup>. Then proceed to Step 11.
- [Step 5] Calculate curvature  $R(a \pm \sqrt{2}\sigma)$  according to (23) and (24). Then, calculate following (26).

$$\left| R(a - \sqrt{2}\sigma) - R(a + \sqrt{2}\sigma) \right| - \left| \frac{2\sqrt{2}H}{\sigma} \right| \approx 0 \quad (26)$$

- [Step 6] Proceed to Step 7 if  $\sqrt{2}\sigma$  satisfies (26).  
 Otherwise modified  $\sqrt{2}\sigma$  and return to Step 6.  
 [Step 7] Calculate variance  $\sigma^2$  according to (25).  
 [Step 8] Calculate the reference histogram by using variance  $\sigma^2$  and average  $a$ . Then perform HMGD.  
 [Step 9] Output the processed image.

#### 4. Experimentation

Fig. 5 (a) shows example of results of HMGD and VE-HMGD processing which the original image have single peakedness histogram. The set of histogram and cumulative histogram (original image, HMGD image, and VE-HMGD image) are shown in Fig. 5 (b) and (c), respectively. In this case, VE-HMGD have a good feeling impression (or Kansei effect) than HMGD. And we found that shading of VE-HMGD is enhancing than HMGD.

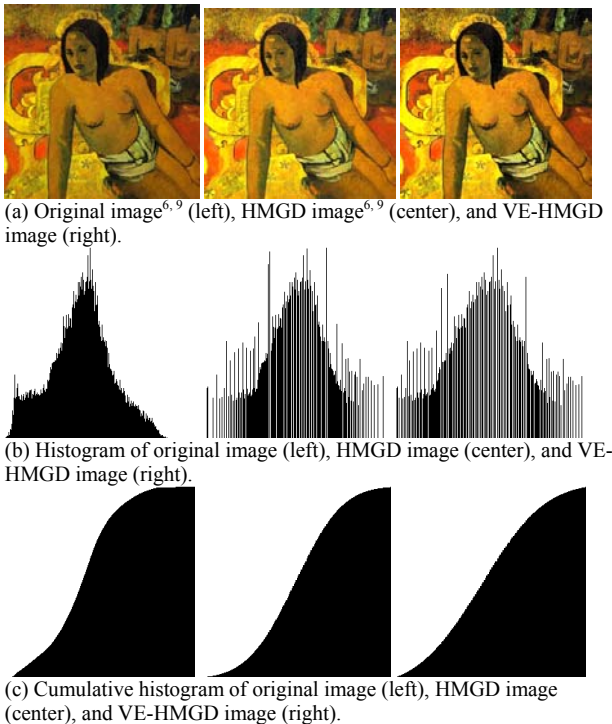


Fig. 5. Example of results by HMGD, VE-HMGD, and the corresponding histograms.

#### 5. Conclusion

Aiming at improvement Histogram Matching based on Gaussian Distribution (HMGD), we have described principal of HMGD, and we have proposed a method for estimate variance of original image histogram. As for concrete method, we have applied the curvature computation to estimation variance.

Furthermore, we suggested the VE-HMGD as improvement of HMGD and described its processing sequence. Through experimentation, we consider that VE-HMGD processing method will be useful and promising than previous HMGD. For further study, we have to verify the effect of VE-HMGD through questionnaire survey.

#### References

1. C. R. Gonzalez and E. R. Woods, *Digital Image Processing* (Addison-Wesley Publishing Company, 1993).
2. B. Jahne, *Digital Image Processing --Concepts, Algorithms, and Scientific Applications-- 4th edition* (Springer, 1995).
3. E. S. Umbaugh, *Computer Vision and Image Processing: A Practical Approach Using C/VItools* (Prentice Hall PTR, 1998).
4. W. Burger and J. M. Burge, *Principles of Digital Image Processing: Fundamental Techniques* (Springer 2009).
5. T. Izumi, T. Hattori, S. Sugimono, and T. Takashima, Color Image Arrangement Using Elastic Transform on Principal Component Axis (in Japanese), *Journal of Japan Society of Kansei Engineering* **8**(3) (2009) 667-674.
6. Y. Kawakami, T. Hattori, D. Kutsuna, H. Matsushita, Y. Imai, H. Kawano, and R. P. C. Janaka Rajapakse, An automated color image arrangement method based on histogram matching, in *Proceedings of 2013 International Conference on Biometrics and Kansei Engineering* (Japan, Tokyo, 2013), ISBN 978-0-7695-5019-0, pp. 31-34.
7. Y. Kawakami, T. Hattori, Y. Imai, H. Matsushita, H. Kawano, and R. P. C. Janaka Rajapakse, Automated Color Image Arrangement Method and Kansei Impression, in *Proceedings of International Conference on Artificial Life and Robotics 2014* (Japan, Oita, 2014), ISBN 978-4-9902880-8-2, pp. 260-263.
8. Y. Kawakami, T. Hattori, Y. Imai, H. Matsushita, H. Kawano, and R. P. C. Janaka Rajapakse, Kansei Impression and Automated Color Image Arrangement Method and Kansei Impression, *Journal of Robotics*,

*Networking and Artificial Life*, **1**(1) (2014), ISSN 2352-6386, 60-67.

9. Y. Kawakami, *Research on Correlation between Feature Quantity of Sound Signal and Kansei Impression*, Doctoral dissertation, Kagawa University, Graduate School of Engineering (2014) (in printing, in Japanese).

# Change Detection Experimentation for Time Series data by New Sequential Probability Ratio

**Yoshihide Koyama<sup>\*</sup>, Tetsuo Hattori,**  
*Graduate School of Engineering, Kagawa University,  
2217-20, Hayashi-cho Takamatsu, Kagawa 761-0396, Japan*

**Hikomichi Kawano**  
*NTT Advanced Technology Corporation, 19-18, Nakamachi  
Musashino, Tokyo 180-0006, Japan*

**Katsunori Takeda**  
*Canon IT Solutions Inc., Tosabori Dai Bldg. 2-2-4, Tosabori,  
Nishi-ku, Osaka-shi, Osaka 550-0001, Japan*

## Abstract

Previously, we have proposed a novel method using New Sequential Probability Ratio (NSPR) for the structural change detection problem of ongoing time series data instead of using SPRT (Sequential Probability Ratio Test). In this paper, for comparison, we present the experimental results by applying the both methods, i.e., NSPR and SPRT, to time series data that are generated by a multiple regression model in the case where one explanatory variation is a periodic function (sine function). And also we discuss the effectiveness of the both methods.

**Keywords:** Time series data, structural change detection, SPRT, New Sequential Probability Ratio (NSPR)

## 1. Introduction

Change point detection (CPD) problem in time series (see Refs.1-7) is to identify whether the generation structure of monitoring data has changed at some time point by some reason, or not. We consider that the problem is very important and that it can be applied to a wide range of application fields.

For the structural change detection problem of ongoing time series data, we have already proposed some kinds of methods (see Refs. 6, 8-12). In this paper, we present the results of comparison experiment by two methods that are Sequential Probability Ratio Test

(SPRT) and New Sequential Probability Ratio (NSPR) (Refs. 6, 11-12).

## 2. SPRT and Chow Test

### 2.1. SPRT

The Sequential Probability Ratio Test (SPRT) is used for testing a null hypothesis  $H_0$  (e.g. the quality is under pre-specified limit 1%) against hypothesis  $H_1$  (e.g. the quality is over pre-specified limit 1%). And it is defined as follows:

Let  $Z_1, Z_2, \dots, Z_i$  be respectively observed time series data at each stage of successive events, the probability ratio  $\lambda_i$  is computed as follows.

---

<sup>\*</sup>2217-20 Hayashi Cho Takamatsu City, Kagawa, 761-0396 Japan,  
Kagawa University, Email: hattori@eng.kagawa-u.ac.jp

© The 2015 International Conference on Artificial Life and Robotics (ICAROB 2015), Jan. 10-12, Oita, Japan

$$\lambda_i = \frac{P(Z_1 | H_1) \cdot P(Z_2 | H_1) \cdots P(Z_i | H_1)}{P(Z_1 | H_0) \cdot P(Z_2 | H_0) \cdots P(Z_i | H_0)} \quad (1)$$

where  $P(Z | H_0)$  denotes the distribution of  $Z$  if  $H_0$  is true, and similarly,  $P(Z | H_1)$  denotes the distribution of  $Z$  if  $H_1$  is true.

Two positive constants  $C_1$  and  $C_2$  ( $C_1 < C_2$ ) are chosen. If  $C_1 < \lambda_i < C_2$ , the experiment is continued by taking an additional observation. If  $C_2 < \lambda_i$ , the process is terminated with the rejection of  $H_0$  (acceptance of  $H_1$ ). If  $\lambda_i < C_1$ , then terminate this process with the acceptance of  $H_0$ .

$$C_1 = \frac{\beta}{1-\alpha}, \quad C_2 = \frac{1-\beta}{\alpha} \quad (2)$$

where  $\alpha$  means type I error (reject a true null hypothesis), and  $\beta$  means type II error (accept a null hypothesis as true one when it is actually false).

### 2.2 Procedure of SPRT

The concrete procedure of applying the SPRT method to the structural change detection problem is described.

[Step 1] Make a prediction expression and set the tolerance band ( $a$ ) (e.g.  $a=2\sigma_s$ ) that means permissible error margin between the predicted data and the observed one. ( $\sigma_s$  denotes a standard deviation in learning sample data at early stage.)

[Step 2] Set up the null hypothesis  $H_0$  and alternative hypothesis  $H_1$ .

$H_0$  : Change has not occurred yet.

$H_1$  : Change has occurred.

Set the values  $\alpha$ ,  $\beta$  and compute  $C_1$  and  $C_2$ , according to Eq. (2). Initialize  $i = 0$ ,  $\lambda_0 = 1$ .

[Step 3] Incrementing  $i$  ( $i = i+1$ ), observe the following data  $y_i$ . Evaluate the error  $|\varepsilon_i|$  between the data  $y_i$  and the predicted value from the aforementioned prediction expression.

[Step 4] Judge as to whether the data  $y_i$  goes in the tolerance band or not, i.e., the  $\varepsilon_i$  is less than (or equal to) the permissible error margin or not. If it is Yes, then set  $\lambda_i = 1$  and return to Step3. Otherwise, advance to Step5.

[Step 5] Calculate the probability ratio  $\lambda_i$ , using the below Eq.(3) that is equivalent to Eq.(1).

$$\lambda_i = \lambda_{i-1} \frac{P(\varepsilon_i | H_1)}{P(\varepsilon_i | H_0)} \quad (3)$$

where, if the data  $y_i$  goes “OUT” from the tolerance band,  $(P(\varepsilon_i | H_0), P(\varepsilon_i | H_1)) = (\theta_0, \theta_1)$ , otherwise (i.e., the data  $y_i$  goes “IN”),  $(P(\varepsilon_i | H_0), P(\varepsilon_i | H_1)) = ((1-\theta_0), (1-\theta_1))$ .

[Step 6] Execution of testing.

(i) If the ratio  $\lambda_i$  is greater than  $C_2$  ( $= (1-\beta)/\alpha$ ), dismiss the null hypothesis  $H_0$ , and adopt the alternative hypothesis  $H_1$ , and then End.

(ii) Otherwise, if the ratio  $\lambda_i$  is less than  $C_1$  ( $= \beta/(1-\alpha)$ ), adopt the null hypothesis  $H_0$ , and dismiss the alternative hypothesis  $H_1$ , and then set  $\lambda_i = 1$  and return to Step3.

(iii) Otherwise (in the case where  $C_1 \leq \lambda_i \leq C_2$ ), advance to Step7.

[Step 7] Observe the following data  $y_i$  incrementing  $i$ . Evaluate the error  $|\varepsilon_i|$  and judge whether the data  $y_i$  goes in the tolerance band, or not. Then, return to Step5 ( $\lambda_i$  calculation).

### 2.3 Chow Test

The well-known Chow Test checks if there are significant differences or not, among residuals for three Regression Lines, where regression Line 1 obtained from the data before a change point  $t_c$ , Line 2 from the data after  $t_c$ , and Line 3 from the whole data so far, by setting up the change point hypothesis at each point in the whole data (Fig.1).

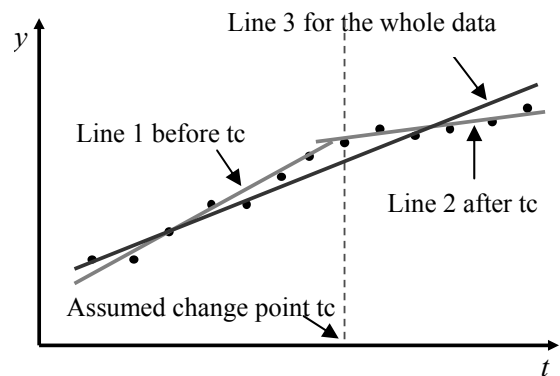


Fig.1. Conceptual image of Chow Test

### 3. New Sequential Probability Ratio (NSPR)

#### 3.1. Definition of NSPR<sup>11-12</sup>

Let  $C_n = a_1 a_2, \dots, a_i, \dots, a_n$   $a_i \in \{IN, OUT\}$  be a string (or symbol sequence) obtained from the observed data.

Let  $\theta_i$  and  $\tilde{\theta}_i$  be the conditional probability that receives the observed data  $a_i$  in the state  $S_0$  and  $S_1$ , respectively, where  $S_0$  and  $S_1$  mean the state of unchanged state and changed state, respectively.

That is, it means that  $\theta_i \in \{R, 1-R\}$  and  $\tilde{\theta}_i \in \{R_c, 1-R_c\}$ , respectively, where  $R = P(OUT | S_0)$ ,  $R_c = P(OUT | S_1)$ . And let  $P(C_n, H_0)$  and  $P(C_n, H_1)$  be the joint probability of the symbol sequence  $C_n$  that happen with the event  $H_0$  (the structural change is not occurred) and  $H_1$  (the change is occurred), respectively. Then, the following equations hold.

$$P(a_1 \dots a_n, H_0) = (1-\gamma)^n \theta_1 \dots \theta_n = (1-\gamma)^n \prod_{i=1}^n \theta_i \quad (4)$$

$$\begin{aligned} P(a_1 \dots a_n, H_1) &= \gamma \prod_{i=1}^n \tilde{\theta}_i + ((1-\gamma)\theta_1)(\gamma \prod_{i=2}^n \tilde{\theta}_i) \\ &\quad + ((1-\gamma)^2 \theta_1 \theta_2)(\gamma \prod_{i=3}^n \tilde{\theta}_i) + \dots \\ &= \sum_{k=1}^n ((1-\gamma)^{k-1} \cdot \prod_{j=0}^{k-1} \theta_j)(\gamma \prod_{i=k}^n \tilde{\theta}_i) \end{aligned} \quad (5)$$

$$P(H_0 | a_1 \dots a_n) \equiv P(H_0 | C_n) = \frac{P(C_n, H_0)}{P(C_n)} \quad (6)$$

$$P(H_1 | a_1 \dots a_n) \equiv P(H_1 | C_n) = \frac{P(C_n, H_1)}{P(C_n)} \quad (7)$$

Using these above equations (Eq.(4)-(7)), the New Sequential Probability Ratio (NSPR) that we propose can be represented as follows.

$$\begin{aligned} \text{NSPR} &\equiv \frac{P(H_1 | a_1 \dots a_n)}{P(H_0 | a_1 \dots a_n)} = \frac{P(H_1 | C_n)}{P(H_0 | C_n)} = \frac{P(C_n, H_1)}{P(C_n, H_0)} \\ &= \frac{\sum_{k=1}^n ((1-\gamma)^{k-1} \cdot \prod_{j=0}^{k-1} \theta_j)(\gamma \prod_{i=k}^n \tilde{\theta}_i)}{(1-\gamma)^n \prod_{i=1}^n \theta_i} \end{aligned} \quad (8)$$

#### 3.2. Recursive Form

When the NSPR is greater than 1.0, we can regard that the structural change has been occurred before the present time.

In the similar way as SPRT (see Eq.(3)), the definition of NSPR can also be described in a recursion formula. Let  $\Lambda_n$  be the value of NSPR defined by Eq.(8), we have the following recursive equation.

$$\Lambda_n = \frac{1}{1-\gamma} (\Lambda_{n-1} + \gamma) \left( \frac{\tilde{\theta}_n}{\theta_n} \right) \quad (9)$$

where  $\Lambda_0 = 0$ ,  $\theta_0 = 1$ ,  $\tilde{\theta}_0 = 1$ .

### 4. Experimentation for Comparison

We have done the comparison experimentation by SPRT and NSPR for a time series data that is generated based on the following equations.

$$\begin{cases} y = x_1 + 20x_2 + 5 + \varepsilon & (t \leq t_c) \\ y = x_1 + 10x_2 + 5 + \varepsilon & (t_c \leq t) \end{cases} \quad (10)$$

where  $\varepsilon \sim N(0, \sigma^2)$ , i.e., the error  $\varepsilon$  is subject to the Normal Distribution with the average 0 and the variation  $\sigma^2$ , and  $t_c$  means the change point. In addition, we have set  $t_c=70$  and  $\sigma=5$ . The number of the time points is 100 (i.e. .

Setting the two kinds (or cases) of coefficients in Eq.(10) as shown in Eq.(11) for Case 1 and Eq.(12) for Case 2, respectively. And we have generated 200 sets of time series data for the two kinds (or cases) of time series, respectively.

$$x_1 = t, x_2 = \sin\left(\frac{1}{8}\pi t\right) \quad (11)$$

$$x_1 = \text{random}, x_2 = \sin\left(\frac{1}{8}\pi t\right) \quad (12)$$

For the two kinds of time series data (400 time series data in total), we have examined the change detection ability and the accuracy of each method (SPRT and NSPR) by setting some various evaluation criteria.

In the experimentation, the prediction model is constructed using the first 40 time points and the rest

of time points from  $t=41$  to  $t=100$  are used for change detection.

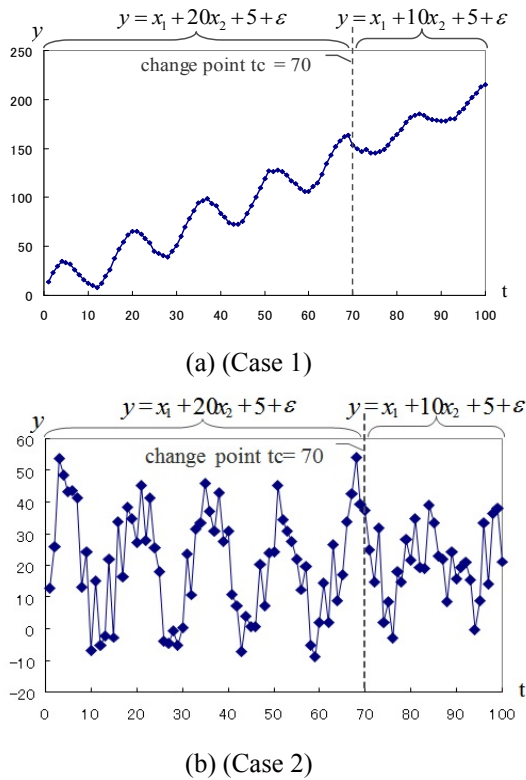


Fig.2. Example of two kinds of time series data generated based on Eq.(10).

(a)Case1 ( $x_1=t$ , and  $x_2 = \sin(\pi/8)$  ).

(b)Case2 ( $x_1=random$ , and  $x_2 = \sin(\pi/8)$  ).

We define a two dimensional vector  $\mathbf{I}=(I_1, I_2)$  as follows.

$$\mathbf{I} = (I_1, I_2) = \left( \sum_{t=41}^{t=70} f_r(t) \times |t - t_c|, \sum_{t=71}^{t=100} f_r(t) \times |t - t_c| \right) \quad (13)$$

where  $t_c=70$ , and  $f_r(t)$  means the detection frequency at time point  $t$  in 200 time series data.

We can consider that the detection ability and the accuracy is high as the absolute value of  $\mathbf{I}$  and  $I_1$  approach to 0.

As a result, in the sense of the abovementioned criteria, the NSPR method has shown that it is superior to SPRT for the both kinds of time series data used in the experimentation.

## References

1. C. G. E. P. Box and G. M. Jenkins, *Time Series Analysis: Forecasting and Control* (Prentice Hall, 1976).
2. Peter J. Brockwell and Richard A. Davis, *Introduction to Time Series and Forecasting*, 2nd edn. (Springer, 2003)
3. C. Han, P. K. Willet and D. A. Abraham, Some methods to evaluate the performance of Page's test as used to detect transient signals, *IEEE Trans. Signal processing.* **47**(8) (1999) 2112-2127.
4. S. D. Blostein, Quickest detection of a time-varying change in distribution, *IEEE Trans. Information Theory.* **37**(4) (1991) 1116-1122.
5. A. Wald, *Sequential Analysis* (John Wiley & Sons, 1947).
6. H. Kawano, T. Hattori, and K. Nishimatsu, Structural Change Point Detection Method of Time Series Using Sequential Probability Ratio Test -Comparison with Chow Test in the ability of early detection- (in Japanese), *IEEJ Trans. EIS.* **128**(4) (2008) 583-592.
7. G. C. Chow, Tests of Equality Between Sets of Coefficients in Two Linear Regressions, *Econometrica.* **28**(3) (1960) 591-605.
8. K. Takeda, T. Hattori, T. Izumi and H. Kawano, Extended SPRT for Structural Change Detection of Time Series Based on Multiple Regression Mode, in *Proceedings of the 15th International Symposium on Artificial Life and Robotics*, (Feb. 2010), ISBN: 978-4-9902880-4-4, pp.755-758.
9. K. Takeda, T. Hattori, Tetsuya Izumi and H. Kawano, Extended SPRT for Structural Change Detection of Time Series Based on Multiple Regression Model, *International Journal of Artificial Life and Robotics* Springer, ISSN: 1433-5298, **15**(4), (2010) 417-420.
10. T. Hattori and H. Kawano, Change Detection Method of Time Series as an Optimal Stopping Problem -- Constructive Proof of Optimal Solution Theorem --, in *Proc. of 2011 International Conference on Biometrics and Kansei Engineering*, (2011), IEEE Computer Society, ISBN: 978-0-7695-4512-7, pp.100-105.
11. Yoshihide Koyama, Tetsuo Hattori, Hiromichi Kawano, Model Introduced SPRT for Structural Change Detection of Time Series (I), in *Proc. of The International Conference on Artificial Life and Robotics* (Jan. 2014), ISBN: 978-4-9902880-8-2, pp.252-255.
12. Yoshihide Koyama, Tetsuo Hattori, Hiromichi Kawano, Model Introduced SPRT for Structural Change Detection of Time Series (II) --- Kansei Channel and Bayes' Estimation ---, in *Proc. of The International Conference on Artificial Life and Robotics* (Jan. 2014), ISBN: 978-4-9902880-8-2, pp.256-259.

# Analysis of Navier-Stokes Equation from the Viewpoint of Advection Diffusion (I) -- Analytical Solution of Diffusion Equation --

Hiroki Sakamoto\*, Tetsuo Hattori, Akiomi Tada, Vanhoa Nguyen

Graduate School of Engineering, Kagawa University, 2217-20, Hayashi-cho Takamatsu, Kagawa 761-0396, Japan

Hikomichi Kawano

NTT Advanced Technology Corporation, 19-18, Nakamachi  
Musashino, Tokyo 180-0006, Japan

## Abstract

We propose an approximate analysis method for Navier-Stokes Equation (NSE) based on the similarity between NSE and Advection Diffusion Equation (ADE). In this paper, we present an analytical solution and a Green function (integral kernel) which are obtained from the diffusion equation over uniform flow field (or velocity field) in three dimensional (3D) boundless region under arbitrary initial condition. The solution shows that the diffusion process is a Markov one and that the Green function becomes a Gaussian-like exponential function.

**Keywords:** approximate analysis method, Navier-Stokes Equation (NSE), Advection Diffusion Equation (ADE)

## 1. Introduction

Navier-Stokes Equation (NSE) is well known as fundamental one in Fluid Mechanics<sup>1</sup>. Because the exact analytical solution of NSE is not yet obtained, we have to use numerical computation for the solution under the arbitrary initial and boundary conditions.

For the numerical computation method, Difference Method, Finite Element Method and Boundary Element Method are well known. However, as for the Difference Method, it tends to be difficult to deal with complicated boundary conditions. In addition, the method has to satisfy the Courant condition to obtain the stable computation solution.

On the other hand, the Finite Element Method takes much time to solve simultaneous equations appeared in the method, and the Boundary Element Method has a

problem in the computation precision for the analysis of viscous flow of high Reynolds number.

Even if we obtain the result by using such numerical computations, those methods take much time and the results are involved by not a little computation error.

So, in order to reach the more accurate solution, it would be desirable to have an analytical approximate solution that is as much as close to the exact one.

In order to obtain such an analytical approximate solution, we focus on the similarity between the NSE and Advection Diffusion Equation (ADE). And in this paper, we derive the exact analytical solution of the ADE over uniform flow field (or velocity field) in three dimensional (3D) boundless region under arbitrary initial condition<sup>2-4</sup>.

---

\*2217-20 Hayashi Cho Takamatsu City, Kagawa, 761-0396 Japan, correspondence Email: hattori@eng.kagawa-u.ac.jp

© The 2015 International Conference on Artificial Life and Robotics (ICAROB 2015), Jan. 10-12, Oita, Japan



## 2. Advection Diffusion Equation

Let  $C$  be a fluid of density (or density of material), and let  $D_x, D_y, D_z$  denote the diffusion coefficient in  $x, y, z$  axis direction, respectively. Similarly, let  $u, v, w$  denote the flow velocity in  $x, y, z$  axis direction, respectively. Moreover, let  $\lambda$  and  $Q$  be the attenuation coefficient that is spatially uniform and the load generation rate function, respectively.

The partial differential equation of the ADE is shown as Eq.(1).

$$\begin{aligned} \frac{\partial C}{\partial t} = & D_x \frac{\partial^2 C}{\partial x^2} + D_y \frac{\partial^2 C}{\partial y^2} + D_z \frac{\partial^2 C}{\partial z^2} \\ & - u \frac{\partial C}{\partial x} - v \frac{\partial C}{\partial y} - w \frac{\partial C}{\partial z} - \lambda C + Q \end{aligned} \quad (1)$$

Here we introduce the Dirac's  $\delta$  function as in the following (2).

$$\left\{ \begin{array}{l} (x=0) \delta(x)=\infty, (x \neq 0) \delta(x)=0, \\ \int_{-\infty}^{\infty} \delta(x) dx=1 \end{array} \right. \quad (2)$$

The initial condition and the load generation rate function are shown in Eq.(3) and Eq.(4), respectively.

$$\begin{aligned} C(x, y, z, 0) = & \int_{-\infty}^{\infty} \int_{-\infty}^{\infty} \int_{-\infty}^{\infty} C_0(\xi, \eta, \zeta) \\ & \delta(x-\xi) \delta(y-\eta) \delta(z-\zeta) d\xi d\eta d\zeta \end{aligned} \quad \dots(3)$$

$$\begin{aligned} Q(x, y, z, t) = & \int_{-\infty}^{\infty} \int_{-\infty}^{\infty} \int_{-\infty}^{\infty} Q(\xi, \eta, \zeta, t) \\ & \delta(x-\xi) \delta(y-\eta) \delta(z-\zeta) d\xi d\eta d\zeta \end{aligned} \quad \dots(4)$$

Next, we think of the Fourier transform for  $C$  in 3 dimensional space. Then, let  $\tilde{C}$  be the Fourier

transformed  $C$ , and we have the following Eq.(5) and Eq.(6).

$$\tilde{C} = \int_{-\infty}^{\infty} \int_{-\infty}^{\infty} \int_{-\infty}^{\infty} C(x, y, z, t) e^{-j(px+qy+rz)} dx dy dz \quad \dots(5)$$

$$C = \frac{1}{(2\pi)^3} \int_{-\infty}^{\infty} \int_{-\infty}^{\infty} \int_{-\infty}^{\infty} \tilde{C}(p, q, r, t) e^{+j(px+qy+rz)} dp dq dr \quad \dots(6)$$

From the Fourier transform (FT) of the left hand side (LHS) and right hand side (RHS) in Eq.(1), we have the following Eq.(7) and Eq.(8), respectively.

$$\begin{aligned} \text{FT of LHS in Eq.(1)} \\ = & \int_{-\infty}^{\infty} \int_{-\infty}^{\infty} \int_{-\infty}^{\infty} \frac{\partial C(x, y, z, t)}{\partial t} e^{-j(px+qy+rz)} dx dy dz \\ = & \frac{\partial}{\partial t} \int_{-\infty}^{\infty} \int_{-\infty}^{\infty} \int_{-\infty}^{\infty} C(x, y, z, t) e^{-j(px+qy+rz)} dx dy dz \\ = & \frac{\partial \tilde{C}}{\partial t} \end{aligned} \quad \dots(7)$$

$$\begin{aligned} \text{FT of RHS in Eq.(1)} \\ = & -\left\{ p^2 D_x + q^2 D_y + r^2 D_z + j(pu + qv + rw) + \lambda \right\} \tilde{C} \\ & + \int_{-\infty}^{\infty} \int_{-\infty}^{\infty} \int_{-\infty}^{\infty} C(x, y, z, 0) e^{-j(px+qy+rz)} dx dy dz \\ = & -\left\{ p^2 D_x + q^2 D_y + r^2 D_z + j(pu + qv + rw) + \lambda \right\} \tilde{C} \\ & + \int_{-\infty}^{\infty} \int_{-\infty}^{\infty} \int_{-\infty}^{\infty} Q(\xi, \eta, \zeta, t) e^{-j(px+qy+rz)} d\xi d\eta d\zeta \end{aligned} \quad \dots(8)$$

As a result from the above Eq.(7) and Eq.(8), the Fourier transform of Eq.(1) becomes as follows.

$$\frac{\partial \tilde{C}}{\partial t} = -\alpha(p, q, r, t) \cdot \tilde{C} + \beta(p, q, r, t) \quad \dots(9)$$

where

$$\alpha(p, q, r, t) = p^2 D_x + q^2 D_y + r^2 D_z + j(pu + qv + rw) + \lambda$$

$$\beta(p, q, r, t) = \int_{-\infty}^{\infty} \int_{-\infty}^{\infty} \int_{-\infty}^{\infty} Q(\xi, \eta, \zeta, t) e^{-j(p\xi + q\eta + r\zeta)} d\xi d\eta d\zeta$$

Since Eq.(9) is a linear differential equation of first order with respect to time t, using an infinitesimal time parameter  $\tau(0 \leq \tau \leq t)$ , the solution is represented as shown in Eq.(10).

$$\tilde{C}(p, q, r, t) = \tilde{C}_0 \cdot \exp\left(\int_0^t \alpha(p, q, r, s) ds\right) + \int_0^t \beta(p, q, r, s) \cdot \exp\left(-\int_{\tau}^t \alpha(p, q, r, s) ds\right) d\tau \dots (10)$$

where  $\tilde{C}_0$  is represented as the following equation in the same way as  $\beta$ ,

$$\tilde{C}_0(p, q, r, 0) = \int_{-\infty}^{\infty} \int_{-\infty}^{\infty} \int_{-\infty}^{\infty} C_0(\xi, \eta, \zeta) e^{-j(p\xi + q\eta + r\zeta)} d\xi d\eta d\zeta$$

Next, we apply the inverse Fourier transform to Eq.(10).

Let the first and second term of the inverse Fourier transform of right hand side be  $C_1(x, y, z, t)$  and

$C_2(x, y, z, t)$ , respectively.

And, let  $\bar{x}$  denote  $\int_0^t X ds$ .

$$C_1 = \frac{1}{(2\pi)^3} \int_{-\infty}^{\infty} \int_{-\infty}^{\infty} \int_{-\infty}^{\infty} \left( \tilde{C}_0 e^{-\int_0^t \alpha(p, q, r, s) ds} \right) e^{j(px + qy + rz)} dpdqdr$$

$$= \frac{1}{8\pi^3} \int_{-\infty}^{\infty} \int_{-\infty}^{\infty} \int_{-\infty}^{\infty} \int_{-\infty}^{\infty} \int_{-\infty}^{\infty} \int_{-\infty}^{\infty} C_0(\xi, \eta, \zeta) e^{+j\{p(x-\xi) + q(y-\eta) + r(z-\zeta)\}}$$

$$\left\{ e^{-\int_0^t [p^2 D_x + q^2 D_y + r^2 D_z + j(pu + qv + rw) + \lambda] ds} \right\} d\xi d\eta d\zeta dpdqdr$$

$$= \frac{1}{8\pi^3} \int_{-\infty}^{\infty} \int_{-\infty}^{\infty} \int_{-\infty}^{\infty} \int_{-\infty}^{\infty} \int_{-\infty}^{\infty} \int_{-\infty}^{\infty} C_0(\xi, \eta, \zeta) \exp\left\{-p^2 \bar{D}_x + jp(x-\xi-\bar{u}) - q^2 \bar{D}_y + jp(y-\eta-\bar{v}) - r^2 \bar{D}_z + jp(z-\zeta-\bar{w}) - \bar{\lambda}\right\} d\xi d\eta d\zeta dpdqdr$$

$$= \frac{1}{8\pi^3} \int_{-\infty}^{\infty} \int_{-\infty}^{\infty} \int_{-\infty}^{\infty} \int_{-\infty}^{\infty} \int_{-\infty}^{\infty} \int_{-\infty}^{\infty} C_0(\xi, \eta, \zeta) \exp\left\{\left\{p\sqrt{\bar{D}_x}\right\} - j\frac{(x-\xi-\bar{u})}{2\sqrt{\bar{D}_x}}\right\}^2$$

$$- \left\{\left\{q\sqrt{\bar{D}_y}\right\} - j\frac{(y-\eta-\bar{v})}{2\sqrt{\bar{D}_y}}\right\}^2 - \left\{\left\{r\sqrt{\bar{D}_z}\right\} - j\frac{(z-\zeta-\bar{w})}{2\sqrt{\bar{D}_z}}\right\}^2\right\}$$

$$* \exp\left\{-\bar{\lambda} - \frac{(x-\xi-\bar{u})^2}{4\bar{D}_x} - \frac{(y-\eta-\bar{v})^2}{4\bar{D}_y} - \frac{(z-\zeta-\bar{w})^2}{4\bar{D}_z}\right\} d\xi d\eta d\zeta dpdqdr \dots (11)$$

First, we perform the integration with respect to  $p, q, r$ , then we have the following Eq.(12)

$$C_1 = \frac{1}{8\sqrt{\pi^3} D_x D_y D_z} \int_{-\infty}^{\infty} \int_{-\infty}^{\infty} \int_{-\infty}^{\infty} C_0(\xi, \eta, \zeta)$$

$$\exp\left\{-\bar{\lambda} - \frac{(x-\xi-\bar{u})^2}{4\bar{D}_x} - \frac{(y-\eta-\bar{v})^2}{4\bar{D}_y} - \frac{(z-\zeta-\bar{w})^2}{4\bar{D}_z}\right\} d\xi d\eta d\zeta \dots (12)$$

As for the  $C_2$ , we have the following equations.

$$C_2 = \frac{1}{(2\pi)^3} \int_{-\infty}^{\infty} \int_{-\infty}^{\infty} \int_{-\infty}^{\infty} \left( \int_0^t \beta(p, q, r, s) \cdot \exp\left(-\int_{\tau}^t \alpha(p, q, r, s) ds\right) d\tau \right)$$

$$e^{j(px + qy + rz)} dpdqdr$$

$$= \frac{1}{8\pi^3} \int_{-\infty}^{\infty} \int_{-\infty}^{\infty} \int_{-\infty}^{\infty} \left[ \int_0^t \int_{-\infty}^{\infty} \int_{-\infty}^{\infty} \int_{-\infty}^{\infty} Q e^{-j(p\xi + q\eta + r\zeta)} d\xi d\eta d\zeta \right] \cdot e^{-\int_0^t \alpha ds} d\tau$$

$$e^{j(px + qy + rz)} dpdqdr$$

$$= \frac{1}{8\pi^3} \int_0^t \int_{-\infty}^{\infty} \int_{-\infty}^{\infty} \int_{-\infty}^{\infty} \int_{-\infty}^{\infty} \int_{-\infty}^{\infty} Q \exp\{jp(x-\xi) + jp(y-\eta) + jr(z-\zeta)$$

$$- \int_{\tau}^t [p^2 D_x + q^2 D_y + r^2 D_z + j(pu + qv + rw) + \lambda] ds\}$$

$$dpdqdr d\xi d\eta d\zeta d\tau$$

$$= \frac{1}{8\pi^3} \int_0^t \int_{-\infty}^{\infty} \int_{-\infty}^{\infty} \int_{-\infty}^{\infty} Q \int_{-\infty}^{\infty} \int_{-\infty}^{\infty} \int_{-\infty}^{\infty} \exp\left\{-\left(p^2 \bar{D}_x + q^2 \bar{D}_y + r^2 \bar{D}_z\right) + jp(x-\xi-\bar{u}) + jq(y-\eta-\bar{v}) + jr(z-\zeta-\bar{w}) - \bar{\lambda}\right\}$$

$$dpdqdr d\xi d\eta d\zeta d\tau$$

$$\begin{aligned}
 &= \frac{1}{8\pi^3} \int_0^t \int_{-\infty}^{\infty} \int_{-\infty}^{\infty} \int_{-\infty}^{\infty} \int_{-\infty}^{\infty} \int_{-\infty}^{\infty} \int_{-\infty}^{\infty} \exp - \left\{ \left\{ p\sqrt{D_x} - j \frac{(x-\xi-\bar{u})}{2\sqrt{D_x}} \right\}^2 \right. \\
 &\quad \left. - \left\{ q\sqrt{D_y} - j \frac{(y-\eta-\bar{v})}{2\sqrt{D_y}} \right\}^2 - \left\{ r\sqrt{D_z} - j \frac{(z-\zeta-\bar{w})}{2\sqrt{D_z}} \right\}^2 \right\} \\
 &\quad * \exp \left[ -\bar{\lambda} - \frac{(x-\xi-\bar{u})^2}{4D_x} - \frac{(y-\eta-\bar{v})^2}{4D_y} - \frac{(z-\zeta-\bar{w})^2}{4D_z} \right] \\
 &\quad dpdqdrd\xi d\eta d\zeta d\tau
 \end{aligned}$$

Therefore, we have

$$\begin{aligned}
 C_2 = &\int_0^t \frac{1}{8\sqrt{\pi^3 D_x D_y D_z}} \int_{-\infty}^{\infty} \int_{-\infty}^{\infty} \int_{-\infty}^{\infty} Q(\xi, \eta, \zeta, \tau) \exp \\
 &\left\{ -\frac{(x-\xi-\bar{u})^2}{4D_x} - \frac{(y-\eta-\bar{v})^2}{4D_y} - \frac{(z-\zeta-\bar{w})^2}{4D_z} - \bar{\lambda} \right\} \\
 &d\xi d\eta d\zeta d\tau \dots(13)
 \end{aligned}$$

By returning the notation “ $\bar{\quad}$ ” to the original integration representation in Eq.(12) and Eq.(13), we have

$$\begin{aligned}
 C_1 = &\frac{1}{8\sqrt{\pi^3 \int_0^t D_x ds \int_0^t D_y ds \int_0^t D_z ds}} \int_{-\infty}^{\infty} \int_{-\infty}^{\infty} \int_{-\infty}^{\infty} C_0(\xi, \eta, \zeta) \\
 &\exp \left\{ \frac{(x-\xi-\int_0^t u ds)^2}{4\int_0^t D_x ds} - \frac{(y-\eta-\int_0^t v ds)^2}{4\int_0^t D_y ds} - \frac{(z-\zeta-\int_0^t w ds)^2}{4\int_0^t D_z ds} - \int_0^t \lambda ds \right\} \\
 &d\xi d\eta d\zeta d\tau \dots(14)
 \end{aligned}$$

$$\begin{aligned}
 C_2 = &\int_0^t \frac{1}{8\sqrt{\pi^3 \int_{\tau}^t D_x ds \int_{\tau}^t D_y ds \int_{\tau}^t D_z ds}} \int_{-\infty}^{\infty} \int_{-\infty}^{\infty} \int_{-\infty}^{\infty} Q(\xi, \eta, \zeta, \tau) \\
 &\exp \left\{ \frac{(x-\xi-\int_{\tau}^t u ds)^2}{4\int_{\tau}^t D_x ds} - \frac{(y-\eta-\int_{\tau}^t v ds)^2}{4\int_{\tau}^t D_y ds} - \frac{(z-\zeta-\int_{\tau}^t w ds)^2}{4\int_{\tau}^t D_z ds} - \int_{\tau}^t \lambda ds \right\} \\
 &d\xi d\eta d\zeta d\tau \dots(15)
 \end{aligned}$$

Because  $C = C_1 + C_2$ , we have the solution as follows.

$$\begin{aligned}
 C(x, y, z, t) &= \int_{-\infty}^{\infty} \int_{-\infty}^{\infty} \int_{-\infty}^{\infty} \{ C_0(\xi, \eta, \zeta) G(x, y, z, t, \xi, \eta, \zeta, 0) \\
 &\quad + \int_0^t Q(\xi, \eta, \zeta, \tau) G(x, y, z, t, \xi, \eta, \zeta, \tau) d\tau \} d\xi d\eta d\zeta
 \end{aligned}$$

where

$$\begin{aligned}
 G(x, y, z, t, \xi, \eta, \zeta, \tau) &= \frac{1}{8\sqrt{\pi^3 \int_{\tau}^t D_x ds \int_{\tau}^t D_y ds \int_{\tau}^t D_z ds}} \\
 &\exp \left\{ \frac{(x-\xi-\int_{\tau}^t u ds)^2}{4\int_{\tau}^t D_x ds} - \frac{(y-\eta-\int_{\tau}^t v ds)^2}{4\int_{\tau}^t D_y ds} - \frac{(z-\zeta-\int_{\tau}^t w ds)^2}{4\int_{\tau}^t D_z ds} - \int_{\tau}^t \lambda ds \right\} \dots(16)
 \end{aligned}$$

### 3. Conclusion

In this paper, we have presented the exact analytical solution of the ADE over uniform flow field (or velocity field) in three dimensional (3D) boundless region under arbitrary initial condition.

### References

1. T. Tanahashi, *Introduction to Computational Fluid Dynamics --Advection Diffusion Equation--*, (in Japanese), (Corona Publishing Co., Ltd., 1996).
2. A. Tada., An Iteration Method Applying Analytical Solution of the Diffusion Equation, (in Japanese), *Japan Society of Civil Engineering*, vol. 2-26, No. 485, (1994) pp.1-10
3. T.Hattori and A.Tada: A Novel Computational Method for Convection Diffusion Equation under Arbitrary Initial and Boundary Condition, *15th IMACS World Congress on Scientific Computation, Modelling and Applied Mathematics*, Edited by A.Sydow, (Wissenschaft & Technik Verlag, vol.3, Berlin, 1997), pp.645-650.
4. T.Hattori, K.Shinagawa, and A.Tada, Averaged Green Function Method for Diffusion Problem, *Proc. of 1998 International Symposium on Nonlinear Theory and Its Applications (NOLTA'98)* 1998, pp.979-982.

# Analysis of Navier-Stokes Equation from the Viewpoint of Advection Diffusion (II) --- Approximate Solution ---

Hiroki Sakamoto\*, Tetsuo Hattori, Akiomi Tada, Vanhoa Nguyen  
Graduate School of Engineering, Kagawa University  
2217-20, Hayashi-cho Takamatsu, Kagawa 761-0396, Japan

Hikomichi Kawano  
NTT Advanced Technology Corporation, 19-18, Nakamachi  
Musashino, Tokyo 180-0006, Japan

## Abstract

We propose an approximate analysis method for the Navier-Stokes Equation (NSE) based on the similarity between NSE and Advection Diffusion Equation (ADE). In the preceding paper titled "Analysis of Navier-Stokes Equation from the Viewpoint of Advection Diffusion (I)", we have presented the analytical solution of the ADE. Subsequently in this paper, we point out the explicit similarity between NSE and ADE by illustrating the corresponding equations. Then, we show an approximate solution of NSE using the aforementioned analytical solution of ADE.

**Keywords:** approximate analysis method, Navier-Stokes Equation (NSE), Advection Diffusion Equation (ADE)

## 1. Introduction

It is well known that Navier-Stokes Equation (NSE) is the most fundamental one in Fluid Mechanics<sup>1</sup>, and also known that the exact analytical solution of NSE is not yet obtained.

Although we have to use numerical computation for solving the NSE under the arbitrary initial and boundary conditions, if possible, it is still desirable to have an analytical approximate solution that is as much as close to the exact one.

In this paper, in order to obtain such an analytical approximate solution, we focus on the similarity between the NSE and Advection Diffusion Equation (ADE). And we apply the exact analytical solution of

the ADE over uniform flow field (or velocity field) in three dimensional (3D) boundless region under arbitrary initial condition<sup>2-4</sup>, that we have presented in the previous paper of ICAROB2015, to the NSE.

## 2. Advection Diffusion Equation (ADE)

Let  $C$  be a fluid of density (or density of material), and let  $D_x, D_y, D_z$  denote the diffusion coefficient in  $x, y, z$  axis direction, respectively. Similarly, let  $u, v, w$  denote the flow velocity in  $x, y, z$  axis direction, respectively. Moreover, let  $\lambda$  and  $Q$  be the attenuation coefficient that is spatially uniform and the load generation rate function, respectively.

---

\*2217-20 Hayashi Cho Takamatsu City, Kagawa, 761-0396 Japan,  
Kagawa University, Email: hattori@eng.kagawa-u.ac.jp

© The 2015 International Conference on Artificial Life and Robotics (ICAROB 2015), Jan. 10-12, Oita, Japan

The partial differential equation of the ADE is shown as Eq.(1).

$$\frac{\partial C}{\partial t} = D_x \frac{\partial^2 C}{\partial x^2} + D_y \frac{\partial^2 C}{\partial y^2} + D_z \frac{\partial^2 C}{\partial z^2} - u \frac{\partial C}{\partial x} - v \frac{\partial C}{\partial y} - w \frac{\partial C}{\partial z} - \lambda C + Q \quad (1)$$

Here we introduce the Dirac's  $\delta$  function as in the following (2).

$$\left\{ \begin{array}{l} (x=0) \delta(x)=\infty, (x \neq 0) \delta(x)=0, \\ \int_{-\infty}^{\infty} \delta(x) dx = 1 \end{array} \right. \quad (2)$$

The initial condition and the load generation rate function are shown in Eq.(3) and Eq.(4), respectively.

$$C(x, y, z, 0) = \int_{-\infty}^{\infty} \int_{-\infty}^{\infty} \int_{-\infty}^{\infty} C_0(\xi, \eta, \zeta) \delta(x - \xi) \delta(y - \eta) \delta(z - \zeta) d\xi d\eta d\zeta \quad (3)$$

$$Q(x, y, z, t) = \int_{-\infty}^{\infty} \int_{-\infty}^{\infty} \int_{-\infty}^{\infty} Q(\xi, \eta, \zeta, t) \delta(x - \xi) \delta(y - \eta) \delta(z - \zeta) d\xi d\eta d\zeta \quad (4)$$

Then, we can obtain the exact solution as follows.

$$\begin{aligned} C(x, y, z, t) &= \int_{-\infty}^{\infty} \int_{-\infty}^{\infty} \int_{-\infty}^{\infty} \{ C_0(\xi, \eta, \zeta) G(x, y, z, t, \xi, \eta, \zeta, 0) \\ &+ \int_0^t Q(\xi, \eta, \zeta, \tau) G(x, y, z, t, \xi, \eta, \zeta, \tau) d\tau \} d\xi d\eta d\zeta \end{aligned} \quad (5)$$

where  $G$  is a Green function and Gaussian-like exponential one as shown in Eq.(6).

$$\begin{aligned} G(x, y, z, t, \xi, \eta, \zeta, \tau) &= \frac{1}{8 \sqrt{\pi^3 \int_{\tau}^t D_x ds \int_{\tau}^t D_y ds \int_{\tau}^t D_z ds}} \\ &\exp \left\{ - \frac{\left( x - \xi - \int_{\tau}^t u ds \right)^2}{4 \int_{\tau}^t D_x ds} - \frac{\left( y - \eta - \int_{\tau}^t v ds \right)^2}{4 \int_{\tau}^t D_y ds} - \frac{\left( z - \zeta - \int_{\tau}^t w ds \right)^2}{4 \int_{\tau}^t D_z ds} - \int_{\tau}^t \lambda ds \right\} \end{aligned} \quad (6)$$

### 3. Navier-Stokes Equation (NSE)

We consider that the NSE shows a Law of conservation of momentum with respect to  $\rho v_i$  ( $i = x, y, z$ ) and that NSE is a kind of Advection Diffusion Equation (ADE) regarding momentum (Eq.(5))

$$\frac{\partial(\rho v_i)}{\partial t} + \text{div}(-\mu \nabla v_i + \rho v_i v) = -\frac{\partial p}{\partial x_i} + f_i \quad (7)$$

where  $\rho, v, \mu, p, f$  are density, velocity, coefficient of viscosity, pressure, and external force, respectively.

#### 3.1. Similarity between ADE and NSE

In Eq.(1), let  $D_x = D_y = D_z = D$ . Using the relational equation in Eq(8), Eq.(1) can be represented as Eq.(9).

$$\begin{aligned} (\mathbf{v} \cdot \nabla) &= (v_x, v_y, v_z) \left( \frac{\partial}{\partial x}, \frac{\partial}{\partial y}, \frac{\partial}{\partial z} \right) \\ &= v_x \frac{\partial}{\partial x} + v_y \frac{\partial}{\partial y} + v_z \frac{\partial}{\partial z} \end{aligned} \quad \dots(8)$$

$$\frac{\partial C}{\partial t} = D \nabla^2 C - (\mathbf{v} \cdot \nabla) C - \lambda C + Q$$

...(9)

From NSE Eq.(7), putting  $\mu = k\rho$  where  $k$  is coefficient of kinematic viscosity, we have

$$\frac{\partial \mathbf{v}}{\partial t} = k\nabla^2 \mathbf{v} - (\mathbf{v} \bullet \nabla) \mathbf{v} - \frac{\text{grad} p}{\rho} + \frac{\mathbf{f}}{\rho} \quad (10)$$

At  $t = t_0$ , we have the following relation.

$$\frac{\partial \mathbf{v}(t_0)}{\partial t} = k\nabla^2 \mathbf{v}(t_0) - \{\mathbf{v}(t_0) \bullet \nabla\} \mathbf{v}(t_0) - \frac{\text{grad} p}{\rho} + \frac{\mathbf{f}}{\rho} \quad (11)$$

Here, we consider that  $\mathbf{v}(t_0) = \mathbf{v}(t_0 - \Delta t)$  where  $\Delta t$  is infinitesimal time parameter. So we have

$$\frac{\partial \mathbf{v}(t_0)}{\partial t} = k\nabla^2 \mathbf{v}(t_0) - \{\mathbf{v}(t_0 - \Delta t) \bullet \nabla\} \mathbf{v}(t_0) - \frac{\text{grad} p}{\rho} + \frac{\mathbf{f}}{\rho} \quad \dots(12)$$

Then putting  $\bar{\mathbf{v}} = \mathbf{v}(t_0 - \Delta t)$ , we have another form of the Eq.(9) and Eq.(10) as follows.

$$\frac{\partial C}{\partial t} = D\nabla^2 C - (\bar{\mathbf{v}} \bullet \nabla) C - \lambda C + Q \quad \dots(13)$$

$$\frac{\partial \mathbf{v}}{\partial t} = k\nabla^2 \mathbf{v} - (\bar{\mathbf{v}} \bullet \nabla) \mathbf{v} - \frac{\text{grad} p}{\rho} + \frac{\mathbf{f}}{\rho} \quad \dots(14)$$

Since the term  $-\lambda C$  in Eq.(9) is attenuation one, letting  $\lambda = 0$ , we have the following correspondent relation.

$$C \leftrightarrow \mathbf{v}, \quad k \leftrightarrow D, \quad Q \leftrightarrow \frac{\text{grad} p}{\rho} + \frac{\mathbf{f}}{\rho}$$

If we regard the  $\bar{\mathbf{v}}$  as a kind of constant comparing with  $\mathbf{v}$ , we can obtain the solution of Eq.(14) in the same way as the solution of ADE, using the aforementioned correspondent relation.

### 3.2. Application of the Solution of ADE to NSE

Since the diffusion coefficient  $D$  appeared in the Green function in Eq.(4), is invariant with respect to time, we can compute the integration term including the  $D$ . Then for the Green function, we have

$$G(x, y, z, t, \xi, \eta, \zeta, \tau) = \frac{1}{8\sqrt{\pi^3} [D(t-\tau)]^3} \exp \left\{ - \frac{\left( x - \xi - \int_{\tau}^t u ds \right)^2}{4D(t-\tau)} - \frac{\left( y - \eta - \int_{\tau}^t v ds \right)^2}{4D(t-\tau)} - \frac{\left( z - \zeta - \int_{\tau}^t w ds \right)^2}{4D(t-\tau)} \right\} \quad \dots(15)$$

Let  $\mathbf{r}_p = (x, y, z)$ ,  $\mathbf{r} = (\xi, \eta, \zeta)$ , that means the position at the present time point and the general position at the past time point, respectively. Since we can regard NSE as a kind of ADE, we can obtain the Green function of the analytical approximate solution of NSE by making an analogy from the solution of ADE, as follows..

$$G(x, y, z, t, \xi, \eta, \zeta, \tau) = \frac{1}{8\sqrt{\pi^3} [D(t-\tau)]^3} \exp \left\{ - \frac{\left\| \mathbf{r}_p - \left( \mathbf{r} + \int_{\tau}^t \bar{\mathbf{v}} ds \right) \right\|^2}{2\sigma^2} \right\}$$

where  $\bar{\mathbf{v}} = (u, v, w)$ ,  $\sigma = \sqrt{2D(t-\tau)}$ ,

$$K = \frac{1}{8\sqrt{\pi^3} [D(t-\tau)]^3} = (\sigma\sqrt{\pi})^{-3} \quad (16)$$

Then we have the approximate solution of NSE using the aforementioned Green function (Eq.(16)) as follows.



# Development of Mouse Cursor Control System Based on Face Direction Using Kinect

**Masayoshi Tabuse**

*Graduate School of Life and Environmental Sciences, Kyoto Prefectural University  
1-5 Hangi-cho, Shimogamo, Sakyo-ku, Kyoto 606-8522, Japan  
E-mail: tabuse@kpu.ac.jp*

**Kaori Tamura**

*ISI Software Corporation  
4-6-17 Honmachi, Chuo-ku, Osaka 541-0053, Japan*

## Abstract

We propose a method of operating mouse cursor and controlling television based on face direction using Kinect. Using our system anyone can control television by motion of a user easily and cheaply. Our system measures face direction and controls mouse cursor using 4 face direction using Kinect. It changes a television's channel and volume by controlling mouse cursor based on face direction using Kinect.

*Keywords:* Mouse Cursor Control System, Kinect, Face detection, Face Direction, Television Tuner Software

## 1. Introduction

In recent years, development of many new kinds of input devices is performed, for example, video and audio input devices. Gaze measurements are used as operation of a mouse cursor. For gaze measurement, input devices are classified into a contacted type and a non-contact type. For a contacted type, detection of a motion is easy and high accuracy. However, equipment and removal of it and adjustment according for a user are required whenever it is used. For a non-contact type, removal of it is not required. However, in order to acquire high accuracy, it is necessary to fix a user's head or to restrict user's head movement, and adjustment according for a user is required. Therefore, the burden on a user is heavy when a user uses a gaze measurement device.

In the present study, we propose a method of operating mouse cursor and controlling television based on face direction using Kinect. Kinect consists of a RGB camera, a depth sensor, a multi-array microphone and software (Kinect for Windows SDK), released by Microsoft. It can recognize a position, a voice, a face,

face direction and skeleton of a user. Kinect was made for the purpose of a game and entertainment, but is applied to the support of medical care and a person with a disability. By using our system, anyone can control television by motion of a user easily and cheaply. It is not necessary to fix a user's head or to restrict user's head movement. Therefore, it can ease a user's burden compared with conventional devices. Furthermore, a person with trouble in a hand can control television easily.

In our system, Kinect is connected to a personal computer. A television tuner is installed in the personal computer. Television tuner software is controlled by a mouse cursor and a mouse wheel. Our system measures face direction and controls mouse cursor using 4 face directions of rightward, leftward, upward and downward directions using Kinect. In the case of a rightward face the system turns a television channel to the forward direction. In the case of a leftward face it turns a television channel to the opposite direction. In the case of an upward face it raises a television's volume. In the case of a downward face it lowers a television's volume in the downward face direction. Our system changes a television's channel and volume by controlling the



mouse cursor and the mouse wheel based on face direction using Kinect in a range with distance less than 4 meters between a user and Kinect. It is also applicable to operation of other application software controlled by mouse cursor, such as a web browser.

### 2. Outline of Our System

Fig.1 shows the flowchart of our system.

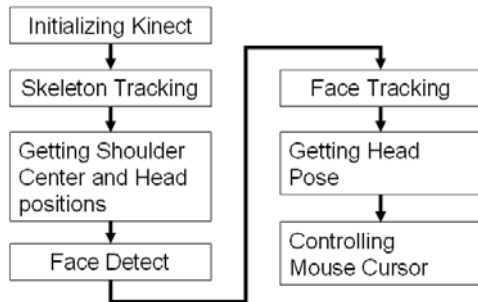


Fig. 1. The flowchart of our system.

### 3. Face Tracking and Face Direction

Microsoft Face Tracking SDK together with Kinect for Windows SDK enables us to track human face in real time.

#### 3.1. Human Body Detection and Skeleton Tracking

Kinect for Windows SDK detects human bodies using depth data acquired from the depth camera in Kinect, estimates 3D joint positions and tracks skeletons<sup>1</sup>. Fig.2 shows joint data.

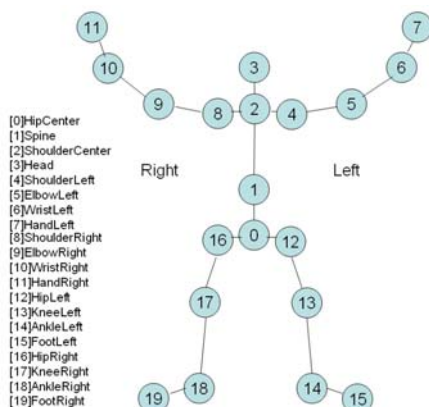


Fig. 2. Joint data

#### 3.2. Face Detection and Face Tracking

Face Tracking SDK extracts human face region in RGB image using Shoulder-Center and Head positions in 3D joint data, depth data and RGB data<sup>2</sup>. It fits a deformable face model in face region and obtains 2D/3D position of 100 landmark points on human face. It tracks these points based on a feature of landmark points in the previous frame.

#### 3.3. Face Direction

Face Tracking SDK tracks the 100 points on human face and outputs tracking status, 2D position of points, 3D head pose. The head pose is expressed by three angles: pitch, roll and yaw, shown in Fig.3. A pitch angle  $\phi$  ranges from -90 degrees (looking down towards the floor) to 90 degrees (looking up towards the ceiling). A roll angle  $\theta$  ranges from -90 degrees (horizontal parallel with right shoulder) to 90 degrees (horizontal parallel with left shoulder). A yaw angle  $\psi$  ranges from -90 degrees (turned towards the right shoulder) to 90 degrees (turned towards the left shoulder). Therefore the face direction is determined by these three angles. In our system we divide face directions into 5 directions: facing up, facing down, facing right, facing left, facing the front. For  $\phi \geq 15^\circ$  and  $-15^\circ < \theta < 15^\circ$  human faces up. For  $\phi \leq -15^\circ$  and  $-15^\circ < \theta < 15^\circ$  human faces down. For  $-15^\circ < \phi < 15^\circ$  and  $\theta < -15^\circ$  human faces right. For  $-15^\circ < \phi < 15^\circ$  and  $\theta \geq 15^\circ$  human faces left. Otherwise human faces the front.

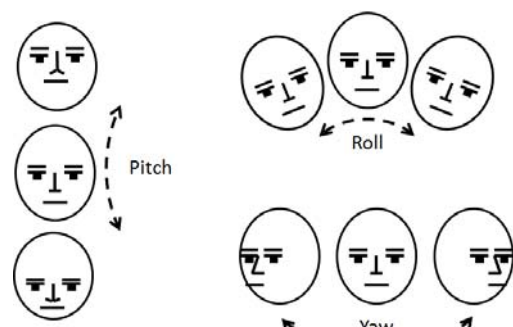


Fig. 3. Head pose<sup>2</sup>.

### 3.4. Mouse Cursor Control by Face Direction

In our system we install a television tuner and television tuner software in a personal computer. The television tuner software is controlled by a mouse cursor and a mouse wheel. In the right region of the software window we roll the mouse wheel, so that the software turns the television channel. In the left region of the software window we roll the mouse wheel, so that the software changes the television's volume. Therefore, our system moves a mouse cursor in response to a face direction and it controls the television tuner software.

## 4. Experiments

### 4.1. Experimental Environment

In our experiments we have used a PC (Dell Optiplex 790; CPU : Core i7-2600, Memory : 4GB) , Kinect for Windows and a television tuner and software (Buffalo DT-F120/U2). For programming, we have used Microsoft Visual C++ 2010, Kinect for Windows SDK v1.7, Kinect for Windows Developer Toolkit v1.7. Fig. 4 shows mouse cursor control system.



Fig. 4. Mouse cursor control system.

### 4.2. Operation Screen

We show a computer operation screen in Fig.5. When our system detects and tracks user's face, it displays image of user's face in the upper right on the window. If our system detects one of 4 face directions of a user (facing up, facing down, facing right, facing left), a region of face direction turns into white, shown in Fig. 6. Then if the user keeps the same direction more than two seconds, the region of face direction turns into yellow, shown Fig 7.



Fig. 5. Computer operation screen.



Fig. 6. A region of face direction turns into white.

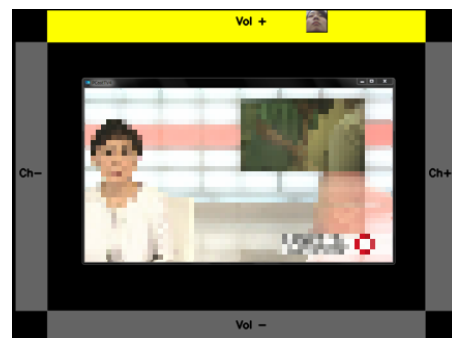


Fig. 7. A region of face direction turns into yellow.

### 4.3. Experiments of television control

We instruct a subject to operate the television and let the subject perform the operation according to the instructions. Subjects are 10 (4 males and 6 females). The evaluation (5 points are perfect) of subjects is as follows.

(i)Arrangement of the region and the design

The evaluation for arrangement of the region and the design is shown in Table 1.

Table 1. The evaluation for arrangement of the region and the design .

Point	5	4	3	2	1	Mean
Frequency	8	4	0	1	0	4.6

(ii)Operability

The evaluation for operability of our system is shown in Table 2.

Table 2. The evaluation for operability.

Point	5	4	3	2	1	Mean
Frequency	3	3	2	1	1	3.6

Comments of subjects are as follows.

(i)Arrangement of the region and the design

(a)Good points

- Reaction of the display when changing the direction of the face is easy to understand.
- It's easy to see, and it's easy to understand.
- It's colored, so it's easy to understand.
- When seeing television screen, a button of the left, right, up or down isn't annoying.

(ii)Operability

(a)Good points

- When a face is recognized once, it reacts accurately.
- It's simple, so it's easy to understand.
- It reacted by a small movement more than I thought.
- A face was turned to the side, but it was possible to look at a screen, so it was good.

(b)Improvement

- The system doesn't detect a face of looking up easily.
- A reaction of looking up wasn't a little good.
- When facing down, it's difficult to look at a screen.

5. Discussions

In our experiments every subject could do operation of a television stably. But after beginning to experiment, a subject wearing glasses couldn't sometimes detect a face.

For a male subject, even if the subject is turning to the front Kinect has often detected it with declining. We setup Kinect which indicates a pitch angle  $\varphi = 0^\circ$  and a roll angle  $\theta = 0^\circ$  when a female of the height of 160cm faces to the front of Kinect. Therefore a taller male has a high location of the head to a RGB camera of Kinect.

We improved our system as a result of the television operation experiments. The calculation of pitch and roll angles was changed as follows.

We calculate average values of pitch and roll angles,  $\bar{\varphi}$  and  $\bar{\theta}$ , in 30 frames after detecting a face, respectively. We redefine pitch and roll angles,  $\varphi'$  and  $\theta'$ , as follows.

$$\begin{aligned} \varphi' &= \varphi - \bar{\varphi} \\ \theta' &= \theta - \bar{\theta} \end{aligned} \tag{1}$$

where  $\varphi$  and  $\theta$  are pitch and roll angles of a face measured by Kinect. For  $\varphi' \geq 15^\circ$  and  $-15^\circ < \theta' < 15^\circ$  human faces up. For  $\varphi' \leq -15^\circ$  and  $-15^\circ < \theta' < 15^\circ$  human faces down. For  $-15^\circ < \varphi' < 15^\circ$  and  $\theta' < -15^\circ$  human faces right. For  $-15^\circ < \varphi' < 15^\circ$  and  $\theta' \geq 15^\circ$  human faces left. Otherwise human faces the front. Two subjects (1 male, 1 female) operate the television using the improvement system. Subjects' comments are as follows.

- It is easy to operate the television.
- Reactions for faces become good.

As a result of the improvement of our system, a subject operates a television whenever the location of the face to a RGB camera of Kinect was different.

6. Conclusion

We have developed a mouse cursor control system based on face direction using Kinect and applied it to a television operating system. Furthermore, by using the average angle of a subject facing the front, a subject operates a television whenever the location of the face to a RGB camera of Kinect was different.

At present, our system operates only channel and volume changes of a television. In the future, we will add various operations, such as on-off of a power supply and recording operation, to our system. It is also applicable to operation of other application software controlled by mouse cursor, such as a web browser.

References

1. *Skeletal Tracking*, Kinect for Windows SDK v1.7, <http://msdn.microsoft.com/en-us/library/hh973074.aspx>.
2. *Face Tracking*, Kinect for Windows SDK v1.7, <http://msdn.microsoft.com/en-us/library/jj130970.aspx>.

# Quantitative Evaluation of Facial Expressions and Movements of Persons While Using Video Phone

**Taro Asada, Yasunari Yoshitomi, Ryota Kato, and Masayoshi Tabuse**

*Graduate School of Life and Environmental Sciences, Kyoto Prefectural University,  
1-5 Nakaragi-cho, Shimogamo, Sakyo-ku, Kyoto 606-8522, Japan  
E-mail: {t\_asada, r\_kato}@mei.kpu.ac.jp, {yoshitomi, tabuse}@kpu.ac.jp*

**Jin Narumoto**

*Graduate School of Medical Science, Kyoto Prefectural University of Medicine,  
Kajii-cho, Kawaramachi-Hirokoji, Kamigyo-ku, Kyoto 602-8566, Japan  
jnaru@koto.kpu-m.ac.jp*

## Abstract

The video is analyzed using image processing and the feature parameters of facial expressions and movements, which are extracted in the mouth area. The feature parameter for expressing facial expressions is defined as the average of facial expression intensity. That for expressing movements of a person is defined as the average of absolute value of vertical coordinate for the center of gravity of mouth area in the relative coordinate system. The experimental result shows the usefulness of the proposed method.

*Keywords:* Facial expression analysis, Movement analysis, Mouth area, OpenCV, and Skype.

## 1. Introduction

In Japan, the average age of the population has been increasing, and this trend is expected to continue. Because of the growing trend of aging, the number of older people with dementia and/or depression living in rural area is increasing very rapidly. Due to mismatch between the number of patients and health care professionals there, it is difficult to provide psychological assessment and support for the patients living there.

We have been developing a method for analyzing facial expressions of a person while speaking with another person using a video phone to improve the QOL of elderly people living in care facility, or at home.<sup>1-3</sup> In the present study, we have developed a method for analyzing facial expressions and movements of a person

while speaking with another person, using our reported method<sup>2</sup>, the standardization of size of face to be analyzed, and the newly proposed feature parameters on facial expressions and movements of a person.

## 2. Proposed Method

### 2.1. System overview and outline of the method

The platform is composed of Skype<sup>4</sup> for video phone. In addition to record the audio and video dialogue, Netralia Pty Ltd's VodBurner<sup>5</sup> and Tapur<sup>6</sup> are introduced. The talks are recorded for the analysis of facial expressions and movements of a person. The recorded data are analyzed using image processing software, Open Source Computer Vision Library for real-time computer vision developed by Intel (Open CV)<sup>7</sup>, the standardization of

© The 2015 International Conference on Artificial Life and Robotics (ICAROB 2015), Jan. 10-12, Oita, Japan

size of face to be analyzed, and the newly proposed feature parameter on facial expressions and movements of a person described in the following subsections. The Y component obtained from each frame in the dynamic image is used for analyzing facial expressions and movements of a person. The proposed method consists of (1) Standardization of lower part of face-area in size, (2) extraction of mouth area, (3) measurement of facial expression intensity, (4) judgment of utterance, (5) calculation of feature parameter on facial expression strength, and (6) calculation of feature parameter on movements of a person. In the following subsections, these six are explained in detail.

### 2.2. Standardization of lower part of face-area in size

First, a face-area obtained from each frame in the dynamic image is extracted using the classifier for a front-view face included in OpenCV. In the classifier, Haar-like feature parameter and Adaboost algorithm for learning are used.<sup>8</sup> It can be assumed that the distance between a subject and the camera is almost always kept during conversation using Skype. The face of the frame where the face-area extracted using OpenCV has the minimum size among those for a period in the dynamic image is assumed to be the most likely front-view among those in the period,<sup>1</sup> and the frame is selected and used. In the present study, we set 1/3 seconds as the period. Then, a low part of face-area extracted by the above method is standardized in length and width for extracting a mouth area. This standardization in size is performed with the aim of not only improving the performance of extracting a mouth area using OpenCV but also normalizing the feature parameter generation using 2D-DCT (Discrete Cosine Transform) there. Under the circumstance that the size of face in a dynamic image cannot be kept constant every time, this standardization in size is indispensable for reliably measuring the feature parameters described in the sections 2.6 and 2.7.

### 2.3. Extraction of mouth area

Next, using OpenCV, the mouth area is extracted as a rectangle shape. The mouth area is selected because the difference between the facial expressions of neutral and happy remarkably appears there. Fig. 1 shows an example

of face image, a lower part of face image before and after standardization of size, and mouth-area image extracted.



Fig. 1. Face image (upper), lower part of face image before (lower & left) and after (lower & center) standardization of size, and mouth-area image extracted (lower & right).

### 2.4. Measurement of facial expression intensity

For the Y component of the frame selected by the processing described above, the feature vector of facial expression is extracted in the mouth area with use of 2D-DCT performed for each domain having 8×8 pixels.

We select 15 low-frequency components of the 2D-DCT coefficients, except for a direct current component, as the feature parameters for expressing facial expression.<sup>2</sup> Then, we obtain the mean of the absolute value for each 2D-DCT coefficient component in the area of mouth.<sup>2</sup> Therefore, we obtain 15 values as the elements of the feature vector. The facial expression intensity, defined as the norm of the difference vector between the feature vector of the neutral facial expression and that of the observed expression, can be used for analyzing a change of facial expression.<sup>2</sup>

### 2.5. Judgment of utterance

The sound data are smoothed and sampled to erase noise. Then, all sampled data that fall within  $[\bar{x}_s - 14\sigma_s, \bar{x}_s + 14\sigma_s]$ , where  $\bar{x}_s$  and  $\sigma_s$  respectively express the average and the standard deviation of the sound data value for one second under the condition of no utterance, are considered to be the range of no utterance. When at least one sampled datum has a value outside  $[\bar{x}_s - 14\sigma_s, \bar{x}_s + 14\sigma_s]$ , our system judges that the sound data contain an utterance after erasing the noise.

### 2.6. Feature parameter on facial expression strength

In diagnosing a patient having dementia and/or depression, it might be useful for health care professionals to evaluate the strength of facial expression using a simple measure. Moreover, it might be more advantageous for a diagnosis of dementia and/or depression to separately evaluate the strength of facial expression as a speaker and a listener. Therefore, we measure as the feature parameter of facial expression strength the average of facial expression intensity in the four cases of (1) both subjects A and B speak, (2) subject A speaks and subject B does not speak, (3) subject A does not speak and subject B speaks, and (4) both subjects A and B do not speak, using the method for judging an utterance described in the section 2.5.

### 2.7. Feature parameter on movements of a person

Head movements such as a nodding during conversation might suggest a mental state and/or recognition ability of a patient having dementia and/or depression. Therefore, we measure as the feature parameter of movements of a person the average of absolute value of vertical coordinate for the center of gravity of mouth area in the relative coordinate system in the four cases described in the section 2.6. The relative coordinate system is defined using the mouth area extracted at the starting point for measuring the feature parameter on movements of a person. At the starting point, the height of the mouth area is set to be one and the vertical coordinate for the center of gravity of the mouth area is set to be 0 in the relative coordinate system.

## 3. Experiment

### 3.1. Condition

Two males (subject A in his 50s and subject B in his 20s) participated in the experiment where they took conversation for about 70 seconds using Skype. The videos saved using VodBurner were transformed into AVI files, and the audios saved using Tapur were transformed into WAV files. The AVI files were used for measuring feature parameters on facial expressions and movements of a subject. The WAVE files were used for judgment of utterance. The size of image frame was 720×480 pixels, and the size of standardized lower part of face image was set to be 240×96 pixels.

### 3.2. Results and discussion

Fig. 2 shows mouth-area images at starting point. Facial expression intensity changes of subjects A and B during their conversation (Fig. 3) and changes of coordinates of center of gravity on mouth area (Fig. 4) are shown respectively. In Fig. 5, face-images are shown at the characteristic timing positions. Feature parameters on facial expressions and movements of subjects are shown in Table.1. The definitions of these parameters are described in the sections 2.6 and 2.7.

As shown in Figs. 3 and 5, facial expression intensity was very sensitive for facial expression change. Both of subjects A and B did not move vertically so much during conversation (Fig. 5 and Table 1). The number of mouth-area images extracted using OpenCV was increased for subject A from 196 to 197 by performing the size



Fig. 2. Mouth-area images of subjects A (left two) and B (right two) at starting point with (left side) and without (right side) size standardization before extracting mouth area.

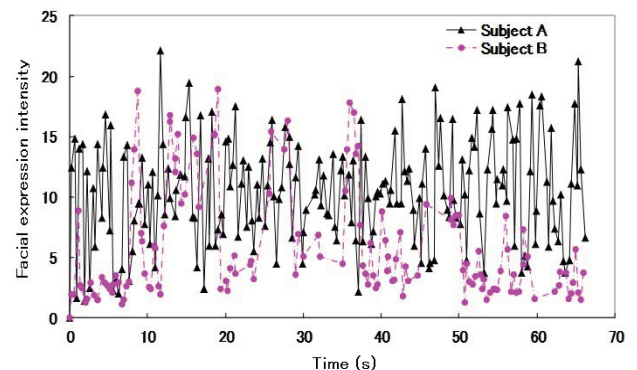


Fig. 3. Facial expression intensity change of subjects A and B during the conversation between these two subjects with size standardization before extracting mouth area.

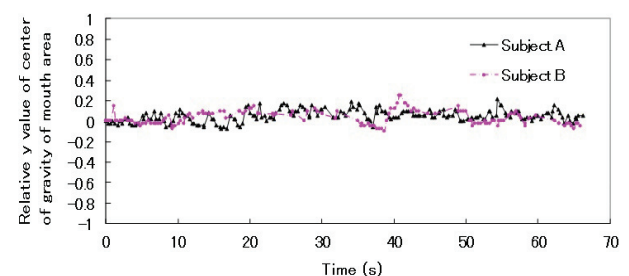


Fig. 4. Changes of coordinates of center of gravity on mouth area with size standardization before extracting mouth area.





Fig. 5. Face-images at characteristic timing positions on facial expression intensity value of subject A; upper: 0 (starting point), lower & left : maximum, lower & right : minimum except that at starting point.

Table 1. Feature parameters on facial expressions and movements.

(1) With size standardization before extracting mouth area

Subject	Utterance		Feature parameter	
	A	B	Facial expression	Movement of person
<b>A</b>	without	without	11.41	0.05
	with	without	9.47	0.08
	without	with	10.50	0.05
<b>B</b>	without	without	4.53	0.05
	with	without	12.51	0.07
	without	with	3.14	0.06

(2) Without size standardization before extracting mouth area

Subject	Utterance		Feature parameter	
	A	B	Facial expression	Movement of person
<b>A</b>	without	without	8.55	0.03
	with	without	8.50	0.04
	without	with	10.06	0.05
<b>B</b>	without	without	5.48	0.04
	with	without	10.88	0.05
	without	with	5.18	0.03

standardization before extracting mouth area, while it was increased for subject B from 27 to 138 by the standardization. Though mouth-area images were influenced by size standardization before extracting mouth area (Fig. 2), the feature-parameter values of both

facial expressions and movements of subjects were not influenced so much by size standardization before extracting mouth area (Table 1). The value of feature parameter of facial expression was relatively high for subject A in the all three cases, while it was relatively high for subject B in the only case that subject B spoke and subject A did not speak (Table 1). Because the period in which both subjects A and B spoke was very short, the data were not described in Table 1.

#### 4. Conclusion

The video is analyzed using image processing and the newly proposed feature parameters of facial expressions and movements. The experimental result shows the usefulness of the proposed method. We will develop the method for estimating a mental state and/or recognition ability of a patient using the proposed method.

#### Acknowledgment

This research is partially supported by COI STREAM of the Ministry of Education, Culture, Sports, Science and Technology of Japan.

#### References

1. T. Asada, Y. Yoshitomi, A. Tsuji, R. Kato, M. Tabuse, N. Kuwahara, and J. Narumoto, Method of facial expression analysis of person while using video phone, in *Proc. of Human Interface Symposium 2013* (Japan, Tokyo, 2013), pp.493-496.
2. T. Asada, Y. Yoshitomi, A. Tsuji, R. Kato, M. Tabuse, N. Kuwahara, and J. Narumoto, Facial expression analysis while using video phone, in *Proc. of Int. Conf. on Artif. Life and Robotics* (Japan, Oita, 2014), pp.230-234.
3. J. Narumoto, N. Kuwahara, Y. Yoshitomi, T. Asada, Y. Kato, H. Kamimura, K. Fukui, Development of support system for patients with dementia through teleconference system, in *Proc. of 4th World Conf. of Asian Psychiatry* (Thailand, Bangkok, 2014), pp.1-4.
4. Skype Web page, <http://www.skype.com/> Accessed 5 November 2013.
5. VodBurner Web page, <http://www.vodburner.com/> Accessed 11 July 2014.
6. Tapur Web page, <http://www.tapur.com/jp/> Accessed 18 December 2014.
7. OpenCV Web page, <http://opencv.willowgarage.com/> Accessed 11 July 2014.
8. P. Viola and M. Jones, Rapid object detection using a boosted cascade of simple features, in *Proc. of the 2001 IEEE Computer Society Conf. on Computer Vision and Pattern Recognition* (USA, Kauai, 2001), Vol.1, pp.511-518.

# Facial Expression Recognition Using Facial Expression Intensity Characteristics of Thermal Image

**Yasunari Yoshitomi, Taro Asada, Ryota Kato, and Masayoshi Tabuse**  
*Graduate School of Life and Environmental Sciences, Kyoto Prefectural University,*  
*1-5 Nakaragi-cho, Shimogamo, Sakyo-ku, Kyoto 606-8522, Japan*  
*E-mail: {yoshitomi, tabuse}@kpu.ac.jp, {t\_asada, r\_kato}@mei.kpu.ac.jp*  
*[http://www2.kpu.ac.jp/ningen/infsys/English\\_index.html](http://www2.kpu.ac.jp/ningen/infsys/English_index.html)*

## Abstract

A video was analyzed using thermal image processing and the feature parameter of facial expression, which was extracted in the area of mouth and jaw using a two-dimensional discrete cosine transform. The facial expression intensity defined as the norm of difference vector between the feature vector of neutral facial expression and that of observed one was used for analyzing facial expression. The feature vector made by facial expression intensity and time at utterance was used for recognizing facial expression.

*Keywords:* Facial expression recognition, Area of mouth and jaw, Thermal image, and Utterance judgment.

## 1. Introduction

The goal of our research is to develop a robot that can perceive human feelings and mental states. Although the mechanism for recognizing facial expressions of human feelings has received considerable attention in computer vision research, it currently falls far short of human capability. This is due to the decreased accuracy of facial expression recognition, which is influenced by the inevitable change of gray levels due to nuances of shade, reflection, and local darkness. To avoid this problem and to develop a robust method for facial expression recognition applicable under widely varied lighting conditions, we use an image registered by infrared rays to describe the thermal distribution of the face.<sup>1-3</sup> The timing of recognizing facial expressions is also important for a robot because the processing can be time-consuming. We adopted an utterance as the key of

expressing human feelings because humans tend to say something when expressing their feelings.<sup>2,3</sup>

In the present study, we proposed a method for recognizing facial expressions using the facial expression intensity<sup>4</sup> and the time at utterance.

## 2. Proposed Method

The proposed method consists of (1) extraction of the area of the mouth and jaw, (2) measurement of facial expression intensity, (3) judgment of utterance, (4) calculation of feature parameters for facial expression and voice.

### 2.1. Extraction of area of mouth and jaw

The frame extracted every 0.1 second in the dynamic image is used for thermal image processing. Six face areas (Fig. 1) are extracted by the thermal image processing reported in our study.<sup>3</sup> The area of mouth and jaw is selected because the difference between the



facial expressions of neutral and happy distinctly appears in this area.<sup>4</sup> Fig. 2 shows an example of thermal face image and image of area of mouth and jaw.

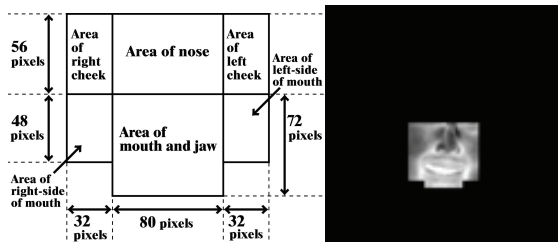


Fig. 1. Blocks for extracting face-part areas (left), thermal image after face part extraction (right).<sup>2, 6</sup>



Fig. 2. Thermal face image (left) and image of area of mouth and jaw (right).<sup>4</sup>

### 2.2. Measurement of facial expression intensity

For the extracted frame, the feature vector of facial expression is extracted in the area of the mouth and jaw by applying a two-dimensional discrete cosine transform (2D-DCT) for each domain of  $8 \times 8$  pixels.<sup>4</sup> We select 15 low-frequency components of the 2D-DCT coefficients, except for a direct current component, as the feature parameters for expressing facial expression.<sup>4</sup> Then, we obtain the mean of the absolute value for each 2D-DCT coefficient component in the area of mouth and jaw.<sup>4</sup> Therefore, we obtain 15 values as the elements of the feature vector. The facial expression intensity, defined as the norm of the difference vector between the feature vector of the neutral facial expression and that of the observed expression, can be used for analyzing a change of facial expression.<sup>4</sup>

### 2.3. Judgment of utterance

The sound data are smoothed and sampled to erase noise. Then, all sampled data that fall within  $[\bar{x}_s - 14\sigma_s, \bar{x}_s + 14\sigma_s]$ , where  $\bar{x}_s$  and  $\sigma_s$  respectively express the average and the standard deviation of the

sound data value for one second under the condition of no utterance, are considered to be the range of no utterance.<sup>4</sup> When at least one sampled datum has a value outside  $[\bar{x}_s - 14\sigma_s, \bar{x}_s + 14\sigma_s]$ , our system judges that the sound data contain an utterance.<sup>4</sup>

### 2.4. Feature parameters

We use two feature parameters as the elements of feature vector. One is a mean of standardized facial expression intensity at each utterance and for 0.3 seconds before and after the utterance. The other is the standardized time at each utterance. The standardization used for making feature parameters is expressed by Eq. (1).

$$x_{i,j}^* = \frac{x_{i,j} - \bar{x}_i}{\sigma_i} \quad (1)$$

,where  $x_{i,j}^*$ ,  $x_{i,j}$ ,  $\bar{x}_i$  and  $\sigma_i$  respectively express the standardized feature parameter, the measured feature parameter, the average and the standard deviation of the measured feature parameters of training data, and  $i, j$  respectively denote no. (1 or 2) of feature parameter and no. (1, 2, ...,  $m$ ) of utterance. Then, clustering using Ward method is performed for each of training and test data to decide major and minor clusters for each class of facial expressions in the feature vector space. Then, for recognizing facial expressions of test data, we use the coordinates of center of gravity of the major cluster for each class of facial expressions for training and test data.

## 3. Experiments

### 3.1. Conditions

The thermal image produced by the thermal video system (Nippon Avionics TVS-700) and the sound captured from an Electret condenser microphone (Sony ECM-23F5), as amplified by a mixer (Audio-Technica AT-PMX5P), were transformed into a digital signal by an A/D converter (Thomson Canopus ADVC-300) and were input into a computer (DELL Optiplex 780, CPU: Intel Core 2 Duo E8400 3.00 GHz, main memory: 3.21 GB, and OS: Windows 7 Professional (Microsoft) with an IEEE1394 interface board (I/O Data Device 1394-PCI3/DV6). We used Visual C++ 6.0 (Microsoft) and Visual C++ 2008 Express Edition (Microsoft) as the programming language. In order to generate a thermal image, we set the condition such that the thermal image had 256 gray levels for the detected temperature range.

The temperature range for generating a thermal image was decided so as to easily extract the face area on the image. We saved the visual and audio information in the computer as a Type 2 DV-AVI file, in which the video frame had a spatial resolution of 720×480 pixels and 8-bit gray levels, and the sound was saved in a stereo PCM format, 48 kHz and 16-bit levels.

Subject A, a male with glasses, performed in alphabetic order each of the intentional facial expressions of “angry,” “happy,” “neutral,” “sad,” and “surprised,” while speaking the semantically neutral utterance of each of the Japanese first names of “taro” (the first and last vowels of which are /a/ and /o/), and “tsubasa” (the first and last vowels of which are /u/ and /a/). In the experiment, Subject A intentionally maintained a front-view in the AVI files, which were saved as both training and test data. We assembled 15 samples as training data and 15 samples as test data. The AVI files were used for measuring the facial expression intensity. The WAV files obtained from the AVI files were used for measuring time at utterance.

### 3.2. Results and discussion

The thermal face image depended on the emotion of subject even at 0.3 seconds before starting to speak (Fig. 3). The deference of the time series of facial expression intensity among those for five kinds of emotion became more distinct in picking up those data in the time range from 0.3 seconds before starting to speak to 0.3 seconds after finishing speaking than that in picking up those data at utterance.



Fig. 3. Thermal face images belonging to major clusters of training data at 0.3 seconds before starting to speak “taro” (upper) and “tsubasa” (lower).

Table 1 shows the number of utterance belonging to each cluster. Fig. 4 shows the facial expression intensity

Table 1. Number of utterance belonging to each cluster.

(1)taro		angry	happy	neutral	sad	surprised
training	major	13	11	10	14	11
	minor	2	4	5	1	4
test	major	13	13	13	8	8
	minor	2	2	2	7	7

(2)tsubasa		angry	happy	neutral	sad	surprised
training	major	12	10	9	11	14
	minor	3	5	6	4	1
test	major	14	12	14	13	10
	minor	1	3	1	2	5

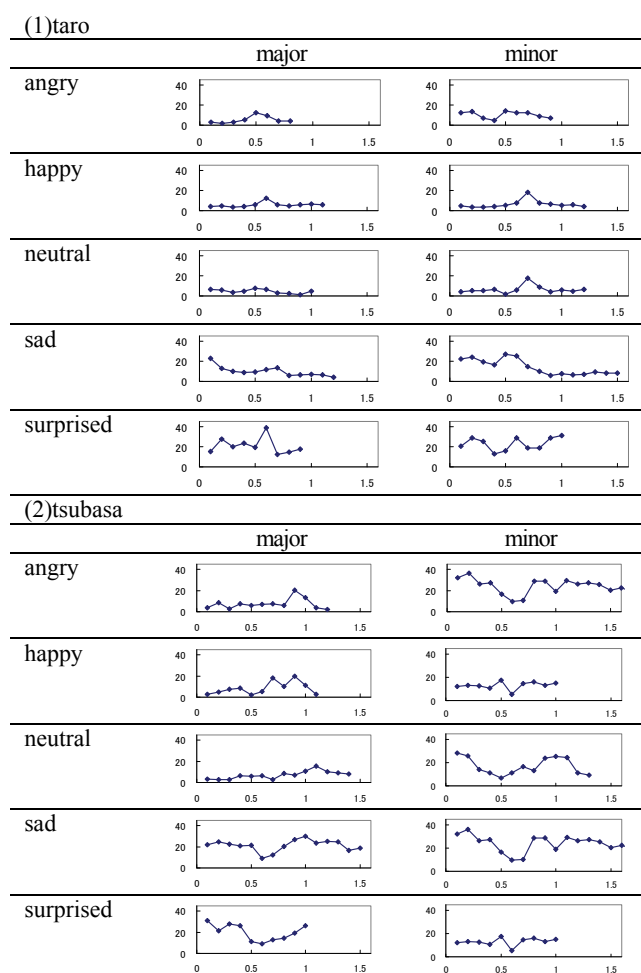


Fig. 4. Example of time series of facial expression intensity corresponding to each cluster of training data; vertical axis: facial expression intensity, horizontal axis: time in second.

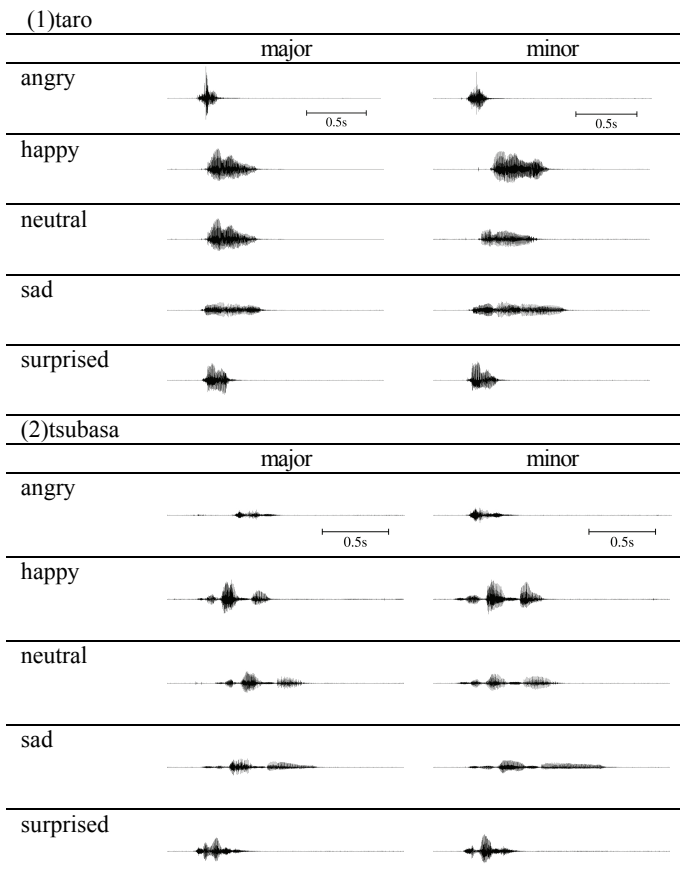


Fig. 5. Example of wave form at utterance corresponding to each cluster of training data.

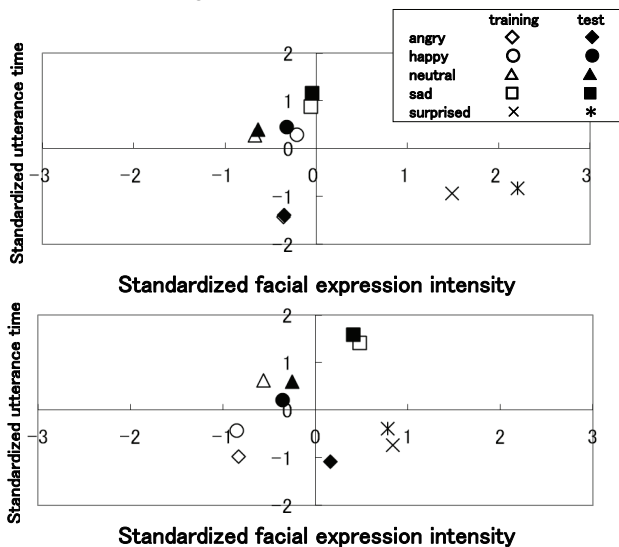


Fig. 6. Two-dimensional distribution of center of gravity of major cluster of training and test data; upper: “taro”, lower: “tsubasa”.

corresponding to each cluster in the time range from 0.3 seconds before starting to speak to 0.3 seconds after finishing speaking. Fig. 5 shows the wave form at utterance corresponding to each cluster. Fig. 6 shows the two-dimensional distribution of center of gravity of the major cluster for each class of facial expressions for training and test data. The recognition accuracy of facial expressions was 100% and 60% for utterance of “taro” and “tsubasa” using the nearest neighbor rule, respectively. In the case of “taro” in Fig. 6, the angry’s mark of training data was almost covered with that of test data.

#### 4. Conclusion

We proposed a method for recognizing facial expressions using the thermal image processing and the facial expression intensity. The standardized mean value of facial expression intensity for a major cluster, and the standardized mean value of time at utterance for a major cluster are used for recognizing facial expression. The experimental results show the usefulness of the proposed method.

#### Acknowledgements

The present study was partially supported by KAKENHI (22300077).

#### References

1. Y. Yoshitomi, N. Miyawaki, S. Tomita, and S. Kimura, Facial expression recognition using thermal image processing and neural network, in *Proc. 6th IEEE Int. Workshop on Robot and Human Communication*, (Japan, Sendai, 1997), pp. 380–385.
2. Y. Yoshitomi, T. Asada, K. Shimada, and M. Tabuse, Facial expression recognition of a speaker using vowel judgment and thermal image processing, *J. Artif. Life and Robotics* **16**(3) (2011) 318–323.
3. Y. Yoshitomi, M. Tabuse, and T. Asada, Facial expression recognition using thermal image processing, in *Image processing: methods, applications and challenges* ed. V. H. Carvalho (Nova Science Publisher, New York, 2012), pp. 57–85.
4. Y. Yoshitomi, T. Asada, R. Kato, M. Tabuse, Method of facial expression analysis using video phone and thermal image, *J. Robotics, Networking and Artif. Life* **1**(1) (2014) 7–11.

# Method for Character Domain Extraction from Image Using Wavelet Transform

**Taiki Taniguchi**

*ZENSHO HOLDINGS Co., Ltd., 2-18-1 Konan Minato-ku Tokyo 108-0075, JAPAN*

**Yasunari Yoshitomi**

*Graduate School of Life and Environmental Sciences, Kyoto Prefectural University,*

*1-5 Nakaragi-cho, Shimogamo, Sakyo-ku, Kyoto 606-8522, Japan*

*E-mail: yoshitomi@kpu.ac.jp*

*[http://www2.kpu.ac.jp/ningen/infsys/English\\_index.html](http://www2.kpu.ac.jp/ningen/infsys/English_index.html)*

## Abstract

The number of images having private information and/or URL of illegal Web site has been increasing in the cyber space on the Internet. These images might cause infringement of human right and/or crime. In the present study, a method for extracting the region(s) having characters on an image has been developed using the discrete wavelet transform and the empirical knowledge that a character has strong vertical and/or horizontal element(s). The experimental results show the usefulness of the proposed method.

*Keywords:* Internet, Private information, URL of illegal Web, Character domain extraction, Wavelet Transform, and Image processing.

## 1. Introduction

The number of images having private information and/or URL of illegal Web site has been increasing in the cyber space on the Internet. These images might cause infringement of human right and/or crime. It is very time-consuming and inefficient to detect them through watching each Web page one by one by naked eyes. The method for checking images to judge whether they have private information and/or URL of illegal Web site has been missing. For achieving the task, firstly, we must extract the region(s) having characters on the image. The algorithm for extracting the region(s) having characters on an image has received considerable attention in computer vision research.<sup>1-3</sup> However, it falls far short of practical capability.

In the present study, a method for extracting the region(s) having characters on an image has been developed using the discrete wavelet transform (DWT). For the course of developing the method, we use the empirical knowledge that a character has strong vertical and/or horizontal element(s).

## 2. Wavelet Transform of Image Signals

Hierarchical decomposition of DWT has been widely used in image compression and other image processing techniques. The image is first decomposed into four subbands, 1LL, 1LH, 1HL, and 1HH. The subbands labeled 1LH, 1HL, and 1HH represent the finest scale wavelet coefficients. Fig.1 describes level 1 decomposition, in which the image is decomposed into four subbands for one scale.

© The 2015 International Conference on Artificial Life and Robotics (ICAROB 2015), Jan. 10-12, Oita, Japan

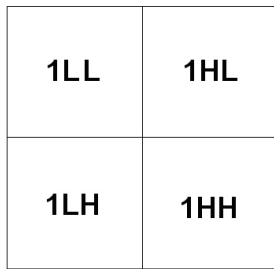


Fig. 1. Mallat division.

In general, the wavelet coefficients on the three domains described as HH, HL and LH are called elements of multi-resolution representation, whereas the wavelet coefficients of LL are called elements of multi-resolution analysis. For further information on the DWT, see Ref.4.

### 3. Proposed Method

Fig.2 illustrates the flowchart of the proposed method. The algorithm of the proposed method is as follows:

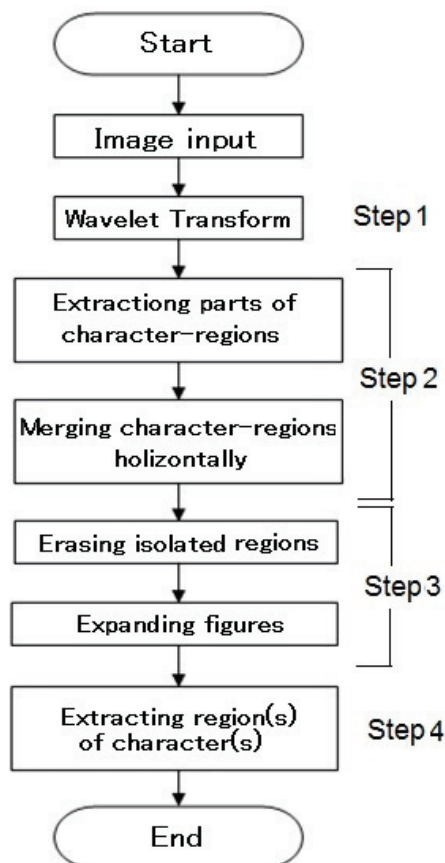


Fig. 2. Flow chart of the proposed method.

**Step 1** : RGB elements of image (Fig.3) are transformed into YCrCb elements (Fig.4) , followed by DWT for each element to obtain 1HL and 1LH elements corresponding to vertical and horizontal elements respectively (Fig.4).



Fig. 3. Sample of input image.



Fig. 4. 1HL (upper & center) and 1LH (upper & right) elements for Y element (upper & left), 1HL (middle & center) and 1LH (middle & right) elements for Cr element (middle & left), and 1HL (lower & center) and 1LH (lower & right) elements for Cb element (lower & left) obtained from input image (Fig. 3).

**Step 2** : A segmentation for both the 1HL and 1LH elements using each threshold for the elements is performed (Fig.5). Then, the scattered regions having '255' in the binary image for each of YCrCb elements are merged with changing the values of pixels existing among pixels of '255' from '0' to '255' when the pixels of '0' have the same value of horizontal coordinate as that of '255' (Fig.6).

**Step 3** : The operations of erasing isolated regions and expanding the regions of the value of '255' are performed (Fig. 7).

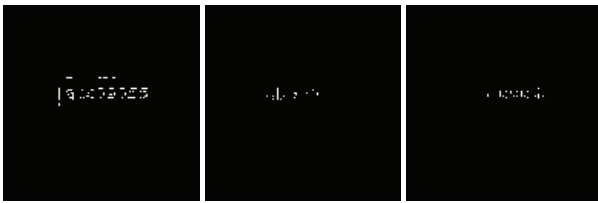


Fig. 5. Binary images obtained for both 1HL and 1LH elements for Y, Cr, and Cb elements, obtained using related images in Fig.4; left: Y, center: Cr, right: Cb.

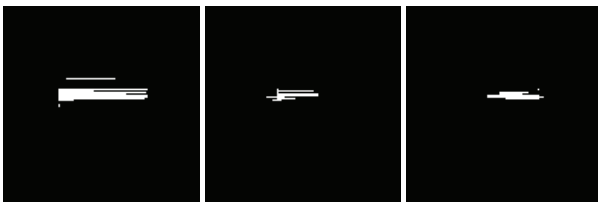


Fig. 6. Binary images after horizontally merging for binary images for Y, Cr, and Cb elements, obtained using related images in Fig.5; left: Y, center: Cr, right: Cb.

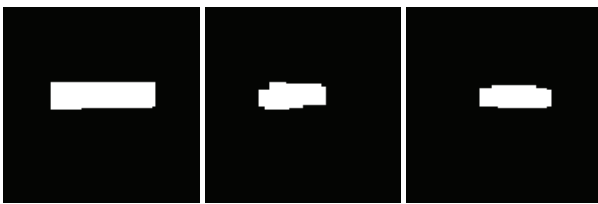


Fig. 7. Binary images just after finishing processing of Step 3 for Y, Cr, and Cb elements, obtained using related images in Fig.6; left: Y, center: Cr, right: Cb.

**Step 4 :** Then a mask image for extracting the region(s) having characters on the input RGB image is generated by merging the regions of '255' with logical sum operation for all of three binary images obtained for Y, Cr, Cb elements. Finally, the output RGB image is generated by the operation that the color of the pixel on the input RGB image is changed into white when the value of corresponding pixel on the mask image is '0', resulting in extracting the region(s) having character(s) on the input RGB image (Fig.8).



Fig. 8. Input image (left) and output image (right).

## 4. Experiments

### 4.1. Conditions

Three standard images (Earth, Couple, and Mandrill) in 24-bit BMP form having  $256 \times 256$  pixels were prepared for evaluation of the proposed method. The images used in this experiment were selected from Standard Image Data-Base (SIDBA). We used the Daubechies wavelet for DWT. Several black characters of abc09056 were written on the original images with one of white, non-white color, and transparent backgrounds (Fig.9). The experiment was performed in the following environment for computation: personal computer; DELL OPTIPLEX780(CPU : Intel(R) Core(TM)2 Duo CPU E8400 3.00GHz, main memory : 4.00GB), OS; Microsoft Windows 7 Professional, Development language; Microsoft Visual C++6.0.

In the process of segmentation in Step 2 described in the section 3, the binary image was obtained by the way that the value of pixel in binary image was set to 255 when the value of 1HL or 1LH element was not higher than each threshold for the elements, and otherwise it was set to be 0. The threshold was set to be half of minimum value for each element except that it was higher than -40. In this exceptional case, the threshold was set to be -40. In the process of segmentation in Step 3 described in the section 3, the regions having 50 pixels or less were erased and the expansion was performed five times.

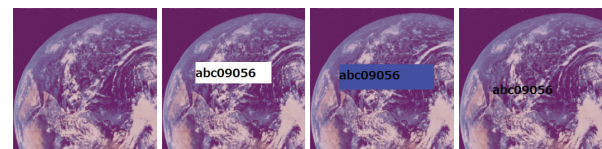


Fig. 9. Examples of original image (left end) and input images with characters (others).



#### 4.2. Results and discussion

Figs. 10, 11 show the input images and the output images obtained using the proposed method. When the background of characters was not transparent, all regions with characters were successfully extracted by the proposed method (Fig.10). However, when the background of characters was transparent, some regions with characters were not extracted and other regions having no characters were extracted by the proposed method (Fig.11).

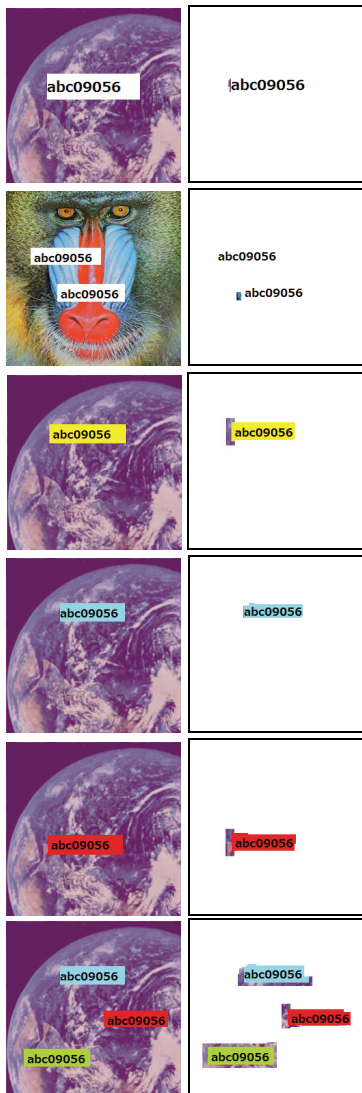


Fig. 10. Input images (left) with characters on color backgrounds, and output images (right).

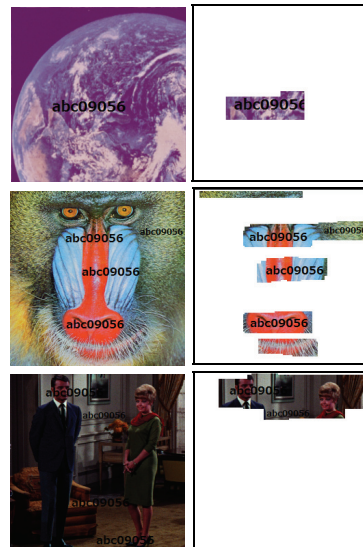


Fig. 11. Input images (left) with characters on transparent backgrounds, and output images (right).

#### 5. Conclusion

A method for extracting the region(s) having characters on an image has been developed using the discrete wavelet transform and the empirical knowledge that a character has strong vertical and/or horizontal element(s). The experimental results show the usefulness of the proposed method.

#### Acknowledgements

The authors would like to express their sincere thanks to Associate Professors M. Tabuse and T. Asada of Kyoto Prefectural University for their useful advices and supports of the present research.

#### References

1. H. Hirano and M. Okabe, Detection of text area inserted by image editing (in Japanese), in *IPSJ SIG Notes*, vol. 2012-CVIM-183, no. 9, (Japan, Koganei, 2012), pp. 1-8.
2. K. Ashida, H. Nagai, M. Okamoto, H. Miyao, and H. Yamamoto, Extraction of characters from scene images (in Japanese), *Trans IEICE J88-D-II(9)* (2005) 1817-1824.
3. S. Masuko, T. Hoshi, and H. Hirano, A system for searching texts in images by using reliability factor and saliency (in Japanese), *J. IPSJ* **51(9)** (2010) 1520-1529.
4. D. Inoue and Y. Yoshitomi, Watermarking using wavelet transform and genetic algorithm for realizing high tolerance to image compression, *J. IEEJ* **38(2)** (2009) 136-144.

# Classification of Japanese Documents and Ranking of Representative Documents Using Characteristic of Frequencies of Words

**Jun Kimura**

*JustSystems Corp., 6-8-1 Nishinjuku, Shinjuku-ku, Tokyo 163-6017*

**Yasunari Yoshitomi, and Masayoshi Tabuse**

*Graduate School of Life and Environmental Sciences, Kyoto Prefectural University,*

*1-5 Nakaragi-cho, Shimogamo, Sakyo-ku, Kyoto 606-8522, Japan*

*E-mail: {yoshitomi, tabuse}@kpu.ac.jp*

*[http://www2.kpu.ac.jp/ningen/infsys/English\\_index.html](http://www2.kpu.ac.jp/ningen/infsys/English_index.html)*

## Abstract

We have developed a method for classification of Japanese documents and ranking of representative documents using characteristic of frequencies of nouns. The representative document is defined as the document whose feature vector is the closest to the center of gravity of the class in the feature vector space among all documents belonging to the class. The ranking of the representative documents is decided in the descending order of the number of documents belonging to the class.

*Keywords:* Document classification, Extraction of representative document, Clustering, and Frequency of nouns.

## 1. Introduction

Recently, Web pages on the Internet have been increasing, resulting in that it is very difficult to read through all of Web pages in which we are interested. However, as a fact, there are too many similar Web pages among them. For efficiently acquiring useful Web pages, it is necessary to select only Web pages having important and independent contents with which we can understand essential parts on an event adequately. A Web page has some kinds of media, such as document, image, and sound.

We focus on selecting Web page on the Internet according to characteristics of document on the page.

Although the classification of documents has received considerable attention in document analysis research,<sup>1-8</sup> there is no research for selecting a representative document in a class of documents, followed by ranking several representative documents in order of importance or in any meaning useful for us, to our best knowledge.

In the present study, we have developed a method for classification of Japanese documents and ranking of representative documents using characteristic of frequencies of nouns.



## 2. Proposed Method

### 2.1. Extraction of nouns

Firstly, all nouns in a document are extracted using MeCab<sup>9</sup> with which the document is resolved into several morphemes (Fig. 1).

```

インターネットを利用する。
インターネット 名詞,一般,*,*,*インターネット,インターネット,インターネット
を 助詞,格助詞,一般,*,*,*を,ヲ,ヲ
利用 名詞,サ変接続,*,*,*利用,リコウ,リコー
する 動詞,自立,*,*,*スル,基本形,する,スル,スル
。 記号,句点,*,*,*。 ,。 ,。
EOS
    
```

Fig. 1. Output of MeCab.

### 2.2. Connection of nouns having a meaning as a set

Some nouns directly connecting each other are treated as one noun in the case that they have a meaning in assuming one noun. For example, 2014 and 年 in Japanese has a meaning as a set of 2014 年. 年 in Japanese means year in English.

### 2.3. Addition of negative attribution

When a sentence expresses a negative meaning with use of 'not', the extracted nouns in the sentence are treated as having a negative attribution. In other words, a noun can have either positive or negative attribution. The noun having a negative attribution is treated as being different from the noun with a positive attribution in making a feature vector for the document where the noun exists.

### 2.4. Feature vector generation

After every noun composing of only one of a hiragana, which is the rounded Japanese phonetic syllabary, or a katakana, which is the angular Japanese syllabary, or a symbol is erased, a feature vector having a relative frequency of each noun as each element is generated for each document. The relative frequency is defined as the ration of frequency of the noun to that of all nouns in the document except nouns erased using the above criterion.

### 2.5. Document classification and extraction of representative one in each class

For clustering, we use Ward method. The representative document is defined as the document whose feature vector is the closest to the center of gravity of the class

in the feature vector space among all documents belonging to the class.

### 2.6. Ranking of representative documents

The first-rank document is defined as the document whose feature vector is the closest to the center of gravity of all documents in the feature vector space. In this case, the number of class is one. Afterward, the number of class is increased one by one, and then the ranking from the second-rank for the representative documents is decided in the descending order of the number of documents belonging to the class for each number of classes. The maximum number  $J$  of classes in the stepwise clustering is given beforehand. Though a document can be selected more than once in the ranking process, the only first selection for the document is accepted.

## 3. Calculation Environment

The development of system and the experiment for evaluation of the proposed method were performed in the following environment for computation: personal computer; DELL OPTIPLEX 780(CPU: Intel Core2 Duo CPU E8400 3.00GHz, RAM: 4.00GB), OS; Microsoft Windows 7 Professional, Development language; Python 2.7.3.

## 4. Experiments and Discussion

### 4.1. Document classification

Firstly, we evaluated the performance of document calcification by the proposed method. We gathered 20 documents on politics (document nos. 1-10) and horse racing (document nos. 11-20) from Yahoo! Japan News<sup>10</sup> in January 2013, and then the number of clusters was set to be two, resulting in that our system gave the outputs shown in Table. 1. The clusters of  $C_1$  and  $C_2$  were composed of the documents on politics and horse racing, respectively (Table 1). Accordingly, the document calcification by the proposed method was perfect.

Table 1. Nos. of documents belonging to each cluster.

Cluster $C_1$	Cluster $C_2$
1, 2, 3, 4, 5,	11, 12, 13, 14, 15,
6, 7, 8, 9, 10	16, 17, 18, 19, 20

## 4.2. Extraction of representative documents

### 4.2.1. Experiment I

Next, we evaluated the performance of extraction of representative document by the proposed method. We gathered top 20 documents obtained by a retrieval from Google News<sup>11</sup> and those from Yahoo! Japan News using the retrieval keyword of '大阪府 高校' in Japanese, which is Osaka Prefecture high school in English, on 22 January 2013. The name of document obtained was set to be the same as the rank by each retrieval, and then all documents were categorized.

The name of category was decided to be the content name when more than two documents having the similar content each other existed, and otherwise the document was assigned to be a category of 'Others'. The categorization was manually performed through our understanding for each document, while the clustering was performed by the proposed method. Therefore, it was not guaranteed for the clustering result to correspond with the document group structure given by the manual categorization.

#### (a) Google News

Table 2 shows the document group structure when we used Google News in our experiment. There were five kinds of categories (Table. 2). Table 3 shows the ranking of representative documents given by the proposed method when using  $J = 4$ .

Table 2. Document group structure I.

Category	Rugby	Board of education	
Document No.	1, 9, 12, 18, 20	2, 4, 5, 11, 16, 17, 19	
Category	Skating	Distress accident	Others
Document No.	3, 14	6, 7, 8, 15	10, 13

Table 3. Result I.

Ranking of representative documents expressed by Nos.
6, 1, 4, 3

The four representative documents were successfully extracted one by one from all categories except the category of 'Others' in the order of 'Distress accident', 'Rugby', 'Board of education', and 'Skating' (Table 3).

#### (b) Yahoo! Japan News

Table 4 shows the document group structure when we used Yahoo! Japan News in our experiment. There were five kinds of categories (Table. 4). Table 5 shows the ranking of representative documents given by the proposed method when using  $J = 4$ .

The four representative documents were successfully extracted one by one from all categories except the category of 'Rugby' in the order of 'Board of education', 'Center exam', 'Distress accident', and 'Others' (Table 5).

Table 4. Document group structure II.

Category	Rugby	Board of education	
Document No.	15, 19	2, 3, 4, 11, 14, 16, 17, 18, 20	
Category	Distress accident	Center exam.	Others
Document No.	8, 12, 13	9, 10	1, 5, 6, 7

Table 5. Result II.

Ranking of representative documents expressed by Nos.
18, 10, 8, 5

### 4.2.2. Experiment II

We gathered top 20 documents obtained by a retrieval from Google News and those from Yahoo! Japan News using the retrieval keyword of 'Microsoft' on 22 January 2013. The name of document obtained was set to be the same as the rank by each retrieval, and then all documents were categorized in the same manner as those in the section 4.2.1.

#### (a) Google News

Table 6 shows the document group structure when we used Google News in our experiment. There were four kinds of categories (Table. 6). Table 7 shows the ranking of representative documents given by the proposed method when using  $J = 4$ . The six representative documents were extracted from all categories in the order of 'Others', 'Others', 'Windows 8', 'MS Essentials', 'Surface' and 'Others' (Table 7).

Table 6. Document group structure III.

Category	Windows 8	MS Essentials
Document No.	3, 5, 14	2, 6, 12
Category	Surface	Others
Document No.	9, 11, 15	1, 4, 7, 8, 10, 13, 16, 17, 18, 19, 20

Table 7. Result III.

Ranking of representative documents expressed by Nos.
18, 4, 3, 6, 11, 20

#### (b) Yahoo! Japan News

There were two kinds of categories (Table. 8). Table 9 shows the ranking for the document group shown in Table 8 by the proposed method.

Table 8. Document group structure IV.

Category	Cannon ITS	Others
Document No.	6, 9, 14	1, 2, 3, 4, 5, 7, 8, 10, 11, 12, 13, 15, 16, 17, 18, 19, 20

Table 9. Result IV.

Ranking of representative documents expressed by Nos.
2, 9, 15, 13, 20, 11

The six documents were extracted in the order of categories of 'Others', 'Cannon ITS', and four sets of 'Others' (Table. 9). In this document group, almost all documents belonged to the category of 'Others'. However, one document was extracted from the category of 'Cannon ITS' in the second order.

### 4.3. Discussion

#### 4.3.1. Document group structure dependency

When the document group had a distinct structure such as that in the sections 4.2.1 (a) & (b) and 4.2.2 (a), the performance of the proposed method was almost sound in the meaning that the documents can be extracted one by one from all categories except 'Others'. On the other hands, when the document group had a scattered structure such as that in the section 4.2.2 (b), it might not be meaningful to try to cover almost all contents by extracting the representative documents using the proposed method.

#### 4.3.2. Performance improvement

It might be necessary to apply the proposed method to many document-groups for finding out assignments of the proposed method. It might be effective to use a thesaurus for reducing the dimension of feature vector space, potentially resulting in extracting more appropriately representative documents and/or reducing the calculation cost.

#### 4.3.3. Definition of representative document

In the present study, the representative document was geometrically defined in the feature vector space. It is necessary to investigate the validity of the definition through questionnaires. In the investigation, other definitions on the representative document might be on the discussion.

## 5. Conclusion

We have developed a method for classification of Japanese documents and ranking of representative documents using characteristic of frequencies of nouns. The experiments where Web pages were collected and used for evaluating the efficiency of the proposed method proved the usefulness of the proposed method.

## References

1. F. Can and E. A. Ozkarahan, Computation of term/document discrimination values by use of the cover coefficient concept, *J. Amer. Soc. for Inf. Sci.*, **38**(3) (1987) 171-183.
2. A. Kawai, An automatic document classification method based on a semantic category frequency analysis (in Japanese), *J. IPSJ* **33**(9) (1992) 1114-1122.
3. N. Yuasa, T. Ueda, and F. Togawa, Classifying articles using lexical co-occurrence in large document databases (in Japanese), *J. IPSJ* **36**(8) (1995) 1819-1827.
4. K. Hatano, R. Sano, Y. Duan, and K. Tanaka, A classification view mechanism for web documents based on self-organizing maps and search engines (in Japanese), *J. IPSJ* **40**(SIG 3(TOD1)) (1999) 47-59.
5. H. Takamura and Y. Matsumoto, Co-clustering for text categorization (in Japanese), *J. IPSJ* **44**(2) (2003) 443-450.
6. H. Takamura and Y. Matsumoto, Constructive induction and text categorization with SVMs (in Japanese), *J. IPSJ* **44**(SIG 3(TOD 17)) (2003) 1-10.
7. R. Kusaya, T. Yamamura, H. Kudo, T. Matsumoto, Y. Takeuchi, and N. Ohnishi, Measuring similarity between documents using term frequency (in Japanese), *Trans IEICE* **J87-D-II**(2) (2004) 661-672.
8. Y. Bamba, K. Shinzato, T. Shibata, and S. Kurohashi, Web information observation using keyword distillation based clustering (in Japanese), *J. IPSJ* **50**(4) (2009) 1399-1409.
9. MeCab, <http://mecab.sourceforge.net/>
10. Yahoo! JAPAN News, <http://headlines.yahoo.co.jp/hl>
11. Google News, <https://news.google.co.jp/>

# Biped Robot Research at Waseda University

**Kenji Hashimoto**

*Research Institute for Science and Engineering, Waseda University,  
#41-304, 17 Kikui-cho, Shinjuku-ku, Tokyo 162-0044, Japan*

**Atsuo Takanishi**

*Department of Modern Mechanical Engineering, Waseda University,  
TWIns Room# 3C-202, 2-2, Wakamatsu-cho, Shinjuku-ku, Tokyo 162-8480, Japan  
E-mail: [contact@takanishi.mech.waseda.ac.jp](mailto:contact@takanishi.mech.waseda.ac.jp)  
[www.takanishi.mech.waseda.ac.jp/top/index.htm](http://www.takanishi.mech.waseda.ac.jp/top/index.htm)*

## Abstract

Waseda University has researched on biped robots since 1967. This paper describes our latest biped robots: (i) WABIAN-2, (ii) a biped running robot, and (iii) WL-16. WABIAN-2 is a biped humanoid robot and has realized a human-like walk with the knees stretched by utilizing a 2-DOF waist mimicking a human's pelvis motion. We are developing a new biped humanoid robot which can jump by utilizing a pelvic movement and leg elasticity. WL-16 is a human-carrying biped vehicle.

*Keywords:* Biped walking, Running, Humanoid robot, Legged robot, Walking chair

## 1. Introduction

Waseda University has researched on biped robots since 1967 and has been one of the leading research sites for humanoid robots since the late Prof. Ichiro Kato and his colleagues started the WABOT Project in 1970. We have developed a variety of humanoid robots including WABOT-1 which is the first full-scale human-like robot made in 1973 and the biped humanoid robot WABIAN in 1997.

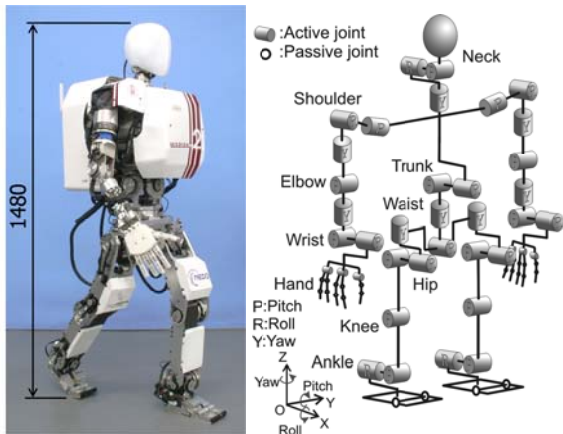
This paper describes our latest biped robots, WABIAN-2<sup>1</sup> (WAseda BIpedal humANoid - No. 2 Refined), a running robot<sup>2</sup> and WL-16<sup>3</sup> (Waseda Leg - No. 16).

## 2. Biped Humanoid Robot, WABIAN-2

We have developed a biped humanoid robot named WABIAN-2 as a human motion simulator to mimic human's motions and mechanisms (see Fig. 1).

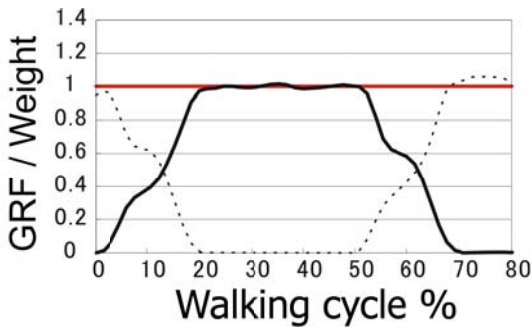
WABIAN-2 has 41 degrees of freedom (DoF) (two 6-DoF legs, a 2-DoF waist, a 2-DoF trunk, two 7-DoF arms, two 3-DoF hands, a 3-DoF neck and two 1-DoF feet having passive toe joint). Its height is 1480 mm with 63.8 kg weight. So far, WABIAN-2 has realized a human-like walk with the knees stretched, heel-contact and toe-off motion by utilizing a foot mechanism having a passive toe joint and a 2-DOF (Roll, Yaw) waist mimicking a human's pelvis motion. A notable feature of human walking is that the vertical ground reaction force (GRF) has two peaks. Two peaks do not appear when a robot walks with bending the knees as shown in Fig. 2(a). On the other hand, during the knee-stretched walking, we can find two peaks of the vertical ground force which are similar to the human ones (Fig. 2(b)).

WABIAN-2 can contribute to quantitatively evaluate welfare and rehabilitation instruments such as a walk-assist machine, an artificial leg and so on instead of human subjects. As one of the applications as the

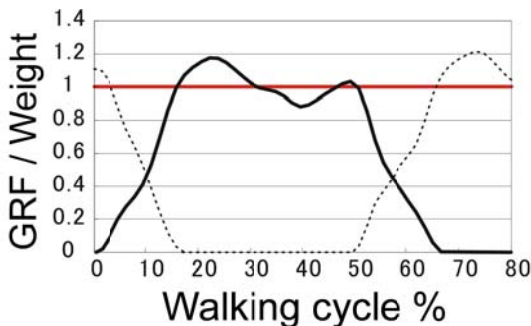


(a) Overview (b) DOF configuration

Fig. 1. Biped humanoid robot, WABIAN-2.



(a) Knee-bent walking



(b) Knee-stretched walking

Fig. 2. Ground reaction force.

human motion simulator, we carried out walking experiments with a walk-assist machine<sup>4</sup> (see Fig. 3). Generally, an armrest of a walk-assist machine is set to equal height of a user’s elbow. It is also known that the severer his/her disability is, the lower we should set the armrest. Measuring the current value of the motors at the knee joints and the forces and torques which are applied to the arms and legs, we can calculate the energy consumption at knee joints and the load to arms. Then we found the fact with quantitative data that the lower we set the height of the armrest, the less the load of knees is. This is a good example that human motion simulator can evaluate empirical facts quantitatively. From the results of these experiments, we confirmed that we can evaluate welfare equipment quantitatively with a human motion simulator.

We also use WABIAN-2 to clarify the function of the foot arch structure.<sup>5</sup> We developed a human-like foot mechanism that mimics the changes of the elasticity of the medial longitudinal arch with the change of the arch height during walking. As experimental results using a biped humanoid robot, WABIAN-2 mounted on the human-like foot mechanism, we confirmed that the arch elasticity could absorb a foot-landing force at the plantar contact phase and the windlass mechanism which caused change of the arch height contributed to a strong thrust at the push-off phase.

### 3. Biped Running Robot

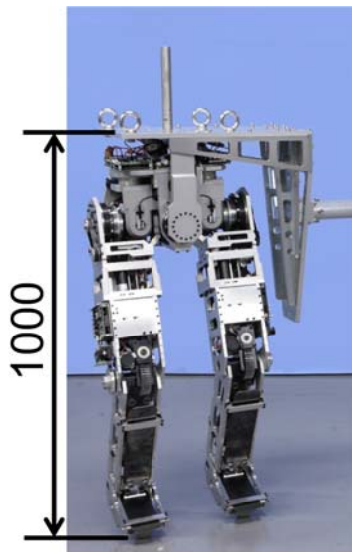
We are now developing a new biped humanoid robot that can mimic various characteristics of human running to investigate human running mechanisms and human motion control. If a biped running robot could perform motions that would improve sports performance, it



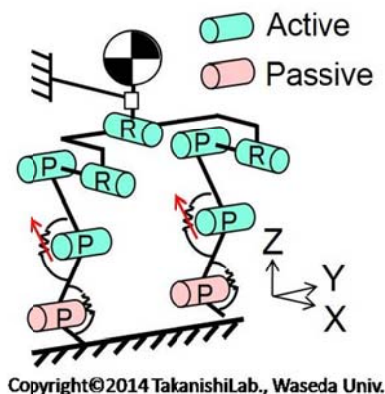
Fig. 3. Quantitative evaluation of walk-assist machine.

would be possible to identify more effective human running motions.

Human running can be modeled by a Spring Loaded Inverted Pendulum (SLIP) model, which is composed of a body mass and spring leg inspired by the linear relationship between the ground reaction force and the vertical body displacement during running.<sup>6</sup> This model describes human running in a simple, straightforward way and is used on the studies of biped running robots. Moreover, the knee and ankle joints of the standing leg act like torsion springs which emerge the leg stiffness.<sup>7</sup>



(a) Overview



(b) DOF configuration

Fig. 4. Biped running robot.

Furthermore, an important characteristic that has not yet been reported is that a human pelvic movement in the frontal plane can help to increase takeoff forces.

On the basis of the analysis of human running motion, we propose a new model named SLIP<sup>2</sup> (Spring Loaded Inverted Pendulum using Pelvis). This model is composed of a body mass, a pelvis, and leg springs. In this model, the knee and ankle joints of the standing leg act like torsion springs and the pelvic sine movement causes the resonance for hopping.

We have developed a biped running robot with a pelvis and a joint stiffness adjustment mechanism that uses two leaf springs to mimic the joint stiffness of a human leg during running (see Fig. 4). The robot has realized hopping motions by utilizing the pelvic movement and leg elasticity.

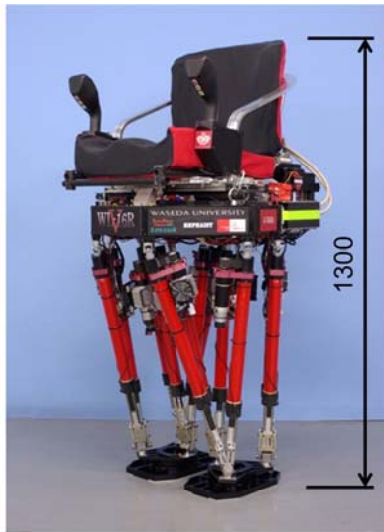
#### 4. Biped Vehicle, WL-16

We consider that a biped walking wheelchair is a viable solution in barrier-free engineering that is much more effective and low-cost than infrastructure improvements. Therefore, we have developed a human-carrying biped walking vehicle named WL-16 as shown in Fig. 5.

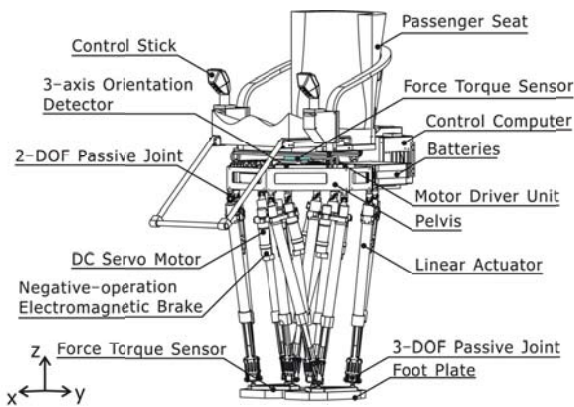
The weight of WL-16 is 74 kg including 11 kg battery weight. We adopt a lithium-ion battery of Micro Vehicle Lab., Ltd., which has no memory effect and is rechargeable without refreshing. Each leg mechanism has six linear actuators and passive joints at the both sides of each linear actuator. The upper passive joints are commercial universal joints using needle bearings which are small, lightweight and have little backlash. The lower passive joints are lightweight 3-DOF combination passive joints, which were newly developed in cooperation with HEPHIST Seiko Co., Ltd.

Each linear actuator consists of a 150W DC servo motor and a ball screw. The control computer is arranged at the rear of the pelvis, and the batteries, DC servo drives and an IMU sensor are arranged inside the pelvis. A passenger seat is on the pelvis, and a control stick is mounted on the passenger seat. A passenger can change the direction of the robot freely by using the control stick.





(a) Overview



(b) Mechanism and sensors

Fig. 5. Biped vehicle, WL-16.

## 5. Conclusions

We introduced our latest biped robots developed at Waseda University. WABIAN-2 is a biped humanoid robot and has realized a human-like walk with the knees stretched, heel-contact and toe-off motion by utilizing a foot mechanism having a passive toe joint and a 2-DOF (Roll, Yaw) waist mimicking a human's pelvis motion. We are developing a new biped running robot mimicking based on the analysis of human running motion. The running robot can jump by utilizing a pelvic movement and leg elasticity. WL-16 is a human-

carrying biped vehicle consisting of two Stewart Platform type legs and waist with a passenger seat. WL-16 can be used as a substitute for a wheel chair.

## Acknowledgements

This study was conducted as part of the Research Institute for Science and Engineering, Waseda University, and as part of the humanoid project at the Humanoid Robotics Institute, Waseda University. It was also supported in part by MEXT/JSPS KAKENHI (Grant Number: 24360099, 25220005 and 25709019), SolidWorks Japan K.K., HEPHIST Seiko Co., Ltd., and DYDEN Corporation whom we thank for their financial and technical support.

## References

1. Y. Ogura, H. Aikawa, K. Shimomura, H. Kondo, A. Morishima, H. O. Lim and A. Takanishi, Development of a Humanoid Robot WABIAN-2, in *Proc. of the 2006 IEEE International Conference on Robotics and Automation* (2006) 76-81.
2. T. Otani, M. Yahara, K. Uryu, A. Iizuka, K. Hashimoto, T. Kishi, N. Endo, M. Sakaguchi, Y. Kawakami, S. H. Hyon, H. O. Lim and A. Takanishi, Running Model and Hopping Robot Using Pelvic Movement and Leg Elasticity, in *Proc. of the 2014 IEEE International Conference on Robotics and Automation* (2014) 2313-2318.
3. K. Hashimoto, H. O. Lim and A. Takanishi, Disturbance Compensation Control for Biped Vehicle, *Advanced Robotics* **25** (3) (2011) 407-426.
4. Y. Ogura, H. Aikawa, K. Shimomura, H. Kondo, A. Morishima, H. O. Lim and A. Takanishi, Development of a humanoid robot capable of leaning on a walk-assist machine, in *Proc. of the IEEE RAS/EMBS International Conference on Biomedical Robotics and Biomechanics* (2006) 835-840.
5. K. Hashimoto, Y. Takezaki, K. Hattori, H. Kondo, T. Takashima, H. O. Lim and A. Takanishi, A Study of Function of the Human's Foot Arch Structure Using Biped Humanoid Robot, in *Proc. of the 2010 IEEE/RSJ International Conference on Intelligent Robots and Systems* (2010) pp. 2206-2211.
6. T. McMahon and G. Cheng, The Mechanics of Running: How does Stiffness Couple with Speed?, *J. Biomechanics* **23** (1990) 65-78.
7. M. Gunther, R. Blickhan, Joint stiffness of the ankle and the knee in running, *J. Biomechanics* **35** (2002) 1459-1474.

# Analysis of Genetic Disease Haemophilia A by Using Machine Learning

**Kenji Aoki**

*Information Technology Center, University of Miyazaki  
Gakuen-kibanadai-nishi 1-1, Miyazaki City, Miyazaki, 889-2192, Japan*

**Makoto Sakamoto and Hiroshi Furutani**

*Faculty of Engineering, University of Miyazaki  
Gakuen-kibanadai-nishi 1-1, Miyazaki City, Miyazaki, 889-2192, Japan  
E-mail: aoki@cc.miyazaki-u.ac.jp, sakamoto@cs.miyazaki-u.ac.jp, furutani@cs.miyazaki-u.ac.jp  
www.miyazaki-u.ac.jp*

## Abstract

Haemophilia A is a genetic disease resulting from deficiency of factor VIII. The database of mutations causing haemophilia A has been developed by the world wide collaboration. In this study, we examined the relation between activity of factor VIII and the missense mutation by using machine learning. As parameters, we used four physical-chemical parameters of amino acids. We predicted the severity of haemophilia A by using machine learning in factor VIII. As the result, logistic regression is not better than other methods in the prediction of haemophilia A severity. The result of the prediction improved in order to SVM, bagging, boosting and random forest. These results suggested that we can predict the haemophilia A severity by using these methods, and random forest was the best method in these five methods to predict the haemophilia A severity.

*Keywords:* Haemophilia A, Machine Learning, Factor VIII, Amino-acid, Mutation

## 1. Introduction

The haemophilia is a group of hereditary genetic disorders, in which one of the coagulation factors is deficient [1]. Haemophilia A is the most common form of disorder caused by low concentration of the coagulation factor VIII. Haemophilia B is another form of disorder caused by deficient factor IX. Haemophilia A accounts for about 85% of this disorder, while haemophilia B for 10–12% [2].

Haemophilia A and B are clinically indistinguishable from each other. Diagnosis must be confirmed by specific factor assay. It becomes very important to study mutations in genes responsible for diseases by biological experiment. However, it is a time-consuming, laborious and expensive task. Thus, it is necessary to develop computational method by

applying various approaches. We used a multiple regression model to predict the effect of a missense mutation in factor IX gene of haemophilia B patients [3]. In the past, we have demonstrated the calculations using Support Vector Machin (SVM) for the analysis of mutant factor VIII genes [4].

There have been reported a variety of defects in factor VIII gene from haemophilia A patients [5], and these are summarized in the haemophilia A database [6]. This database has data of clotting activity, nucleotide No., position, changed amino-acid and mutation type. In this study, we analyzed amino acid changing mutations, or missense mutations in the database described with factor VIII activity values. We adopted 439 cases from the database. We use the distances between 20 amino acids by using the four physical-chemical properties:

©The 2015 International Conference on Artificial Life and Robotics (ICAROB 2015), Jan. 10-12, Oita, Japan



Molecular volume, Hydropathy, Polar requirement and Isoelectric point. These distances are the differences between physical-chemical values before mutation and after mutation. In this study, we used some machine learnings to analyze of haemophilia A severity, and we compared these methods.

## 2. Methods

### 2.1. Haemophilia A Database

The gene coding for human factor VIII consists of 26 exons and 25 introns, and is located on the X chromosome [5]. Factor VIII is an essential blood-clotting protein, and synthesized as a precursor protein of 2351 amino acids. This includes a signal peptide and a mature protein of 2332 amino acids with domain structure A1-A2-B-A3-C1-C2. Classification of haemophilia A is presented in Table 1. Three A domains display approximately 30% homology to each other. The C domains are structurally related to the C domains of factor V. The B domain exhibits no significant homology with any other known protein. We used Haemophilia A Mutation Database [6]. The part of the database is shown in Table 2. This database includes exon number, amino-acid number, amino-acid change and activity of factor VIII (FVIII:C). Activity of factor VIII in a patient's blood depends on a position of the substitution and combination of original and substituting amino acids.

Table 1. Domain structure and number of data in Factor VIII.

Domain	Location	Number of data
A1	1 ~ 329	111
A2	330 ~ 711	131
B	712 ~ 1648	18
A3	1649 ~ 2019	107
C1	2020 ~ 2172	39
C2	2173 ~ 2332	33
total		439

Table 2. Mutation database of haemophilia A.

Exon Number	Amino-acid Number	Amino-acid Change	FVIII:C (%)
1	3	Arg Thr	1
1	6	Tyr Cys	6
1	10	Val Gly	<1

1	11	Glu Lys	1.5
1	14	Trp Gly	5
⋮	⋮	⋮	⋮

### 2.2. Machine Learning

We used five machine learnings for analysis of haemophilia A database. These are logistic regression, support vector machine, bagging, boosting and random forest. We used statistical application software “R” and packages for calculations. The packages are ‘kernlab’, ‘ipred’, ‘ada’ and ‘randomForest’.

#### 2.2.1. Logistic Regression

Logistic regression is a probabilistic statistical classification (regression) model. It is used for predicting the outcome of a categorical dependent variable based on predictor variables. It is a kind of generalization linear model using a logistic function.

#### 2.2.2. Support Vector Machine

SVM (Support Vector Machine) is supervised learning models with associated learning algorithms [7]. It is used for classification and regression analysis. Given a set of training data, SVM builds a model. It assigns new data into one category or the other. It is a non-probabilistic binary linear classifier.

#### 2.2.3. Bagging

Bagging is a method for generating multiple versions of a predictor and using these to get an aggregated predictor [8]. The aggregation does a plurality vote when predicting a class. The multiple versions are formed by making bootstrap replicates of the learning set. Tests on data sets using classification and regression trees show that bagging can give substantial gains in accuracy.

#### 2.2.4. Boosting

Boosting is a machine learning based on the idea of creating a highly accurate predictor by combining many weak rules of thumb [9]. A remarkably rich theory has evolved around boosting with connections to a range of several topics. Boosting algorithms have also made practical success in such fields as biology, vision, and speech processing.

### 2.2.5. Random Forest

Random forests are an ensemble learning method for classification and regression [10]. It operate by constructing a multitude of decision trees at training time and outputting the class that is the mode of the classes output by individual trees. The method combines bagging idea and the random selection of features, introduced in order to construct a collection of decision trees with controlled variance.

### 2.3. Dataset

We used data of haemophilia A Mutation Database. The number of data in A1, A2, B, A3, C1 and C2 domain are 111, 131, 18, 107, 39 and 33 respectively. We used all data in each domain for training data and test data in machine learning. We considered serious illness with less than 1% of factor VIII activity, and slight illness with more than 1% of one. We predicted the serious or slight illness of haemophilia A by machine learning based on these data.

We used a distance between amino acids for each four amino acid physical-chemical parameters (Molecular volume, Hydrophathy, Polar requirement and Isoelectric point). The k-th distance between amino acid  $A_i$  and  $A_j$  is defined as

$$D_{ij}^{(k)} = |f_k(A_i) - f_k(A_j)| \quad (1)$$

In this study,  $A_i$  is a normal amino acid, and  $A_j$  is a substituting amino acid.

## 3. Results

At first, we predicted the severity of haemophilia A by logistic regression, SVM, bagging, boosting (adaboost) and random forest using all domain data. Furthermore, we predicted severity of haemophilia A using each domain data.

In all figures, the horizontal axis is the false positive ratio, and the vertical axis is the true positive ratio. False positive means that the predicted result is positive (serious), but observed result is negative (slight). True positive means that both the prediction result and observed result are positive. False negative and true negative are similar to these. We plot the relationship between the false positive ratio and the true positive ratio in the figures. Such a figure is called ROC curve. ROC curve is used for a comparison of the inspection

performance, which in the upper left indicates more superior performance.

The result of prediction using all data is shown in Fig. 1. In Fig. 1, there are five curve these are the result of prediction by each machine learning method. The result of using logistic regression lies in more down right than other methods in the prediction of haemophilia A severity. The result of using random forest situated in the most upper left than other curves. Therefore, this result suggested that the predictions by random forest is the most superior performance in five machine learnings.

The result of prediction using one domain data is shown in Fig. 2, 3 and 4. Fig. 2, Fig. 3, Fig. 4 show the ROC curve of prediction using A1, A2, and A3 domain data, respectively. In all figures, the ROC curve using random forest method lies in upper left than other curves. This result is more remarkable in Fig. 2, 3 and 4 than Fig. 1. This result suggested that the predictions by random forest is also the most superior performance in five machine learnings using each domain data. We were not able to get a clear result in other domains, because number of data is too small in these domains.

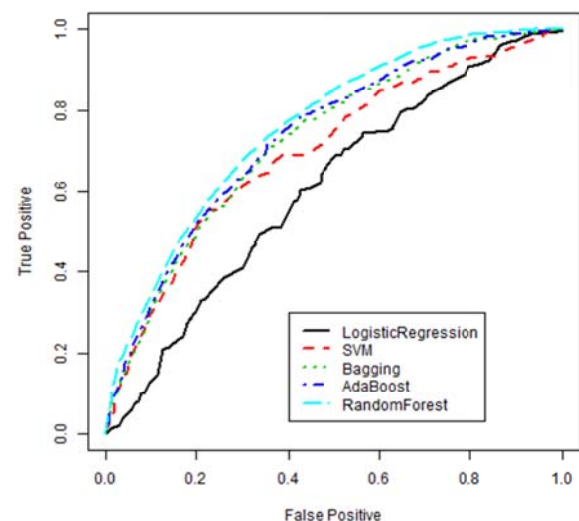


Fig. 1. ROC curve of prediction of haemophilia A severity using all domain data.

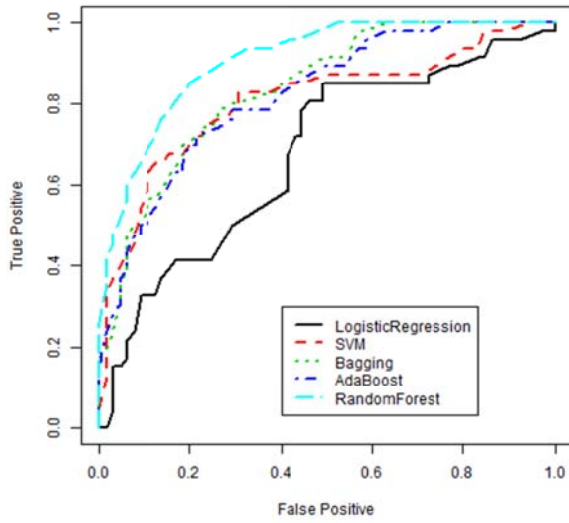


Fig. 2. ROC curve of prediction of haemophilia A severity using A1 domain data.

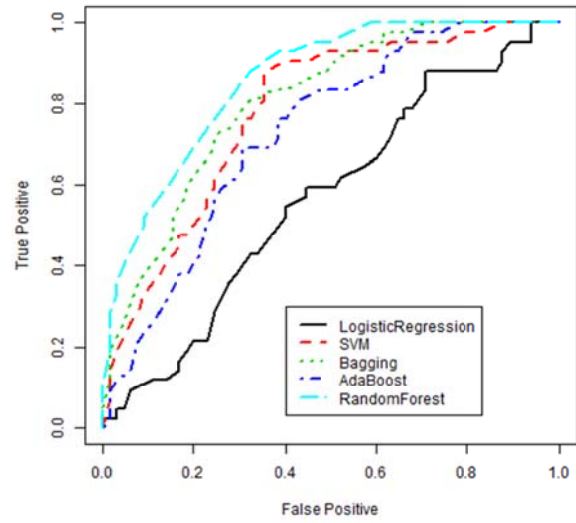


Fig. 4. ROC curve of prediction of haemophilia A severity using A3 domain data.

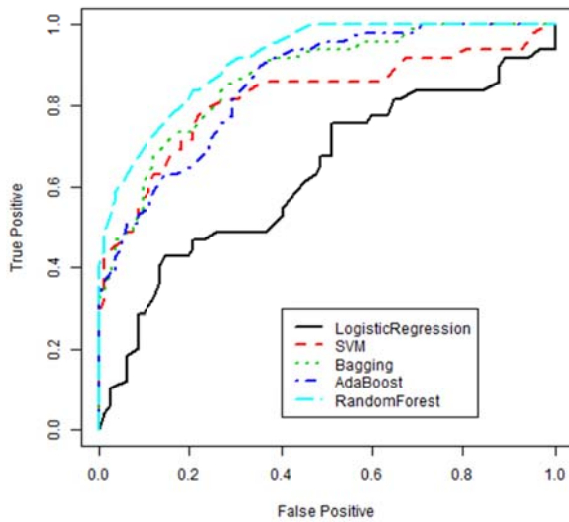


Fig. 3. ROC curve of prediction of haemophilia A severity using A2 domain data.

### References

1. P.H.B. Bolton-Maggs, K.J. Pasi, Haemophilias A and B, *The Lancet* **361** (2003) 1801-1809
2. B. Furie, B.C. Furie, The Molecular Basis of Blood Coagulation, *Cell* **53** (1988) 505-518
3. M. Utsunomiya, M. Sakamoto, H. Furutani, Regression Analysis of Amino Acid Substitutions and Factor IX Activity in Hemophilia B, *Artificial Life and Robotics* **13** (2008) 531-534
4. K. Aoki, K. Yamamori, M. Sakamoto, H. Furutani, SVM Analysis of Hemophilia A by Using Protein Structure, *Lecture Notes in Computer Science, Springer* **8227** (2013) 681-688
5. J. Gitschier, W.I. Wood, T.M. Goralka, et al. Characterization of the Human Factor VIII Gene. *Nature* **312** (1984) 326-330
6. G. Kemball-Cook, The Haemophilia A Mutation, Structure, Test and Resource Site (HAMSTeRS), <http://hadb.org.uk/> (11 February 2013 updated)
7. B. Schölkopf, C.J.C. Burges, A.J. Smola, Advances in Kernel Methods, The MIT Press, London (1999)
8. L. Breiman, Bagging Predictors, *Machine Learning* **24**(2) (1996) 123-140
9. J. Friedman, T. Hastie, R. Tibshirani, Additive Logistic Regression: A statistical view of boosting, *Annals of Statistics* **28**(2) (2000) 337-374
10. L. Breiman, Random Forest, *Machine Learning* **45**(1) (2001) 5-32

# Analysis of Asymmetric Mutation Model in Random Local Search

**Hiroshi Furutani\*** and **Makoto Sakamoto**

*Faculty of Engineering, University of Miyazaki, Gakuen Kibanadai-nishi 1-1  
Miyazaki City, Miyazaki Prefecture, 889-2192, Japan*

**Yifei Du**

*Graduate School of Engineering, University of Miyazaki, Gakuen Kibanadai-nishi 1-1  
Miyazaki City, Miyazaki Prefecture, 889-2192, Japan*

**Kenji Aoki**

*Information Technology Center, University of Miyazaki, Gakuen Kibanadai-nishi 1-1  
Miyazaki City, Miyazaki Prefecture, 889-2192, Japan*

*E-mail: furutani@cs.miyazaki-u.ac.jp*

## Abstract

In a standard Evolutionary Algorithms (EAs), one uses the same rate for mutations from bit 1 to bit 0 and its reverse direction. There are many reports that the asymmetric mutation model is a very powerful strategy in EAs to obtain better solutions more efficiently. In this paper, we report stochastic behaviors of algorithms that are asymmetric mutation models of Random Local Search (RLS). The mathematical structure of asymmetry model can be derived in terms of a finite Markov chain. We demonstrate some useful results representing the effects of asymmetric mutation.

*Keywords:* Random Local Search, Asymmetric mutation, Hitting time, Markov chain

## 1. Introduction

Theoretical studies of EAs have been performed from various viewpoints. One of the most attractive objects of them is the convergence properties of EAs [1]. In the previous conference, we have reported a randomized heuristics, which mainly treated the computational complexity of Random Local Search (RLS) [2]. Our study used the results obtained in researches on Coupon Collector Problem (CCP), and made a mathematical analysis of hitting time in RLS by extending the original model of CCP.

In this conference, we report another extension of RLS, an asymmetric mutation model. We apply the asymmetric mutation in evolution of RLS; that is,  $p_a$  for mutation  $0 \rightarrow 1$  and  $p_b$  for  $1 \rightarrow 0$ , respectively. We carry out a theoretical analysis for the evolution of strings in the framework of a finite Markov chain [3].

The asymmetric mutation model is a very powerful strategy in EAs to obtain better solutions more efficiently [4]. In biology, spontaneous misreading of bases during DNA synthesis, mutation, is considered as a major factor contributing to evolution [5]. Nei stated that the driving force behind evolution is mutation, with natural selection being of only secondary importance. Wada et al. showed that double-stranded DNA type strings can solve the knapsack problem effectively by using the asymmetric machinery of DNA replication [6]. They used different mutation rates for the leading and lagging DNA strands.

To analyze the behavior of the evolution processes, it is necessary to take into account of effects due to stochastic fluctuations. During the study of asymmetric mutation model of RLS, we noted mathematical papers in learning model with reinforcement, which gave the Markov chain model of learning processes [3]. We found that results in these papers can be interpreted as a

model of RLS with asymmetric mutation rates, and apply these results in the present study.

In this model, we obtained an explicit form of Markov chain transition matrix, and furthermore the eigenvalues of this matrix were calculated by using rather technical methods. The largest eigenvalue is naturally  $\lambda_0 = 1$ , and the second largest one is  $\lambda_1 = 1 - (p_a + p_b)/l$ . Since the most important factor to decide the speed of convergence is the second largest eigenvalue, we know the averaged value of two mutation rates mainly controls the speed of evolution. We will show in our report the behavior of solutions from the aspects of mathematical analysis and numerical simulations.

## 2. Evolutionary Algorithms

As a test function, we adopt OneMax function  $f(x)$

$$f(x) = \sum_{i=1}^l x_i, \quad x_i \in \{0,1\},$$

where  $x$  is a binary string of length  $l$ . We consider the maximization of OneMax function. The optimum solution is  $x_{opt} = \{1\}^l$ , and  $f(x_{opt}) = l$ .

1. The first choice of Evolutionary Algorithm is the Random Local Search (RLS). We define RLS as

---

### Algorithm 1 Random Local Search

---

- 1: Initialize  $x \in \{0,1\}^l$  uniformly at random.
- 2: Create  $x'$  by flipping one bit in  $x$  which is selected at random.
- 3: Select if  $f(x') > f(x)$  then  $x := x'$ .
- 4: Go to 2 until a termination condition is fulfilled.

2. The next one is RLS with asymmetric mutation (ARLS). The ARLS is defined as

---

### Algorithm 2 RLS of Asymmetric Mutation

---

- 1: Initialize  $x \in \{0,1\}^l$  uniformly at random.
- 2: Select one bit  $x[j]$  in  $x$  at random.
- 3: With probability  $1 - (p_a + p_b)$ ,  $x'[j] = x[j]$ .  
If  $x[j] = 0$  then  $x'[j] = 1$  with probability  $p_a$ .  
If  $x[j] = 1$  then  $x'[j] = 0$  with probability  $p_b$ .
- 4: If  $x[j]$  is flipped then  $x := x'$ .
- 5: Go to 2 until a termination condition is fulfilled.

3. The third one is a lazy version of RLS, which is defined as

---

### Algorithm 3 Lazy RLS

---

- 1: Initialize  $x \in \{0,1\}^l$  uniformly at random.
- 2: Select one bit  $x[j]$  in  $x$  at random.

- 3: Does not change  $x[j]$  with probability  $1 - p_a$ .

If  $x[j] = 0$  then  $x'[j] = 1$  with probability  $p_a$ .

- 4: If  $x[j]$  is flipped then  $x := x'$ .

- 5: Go to 2 until a termination condition is fulfilled.

This model is also defined as the variation of ARLS by putting  $p_b = 0$ .

## 3. Markov Chain Model

This section presents the Markov chain approaches to the EAs. The search space of OneMax function is  $\Omega = \{0,1\}^l$ , and we divide  $\Omega$  into  $(l + 1)$  subsets  $\Omega = S_0 \cup S_1 \cup \dots \cup S_l$ , where  $f(S_i) = i$ .

### 3.1. Asymmetric mutation model of RLS

The transition matrix  $P_{i,j} = P(j|i)$  represents the evolution of ARLS.

1. For  $j = i + 1$ ,  $0 \leq i < l$

$$P_{i,i+1} = p_a \left(1 - \frac{i}{l}\right).$$

2. For  $j = i - 1$ ,  $0 < i \leq l$

$$P_{i,i-1} = p_a \frac{i}{l}.$$

3. For  $i = j$ ,  $0 \leq i \leq l$

$$P_{i,i} = 1 - p_a \left(1 - \frac{i}{l}\right) - p_a \frac{i}{l}.$$

For example, the transition matrix for  $l = 3$  is given by

$$P = \begin{pmatrix} 1 - p_a & p_a & 0 & 0 \\ \frac{1}{3}p_b & 1 - \frac{2}{3}p_a - \frac{1}{3}p_b & \frac{2}{3}p_a & 0 \\ 0 & \frac{2}{3}p_b & 1 - \frac{1}{3}p_a - \frac{2}{3}p_b & \frac{1}{3}p_a \\ 0 & 0 & p_b & 1 - p_b \end{pmatrix}$$

The left eigenvectors  $\mathbf{u} = (u_0, u_1, \dots, u_l)$  satisfy, in the case of  $l = 3$ ,

$$\begin{aligned} (1 - p_a)u_0 + \frac{1}{3}p_b u_1 &= \lambda u_0, \\ p_a u_0 + \left(1 - \frac{2}{3}p_a - \frac{1}{3}p_b\right)u_1 + \frac{2}{3}p_b u_2 &= \lambda u_1, \\ \frac{2}{3}p_a u_1 + \left(1 - \frac{1}{3}p_a - \frac{2}{3}p_b\right)u_2 + p_b u_3 &= \lambda u_2, \\ \frac{1}{3}p_a u_2 + (1 - p_b)u_3 &= \lambda u_3. \end{aligned}$$

We define the  $l$ th order polynomial function

$$f(z) = u_0 + u_1 z + u_2 z^2 + u_3 z^3 + \dots + u_l z^l.$$

Multiplying eigenvalue equations with  $1, z, z^2, \dots, z^l$ , respectively, and summing them up, we have

$$l(p_a z + 1 - p_a - \lambda)f(z) - (z - 1)(p_a z + p_b)f'(z) = 0.$$

Considering this as a differential equation of  $f$ , we have

$$f(z) = C(z - 1)^k (p_a z + p_b)^{l-k},$$

$$k = \frac{l(1 - \lambda)}{p_a + p_b},$$

where  $C$  is an arbitrary constant. Since  $f(z)$  is a polynomial of  $l$ th order,  $k$  must be an integer of  $\{0, 1, \dots, l\}$ . Then the eigenvalues are given by

$$\lambda_k = 1 - \frac{k}{l}(p_a + p_b), \quad k = 0, 1, \dots, l. \quad (1)$$

The largest eigenvalue is  $\lambda_0 = 1$ , and the second largest one is  $\lambda_1 = 1 - (p_a + p_b)/l$ , which determines the convergence speed of the chain.

The eigenvector corresponding to the largest eigenvalue  $\lambda_0 = 1$  presents the distribution of the stationary state. In this case of  $k = 0$ , we have

$$f(z) = (p_a z + p_b)^l = \sum_{i=0}^l \binom{l}{i} p_a^i p_b^{l-i} z^i,$$

thus the components of eigenvector with normalization are given by

$$u_i = \binom{l}{i} p_a^i p_b^{l-i} / (p_a + p_b)^l, \quad (0 \leq i \leq l). \quad (2)$$

From this, we can obtain the average number of bit ones,

$$\bar{i} = l \frac{p_a}{p_a + p_b}.$$

Similarly, we have the variance

$$V(i) = l \frac{p_a \cdot p_b}{(p_a + p_b)^2}.$$

Both quantities depend on the ratio of two mutation rates  $p_b/p_a$ .

### 3.2. Lazy RLS

The transition matrix for the lazy RLS is given by

$$P = \begin{pmatrix} 1 - p_a & p_a & 0 & \dots & 0 \\ 0 & 1 - \frac{l-1}{l} p_a & \frac{l-1}{l} p_a & \dots & \vdots \\ \vdots & \vdots & \ddots & \ddots & \vdots \\ 0 & 0 & \dots & 1 - \frac{p_a}{l} & \frac{p_a}{l} \\ 0 & 0 & \dots & 0 & 1 \end{pmatrix} \quad (3)$$

This equation shows that the Markov chain is absorbing one, and there are  $l$  transient and one absorbing states, respectively. For absorbing Markov chains, the transition matrix is represented as

$$P = \begin{pmatrix} Q & R \\ 0 & I \end{pmatrix} \quad (4)$$

The  $l \times l$  submatrix  $Q$  shows transition probabilities among transient states  $S_0, S_1, \dots, S_{l-1}$ . Since there is only one absorbing state, the unit matrix  $I$  is a scalar 1.

For the calculation of the hitting time of the optimum solution, we use the fundamental matrix

$$N = (I - Q)^{-1}. \quad (5)$$

After some calculations, we have

$$N_{i,j} = 0, \quad (i > j)$$

$$= \frac{l}{(l-j)p_a}, \quad (i \leq j).$$

The expected step  $E_i(t)$  to enter into the absorbing state from the initial state  $i$  is given by the vector  $\mathbf{m}$  of  $(l \times 1)$  [3]

$$\mathbf{m} = N\mathbf{1},$$

where  $m_i$  is the expected step from  $i$ th state, and  $\mathbf{1}$  is a column vector whose all entries are 1. Thus, we have

$$m_i = \frac{l}{p_a} \sum_{j=i}^{l-1} \frac{1}{l-j} = \frac{l}{p_a} H_1(l-i) \quad (0 \leq i \leq l-1), \quad (6)$$

where  $H_1$  is the  $n$ -th harmonic number

$$H_1(n) = 1 + \frac{1}{2} + \dots + \frac{1}{n}.$$

The variance of  $t$  is given by

$$V(t) = (2N - I)\mathbf{m} - \mathbf{m}^2,$$

where  $\mathbf{m}^2$  is a column vector whose elements are  $m_i^2$ .

The explicit form of the variance is given by

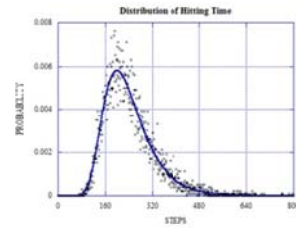
$$V_i(t) = \frac{l^2}{p_a^2} H_2(l-i) - \frac{l}{p_a} H(l-i), \quad (7)$$

where  $H_2(n)$  is the generalized harmonic number

$$H_2(n) = 1 + \frac{1}{2^2} + \dots + \frac{1}{n^2}.$$

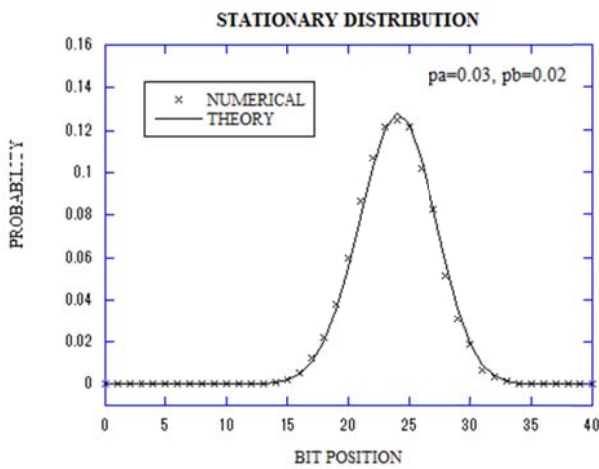
We have used the identity

$$2 \sum_{i=1}^n \frac{1}{i} H_1(i) - H_1(n)^2 = H_2(n).$$



#### 4. Numerical Experiment

In this section, we demonstrate theoretical predictions for ARLS and Lazy RLS, and present results of numerical calculations for comparison. We performed 10000 runs for each calculation, and obtained statistical quantities from them.



in  
10.  
12,  
the

Figure 1 shows the stationary distribution of the asymmetric mutation model. The string length  $l = 40$ ,  $p_a = 0.03$  and  $p_b = 0.02$ . The crosses are the result of numerical calculation. The solid line is the theoretical prediction obtained by eq.(2).

Figure 2 shows the distribution of the first hitting time of the optimum solution in Lazy RLS. The string length  $l = 20$  and mutation rate  $p_a = 0.3$ . The initial state is a bit string of all zeros. Dots are the numerical results. The solid line is the theoretical prediction obtained by using Markov chain transition matrix.

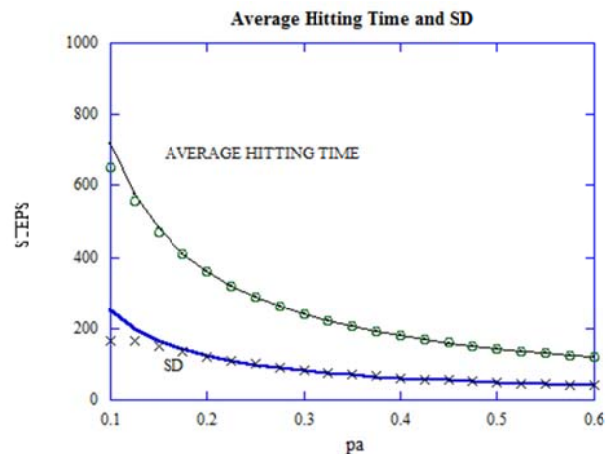


Figure 3 shows the dependence of the average hitting time and its standard deviation (SD) on mutation rate  $p_a$  in Lazy RLS. The string length  $l$  is 20. The initial state is a bit string of all zeros. The thin solid line is the theoretical prediction of the average hitting time, and the thick solid line represents the theoretical SD. Circles and crosses are numerical results.

#### 4. Summary

In this paper, we considered the behavior of the asymmetric mutation in the solving the optimization of OneMax function. This problem can be solved analytically in terms of a finite Markov chain [3]. We derived the explicit form of eigenvalues and eigenvectors, and obtained various quantities theoretically.

In genetic biology, it has been suggested by many statistical studies that asymmetric directional mutation pressures are commonly observed in weakly selected positions [7]. It is interesting to study the phenomena using the theoretical approach presented in this paper.

#### References

1. P. S. Oliveto and X. Yao (2011), Runtime analysis of evolutionary algorithms for discrete optimization, in *Theory of Randomized Search Heuristics*, A. Auger and B. Doerr (eds), World Scientific, Singapore, pp.21--52.
2. H. Furutani, H. Tagami, Y. Du, and M. Sakamoto (2014), Markov chain analyses of Random Local Search and Evolutionary Algorithm, in *Proceedings of the International Conference on Artificial Life and Robotics 2014*.
3. M. Iosifescu (1980), *Finite Markov chain processes and their applications*, John Wiley & Sons, New York.
4. B. Doerr, N. Hebbinghaus and F. Neumann (2007), Speeding up Evolutionary Algorithms through asymmetric mutation operator, *Evolutionary Computation* **15**, pp.401--410.
5. M. Nei (2013), *Mutation-Driven Evolution*, Oxford University Press, Oxford.
6. K. Wada, H. Doi, S. Tanaka, Y. Wada and M. Furusawa (1993), A neo-Darwinian algorithm: Asymmetrical mutation due to semiconservative DNA-type replication promote evolution, *Proceedings of National Academy of Science*, USA **90**, pp.11934--11938.
7. J. R. Lobry and N. Sueoka (2002), Asymmetric directional mutation pressures in bacteria, *Genome Biology* **3**, pp.58.1--58.14.



# Hitting Time Analysis of OneMax Problem in Genetic Algorithm

**Yifei Du**

*Graduate School of Engineering, University of Miyazaki, Gakuen Kibanadai-nishi 1-1  
Miyazaki City, Miyazaki Prefecture, 889-2192, Japan*

**QinLian Ma**

*Interdisciplinary Graduate School of Agriculture and Engineering, University of Miyazaki*

**Kenji Aoki**

*Information Technology Center, University of Miyazaki*

**Makoto Sakamoto and Hiroshi Furutani**

*Faculty of Engineering, University of Miyazaki*

**Yu-an Zhang**

*Department of Computer Science and Technology, Qinghai University, No. 251, Ning Road  
Xining City, Qinghai Province, 810016, China*

*E-mail: furutani@cs.miyazaki-u.ac.jp*

## Abstract

Genetic algorithms (GAs) are stochastic optimization techniques, and we have studied the effects of stochastic fluctuation in the process of GA evolution. A mathematical study was carried out for GA on OneMax function within the framework of Markov chain model. We treated the task of estimating convergence time of the Markov chain for OneMax problem. Then, in order to study hitting time, we study the state after convergence.

*Keywords:* genetic algorithms, OneMax problem, Markov model, convergence time, hitting time

## 1. Introduction

Since GAs are stochastic optimization methods, we have to take into account a stochastic fluctuation to explain the behaviors of evolution. To do this, we made use of the Wright-Fisher model<sup>1</sup>, a type of Markov chain method. For example, we considered the effects of crossover on the evolution speed of OneMax problem<sup>2</sup>, and carried out the microscopic investigation in terms of linkage analysis<sup>3</sup>. We also studied the convergence time of Markov chain in OneMax problem<sup>4</sup>. This analysis was performed by using the eigenvalues of transition matrix representing the behavior of population in the GA. From this analysis, we found that the convergence of GA to the stationary state can be represented approximately by mutation rate and string length. It is well known from the theory of finite Markov chain that ergodic Markov chain converges to the stationary distribution<sup>5</sup>. We obtained the approximate expression

for predicting the convergence time to the stationary state in terms of one parameter.

In this paper, we report the hitting time analysis of GA by the use of Markov chain theory. The hitting time is the step at which the optimum solution appears in a population for the first time during the process of GA evolution. To simplify the analysis, we have separated the process into convergence time  $T_c$  and hitting time after convergence  $T_h$ .

The convergence time  $T_c$  can be estimated by using the Markov chain theory. On the other hand, we estimate  $T_h$  by experiments of OneMax function, and survey the impact of parameters on the hitting time after convergence. Our results demonstrate that the hitting time distribution  $h(t)$  has an exponential form, and the logarithmic of  $h(t)$  is linearly decreasing function. This means the distribution is almost determined by one parameter  $b$ . We estimate the value of  $b$  from the experiments, and report the dependence of  $b$  on the

© The 2015 International Conference on Artificial Life and Robotics (ICAROB 2015), Jan. 10-12, Oita, Japan

population size and mutation rate.

## 2. Mathematical Model

We treat the evolution process of a population with  $N$  individuals. The individuals are represented by binary strings of length  $l$ , and there are  $n = 2^l$  genotypes,

$$i = \langle i(l), \dots, i(1) \rangle, i(k) \in \{0,1\}. \quad (1)$$

The OneMax fitness function  $f_i$  is defined as

$$f_i = \sum_{k=1}^l i(k). \quad (2)$$

Thus the string of all ones  $\langle 1,1, \dots, 1 \rangle$  is the optimum solution of this function.

## 3. Analysis of Hitting Time

In our model, we will investigate the distribution of hitting time  $H(t)$  approximately. Though it is difficult to obtain the theoretical expression of  $H(t)$ . Therefore, in order to study the hitting time  $T_H$  directly, we have separated  $T_H$  into converge time  $T_c$  and hitting time after converge  $T_h$ . By analyzing  $T_c$  and  $T_h$ , we can estimate the upper bound of hitting time<sup>1</sup>. So we assume

$$T_H \leq T_c + T_h. \quad (3)$$

We have used the concept of Markov chain to analyze convergence time  $T_c$ . In this study, we used experimental method to estimate the hitting time after convergence  $T_h$ . In this study, we obtained the hitting time distribution after convergence  $h(t)$  by the experiments.

### 3.1. Analysis of convergence

In our study, we used the Wright-Fisher model to theoretically analyze the process of population convergence. The Wright-Fisher model is one of the Markov model in population genetics<sup>6,7</sup>.

We consider the GA under positive mutation rate  $p_m > 0$ . In this case, all elements of the transition matrix  $P$  are positive, and the Markov chain of schema evolution is irreducible and aperiodic. The Markov chain theory states that an irreducible and aperiodic Markov chain converges to the stationary distribution  $\pi$

$$\lim_{t \rightarrow \infty} \mu(t) = \pi, \quad (4)$$

and all elements  $\pi_i$  are positive<sup>5</sup>.

In order to analyze the evolution of the first order schema, we referenced the total variation distance<sup>9</sup>. The total variation distance between the stationary distribution and the first order schema at generation  $t$

is defined as

$$TV(t) = \frac{1}{2} \sum_{i=0}^N |\mu_i(t) - \pi_i|. \quad (5)$$

By analyzing Markov chain, we have at large  $t$

$$TV(t) = C a^t, \quad (6)$$

where  $C$  is a constant. It should be noted that the convergence behavior is determined by only one parameter  $a$ . The parameter  $a$  is the second largest eigenvalue of the transition matrix<sup>8</sup>  $P$ .

$$a = \left(1 - \frac{1}{l}\right) (1 - 2p_m). \quad (7)$$

### 3.2. Analysis of hitting time after convergence

In this study, we obtained the hitting time distribution after convergence  $h(t)$  by using the experiments of OneMax problem. The distribution  $h(t)$  is the result of resetting generation  $t = 0$  when the population achieves the convergence state.

Our results demonstrate that the hitting time distribution  $h(t)$  is an exponential form,

$$h(t) = B(t)^t, \quad (8)$$

and the logarithmic of  $h(t)$  is linearly decreasing function

$$\log h(t) = t \log B(t). \quad (9)$$

Then, we transform this equation to

$$\log B(t) = \frac{\log h(t)}{t}. \quad (10)$$

We calculated the average of  $\log B(t)$ ,

$$\overline{\log B(t)} = \frac{\sum_t \log B(t)}{t}, \quad (11)$$

and defined a constant,

$$b = \exp(\overline{\log B(t)}). \quad (12)$$

We can defined that the distribution is almost determined by one parameter  $b$

$$h(t) \approx b^t. \quad (13)$$

We report the dependence of  $b$  on the parameters of GA, population size, mutation rate, and so on.

## 4. Experiments

We compared results of the theoretical prediction with GA experiments. Crossover is uniform crossover with crossover rate = 1. Mutation rate is  $p_m$  for each bit. Selection is roulette wheel selection. We averaged the results obtained by repeating 10000 calculations. The initial state was randomly generated with  $p^{(1)} = 1/2$ .

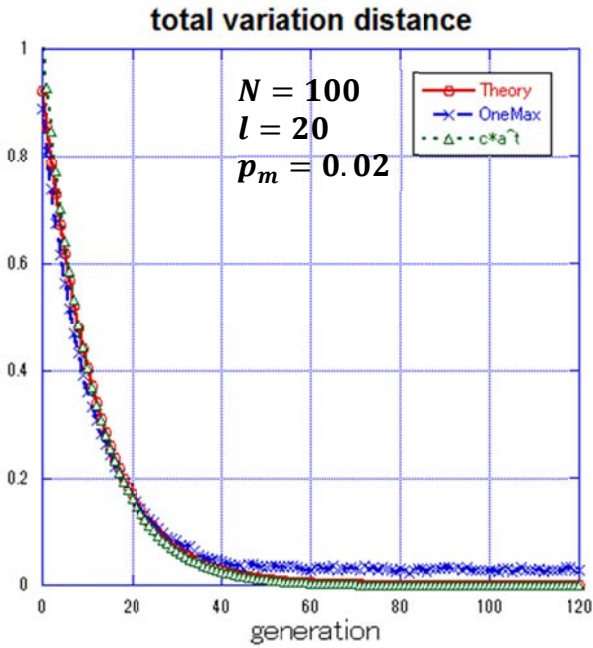


Figure 1 shows the results with  $N=100$ ,  $l=20$  and  $p_m = 0.02$ . We used the matching time  $tm=10$ . The dotted line is the approximate curve obtained by eq.(6). We found that the convergence behavior of the GA calculation is well reproduced by eq.(6).

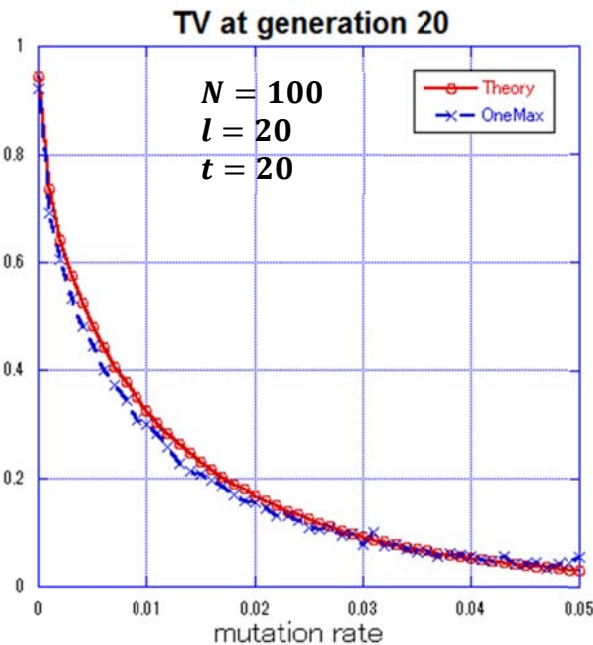


Figure 2 shows the results with  $N=100$  and  $l=20$ . We

© The 2015 International Conference on Artificial Life and Robotics (ICAROB 2015), Jan. 10-12, Oita, Japan

used the total variation distance at generation 20 to show convergence rate. The line of “Theory” is the result of theoretical calculations. The line of “OneMax” is the result of experiments. We can know that at the same time the smaller the total variation distance is, the faster the convergence rate is. Therefore we can know the result of experiments consists with the result of theoretical calculations. The consistent result is that mutation rate is larger while convergence rate is faster.

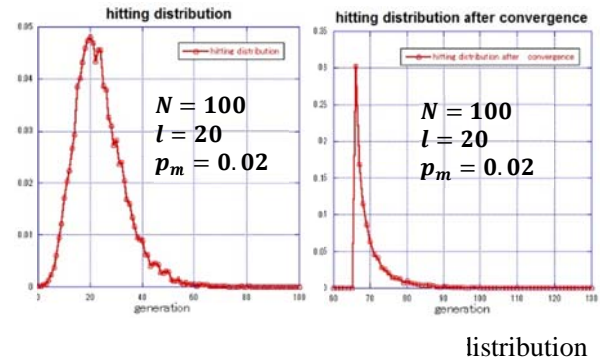


Figure 3 shows the results with  $N=100$ ,  $l=20$  and  $p_m = 0.02$ . The left figure is hitting time distribution  $H(t)$ . The right figure is hitting time distribution after convergence  $h(t)$ .

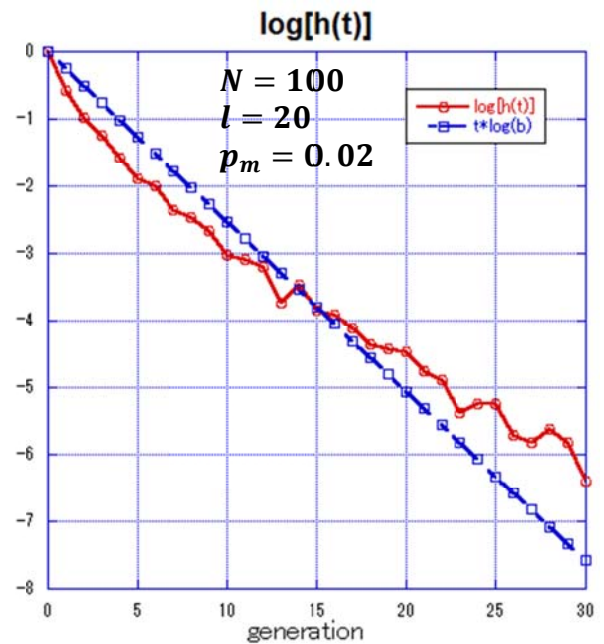


Figure 4 shows the results with  $N=100$ ,  $l=20$  and  $p_m = 0.02$ . We calculated the results by eq.(10) and eq. (11).

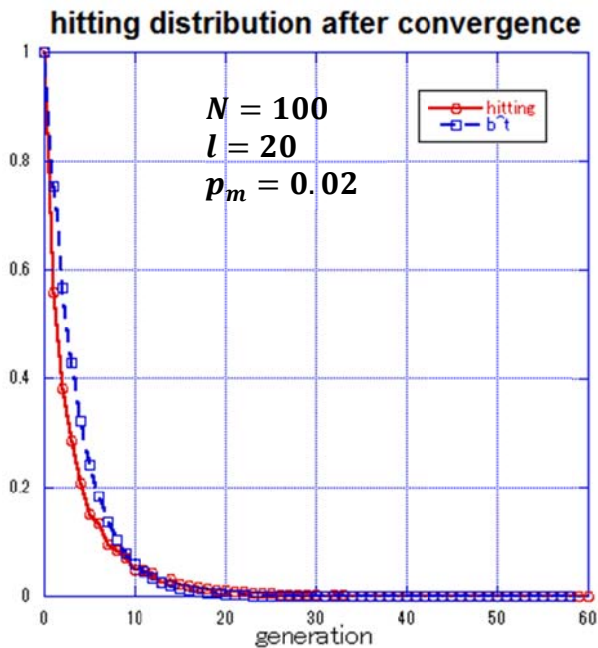
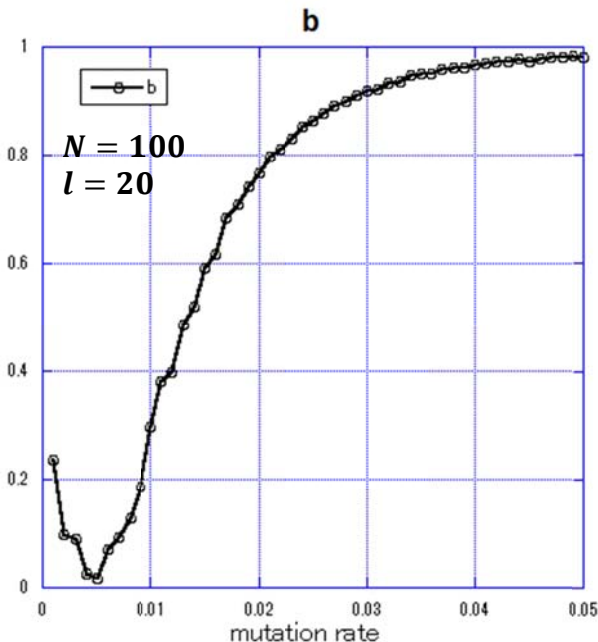


Figure 5 shows the results with  $N=100$ ,  $l=20$  and  $p_m = 0.02$ . The line of “hitting” is the distribution  $h(t)$  is the result of resetting generation when the population achieves the convergence state. The line of “ $b^t$ ” is the result of eq.(13). The two results are roughly consistent. So it means that the distribution is almost determined by one parameter  $b$ .



e

Figure 6 shows the results with  $N=100$  and  $l=20$ . From the results we can know that the larger mutation rate is, the slower hitting time is.

### 5. Summary

We studied the hitting time of GA calculation using the fitness function of OneMax. We have separated hitting time into convergence time and hitting time after convergence. We analyzed the effects of mutation rate on hitting time. In our previous results, we found that if mutation rate goes to large, convergence time becomes fast. In the present experiments, if mutation rate is larger, the hitting time after convergence becomes slower. Thus, we consider that there is a optimal value of mutation rate which can make the hitting time fastest.

### References

1. H. Furutani, S. Katayama, M. Sakamoto, M. Ito (2007), Stochastic Analysis of Schema Distribution in a Multiplicative Landscape, *Artificial Life and Robotics* 11:101–104.
2. Y. Du, Q. Ma, Y. Zhang, M. Sakamoto and H. Furutani (2014), Runtime Analysis of OneMax Problem in Genetic Algorithm, *Journal of Robotics, Networks and Artificial Life*, Vol. 1, No. 3.
3. H. Furutani, Y. Zhang and M. Sakamoto (2009), Study of the Distribution of Optimum Solution in Genetic Algorithm by Markov Chains, *IPSI, Transactions on Mathematical Modeling and its Applications*, 2:54-63.
4. H. Furutani (2003), Schema Analysis of OneMax Problem–Evolution Equation for First Order Schemata. in *Foundations of Genetic Algorithms 7*, Morgan Kaufmann, San Francisco, 9–26.
5. Q. Ma, Y. Zhang, K. Koga, K. Yamamori, M. Sakamoto and H. Furutani (2013), Stochastic analysis of OneMax problem by using Markov chain, *Artificial Life and Robotics* 17: 395-399.
6. J. W. J. Ewens (2004), *Mathematical Population Genetics. I. Theoretical Introduction*, Second Edition. Springer-Verlag, New York.
7. J. F. Crow and M. Kimura (1970), *An Introduction to Population Genetics Theory*, Harper and Row, New York.
8. W. Y. Tan (2002), *Stochastic Models with Applications to Genetics, Cancers, AIDS and Other Biomedical Systems*, World Scientific, Singapore.
9. D. A. Levin, Y. Peres and E. L. Wilmer (2008), *Markov Chains and Mixing Times*, American Mathematical Society, Providence.

# An Authentication Method for Mobile Devices that is Independent of Tap-Operation on a Touchscreen

<sup>1</sup>Hisaaki Yamaba, <sup>1</sup>So Nagatomo, <sup>2</sup>Kentaro Aburada, <sup>1</sup>Shinichiro Kubota,  
<sup>1</sup>Tetsuro Katayama, <sup>3</sup>Mirang Park, <sup>1</sup>Naonobu Okazaki

<sup>1</sup>University of Miyazaki, 1-1, Gakuen-kibanadai nishi, Miyazaki, 889-2192, Japan

<sup>2</sup>Oita National College of Technology, 1666, Maki, Oita, 870-015, Japan

<sup>3</sup>Kanagawa Institute of Technology, 1030, Shimo-ogino, Atsugi, Kanagawa, 243-0292, Japan

yamaba@cs.miyazaki-u.ac.jp, hf11036@student.cs.miyazaki-u.ac.jp, y.kita@ccy.kanagawa-it.ac.jp,

aburada@oita-ct.ac.jp, kubota@cs.miyazaki-u.ac.jp, kat@cs.miyazaki-u.ac.jp,

mirang@nw.kanagawa-it.ac.jp, oka@cs.miyazaki-u.ac.jp

## Abstract

At the present time, mobile devices such as tablet-type PCs and smart phones have widely penetrated into our daily lives. Therefore, an authentication method that prevents shoulder surfing is needed. We are investigating a new user authentication method for mobile devices that uses surface electromyogram (s-EMG) signals, not screen touching. The s-EMG signals, which are generated by the electrical activity of muscle fibers during contraction, are detected over the skin surface. Muscle movement can be differentiated by analyzing the s-EMG. In this paper, a series of experiments was carried out to investigate the prospect of an authentication method using s-EMGs. Specifically, several gestures of the wrist were introduced, and the s-EMGs generated for each motion pattern were measured. We compared the s-EMG patterns generated by each subject with the patterns generated by other subjects. As a result, it was found that each subject has similar patterns that are different from those of other subjects. Thus, s-EMGs can be used to confirm one's identification for authenticating passwords on touchscreen devices..

*Keywords:* mobile device, user authentication, shoulder surfing, electromyogram.

## 1. Introduction

This paper proposes a new user authentication method for mobile devices by using surface electromyogram (s-EMG) signals, not screen touching.

At the present time, mobile devices such as tablet type PCs and smart phones have widely penetrated into our daily lives. Therefore, an authentication method that prevents shoulder surfing is needed. Shoulder surfing is the direct observation of a user's personal information,

such as passwords. Authentication operations on mobile devices are performed in many public places, so we have to ensure that no one can view our passwords. However, many mobile devices have no keyboards, so the authentication method must use a touchscreen. When using a touchscreen, the owner of the mobile device inputs his or her authentication information through simple or multi-touch gestures. These gestures include, for example, designating his/her passcode from displayed numbers, selecting registered pictures or icons

from a set, or tracing a registered one-stroke sketch on the screen. People positioned close to the mobile device owner can easily grasp these actions and obtain the user's authentication information.

The s-EMG signals, which are generated by the electrical activity of muscle fibers during contraction, are detected over the skin surface. These s-EMGs have been used to control various devices, including artificial limbs and electrical wheelchairs. Muscle movement can be differentiated by analyzing the s-EMG<sup>1</sup>. For example, fast Fourier transform (FFT) can be adopted for the analysis. Feature extraction is carried out through the analysis of the s-EMGs. The extracted features are used to differentiate the muscle movement, including hand gestures.

In this paper, a series of experiments was carried out to investigate the prospect of realizing an authentication method using s-EMGs. Specifically, several gestures of the wrist were introduced, and the s-EMG signals generated for each motion pattern were measured. We compared the s-EMG signal patterns generated by each subject with the patterns generated by other subjects. As a result, it was found that the patterns of each individual subject are similar but they differ from those of other subjects. Thus, s-EMGs can confirm one's identification for authenticating passwords on touchscreen devices.

## **2. Characteristics of authentication method for mobile devices**

User authentication of mobile devices has two characteristics.

One is that an authentication operation is performed when a user wants to start using their mobile devices. The authentication often takes place around strangers. Therefore, the strangers around the user can possibly see the user's unlock actions. Some of these strangers may scheme to steal information such as passwords for authentication.

The other characteristic is that much user authentication of mobile devices is now performed on a touchscreen. Many current mobile devices do not have hardware keyboards, and so it is not easy to input long strings into such mobile devices. When users unlock mobile touchscreen devices, they input passwords or

personal identification numbers (PINs) by tapping numbers or characters displayed on the touchscreen. In many cases, the user moves only one finger. Since users have to look at their touchscreens while unlocking their devices, strangers around them can easily see the unlock actions, and so it becomes very easy for thieves to steal passwords or PINs.

To prevent shoulder-surfing attacks, many studies have been conducted. The secret tap method introduces a shift value to avoid revealing pass-icons<sup>2</sup>. The user may tap other icons in the shift position on the touchscreen, as indicated by a shift value, to unlock the device. By keeping the shift value secret, people around the user cannot know the pass-icons, although they can still watch the tapping operation. The rhythm authentication method relieves the user from looking at the touchscreen when unlocking the device<sup>3</sup>. In this method, the user taps the rhythm of his or her favorite music on the touchscreen. The pattern of tapping is used as the password. In this situation, the users can unlock their devices while keeping them in their pockets or bags, and the people around them cannot see the tap operations that contain the authentication information.

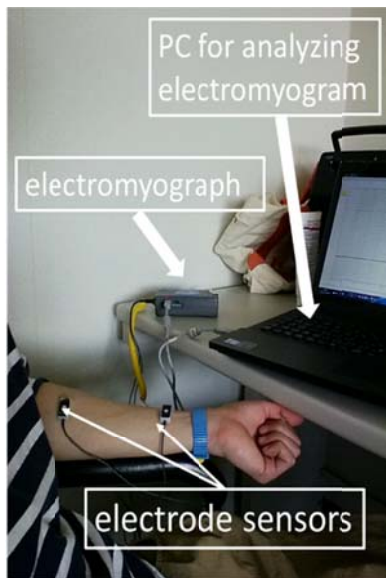
## **3. Surface electromyogram signals**

The s-EMG signals are detected over the skin surface and are generated by the electrical activity of muscle fibers during contraction. Muscle movement can be differentiated by analyzing the s-EMG. Usually, FFT is adopted for the analysis, and feature extraction is carried out through analysis of the s-EMG.

However, since measured s-EMG signals vary by subject, the extracted features do not show enough performance to correctly differentiate the muscle movement in multiple subjects. Therefore, researchers have explored other methods to improve the performance of feature extraction. Since some methods demonstrate good performance for some subjects but other methods show better performance for other subjects, a feature that can be used to distinguish gestures for everyone is desired. For example, a method that uses the maximum value and the minimum value of raw s-EMG signals was proposed<sup>4</sup>.

## **4. User authentication using s-EMG**





m

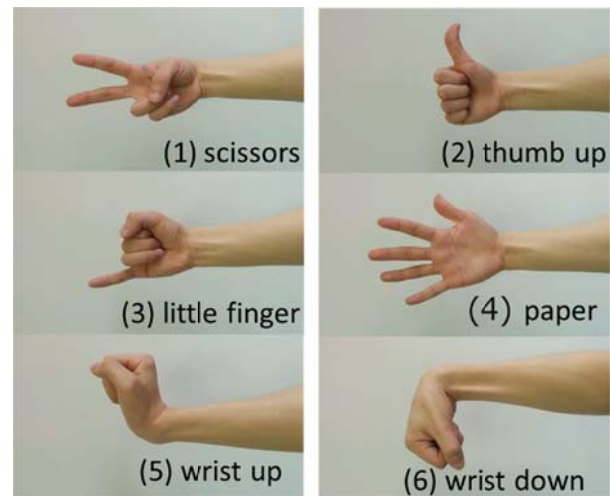
In this section, the method of user authentication by using s-EMGs, which do not require looking at a touchscreen, is presented.

The s-EMG signals are measured, and the features of the measured raw signals are extracted. We estimate gestures of a user of a mobile device from the extracted features. Next, combinations of the gestures are converted into a code for authentication. These combinations are inputted into the mobile device and used as a password for user authentication.

Adopting s-EMGs for authentication of mobile devices has two advantages. First, the user does not have to look at his/her device. Since the user can make a gesture that is used as a password on a device inside a pocket or in a bag, it is expected that the authentication information can be concealed. No one can see what gesture is made. In addition, it is expected that if another person reproduces a sequence of gestures that a user has made, the authentication will not be successful, because the extracted features from the s-EMG signals are usually not the same between two people.

## 5. Experiments

A series of experiments was carried out to investigate the prospect of the authentication method using s-EMGs.



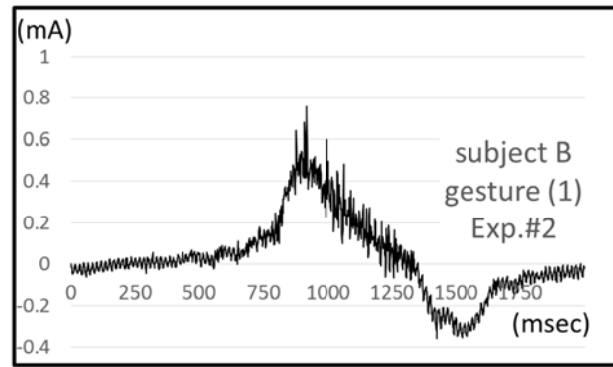
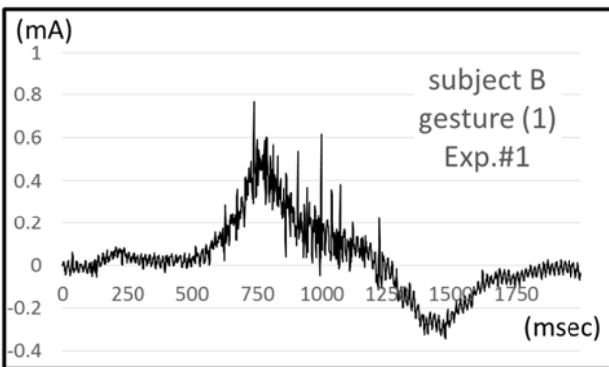
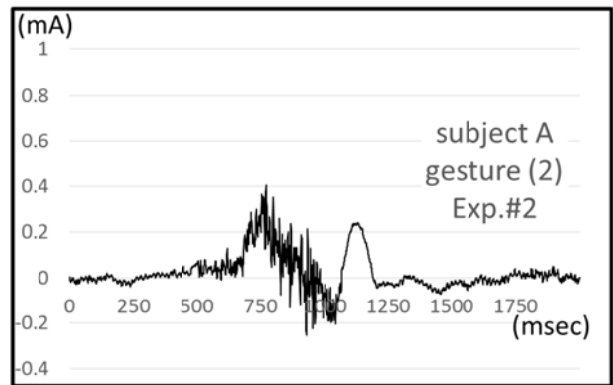
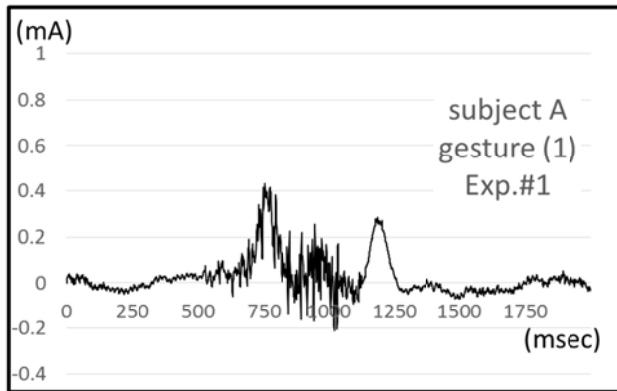
iments

Specifically, we investigated whether the measured s-EMG signals of one experimental subject were similar and whether the signals of different subjects were different from each other.

Figure 1 shows the experimental system used in these experiments. An electromyograph measured the s-EMG of each movement pattern with two electrode sensors. The measured data were stored and analyzed on a PC. Ten healthy persons whose ages were in the twenties (students of University of Miyazaki) participated as experimental subjects (Subjects A–J). The six hand gestures (1–6) shown in Figure 2 were introduced in the experiments. First, each subject made each gesture ten times in succession and their s-EMG signals were recorded (Exp. #1). Approximately one week later, the same experiment was carried out again (Exp. #2).

Some of the results are shown in Figure 3. The raw s-EMG signals of gesture 1 made by experimental subjects A and B are displayed. The signals of Exp. #1 and #2 are similar for each subject. On the other hand, the signals of subjects A and B are not similar to those of the other subject. The same results were obtained for every pair of subjects and all gestures.

These results show that the s-EMG is promising as identification input for a new user authentication method.



## 6. Conclusion

We investigated a new user authentication method that can prevent shoulder-surfing attacks in mobile devices. We know that the unlocking operations of mobile devices such as tablet-type PCs or smart phones can often be viewed by other people. Users can hide such operations from others by not looking at the touchscreen of a mobile device while unlocking it. To realize such an authentication method, we assigned a set of gestures to obtain the s-EMG signals. A series of experiments was carried out to confirm that the s-EMG signals of each person are similar for that person and the signals of different people are not similar to other people's signals. These results showed that s-EMG signals can be used as input for a new user authentication method. We will conduct a quantitative evaluation of this approach in future work.

## Acknowledgements

Useful advice and the experiment system were offered by Prof. K. Tanno, Prof. H. Tamura and Mr. K. Nagatomo of University of Miyazaki.

## References

1. H. Tamura, et al., A study on motion recognition without FFT from surface-EMG, IEICE-part D, J90-D(9), (2007) 2652-2655.
2. Y. Kita, et al., Implementation and evaluation of shoulder-surfing attack resistant users (In Japanese), IEICE-part D, J97-D(12), (2014) 1770-1784.
3. Y. Kita, et al., A Study of Rhythm Authentication and its Accuracy using the Self-Organizing Maps (In Japanese), Proceedings of DICOmO 2014, (2014) 1011-1018.
4. H. Tamura, et al., A study on the s-EMG pattern recognition using neural network, IJICIC, 5(12) (2009) 4877-4884.



# Proposal of Security Evaluation System using User's Reviews and Permissions for Android Applications

**Naonobu Okazaki**

*University of Miyazaki,  
1-1 Gakuen-Kibanadai-Nishi, Miyazaki, 889-2192, Japan*

**Yoshihiro Kita**

*Kanagawa Institute of Technology,  
1030 Shimo-Ogino, Atsugi, 243-0292, Japan*

**Kentaro Aburada**

*Oita National College of Technology,  
1666 Ooaza-Maki, Oita, 870-0152, Japan*

**Mirang Park**

*Kanagawa Institute of Technology,  
1030 Shimo-Ogino, Atsugi, 243-0292, Japan  
E-mail: oka@cs.miyazaki-u.ac.jp, y.kita@ccy.kanagawa-it.ac.jp,  
aburada@oita-ct.ac.jp, mirang@nw.kanagawa-it.ac.jp*

## Abstract

Leakage of the personal information in Android OS powered device by mal-applications is becoming the heavy matter. The Android OS users must be careful not to install mal-applications. The reviews and the using permissions of applications are useful by users to detect mal-application. However, the most of users read the reviews only. All users must be cautious about not only the using permissions but also the combination of them. In this paper, we propose the security evaluation system to prevent the installation of mal-applications on Android OS. This system indicates the user reviews with the using permission information of application to new users. *Keywords:* Security for applications, Mal-applications, User's reviews, Permissions, Android OS.

## 1. Introduction

Recently, leakage of the personal information in Android OS powered device by mal-applications is becoming heavy matter. Google implements mal-application detection system "Bouncer" for Google play[1]. However, mal-applications are not eliminated completely, even how to defeat Bouncer legally has been found also.

Google Play provides the using permissions of application to users when downloads there. The users

not read the permissions, because it is need to consider combination of permissions, and have specialized knowledge for permissions.

The most of the users get the information of application from user reviews. A part of exist reviews is useless review that is the malicious review or the unrelated review to contents of the application. There is the problem that it is difficult to determine the mal-application by users using the existing user reviews.

In this paper, we propose the security evaluation system using user reviews for Android OS. This system

© The 2015 International Conference on Artificial Life and Robotics (ICAROB 2015), Jan. 10-12, Oita, Japan

shows the user reviews with the using permission information of application to new users. New user evaluates the one of reviews, and determines to download or not download the application. The evaluation of the review is transmitted to reviewer. The reviewer refers to the evaluation of review for next review.

## 2. Preceding Studies

Reviews are useful as guidelines for new users to download the application. However, if the mal-application developer writes the review of the application in order to be installed it by users, this review is exaggerated review or fake review. The other users trust these review, and are suffered damage by mal-applications.

It is impossible to remove the vulnerability of applications completely, but guidelines of secure applications for Android developers (i.e. iSEC Partner[2]) are issued by various organizations for security information.

Existing review system (i.e. Google play[1]) show reviews of user and using permissions to new users. It is possible to predict the risk of application from reviews and permissions, because these are indicate the behavior of application. But, users can not understand the risk of application adequately, because these are not indicate the risk of application in combination with other permissions, and it is difficult to understand the behavior of application by users who do not understand the expertise of security and function of mobile terminals.

Matsudo[3] proposed security advisor system, which indicates the risk of application by the combination of permissions. This system shows the number of download and the risk level of application to new users. However, these values are not objective and fair measure, because other users can manipulate these values intentionally, and new users do not have information enough to determine the application downloading by these values only. It needs for new users to show the user's reviews of applications in order to get the information of applications.

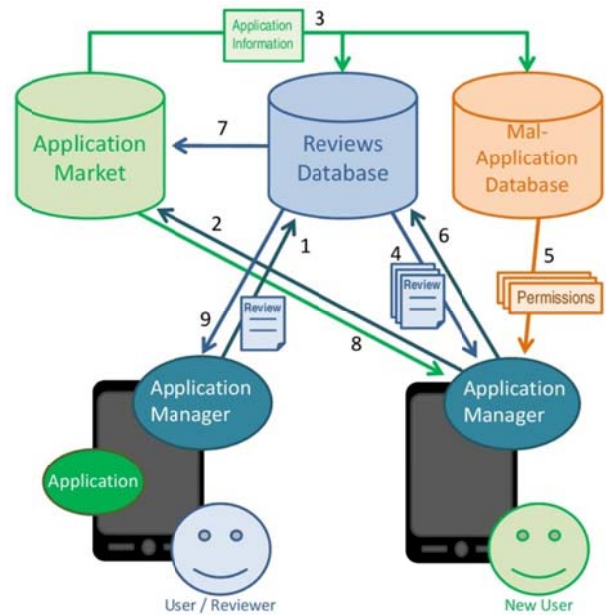


Fig. 1. Structure of security evaluation system.

## 3. Security Evaluation System

We propose security evaluation system, which indicate the risk of application by the reviews and using permissions. This system indicates the reviews and the evaluation of them. Fig.1 shows the structure of security evaluation system. This system consists of three parts as follows:

- **Reviews Database**  
This is storage of reviews and the evaluation of reviews, which are sent from all users.
- **Mal-Application Database**  
This is the storage of permissions and the information of mal-applications (i.e. application's name, version, developer).
- **Application Manager**  
This is the application which indicates the reviews and the risk of applications by the combination of permissions to terminal user, and transmits the user's review to review database.

Table 1. Risk allowances of applications.

	Safety	Caution	Danger
Does the application have the one or more dangerous permission?	NO	YES	YES
Does the application have the dangerous combination of permissions?	NO	NO	YES
Is the application reported as mal-application?	NO	NO	YES/NO

The procedure of this system is described as follows:

1. The user which is using the application sends a review to review database through the user's application manager.
2. New user requests the download of the application to the application market.
3. The application market sends the information of the application (i.e. name, developer, request user's name) to reviews database and mal-application database.
4. Reviews database shows the all review and the evaluation of them for the application to new user through the new user's application manager.
5. Mal-application database shows the information of using permissions and the information of mal-application to new user.
6. New user gives the evaluation "Good" or "Bad" for the one of the reviews, and reports the evaluation of the review to reviews database through the application manager.
7. Reviews database stores the evaluation of review, and permit the download of the application to application market.
8. New user downloads the application to application market through the application manager.
9. Reviews database reports the evaluation of the review to existing user as reviewer.

Reviews have two types: positive reviews and negative reviews. Positive reviews include selling points or good features for the application. Negative reviews include wrong points or problems of the application. The

Table 2. The permissions concern the personal information or the information leak.

Permissions concern personal information	Permissions concern information leak
READ_CONTACTS	INTERNET
WRITE_CONTACTS	SEND_SMS
READ_CALENDAR	BLUETOOTH
WRITE_CALENDAR	NFC
READ_LOGS	USE_SIP
BIND_APPWIDGET	CHANGE_NETWORK_STATE
READ_PROFILE	BLUETOOTH_ADMIN
WRITE_PROFILE	
ACCESS_FINE_LOCATION	
ACCESS_COARSE_LOCATION	
ACCESS_MOCK_LOCATION	
GET_ACCOUNT	
READ_EXTRNAL_STORAGE	
WRITE_EXTRNAL_STORAGE	

reviews are evaluated not only new users but also existing user instead of writing the review.

The permissions have the four protection levels[4]: "normal," "dangerous," "signature," and "signatureOfSystem." Table.1 shows the risk allowances of applications that we defined. We divide the risk of applications into three levels as follows according to the protection levels and the combination of permissions.

- Safety  
All permissions use the protection level "normal" only.
- Caution  
Permissions use the protection level "dangerous," "signature," or "signatureOfSystem."
- Danger  
The application is permitted the functions which include both connecting internets and accessing the personal information, plus the condition of "Caution."

Table.2 shows the permissions concern the personal information or the information leak. The applications include these permissions are allocated the risk of applications "Danger."

Fig.2 shows the example of indication for risk allowances of applications. The application manager indicates the risk of the application using the kinds of



# Evaluation of Neighbors Based Routing for ad hoc networks

**Kentaro Aburada**

*Oita National College of Technology, Japan*

**Hisaaki Yamaba, Shinichiro Kubota, Tetsuro Katayama**

*University of Miyazaki, Japan*

**Mirang Park**

*Kanagawa Institute of Technology, Japan*

**Naonobu Okazaki**

*University of Miyazaki, Japan*

## Abstract

In ad hoc networks, due to the mobility of nodes, communication links are unstable and restricted. As such, an efficient routing protocol is needed in order to solve these problems. In the present paper, we propose a neighbors based routing (NBR) protocol by constructing paths in an area in which a large number of nodes exists.

*Keywords:* Ad hoc networks, Routing Protocol, Route Repair, AODV-BR

## 1. Introduction

In recent years, mobile ad hoc networks (MANET) have attracted attention because of the development and popularization of wireless communication technology [1].

Mobile ad hoc networks can be constructed by mobile nodes without a fixed infrastructure. These nodes can send packets directly to each other by wireless communication. Moreover, a node can communicate with other distant nodes, which are outside radio range, by relaying packets. Therefore, MANET is expected to be used as communication tool in emergency situations, for example, at disaster sites, and for data-gathering using sensors. However, due to the mobility of nodes and the limitation of battery capacity, MANET has

problems such as route disconnection and a decrease in the packet reception ratio (PRR).

In MANET, various routing protocols are actively being investigated [2]–[5]. It is important to reduce the risk of route disconnections, for example due to increases in power consumption and waiting time, in wireless routing.

Accordingly, methods for repairing disconnected links in

[2] and avoiding an interference region in [4] [5] have been proposed. As an expansion of the ad hoc on-demand distance vector (AODV) [3]), which is the typical routing protocol used in MANET, the AODV-BR (AODV with backup routes) was proposed to repair disconnected links

[2]. In the AODV-BR, nodes around the constructed route have alternate paths to other nodes on the route, which are used in order to repair disconnected links. When the AODV-BR detects a disconnected link, the node at the link broadcasts data packets. Thus, nodes that receive these packets can restart communication using an alternate path. A method of using a node as position information by GPS as a means of routing instead of flooding was proposed in previous studies [4] and [5]. In [4],  $PRR \times Distance$  was proposed in order to avoid the interference region based on the packet reception rate (PRR) and the distance to the destination. In addition, in [5], interference-aware energy efficient geographical (IEG) routing was proposed based on the power efficiency of each link.  $PRR \times Distance$  measures the PRR by packet exchange with neighbor nodes. However, the effectiveness of the PRR decays due to frequent node mobility. Thus, each node must measure PRR repeatedly. Consequently,  $PRR \times Distance$  cannot immediately adapt to changes in a network. In the IEG, a route that has high power efficiency is constructed by means of measuring the radio field strength instead of the PRR. Therefore, links on the route are shorter than  $PRR \times Distance$  and, as a result of node mobility, are difficult to disconnect.

## 2. Problems with Existing Protocols

In the AODV-BR, a route that does not consider neighbor nodes is constructed. Hence, the number of alternate paths is reduced and it is difficult to repair disconnected links. The AODV-BR cannot repair the route flexibly because the disconnected of the alternate path is not considered. In addition, although a route is not constructed in the interference region the route can be constructed around the interference region (Fig. 1). In this case, some of the nodes around the route are in the interference region and may be not available for repairing the route.

In the IEG, each node requires a device that can measure the radio field strength. In addition, since position information is used to choose the next node, the IEG ceases routing in topologies such as that shown in Fig. 1. In Fig.1, as a next hop, node N must choose a neighbor node that is closer to the destination. These topologies frequently appear upon expansion of the interference region. Once the routing ceases, the IEG

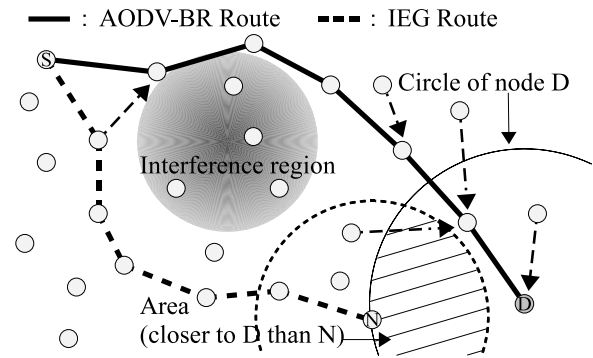


Fig. 1. Problems of existing protocols.

switches over to the AODV and resumes communication. However, the AODV has problems with packet loss and power consumption because packets are sent to nodes to which the IEG has already sent an RREQ.

## 3. Proposed Method

In the present paper, we propose an NBR protocol that can easily repair disconnected links by constructing a route based on a number of neighbor nodes and alternative paths.

First, the source node floods RREQs, and each node confirms the state of links with neighbor nodes. The destination node then sends back an RREP upon receiving an RREQ. The RREP is then transmitted to the source node while constructing routes and alternative paths. The source node can receive route information but communicates using the route that has the largest number of neighbor nodes on these routes. In addition, each node can use its route information as an alternative path to repair a disconnected link. Consequently, the NBR can easily repair the disconnected link. Moreover, the NBR introduces the concept of the extension variable in order to increase the number of alternative paths and broaden the route construction area.

### 3.1. Route Evaluation Formula

In the NBR, alternative paths are recorded in the route table of each node around the route as the AODV-BR. In addition, in the NBR, each node on the route records the paths in the same manner. These paths are the reutilization of received route information. Hence, a

significant amount of route information may lead to easier repair. In the NBR, a node that has several neighbor nodes can receive a great deal of route information. Therefore, the evaluation value  $E$  of the route can be derived as follows:

$$E = \frac{N_{sum}}{h}$$

where  $N_{sum}$  denotes the sum of the neighbor nodes of each node on a route, and  $h$  denotes the number of intermediate nodes between the destination and the node that has received the route information. The source node decides the route that has the highest  $E$  using Eq and uses this route for communication. In addition, each node can reduce traffic by relaying only route information that has a higher  $E$ .

### 3.2. Extension Value

The NBR obtains the hop count from the source node by receiving an RREQ. Each node constructs a route by sending an RREP to a node that has a lower hop count. Thus, an RREP does not reply to a node that has a high hop count. As a result, the NBR cannot construct a route that has several alternative paths, and cannot sufficiently respond to disconnected link. Therefore, the NBR introduces the concept of Extension Variable for transmitting an RREP to a node that has a high hop count.

In the present paper,  $k$  denotes the value of Extension Variable. Here,  $k$ , which is configured in advance, refers to the number of times that a node can rule out the limit of hop count in the transfer condition of an RREP. The NBR can increase the number of alternative paths and broaden the route construction area.

Fig.2 shows an example of a route with  $k = 2$ . The route has 20 neighbor nodes and contains five intermediate nodes. Therefore, the evaluation value of the route is 4. When  $k = 0$ , the route is constructed by under route (Fig.2).

### 4. Evaluation

In order to evaluate the performance of the proposed method NBR, we compare the simulation results of NBR with the traditional AODV-BR method. The simulation measured the packet delivery ratio and the control overhead using Network Simulator-2 (NS-2) [6].

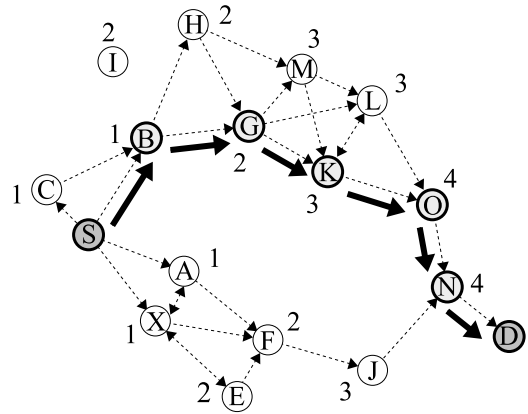


Fig. 2. Example of NBR ( $k = 2$ ).

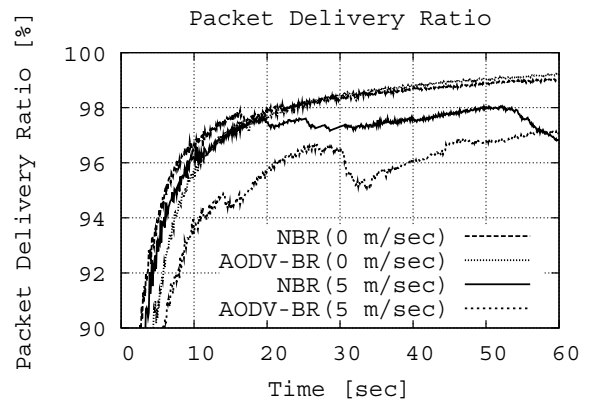


Fig. 3. Packet delivery ratio.

In the simulation, we compare the results for a topology with a moving node to the results for a topology without a moving node. We evaluate the wait time until route construction, the packet delivery ratio, and the control overhead.

#### 4.1. Simulation Environment

The proposed simulation modeled a network of 100 mobile nodes placed randomly within a 1,000 meter x 1,000 meter area. Two of the nodes were placed at (100, 100) and (900, 900) as a source node and a destination node, respectively. We used IEEE 802.11 as the medium access control protocol. The radio propagation range for each node was 250 meters, and the channel capacity was 2Mbps. During the simulations, each node

moves according to the random waypoint model at a speed of up to 5 m/s.

The source node transmits data packets to the destination at a rate of five packets per second. The size of the data payload is 1,024 bytes. Each run is executed for a simulation time of 60 seconds. These parameter uses [2] as a reference.

#### 4.2. Packet delivery ratio

The packet delivery ratios with NBR and the AODV-BR are shown in Fig. 3. Note that both NBR and the AODV-BR have high packet delivery ratios in topologies without node mobility. However, in topologies with moving nodes, the packet delivery ratio of the AODV-BR decreases more than that of NBR. Since NBR constructs several alternate paths, NBR can repair broken links due to moving nodes.

On the other hand, the AODV-BR cannot repair such broken links because the AODV-BR has relatively few alternate paths. Therefore, the individual nodes cannot forward data packets to the destination, and the packet delivery ratio of the AODV-BR decreases in topologies with moving nodes.

#### 4.3. Control overhead

Fig.4 shows the control overhead with NBR and the AODV-BR. Both NBR and the AODV-BR have slightly increased control overheads in topologies without moving nodes. However, in topologies with moving nodes, the control overhead of the AODV-BR increases significantly to approximately 120 kbytes. The control overhead of NBR increased but eventually settled at approximately 30 kbytes. The frequency of route reconstruction by the AODV-BR is higher than that for NBR for all simulations. On average, the route reconstruction frequency is 1.2 times per simulation for NBR and 10.2 times per simulation for the AODV-BR. This indicates that the control overhead of the AODV-BR was increased due to the numerous route reconstructions performed by the AODV-BR.

#### 5. Conclusion

We proposed neighbors-based routing (NBR), which constructs alternative paths and routes based on the number of neighbor nodes. Since NBR uses extension

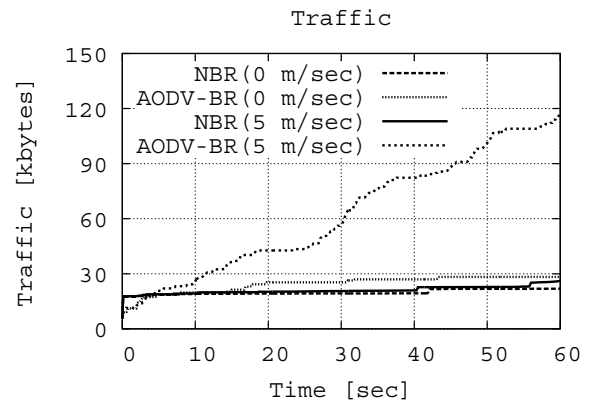


Fig. 4. The control overhead.

variable  $k$  to increase the number of alternative paths and broaden the route construction area, NBR can easily repair disconnected links using alternative paths. In order to evaluate NBR, we compare the packet delivery ratio with the control overhead of NBR and the traditional AODV-BR method using NS-2. The results indicate that

NBR maintains a high packet delivery ratio in topologies with moving nodes, and the present simulations confirmed that the proposed protocol has a higher connectivity and a lower control overhead than existing protocols in topologies with moving nodes.

#### References

- [1] C-K.Toh.: "Ad Hoc Mobile Wireless Networks: Protocols and Systems", Prentice Hall (2001).
- [2] S-J, Lee. and M, Gerla.: "AODV-BR: Backup Routing in Ad hoc networks", Proc. of IEEE Wireless Communications and Networking Conference, Vol. 3, pp. 1311-1511 (2000).
- [3] C, Perkins., E, Belding-Royer. and S, Das.: "Ad hoc on-demand distance vector (AODV) routing", <http://www.ietf.org/rfc/rfc3561.txt> (2003).
- [4] K, Seada., M, Zuniga., A, Helmy. and B, Krishnamacharim.: "Energy-efficient forwarding strategies for geographic routing in lossy wireless sensor networks", Proc. ACM SenSys, pp. 108-121 (2004).
- [5] J, Kim. and Y, Kwon.: "Interference-Aware Energy-Efficient Geographical Routing for IEEE 802.15.4a Networks", IEICE TRANSACTIONS on



Communications, Vol. E93-B, No. 4, pp. 1024-1028  
(2010).  
[6] <http://www.isi.edu/nsnam/ns>.

# Sufficient spaces for seven-way four-dimensional Turing machines to simulate four-dimensional one-marker automata

**Makoto Nagatomo, Makoto Sakamoto, Hikaru Susaki, Tuo Zhang, Satoshi Ikeda and Hiroshi Furutani**  
*Faculty of Engineering, University of Miyazaki, 1-1 Gakuen Kibanadai Nishi*  
*Miyazaki, Miyazaki 889-2192, Japan*  
*E-mail: sakamoto@cs.miyazaki-u.ac.jp*

**Takao Ito**  
*Institute of Engineering, Hiroshima University, 4-1, Kagamiyama1-chome*  
*Higashi-Hiroshima, Hiroshima 739-8527, Japan*  
*E-mail: itotakao@horoshima-u.ac.jp*

**Yasuo Uchida**  
*Department of Business Administration, Ube National College of Technology, Tokiwadai*  
*Ube, Yamaguchi 755-8555, Japan*  
*E-mail: uchida@ube-k.ac.jp*

**Tsunehiro Yoshinaga**  
*Department of Computer Science & Electronic Engineering,*  
*National Institute of Technology, Tokuyama College, Gakuendai*  
*Shunan, Yamaguchi 745-8585, Japan*  
*E-mail: yosinaga@tokuyama.ac.jp*

## Abstract

A multi-marker automaton is a finite automaton which keeps marks as ‘pebbles’ in the finite control, and cannot rewrite any input symbols but can make marks on its input with the restriction that only a bounded number of these marks can exist at any given time. An improvement of picture recognizability of the finite automaton is the reason why the marker automaton was introduced. That is, a one-marker automaton can recognize connected picture. This automaton has been investigated in the two- or three-dimensional case. As is well known among the researchers of automata theory, one-marker automata are equivalent to ordinary finite state automata. In other words, there is no working space usage such as Turing machines to calculate the space complexities. In this paper, we deal with four-dimensional one-marker automata in terms of the space complexities that seven-way four-dimensional Turing machines, which can move east, west, south, north, up, down, or in the future, but not in the past on four-dimensional rectangular input tapes, suffice to simulate one-marker automata.

*Keywords:* computational complexity, finite automaton, marker, simulation, Turing machine, upper bounds.

## 1. Introduction

A multi-marker automaton is a finite automaton which keeps marks as ‘pebbles’ in the finite control, and cannot rewrite any input symbols but can make marks on its input with the restriction that only a bounded number of these marks can exist at any given time[1]. An improvement of picture recognizability of the finite automaton is the reason why the marker automaton was

introduced. That is, a two-dimensional one-marker automaton can recognize connected pictures. This automaton has been widely investigated in the two- or three-dimensional case [2].

As is well known among the researchers of automata theory, one-dimensional one-marker automata are equivalent to ordinary finite state automata. In other words, there is no need of working space usage for

one-way Turing machines to simulate one-marker automata, as well as finite state automata.

In the two-dimensional case, the following facts are known : the necessary and sufficient space for three-way two-dimensional deterministic Turing machines *TR2-DTM*'s to simulate two-dimensional deterministic (nondeterministic) finite automata *2-DFA*'s (*2-NFA*'s) is  $m \log m$  ( $m^2$ ) and the corresponding space for three-way two-dimensional nondeterministic Turing machines *TR2-NTM*'s is  $m$  ( $m$ ), whereas the necessary and sufficient space for three-way two-dimensional deterministic Turing machines *TR2-DTM*'s to simulate two-dimensional deterministic (nondeterministic) one-marker automata *2-DMA<sub>1</sub>*'s (*2-NMA<sub>1</sub>*'s) is  $2^{m \log m}$  ( $2^{m^2}$ ) and the corresponding space for *TR2-NTM*'s is  $m \log m$  ( $m^2$ ), where  $m$  is the number of columns of two-dimensional rectangular input tapes.

In the three-dimensional case, the following facts are known : the necessary and sufficient space for five-way three-dimensional deterministic Turing machines *FV3-DTM*'s to simulate three-dimensional deterministic (nondeterministic) finite automata *3-DFA*'s (*3-NFA*'s) is  $m^2 \log m$  ( $m^3$ ) and the corresponding space for five-way three-dimensional nondeterministic Turing machines *FV3-NTM*'s is  $m^2$  ( $m^2$ ), whereas the necessary and sufficient space for five-way three-dimensional deterministic Turing machines *FV3-DTM*'s to simulate three-dimensional deterministic (nondeterministic) one-marker automata *3-DMA<sub>1</sub>*'s (*3-NMA<sub>1</sub>*'s) is  $2^{l \log l m}$  ( $2^{l^2 m^2}$ ) and the corresponding space for *FV3-NTM*'s is  $l m \log l m$  ( $l^2 m^2$ ), where  $l(m)$  is the number of rows (columns) on each plane of three-dimensional rectangular input tapes.

In this paper, we deal with four-dimensional one-marker automata in terms of the space complexities that seven-way four-dimensional Turing machines suffice to simulate four-dimensional one-marker automata.

## 2. Preliminaries

An ordinary finite automaton cannot rewrite any symbols on input tape, but a marker automaton can make a mark on the input tape. We can think of the mark as a 'pebble' that  $M$  puts down in a specified

position. If  $M$  has already put down the mark, and wants to put it down elsewhere,  $M$  must first go to the position of the mark and pick it up. Formally, we define it as follows.

**Definition 2.1.** A *four-dimensional nondeterministic one-marker automaton* (*4-NMA<sub>1</sub>*) is defined by the 6-tuple  $M = (Q, q_0, F, \Sigma, \{+, -\}, \delta)$ , where

- (1)  $Q$  is a finite set of *states* ;
- (2)  $q_0 \in Q$  is the *initial state* ;
- (3)  $F \subseteq Q$  is the set of *accepting states* ;
- (4)  $\Sigma$  is a finite input *alphabet* ( $\# \notin \Sigma$  is the *boundary symbol*);
- (5)  $\{+, -\}$  is the pair of *signs of presence and absence of the marker* ; and
- (6)  $\delta : (Q \times \{+, -\}) \times ((\Sigma \cup \{\#\}) \times \{+, -\}) \mapsto \times 2^{Q \times \{+, -\}} \times ((\Sigma \cup \{\#\}) \times \{+, -\}) \times \{\text{east, west, south, north, up, down, future, past, no move}\}$  is the *next-move function*, satisfying the following : For any  $q, q' \in Q$ , any  $a, a' \in \Sigma$ , any  $u, u', v, v' \in \{+, -\}$ , and any  $d \in \{\text{east, west, south, north, up, down, future, past, no move}\}$ , if  $((q', u'), (a', v'), d) \in \delta((q, v), (a, v))$  then  $a = a'$  and  $(u, v, u', v') \in \{(+, -, +, -), (+, -, -, +), (-, +, -, +), (-, +, +, -), (-, -, -, -)\}$ .

We call a pair  $(q, u)$  in  $Q \times \{+, -\}$  an *extended state*, representing the situation that  $M$  holds or does not hold the marker in the finite control according to the sign  $u = +$  or  $u = -$ , respectively. A pair  $(a, v)$  in  $\Sigma \times \{+, -\}$  represents an input tape cell on which the marker exists or does not exist according to the sign  $u = +$  or  $u = -$ , respectively.

Therefore, the restrictions on  $\delta$  imply the following conditions. (i) When holding the marker,  $M$  can put it down or keep on holding. (ii) When not holding the marker, and ① if the marker exists on the current cell,  $M$  can pick it up or leave it there, or ② if the marker does not exist on the current cell,  $M$  cannot create a new marker any more.

**Definition 2.2.** Let  $\Sigma$  be the input alphabet of *4-NMA<sub>1</sub>*  $M$ . An *extended input tape*  $\tilde{x}$  of  $M$  is any four-dimensional tape over  $\Sigma \times \{+, -\}$  such that for some  $x \in \Sigma^{(4)}$ ,

- (i) for each  $j(1 \leq j \leq 4)$ ,  $l_j(\tilde{x}) = l_j(x)$ ,
- (ii) for each  $i_1(1 \leq i_1 \leq l_1(\tilde{x}))$ ,  $i_2(1 \leq i_2 \leq l_2(\tilde{x}))$ ,  $i_3(1 \leq i_3 \leq l_3(\tilde{x}))$ , and  $i_4(1 \leq i_4 \leq l_4(\tilde{x}))$ ,  $\tilde{x}(i_1, i_2, i_3, i_4) = x((i_1, i_2, i_3, i_4), u)$  for some  $u \in \{+, -\}$ .

**Definition 2.3.** A configuration of 4-NMA<sub>1</sub>  $M = (Q, q_0, F, \Sigma, \{+, -\}, \delta)$  is a pair of an element of  $((\Sigma \cup \{\#\}) \times \{+, -\})^{(4)}$  and an element of  $C_M = (\mathbf{N} \cup \{0\})^{(4)} \times (Q \times \{+, -\})$ . The first component of a configuration  $c = (\tilde{x}, ((i_1, i_2, i_3, i_4), (q, u)))$  represents the extended input tape of  $M$ . The second component  $(i_1, i_2, i_3, i_4)$  of  $c$  represents the input head position. The third component  $(q, u)$  of  $c$  represents the extended state. An element of  $C_M$  is called a *semi-configuration* of  $M$ . If  $q$  is the state associated with configuration  $c$ , then  $c$  is said to be an *accepting configuration* if  $q$  is an accepting state. The *initial configuration* of  $M$  on input  $x$  is  $I_M(x) = (x^-, ((1, 1, 1, 1), (q_0, +)))$ , where  $x^-$  is the special extended input tape of  $M$  such that  $x^-(i_1, i_2, i_3, i_4) = (x(i_1, i_2, i_3, i_4), -)$  for each  $i_1, i_2, i_3, i_4$  ( $1 \leq i_1 \leq l_1(x^-), 1 \leq i_2 \leq l_2(x^-), 1 \leq i_3 \leq l_3(x^-), 1 \leq i_4 \leq l_4(x^-)$ ). If  $M$  moves deterministically, we call  $M$  a four-dimensional deterministic one-marker automaton (4-DMA<sub>1</sub>).

**Definition 2.4.** Given a 4-NMA<sub>1</sub>  $M = (Q, q_0, F, \Sigma, \{+, -\}, \delta)$ , we write  $c \vdash_M c'$  and say  $c'$  is a *successor* of  $c$  if configuration  $c'$  follows from configuration  $c$  in one step of  $M$ , according to the transition rules  $\delta$ .  $\vdash_M^*$  denotes the reflexive transitive closure of  $\vdash_M$ . The relation  $\vdash_M$  is not necessarily single-valued, because  $\delta$  is not. A *computation path* of  $M$  on  $x$  is a sequence  $c_0 \vdash_M c_1 \vdash_M \dots \vdash_M c_n$  ( $n \geq 0$ ), where  $c_0 = I_M(x)$ . An *accepting computation path* of  $M$  on  $x$  is a computation path of  $M$  on  $x$  which ends in an accepting configuration. We say that  $M$  *accepts*  $x$  if there is an accepting computation path of  $M$  on input  $x$ .

Let  $S(l, m, n, t): \mathbf{N}^4 \mapsto \mathbf{R}$  be a function. A seven-way four-dimensional Turing machine  $M$  is said to be  $S(l, m, n, t)$  *space-bounded* if for each  $l, m, n, t \geq 1$  and for each  $x$  with  $l_1(x) = l, l_2(x) = m, l_3(x) = n$ , and  $l_4(x) = t$ , if  $x$  is accepted by  $M$ , then there is an accepting computation path of  $M$  on  $x$  in which  $M$  uses no more than  $S(l, m, n, t)$  cells of the storage tape. We denote an  $S(l, m, n, t)$  space-bounded SV4-DTM (SV4-NTM) by  $SV4-DTM(S(l, m, n, t))$  (SV4-NTM  $(S(l, m, n, t))$ ).

Let  $L(l, m, n): \mathbf{N}^3 \mapsto \mathbf{R}$  be a function. A seven-way four-dimensional Turing machine  $M$  is said to be  $L(l, m, n)$  *space-bounded* if for each  $l, m, n \geq 1$  and for each  $x$  with  $l_1(x) = l, l_2(x) = m$ , and  $l_3(x) = n$ , if  $x$

is accepted by  $M$ , then there is an accepting computation path of  $M$  on  $x$  in which  $M$  uses no more than  $L(l, m, n)$  cells of the storage tape. We denote an  $L(l, m, n)$  space-bounded SV4-DTM (SV4-NTM) by  $SV4-DTM(L(l, m, n))$  (SV4-NTM  $(L(l, m, n))$ ).

**Definition 2.5.** For any four-dimensional automaton  $M$  with input alphabet  $\Sigma$ , define  $T(M) = \{x \in \Sigma^{(4)} \mid M \text{ accepts } x\}$ . Furthermore, for each  $X \in \{D, N\}$ , define

$$\mathcal{L}[4-XMA_1] = \{T \mid T = T(M) \text{ for some } 4-XMA_1\},$$

$\mathcal{L}[SV4-XTM(S(l, m, n))] = \{T \mid T = T(M) \text{ for some } SV4-XTM(S(l, m, n)) M\}$ , and

$\mathcal{L}[SV4-XTM(L(l, m))] = \{T \mid T = T(M) \text{ for some } SV4-XTM(L(l, m)) M\}$ .

By using the same technique as in the proof of Lemma 5.4 in [2], we can easily prove the following theorem.

**Lemma 2.1.** For any function  $L(l, m, n) \geq \log lmn$ ,

$$\mathcal{L}[SV4-XTM(L(l, m, n))] \subseteq \bigcup_{c>0} \mathcal{L}[SV4-DTM(2^{c(L(l, m, n))})].$$

### 3. Sufficient spaces

In this section, we investigate the sufficient spaces (i.e., upper bounds) for seven-way Turing machines to simulate one-marker automata. We first show that  $lmn \log lmn$  space is sufficient for SV4-NTM's to simulate 4-DMA<sub>1</sub>'s.

**Theorem 3.1.**  $\mathcal{L}[4-DMA_1] \subseteq \mathcal{L}[SV4-NTM(lmn \log lmn)]$ .

**Proof :** Suppose that a 4-DMA<sub>1</sub>  $M = (Q, q_0, F, \Sigma, \delta)$  is given. We partition the extended states  $Q \times \{+, -\}$  into disjoint subsets  $Q^+ = Q \times \{+\}$  and  $Q^- = Q \times \{-\}$  which correspond to the extended states when  $M$  is holding and not holding the marker in the finite control, respectively. We assume that  $M$  has a unique accepting state  $q_a$ , i.e.,  $|F| = 1$ . In order to make our proof clear, we also assume that  $M$  begins to move with its input head on the position  $(l + 1, m + 1, n + 1, t + 1)$  and, when  $M$  accepts an input, it enters the accepting state at the same position  $(l + 1, m + 1, n + 1, t + 1)$  with the marker held in the finite control.

Suppose that an input tape  $x$  with  $l_1(x) = l, l_2(x) = m, l_3(x) = n$ , and  $l_4(x) = t$  is given to  $M$ . For  $M$  and  $x$ , we define three types of mappings

$$f_r^{\uparrow-} : S^- \times \{0, 1, \dots, l + 1\} \times \{0, 1, \dots, m + 1\} \\ \times \{0, 1, \dots, n + 1\} \mapsto S^- \times \{0, 1, \dots, l + 1\}$$

$$\begin{aligned} & \times \{0,1, \dots, m+1\} \times \{0,1, \dots, n+1\} \cup \{l\}, \\ f_r^{\uparrow+} : S^+ \times \{0,1, \dots, l+1\} \times \{0,1, \dots, m+1\} \\ & \times \{0,1, \dots, n+1\} \mapsto S^+ \times \{0,1, \dots, l+1\} \\ & \times \{0,1, \dots, m+1\} \times \{0,1, \dots, n+1\} \cup \{l\}, \quad \text{and} \\ f_r^{\downarrow-} : S^- \times \{0,1, \dots, l+1\} \times \{0,1, \dots, m+1\} \\ & \times \{0,1, \dots, n+1\} \mapsto S^- \times \{0,1, \dots, l+1\} \\ & \times \{0,1, \dots, m+1\} \times \{0,1, \dots, n+1\} \cup \{l\}, \end{aligned}$$

( $r = 0, 1, \dots, t+1$ ) as follows. (Below, we attach the superscripts ‘+’, ‘-’ to any extended states in  $(Q^+, Q^-$ , respectively.)

$f_r^{\downarrow-}(q^-, i, j, k) = (q'^-, i', j', k')$ : Suppose that we make  $M$  start from the configuration  $(x^-, ((i, j, k, r-1), q^-))$ , i.e., no marker existing either on the input  $x$  or in the finite control of  $M$ . After that, if  $M$  reaches the  $r$ -th three-dimensional rectangular array of  $x$  in some time, the configuration corresponding to the first arrival is  $(x^-, ((i', j', k', r), q'^-))$ ;

$f_r^{\downarrow-}(q^-, i, j, k) = l$  : Starting from the configuration  $(x^-, ((i, j, k, r-1), q^-))$  with no marker on the input tape,  $M$  never reaches the  $r$ -th three-dimensional rectangular array of  $x$ .

$f_r^{\uparrow+}(q^+, i, j, k) = (q'^+, i', j', k')$  : Suppose that we make  $M$  start from the configuration  $(x^-, ((i, j, k, r-1), q^+))$ , i.e., holding the marker in the finite control of  $M$ . After that, if  $M$  reaches the  $r$ -th three-dimensional rectangular array of  $x$  with its marker held in the finite control in some time ( so, when  $M$  puts down the marker on the way, it must return to this position again and pick up the marker), the configuration corresponding to the first arrival is  $(x^-, ((i', j', k', r), q'^+))$  ;

$f_r^{\uparrow+}(q^+, i, j, k) = l$  : Starting from the configuration  $(x^-, ((i, j, k, r-1), q^+))$ ,  $M$  never reaches the  $r$ -th three-dimensional rectangular array of  $x$  with its marker held in the finite control.

$f_r^{\downarrow-}(q^-, i, j, k) = (q'^-, i', j', k')$  : Suppose that we make  $M$  start from the configuration  $(x^-, ((i, j, k, r+1), q^-))$ , i.e., no marker existing either on the input tape or in the finite control of  $M$ . After that, if  $M$  reaches the  $r$ -th three-dimensional rectangular array of  $x$  in some time, the configuration corresponding to the first arrival is  $(x^-, ((i', j', k', r), q'^-))$ ;

$f_r^{\downarrow-}(q^-, i, j, k) = l$  : Starting from the configuration  $(x^-, ((i, j, k, r+1), q^-))$ ,  $M$  never reaches the  $r$ -th three-dimensional rectangular array of  $x$ .

Then, we can show that there exists an  $SV4\text{-}NTM(lm \log lm)$   $M'$  such that  $T(M') = T(M)$ . Roughly speaking, while scanning from the top three-dimensional rectangular array down to the bottom three-dimensional rectangular array of the input,  $M'$  guesses  $f_r^{\downarrow-}$ , constructs  $f_{r+1}^{\uparrow-}$  and  $f_{r+1}^{\uparrow+}$ , checks  $f_{r-1}^{\downarrow-}$ , and finally at the bottom three-dimensional rectangular array of the input,  $M'$  decides by using  $f_{t+1}^{\uparrow-}$  and  $f_{t+1}^{\uparrow+}$  whether or not  $M$  accepts  $x$ .

In order to record these mappings for each  $r$ ,  $O(lmn)$  blocks of  $O(\log lmn)$  size suffice, so in total,  $O(lmn \log lmn)$  cell of the working tape suffice. More precisely, the working tape must be used as a ‘multi-track’ tape, but we omit the detailed construction of the working tape of  $M'$ . It will be obvious that  $T(M) = T(M')$ .  $\square$

From Lemma 2.1 and Theorem 3.1, we get the following.

**Corollary 3.1.**  $\mathcal{L}[4\text{-}DMA_1] \subseteq$

$$\mathcal{L}[SV4\text{-}DTM(2^{O(lmn \log lmn)})].$$

Next, we can show that  $l^2 m^2 n^2$  space is sufficient for  $SV4\text{-}NTM$ 's to simulate  $4\text{-}NMA_1$ 's. The basic idea and outline of the proof are the same as those of Theorem 2.1.

**Theorem 3.2.**  $\mathcal{L}[4\text{-}NMA_1] \subseteq \mathcal{L}[SV4\text{-}NTM(l^2 m^2 n^2)]$ .

From Lemma 2.1 and Theorem 3.2, we get the following.

**Corollary 3.2.**  $\mathcal{L}[4\text{-}NMA_1] \subseteq$

$$\mathcal{L}[SV4\text{-}DTM(2^{O((l^2 m^2 n^2)})].$$

#### 4. Conclusion

In this paper, we showed the sufficient space for  $SV4\text{-}DTM$ 's to simulate  $4\text{-}DMA_1$ 's ( $4\text{-}NMA_1$ 's) is  $2^{lmn \log lmn} (2^{l^2 m^2 n^2})$  and the sufficient space for  $SV4\text{-}NTM$ 's to simulate  $4\text{-}DMA_1$ 's ( $4\text{-}NMA_1$ 's) is  $lmn \log lmn (l^2 m^2 n^2)$ . It will be interesting to investigate how much space is necessary for  $SV4\text{-}DTM$ 's ( or  $SV4\text{-}NTM$ 's) to simulate  $4\text{-}DMA_1$ 's ( or  $4\text{-}NMA_1$ 's).

#### References

1. M. Blum and C. Hewitt, “Automata on a two-dimensional tape”, IEEE Symposium on Switching and Automata Theory (1967), pp.155-160.
2. M. Sakamoto, “Three-dimensional alternating Turing machines”, Ph.D. Thesis, Yamaguchi University (1999).

## **Some properties of $k$ -neighborhood Template $A$ -type two-dimensional bounded cellular acceptors**

**Makoto Sakamoto, Makoto Nagatomo, Hikaru Susaki, Tuo Zhang, Satoshi Ikeda and Hiroshi Furutani**

*Faculty of Engineering, University of Miyazaki, 1-1 Gakuen Kibanadai Nishi*

*Miyazaki, Miyazaki 889-2192, Japan*

*E-mail: sakamoto@cs.miyazaki-u.ac.jp*

**Takao Ito**

*Institute of Engineering, Hiroshima University, 4-1, Kagamiyama1-chome*

*Higashi-Hiroshima, Hiroshima 739-8527, Japan*

*E-mail: itotakao@horoshima-u.ac.jp*

**Yasuo Uchida**

*Department of Business Administration, Ube National College of Technology, Tokiwadai*

*Ube, Yamaguchi 755-8555, Japan*

*E-mail: uchida@ube-k.ac.jp*

**Tsunehiro Yoshinaga**

*Department of Computer Science & Electronic Engineering,*

*National Institute of Technology, Tokuyama College, Gakuendai*

*Shunan, Yamaguchi 745-8585, Japan*

*E-mail: yosinaga@tokuyama.ac.jp*

### **Abstract**

In this paper, we investigate multi-dimensional computational model,  $k$ -neighborhood template  $A$ -type three-dimensional bounded cellular acceptor on four-dimensional tapes, and discuss some basic properties. This model consists of a pair of a converter and a configuration-reader. The former converts the given four-dimensional tape to three-dimensional configuration. The latter determines whether or not the derived three-dimensional configuration is accepted, and concludes the acceptance or non-acceptance of given four-dimensional tape. We mainly investigate some open problems about  $k$ -neighborhood template  $A$ -type three-dimensional bounded cellular acceptor on four-dimensional tapes whose configuration-readers are  $L(m)$  space-bounded deterministic (nondeterministic) three-dimensional Turing machines.

*Keywords:* configuration-reader, converter, four-dimension, neighbor, space-bounded, Turing machine.

### **1. Introduction**

Due to the advances in many application areas such as computer animation, dynamic image processing, and so on, the study of four-dimensional pattern processing has been of crucial importance. Thus, the study of four-

dimensional automata as the computational models of four-dimensional pattern processing has been meaningful. From this point of view, we first proposed four-dimensional automata as computational models of four-dimensional pattern processing in 2002, and investigated their several accepting powers[2]. By the

© The 2015 International Conference on Artificial Life and Robotics (ICAROB 2015), Jan. 10-12, Oita, Japan



$q_{i+1,j,k-1}(t), q_{i+1,j+1,k-1}(t), q_{i-1,j-1,k}(t), q_{i-1,j,k}(t), q_{i-1,j+1,k}(t), q_{i,j-1,k}(t), q_{i,j,k}(t), q_{i,j+1,k}(t), q_{i+1,j-1,k}(t), q_{i+1,j,k}(t), q_{i+1,j+1,k}(t), q_{i-1,j-1,k+1}(t), q_{i-1,j,k+1}(t), q_{i-1,j+1,k+1}(t), q_{i,j-1,k+1}(t), q_{i,j,k+1}(t), q_{i,j+1,k+1}(t), q_{i+1,j-1,k+1}(t), q_{i+1,j,k+1}(t), q_{i+1,j+1,k+1}(t), a$ ,

where  $a$  is the symbol on the  $A(i,j,k)$  at time  $t$ . If  $q_{i,j,k}(t) = q_{\#}$ , however,  $q_{i,j,k}(t+1) = \{q_{\#}\}$  for each  $(i,j,k) \in \mathbb{Z}^3$  and each  $t \geq 0$ .

- (2) A set of input symbols of  $B$  is  $K - \{q_{\#}\}$  (where  $B \in A$ ). Intuitively,  $M=(R,B)$  moves as follows, given a four-dimensional input tape  $x \in \Sigma^{(m_1,m_2,m_3,m_4)}$  ( $m_1, m_2, m_3, m_4 \geq 1$ ) ( $x$  is surrounded by the boundary symbol  $\#$ ). First, each cell  $A(i,j,k)$  of  $R(1 \leq i \leq m_1, 1 \leq j \leq m_2, 1 \leq k \leq m_3)$  reads each symbol on the first three-dimensional rectangular array  $x(i,j,k,1)$  in the initial state  $q_0$ , and all of the other cells read the boundary symbols  $\#$ 's in the boundary state  $q_{\#}$ 's at time  $t=0$ . Starting from this condition,  $R$  keeps reading  $x$  according to the cell state transition function, and moving down the cell array by one three-dimensional rectangular array, every time  $R$  reads one three-dimensional rectangular array all. Next,  $B$  starts to move regarding a *three-dimensional configuration* of  $R$  just after  $R$  finished reading  $x$  as a three-dimensional input tape and determines whether or not can accept the configuration. If  $B$  accepts it,  $x$  is said to be *accepted* by  $M$ . Let  $T(M)$  be the set of all accepted three-dimensional tape by  $M$ .

**Definition 2.3.** An  $A$ -3BCA in Definition 2.2 is called a 27-neighborhood template  $A$ -3BCA. If we deal with east, west, south, north, up, down neighboring cells and remarkable cell, we call it 7-neighborhood template  $A$ -3BCA. If we deal with only remarkable cell, we call it 1-neighborhood template  $A$ -3BCA. From now on, we denote  $k$ -neighborhood template  $A$ -3BCA by  $A$ -3BCA( $k$ ) ( $k \in \{1,7,27\}$ ).

**Definition 2.4.** If the image generated by  $\sigma$  in Definitions 2.2 and 2.3 is a singleton, the converter is said to be *deterministic*, and if not, it is said to be *nondeterministic*. An  $A$ -3BCA( $k$ ) ( $k \in \{1,7,27\}$ ), which converter is deterministic (nondeterministic), is said to be a *deterministic (nondeterministic)*  $A$ -3BCA( $k$ ) and denoted by  $A$ -3DBCA( $k$ ) ( $A$ -3NBCA( $k$ )).

We now consider the class of three-dimensional automata described by the following abbreviations as the class of the configuration-reader of  $A$ -3BCA( $k$ )  $A$ . In this paper, we assume that the reader is familiar with the definition of these automata. If necessary, see[2].

3-*DTM*( $L(m)$ ) ... The class of  $L(m)$  space-bounded deterministic three-dimensional Turing machine

3-*NTM*( $L(m)$ ) ... The class of  $L(m)$  space-bounded nondeterministic three-dimensional Turing machine

*DO* ... The class of deterministic three-dimensional on-line tessellation acceptor

*DB* ... The class of deterministic two-dimensional bounded cellular acceptor

For example 3-*DTM*( $L(m)$ )-3DBCA(27) represents such the class as its converter is deterministic and 27-neighborhood, and its configuration-reader is an  $L(m)$  space-bounded deterministic three-dimensional Turing machine. Moreover, for any  $A \in \{3\text{-DTM}(L(m)), 3\text{-NTM}(L(m))\}$ , for any  $X \in \{D, N\}$  and for any  $k \in \{1,7,27\}$ , the class of set of all four-dimensional tapes accepted by  $A$ -3XBCA( $k$ ) is denoted by  $\mathcal{L}[A\text{-3XBCA}(k)]$ . We let each side-length of each input tape of these automata be equivalent in order to increase the theoretical interest.

### 3. Main results

In this section, we discuss some properties of  $A$ -3BCA( $k$ )'s whose configuration-readers are  $L(m)$  space-bounded deterministic (nondeterministic) three-dimensional Turing machines.

First, we show that a relationship between determinism and nondeterminism, when we use  $L(m)$  space-bounded three-dimensional Turing machines for any  $L(m) > m^3$  as the configuration-readers.

**Theorem 3.1.** For any  $X \in \{D,N\}$ ,  $\mathcal{L}[3\text{-XTM}(m^3)\text{-3DBCA}(1)] = \mathcal{L}[3\text{-XTM}(m^3)\text{-3NBCA}(1)]$ .

**Proof:** From above definition, it is obvious that  $\mathcal{L}[3\text{-XTM}(m^3)\text{-3DBCA}(1)] \subseteq \mathcal{L}[3\text{-XTM}(m^3)\text{-3NBCA}(1)]$ . We below show that  $\mathcal{L}[3\text{-XTM}(m^3)\text{-3NBCA}(1)] \subseteq \mathcal{L}[3\text{-}$



DTM( $m^3$ )-3DBCA(1)] (we can prove another case (i. e.,  $X=N$ ) in the same way).

Now, let  $M=(R,B)$  ( $R=Z^2, N^2, K, \Sigma, \sigma, q_0$ ),  $B=(K, Q, \Sigma, \Gamma, \delta, p_0, F)$ ) be some 3- $DTM(m^3)$ -3NBCA(1). Then, we consider an  $M'=(R',B')$  ( $R'=Z^3, N^3, K', \Sigma, \sigma', q_0$ ),  $B'=(K', Q, \Sigma, \Gamma, \delta', p_0', F')$ ) constructed as follows.

(1) Construction of  $R'$

- ①  $K'=2^{(K-\{q_\#\})} \cup \{q_\#\}$ ,  $q_0'=\{q_0\}$ .
- ② For any  $a \in \Sigma$  and any  $K'' \in K'-\{q_\#\}$ ,  
 $\sigma'(K'', a) = \bigcup_{p \in K''} \sigma(p, a)$ .

(2) Construction of  $B'$

For any  $p \in Q$  and any  $K'' \in K'-\{q_\#\}$ ,

$$\delta'(p, K'') = \bigcup_{r \in K''} \delta(p, r).$$

Intuitively, we explain the movement of  $M'=(R', B')$  constructed in this way. Let us suppose that a four-dimensional tape  $x \in \Sigma^{(4)+}$  is given to  $M'$ .  $R'$  is one-neighborhood, so we can consider each cell of  $R'$  as usual one-dimensional finite automata. Then, each cell of  $R'$  moves to store all states that each corresponding cell of  $R$  can enter in each state at each time by using the well-known subset construction method (see (1)).

$B'$  nondeterministically chooses only one state from each state of each cell of  $R'$ , and simulates the movement of  $B$  regarding the selected states as the input symbol. If  $B'$  can not accept the input,  $B'$  selects the next input and simulates the movement of  $B$ . From the way such as the above manner,  $B'$  checks the all input patterns, and if  $B'$  can accept one input,  $B'$  can accept the configuration of  $R'$  (see (2)).

It is clear that  $T(M')=T(M)$  for  $M'=(R',B')$  constructed in this manner.  $\square$

Next, we show that there exists a language accepted by a 3- $DTM(0)$ -3NBCA(1), but not accepted by any 3- $NTM(L(m))$ -3DBCA(27) for any  $L(m) = o(\log m)$ .

**Theorem 3.2.** For any function  $L(m) = o(\log m)$ ,  $\mathcal{L}[3\text{-}DTM(0)\text{-}3NBCA(1)] - \mathcal{L}[3\text{-}NTM(L(m))\text{-}3DBCA(27)] \neq \phi$ .

**Proof:** Let  $C = \{w_0 2 w_1 2 \cdots 2 w_k \mid k \geq 1 \ \& \ \forall i (0 \leq i \leq k) [w_i \in \{0,1\}^+] \ \& \ \exists j (0 \leq j \leq k) [w_0 = w_j^{-1}]\}$  (where, for any one-dimensional tape  $w$ ,  $w^f$  denotes the reversal of  $w$ ), and  $T_1 = \{x \in \{0,1,2\}^{(4)+} \mid \exists m > 3 [\ell_1(x) = \ell_2(x) = \ell_3(x) = \ell_4(x) = m \ \& \ x[(1,1,m,m), (1,m,m,m)] \in C]\}$ . Then, by using a technique similar to that in the proof of Lemma 2(1) in [4], we can show that  $T_1$  is accepted by 3- $DTM(0)$ -

3NBCA(1), but not accepted by any 3- $NTM(L(m))$ -3DBCA(27) for any  $L(m) = o(\log m)$ .  $\square$

**Corollary 3.1.** For any  $L(m) = o(\log m)$  and any  $X \in \{D, N\}$ ,  $\mathcal{L}[3\text{-}XTM(L(m))\text{-}3DBCA(1)] \subseteq \mathcal{L}[3\text{-}XTM(L(m))\text{-}3NBCA(1)]$ .

**Remark 3.1.** By using a technique to that in the proof of Theorem 3 in [4], we can show that for any function  $L(m)$  and any  $k \in \{7, 27\}$ ,  $\mathcal{L}[3\text{-}XTM(L(m))\text{-}3DBCA(k)] \subseteq \mathcal{L}[3\text{-}XTM(L(m))\text{-}3NBCA(k)]$ .

Finally, by using the well-known technique, we can show that there exists a language accepted by a  $DO$ -3NBCA(1) and a  $DB$ -3NBCA(1), but not accepted by any 3- $DTM(L(m))$ -3DBCA(27) for any function  $L(m) = o(\log m)$ .

**Theorem 3.3.** For any function  $L(m) = o(\log m)$ ,  $(\mathcal{L}[DO\text{-}3NBCA(1)] \cap \mathcal{L}[DB\text{-}3NBCA(1)]) - \mathcal{L}[3\text{-}DTM(L(m))\text{-}3DBCA(27)] \neq \phi$ .

#### 4. Conclusion

We conclude this paper by giving the following problem. For any  $X \in \{D, N\}$  and any  $L(m)$  ( $\log m \leq L(m)$  and  $L(m) = o(m^2)$ ),  $\mathcal{L}[XTM(L(m))\text{-}3DBCA(1)] \subseteq \mathcal{L}[XTM(L(m))\text{-}3NBCA(1)]$ ?

#### References

1. M. Sakamoto, H. Okabe, and K. Inoue, "Some properties of four-dimensional finite automata", 2002 Chugoku-Section Joint Convention Record of Institutes of Electrical and Information Engineering, Shimane, Japan (2002), p.351.
2. M. Sakamoto, "Three-dimensional alternating Turing machines", Ph.D. Thesis, Yamaguchi University (1999).
3. M. Sakamoto, M. Nagatomo, X. Feng, T. Kurogi, T. Zhang, T. Ito, Y. Uchida, T. Yoshinaga, S. Ikeda, M. Yokomichi, and H. Furutani, "Hierarchy based on k-neighborhood template about k-neighborhood template A-type three-dimensional bounded cellular acceptor", Proceedings of the International Conference on Artificial Life and Robotics (ICAROB2014), Compal Hall, Oita, Japan, OS9-1 (2014)
4. H. Taniguchi, K. Inoue, and I. Takanami, "k-neighborhood template A-type 2-dimensional bounded cellular acceptor", IECE of Japan Transactions (D), Vol.69, No.3 (1986), pp.291-301.

# Perfect Analysis in miniature Othello

**Yuki Takeshita\***

*Department of Computer Science and System Engineering, Miyazaki University,  
Japan, hf11031@student.miyazaki-u.ac.jp*

**Satoshi Ikeda\***

*Department of Computer Science and System Engineering, Miyazaki University,  
Japan, bisu@cs.miyazaki-u.ac.jp*

**Makoto Sakamoto\***

*Department of Computer Science and System Engineering, Miyazaki University,  
Japan, sakamoto@cs.miyazaki-u.ac.jp*

**Takao Ito†**

*Graduate School of Engineering, Hiroshima University,  
Japan, itotakao@hiroshima-u.ac.jp*

## Abstract

More than 20 years has passed after J. Feinstein (1993) found that a perfect play on 6×6 board of Othello gives a 16-20 win for the second player, but standard 8×8 board has not yet been. In this paper, we analyzed for 4×4, 4×6, 4×8, 4×10 and 6×6 boards of Othello. From these results, we discuss which it is, win/loss/draw in 8×8 board or more board.

*Keywords:* perfect analysis, perfect play, Alpha-Beta Pruning, rectangular Othello

## 1. Introduction

Othello is categorized into two-player zero-sum finite deterministic games of perfect information [1]. Games in this class are possible to look ahead in theory, thus if both players play the best move, these are classified into a win, loss or draw game [2].

In 1993, Joel Feinstein found that a perfect play on 6×6 board of Othello gives a 16-20 win for the second player [3]; he looked at 40 billion positions, run time

was 2 weeks. Then computer Othello surpasses a much more human since more than 20 years has been passed. However, standard 8×8 board of Othello has not been solved (we couldn't find the articles solved it). The cause is that number of the positions is too large: in 8×8 board, perfect analysis in a realistic time is impossible even if we use the latest supercomputer.

In this paper, we show the perfect play of 4×4, 4×6, 4×8, 4×10 and 6×6 boards of Othello. From these results, we discuss the feature of the Othello game in

---

\* University of Miyazaki, 1-1, Gakuen Kibanadai Nishi, Miyazaki, 889-2192

† University of Hiroshima, 1-4-1, Kagamiyama, Higashi-Hiroshima, 739-8527

8×8 board or more. In Section 2, we introduce the rules of Othello. In Section 3, we introduce computer Othello. In Section 4, we explain perfect play. In Section 5, our experimental results are presented. We ran the perfect analysis in 4×4, 4×6, 4×8, 4×10 and 6×6 board of Othello. In Section 6, we discuss conclusion.

## 2. Othello<sup>‡</sup>

First of all, we will introduce the rules of Othello. See Figure 1. The game always begins with this setup. In the case of Reversi, we put randomly by two in central squares, thus there may be a parallel. One player uses the black side of the pieces (circular chips), the other the white sides. Black always moves first.

Both players put the pieces of own color to an empty board in turn. A player's move consists of outflanking his opponent's the pieces. Then, He flip outflanked the pieces to his color. To outflank means to place the piece on the board so that his opponent's rows of the piece are bordered at each end by the piece of his color. If a player cannot make a move that flips at least one of his opponent the pieces, then he has to pass. If he is able to make a valid move however, then passing is not allowed. The game ends when neither player can make a valid move. The winner is the player who has more the pieces than his opponent.

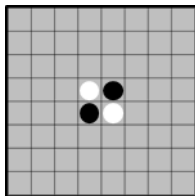


Fig. 1. Board and Starting position.

## 3. Computer Othello

The making of the thinking routines is indispensable in studying perfect analysis of the board game. This is because the end-game routine is the perfect analysis, the evaluation function in the middle-game routine is available for the ordering of the search in perfect analysis.

<sup>‡</sup> Othello is a registered trademark.

In addition, end-game is classified into solver for WLD (win/loss/draw) score and solver for exact score. Both the perfect analyses, but there is a difference in the evaluation of the end. In solver for exact score, the end is evaluated with the piece difference. However, it is necessary to consider if one was wiped out in the middle<sup>§</sup>. This routine can find best one move. In solver for WLD score, the end is evaluated in three ways win, loss, and draw. In this way, if the range of the evaluation value is small, pruning (Alpha-Beta Pruning [4]) occurs relatively large. Therefore, the solver for exact score can estimate that it is several times of the execution time by run the first WLD.

### 3.1. Speed up of the program

Currently, our program read approximately 1.5-2 million moves per second. There are some ideas for this.

At first, we implemented doubly-linked list storing the empty the pieces. This function reduce search cost so as to go to the end-game. From this, Search speed is approximately two times faster than previous version.

Next, our program had a function to count number of the pieces in specified the color, but we have removed it. Instead, it was adjusted from the time of reversal and restoration by adding a variable that stores number of the pieces into structure. This effect was approximately 1.5 times. In addition, we planned the shift to the Bid Board (way to represent the board in only logical operations and bit shifting) which helped speedup of the processing. Unfortunately, we have not yet implemented it.

## 4. Perfect Play

The perfect play is a sequence when both sides continue to choosing the best move. In computer Othello, the sequence to an end is not saved because we should just find even the best move of next; a return value is sufficient. Because our program is based on the thinking routines for such a game, it has become inefficient program to repeat the perfect analysis again after finding the next move. There is little harmful effect until perfect analysis of the 6×6 board. For example, it will takes 11 months to select the after next

<sup>§</sup> For example, in 4×8 board, the evaluation value at 26-0 must be +32.

move if we search the board to take one year to perfect analysis.

### 5. Experiments

We derived the perfect play of 4x4, 4x6, 4x8, 4x10 and 6x6 boards. CPU that we used for the experiments is Intel Core i7-4770 processor. First, see Table 1.

Table 1. Execution results of perfect analysis in each Othello board. P means number of the positions, T means execution time and R means results.

	4x4	6x6
P	218	884,392,099,420
T	0.001s	5d12h16m
R	LOSS(-8) B:3,W:11	LOSS(-4) B:16,W:20

	4x6	4x8	4x10
P	139,803	294,430,331	1,195,804,922,641
T	0.1s	2m15s	6d6h22m
R	WIN(+16) B:20,W:4	WIN(+32) B: 28, W: 0	WIN(+40) B: 39, W: 0

It turned out that the result of 6x6 board is consistent with the result of Feinstein. However, we have took about one week to perfect analysis because number of the positions was about 890 billion. Second, see Table 2.

Table 2. Execution results of perfect analysis in each Reversi board.

	4x4	6x6
P	524	1,628,664,185,199
T	0.001s	8d12h42m
R	LOSS(-3) B:6,W:9	LOSS(-2) B:17,W:19

	4x6	4x8	4x10
P	274,549	299,987,758	842,204,125,277
T	0.15s	2m12sec	4d12h22m
R	WIN(+18) B:21,W:3	WIN(+32) B: 28, W: 0	WIN(+40) B: 32, W: 0

We ran a similar experiment in Reversi version (starting position is parallel). However, we obtained similar experimental results.

### 6. Conclusion

See Figure 2 and Figure 3. The horizontal axis shows each board and the vertical one shows the ration number of the pieces acquired by the first move relative to the total number of the pieces. The central dashed line shows the boundary of the win/loss. Figure 2 shows the ration is increased in the transition from the 4x4 board to the 6x6 board. Figure 3 shows the feature that the first move becomes advantageous along with the expansion of the board in rectangular Othello.

From these, we guess that the first move will become advantageous along with the expansion of the board in square Othello.

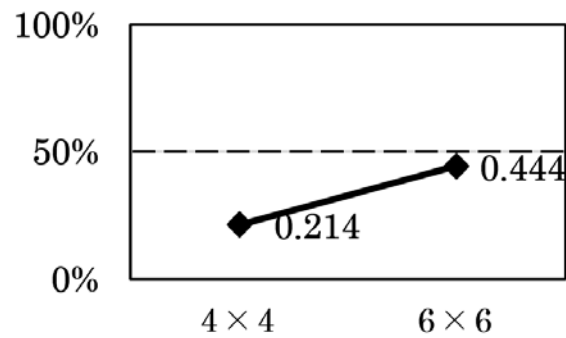


Fig. 2. Ration number of the pieces by first move (square).

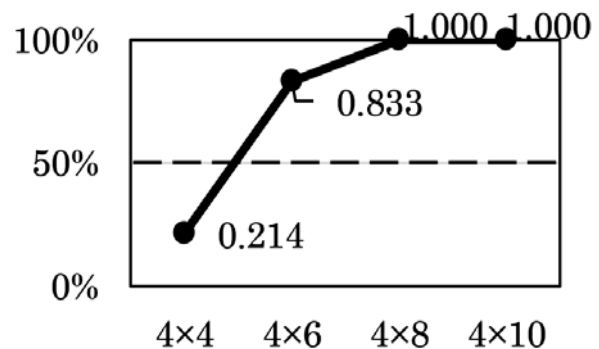


Fig. 3. Ration number of the pieces by first move (rectangle).

Also, considering the increased range in Figure 2, we consider the standard 8×8 board is likely to be a win for the first move or draw. Moreover, there is a high possibility that first move wins in 10×10 or more board.

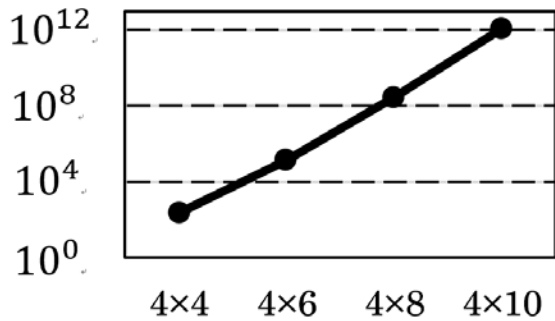


Fig. 4. Number of the positions in rectangular Othello.

Besides, Figure 4 shows the transition in number of the positions in rectangular board. The horizontal axis shows each board size and the vertical one represents number of the positions by the exponent. From this graph, we can see that number of the positions increases curvedly. Additionally, it can be guessed that number of the positions of 4×12 board is about 10<sup>4</sup> times of 4×10 board.

## 7. Future work

In this paper, we were able to obtain the perfect play of 6×6 board and 4×10. We confirm that this consideration is correct by continue to challenge the perfect analysis which extended this (4×12, 4×14 and 6×8 boards). In addition, in 8×8 board, we continue to further consideration by the perfect analysis of some advanced boards from starting position to occur well in between the high-level players.

### 7.1. Improvement

Alpha-Beta Pruning becomes more effective by the move ordering. Because our program is low this quality, it is necessary to improve.

We have to implement a hash table in order to cut the boards with duplicate and symmetry. However, it will slow down the search to take the access time to it.

In addition, we improve the Bid Board mentioned in Section 3.1 and the drawbacks mentioned in Section 4.

## Acknowledgements

This work was supported by JSPS KAKENHI Grant Number 24510217.

## References

- [1] J. v. Neumann, O. Morgenstern, *Theory of Games and Economic Behavior* (Princeton Univ Pr, 1944)
- [2] J. Schaeffer, N. Burch, Y. Björnsson, A. Kishimoto, M. Müller, R. Lake, P. Lu and S. Sutphen. Checkers Is Solved, *Science*, Vol. 317 (2007), pp. 1518-1522.
- [3] British Othello Federation. Forty Billion Nodes Under The Tree: The Newsletter of the British Othello Federation (1993), pp. 6-8.
- [4] D. E. Knuth, R. W. Moore. An Analysis of Alpha-Beta Pruning, *Artificial Intelligence*, Vol. 6 (1975), pp. 293-326.

# **A proposal for teaching programming through the Five-Step Method**

**Yasuo Uchida**

*National Institute of Technology, Ube College  
Ube, 755-8555, Japan  
E-mail: uchida@ube-k.ac.jp*

**Seigo Matsuno**

*National Institute of Technology, Ube College  
Ube, 755-8555, Japan*

**Takao Ito**

*Hiroshima University  
Higashi-Hiroshima, 739-8527, Japan*

**Makoto Sakamoto**

*University of Miyazaki  
Miyazaki, 889-2192, Japan*

## **Abstract**

We have proposed a new method of advancing from CS Unplugged through the new process of CS Plugged to full-fledged computer programming languages, as a means of deepening understanding in computer programming education. We also have proposed a new Five-Step Method consisting of the following steps: Step 1, A CS Unplugged activity; Step 2, A CS Plugged activity; Step 3, A trace table, Step 4, Preparing pseudocode; and Step 5, Writing Java source code.

*Keywords:* CS Unplugged, CS Plugged, Programming, Five-Step Method.

## **1. Introduction**

The course we teach has about 40 students per class, aged 17 through 18 years. Since the students' major field of study is Management Information, they need to learn programming [1] techniques. However, the results of the survey described below show that not a few students consider themselves to have insufficient

understanding of programming or think that they are not good at programming. We are examining ways to improve this situation. CS Unplugged [2] is a method of teaching information science without using computers, first proposed by Tim Bell of the University of Canterbury in New Zealand. While CS Unplugged is said to be effective in teaching information science [3], there have been concerns that its success or failure may be an effect of the skill and experience of instructors. To

© *The 2015 International Conference on Artificial Life and Robotics (ICAROB 2015), Jan. 10-12, Oita, Japan*

address this topic, we implemented CS Unplugged for a group of students of a different age group, from fifth through ninth grades, and looked at their responses. The results showed that after first making sufficient preparations the method could generate results without necessarily depending on the skill or experience of instructors. Other research underway in Japan includes a study on use of teaching aids in learning about algorithms through CS Unplugged [4] and a study on learning the fundamentals of computer programming through a programming learning environment for beginners [5]. A study by Y. Feaster et al [6] concerns practice in teaching high-school students, and it has been reported to have had some, albeit limited, success. However, at present almost no research has been conducted on advancement from CS Unplugged to full-fledged programming languages. Accordingly, we propose a new method of advancing from CS Unplugged to full-fledged programming. The proposed method begins with conducting a CS Unplugged activity, and then continues on to writing a program on the same theme and further to its abstraction in Java. Accordingly, we propose advancing from CS Unplugged to full-fledged programming through a new Five-Step Method. The proposed method consists of the following steps: Step 1, A CS Unplugged activity; Step 2, A CS Plugged activity; Step 3, A trace table, Step 4, Preparing pseudocode; and Step 5, Writing Java source code.

## 2. Background of this study

Every year we conduct a survey following our first-term course of two 90-minute sessions per week held over 30 weeks. Here we will look at numbers of students who answered “yes” or “no” to this survey’s question, “Do you think you largely understand Java?”

As seen in Fig. 1, the survey’s results show that not a few students consider themselves to have insufficient understanding of programming or think that they are not good at programming. As such, there is a need to improve this situation.

## 3. CS Unplugged in practice

For about 50 minutes on August 2, 2014 we used the CS Unplugged method for approximately 30 students from

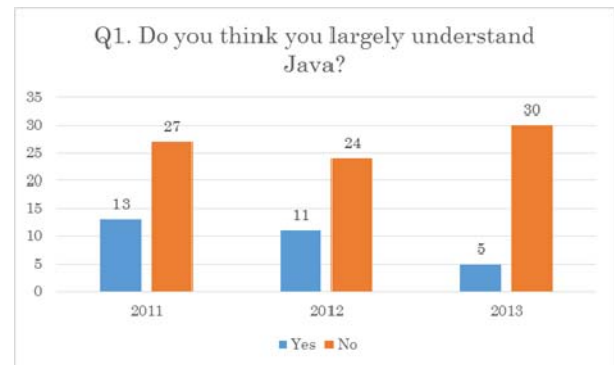


Fig. 1. Survey results on understanding of Java.

fifth through ninth grades as part of a summer-vacation junior science course. The activity we implemented was CS Unplugged’s Image Representation activity. Fig. 2 shows examples of students’ work.

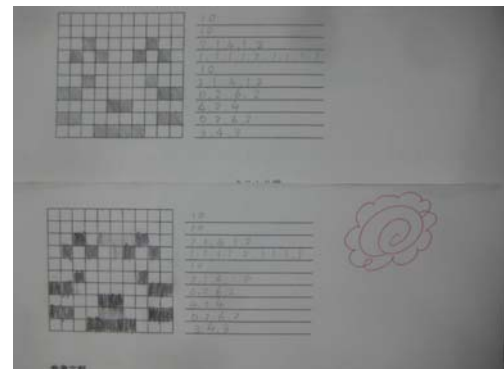


Fig. 2. Examples of students’ work

## 4. The Five-Step Method

In this paper, we use the name CS Plugged to refer to implementing a CS Unplugged activity through a computer program. The goal is to advance to computer programming through using a computer program to conduct the work done by human beings in a CS Unplugged activity.

Accordingly, we propose advancing from CS Unplugged to full-fledged programming through a Five-Step Method. The proposed method consists of the following steps: Step 1, A CS Unplugged activity; Step 2, A CS Plugged activity; Step 3, A trace table, Step 4, Preparing pseudocode; and Step 5, Writing Java source code.





#### 4.5. Step 5: Writing Java source code

In this step students create a program by converting the pseudo-language from the previous step to Java source code. The subsequent debugging process is handled by going back and examining each previous step depending on the content of the error messages.

- Java source code

```
public class Image2Code {
    public static void main(String args[]) {
        char[][] image = {{'□', '■', '■', '■', '□'},
                          {'□', '□', '□', '□', '■'},
                          {'□', '■', '■', '■', '■'},
                          {'■', '□', '□', '□', '■'},
                          {'■', '□', '□', '□', '■'},
                          {'□', '■', '■', '■', '■'}
        };
        // Iterate only number of lines in an array
        for(int i = 0; i < image.length; i++) {
            char previous = '□';
            int count = 0;
            // Display the image in pixels
            for(int j = 0; j < image[0].length; j++) {
                System.out.print(image[i][j]);
            }
            System.out.print(" ");
            // Count number of adjoining pixels of same color and
            display in numerical form (code)
            for(int j = 0; j < image[0].length; j++) {
                if (image[i][j] == previous) {
                    count++;
                } else {
                    previous = image[i][j];
                    System.out.print(count + " ");
                    count = 1;
                }
            }
            System.out.println(count);
        }
    }
}
```

- Results of running the above program

```
□■■■■ 1, 3, 1
□□□■ 4, 1
□■■■■ 1, 4
■□□■ 0, 1, 3, 1
■□□■ 0, 1, 3, 1
□■■■■ 1, 4
```

#### 5. Conclusion

We have proposed a new method of advancing from CS Unplugged through the new process of CS Plugged to full-fledged computer programming languages, as a

means of deepening understanding in computer programming education. We also have proposed a new Five-Step Method consisting of the following steps: Step 1, A CS Unplugged activity; Step 2, A CS Plugged activity; Step 3, A trace table, Step 4, Preparing pseudocode; and Step 5, Writing Java source code. Topics for the future are those of putting together detailed procedures for abstraction of pseudocode from trace table as well as continually implementing the proposed method and measuring its results.

#### References

1. D. Everitt, Introducing programming skills in education, [https://www.academia.edu/1478617/Introducing\\_programming\\_skills\\_in\\_education](https://www.academia.edu/1478617/Introducing_programming_skills_in_education).
2. The Unplugged Community: Computer Science Unplugged, <http://csunplugged.org/>.
3. Y. Idosaka, Y. Kuno, and S. Kanemune, Attempt and the Practice of Class Method Improvement Based on "Computer Science Unplugged", *Journal of the Japan Society of Technology Education*, vol.53, no.2 (2011), pp. 115-123 (in Japanese).
4. H. Manabe, S. Kanemune, and Namiki M., Effects of Teaching Tools in CSU Algorithm Education, *IPJS Journal*, vol.54, no.1 (2013), pp. 14-23 (in Japanese).
5. T. Nishida, A. Harada, R. Nakamura, Y. Miyamoto, and T. Matsuura, Implementation and Evaluation of PEN: The Programming Environment for Novices, *IPJS Journal*, vol.48, no.8 (2007), pp. 2736-2747 (in Japanese).
6. Feastery Y., Segarsz L., Wahbay S.K., Hallstrom J.O.: Teaching CS Unplugged in the High School (with Limited Success). Proceedings of the 16th annual joint conference on Innovation and technology in computer science education, pp. 248--252 (2011)
7. Cambridge International Examinations, SYLLABUS Cambridge O Level Computer Studies 7010 For examination in June and November 2014, *University of Cambridge International Examinations*, <http://www.cie.org.uk/images/90258-2014-syllabus.pdf>.
8. Information-technology Promotion Agency Japan, Kyotsu ni shiyo sareru gijigengo no kijutsukeishiki ("Symbolic conventions of commonly used pseudo-language"), [https://www.jitec.ipa.go.jp/1\\_13download/gijigengo\\_keisiki.pdf](https://www.jitec.ipa.go.jp/1_13download/gijigengo_keisiki.pdf) (in Japanese).
9. S. Mimura: Gijigengo shimyureta SARA ("SARA pseudo-language simulator"), <http://mimumimu.net/software/#sara> (in Japanese).

# The role of national standards setter in the global convergence era: the case of the Japanese setter from 2001 to 2008

**Kensuke Ogata**

*Economic Department, University of Nagasaki,  
123 Kawashimo, Sasebo, Nagasaki, 858-8580, Japan  
E-mail: ogata@sun.ac.jp*

## Abstract

An aim of this paper is to explain that the change of standard-setting activities of ASBJ in the 2000s was caused by its own standard-setting development strategy. An analysis of organizational structure using graph theory showed that the ASBJ strategically alter its structure, and that the structure can trigger the change of setting activities.

*Keywords:* ASBJ, social network analysis, standards-setting process, accounting regulations

## 1. Introduction

Since International Accounting Standards Board (IASB) was founded in 2001, far more one hundred countries adopted International Financial Reporting Standards (IFRSs) which the IASB produced; currently both the Board and its standards should not be ignored. As accompanying with these increasing attentions, it is expected to draw a lot of interests in roles of national standard-setters as mediators between the IASB and wide ranges of stakeholders in the country (Büthe and Mattli [1]).

In Japan, although giving the listed companies permission to preparing their consolidated statements with IFRSs, the national setter, Accounting Standards Board of Japan (ASBJ), has kept producing its own standards; the great majority of companies furthermore use Japanese standards. When turning to the activities of ASBJ over times (shown in Table 1), we can see major difference in terms of volume and content of the standards according to time. In particular, its activities varied greatly before or after 2005. Based on traditional organizations theory (See Rumelt [2], Miles and Snow [3]), it is presumed that organizations change their structure to achieve their desired results. Following this presumption, the ASBJ might change its structure around then. In this paper, we focus on the activities of ASBJ in the first eight years, and determine what kinds of organiza-

tional structure the IASB respectively constructed before or after 2005. This examination process is the first step to approach standard-setting motivations of ASBJ.

## 2. Overview of ASBJ

For getting over the long-term recession, Japanese government put efforts into huge economic structural reforms. Also, in order to respond to the appearance of IASB, standard-setting regime in Japan was transformed from a public body to a private in order to make the most of the private sector vitality. Subsequently, ASBJ was created as the first private setter for establishing accounting standards in Japanese history in September 2001. The creation was initiated by Japanese government, Financial Service Agency, with some stakeholders related to securities markets in private sector (ASBJ/FASF [4]).

The ASBJ has completed a total of fifty-seven standards from September 2001 to September 2014. Graph 1 shows the activities of ASBJ during this period with one polygonal line and two bars. The line indicates the number of standards the Board developed every year, while the two bars respectively denote the number of “Liberal” standards and of “Non-Liberal” ones. Herein, “Liberal” standards are synonymous with the term “investor-oriented,” including standards to include accounting techniques which have never been used in

© The 2015 International Conference on Artificial Life and Robotics (ICAROB 2015), Jan. 10-12, Oita, Japan

practices, to reduce alternative accounting procedures, and to introduce the fair value measurement; “Non-Liberal” give the preparers their favorable consequences, for example, the increment of alternative procedures and the clarification of accounting procedures simply in response to changes of other standards or related laws.



According to this graph, we can separate the standard-setting activities of ASBJ into three parts. The first is period from 2001 to 2004; the second is from 2005 to 2008; and the third is since 2009. In the first period, the ASBJ set very little accounting standards. The Board made thirty standards public, which accounts for 52.6% of the total. In addition, the Board issued fifteen “Liberal” standards. It accounts for 68.2% of the total “Liberal” standards over the whole period. In the next four years, the Board actively developed standards from both quantitative and qualitative aspects. In the last period, the activities of ASBJ slowed down.

Due to space limitation, we focus on a big difference between the activities in the first four years and the second four in this paper. Therefore, we mention characteristics of standard-setting of ASBJ in two periods as follows: the ASBJ developed quite passive standard-setting attitude during the period of 2001-2004; the Board contrastingly exhibited the most positive behavior during the period of 2005-2008. In taking account for a reason of that difference, it seems effective to shed light on difference of organizational structure, based on the traditional organizations theory.

### 3. Organizational Structure of ASBJ

#### 3.1 Social network analysis and using data

We extract structural feature of ASBJ with social network analysis<sup>1</sup>. We particularly use continuous coreness analysis to identify a set of actors who have a high density of ties among themselves (the core) and another set

of actors who have a low density of ties among themselves (the periphery) by having few events in common (Borgatti and Everett [8]). Herein, the term “coreness” refers to who has a high density of ties in the network by many common events.

In analyzing the structure of ASBJ, we use data associated with existing organizations to which members of some bodies inside Financial Accounting Standards Foundation (FASF), which is a parent organization of ASBJ, belong. An underlying idea to use such data is that individual preferences and opinions on the accounting standards or techniques should be depended upon his/her background or career. In sum, shedding light on the relations based on the career of members who engaged in the accounting standard-setting process can demonstrate what kinds of actors dominate and what values are prevailing in the setter.

To do so, first of all, we prepare a matrix data-set, composed of both the existing organization of members shown in FASF’s annual reports and the bodies inside FASF<sup>2</sup> by period. This data-set tells us that the more and the longer the organizations send their members to the bodies inside FASF, the higher the coreness scores of the organizations get. Second, we transform each data-set to the organization-to-organization data-set through the affiliation process, included in the software of social network analysis, UCINET 6 (Borgatti, Everett and Freeman [9]). Third, we conduct coreness analysis using the organization-to-organization data-set and, at once, draw a graph on the basis of degree centrality analysis performed over the same data-set, using Net-Draw (Borgatti [10]).

We prepare two original matrix data: one is the data pertain to the first half, a period of 2001-2004; another is the data related to the second half, a period of 2005-2008. We confirm that 69 organizations engaged in the standard-setting process of ASBJ in the first period; and 77 organizations in the second period.

#### 3.2 Analytical results

##### 3.2.1 Analytical results in Period 1

A result of the coreness analysis on the first period is shown in Table 1. The top 30 organizations are shown in this table. This result tells us some interesting facts.

<sup>1</sup> Some recent studies on accounting standard setters applied social network analysis. See Perry and Noëlke [5], Richardson [6], Ogata [7].

© The 2015 International Conference on Artificial Life and Robotics (ICAROB 2015), Jan. 10-12, Oita, Japan

<sup>2</sup> Included are Board of Directors, Board of Councilors, Board, Theme Advisory Council, Advisors, and Standards Advisory Council.

First of all, the top four actors, that is, Tokyo Stock Exchange, University of Tokyo, Chuo-Aoyama, and Japanese

1 period 1	
ite	Coreness
-	0.392
-	0.343
-	0.336
-	0.302
-	0.248
in	0.203
in	0.172
-	0.163
-	0.152
-	0.151
-	0.149
in	0.147
-	0.141
-	0.138
-	0.122
in	0.120
-	0.120
-	0.104
-	0.104
-	0.104
in	0.104
-	0.104
r	0.101
-	0.096
-	0.096
in	0.096
in	0.094
-	0.088
in	0.077
in	0.077

Bankers Association, got strikingly high coreness scores among a total of 69 organizations. It is an unprecedented feature that organizations from stock markets and academic community played central roles in the standard-setter. Although very few user actors existed in this network, some academic

actors appeared, for example, Waseda University, Hitotsubashi University, and University of Shizuoka. Second, prepare of financial statements, including both financial community and non-financial community, belonged to half of the top 30 organizations. Among these organizations, non-financial community, for example, Hitachi, Panasonic, Sumitomo Electric, and Tokyo Electric Power, obtained relatively high marks.



Also, we see the organizational structure of ASBJ at that time (see Graph 2). As is the case with the above coreness result, we can tell that the four main organizations (Tokyo Stock Exchange, University of Tokyo, Chuo-

Aoyama, and Japanese Bankers Association) were dominant actors. In addition to that, more organizations from preparers appeared on this graph, compare to other kinds of groups.

### 3.2.2 Analytical results in Period 2

We confirm the coreness result of ASBJ in the following four years:

2005-2008 (see Table 2). According to this Table, we can see that there was a considerable difference in coreness scores between the top four organizations and the others. With regard to the top four, included were Azusa, Tohmatsu, ShinNihon, and FASF. These three accounting



firms are member firms of the Big Four<sup>3</sup>. Also, the FASF has gotten staffs on the payroll; as a result, the coreness score of FASF sharply increased. Secondary, prepares of financial statements occupied a half of the top 30 organizations alike the first period. However, its composition changed as financial sectors including



<sup>3</sup> Azusa belongs to KPMG group; Tohmatsu to Deloitte; and ShinNihon to Ernst & Young.

Nomura Securities, Mitsui Sumitomo Insurance, and Meiji Yasuda Life, had relatively high scores.

Then, we make sure of a network graph of ASBJ during the same period (*see* Graph 3). According to this Graph, we can point out that the actors as described below existed at the heart of this network: Tohmatsu, Azusa, ShinNihon, FASF, Tokyo Stock Exchange, and several financial and non-financial companies. Among others, accounting profession group occupied a central position in this network, in terms of the strength of connection shown by line thickness.

#### 4. Discussion

To emphasize the change of the ASBJ's organization structure between the first period and the second, we show the transition of central actors by attributes in Table 3. This table presents the proportions of each attribute group to all groups between the both periods on the basis of coreness scores and the difference. Herein, attribute group are divided into seven groups as follows: academic community (Aca); financial community (Fin); non-financial community (Non-Fin); accounting professions (Pro); regulators (Reg); the users of financial statements (User); and the others (Other).

In the first period, the preparer group (47.3%) obtained the highest rank. Among this group, non-financial community group (25.5%) had superiority over financial group (21.8%) to a small extent. Academic community group (21.1%) and accounting profession group (20.2%) followed these groups. The ASBJ thus orchestrated the various powers of Japanese actors, including preparer group, academic community, accounting profession community, at that time. Among them, preparer group was a pillar to the ASBJ. On the other hand, the accounting profession group (43.5%) became the most powerful player in the second period. Preparer group (34.3%), composed of non-

financial community (18.1%) and financial community (16.2%), followed this group. To focus attention on the difference between the both periods, the profession group significantly increased the proportion (+23.3%), and the regulators came next (+11.0%); but all other groups, for example, the academic group (-15.9%), the non-financial group (-7.5%), and the financial group (-5.6%), lowered their importance.

#### 5. Conclusions

Thus, it seems that the ASBJ, during the first period, constructed the organization, in which the preparer group was the most central player, although orchestrating the various powers of Japanese actors, for the purpose of setting very few standards. On the other hand, the Board formed an accounting profession-centric organization to develop the standards, which contained new accounting techniques to have never been used in Japanese practices, in an active attitude.

#### References

- [1] Büthe T and Mattli W (2011), *The New Global Rulers: The Privatization of Regulation in the World Economy*. Princeton University Press
- [2] Rumelt RP (1974), *Strategy, Structure, and Economic Performance*. Harvard University Press
- [3] Miles RE and Snow CC (1978), *Organizational Strategy, Structure, and Process*. McGraw-Hill
- [4] ASBJ/FASF (2012), *The 10-year history of ASBJ/FASF* (in Japanese). FASF
- [5] Perry J and Noëlke A (2005), International Accounting Standards Setting: A Network Approach. *Business and Politics* 7(3.5): 1-32
- [6] Richardson AJ (2009), *Regulatory Networks for Accounting and Auditing Standards: A Social Network Analysis of Canadian and International Standard-Setting*. *Accounting, Organizations and Society* 34: 571-588
- [7] Ogata K (2010), A Study of Accounting Standard-Setting Using Graph Theory. *Artificial Life and Robotics* 15: 279-283
- [8] Borgatti SP and Everett MG (1999), Models of Core/Periphery Structures. *Social Networks* 21: 375-395
- [9] Borgatti SP, Everett MG, Freeman LC (2002), *Ucinet for Windows: Software for Social Network Analysis*. Harvard, MA: Analytic Technologies
- [10] Borgatti SP (2002), *Netdraw: Network Visualization*. Harvard, MA: Analytic Technologies

## **An Empirical Research on Inter-firm Capital Relationship in Yokokai Using IDE Spatial Model**

**Takao Ito**

*Graduate School of Engineering, Hiroshima University, Higashi-Hiroshima, 739-8527 Japan*  
[itotakao@hiroshima-u.ac.jp](mailto:itotakao@hiroshima-u.ac.jp)

**Makoto Sakamoto and Satoshi Ikeda**

*Dept. of Computer Science and Systems Engineering, University of Miyazaki, Miyazaki, 889-2192 Japan*  
[sakamoto@cs.miyazaki-u.ac.jp](mailto:sakamoto@cs.miyazaki-u.ac.jp) [bisu@cs.miyazaki-u.ac.jp](mailto:bisu@cs.miyazaki-u.ac.jp)

**Rajiv Mehta**

*School of Management, New Jersey Institute of Technology, New Jersey, NJ 07102-1982 U.S.A*  
[mehta@njit.edu](mailto:mehta@njit.edu)

**Tsutomu Ito**

*Hamura Factory, Hino Motors, Ltd, Tokyo, 205-8660 Japan*  
[fw.eldorado.500cuin@gmail.com](mailto:fw.eldorado.500cuin@gmail.com)

### **Abstract**

This paper introduces recent fundamental modifications to Japanese alliance system known as the keiretsu, and analyses how these changes have affected corporate performance. Specially, the performance of Japanese auto manufacturers, such as Toyota, Nissan and others, has significantly improved due to sophisticated production system technologies, highly productive workers, and recurring transaction relationship with other partners in their network family. One possible determinant of their success could be due to their unique organization forms –the keiretsu– which provides a strong platform to forge their strategic alliance relationship with their parts suppliers as well as collaboration in research and development with other automobile makers. After economic bubble of the 1990', the strong ties between automobile makers and their supplier partners experienced significant changes, which are known as “keiretsu loosening”. Consequently, what is the status quo of automotive keiretsus? Does cross-shareholding, which is one specific form of capital relationship in keiretsu, still contribute to improving corporate performance? To answer these questions, this paper reports the results of a study that collected data on cross-shareholdings to shed light on the relationship between inter-firm capital relationship and corporate performance. The findings of this empirical investigation reveal that: (1) Keiretsu is a flexible, highly adaptive organizational form; its scale changes in response to economic situations; (2) Capital relationship is still a significant determinant of increasing profits for keiretsu partners even after the bubble burst in the 1990s.

*Keywords:* Influence, Degree, Effective Size, the IDE model, keiretsu loosening.

© The 2015 International Conference on Artificial Life and Robotics (ICAROB 2015), Jan. 10-12, Oita, Japan

### 1. Introduction

Japanese automobile manufacturers still show signs of performing at a significantly higher level than their global counterparts. This could possibly be due to the sophisticated technologies deployed for their production systems, highly productive employees, and continuous transaction relationships with other member-partners in the keiretsu network. Possibly, one explanatory factor contributing to their success could be due to their unique organization forms –the keiretsu– which provides a strong platform to forge strategic alliances with their parts suppliers, as well as collaboration in research and development with other automobile makers. This manuscript is organized as follows: Section 2 reviews the relevant literature associated with keiretsu networks. Section 3 describes the data collection process and the new network model. Based upon the findings, the managerial implications are discussed in section 4. In section 5, the study limitations are identified and avenues of future research are proffered.

### 2. Variables Selection

To shed light on these issues and to examine the network relationship between cross shareholdings and corporate performance, data were collected from Mazda’ keiretsu, Yokokai,. The Mazda’s keiretsu is composed of three sub-organizations: Nishi-Nihon Yokokai, Kanto Yokokai and Kansai Yokokai.

As previously noted, many structural indices of network analysis have been developed. This study selected degree, influence and effective size of the firms included in Yokokai to analyze the relationship between those indices and corporate performance.

Degree is an index of a firm’s potential communication activity. In a network, cross shareholding degree includes two categories: in-degree and out-degree. This is because cross shareholding networks are considered to be asymmetric organizations. In-degree refers to a firm accept investment from other member firms, whereas out-degree reflects a firm that only buy stocks from other firms within the network. Degree is calculated as below [7].

$$C_D(p_k) = \sum_{i=1}^n a(p_i, p_k) \tag{1}$$

where

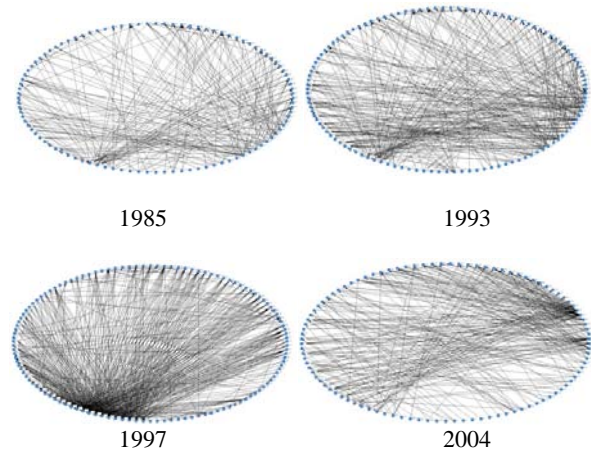


Fig.1. Capital Networks in Yokokai.

$$a(p_i, p_k) = 1; \text{ if and only if } p_i \text{ and } p_k \text{ are connected by a line}$$

$$= 0; \text{ otherwise}$$

Percentage data of inter-firm’s transactions were collected from Yokokai. In a transactional network, high value of degree is positively associated with its corporate performance such as sales and profit [9-10]. Based upon this prior work, the following hypothesis is postulated:

H1: Out-degree will be positively associated with its profit, and in-degree will be negatively associated with its profit.

Influence reflects the power to influence or have an impact on other member firms directly and indirectly in a network. Consequently, influence is being divided into two parts: direct influence and indirect influence. Suppose that A is the matrix of the direct network, and A<sup>n</sup> means the indirect influence from one firm to another firm by n steps. Then influence is calculated as follows.

$$T = A + R = A + A^2 + A^3 + \dots + A^n$$

$$= A(I - A)^{-1} \tag{2}$$

where

- T: Total influence;
- A: direct influence;
- R: indirect influence;
- I: Identity matrix.

In an asymmetric network, cross shareholding influence includes two categories: influence and affectedness. Influence refers to a firm have strong impact on other member firms, whereas affectedness reflects a firm that only is influenced by other firms within the network. In same network, influence has strong impact on its corporate performance [4, 10]. Consequently, the following hypothesis proffered:

H2: *Influence will be positively associated with its performance and affectedness## will be negatively associated with its profit.*

Effective size of the network refer to the number of alters that ego has, minus the average number of ties that each alter has to other alters. It can be calculated as follows [8].

$$ES(p_k) = (n - 1) - \frac{1}{n - 1} \sum x_{pk} \quad (3)$$

where

- n: number of ego network (pk is not included);
- x<sub>pk</sub>: node k's connection line in k's ego network.

A recent study investigated the relationship between firm network position and corporate venture capital investment [11]. In another study, Sakamoto et al. reported effective size is one of the key determinants associated with corporate performance in transaction network [12]. Accordingly, the following hypothesis is posited:

H3: *Effective-size will be positively associated with its profit.*

### 3. Analysis and Discussion

The implications of our results can be considered as follows.

#### 3.1. Out-degree and In-degree

In capital network, out-degree means the amount of investment in other partner companies, and in-degree refers to the amount of investment accepted from other companies. From 1985 to 2004, the partial correlation coefficient of out-degree is -0.2756, -0.863, -0.3822,

and -0.319 respectively. In-degree is significant only in 1985 and 1993. The value of in-degree is -0.2191 and -0.3493, which is illustrated in Fig. 2.

All of the out-degree is significant, but the relationship is the inverse. This means that higher investments are associated with less profit. According to the findings reported by Sakamoto et al., hypothesis 1 holds in transactional network, but in capital network, out-degree is negatively associated with profit. However, in McGuire and Dow's study, one of the conclusions is inconsistent because out-degree is negative even before the bubble economy collapsed. Much more quantitative research should be done to find support for their arguments. As interesting findings is that value in 1997 is very high. And the value returned to normal levels in 4 years after its adjustment. The values of in-degree in 1985 and 1993 are significant, but in 1997 and 2004 they are not significant. The bubble economy occurred at the beginning of 1990. Evidently, keiretsu began to adjust their structure after bubble economy collapsed. Therefore, it is apparent that the dramatic loosening of keiretsu occurred in Yokokai. Out-degree is a reflex of this change. Upon close investigation, the member of Yokokai is found to have been significantly changed. Most firms with weak competition disappeared and some strong firms such as Toyota's suppliers become new members in Yokokai. Thus, based upon the analysis described above, H1 partially holds.

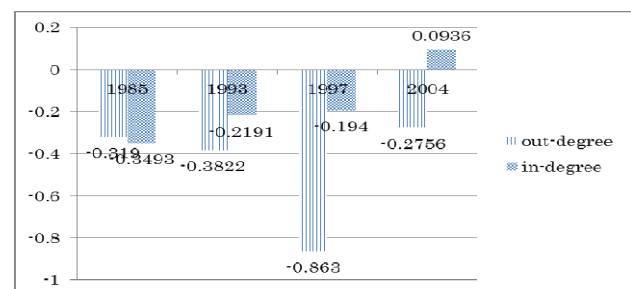


Fig.2. Out-degree and in-degree in Yokokai (1985-2004).

#### 3.2. Influence

Influence means one kind of power to affect persons or events without any direct or discernible effort. Influence reflects the power to influence or have an impact on other member firms directly and indirectly in a network. Influence depends on network depth. The depth of



Yokokai is 3, which means that depth still has impact on its influence. From 1985 to 2004, the partial correlation coefficient of influence is 0.3023, 0.864, 0.3874, and 0.3146 respectively. It can be shown as Fig. 3.

Fig. 3 shows that all partial correlation coefficients are positive and significant. The value in 1997 is extra high. And the value returned to normal by 7 years after its adjustment. This result coincides with the result of out-degree. Invest or buy stock from other companies is an effective way to maintain its influence in network. This means that higher influence is associated with higher profits. Therefore, H2 holds completely.

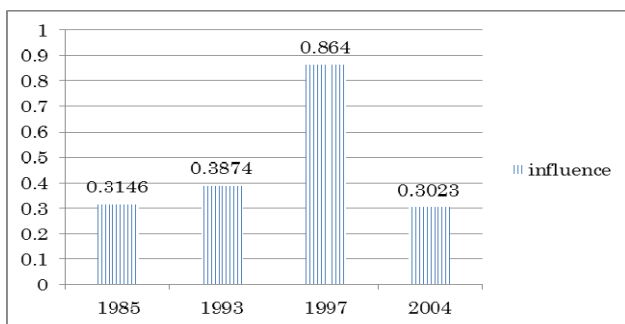


Fig.3. Influence in Yokokai (1985-2004).

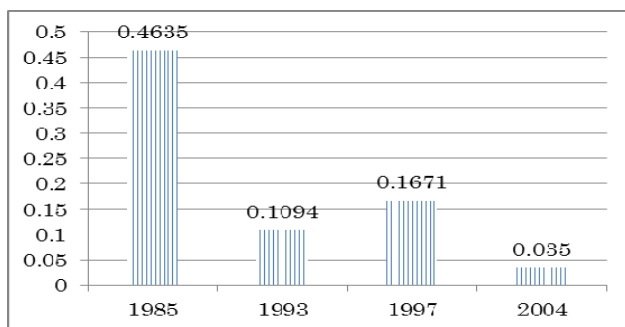


Fig.4. Effective Size in Yokokai (1985-2004).

### 3.3. Effective Size

All partial correlation coefficients of effective size can be drawn as Fig. 4.

Effective size refers to the situation of ego's network. The firm has strong connected neighbors if the value of effective size is high. Basically, strong connected neighbors can be considered as good condition to invest because all of the firms invest with each other in keiretsu. The value of effective size only in 1985 is high

and significant. Therefore, there is support for H3 only before bubble economy collapsed. The evidence reveals that keiretsu has already made a major policy shift by breaking with the so-called convoy system of alliance organization.

## 4. Conclusion and Future Research Avenues

This paper proposed three hypotheses between profit and network indexes including degree, influence and effective size. The relationship between profit and influence is supported, but the association between profit and degree is partially supported. The linkage between profit and effective size holds only before bubble economy collapsed. On analyzing the background of the membership change in Yokokai, the results show that rational inter-firm relationships in keiretsu are still associated with corporate performance. This suggests that keiretsu loosening resulted in performance improvement as cross share-holdings still maintained.

Some factors, such as affectedness and effective size are not statistically significant. Thus, additional factors should be identified as potential determinants of profit. Data were drawn from Mazda's Yokokai to test the hypotheses. Thus, additional studies should replicate these findings by drawing data from other keiretsus, such as Toyota's Kyohokai and Nissan's Nishokai, thus testing the validity of these research findings.

## ACKNOWLEDGMENT

This work was supported by JSPS KAKENHI Grant Number 24510217.

## References

1. McGulre J, Dow S., (2009) *Japanese keiretsu: Past, present, future*, [http://download.springer.com/static/pdf/983/art%253A10.1007%252Fs10490-008-9104-5.pdf?auth66=1399794791\\_ce53db11bd93d8098b0304e16dae06f&ext=.pdf](http://download.springer.com/static/pdf/983/art%253A10.1007%252Fs10490-008-9104-5.pdf?auth66=1399794791_ce53db11bd93d8098b0304e16dae06f&ext=.pdf), retrieved May 9, 2014
2. Ito T. (2004) *Quantitative analysis of the firm's relationship in the Keiretsu of Toyota group*, *Proceedings of the 2004 Information Resources Management Association, International Conference, Innovations Through Information Technology*, pp.1078-1079, May 23-26, 2004, New Orleans, USA.

# Design and Experimental Evaluation of a Human Skill-Based PID Controller

**Yuntao Liao\***

*Graduate School of Engineering, Hiroshima University,  
Hiroshima Japan*

**Toru Yamamoto**

*Faculty of Engineering, Hiroshima University  
Hiroshima Japan*

*E-mail: liao-yuntao@hiroshima-u.ac.jp, yama@hiroshima-u.ac.jp  
www.hirosima-u.ac.jp*

## **Abstract**

Nowadays less and less people are willing to do hard works. Which makes that the controller based on human skill is needed. Cerebellar model articulation controller (CMAC) is a kind of neural networks (NNs) that can easily solve problems of nonlinear system. Compared with other NNs the advantage of CMAC is that it takes shorter learning time. Moreover because of the widely used of PID controller a human skill-based PID controller using CMACs has been proposed in this paper.

*Keywords:* Cerebellar model articulation controller, Neural network, Human skill, PID controller.

## **1. Introduction**

In the last decades, the automatic controller has been widely used in many fields. But still there are a lot of fields that human skill cannot be taken place by automatic controllers. However, the skilled workers become less and less due to the change of modern thoughts. As the result these specific skills will not be taken to the next generations. Therefore, to develop human skill based controller is necessary.

Human skill is a kind of nonlinear system. In order to deal with such nonlinear system, it is effective that some neural networks (NNs) are utilized. So far many NNs have been proposed and parts of them have been successfully used to design controllers<sup>1-4</sup>. But there is a problem that the conventional NNs need large learning

time to adjust weights of neurons, which makes it impossible for NNs to be applied widely. However the appearance of cerebellar model articulation controller (CAMC) that was proposed at 1975 by Albus partly solves this problem. CMAC has simple structure and like other NNs weights of CMAC also need to be adjusted, but this kind of adjustment has generalization ability. This kind of ability brings CMAC good real-time performance and some CMAC controllers have already been proposed<sup>5</sup>. Due to the above reasons using CMAC to design a controller based on human skill is feasible.

Furthermore PID controller has been widely used in various control systems. And the experienced human experts have been inevitably required in tuning PID gains. For the above proposal a human-skill based PID controller using CAMCs have been proposed.

## 2. Design of a Human Skill-Based Controller

### 2.1. CMAC

The following figure is a sample of simplified 2-dimensional input CMAC model to explain the structure of CMAC.

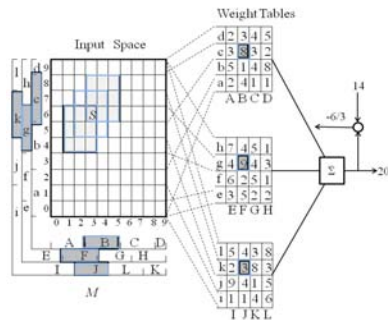


Fig. 1. 2-dimensional input CMAC model

In Fig.1, it is a CMAC with 3 weight tables and 4 labels. The set of input signals  $S$  (3,6) is mapped to B, F, J and c, g, k as set of labels M. Then, from each weight table 8,9 and 3 are selected. The sum of the selected weights is 20. Assume that the wished output value is 14, there will be  $-6/3$  added to all referred weights in the tables because of the difference between obtained value and wished value is  $-6$  and the number of selected weight tables is 3. As explained in the example CMAC usually works as follows: First the set of input signals  $S$  is mapped to the set of labels M. Then, according to the set of tables weights will be selected from each table. At last, output signals will be performed as the sum of the weights. From the explanation, when CMAC updating weights for one input signal the weights for the nearest input signals are also being updated, this kind of ability makes CMAC can obtain approximately wished value in shorter learning time than conventional NNs.

### 2.2. Controller design

In this paper, the following PID structure is considered:

$$\begin{aligned}
 u(t) = & u(t-1) \\
 & + K_p (y(t-1) - y(t)) \\
 & + K_i e(t) \\
 & + K_d (2y(t-1) - y(t) - y(t-2))
 \end{aligned} \tag{1}$$

where  $K_p$ ,  $K_i$  and  $K_d$  denote the proportional gain, the integral gain and the differential gain. Moreover  $r(t)$  denotes the target value and  $e(t)$  means the control error signal. The block diagram that shows the process how proposed method works is Fig.2.

© The 2015 International Conference on Artificial Life and Robotics (ICAROB 2015), Jan. 10-12, Oita, Japan

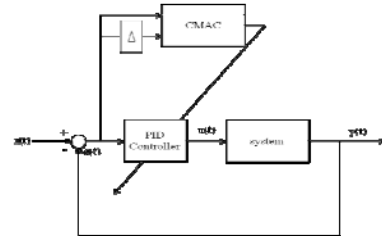


Fig.2. Block diagram of proposed method

In figure human skill data has already been learned by the CMAC and PID gains that tuned by these CMACs are used to control the system. The CMAC here sets  $e(t)$  and  $\Delta e(t)$  as the input space to calculate weights. And  $\Delta e(t)$  is the signal defined as:

$$\Delta e(t) := e(t) - e(t-1) \tag{2}$$

PID parameters are tuned by CMACs according to the following equations:

$$\begin{aligned}
 K_p &= \sum_{h=1}^K W_{p,h}(t) \\
 K_i &= \sum_{h=1}^K W_{i,h}(t) \\
 K_d &= \sum_{h=1}^K W_{d,h}(t)
 \end{aligned} \tag{3}$$

Where  $h=1,2,\dots,K$  and  $K$  denotes the total number of the selected weights in CMAC. From above the human skill based controller is designed through PID gains. And the performance of the controller is strongly depended on these PID gains.

Then the process of how CMACs learn human-skill data is shown in Fig.3.

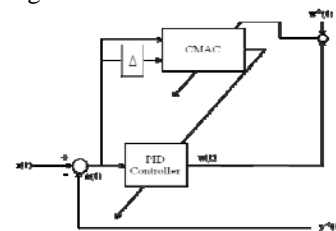


Fig.3. Block diagram of learning process

From Fig.3 there are two signals that attached asterisk (\*) which means they are human-skill data. And the human-skilled signals are set as the teacher signals. The learned result  $u(t)$  approaches teacher signal  $u^*(t)$  by updating weights  $W_h(t)$ . The CMAC weight tables are modified by steepest descent method and shown in Eq.4. In the equation  $g(t)$  means the gradient that used to update weights,  $J$  means the error criterion. And they are expressed as Eq.5 and Eq.6. In Eq.5  $a$ ,  $b$  and  $c$  are the appropriate positive constants set by designer.

$$W_{p,h}^{new}(t) = W_{p,h}^{old}(t) - g(t) \frac{\partial J}{\partial K_p} \frac{1}{K}$$

$$W_{i,h}^{new}(t) = W_{i,h}^{old}(t) - g(t) \frac{\partial J}{\partial K_i} \frac{1}{K}$$

$$W_{d,h}^{new}(t) = W_{d,h}^{old}(t) - g(t) \frac{\partial J}{\partial K_d} \frac{1}{K}$$
(4)

$$g(t) = \frac{1}{c + a * \exp(-b |u^*(t) - u(t)|)}$$
(5)

$$J := \frac{1}{2} \varepsilon(t)^2$$
(6)

$$\varepsilon = (u^*(t) - u(t))$$
(7)

Moreover, the partial differential of Eq. (4) is developed as follows:

$$\begin{aligned} \frac{\partial J}{\partial K_p} &= \frac{\partial J}{\partial \varepsilon(t)} \frac{\partial \varepsilon(t)}{\partial u(t)} \frac{\partial u(t)}{\partial K_p} \\ &= \varepsilon(t)(y(t) - y(t-1)) \\ \frac{\partial J}{\partial K_i} &= \frac{\partial J}{\partial \varepsilon(t)} \frac{\partial \varepsilon(t)}{\partial u(t)} \frac{\partial u(t)}{\partial K_i} \\ &= -\varepsilon(t)e(t) \\ \frac{\partial J}{\partial K_d} &= \frac{\partial J}{\partial \varepsilon(t)} \frac{\partial \varepsilon(t)}{\partial u(t)} \frac{\partial u(t)}{\partial K_d} \\ &= \varepsilon(t)(y(t) - 2y(t-1) + y(t-2)) \end{aligned}$$
(8)

### 3. Experimental Evaluation

#### 3.1. Experimental Equipment

In order to illustrate the effectiveness of the proposed method, an experiment has been performed by using a beam and ball control model. The experiment equipment is shown in Fig.4. As the figure shows, there is an input manipulator for human to operate. It is set to record the data of human skill. Also there is a distance sensor on beam to read output data of the system. Moreover there is an Arduino board to transfer data between computer and system. And the ball on the beam is the target to be controlled.

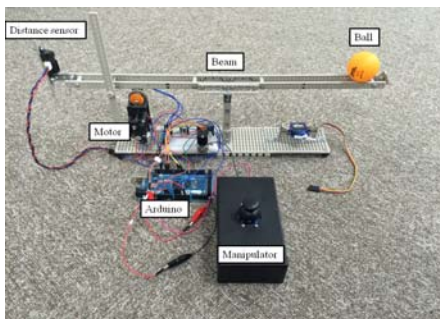


Fig. 4. Beam and Ball control Equipment

#### 3.2. Simulation and Experiment Result

The aim of the experiment is to control the ball staying at the middle of the beam, where  $r=0$ . Position of ball will be considered as output  $y$  and in this experiment the initial  $y$  is 20, it means at the beginning the ball stays at the right side of the beam. And angle of the beam is considered as the input of the system and the initial input is 0. The limit of  $u$  is set as:

$$-45^\circ \leq -u(t) \leq 45^\circ$$

And the output  $y$  is limited as:

$$-20[cm] \leq y(t) \leq 20[cm]$$

Human skill data  $u^*$  and  $y^*$  are obtained by skilled operator and they are shown in Fig.5. And based on the human skill data the learning process of CMACs is performed. In this design the CMACs with 4 weight tables and 3 labels are chosen. And the coefficients of learning ratio are set to be  $a=10^2$ ,  $b=10^2$ ,  $c=10^2$ . In addition, the initial values of the weights were fixed PID gains obtained by pole placement method based on the model of the system. And these PID gains are  $K_p = 0.0056$ ,  $K_i = 0.0019$ ,  $K_d = 0.0045$ .

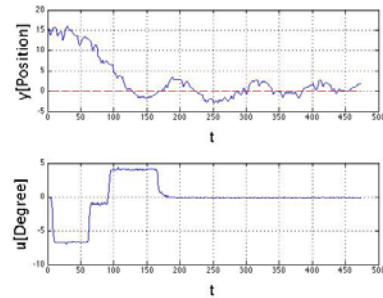


Fig.5. Control result by skilled operator

And the performance of learning process is evaluated by the following integrated squared error (ISE) equation:

$$ISE = \sum_{t=1}^{30} (u^*(t) - u(t))$$
(9)

As Fig.6 shows, the learning process stops when the integrated squared error is less than 0.00056.

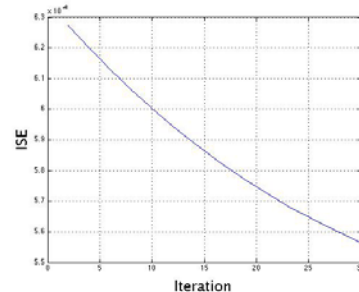


Fig.6. Performance of learning process

Fig.7 shows the comparison between learning result  $u$  and teacher signal  $u^*$ , where 30 iterations were performed. Fig.8 shows the PID gains trajectories corresponding to Fig.7. By using the PID gains that shown in Fig.8 an experiment has been done and the result is shown in Fig.9. From figure  $y$  is close to  $y^*$  shows that by using proposed method human skill can be learned.

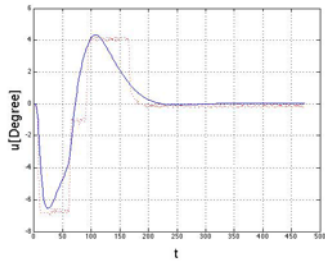


Fig.7. Comparison between  $u$  and  $u^*$

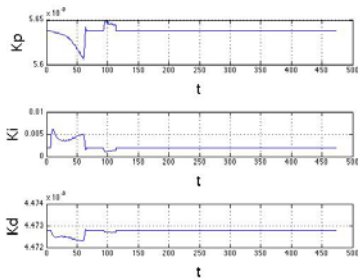


Fig.8. PID gains corresponding to Fig.7

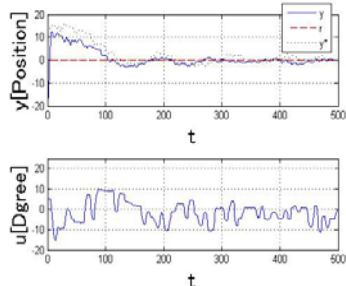


Fig.9. Control result by proposed method

### 3.3. Human Skill Analysis

Fig.13 shows the trajectories of  $kc$ ,  $Ti$  and  $Td$  they are got by following equations:

$$kc = Kp \quad Ti = \frac{kc}{Ki} Ts \quad Td = \frac{Kd}{kc} Ts \quad (10)$$

where  $Ts$  is sampling time and  $Ts=0.02$ . From the figure human skill is analyzed as follows: At first  $kc$  and  $Ti$  become smaller and  $Td$  becomes bigger because manipulator tries to move the ball to target stably. And then  $kc$  and  $Ti$  becomes bigger and  $Td$  becomes smaller shows human thinks the ball is going to reach the target

and he is trying to stop moving the ball. Next  $kc$  and  $Ti$  become smaller again and  $Td$  becomes bigger because his prediction was wrong the ball is not reach the target.

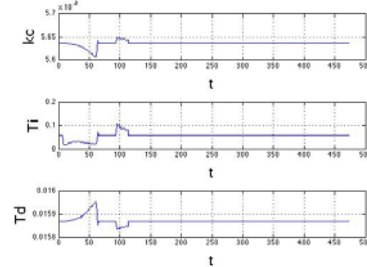


Fig.13. Trajectories of PID parameters

Then  $kc$  and  $Ti$  becomes bigger and  $Td$  becomes smaller because the manipulator predicts the ball is going to reach the target again and after that the change of  $kc$ ,  $Ti$  and  $Td$  is not obvious shows human is maintain his input to move the ball to target. At last,  $kc$  and  $Ti$  become smaller and  $Td$  becomes bigger to stop the ball at the target after that there is no change of  $kc$ ,  $Ti$  and  $Td$  shows human thinks the ball stops at the target. From analysis, the manipulator wants to control the ball stably approach to the target without overshoot.

### 4. Conclusions

In this paper, a human skill based PID controller using CMAC has been proposed. And the effectiveness of method has been experimentally examined on a beam and ball model. According to the control results the proposed method can replace human skill and based on the PID parameters human skill can be analyzed.

### 5. References

1. S.Liu and H.Asada "Adaptive Control of Deburring Robots Based on Human Skill Models," *Proc.of IEEE Conf. on Decision and Control, Brighton*, pp.348-353,1991.
2. K.S.Narendra and K.Parthasarathy "Identification and Control of Dynamical Systems Using Neural Networks," *IEEE Trans.on Neural Networks*, Vol.1,No.1,pp.4-27,1990.
3. S.Omatu, K.Marzuki and Y.Rubiyah "Neuro-Control and Its Applications," *Springer-Verlag*, 1995.
4. M.Kato, T.Yamamoto and S.Fujisawa "A Skill-Based PID Controller Using Artificial Neural Networks," *Proc.of Int. Conf. on Computational Intelligence for Modeling, Control and Automation, Vienna*, pp.702-705,2005.
5. K.Koiwai, K.Kawada and T.Yamamoto, "Design of a Human-Skill Based PID Controller using CMACs," *Int. Conf. on Control, Automation and Systems*, 2008

# Prototype of a Supporting Tool to Generate Testing Communication Diagram

Tetsuro Katayama\*, Seiya Urata\*, Yohei Ogata\*, Yoshihiro Kita†,  
Hisaki Yamaba\*, Kentaro Aburada‡ and Naonobu Okazaki\*

\*University of Miyazaki, 1-1 Gakuen-kibanadai nishi, Miyazaki, 889-2192 Japan

†Kanagawa Institute of Technology, 1030 Shimo-ogino, Kanagawa, 243-0292 Japan

‡Oita National College of Technology, 1666 Maki, Oita, 870-0152 Japan

E-mail: kat@cs.miyazaki-u.ac.jp, urata@earth.cs.miyazaki-u.ac.jp, ogata@earth.cs.miyazaki-u.ac.jp,  
y.kita@ccy.kanagawa-it.ac.jp, yamaba@cs.miyazaki-u.ac.jp, aburada@oita-ct.ac.jp, oka@cs.miyazaki-u.ac.jp

## Abstract

This research has implemented a prototype of a supporting tool to generate testing communication diagram. The testing communication diagram helps a developer to understand where the software system is tested by a large quantity of test cases written in text, and it is generated by adding the information of test cases to communication diagram in UML (Unified Modeling Language). The implemented prototype can detect more efficiently deficiency and/or contradiction in communication diagram and/or test cases.

*Keywords:* Software development, Software testing, Test cases, Visualization, UML(Unified Modeling Language)

## 1. Introduction

In recent years, test cases used in software testing have become a larger scale as a software system becomes a larger. It is difficult to understand where the software system is tested by a large quantity of test cases written in text. Moreover, test cases or models to describe a software system with UML (Unified Modeling Language)<sup>1</sup> may have deficiency and/or contradiction because the work to design the test cases and to model the system manually. It causes a situation that defects included in the system are not detected, leads to system failure after its operation, and gives users a great trouble.

The testing communication diagram has been proposed already.<sup>2</sup> It visualizes messages, which are written in a part of test cases, between objects in software system. It helps a developer to understand where the software system is tested by test cases written in text.

The testing communication diagram is generated by comparing test cases with communication diagram in UML and then adding the information of the test cases to the communication diagram. After the generation, a developer confirms whether or not deficiency and/or contradiction exist in communication diagram and/or test cases. Here, this process was gone manually.

In drawing testing communication diagram manually, one of problems is troublesome points to draw it and to confirm that the drawn diagram does not have any mistake. In confirming existence of deficiency and/or contradiction manually, one of problems is troublesome points to check it and to the checking process become more difficult as testing communication diagram becomes larger and more complex.

This research has implemented the prototype which can support to reduce the burden to generate testing communication diagram and to detect deficiency and/or contradiction in communication diagram and/or test cases. Because the prototype generates testing

communication diagram automatically, it can reduce the burden to draw the diagram and it can rid the work to confirm that the drawn diagram does not have any mistake. And also, because highlight display in a table of test cases and testing communication diagram are implemented as a function of the prototype, it can reduce the burden to detect deficiency and/or contradiction in communication diagram and/or test cases. Here, test cases are need to write in a template, a file format for test cases is CSV (Comma Separated Values), and a test suite means a collection of test cases.

## 2. Testing Communication Diagram

We explain steps to generate testing communication diagram.

- (i) Select one of the test cases that are not yet in comparison with communication diagram.
- (ii) Compare precondition with “participant name of sending side.”
- (iii) Compare input with “message name.”
- (iv) Compare precondition with “participant name of receiving side.”
- (v) When these agree, enclose the part represented an arrow of message in the diagram with a solid line. And, add a test case ID to inside the solid line.
- (vi) If you have a test case that not yet compared, return to (i). Otherwise, testing communication diagram is completed.

The completed testing communication diagram supports to detect deficiency and/or contradiction in communication diagram and/or test cases by confirming whether arrows of messages is encircled, or whether each test case ID exists.

## 3. Prototype of a Supporting Tool to Generate Testing Communication Diagram

The implemented prototype has two major characteristics to reduce the burden to find deficiency and/or contradiction in communication diagram and/or test cases.

- Highlight display in a table of test cases. Background color of a cell in a table of test cases is highlighted red from white based on a comparison

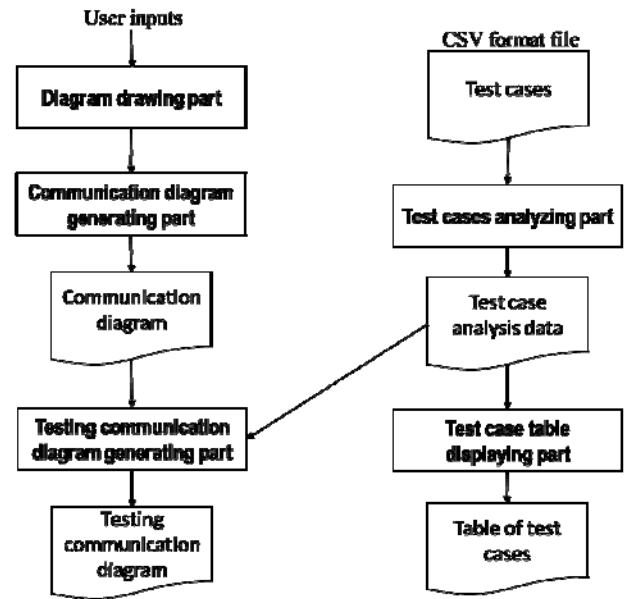


Fig. 1. Structure of the implemented prototype

result between communication diagram and a CSV file in which test cases are written.

- Highlight display in testing communication diagram. Based on the comparison result, test case IDs are added each of message name in the communication diagram as “message name : test case ID”, and their color is highlighted red from black.

Fig. 1 shows structure of the prototype. The prototype consists of five parts: diagram drawing part, communication diagram generating part, test cases analyzing part, test case table displaying part, and testing communication diagram generating part.

The diagram drawing part has two panels: mode panel and paint panel, and supports a user to draw communication diagram. In the mode panel, the user can choose any objects the user want to draw. The paint panel send data to the communication diagram generating part. The data is both a type of the object generated by the user and the coordinates of the place clicked by the user.

The communication diagram generating part generates communication diagram by receiving the user’s drawing requests through the diagram drawing part. It is regarded as communication diagram is



completed when a request to generate objects from the diagram drawing part disappears.

The test cases analyzing part generates test case analysis data. This part reads information by using *java.io.FileReader* class<sup>3</sup> and *java.io.BufferedReader* class<sup>3</sup> each line from the CSV file in which test cases are written along a form “test case ID, pre-condition, operation, post-condition”. And then, it gets test case analysis data from the information by using *split* method of *java.lang.String* class<sup>3</sup>. The test case analysis data are generated by storing each string to arrays in order of test case ID, pre-condition, operation, and post-condition

The test case table displaying part generates a table of test cases. This part adds the array outputted from the test case analyzing part as one line of a table on the window. After finishing to add all elements of the array, this part compares test case IDs which is one of data stored to cells in the table with all test case IDs of each message object on the testing communication diagram. Here, a message object means one to express a message. The background color of cells is managed per a line of the table. The background color of the line where a comparison result is accorded is highlighted red from white. When all test case IDs are compared, this part displays a table of test cases.

The testing communication diagram generating part generates testing communication diagram. This part compares pre-conditions, operations, and post-conditions in the array stored test case analysis data with each attribute data of message objects in communication diagram. If all of them match after comparison, the font color of message name of its message object is highlighted red from black. In addition, its test case ID is added to the test case ID list which is an attribute of the message object. And then, this part generates testing communication diagram by redrawing each object on the window and highlighting message names and test case IDs. Here, the message name of the message object which has a test case ID is drawn as a form “message name : test case ID”.

#### 4. Overview of the Prototype

Fig. 2 shows an overview of the implemented prototype. The window consists has four parts: “File menu”,

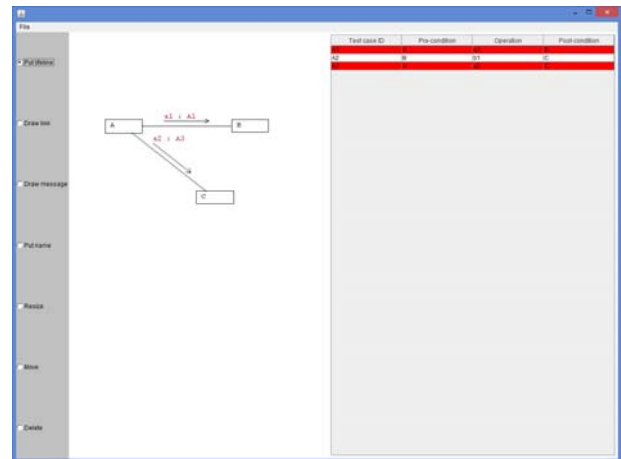


Fig. 2. An overview of the implemented prototype

“Mode panel”, “Paint panel”, and “Table of test cases”. Each part is described as follows.

- File menu  
It is placed in the leaning to the left of the window. If “open” is selected, a file dialog is displayed.
- Mode panel  
It is placed in the left of the window. In drawing communication diagram, each mode can be changed by user’s click. At present, we have implemented seven modes: “Put lifeline”, “Draw link”, “Draw message”, “Put name”, “Resize”, “Move”, and “Delete”.
- Paint panel  
It is placed in the middle of the window. It displays elements in communication diagram and testing communication diagram.
- Table of test cases  
It is placed in the right of the window. It is a table which displays test cases list.

We applied the prototype to some examples and confirmed that it worked properly. Elements which a comparison result is accorded in a table of test cases and testing communication diagram are highlighted red correctly. Moreover, elements which do not accorded do not highlighted.

In Fig. 2, test case ID A1 and A3 are highlighted and. ID A2 is not highlighted.



## 5. Discussion

In this chapter, we discuss the usefulness of the implemented prototype.

We confirm the usefulness of our tool by experiments using examinees. The examinees draw testing communication diagram in hand by giving a communication diagram and test suits. For this work, it took an average of 232 seconds. In contrast, the time when the tool uses the same diagram and test suits as an input was an average of 5.2 seconds. Hence, the prototype can reduce 92% of the burden to generate testing communication diagram. Moreover, in chapter 4, we showed that our prototype generated testing communication diagram properly. Works to confirm that the generated testing communication diagram is not included human errors are not necessary because using our prototype prevents the human errors in generating testing communication diagram.

In addition, by the function of highlight display in a table of test cases and testing communication diagram, users can find deficiency and/or contradiction in them at glance. Hence, our tool can reduce the burden to detect deficiency and/or contradiction in communication diagram and/or test cases.

Some studies have been reported visualization of test results (e.g. Refs. 4) and some tools have functions of visualization of test results (e.g. Refs. 5). Also, research to automatically generate test cases from communication diagrams has been reported.<sup>6</sup> In contrast, our research attempts to visualize test cases which are usually described in text.

## 6. Conclusion

This research has implemented the prototype which can support to reduce the burden to generate testing communication diagram and to detect deficiency and/or contradiction in communication diagram and/or test cases. Because the prototype generates testing communication diagram automatically, it can reduce the burden to draw the diagram and it can rid the work to confirm that the drawn diagram does not have any mistake. And also, because highlight display in a table of test cases and testing communication diagram are implemented as a function of the prototype, it can reduce the burden to detect deficiency and/or

contradiction in communication diagram and/or test cases. It contributes to improve the software reliability.

Future issues as follows.

- Improvement in inputting communication diagram. To generate testing communication diagram with our prototype, users need to draw communication diagram on the prototype. To improvement of convenience of the users, the prototype will be accept diagram drawn on other tools.
- Improvement in displaying message names. In implementation of our tool, only one arrow in message is drawn. Because of this, plural message names are displayed parallel to the up of the arrow. We consider improvement to be easy to see the message name.
- Adaptation extension of comparable elements of communication diagram. At present, our prototype does not support communication diagram which has messages including loop condition. To support them, a part of the method to generate testing communication diagram will be reconstructed.
- Extension of a table of test cases. Test cases in this paper does not have expected outputs. We need to add a field to a table to describe the expected outputs.

## References

1. UML Resource Page, <http://uml.org/>
2. S. Urata and T. Katayama, Proposal of testing diagrams for visualizing test cases, *Proc. 6th Int'l Conf. on Software Testing, Verification and Validation (ICST2013)* (2013).
3. Java™ Platform, Standard Edition 8 API Specification, <http://docs.oracle.com/javase/8/docs/api/>
4. J. A. Jones, Fault localization using visualization of test information, *Proc. 26th Int'l Conf. on Software Eng. (ICSE 2004)* (2004) 54-56.
5. Hertland.Data Inc., Dynamic Test tool DT10, <http://hlcd.co.jp/english/products/dt10/>
6. P. Samuel, R. Mall, and P. Kanth, Automatic test case generation from UML communication diagrams, *Information and Software Technology, ScienceDirect*, **49**(2) (2007) 158-171.

# Code Coverage Visualization on Web-Based Testing Tool for Java Programs

Mochamad Chandra Saputra<sup>\*</sup>, Tetsuro Katayama<sup>†</sup>

<sup>\*</sup>Universitas Brawijaya, Jl. Veteran, Malang 65145, Indonesia

<sup>†</sup>University of Miyazaki, 1-1 Gakuen-kibanadai nishi, Miyazaki, 889-2192 Japan

E-mail: andra@ub.ac.id, kat@cs.miyazaki-u.ac.jp

## Abstract

The visualization of statement coverage (C0) and branch coverage (C1) measurement output can be used in several ways to improve the verification and validation process. The result displays are percentage of a successful tested code and visual information with highlighted in bright green as information of executed lines, bright yellow for statement coverage and dark green The web-based testing tool significantly reduces the time for testing the code and help user to understand the behavior of the tested code.

*Keywords:* Visualization on software testing, Code coverage, Web-based testing tool, Java

## 1. Introduction

There are many ways to measure software development incorrectly. Testing can be the process of validating and verifying the software product to ensure the business and technical requirements to work as expected.<sup>1</sup>

A common way to evaluate tests is to measure code coverage. Code coverage helps software engineers to understanding which portion of code has been executed, measure the percentage of source code executed during the run and also the software engineering using a given test suite throughout the software testing process.<sup>2</sup>

Since software testing is a long and complex process with probably huge result data collection, visual information will provide testers with a quick and general perspective, which leads to a better understanding of a system's software behavior.<sup>3</sup> Implementing software testing as a web application for visualizing the result of testing is one of the solution to easily understand the behavior of a software code.

The main advantages of adopting the web applications are (1) no installation costs, (2) automatic upgrade with new features for all users, (3) universal

access from any machine connected to the Internet, and (4) independence from the operating system.<sup>4</sup>

To display the testing process and to understand the behavior of a code, this research has implemented a code coverage visualization on web-based testing tool for java programs. The testing process is shown the executed each line of tested code and calculation of the lines that executed several times using statement coverage.

## 2. Specifications and Implementation Policies For The Tool

### 2.1 Specifications

This research uses statement coverage (C0) and branch coverage (C1).<sup>5</sup>

The testing tool has three parts: uploader code, java service testing, and insertion of temporary database. The java service testing has four sub-parts: analyzer, C0 and C1 instrument code generator, testing part, and random data generator as shown the design system in Fig.1.

To implement this model, several steps are followed.

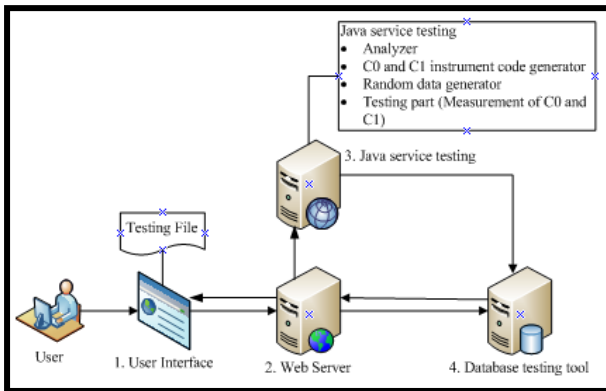


Fig. 1. Design of the testing tool.

1. Uploader code is an input of testing tool.

The input is tested code from a user into the server that used for the java service testing. Tested code is a java program.

2. Java service testing

a) Analyzer loads the original tested code and then the original tested code used by the C0 and C1 instrument code generator, testing part, and random data test generator. The testing tool will execute the java service testing to analyze and read the original code based on the information on the specified file, then testing the code and inserting it into a temporary database for javascript visualization.

b) The C0 and C1 instrumented code generator generates a C0 and C1 instrumented code. It is inserted or rewritten instrument code at each line of the original code, and it is used for calculating the number of executions of C0 and C1.

c) Testing part views the covering status of statements and branches by inputting random data during the background process. Java service testing finds the class name of the original code by pattern matching. The class name is used when the C0 and C1 instrumented code generator generates the instrumented code.

The testing method process will insert the data execution line by line into the database. Data stored in the database are the line number, number of executions of each line, and tested code.

When the java service testing executes a testing, the service assigns 1 to an element of the array that

```

1 package checker;
2 public class CheckNumber {
3     public static void main(String[] args) {
4         int i;
5         int[] C0 = new int[10];
6         int[] C1 = new int[10];
7         int[] C2 = new int[10];
8         int[] C3 = new int[10];
9     }
10    public static void Check(int n) {
11        for (int i = 0; i < n; i++) {
12            if (i % 2 == 0) {
13                C0[i] = 1;
14                C1[i] = 1;
15                C2[i] = 1;
16                C3[i] = 1;
17            } else {
18                C0[i] = 0;
19                C1[i] = 0;
20                C2[i] = 0;
21                C3[i] = 0;
22            }
23        }
24    }
25 }

```

Fig. 2. Example of the C0 and C1 instrumented Code CheckNumber tested code.

corresponds to the executed statement. When all elements of the array C0 are assigned 1, the java service testing judges C0 satisfies 100% and also for C1.

d) Random data generator generates random test data. Users of the testing tool do not need to describe the test data. The random data generator starts after generating the C0 and C1 instrumented code. The testing part executes the C0 and C1 instrumented code. The random data generator inputs random data into the C0 and C1 instrumented code on behalf of the users inputting data per standard input instructions.

After each execution of the C0 and C1 instrumented code by the testing part, the testing tool obtains the covering status of statements and measures C0 and C1. The testing tool visualizes the covering status of the statements by highlighting the original code that is displayed and animated as the sequence process executes the tested code.

2.2 Implementation

This research implements the web-based software testing tool of an automatic unit testing tool using random testing for java programs. This testing tool can automatically test a program based on statement coverage (C0) and branch coverage (C1), without preparing test data by user. As an example of the tested code is Class CheckNumber. Fig.2 shows the tested code with C0 and C1 instrumented Code. To test the code, the following steps are used to generate the code:

- Insert a package before the first line of Fig.2, to generate the C0 and C1 instrumented code.

```

0 public class CheckNumber {
1 public static void main(String[] args) {
2 int i;
20 for(i=1 ; i<=20 ; i++){
20 fungsi(i);
0 }
0 }
20 public static void fungsi(int n){
2 if(n % 10 == 0){
2 System.out.println("Value 1.1");
6 }else if(n % 3 == 0){
6 System.out.println("Value 1.2");
1 }else if(n % 5 == 0){
1 System.out.println("Value 1.3");
2 }else if(n < 10){
2 System.out.println("Value 1.4");
8 }else if(n*n > 100){
8 System.out.println("Value 1.5");
0 }
1 else{}
0 }
0 }

Statement Coverage=100%
Branch Coverage=100%
Number Of Runs=1

Time Execution : 716 ms

```

Fig. 3. Static display for investigation of the CheckNumber tested code

- Rewrite an original class name as a class name "MyCheckNumber" specified in advance by the testing part.
- Insert an assignment statement after all statements to gain the covering status of the statements.
- Insert an assignment statement to store outputs after standard input instruction "System.out.println".
- Random data are used for data test the code and then automatically tested for the CheckNumber2 using C0 and C1 instrumented code to verify the branch condition. Each data testing process are insert into the database using for visual information.

Code instrumentation in this research consists of inserting some additional codes to measure coverage results. Instrumentation can be done at the source level in a separate pre-processing phase with pattern matching or at runtime by measure of coverage result. Data gathering consists of storing coverage data collected during test runtime.

Random data tests provide the application under testing with input data generated at random. Typically, testers pay no attention to expected data types.<sup>6</sup> The type of random data used in the testing tool is integer only.

The testing tool has two result displays. The first is a static display as shown in Fig.3. The testing tool displays the static result of testing as the number of each

© The 2015 International Conference on Artificial Life and Robotics (ICAROB 2015), Jan. 10-12, Oita, Japan

1	public static void main(String[] args) {
1	int i;
15	for(i=1 ; i<=20 ; i++){
14	fungsi(i);
15	public static void fungsi(int n){
1	if(n % 10 == 0){
1	System.out.println("Value 1.1");
5	else if(n % 3 == 0){
4	System.out.println("Value 1.2");
1	else if(n % 5 == 0){
1	System.out.println("Value 1.3");
2	else if(n < 10){
2	System.out.println("Value 1.4");
5	else if(n*n > 100){
5	System.out.println("Value 1.5");
1	else{

**Estimation Time For Visualization :**  
**00 Hours : 02 Minutes : 31 Second**

Fig. 4. Dynamic display for investigation of the CheckNumber tested code

line execution, measurement percentage of success from the statement and branch coverage, and time execution for testing as how many times the line was executed by the java service testing.

The second result display is dynamic with Ajax. The result display visualizes the behavior of the tested code as shown in Fig.4. Certain coverage analysis tools also depict coverage visually, often by highlighting portions of code that are unexecuted by a test suite.<sup>7</sup> In this research, the visual information resets every time a tester select a new code and then tests the code. The testing tool performs new visualizations to know the behavior of the code, and that it does not accumulate with each successive test run before the testing.

### 3. Discussion

The testing tool can show the correlation between visual information and software testing. This correlation means results collection and a better perspective of software testing. The testing tool shows the correlation as visual information, and it allows a better understanding of the behavior of the tested code.

Visual information describes the behavior of the tested code as a sequence of the line executed by the testing tools. Visual information helps to understand the behavior of the tested code. The result displays for visual information have been highlighted in bright green as information on executed lines, bright yellow for

Table 1. Time comparison between using the testing tools and manual testing (by human)

Testing Tool	No.	Manual Testing
716 ms	1	3' 54 "
	2	2' 54 "
	3	5' 40 "
	Average	4' 15 "

statement coverage and dark green for branch coverage. Visual information describes the behavior of the tested code as a sequence of the line being executed.

Code coverage visualizations are supposed to improve developer efficiency and knowledge and promote more productive testing strategies. The research for the visualization leads developers toward a better standard of test effectiveness.

The testing tool uses java file CheckNumber that inputs 19 lines and then to measure statement coverage, branch coverage, number of runs and the input of each program to the end of testing by C0 and C1 to reach 100%. The testing measured at the web server with CentOS release 5.9 (Final), Apache/2.2.3, Intel(R) Xeon(R) CPU 3050 @2.13GHz, PHP Version 5.3.3.

The times execution for testing the class CheckNumber is 716 ms and if we test manually (by humans), the average time is 4 minutes 15 second as shown in Table 1. The testing tool can reduce time to describe a tested code and execute unit testing in a shorter time.

Visualization concerns the graphical representation of information to assist human comprehension of and reasoning about that information.<sup>8</sup> The testing tool result makes possible distribution of the software testing scalability problem, making certain key choices instead a technical distribution of responsibilities.

#### 4. Conclusion

To improve the efficiency of testing in software development, this research has implemented a web-based software testing tool with java service testing of an automatic unit testing tool for java programs with random testing. The implemented testing tool generates the C0 and C1 instrumented code from the original code. The testing tool uses java service testing to automatically test a program by inputting random data into the C0 and C1 instrumented code. After testing, the

obtained result is output as a static html page and dynamic display for visual information with Ajax.

The testing tool can show the correlation between visual information and software testing as a result collection and perspective of software testing as a sequence of the line executed by the testing tools. The testing tool can reduce the time needed to describe a tested code and execute unit testing. The time execution needed to test CheckNumber was 716 ms.

Future issues are as follows:

- Expand the type of a data test can input data tests other than type int.
- Measurement with key performance indicators for software development like resources and cost, product size and stability, product quality, process performance, technology effectiveness.

#### References

1. Sivakumar.N.,Vivekanandan.K. “Comparing the Testing Approaches of Traditional, Object-Oriented and Agent-Oriented Software System”, *International Journal of Computer Science & Engineering Technology (IJCSET)*, 3(10) (2012) 498-504.
2. Heed. Per., Westrup. Alexander., Runeson.Per. “Automated Platform Testing Using Input Generation and Code Coverage”. Master Thesis Document. Lund University, Faculty of Engineering (2009).
3. Wang.Huansong., Zhang.Xiang., Zhou.Mingqi . “MaVis: Feature-based Defects Visualization in Software Testing”, *Engineering and Technology (S-CET) 2012 Spring Congress on* (2012) 1-4.
4. Dogana.Serdar., Betin-Cana.Aysu., Garousia.Vahid. “Web application testing: A systematic literature review”, *The Journal of Systems and Software (ELSEVIER)*, (2014) 174-201.
5. ISTBQ. “How to Calculate Statement, Branch/Decision and Path Coverage for ISTQB Exam Purpose”. <http://www.ajoyingha.info>
6. Agarwal,B. B., Tayal, S. P., Gupta, M. “Software Engineering & Testing An Introduction”, *Jones and Bartlett Publishers*, (2010) 161-179.
7. Lawrance, Joseph., Clarke, Steven., Burnett, Margaret., Rothermel, Gregg. “How Well Do Professional Developers Test with Code Coverage Visualizations? An Empirical Study”, *IEEE Computer Society*, (2005) 53-60.
8. Petre, Marian.,Quincey, Ed de. “A gentle Overview of Software Visualisation”, *Computer Society of India Communications*, (2006) 1- 10.

# TFVIS: a Supporting Debugging Tool for Java Programs by Visualizing Data Transitions and Execution Flows

Hiroto Nakamura<sup>\*</sup>, Tetsuro Katayama<sup>\*</sup>, Yoshihiro Kita<sup>†</sup>  
Hisaki Yamaba<sup>\*</sup>, Kentaro Aburada<sup>‡</sup>, Naonobu Okazaki<sup>\*</sup>

<sup>\*</sup>University of Miyazaki, 1-1 Gakuen-kibanadai nishi, Miyazaki, 889-2192 Japan

<sup>†</sup>Kanagawa Institute of Technology, 1030 Shimo-ogino, Kanagawa, 243-0292 Japan

<sup>‡</sup>Oita National College of Technology, 1666 Maki, Oita, 870-0152 Japan

E-mail: [tf13006@student.miyazaki-u.ac.jp](mailto:tf13006@student.miyazaki-u.ac.jp), [kat@cs.miyazaki-u.ac.jp](mailto:kat@cs.miyazaki-u.ac.jp), [kita@earth.cs.miyazaki-u.ac.jp](mailto:kita@earth.cs.miyazaki-u.ac.jp),  
[yamaba@cs.miyazaki-u.ac.jp](mailto:yamaba@cs.miyazaki-u.ac.jp), [aburada@oita-ct.ac.jp](mailto:aburada@oita-ct.ac.jp), [oka@cs.miyazaki-u.ac.jp](mailto:oka@cs.miyazaki-u.ac.jp)

## Abstract

TFVIS(transitions and flow visualization) can perform the visualization of data transitions and the visualization of execution flows. The visualization of data transitions shows the flow of variable renewals in executing programs. It becomes easier to grasp the behavior in executing the programs whose behavior is unexpected by a bug. The visualization of execution flows shows an entire flow of the execution. It is useful to select the part where users want the visualization of the data transitions.

*Keywords:* Debugging, Java, Dynamic analysis, Visualization, Slicing

## 1. Introduction

We need much time in order to find the cause of a bug in programs.<sup>1</sup> We need to find the behavior of programs which is different from ideal behavior in order to find the cause of a bug. However, grasping the behavior is difficult because the behavior of the program which includes a bug becomes unexpected behavior.

We had implemented the visualization tool called TVIS<sup>2</sup> in our previous research. TVIS visualizes the data transitions. The data transitions in our research show the flow of variable renewals in executing a program.

TVIS expresses when and what value of each variable is renewed. Programmers can grasp behavior of a program because they can prefigure the behavior of each variable at arbitrary timing in the program execution by grasping the data transitions.

However, the efficiency of TVIS is lost, if the program which TVIS uses becomes large. Moreover,

TVIS can't visualize the data transitions between different methods.

Therefore, this paper implements the visualization tool TFVIS(transitions and flow visualization) which visualizes the data transitions and the execution flows, and shows the effectiveness of TFVIS. That is, we combine the visualization of the execution flows with the visualization of the data transitions in order to visualize a larger program. Moreover, we improve the visualization of the data transitions in order to realize the more effective one.

## 2. TFVIS

We have developed the visualization tool called TFVIS. TFVIS visualizes the data transitions and the execution flows of Java programs. Fig.1 shows an example of the window of TFVIS. Two small windows on the right of the window are called the data transitions diagrams. The diagram on the left-hand side of them is called the execution flows diagram.

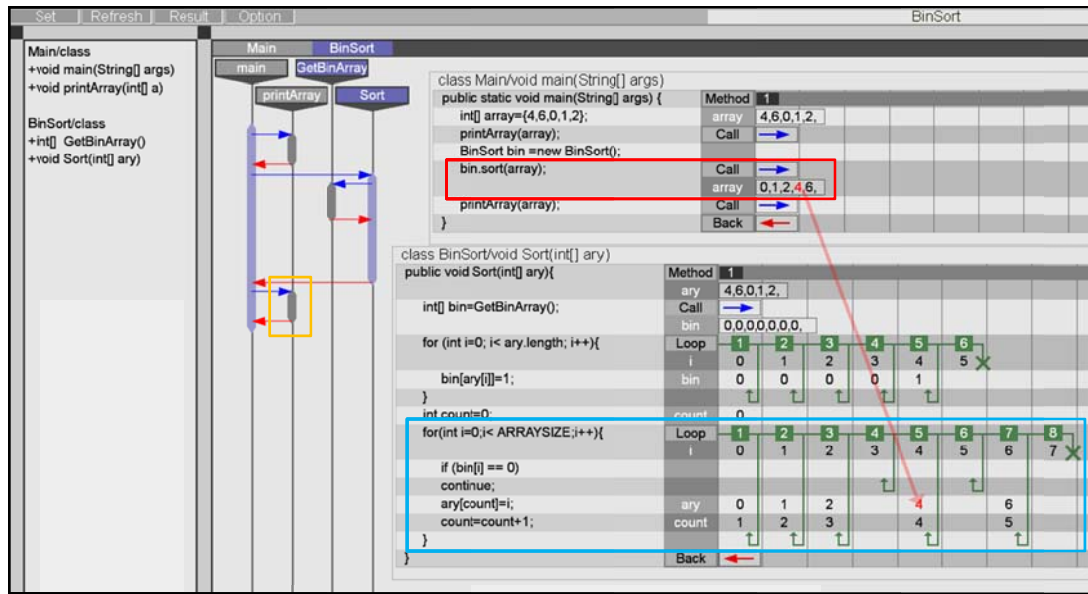


Fig. 1. An example of the window of TFVIS.

The list of the left side of the window of TFVIS shows list of methods of a program. The functions of TFVIS are as follows.

**2.1. Program analysis**

Firstly, we explain the program analysis used to the visualization. TFVIS performs two types of analysis: the structure analysis and the executions analysis.

The structure analysis is static analysis for obtaining the information which is used to insert probes for the execution analysis and visualize. The information which is obtained by the structure analysis is the information about a location where statements occur: generations and renewals of variables, loops, and method calls. Moreover, it includes the information about the relation of a class and a method.

The execution analysis is dynamic analysis for obtaining the information about behavior in executing the programs. The information which is obtained by the execution analysis is the information about renewals of variables, behavior of loops and method calls, and so on. TFVIS obtains the information by using the probes, inserted based on the result of the structure information.

**2.2. Data transitions diagram**

The data transitions diagram is generated by the visualization of the data transitions. TFVIS in Fig.1

shows the two windows of the data transitions diagram. TFVIS can show the plural windows of the data transitions diagram in this way.

The data transitions diagram shows renewals of a variable. It is a table and indicates the number of iterations of execution in a lateral direction and indicates the line number of a source code in a vertical direction. Normally, its table shows renewal value of variables to where the renewal of the variable occurs. The area surrounded by the red frame in Fig.1 shows that the values of the array “array” become “0, 1, 2, 4, 6” after the method “sort” is executed. The method “printArray” has “array” as an argument the same as “sort”. However, the renewal value of “printArray” is not showed, because “printArray” only refers to the value of “array” without updating it.

The green pattern on the data transitions diagram shows a loop, and the number on it shows the number of the iteration of the loop. The green arrows extending from the right of each number show the process of iteration of the loop. In the statement “for” is surrounded by the blue frame in Fig.1, the arrow at the fourth loop in this example is shorter than the arrow at the third loop; it expresses “jump” by using statement “continue”. The mark “x” on the seventh loop expresses the end of a loop caused by using the “break” statement or failing the condition of a loop.



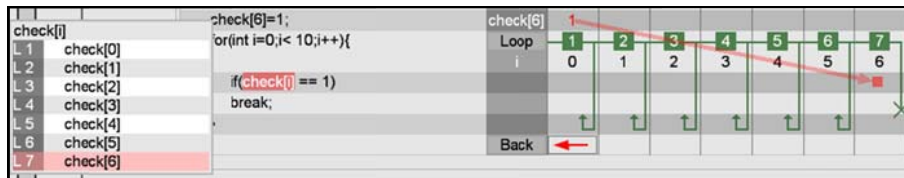


Fig. 2. An example of the window of the data transitions search.

### 2.2.1. Data transitions arrow

The data transitions arrow is a function of the data transitions diagram, and visualizes the dependence relations between each renewal of variables. The dependence relations mean ones between state of a variable and the state of other variables which is used for the renewal of its state.

The data transitions arrow is based on the technique of the program slicing.<sup>3</sup> It becomes easy to grasp behavior of the data transitions in the loop and select the standard value of the program slicing by combining the technique of the program slicing and the data transitions diagram.

TFVIS shows the data transitions arrow, when users click a value of a variable on the data transitions diagram. The data transitions arrow is the red arrow and connects the two values which the data transitions diagram shows with red font color. Fig.1 shows an example of it. It can visualize the relation of the values between methods. Therefore, it is not necessary that the start point and the end point of the data transitions arrow exists in the same method.

Fig.1 shows the data transitions arrow in the window when users select the fourth value of the array “array” which the method “sort” updates. The tip of the data transitions arrow of Fig.1 shows the state which finally updated the value which the user selected. When users find the suspicious state of a variable, the data transitions arrow supports to find the cause of it.

### 2.2.2. Data transitions search

The data transitions search shows the data transitions arrow by selecting the variable and its state from the source code on the left side of the data transitions diagram. Fig.2 shows an example of the data transitions search, it is the window when users selected the state of the seventh loop of the variable “check[i]” which is used as the conditions of the “if” statement.

### 2.2.3. Selection of the target for the visualization

The data transitions diagram can't visualize the whole of the program at a time, because visualization typically has the issue<sup>4</sup> that the output of it becomes huge even if the visualized program is moderate size.

Therefore, users must select the part where they want the visualization of the data transitions. The execution flow diagram, which we explain in the next section, can support this selection.

## 2.3. Execution flow diagram

The visualization of the execution flow visualizes an entire flow of execution of a program and generates the execution flow diagram. The execution flow diagram provides the useful information in order to select the part where users want the visualization of the data transitions. It is based on the sequence diagram and shows status of use of each methods and the relation of method calls.

We explain the usage of the execution flow by using an example of Fig.1. The column in topmost of the execution flow diagram shows each class name, and the figures at under of it express each method. The black lines extending from methods are their lifelines, and the thick parts on their lifelines are their execution specification which means execution of the method. When users click a execution specification, TFVIS shows the data transitions diagram of corresponding with it. Normally, the execution specification uses the gray color. However, the execution specification uses the light blue color, if the window of the data transitions diagram of corresponding with it is being displayed. The blue arrows on the execution flow diagram express method calls, and the red arrows express completion of methods.

The execution specification is surrounded by the orange frame in Fig.1 expresses the execution which is



called by the only execution of the method “main” and is the second execution of the method “printArray”.

### 3. Discussion

We discuss the usefulness of TFVIS.

Programmers normally use the dynamic slicing<sup>5</sup> or trace tools<sup>6,7</sup> in order to obtain data transitions in executing a program. However, it is difficult to grasp positional relations of each renewal, if data transitions include the process of a loop, and so on. The visualization of data transitions of TFVIS uses the representation which exploits the source code and the processes of a loop as shown in Fig.1, and can show the data transitions in a way that is easy to understand. Moreover, the above-mentioned technique or tools need that users search a reference point when they analyze a program. In the case of TFVIS, it becomes easy to decide a reference point because the data transitions diagram shows renewals of variables and behavior of loops so that users understand them at a glance.

On the other hand, the range of the program which TFVIS can visualize is still narrower than other tools because the abstraction degree of the visualization of TFVIS is lower. TFVIS is inferior compared with the tool<sup>8</sup> which can visualize the multi-threading because TFVIS can't visualize multi-threading.

We will be able to adjust the abstraction degree of the visualization of the execution flow in order to enlarge the range of the program which TFVIS can visualize. The abstraction degree of the execution flow diagram is too low to prevent excessive expansion of its diagram, if users want to visualize the program which has the process of multi-thread or a larger program. However, if it merely becomes higher, the users become unable to grasp behavior of a program in detail. Therefore, the information which the users obtain by the execution flow diagram becomes not enough to select the part where they want the visualization of the data transitions. We combine the visualization which the abstraction degree is low and the visualization which the abstraction degree is high by using an idea of the fisheye view<sup>9</sup>. Therefore, we will enable TFVIS to provide the enough information which users select the part where they want the visualization of the data transitions and visualize the larger programs.

### 4. Conclusion

We have implemented TFVIS in order to improve the efficiency of debugging of Java program.

TFVIS can support to grasp behavior in executing a program by visualizing the data transitions. The data transitions diagram visualizes renewals of variables and behavior of loops. Even if the data transition is the relation between methods, the data transitions arrow can visualize it.

Moreover, we have implemented the visualization of execution flow in order to improve the narrowness of the range of the visualization of the data transitions. It improves convenience when TFVIS visualizes a large program. Therefore, we judge that TFVIS can support to find the cause of a bug, and is effective of debugging for Java programs.

The future issues are as follows.

- The realization of the visualization of the multi-thread process.
- The improvement of the execution flow diagram by using an idea of the fisheye view.

### References

1. Roger S. Pressman, Software Engineering A Practitioner's Approach 5thEdition, *McGraw-Hill Science* (2001).
2. Tetsuro Katayama et al, Proposal of a Visualizing Method of Data Transitions to Support Debugging for Java Programs, *Journal of Robotics Networks and Artificial Life*, **1**(2) (2011) 111-115.
3. Mark Weiser, Programmers Use Slices When Debugging, *Communications of the ACM*, **25** (1982) 446-452.
4. W. De Pauw et al, Execution patterns in object-oriented visualization, In *Proc. 4th COOTS* (1998) 219-234.
5. H Agrawal, JR Horgan, Dynamic Program Slicing, *SIGPLAN Notices* **25**(6) (1990) 246-256 .
6. Kouhei Sakurai et al, Traceglasses: A Trace-based Debugger for Realizing Efficient Navigation, *Information Processing Society of Japan*, **3**(3) (2010) 1-17.
7. Salman Mirghasemi et al, Querypoint : Moving Backwards on Wrong Values in the Buggy Execution, *ESEC/FSE* (2011) 436-439.
8. Jan Lönnberg et al, Java replay for dependence-based debugging, *PADTAD '11* (2011) 15-25.
9. W Furnas, Generalised sheye views, In *Proc ACM SIGCHI 86 Conference on Human Factors in Computing Systems* (1986) 16-23.

# Proposal of a Testing Method Using Similarity of Interleaving for Java Multi-threaded Programs

Shoichiro Kitano\*, Tetsuro Katayama\*, Yoshihiro Kita†,  
Hisaki Yamaba\*, Kentaro Aburada‡ and Naonobu Okazaki\*

\*University of Miyazaki, 1-1 Gakuen-kibanadai nishi, Miyazaki, 889-2192 Japan

†Kanagawa Institute of Technology, 1030 Shimo-ogino, Kanagawa, 243-0292 Japan

‡Oita National College of Technology, 1666 Maki, Oita, 870-0152 Japan

E-mail: kitano@earth.cs.miyazaki-u.ac.jp, kat@cs.miyazaki-u.ac.jp, y.kita@ccy.kanagawa-it.ac.jp,  
yamaba@cs.miyazaki-u.ac.jp, aburada@oita-ct.ac.jp, oka@cs.miyazaki-u.ac.jp

## Abstract

In order to improve the efficiency of testing Java multi-threaded programs, this research proposes a testing method to detect order violation in them using similarity of interleaving. The proposed method improves the efficiency of testing by executing interleaving which can test the places where lead the order violation easily in source codes and by reducing interleaving which is similar to executed one already. The efficiency of the method is shown by experiments for confirmation.

*Keywords:* multi-threaded program, testing, similarity, Java

## 1. Introduction

In recent years, many computers are adapted multi-core CPUs. In order to use such resources effectively, the demand of multi-threaded programs increases.

It is difficult for even expert programmer to implement multi-threaded programs. And it is easier to embed bugs than single-threaded programs[1]. There are some distinctive bugs in a concurrent program which are different from the bugs in a single-threaded program. Those bugs often appear in the latter of development process or when the program is used by the users. In this case, it is difficult to fix the detected bugs. In order to prevent this problem, we need to detect the bugs and to fix them in unit testing. However, normal unit testing cannot test multi-threaded programs enough. Unit testing tests often only single interleaving because executed tasks are too small in unit testing. Therefore, the bugs appear when the modules are

integrated. One of the testing methods for multi-threaded programs in unit testing is to execute programs in the plural interleaving by staggering the timing of execution between each thread. That method can detect the existing bugs in multi-threaded programs. However, there is too large number of interleaving that we must execute and many interleaving cannot detect the distinctive bugs in a concurrent program. It takes the same result to test by the interleaving that is similar to tested one already and it is excessive testing. Moreover, each distinctive bug in a concurrent program has the own causes each other. It is not effective to detect all such bugs by an only testing method.

In order to improve the efficiency of testing for Java multi-threaded programs, this research proposes a testing method to detect order violation in them using similarity of interleaving. Our proposed method improves the efficiency of testing by executing interleaving which can test all places which lead the

```

Ham ham = null;
void methodA(){
    ...
    ham = createHam(); //A
    ...
}
void methodB(){
    ...
    ham.doSomething(); //B
    ...
}
    
```

Fig. 1. An example of a source code which includes order violation.

Table 1. The number of threads which involved to detect concurrency bugs.

Application	Total	> 2 threads	2 threads	1 threads
MySQL	22	1	17	4
Apache	17	0	17	0
Mozilla	56	1	54	1
OpenOffice	8	0	6	2
Overall	103	2	94	7

order violation easily in source codes and by reducing interleaving which is similar to executed one already.

## 2. The Kinds of Bugs That Our Proposal Method Can Detect

In this chapter, we explain the kinds of bugs that our proposed method targets.

### 2.1. Target bug in multi-threaded programs

The kinds of bug patterns in concurrency programs are classified[2]. The patterns are classified into dead lock, atomicity violation, order violation, and so on.

Order violation means that some threads can be executed as an access to a certain memory in an unexpected order. It occurs when a synchronization protocol for several threads is deficient. Fig.1 shows an example of a source code which includes order violation. Consider the case which methodA and methodB are executed in different threads each other. Statement B expects that ham has been initialized by statement A before statement B accesses to ham. However, this program can execute statement B before statement A. That leads the incident. The cause of this problem seems like atomicity of flag. However, Accessing to ham is unacceptable before ham has been initialized. Even if accessing to ham is serialized, the incident occurs because the initial value of ham is null.

In this research, we propose a testing method which can detect order violation as above.

```

public void run(){
    PreemptionPointer.preemptionPoint(0); // (iii)
    PreemptionPointer.preemptionPoint(1); // (ii)
    synchronized(lock){
        PreemptionPointer.preemptionPoint(2); // (i)
        flag = true;
    }
    PreemptionPointer.preemptionPoint(3); // (iv)
}
    
```

Fig. 2. An example of a source code which is inserted the probes.

### 2.2. Number of thread used in testing

In multi-threaded programs, the number of thread used in testing is important. Table 1 is a result of the research[2] which shows how many threads are necessary to detect the distinctive bugs in a concurrent program.

Table 1 shows that two threads can detect the most number of bugs. Hence, our proposed method uses two threads that can detect bugs the most effectively.

## 3. Proposal Method

### 3.1. The four places which can lead the order violation easily

In order to detect the distinctive bugs in a concurrent program, we have to enforce the testing which relates on timing of execution between threads. However, each bug pattern has own causes each other. Therefore, we need to enforce effective testing the each bug pattern.

In this research, we propose the four places which can lead order violation easily in source codes. We detect the order violation by executing the interleaving which can test the all places.

The places and reasons that we choose them are following.

- (i) Substitution for a shared flag variable used for synchronization of threads  
This place can detect the bugs caused by incorrect place of statements that rewrite the value of a flag variable.
- (ii) The entry point of synchronized blocks  
This place can detect the bugs caused by defectiveness of logic for a synchronization protocol implemented in a synchronized block.

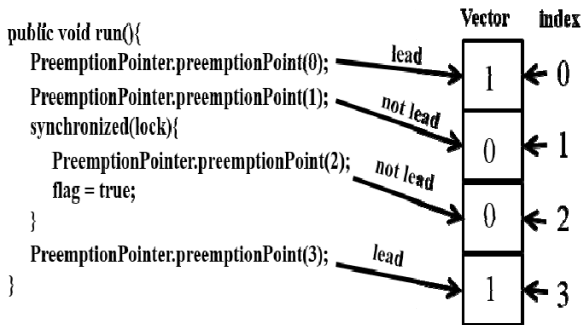


Fig. 3. An example of a vector generation.

- (iii) The start of execution of a thread  
This place can detect the bugs caused when synchronization protocol is not implemented because programmers suppose that a program is executed in only one interleaving.
- (iv) The end of execution of a thread  
This place can detect the bugs caused by a logic which depends on the termination of other threads.

### 3.2. Test codes

In this research, we execute the interleaving which can test all places explained in section 3.1. Therefore, we describe the test code inserted some probes at the places in a source code of a test target program.

Fig.2 shows an example of the test code. “preemptionPoint(int number)” method which is member of “PreemptionPointer” class is probes. We explain integer values of arguments in the next section. This method can lead a context switch, as needed. This provides various interleaving which can test each place. The numbers in comments correspond to the numbers which are labeled each place in section 3.1.

### 3.3. Reduction of number of test execution by using similarity of interleaving

Our proposed method improves efficiency of testing by reducing interleaving which is similar to executed one already. It is necessary to change interleaving to the value which can be calculated similarity. Therefore, we generate vectors from the order and the number of probes in a test code. The values of the generated vectors are 1 or 0. 1 shows that the probe leads a context switch and 0 shows that the probe does not.

Fig.3 shows an example of vector generation. When the number of probes is n, the number of generated vectors is the n-th power of two. We treat this vector as

Table 2. Result of experiments.

Number of Places	All or Reduced	Number of Testing	Number of Testing in Buggy Interleaving
4	All	16	7.4
4	Reduced	9	4.8
7	All	128	66.4
7	Reduced	59	27.9

interleaving and enforce testing each generated vector. The method “preemptionPoint(int number)” leads context switch to execute any interleaving by using generated vector. The integer number of arguments expresses index of elements that a vector has. “preemptionPoint(int number)” chooses to lead context switch or not to lead by using the elements at number of arguments. Here, the first index of elements is 0.

Then, we calculate the similarity between vectors. In this research, we use cosine similarity to calculate similarity between vectors. When the similarity between any vector and the vector which has used already is more than a threshold, “preemptionPoint(int number)” does not use that vector. This reduces the interleaving which leads the same result as the result of executed one already. Therefore, we can improve the efficiency of testing in multi-threaded programs.

## 4. Discussion

### 4.1. Experiment for Confirmation

We have conducted experiments to confirm efficiency of our proposed method.

The method in experiment is that we prepare two programs which include an order violation. And we execute the test codes that have some probes at places which can lead order violation easily in the source codes of those programs. They include four places and seven places in their source codes. We enforce two tests that use all generated vectors and reduce the vectors which are similar to vector which has used already. We confirm the efficiency of proposed method by comparing the number of testing that are result of each testing and by verifying that a bug can be detected when tests are reduced. Here, threshold used by deciding to reduce vectors is 0.8.

Table 2 shows the results of the experiments. Each number is the mean value of the result of executing the programs 10 times for each condition. “Number of Testing Buggy Interleaving” on the line of “All” shows that the proposed method can detect the bug definitely. Therefore, we confirmed that the proposed method can

detect the order violation, which is one of the distinctive bugs in a concurrent program definitely.

“Number of Testing” shows that proposed method can reduce the number of each test execution by 56% and 46%. And “Number of Testing Buggy Interleaving” on the line of “Reduced” shows that the proposed method can execute the interleaving which can lead the bug definitely even if tests are reduced. These results show that the proposed method reduces the number of execution of testing by about 51% and can test to detect order violation enough. Therefore, we confirmed that proposed method can improve the efficiency of testing in multi-threaded programs.

#### 4.2. Related works

Concuerror[3] is a testing tool for Erlang. Concuerror can test programs by executing plural interleaving and can reduce the interleaving by preemption bounding[4]. Therefore, Concuerror can enforce testing efficiency. However, executed interleaving is not focused on detecting the distinctive bugs in a concurrent program. Therefore, it has possibility not to detect such bugs.

Our proposed method executes the interleaving which can test all places which can lead order violation easily. Therefore, our proposed method can test more efficiently for the distinctive bugs in concurrent programs.

ConTest[5] is a testing tool for Java multi-threaded programs. ConTest can enforce testing that relates on timing by executing plural interleaving. However, it does not ensure to detect bugs definitely even if increasing the number of tests execution because it executes plural interleaving in an ad hoc basis. Therefore, the efficiency of its testing is poor.

Our proposed method executes the interleaving which can test the all places which can lead order violation easily. It reduces testing in the interleaving which is similar to executed one already and can detect order violation definitely. Therefore, our proposed method tests more efficiently.

#### 5. Conclusion

In this research, we have proposed a testing method for order violation using similarity of interleaving. In order to realize it, we have defined four places which can lead order violation easily in source codes. The proposed method reduces the interleaving by changing interleaving to vectors which can be calculated and calculating the similarity between a vector and used vectors in testing already by cosine similarity. We

conducted experiments that use the proposed method. The results show that the proposed method can detect the order violation definitely. And it can also detect the bugs even if it reduces the number of test execution by about 51%. That shows it is effective for improving the efficiency of testing in multi-threaded programs to use our proposed method.

Future issues are as following.

- Considering the testing methods which can detect other bug patterns  
Our proposed method is focused on only order violation. Therefore, it is not enough to detect other bug patterns like dead lock or atomicity violation. We need to consider the testing methods which can detect these bugs efficiently.
- Investigating the threshold of similarity for reducing the vectors  
Depending on the length of generated vector, there is a case that the number of generated vector which has similarity less than threshold is too large. In such a case, the number of vectors which is reduced is much the same as the number of vectors which are not reduced. We need to investigate the appropriate threshold which is based on length of the vectors.
- Consider the testing method which use more than two threads  
Our proposed method uses two threads for testing. Therefore, it cannot detect the bugs which occur in testing using more than two threads. We need to consider it.

#### References

1. J. K. Ousterhout, Why Threads Are A Bad Idea(Usenix Annual Technical Conference, San Diego, 1996) <http://www.softpanorama.org/People/Ousterhout/Threads>
2. S. Lu, S. Park, E. Seo and Y. Zhou, Learning from Mistakes - A Comprehensive Study on Real World Concurrency Bug Characteristics, (ASPLOS '08, Washington, 2008), pp. 329-339.
3. A. Gotovos, M. Christakis, and K. Sagonas, Test-DrivenDevelopment of Concurrent Programs using Concuerror, (Erlang'11, New York, 2011), pp.51-61.
4. M. Madan, Q. Shaz, Iterative Context Bounding for Systematic Testing of Multithreaded Programs, (PLDI '07, Sam Diego, 2007), pp.11-13.
5. ConTest - A Tool for Testing Multi-threaded Java Applications, <https://www.research.ibm.com/haifa/projects/verification/contest/>

# Proposal of a Modification Method of a Source Code to Correspond with a Modified Model in MDA

Yuuki Kikkawa<sup>\*</sup>, Tetsuro Katayama<sup>\*</sup>, Yoshihiro Kita<sup>†</sup>,  
Hisaki Yamaba<sup>\*</sup>, Kentaro Aburada<sup>‡</sup> and Naonobu Okazaki<sup>\*</sup>

<sup>\*</sup>University of Miyazaki, 1-1 Gakuen-kibanadai nishi, Miyazaki, 889-2192 Japan

<sup>†</sup>Kanagawa Institute of Technology, 1030 Shimo-ogino, Kanagawa, 243-0292 Japan

<sup>‡</sup>Oita National College of Technology, 1666 Maki, Oita, 870-0152 Japan

E-mail: kikkawa@earth.cs.miyazaki-u.ac.jp, kat@cs.miyazaki-u.ac.jp, y.kita@ccy.kanagawa-it.ac.jp,  
yamaba@cs.miyazaki-u.ac.jp, aburada@oita-ct.ac.jp, oka@cs.miyazaki-u.ac.jp

## Abstract

This paper proposes a modification method of a source code to correspond with a modified model in MDA. The proposed method generates, translates, and modifies EAD (Extended Activity Diagram). Also, it generates a source code from the activity diagram. We use a simple ATM example to confirm availability of the method. The method can reduce time and effort to keep consistency between models and a source code after requirement specification is modified.

*Keywords:* MDA (Model Driven Architecture), Extended Activity Diagram, Activity diagram, Detail specification.

## 1. Introduction

MDA (Model Driven Architecture) is a concept of software development.<sup>1</sup> MDA defines five models: business model, requirement model, platform independent model (PIM), platform specific model (PSM), physics model.<sup>2</sup> Each Model has different abstraction level. A developer defines models and generates a less abstract model by software development in MDA. Here, MDA Tool is used to generate a less abstract model. A developer uses UML for modeling PIM and PSM.

One of the MDA's problems is how to keep consistency between the original model and an edited model which is generated from the original. A modification method of PIM to keep consistency with PSM is researched.<sup>3</sup>

Also, there is no consistency way if a developer edits the original model. A developer can keep consistency if MDA Tool generates models from the edited models again. However, MDA Tool cannot generate complete

models from abstract models because these models do not have detail specification of a system. The developer must modify generated models to fit the modified original models or generate a new model from the modified models with MDA Tool and then add the detail specification to the new model by hand again.

The purpose of this study is to improve the efficiency of software development using MDA. This paper proposes a modification method of a source code to correspond with a modified model in MDA.

## 2. Proposal Method

As shown in Fig. 1, the proposed method has four functions: generate a source code from the activity diagram, generate EAD, modify EAD to correspond with the modified activity diagram, and generate a source code from the modified EAD. The proposed method consists of six steps as below.

- (i) generate a source code from the activity diagram
- (ii) add detail specification to the generated source code

- (iii) generate EAD
- (iv) modify the activity diagram
- (v) modify EAD
- (vi) generate a source code from the modified EAD

### 2.1. Generate a source code from the activity diagram

The proposed method generates a source code from the activity diagram. The steps to generate source code are shown as below.

- (i) Acquire the function name
  - The method generates a skeleton of source code.
  - The function name is the activity name that is described in the activity diagram. Here, the type and the parameter of the function is void.
- (ii) Select the initial node
- (iii) Implement the function
  - The method executes the process as below depending on the type of the selected node.
    - Call activity node
      - Write the name of the call activity node to the source code.
    - Decision node
      - Write an if-statement to the source code.
      - Condition of if-statement is guard condition of this node.
    - Activity final node
      - Finish the generation of the source code.
    - Other than the above
      - Do nothing.
- (iv) Select another node
  - The method reselects the node connected by the outgoing edge of the selected node and go to (iii)

### 2.2. Add detail specification to the generated source code

A developer adds detail specification to the generated source code.

### 2.3. Generate EAD

The method generates EAD from an activity diagram and a source code added detail specification. At the first step, the method selects the first line of the source code added detail specification. Thereafter, we call the selected source code “LOS (line of selected)”. The method executes the process shown as below.

© The 2015 International Conference on Artificial Life and Robotics (ICAROB 2015), Jan. 10-12, Oita, Japan

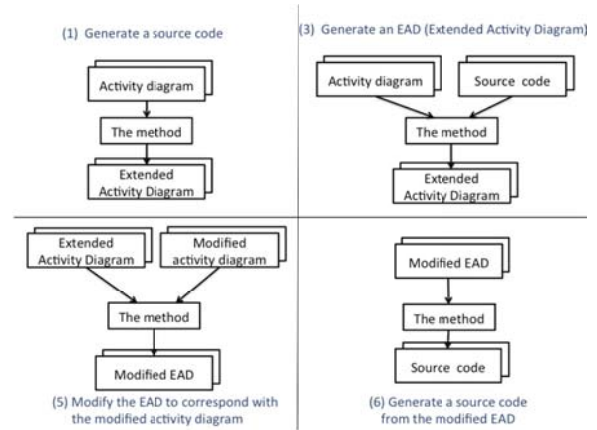


Fig. 1. Functions of the proposed method.

- (i) Generate a source code from activity diagram by the steps shown in section 2.1.
- (ii) Select the next line of LOS
- (iii) If (i) and (ii) are not same character string, the method executes the process shown as below
  - (a) Write LOS to the activity diagram
  - (b) Encircle lines written in (a) as a node
  - (c) Select the original node of the generated source code in (i)
  - (d) Connect the outgoing edge for the selected node to the node generated in (b)
  - (e) Make an edge connected with the selected node and the node generated in (a)
  - (f) Go to (ii)
- (iv) If encircled nodes are connected each of them, the method collects them as one node
- (v) Go to (i)

### 2.4. Modify the activity diagram

At the second step, a developer modifies the activity diagram to fit the changed requirement specification.

### 2.5. Modify EAD

The method modifies EAD to correspond with the modified activity diagram. The method selects initial nodes of the EAD and the modified activity diagram. We call the node extended in EAD “EAD selected node”. We call the node extended in activity diagram “AD selected node”. The method executes the process shown as below.

- (i) Check whether AD selected node and EAD selected node have the same name or not

- (ii) Execute the process shown as below depending on the result of (i)
  - They have the same name.
    - (a) Change EAD selected node to the next node of the current EAD selected node
    - (b) Change node to the next node of current AD selected node
  - They do not have the same name.
    - (a) Write the EAD selected node to the activity diagram
    - (b) Make an edge to connect the EAD selected node and the node written in (a)
    - (c) Change AD selected node to the next node of the current AD selected node

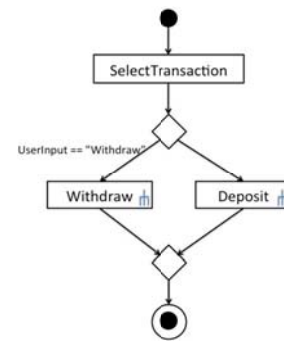


Fig. 2. The activity diagram.

**2.6. Generate a source code from the EAD**

The method generates a new source code from the modified EAD. It has information about detail specification and is applied the changed requirement specification. Therefore, a new source code generated from the modified EAD corresponds with the changed requirement specification and has information about detail specification.

Here, the method can treat only if-statement. The way to treat other statements is a future issue. In addition, the method can treat with addition only to a generated source code and an activity diagram, but it cannot treat with deletion or revision. Correspondence to them is a future issue.

**3. Application Example**

We use a simple ATM as an example to confirm availability of the method. This ATM system executes a withdrawal process or a depositing process depending on a user input. Fig. 2 shows the activity diagram that expresses processing flow of the ATM system.

The method generates a source code from the activity diagram. Fig. 3 shows a generated source code.

The developer adds the detail specification to the generated source code in order to execute it. The source code added the detail specification shown in Fig. 4.

Suppose a case that the requirement of specification is changed to add a process of balance checking after adding the detail specification.

```
void Transaction(){
    if(UserInput == "Withdraw"){
        Withdraw();
    }else{
        Deposit();
    }
}
```

Fig. 3. The source code generated from activity diagram.

```
void Transaction(){
    string UserInput;
    cin>>UserInput;

    if(UserInput == "Withdraw"){
        Withdraw();
    }else{
        Deposit();
    }
}
```

Fig. 4. The source code added detail specification.

The method generates the EAD from source code added the detail specification and the activity diagram shown in Fig. 2. Fig. 5 shows the generated EAD.

A developer adds the process of balance checking to the activity diagram as shown in Fig. 2. Fig. 6 shows the activity diagram added the process of balance checking.

The method modifies EAD to correspond with the modified activity diagram. Fig. 7 shows the modified EAD.

The method generates the source code from the modified EAD. Fig. 8 shows the generated source code. This source code has the detail specification.



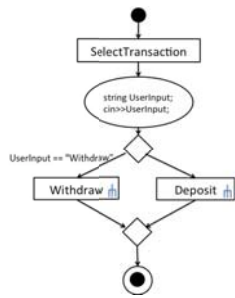


Fig. 5. The Extended Activity Diagram.

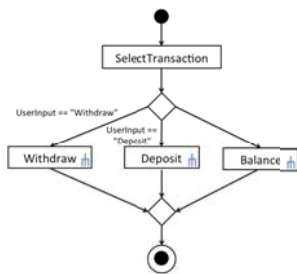


Fig. 6. The modified activity diagram.

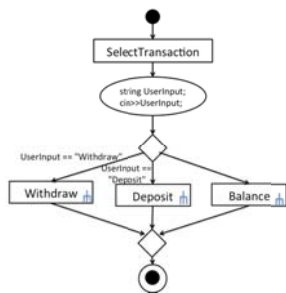


Fig. 7. The modified EAD.

#### 4. Discussion

MDA Tool such as EA<sup>4</sup> (Enterprise Architecture) can generate a skeleton of a source code from a class diagram. In addition, EA can generate a source code from an activity diagram or a state machine diagram. However, The source code generated by EA does not have detail specification. It takes time and effort that the developer adds detail specification to the source code generated from the modified activity diagram.

The method can generate a source code including detail specification. The method can reduce time and effort to add detail specification to the source code generated from the modified activity diagram. Moreover,

```
void Transaction(){
    string userInput;
    cin>>UserInput;

    if(UserInput == "Withdraw"){
        Withdraw();
    }else if(UserInput == "Deposit"){
        Deposit();
    }else{
        Balance();
    }
}
```

Fig. 8. The source code generated from EAD.

it can reduce time and effort to keep consistency between models and a source code after requirement specification is modified. Therefore, the method is useful for efficiency of software development.

#### 5. Conclusion

This paper has proposed a modification method of a source code to correspond with a modified model in MDA. The method can generate the source code that corresponds with the modified activity diagram and has information about detail specification. We have confirmed that the method can generate a source code including the detail specification from the original activity diagram, the modified activity diagram, and the original source code. Therefore, the method is useful for efficiency of software development.

Future issues are as follows.

- Development of the tool implemented the method
- Improvement of the method to treat with deletion or revision to source code and activity diagram.
- Improvement of the method to treat with other statements except if-statement.

#### References

1. Yamashiro A, Sugimoto N, Hosoya R, From Program Coding to Software Modeling (in Japanese), TOSHIBA review, **58** (2003) 65-69.
2. Wada H, Yasutake Y, MDA (Model Driven Architecture) and Actual Development Process (in Japanese), UNISYS TECHNOLOGY REVIEW, No.61 (2004).
3. Ueno M, Omori M, An Approach to Keep Coherence between PIM and PSM of MDA (in Japanese), IPSJ SIG Technical Report, SE-156 (7), (2007).
4. Enterprise Architect, <http://www.sparxsystems.jp> (accessed December 10, 2014).

# Prototype of a Decision Table Generation Tool from the Formal Specification

Kenta Nishikawa<sup>\*</sup>, Tetsuro Katayama<sup>\*</sup>, Yoshihiro Kita<sup>†</sup>  
Hisaki Yamaba<sup>\*</sup>, Kentaro Aburada<sup>‡</sup> and Naonobu Okazaki<sup>\*</sup>

<sup>\*</sup>University of Miyazaki, 1-1 Gakuen-kibanadai nishi, Miyazaki, 889-2192 Japan

<sup>†</sup>Kanagawa Institute of Technology, 1030 Shimo-ogino, Kanagawa, 243-0292 Japan

<sup>‡</sup>Oita National College of Technology, 1666 Maki, Oita, 870-0152 Japan

E-mail: nishikawa@earth.cs.miyazaki-u.ac.jp, kat@cs.miyazaki-u.ac.jp, kita@earth.cs.miyazaki-u.ac.jp,  
yamaba@cs.miyazaki-u.ac.jp, aburada@oita-ct.ac.jp, oka@cs.miyazaki-u.ac.jp

## Abstract

This research has implemented a prototype of a decision table generation tool from the specification (the formal specification) described in a formal specification language. This paper uses the formal specification description language VDM++ which is the lightweight formal methods VDM (Vienna Development Method) to write the formal specification. We applied some general specifications to the prototype, in order to evaluate its usefulness. As a result, the prototype has improved the efficiency in test design with formal methods.

*Keywords:* automatic generation, decision table, formal method, formal specification, VDM++, test design

## 1. Introduction

In recent years, the software quality cannot be maintained with the conventional software development methods because software system becomes large scale and high performance. At the same time, effect of defects in the system becomes one of the major social problems with the economy and life.

Hence, the software quality becomes more important. A demand for reliability and safety of the system is growing.

In general, many defects are embedded in the upstream process of the software development.<sup>1</sup> As one reason of the above, each step in the software development process moves to the next step with specifications included ambiguous description. Therefore, specifications should be written strictly. As a means for writing specifications strictly, formal methods<sup>2</sup> are proposed. The formal methods are a means for using strict specifications in each step in the software development process. They express the system

with a specification description language based on mathematical logic. Using the formal methods can remove defects or ambiguity of the specifications. They attract attention as a means to improve software quality.

By the way, as one of the test techniques, the decision table<sup>3</sup> is proposed in the testing process of the software cycle. The decision table uses a matrix divided the logical relationships in specifications into items of conditions and actions. However, it takes much time and effort to design the decision table. It is needed to extract test items and understand contents written on specifications. It is no exception even if you write strict specifications with formal methods.

This research has implemented a prototype of a decision table generation tool from the specification (the formal specification) described in a formal specification language, in order to improve efficiency of the test design with formal methods.<sup>4</sup> This prototype generates a decision table from the formal specifications, and displays it. This paper uses the formal specification description language VDM++ which is the lightweight

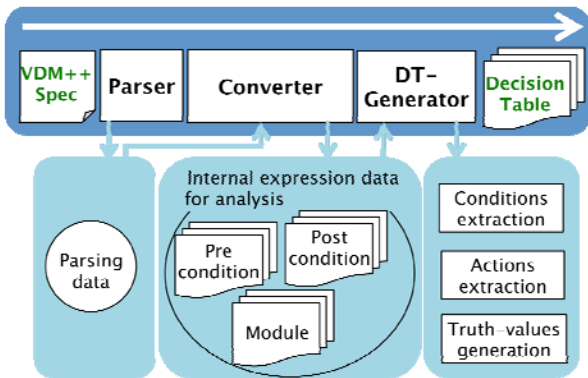


Fig. 1. A process to generate a decision table of the prototype.

Table 1. Extraction rules.

Pattern of condition extraction	Pattern of action extraction
if “condition” then	then “action” elseif
elseif “condition” then	then “action” else
	else “action” if
	else “action” elseif
	else “action” else
	else “action” EOF
cases “condition” ->	-> “action” cases
	others “action” EOF
pre “condition” post	
pre “condition” EOF	
post “condition” EOF	

EOF(End Of File)

formal methods VDM (Vienna Development Method) to write the formal specification.

## 2. Process to Generate a Decision Table of the Prototype

Fig. 1 shows a process to generate a decision table of the prototype. The prototype consists of three parts: Parser, Converter, and DT-Generator. We use a parser of Overture Toolset as a Parser.<sup>5</sup>

First, Parser reads a VDM++ specification inputted by a user, parses VDM++ specification, and outputs a parsing data. The parsing data has an abstract syntax tree and tokens.

Next, Converter converts the parsing data into an internal expression data for analysis by a module unit. The internal expression data for analysis is a data converted an abstract syntax tree of a parsing data into information suitable for analysis such as the division of a module or the correspondence of “if” and “else”.

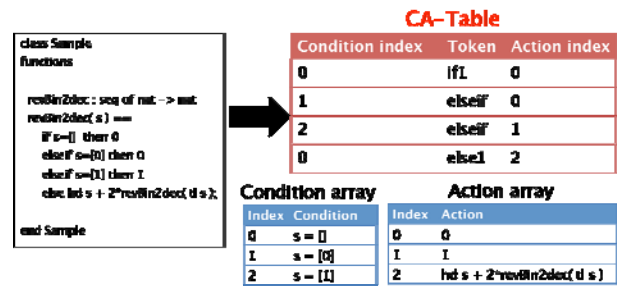


Fig. 2. An example of CA-Table.

Then, DT-Generator extracts conditions and actions from an internal expression data for analysis. After, DT-Generator stores conditions and actions in an array of String type. Table 1 shows extraction rules of conditions and actions. DT-Generator makes CA-Table, when DT-Generator extracts conditions and actions. Fig. 2 shows an example of CA-Table. CA-Table is a table which is correspondence of conditions and actions. CA-Table is three columns of condition index, token, and action index. DT-Generator generates truth-values based on this CA-Table.

We show truth-values generating process as follows.

- (i) Make an array to store truth-values
- (ii) Select the first column of this array
- (iii) Select a row of CA-Table
- (iv) Compare a token of the selected row of CA-Table
  - (a) If this token matches “if”, “elseif”, or “cases”
    - (I) Store “Y” into the condition index row of this column, then store “N” from the next column to the last column
    - (II) Store “X” into the action index row of this column
  - (b) If this token matches “else”, or “others”
    - (I) Store “N” into the condition index row of this column, then store “-” from the next column to the last column
    - (II) Store “X” into the action index row of this column
- (v) If there is a row that we have not yet selected, we select the next column of this array and return to third step. Otherwise truth-values is filled

Finally, DT-Generator generates a decision table from conditions, actions, and truth-values.

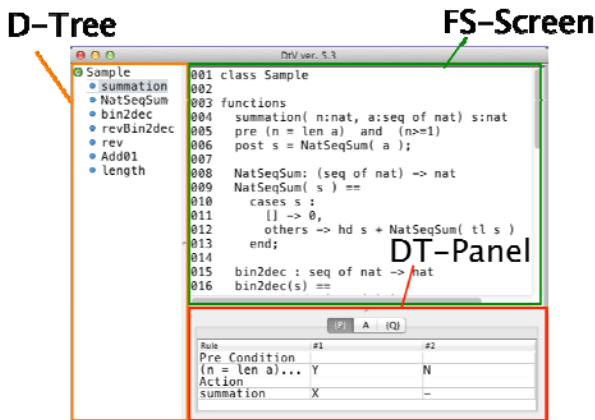


Fig. 3. Overview of the prototype.

### 3. Overview of the Prototype and Application Example

Fig. 3 shows overview of the prototype. The prototype consists of three displays: D-Tree, FS-Screen, and DT-Panel. FS-Screen displays a VDM++ specification inputted by a user. DT-Panel consists of three tabs: P-Tab, A-Tab, and Q-Tab. P-Tab displays a decision table of preconditions. A-Tab displays a decision table of a module. Q-Tab displays a decision table of post conditions. D-Tree displays a list of the definition names of the VDM++ specification. D-Tree redraws a decision table, when a user selects any the definition names of a VDM++ specification.

We confirm that this prototype works properly by adapting it to an example. Fig. 4 shows an example formal specification. It stores a positive integer  $X$  in a binary expression array  $b$ . Here, the highest-order digit must become one.

Fig. 5 shows the application example results. These results shows that this prototype extracts conditions and actions from a specification. Also, these results shows that this prototype generates truth-values. Therefore, we have confirmed that this prototype works properly.

### 4. Discussion

This research has implemented a prototype of a decision table generation tool from the formal specification, in order to improve efficiency of the test design with formal methods. This prototype generates a decision table from the formal specifications, and displays it.

© The 2015 International Conference on Artificial Life and Robotics (ICAROB 2015), Jan. 10-12, Oita, Japan

```

class Dec2bin
functions

dec2bin( X : nat ) b : seq of nat
pre X >= 1

post (forall i in set inds b & b(i)=1 or b(i)=0) and
b(1) = 1 and
X = NatSeqSum( [ b(i)*2**(len b - i) | i in set inds b ] );

NatSeqSum : seq of nat -> nat
NatSeqSum( s ) ==
cases s :
[] -> 0,
others -> hd s + NatSeqSum( tl s )
end;

end Dec2bin
    
```

Fig. 4. The formal specification of converting decimal to binary.

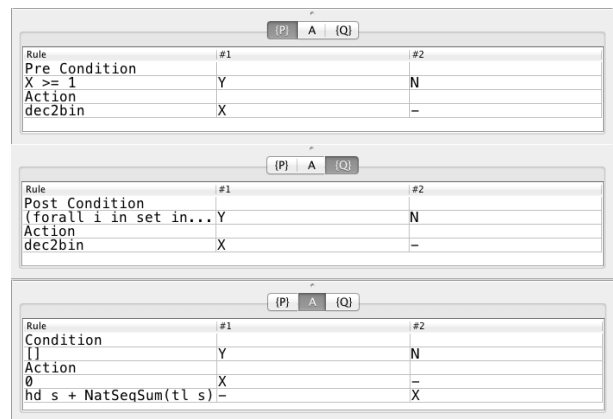


Fig. 5. The application example results.

We discuss our prototype in this chapter.

#### 4.1. Evaluation of the usefulness

We confirm the usefulness of this prototype by using the examinees.

Specifically, we apply three specifications, which is ways of combination of truth-values of the conditions are different. Then, we measure the time of examinees and the prototype, which is required until completion for the decision table, and compares it.

Table 2. The measured results.

Formal Specifications (ways of combination of truth-values of the conditions)	Examinee A (sec)	Examinee B (sec)	Examinee C (sec)	Examinee D (sec)	Examinee E (sec)	Average (sec)	Prototype (sec)
Specification A (4)	252	213	169	240	134	216	0.012
Specification B (16)	405	559	499	435	557	498	0.016
Specification C (256)	1131	1292	1194	1859	1397	1629	0.02

Table 2 shows the measured results. By using the tool, we could automatically generate a decision table which has 256 ways of combination of truth-values of the conditions in about 20 milliseconds.

That is, we have confirmed the usefulness of this prototype.

#### 4.2. Related work

Few researches of test design from the formal specification are reported<sup>6</sup>, and the method is not well established.

Also, CEGTest<sup>7</sup> is a tool supporting the generation of the decision table. CEGTest automatically generates from a cause effect graph created by a user. However, a user must make a cause effect graph created, manually. Therefore, it takes much time and effort. It is needed to extract test items and understand contents written on the formal specification.

In addition, some test tools that inputs the formal specification are proposed<sup>8, 9</sup>, but those tools do not support the generation of the decision table from a formal specification such as our prototype. In contrast, our prototype can automatically get a decision table from the formal specification inputted by a user.

#### 5. Conclusions

This research has implemented a prototype of a decision table generation tool from the formal specification, in order to improve efficiency of the test design with formal methods. This prototype generates a decision table from the formal specifications, and displays it.

We have confirmed that our prototype extracts conditions and actions from the formal specification. Also, we confirmed that the prototype generates truth-values.

By using the tool, we could automatically generate a decision table which has 256 ways of combination of truth-values of the conditions in about 20 milliseconds.

Future issues are as follows.

- The usefulness improvement of the prototype
- Application to large-scale system specifications
- Automatic generation of test data
- Expansion to other test design techniques

#### References

1. G. Tasse, The Economic Impacts of Inadequate Infrastructure for Software Testing, National Institute of Standards and Technology, Planning Report 02-3 (2002).
2. John Fitzgerald, Peter Gorm Larsen, Paul Mukherjee, Nico Plat, Marcel Verhoef, Validated Designs for Object-Oriented Systems, Springer (2005).
3. ISO 5806, Specification of single-hit decision tables.
4. Kenta Nishikawa, Tetsuro Katayama, Yoshihiro Kita, □Hisaaki Yamaba and Naonobu Okazaki, Proposal of a Supporting Method to Generate a Decision Table from the Formal Specification, *International Conference on Artificial Life and Robotics*, (2014) 222-225. □
5. A Scanner/Parser for the Overture Toolset, <http://overturetool.hosting.west.nl/twiki/bin/view/Main/OvertureParser/> (accessed October 30, 2014).
6. Jeremy Dick, Alain Faiver, Automating the Generation and Sequencing of Test Cases from Model-Based Specifications, *FME'93: Industrial-Strength Formal Methods*, Lecture Notes in Computer Science, **670** (1993) 268-284.
7. CEGTest, <http://softest.jp/tools/CEGTest/> (accessed October 30, 2014).
8. Y. Ledru, L. du Bousquet, O. Maury, and P. Bontron, Filtering TOBIAS combinatorial test suites, *Fundamental Approaches to Software Engineering*, (2004) 281-294.
9. Adriana Sucena Santos, Combinatorial Test Automation Support for VDM++, *VDM/Overture Workshop*, (2008) 45-53.

Table 2. The measured results.

Formal Specifications (ways of combination of truth-values of the conditions)	Examinee A (sec)	Examinee B (sec)	Examinee C (sec)	Examinee D (sec)	Examinee E (sec)	Average (sec)	Prototype (sec)
Specification A (4)	252	213	169	240	134	216	0.012
Specification B (16)	405	559	499	435	557	498	0.016
Specification C (256)	1131	1292	1194	1859	1397	1629	0.02

Table 2 shows the measured results. By using the tool, we could automatically generate a decision table which has 256 ways of combination of truth-values of the conditions in about 20 milliseconds.

That is, we have confirmed the usefulness of this prototype.

#### 4.2. Related work

Few researches of test design from the formal specification are reported<sup>6</sup>, and the method is not well established.

Also, CEGTest<sup>7</sup> is a tool supporting the generation of the decision table. CEGTest automatically generates from a cause effect graph created by a user. However, a user must make a cause effect graph created, manually. Therefore, it takes much time and effort. It is needed to extract test items and understand contents written on the formal specification.

In addition, some test tools that inputs the formal specification are proposed<sup>8, 9</sup>, but those tools do not support the generation of the decision table from a formal specification such as our prototype. In contrast, our prototype can automatically get a decision table from the formal specification inputted by a user.

#### 5. Conclusions

This research has implemented a prototype of a decision table generation tool from the formal specification, in order to improve efficiency of the test design with formal methods. This prototype generates a decision table from the formal specifications, and displays it.

We have confirmed that our prototype extracts conditions and actions from the formal specification. Also, we confirmed that the prototype generates truth-values.

By using the tool, we could automatically generate a decision table which has 256 ways of combination of truth-values of the conditions in about 20 milliseconds.

Future issues are as follows.

- The usefulness improvement of the prototype
- Application to large-scale system specifications
- Automatic generation of test data
- Expansion to other test design techniques

#### References

1. G. Tasse, The Economic Impacts of Inadequate Infrastructure for Software Testing, National Institute of Standards and Technology, Planning Report 02-3 (2002).
2. John Fitzgerald, Peter Gorm Larsen, Paul Mukherjee, Nico Plat, Marcel Verhoef, Validated Designs for Object-Oriented Systems, Springer (2005).
3. ISO 5806, Specification of single-hit decision tables.
4. Kenta Nishikawa, Tetsuro Katayama, Yoshihiro Kita, Hisaaki Yamaba and Naonobu Okazaki, Proposal of a Supporting Method to Generate a Decision Table from the Formal Specification, *International Conference on Artificial Life and Robotics*, (2014) 222-225. □
5. A Scanner/Parser for the Overture Toolset, <http://overturetool.hosting.west.nl/twiki/bin/view/Main/OvertureParser/> (accessed October 30, 2014).
6. Jeremy Dick, Alain Faiver, Automating the Generation and Sequencing of Test Cases from Model-Based Specifications, *FME'93: Industrial-Strength Formal Methods*, Lecture Notes in Computer Science, **670** (1993) 268-284.
7. CEGTest, <http://softest.jp/tools/CEGTest/> (accessed October 30, 2014).
8. Y. Ledru, L. du Bousquet, O. Maury, and P. Bontron, Filtering TOBIAS combinatorial test suites, *Fundamental Approaches to Software Engineering*, (2004) 281-294.
9. Adriana Sucena Santos, Combinatorial Test Automation Support for VDM++, *VDM/Overture Workshop*, (2008) 45-53.